United States Committee on Large Dams

USCOLD

Proceedings

Fifth Benchmark Workshop on Numerical Analysis of Dams

Denver, Colorado, U.S.A.
June 1999

CIGB ICOLD

USCOLD

U.S. DEPARTMENT OF THE INTERIOR BUREAU OF RECLAMATION

Zenz

United States Committee on Large Dams

Proceedings

Fifth Benchmark Workshop on Numerical Analysis of Dams

Organized by the ICOLD Ad Hoc Committee on
Computational Aspects of Analysis and Design of Dams

Sponsored by USCOLD and the Bureau of Reclamation

USCOLD

The United States Committee on Large Dams (USCOLD), a Member of the International Commission on Large Dams, is a professional organization dedicated to:

- advancing the technology of dam engineering, construction, operation, maintenance and safety;
- fostering socially, environmentally and financially responsible water resources projects; and
- promoting public awareness of the role of dams in the beneficial and sustainable development of the nation's water resources.

Printed in the United States of America

Library of Congress Catalog Card Number: 00-107394

ISBN 1-884575-17-X

U.S. Committee on Large Dams
1616 Seventeenth Street, Suite 483
Denver, CO 80202
Telephone: 303-628-5430
Fax: 303-628-5431
E-mail: stephens@uscold.org
Internet: www.uscold.org/~uscold

Foreword

The **Fifth Benchmark Workshop on Numerical Analysis of Dams** was held June 2-5, 1999, in Denver, Colorado, USA. The Workshop was the latest in a series of workshops organized by the ICOLD Ad Hoc Committee on Computational Aspects of Analysis and Design of Dams.

Consistent with previous Workshops, four problems were featured, two on concrete dams and two on embankment dams. Computational analyses of the problems were submitted in advance to the problem formulators and presented during the Workshop. The problem formulators then prepared synthesis reports which summarized the problem, analysis data and results. Also included in these Proceedings are three papers presented during the Workshop Poster Session.

During the three years since the Fourth Benchmark Workshop was held in 1996, the ICOLD Ad Hoc Committee finalized the report ***Reliability and Applicability of Computational Procedures for Dam Engineering***. I think that the report enables the readers to recognize a hierarchy among phenomena which contribute to determine the safety of a dam — hierarchy which is based on two precise criteria of selection. First, the relevance in applications must be considered, i.e. major emphasis has to be paid to phenomena most commonly faced by dam engineers; second, emphasis must be placed on the reliability of available numerical procedures.

Accordingly, the topics developed for the Fifth Benchmark Workshop reflect this philosophy and try to respond to recommendations in the report.

Undoubtedly the addressed topics (the role played by peripheral joint and uplift pressure in arch dams, the failure mode of overtopped gravity dams, the comparison between classical analysis procedure and advanced methods in embankments, the simulation of first filling of rockfill dams) are of great interest both for practicing engineers and for analysts.

It is my hope that the solutions presented in this Proceedings will become the terms of reference for the validation of numerical procedures and, at the same time, constitute a useful reference in making modeling choices.

G. Giuseppetti
Chairman, ICOLD Ad Hoc Committee on
Computational Aspects of Analysis and
Design of Dams
Milan, Italy

Scientific Committee

(Members, ICOLD Ad Hoc Committee on
Computational Aspects of Analysis and Design of Dams)

G. Giuseppetti, Chairman (Italy)
B. Tardieu, Vice Chairman (France)
R. Dungar (Switzerland)
P. J. Pahl (Germany)
M. Fanelli (Italy)
J. Polimon (Spain)
W. Liam Finn (Canada)
A. Popovici (Romania)
Y. P. Liapichev (Russia)
D. Ravaska (Finland)
S. N. Soheili (Iran)
C. H. Yeh (U.S.A.)
P. Obernhuber (Austria)
K. Yoshikoshi (Japan)

Organizing Committee

D. Harris, Bureau of Reclamation (U.S.A.)
G. Mazza, ENEL S.p.A. Ricerca (Italy)
V. Saouma, University of Colorado (U.S.A.)
F. Chille, ENEL S.p.A. Ricerca (Italy)
G. Zenz, Verbundplan GmbH (Austria)
G. La Barbera, ISMES S.p.A. (Italy)
A. Carrere, Coyne & Bellier (France)
P. Palumbo, ISMES S.p.A. (Italy)

Technical Secretariat

ISMES
Attention: Pasquale Palumbo
Permanent Benchmark Workshop Technical Secretariat
Via Pastrengo, 9
24068 Seriate (BG), Italy
Telephone: 39-35-307-111
Fax: 39-35-302-999
E-mail: ppalumbo@ismes.it

Table of Contents

Poster Session

5th International Benchmark Workshop
on
Numerical Analysis of Dams

Theme A1 - Concrete Dam

Uplift Pressure and Stress Analysis of an Arch Dam Foundation

1. Introduction
2. Analysis Data
3. System Requirements
4. Requested Results

- Appendix A
- Appendix B

1. INTRODUCTION

Dam Description

Schlegeis Arch Dam was constructed under favourable geological site conditions as double curvature arch-gravity dam with a crest/height ratio of 5.5. The horizontal sections designed in an elliptical shape, which permitted optimum fitting into the unsymmetrical valley configuration. The dam consists of 43 blocks, each 17 m wide. The blocks have plane vertical joints (fig. 1).
The dam is provided with 4 horizontal inspection galleries and the base gallery located at the foundation rock. The upstream grout curtain originally consisted of a vertical main curtain beneath the dam base extending to a depth of 50 m, and a shallower secondary grout curtain extending from the base gallery and inclined towards the upstream (fig. 2). Because of the large span in relation to its height the dam is monitored with a wide range instrumentation. The most important surveillance instruments are five shafts with direct and inverted pendulums extending to a depth of 80 m below the dam base.
When top storage level was first reached in 1973, seepage rates of 200 l/s where measured in the middle part of the base gallery. This water inflow was due to cracking in the foundation rock caused by tensile stresses. To reduce this amount of seepage water a cut off wall was built in a total of a eleven blocks. Since than the seepage rate at top storage level has not exceeded of about 25 l/s.
The objective of Theme A1 is to investigate the performance of a wide spanned arch dam. The basic model assumption is, that the dam body may decouple from rock foundation within the interface tensile stresses evolve. The reason for that assumption is the monitored system behaviour during the first years of operation.
The assumed loading sequence for this benchmark is:

- dead weight loading - with independent columns
- water loading
- temperature loading
- and uplift pressure loading.

The provided model is to investigate the possible opening of a predefined joint between concrete dam and rock foundation. Under full loading conditions the amount and extension of the opening of the base joint as well as the influence on the overall observed dam behaviour and block sliding stability has to be calculated. This explanation is related to figures

shown in appendix A.
A model with a reduced set of dof's (degree of freedoms) is provided in appendix B. The influence of different model size on results will be elaborated.

2. ANALYSIS DATA

The main geometric data of the Schlegeis dam are:

- crest elevation 1783 m a.s.l.
- dam height 131 m
- crest length 725 m
- crest thickness 9 m
- base thickness 34 m

Two different kind of finite element models are suggested. One fine discretized model and a model with coarser discretization. Numbers in [] give the appropriate value for the coarse model.
The Finite-Element Mesh for the dam and a sufficient portion of the foundation on the basis of quadratic, isoparametric 20 and 15 node volume elements. Six [three] elements are foreseen in radial direction at the base of the highest blocks and three at the crest. Provision is made to introduce contact elements in the interface between dam and foundation. The mesh has about 50.000 nodes and resulting into around 150000 degrees of freedom.

	Elements		Nodes	
Dam	2553	[246]	12904 + 798	[1369 + 108]
Rock	8170	[896]	39379 + 798	[4713 + 108]
Interface	399	[54]		

Table 1: Basic Data - Finite Element Mesh

	Rock	Concrete
Young's modulus E [GPa] (for rock E_{II})	30	25
Young's modulus E [GPa] (for rock $E\perp$)	10	
Poisson ratio ν	0.17	0.17
Density [kg/m^3]		2400
α_T		8.10^{-6}

Table 2: Basic Data - Material Parameters

For the rock foundation an orthotropic behaviour is assumed. The rock is assumed as massless during analysis steps. The plane of schistosity is defined in fig. 6. The rock consists of Granite-Gneiss with a schistosity of 340/75 related to Gauss-Krüger-System.
The loadings to be considered are

- selfweight of the dam
- water load for full impounded reservoir
- uplift pressure
- temperature

The selfweight of the dam has to be applied on the individual blocks (open block joints). Water load and uplift pressure are as indicated in fig. 5. Temperature (relative to that during joint grouting) will be prescribed at the upstream and downstream surfaces of the central cross section and assumed constant along the arches.
The joint behaviour is described by the following normal to shear stress relation

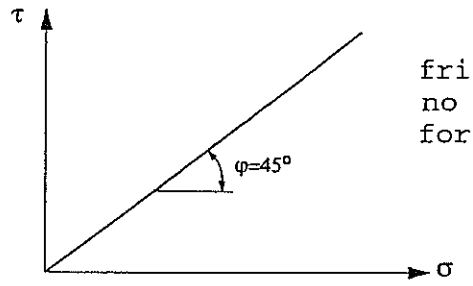

friction angle $\varphi=45^{\circ}$
no tensile stresses allowed
for being transmitted

Two sequences of analyses are suggested, a linear and a nonlinear one. The linear analysis is referred to as reference model. The nonlinear one should include the opening of the dam-foundation interface and the influence of the uplift pressure.

3. SYSTEM REQUIREMENTS

Model presented in appendix A [B]

The full model needs:

- 3.7GB [255MB] . ...Scratch file sizes
- 100MB [10MB] . ...Result file (last step only)
- 200MB ....Memory

4. REQUESTED RESULTS

For each Case examined, results should be provided (on paper and diskette) using the following instructions (requested file format is attached).

- Deformation in radial direction for block 0, 15 and 16 (nodes see fig. 9)
  (def.dat)
- Extension and opening of base joint (1364 [205])
  (open.dat)
- Maximum and Minimum principal stresses at the upstream and downstream surfaces of the dam and for block 0 in the cross section.
  Stresses are required at nodes in Ascii file-list
  (up.dat + do.dat)
- Normal and shear stresses at the dam foundation interface along a radial line (block 0, 15 and 16) - nodes see fig.9
  (nor.dat)

- Resultant forces (stresses integrated over block 0, 15 and 16) for fine model only acting on the foundation and evaluating the safety margins (Mohr-Coulomb criteria) - (s = N/T), see fig. 10
  (force.dat)

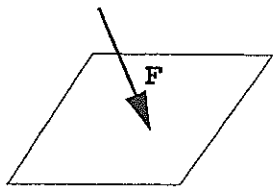

$$s = \frac{N}{T_{max}}$$

F = {Fx, Fy, Fz}

Appendix A

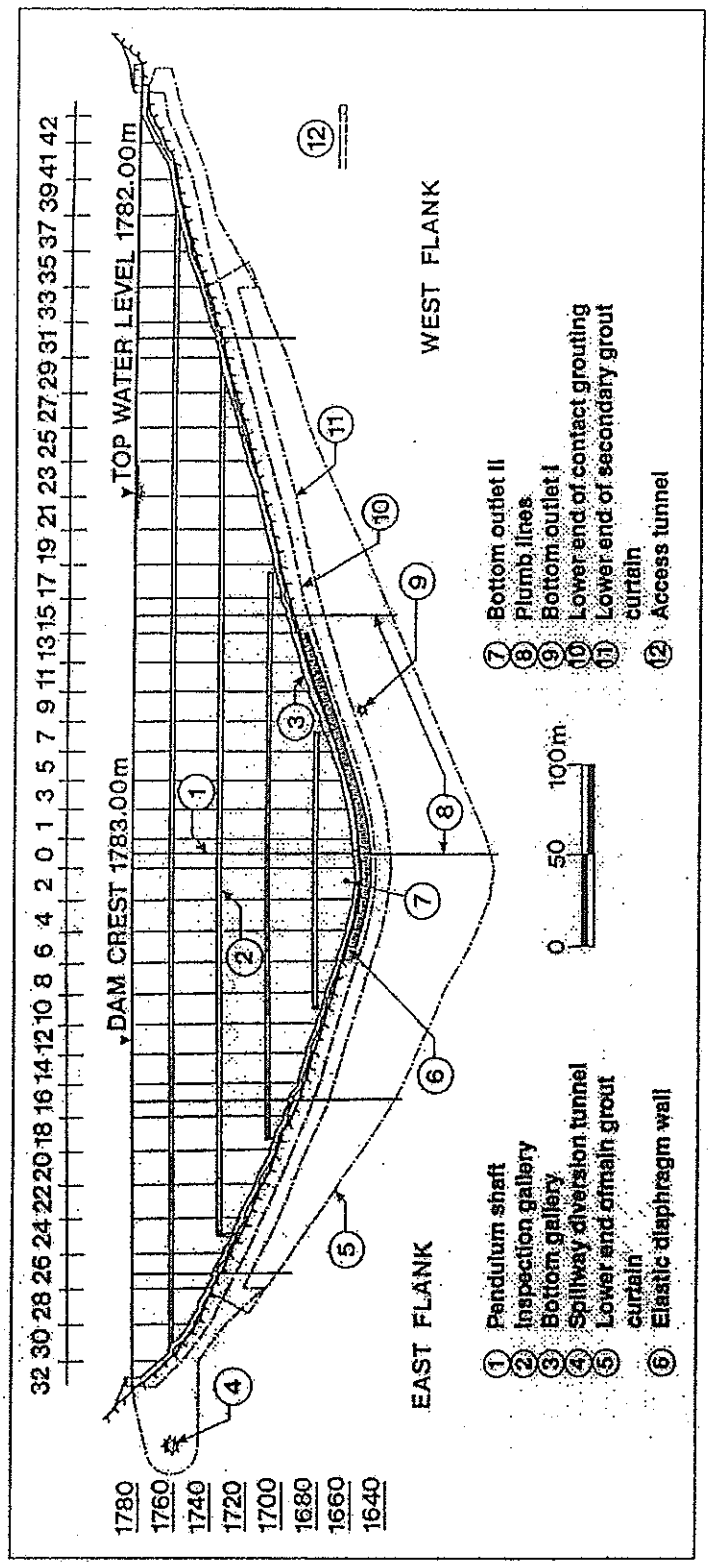

Figure 1: Overview of the Schlegeis Arch Dam

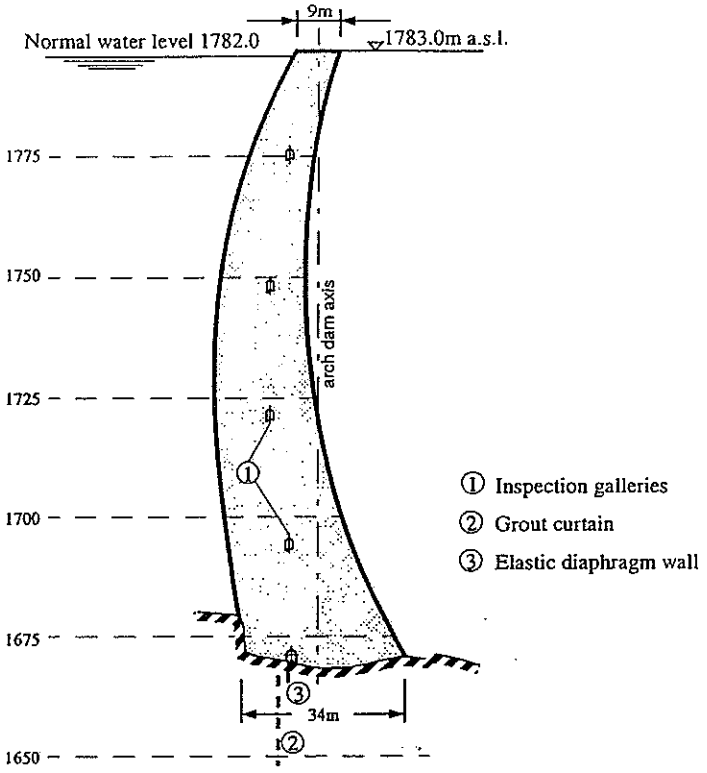

Figure 2: Central Cross Section

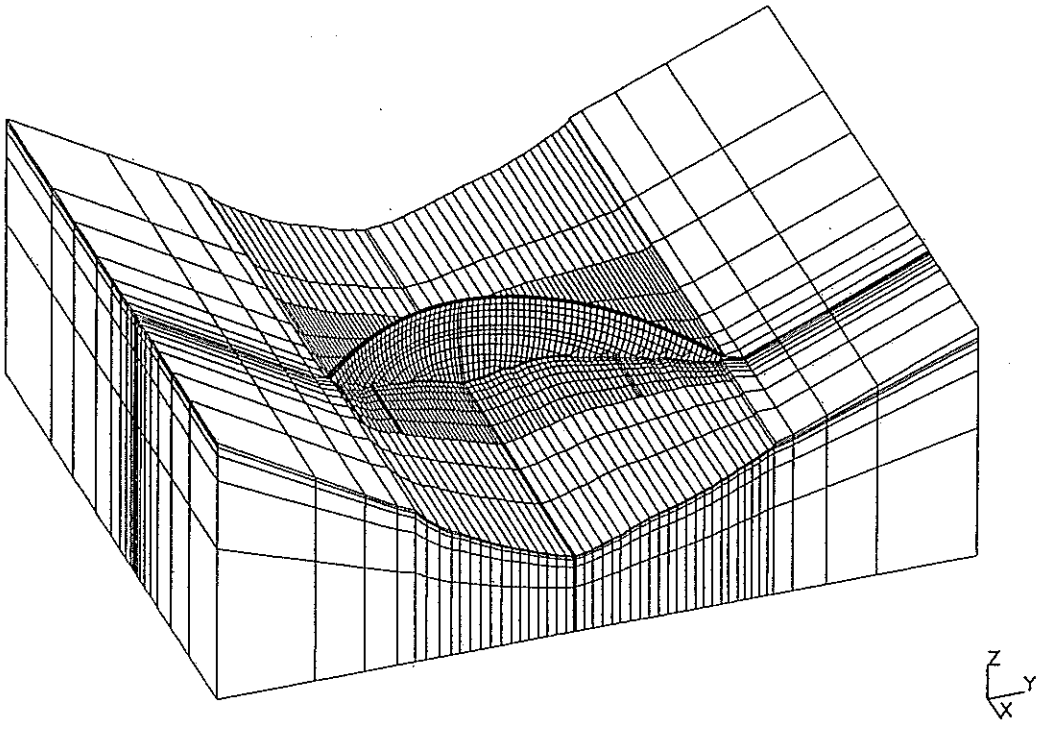

Figure 3: Downstream View of the provided Finite Element Mesh

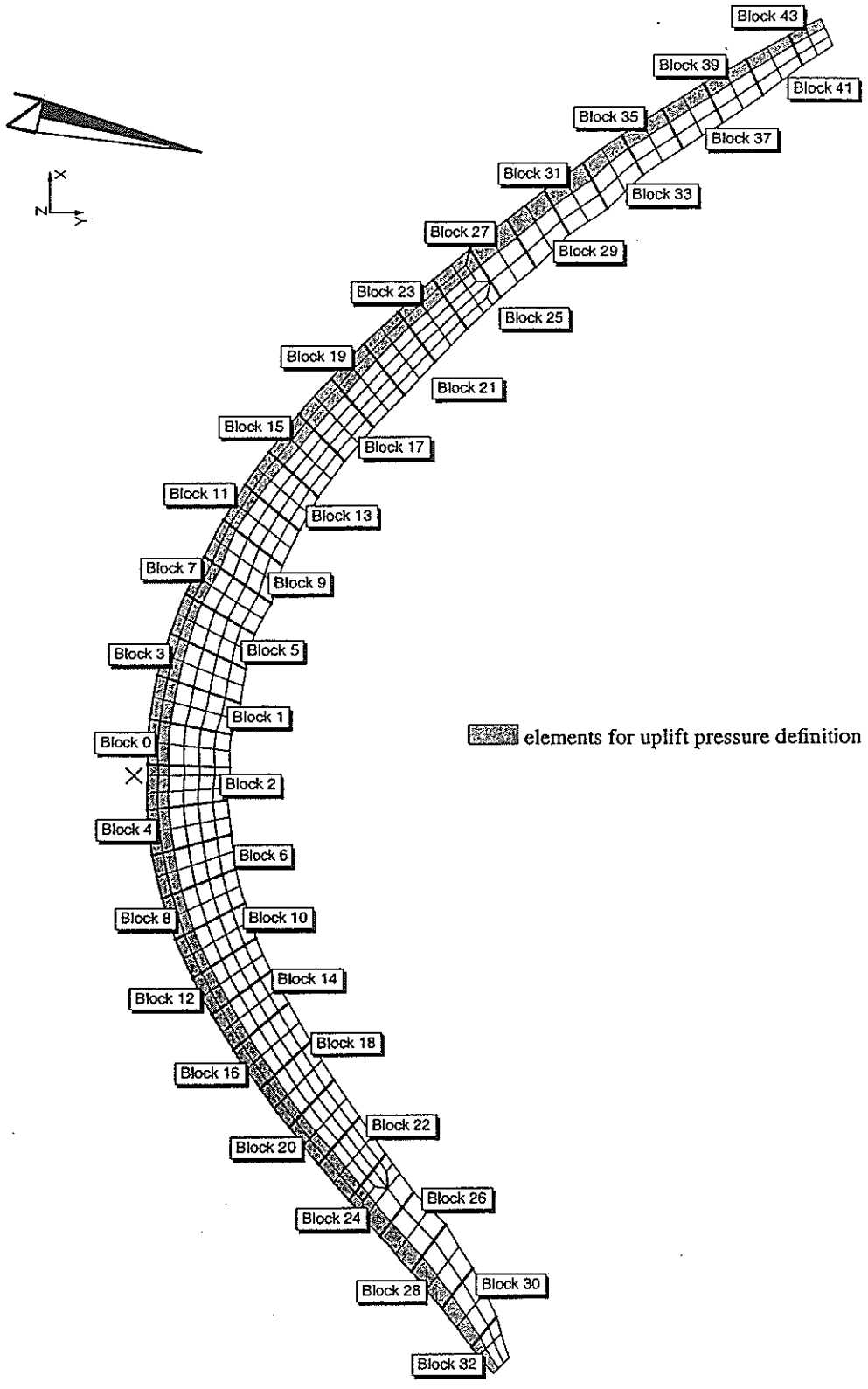

Figure 4: Interface Elements and Block Distribution

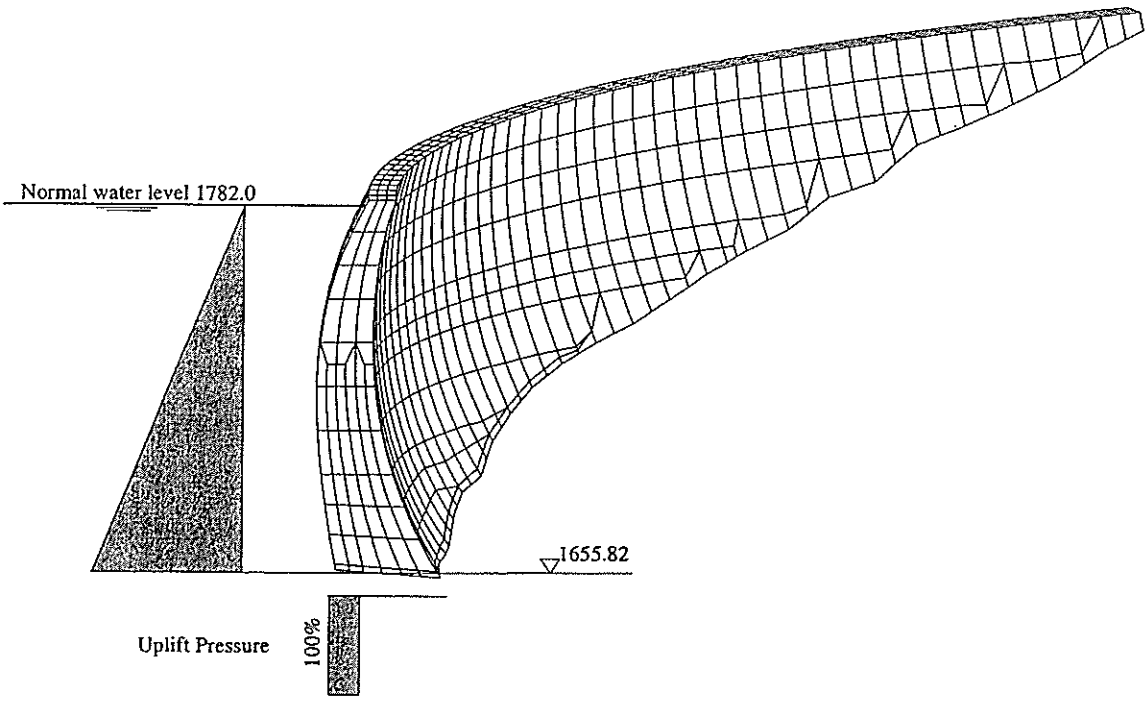

Figure 5: Dam Model, Water and Uplift Loading

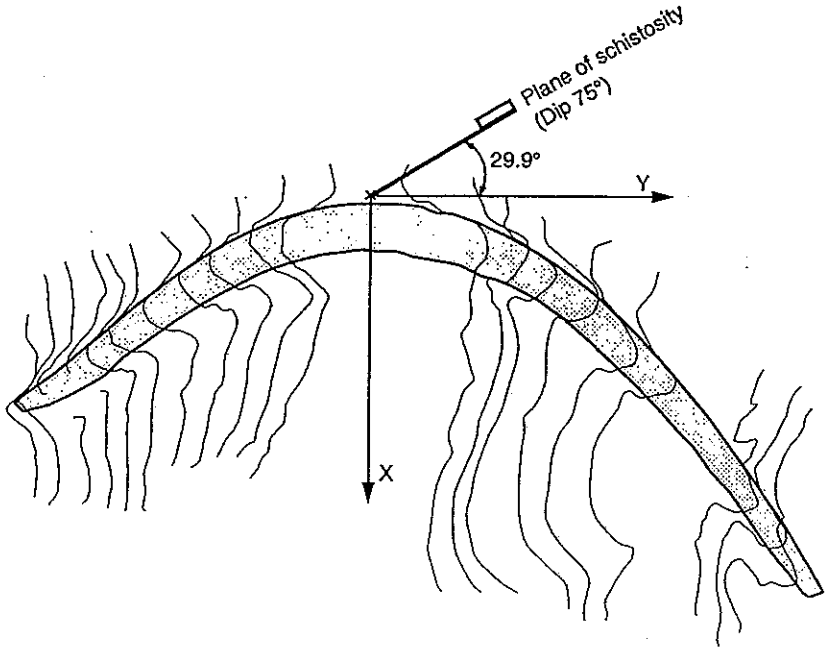

Figure 6: Description of Schistosity

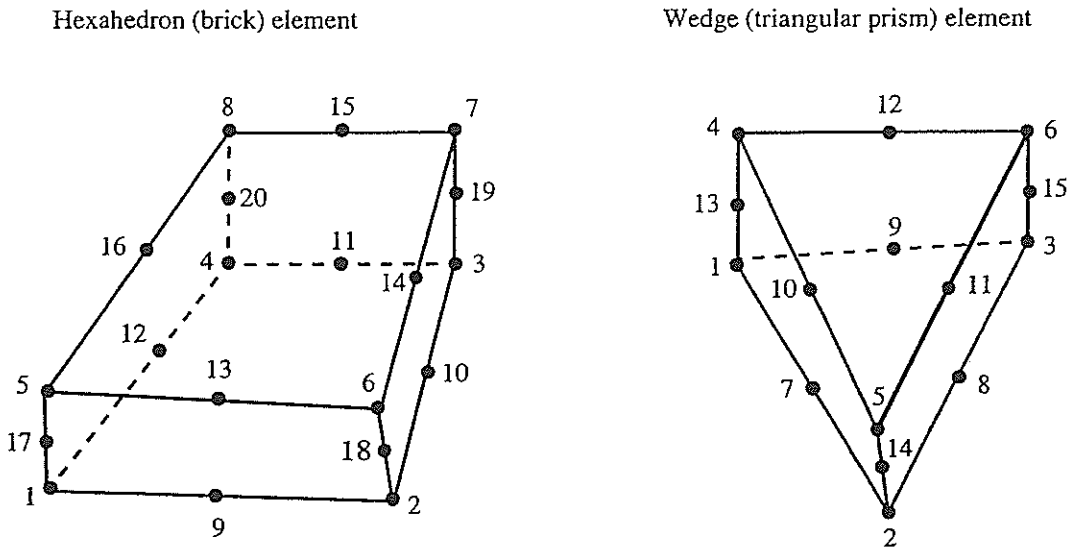

Figure 7: Node Order of the Brick and Wedge Element

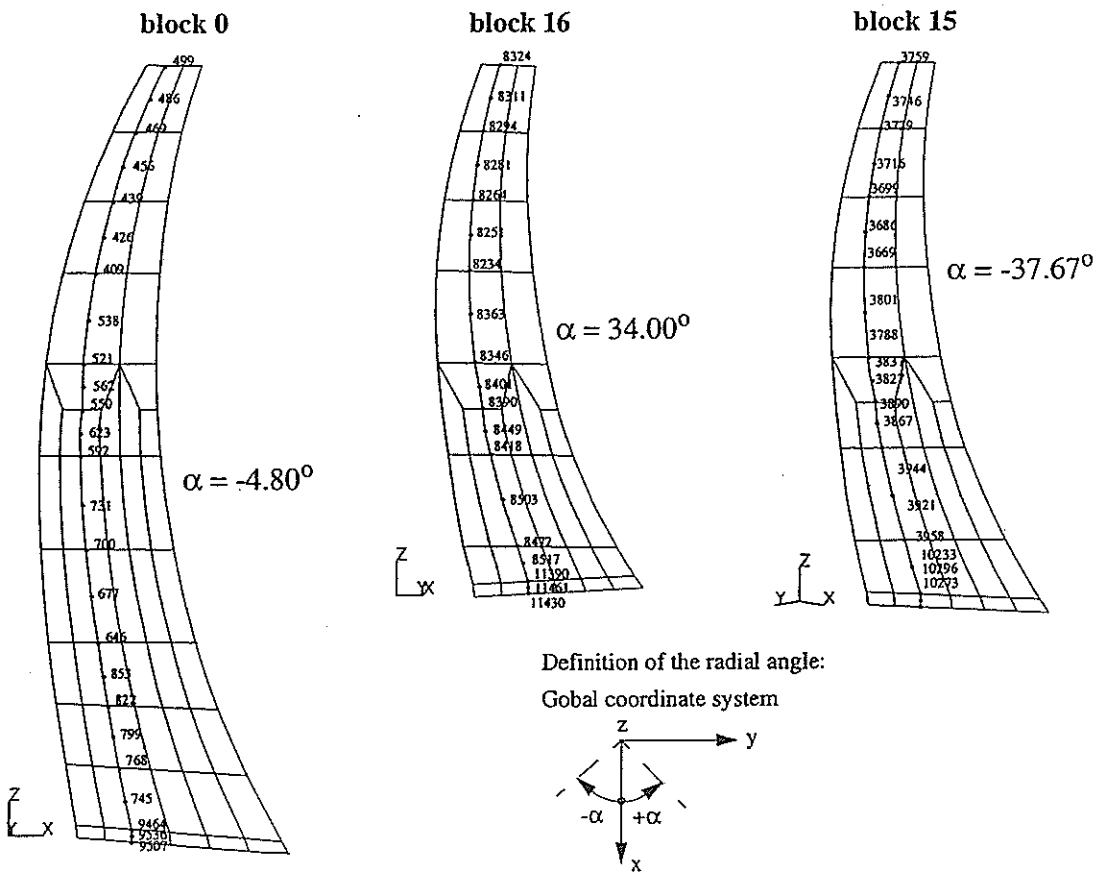

Figure 8: Nodes for Evaluating of Deformation in Radial Direction

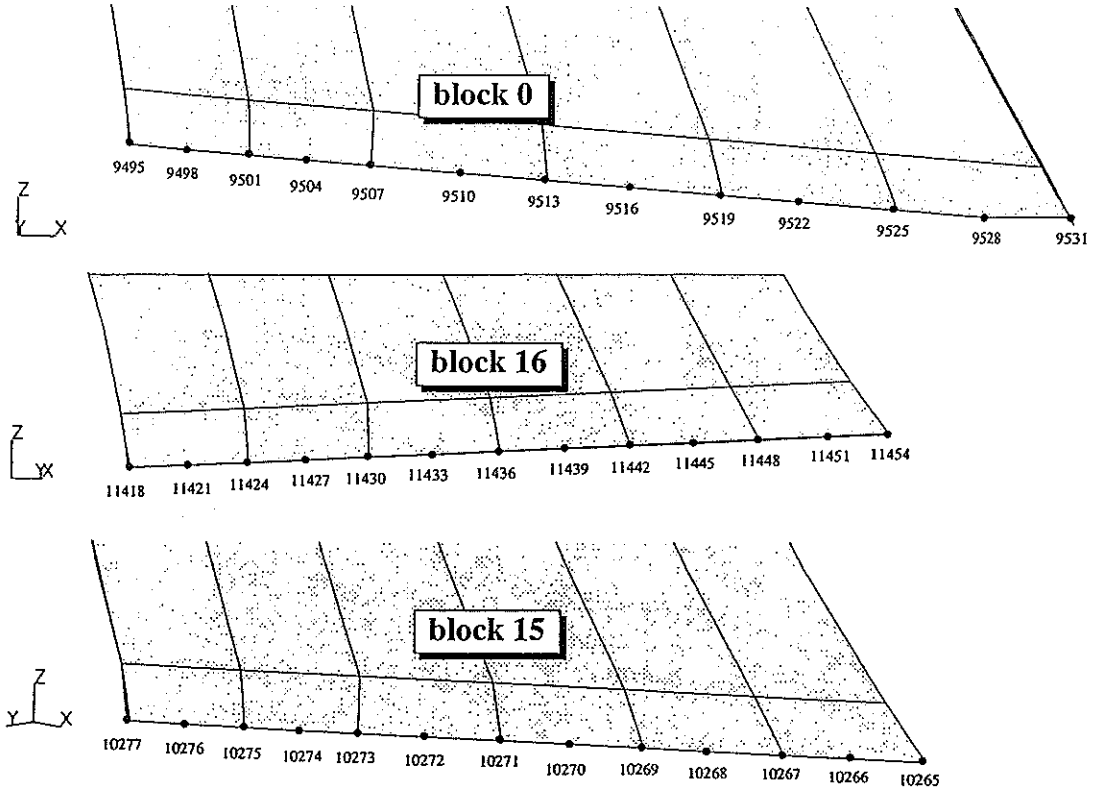

Figure 9: Nodes for Normal and Shear Stress Evaluation

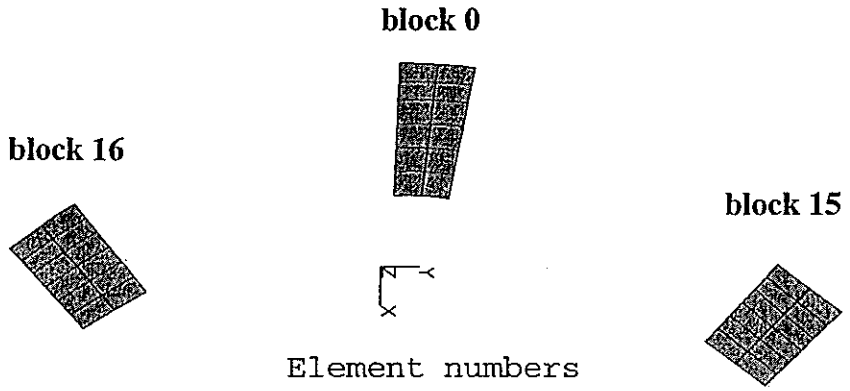

Figure 10: Abutment Elements for Block 0, 15 and 16

Appendix B

Fig.3: Downstream View of the provided Finite Element Mesh

Fig.4: Interface Elements and Block Distribution

Fig.5: Dam Model, Water and Uplift Loading

Fig.8: Nodes for Evaluating of Deformation in Radial Direction

Fig.9: Nodes for Normal and Shear Stress Evaluation

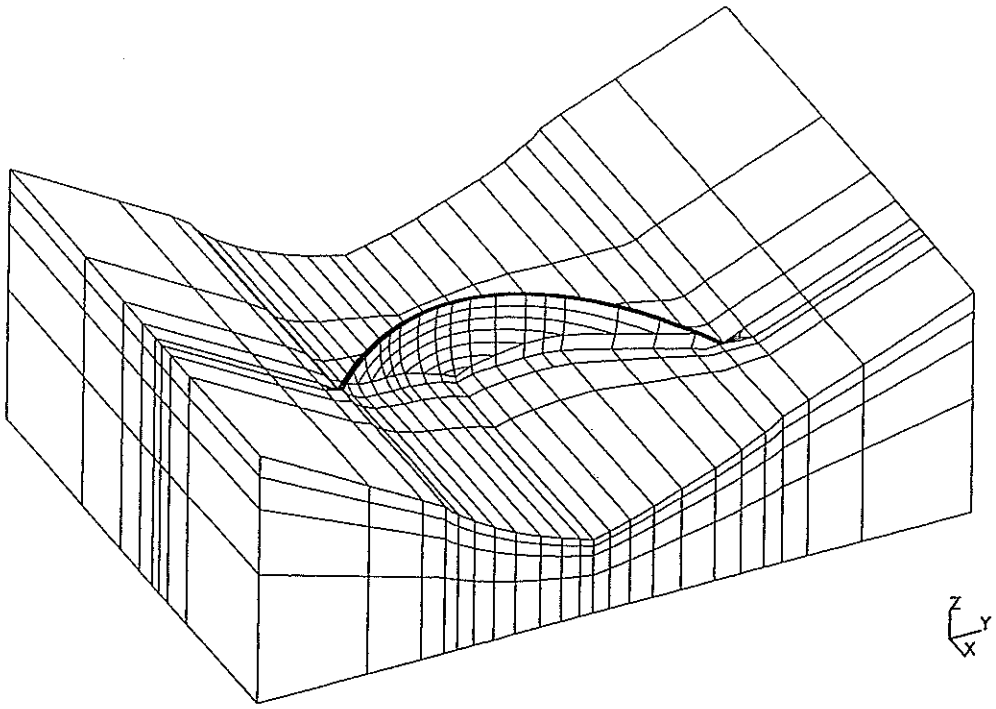

Figure 3: Downstream View of the provided Finite Element Mesh

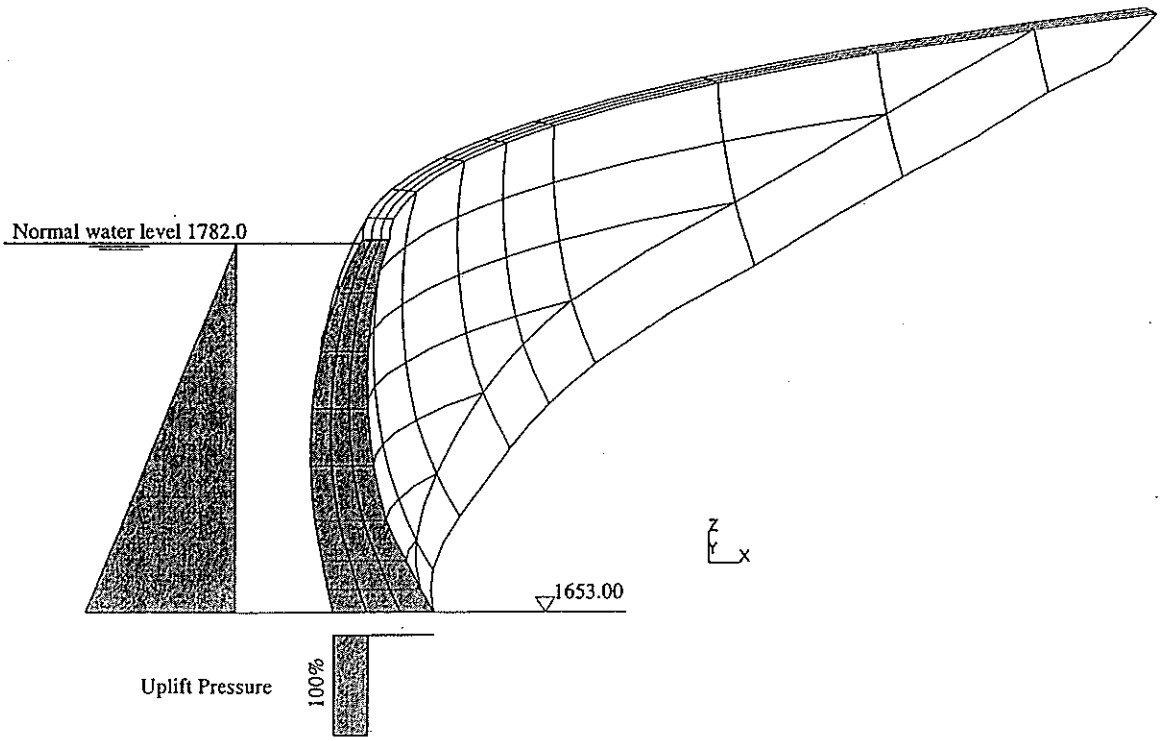

Figure 5: Dam Model, Water and Uplift Loading

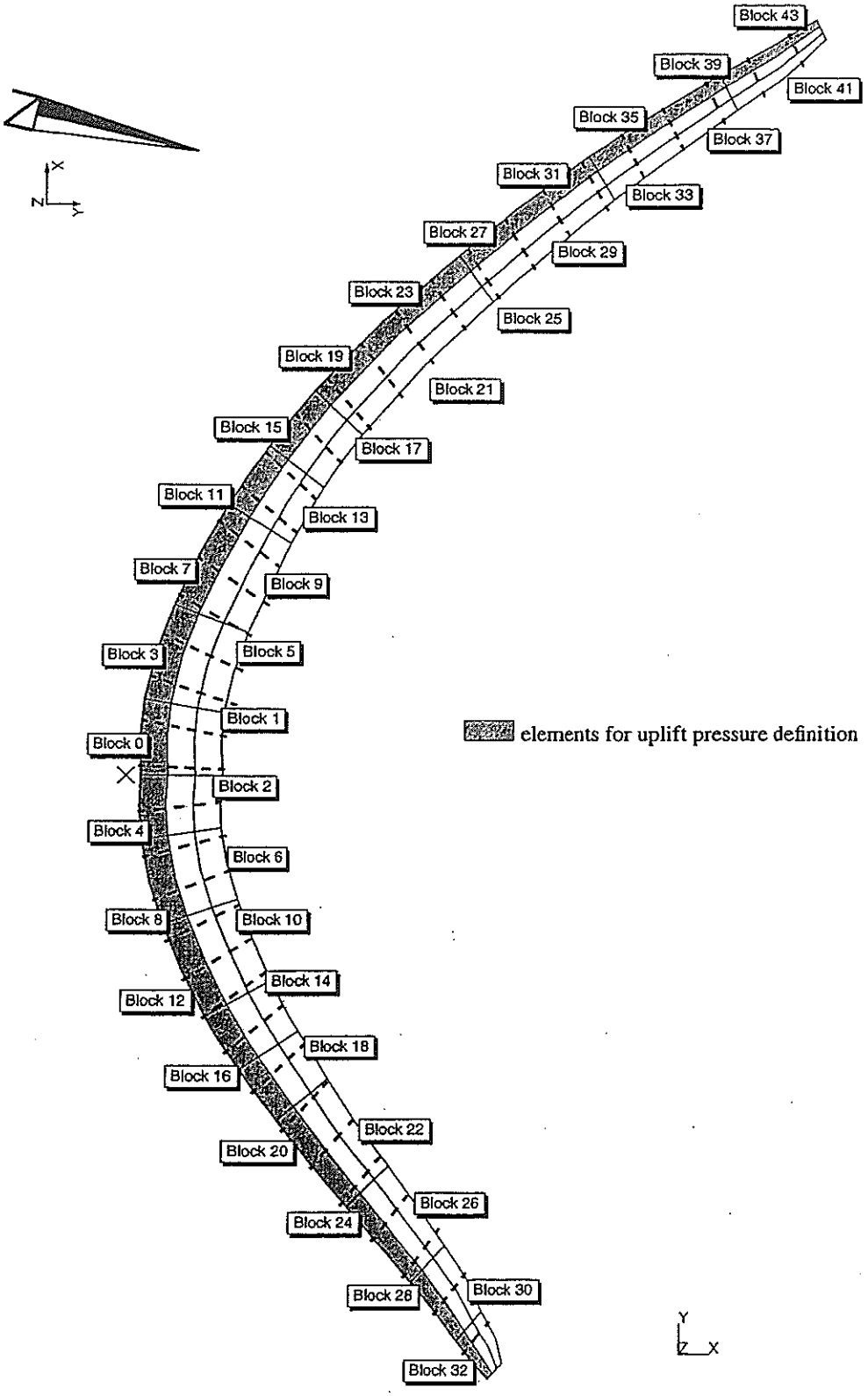

Figure 4: Interface Elements and Block Distribution

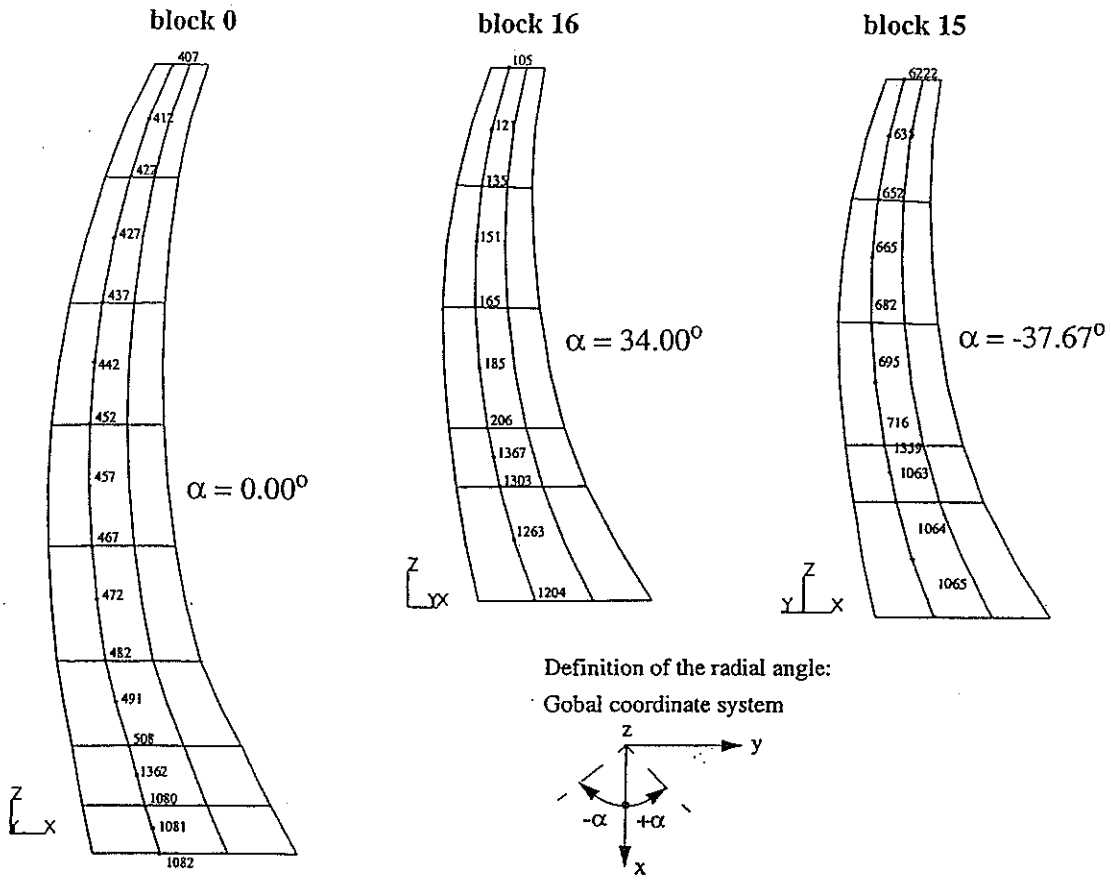

Figure 8: Nodes for Evaluating of Deformation in Radial Direction

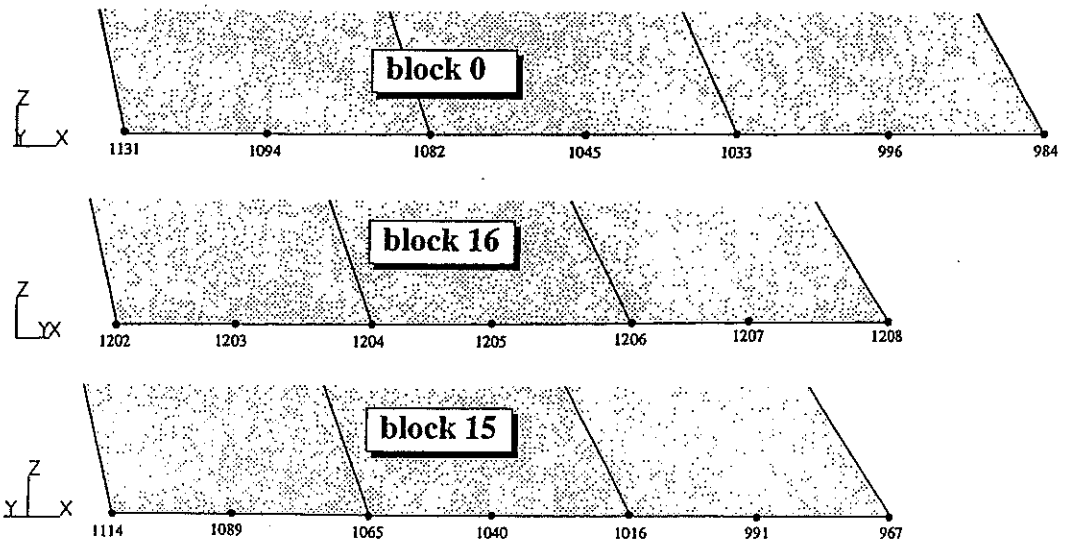

Figure 9: Nodes for Normal and Shear Stress Evaluation

UPLIFT PRESSURE AND STRESS ANALYSIS OF AN ARCH DAM AND FOUNDATION

SYNTHESIS REPORT

Gerald Zenz*, Ernst Aigner*

1. INTRODUCTION

International Benchmark Workshops on Numerical Analysis of Dams are intended to provide an in-depth examination of the computational methods and software used for dam analysis. This is an international forum to share the latest information regarding state-of-the-art software and techniques available for analysis of dam behavior. For this theme all participants used commercial software packages, which shows that for this special purpose of analysis developed programs are available.

This Benchmark Workshop theme A1 is devoted to examine the Schlegeis arch dam behavior based on idealizations of numerical, geometrical and physical nature as explained in the description of the problem formulation. Few additional assumptions - described in the paper of the individual authors - were taken by participants to carry out the analysis with their available software.

From a high number of initially interested participants five provided results which are the basis of this synthesis report.

With these participations a possibility is given to the community of Dam Engineers to discuss on assumptions, results and conclusions drawn by the help of numerical analyses.

* Verbundplan Consulting Engineers, Austria

2. PARTICIPANTS - GENERAL REMARKS

Five Participants faced the challenging complexity of the problem and provided results based on the given problem formulation. An existing arch-gravity dam had to be analyzed by means of the finite element technique together with an entire discontinuity at its dam base.

The calculations were carried out with three different finite element programs, using penalty and/or the Lagrange multiplier method for formulation of the contact condition. Either quadratic or linear contact elements were used.

The applicability of numerical parameters to steer the contact condition are on the participants responsibility and were introduced according to the program code requirements.

Short Cut	Authors	Company		Country	Program used
P1	H. Durieux Cai Qingbo	DWA	Department of Water Affairs	South Africa	Abaqus
P2	P. Divoux	EDF	Electricite de France	France	Gefdyn
P3	V. Rebecchi P. Palumbo G. Mazza	ISMES ENEL	ISMES, ENEL	Italy	Abaqus
P4	A. Popovici L. Lefter R. Sarghiuta V. Vacarescu	UNIB	University of Bucharest	Romania	Ansys
P5	G. Zenz E. Aigner F. Perner	VPL	Verbundplan Consulting Engineers	Austria	Abaqus

Figure 1: Table of Participants

For comparison reasons for the contact condition itself a coarse and a fine discretized finite element model were provided for the participants. However, the results calculated with both models in general as well as to a certain extent in detail are equivalent.

3. COMPARISON OF RESULTS

By making reference to the table of participants (figure 2), the shortcut mentioned there are used for each participant.

In addition to that the loading steps are marked with the following step numbers:

- Dead Weight Loading - Step 1
- Water Loading - Step 2
- Temperature Loading - Step 3
- Uplift Pressure Loading - Step 4.

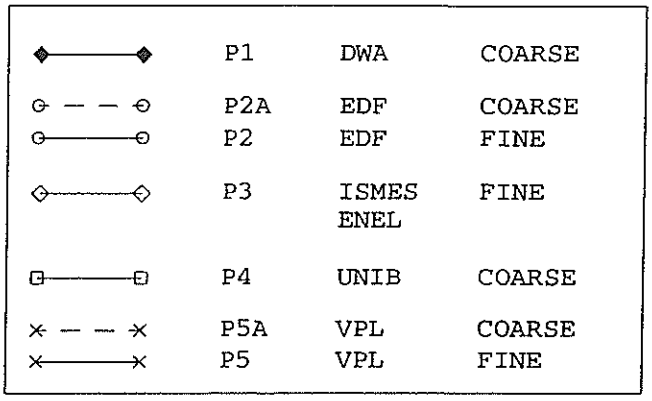

P1	DWA	COARSE
P2A	EDF	COARSE
P2	EDF	FINE
P3	ISMES ENEL	FINE
P4	UNIB	COARSE
P5A	VPL	COARSE
P5	VPL	FINE

Figure 2: Used Symbols for Participants

Participants P2 and P5 provided results for the coarse and fine discretized model. In this case the coarse model is indicated by dashed lines.
Throughout this text the shortcut shown in figure 2 for each relevant participant is used.

Herein the block 0 is compared with minimum principal stress values at up- and downstream side of the dam (no comparison is made upon the direction of stress values) and opening of the dam base and its resultant compressive normal stress are discussed. The radial displacements of block 0 are prepared to see the overall deformation behaviour of the dam.
All additionally provided and detailed results for the blocks 15 and 16 are attached in appendix A.

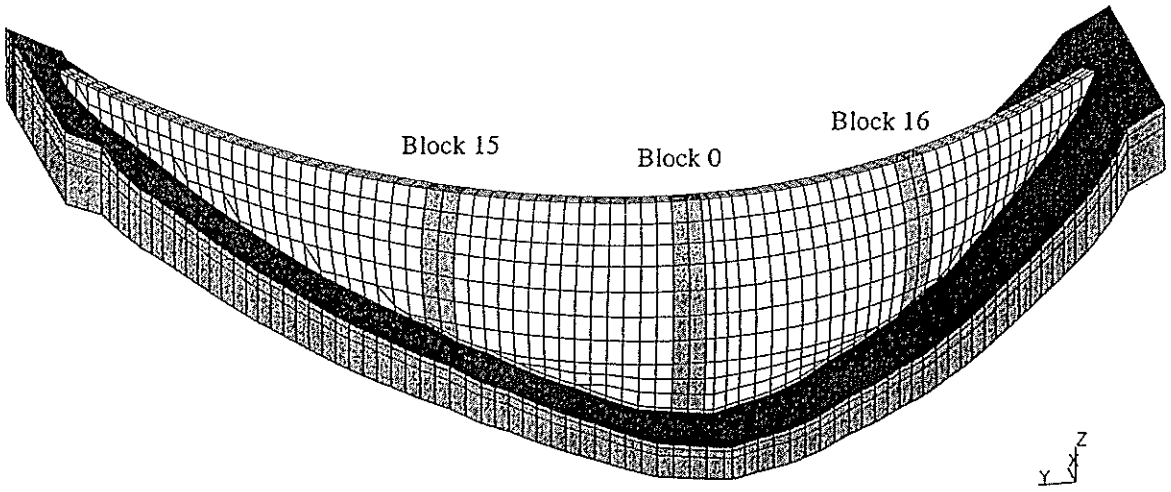

Figure 3: Results evaluated at concrete blocks 0/15/16

Dead Weight Loading - Step 1

The dead weight loading of the dam was suggested (in the problem formulation) by simulating independent concrete blocks.

The stress distribution at the upstream heel of the dam gives for most of the participants values above -6MPa. The compressive stresses are lower for the coarse discretized model. P2 uses a tension cut off model which explains the zero stress values at dams downstream face (figure 4).
The model assumed by P4 results in compressive stress of 4.2MPa at the upstream side and shows higher compressive stresses compared to others at the downstream dam face. This behavior is explained due to the model modifications with linear elements. The linearization of P4 results in a linear stress distribution at the abutment.
The coarse model results of P2 and P5 present lower compressive stresses at the heel of the dam.

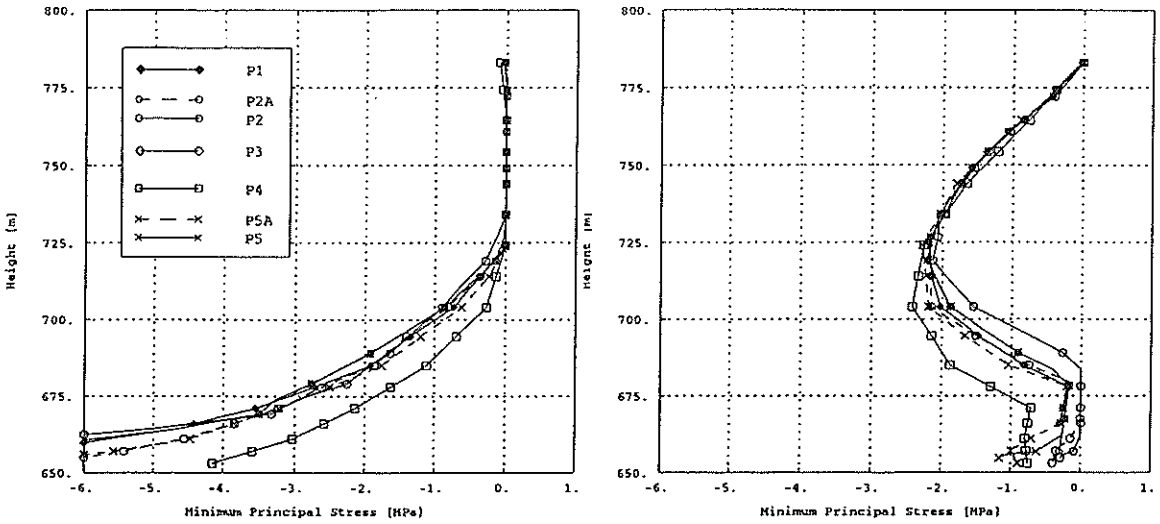

Figure 4: Dead Weight - Min.Prin.Stress Up-/ Downstream Block 0

The normal stress distribution provided by P1 along the base of the dam in radial direction is always nearly twice as high as the other results. With the provided data no direct explanation could be found; the results found for blocks 15/ 16 agree to other results provided

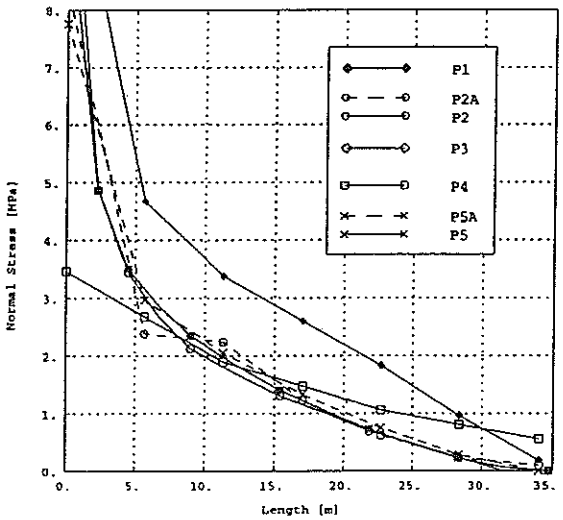

Figure 5: Dead Weight - Normal Stress Block 0

Water Loading - Step 2

For the dam upstream side the variation of min. principle stresses are from 4.9 to 5.4MPa and are due to fine and coarse model discretization (comparison e.g. P2/P2A and P5/P5A in figure 6).
At the dams downstream face the model linearization of P4 results in smaller minimum principal stress values.

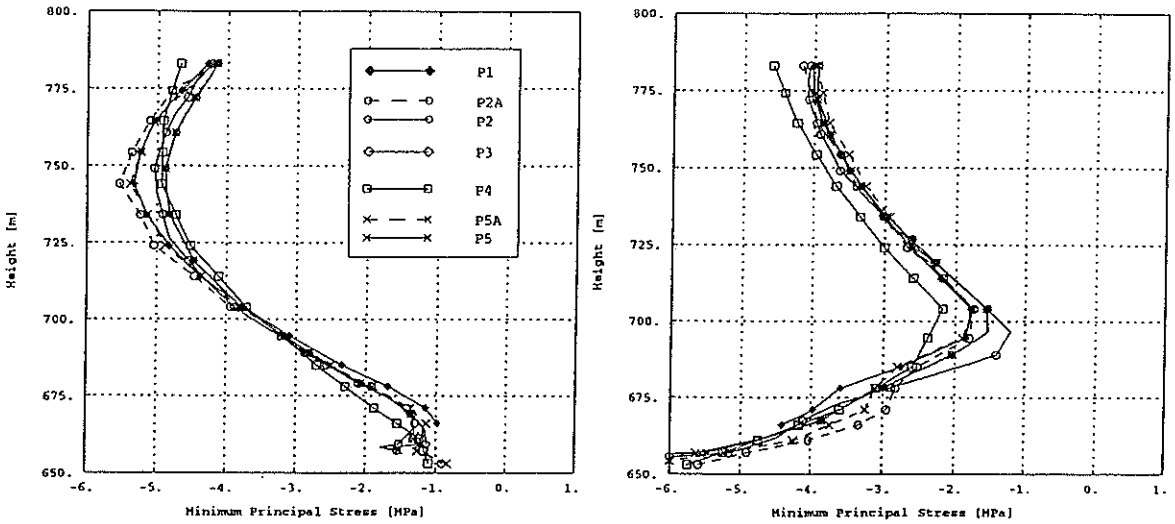

Figure 6: Step2 - Min. Prin.Stress Up-/ Downstream Block 0

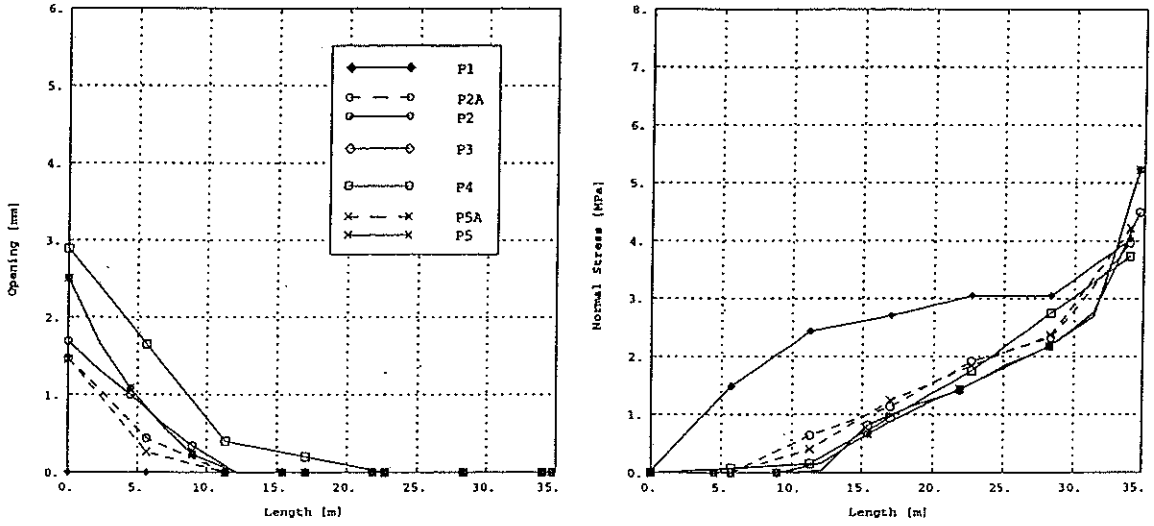

Figure 7: Step2 - Base Opening / Normal Stress Block 0

The base joint opening calculated by P3/P4 is 2.5mm in maximum. P2 evaluated with the same model discretization 1.8mm. With the coarse model P2/P5 evaluated 1.5mm opening at the heel of the dam. P1 calculated zero opening.
The general tendency of normal stress distribution is differently evaluated by P1. An adhoc explanation for that behavior could not be found.

Full Loading Condition - Step 4

More or less the same stress distribution as seen for step 2 appears under full loading condition (figure 8). The uplift pressure acting in the base joint can be seen on the stress diagrams.

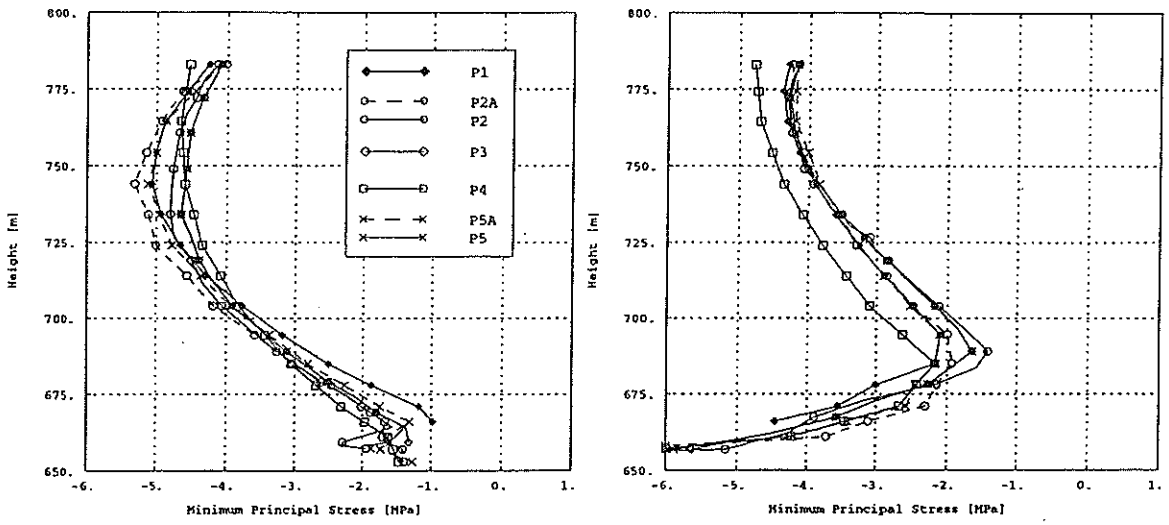

Figure 8: Step4 - Min. Prin.Stress Up-/ Downstream Block 0

The participants P2 and P3/P5 calculated openings at the heel of the base joint between 4.5 to 4.9mm. The shape of the deforming dam concrete surface at the abutment is slightly different. The results of P1 show significant differences in the opening.

P2 evaluated for the fine model for concrete blocks 15/16 a different behaviour in the opening (to seen in Appendix A) - this might be influenced by the contact condition.

The normal stress distribution are in general in accordance with the joint opening. However, P1 evaluates a different

shape of the stress distribution, which can be explained from the differences already seen starting from dead weight loading.

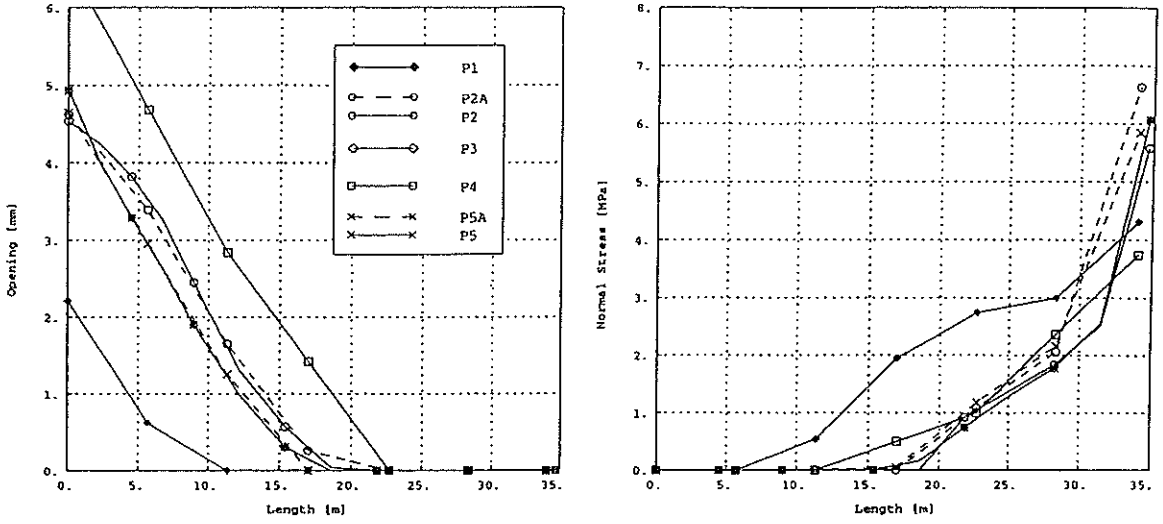

Figure 9: Step4 - Base Opening / Normal Stress Block 0

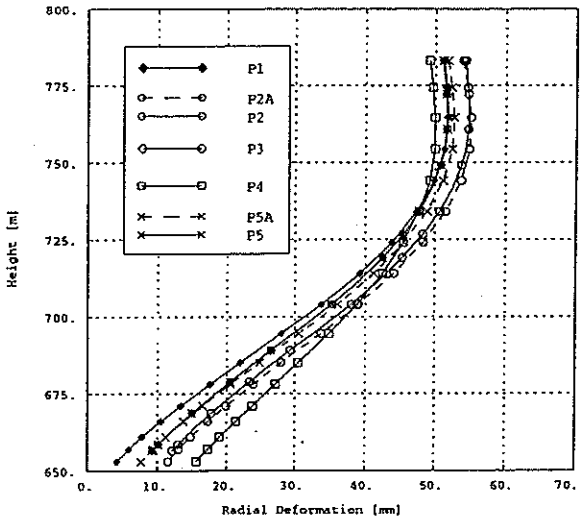

Figure 10: Step4 - Radial Displacement Block 0

The overall radial displacements provided by each participant are shown on figure 10. At the abutment differences of about 10mm in the radial deformation appear. This is due to individual sliding conditions assumed by the participants.

	Block	Global [MPa]			Local [MPa]		Safety
		Fx	Fy	Fz	Tmax	N	
P2	0	401.6	42.2	448.4	427.0	426.3	1.00
	15	751.0	19.8	536.8	591.4	709.1	1.20
	16	821.3	185.6	591.0	680.8	771.2	1.13
P3	0	-	-	-	436.0	436.0	1.00
	15	-	-	-	707.0	800.0	1.13
	16	-	-	-	640.0	740.0	1.16
P5	0	412.1	53.1	457.5	437.7	436.4	1.00
	15	773.1	15.8	564.1	607.1	739.9	1.22
	16	801.2	190.1	597.8	659.6	774.9	1.18

Table 1: DEAD W., WATER L., TEMP., UPLIFT - Safety Factor: Block 0/15/16

As a result of this investigation a sliding factor of safety in the plane of the abutment is evaluated. Due to different assumptions of participants only for P2/P3/P5 these values could be evaluated. The results show, that for block 0 the sliding factor of safety is 1.0 for all participants. For block 15 the sliding factor of safety is 1.20/1.13/1.22 and for block 16 these values are 1.13/1.16/1.18.
The maximum differences for the sliding factor of safety are at about 6%.

4. CONCLUSIONS

In general a converging solution for the analysis of a dam based on an entire foundation joint could be found. The numerical stability of the procedure implemented into the finite element codes - with physical interpretable parameters - were shown by the participants.

The radial displacements at the dam crest are calculated by all participants within a range of 10% only. However, the most comparable analyses are in a closer range. For example provides the linearized model of P4 due to its less flexible behaviour results of smaller radial displacement values.

At the abutment of block 0 the differences are due to the different shearing flexibility of contact condition under closed joint - which can be explained by the influence of different numerical parameters on the simulated physical behaviour. At this level P4 calculated the highest sliding values and P1 the smallest. For Step 4 participant P4 calculated 16mm and P1 calculated 4mm sliding only.

The vertical stress distribution calculated equivalent under dead weight by P2, P3 and P5 respectively. The provided results of P1, which are - in concrete block 0 - about twice of the aforementioned results and are not explained. Due to the model linearization the results of P1 give a more linear stress distribution with lower stress gradients.

The openings calculated by P2, P3 and P5 are comparable. P1 presents small openings in block 0 due to the high vertical stress but presents for block 15, 16 results comparable to others. P4 calculated larger openings for block 0. For P2 and the fine model, the opening provided for block 15/16 are diverging from other results.

In general a comparable solution (with more or less the same additional numerical assumptions) for the problem were found by three participants.

APPENDIX A

UPLIFT PRESSURE AND STRESS ANALYSIS OF AN ARCH DAM AND FOUNDATION

SYNTHESIS REPORT

Content of Comparison

DEAD WEIGHT - Step 1		
Block 0	Minimum Principle Stress	
	Upstream	Downstream
Block 0	Middle Principle Stress	
	Upstream	Downstream
Block 0	Opening - Normal Stress	
Block 15	Opening - Normal Stress	
Block 16	Opening - Normal Stress	

DEAD WEIGHT, WATER LOADING - Step 2		
Block 0	Minimum Principle Stress	
	Upstream	Downstream
Block 0	Middle Principle Stress	
	Upstream	Downstream
Block 0	Opening - Normal Stress	
Block 15	Opening - Normal Stress	
Block 16	Opening - Normal Stress	
Block 0	Radial Deformation	
Block 15	Radial Deformation	
Block 16	Radial Deformation	

DEAD WEIGHT, WATER LOADING, TEMPERATURE Step 3		
Block 0	Minimum Principle Stress	
	Upstream	Downstream
Block 0	Middle Principle Stress	
	Upstream	Downstream

DEAD WEIGHT, WATER LOADING, TEMPERATURE Step 3	
Block 0	Opening - Normal Stress
Block 15	Opening - Normal Stress
Block 16	Opening - Normal Stress
Block 0	Radial Deformation
Block 15	Radial Deformation
Block 16	Radial Deformation

FULL LOADING CONDITION - Step 4		
Block 0	Minimum Principle Stress	
	Upstream	Downstream
Block 0	Middle Principle Stress	
	Upstream	Downstream
Block 0	Opening - Normal Stress	
Block 15	Opening - Normal Stress	
Block 16	Opening - Normal Stress	
Block 0	Radial Deformation	
Block 15	Radial Deformation	
Block 16	Radial Deformation	

FULL LOADING CONDITION with and without UPLIFT	
Block 0	Normal Stress - Shear Stress

DEAD WEIGHT - Step1		
Block 0	Minimum Principle Stress	
	Upstream	Downstream
Block 0	Middle Principle Stress	
	Upstream	Downstream
Block 0	Opening - Normal Stress	
Block 15	Opening - Normal Stress	
Block 16	Opening - Normal Stress	

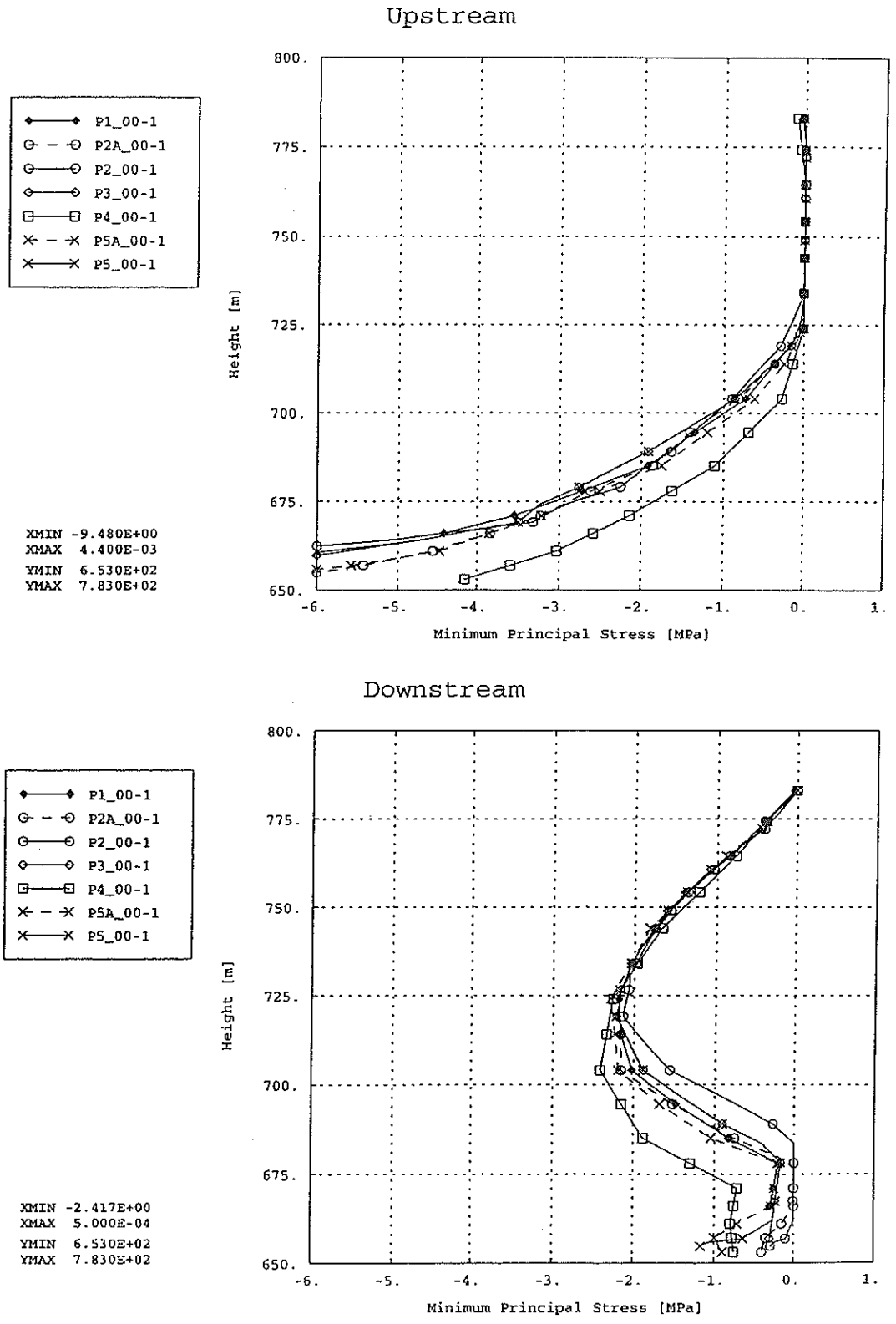

Figure 1: DEAD WEIGHT - Minimum Principle Stress: Block 0

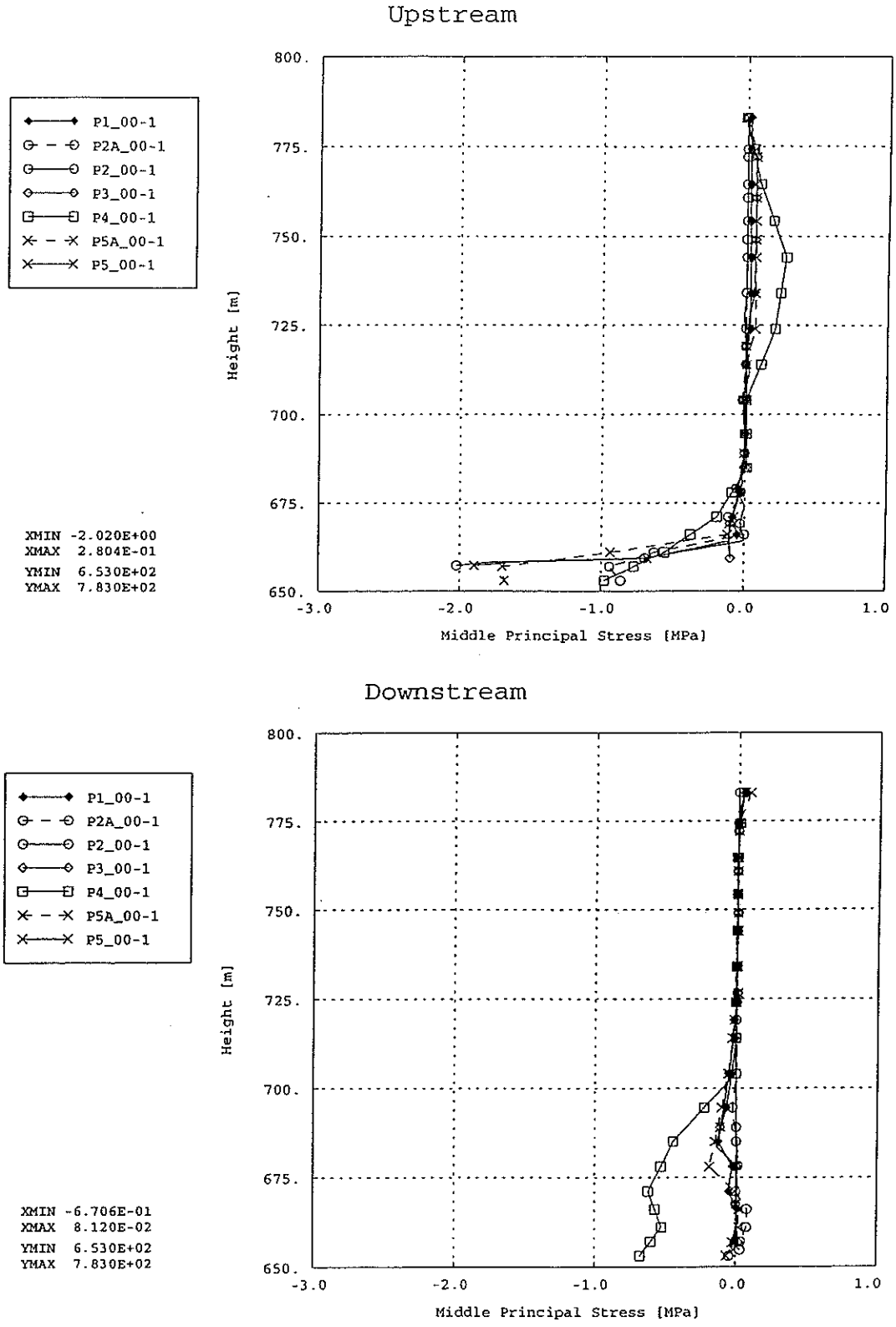

Figure 2: DEAD WEIGHT - Middle Principle Stress: Block 0

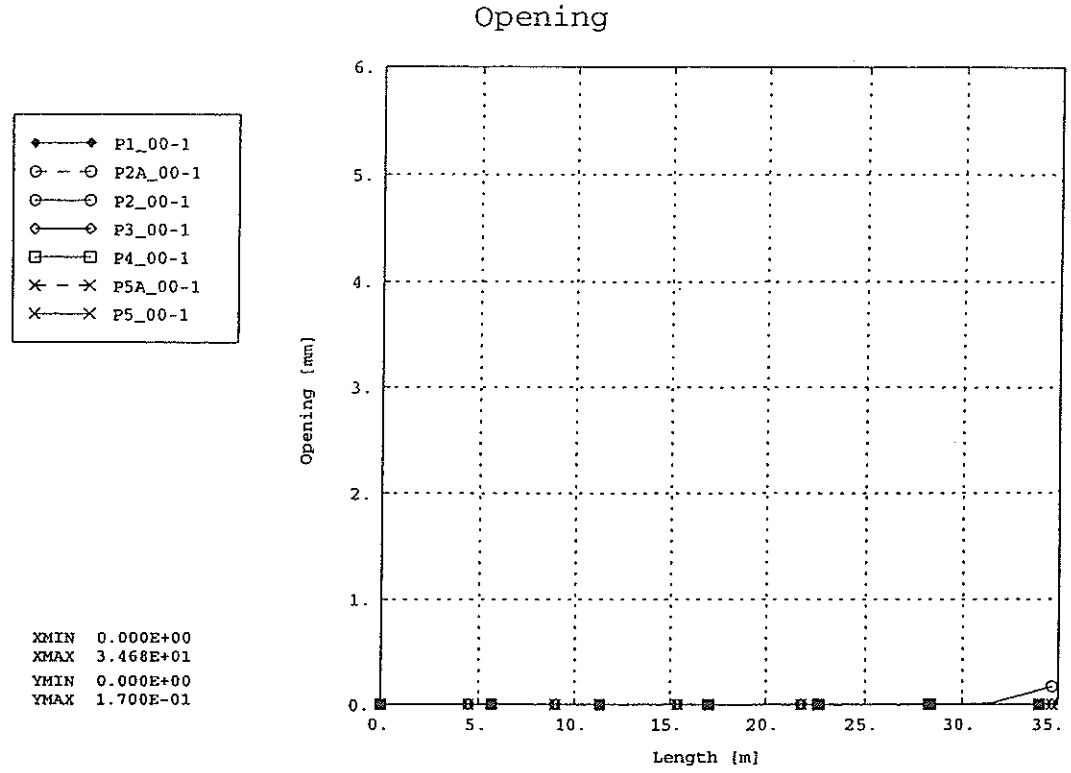

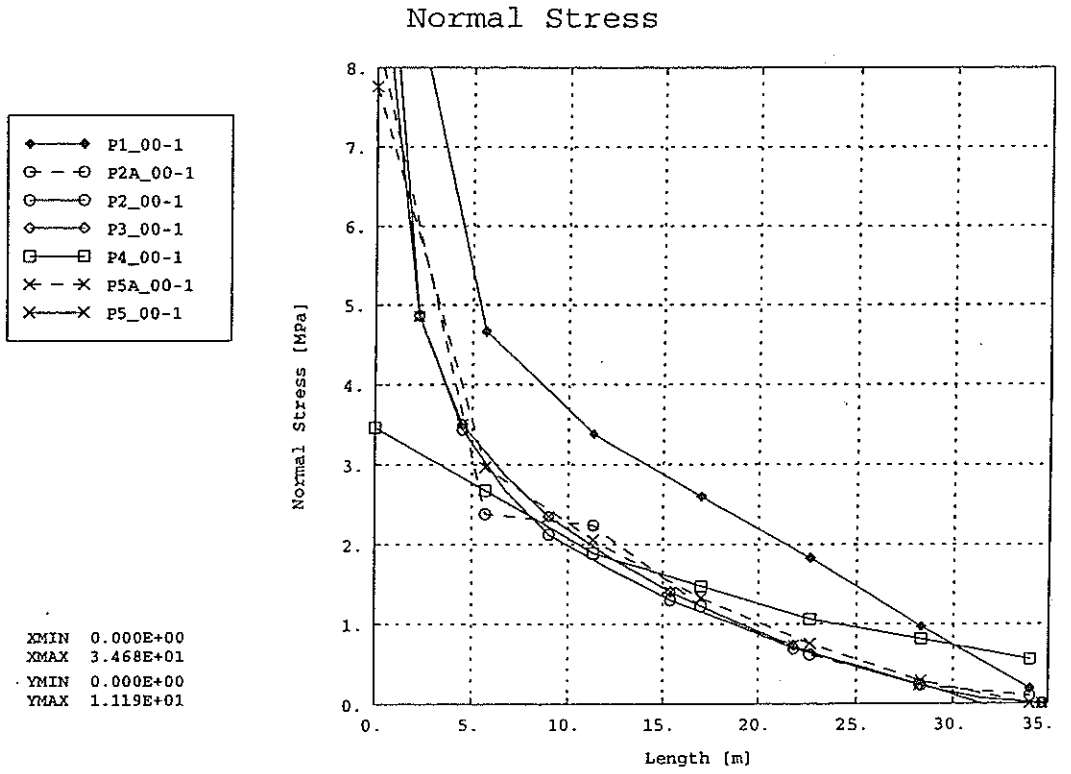

Figure 3: DEAD WEIGHT - Opening & Normal Stress: Block 0

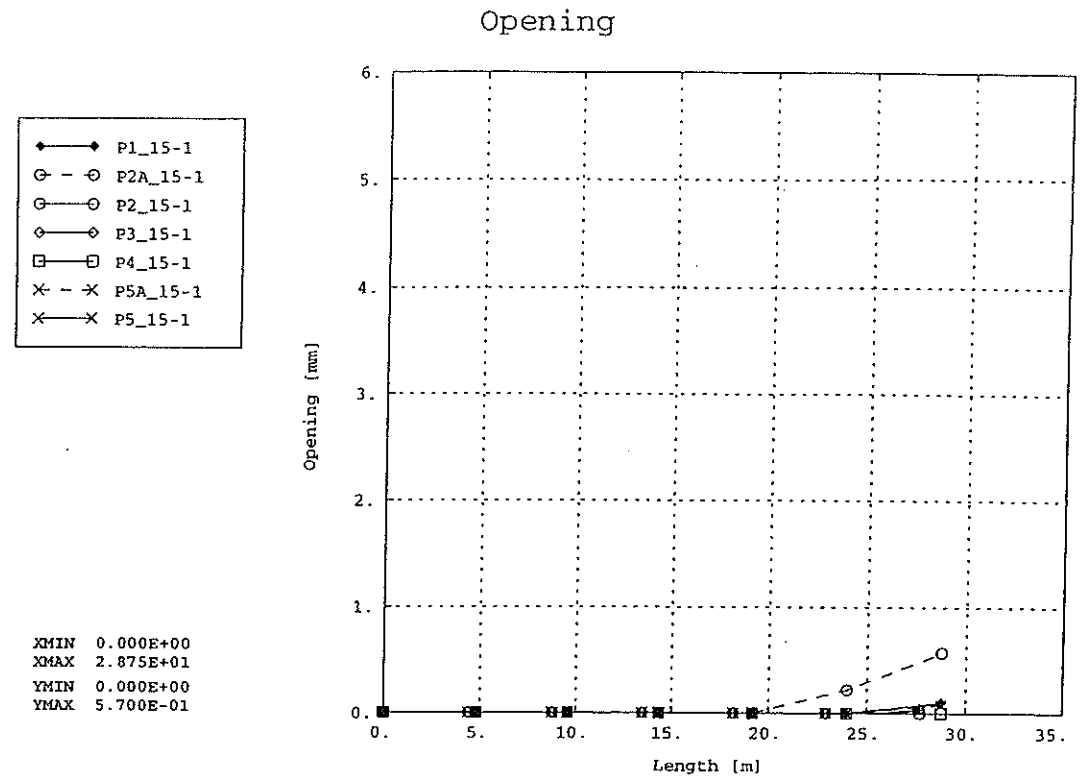

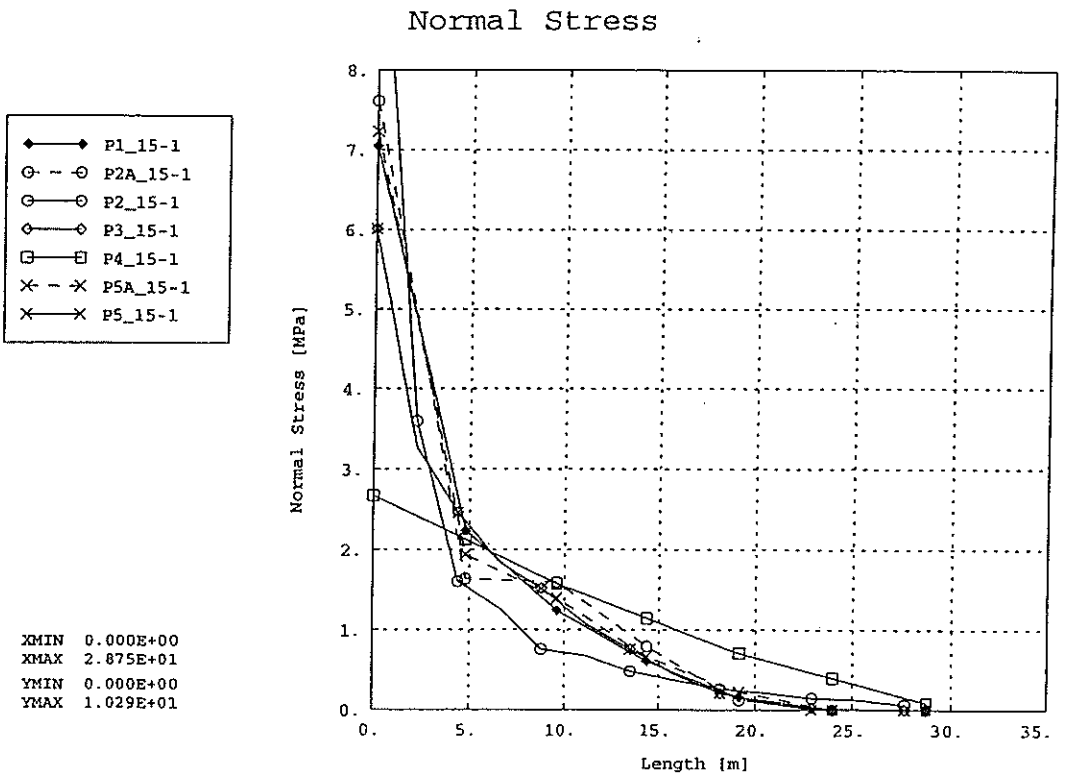

Figure 4: DEAD WEIGHT - Opening & Normal Stress: Block 15

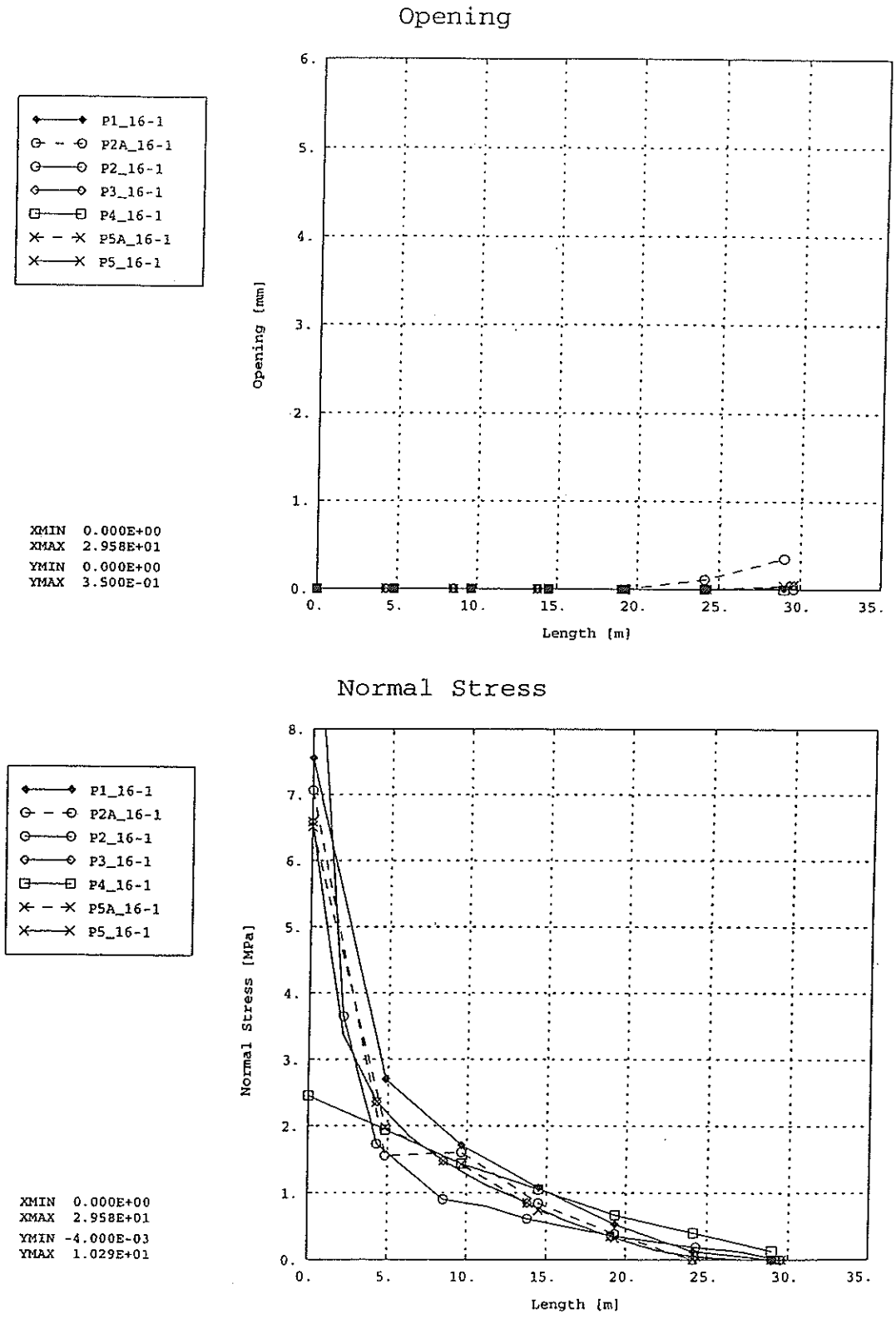

Figure 5: DEAD WEIGHT - Opening & Normal Stress: Block 16

DEAD WEIGHT, WATER LOADING - Step 2		
Block 0	Minimum Principle Stress	
	Upstream	Downstream
Block 0	Middle Principle Stress	
	Upstream	Downstream
Block 0	Opening - Normal Stress	
Block 15	Opening - Normal Stress	
Block 16	Opening - Normal Stress	
Block 0	Radial Deformation	
Block 15	Radial Deformation	
Block 16	Radial Deformation	

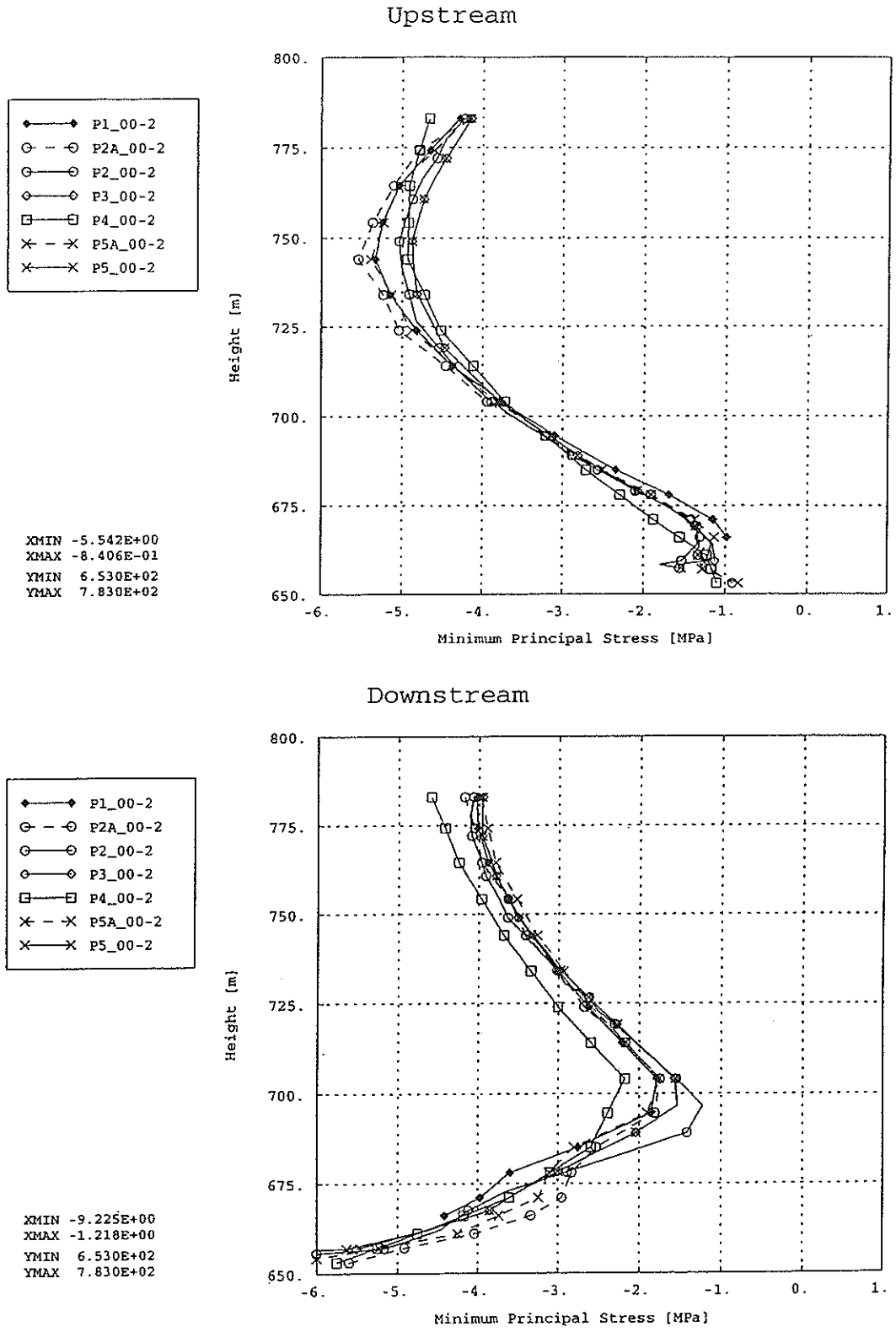

Figure 6: DEAD WEIGHT, WATER LOAD - Min. Prin. Stress: Block 0

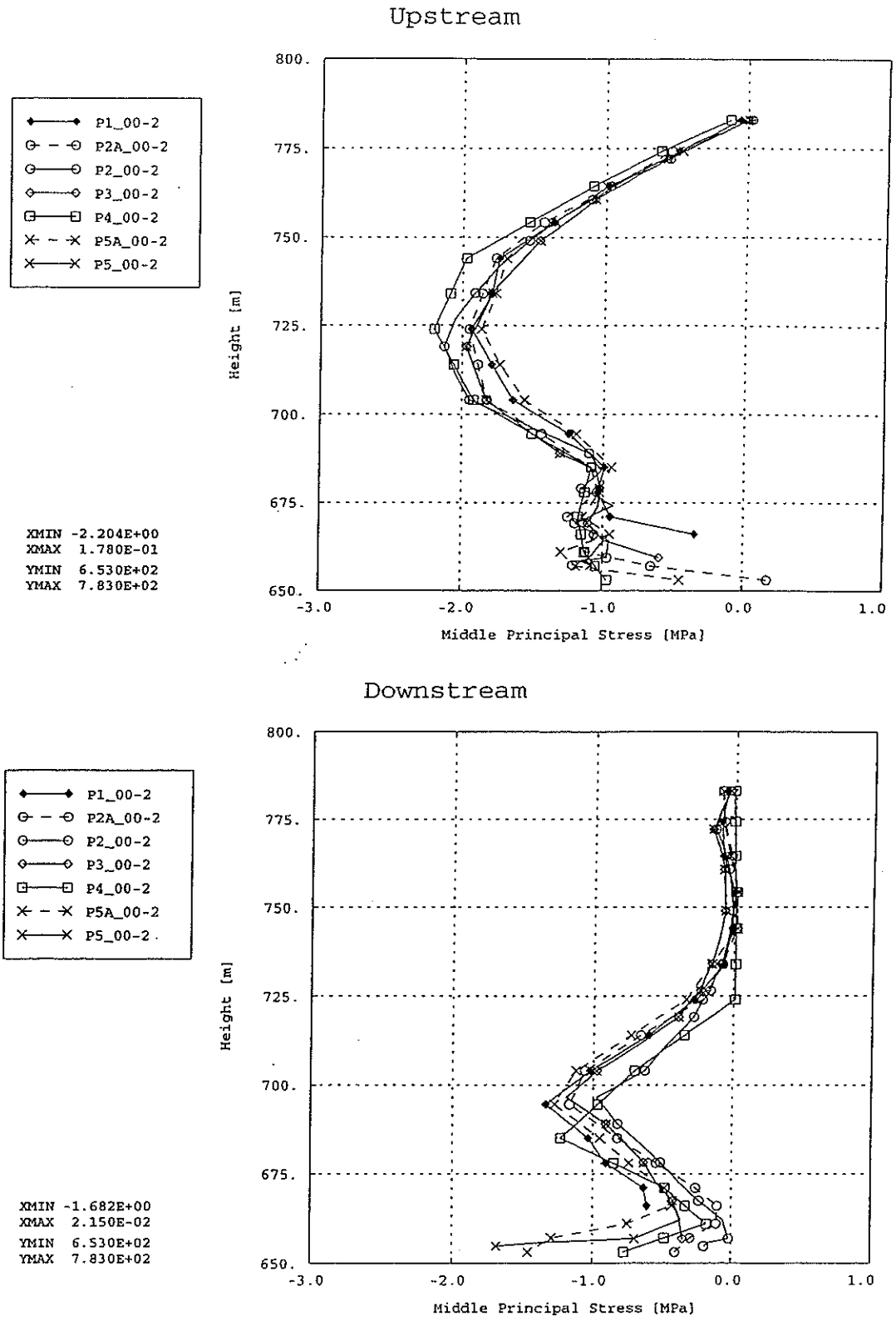

Figure 7: DEAD WEIGHT, WATER LOAD - Middle Prin. Stress: Block 0

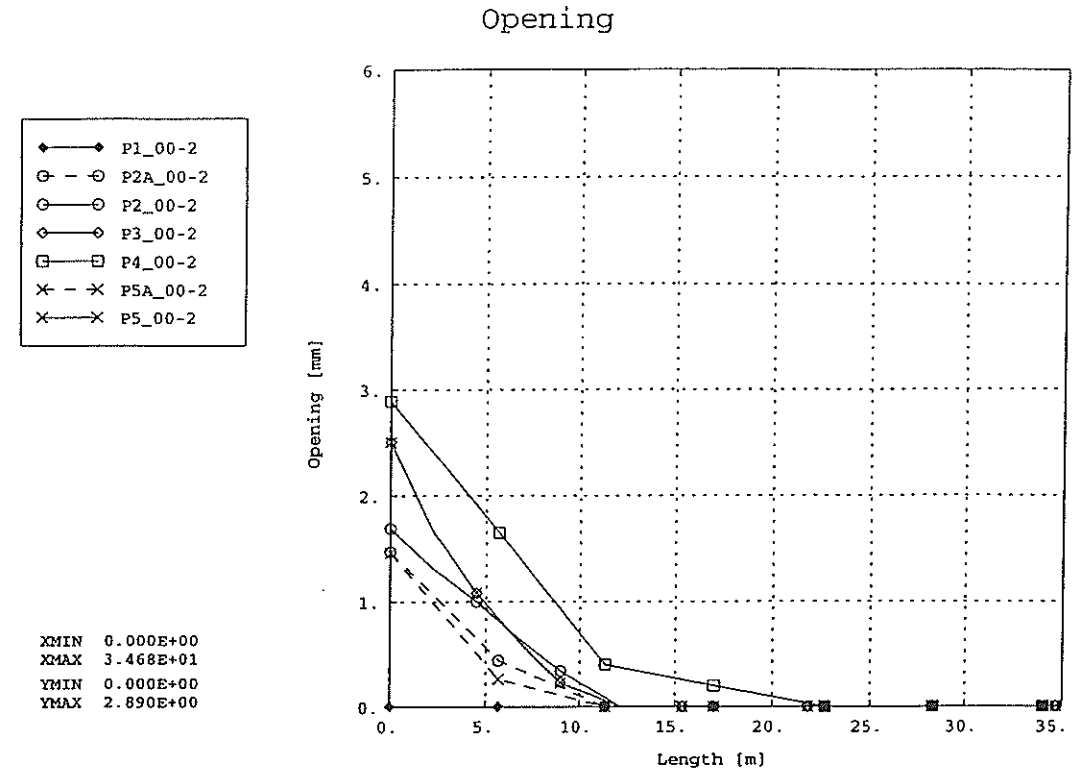

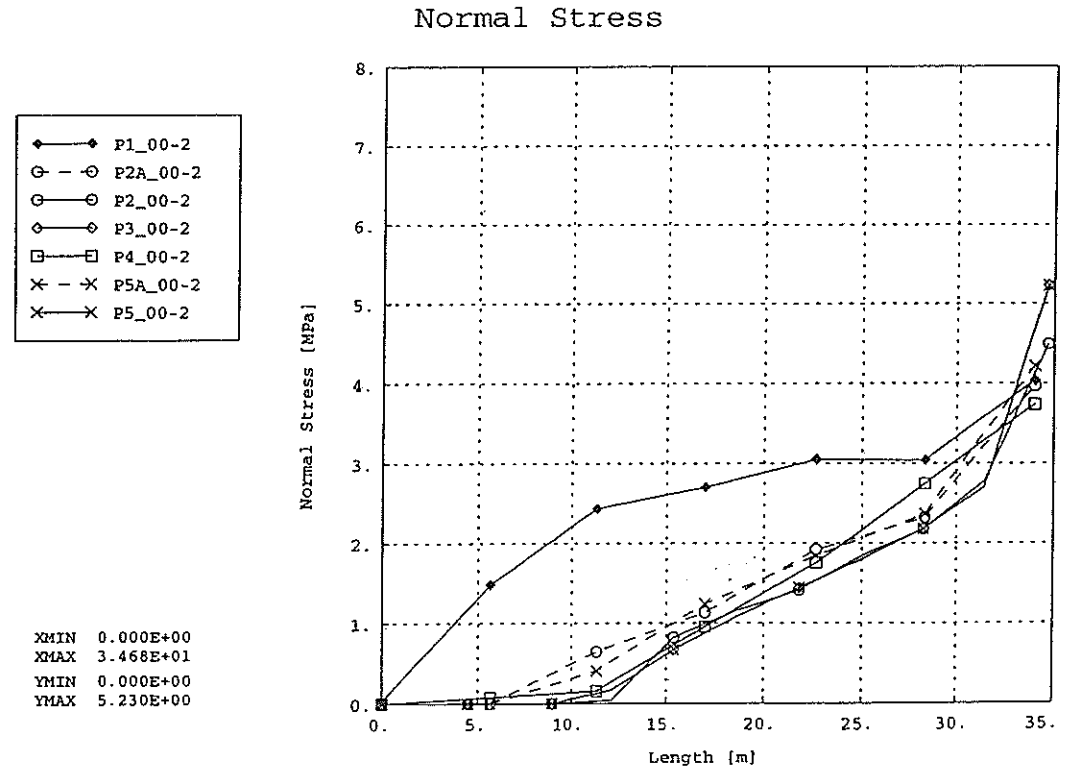

Figure 8: DEAD WEIGHT, WATER LOAD - Opening & Normal Stress: Block 0

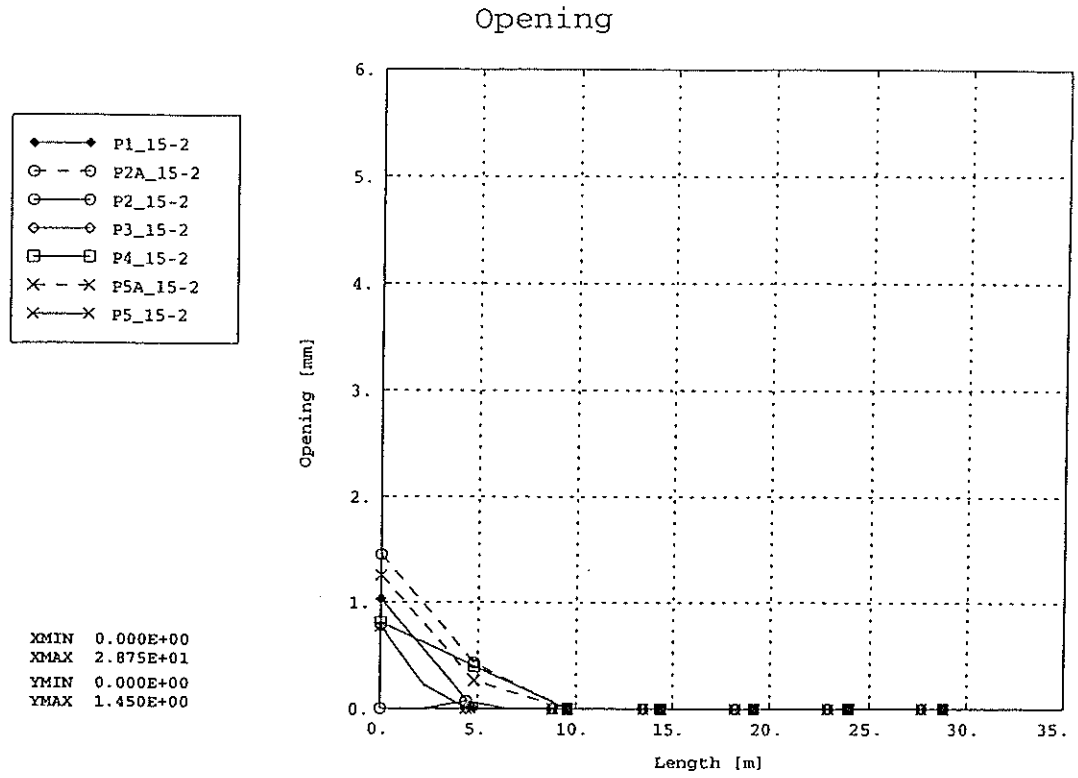

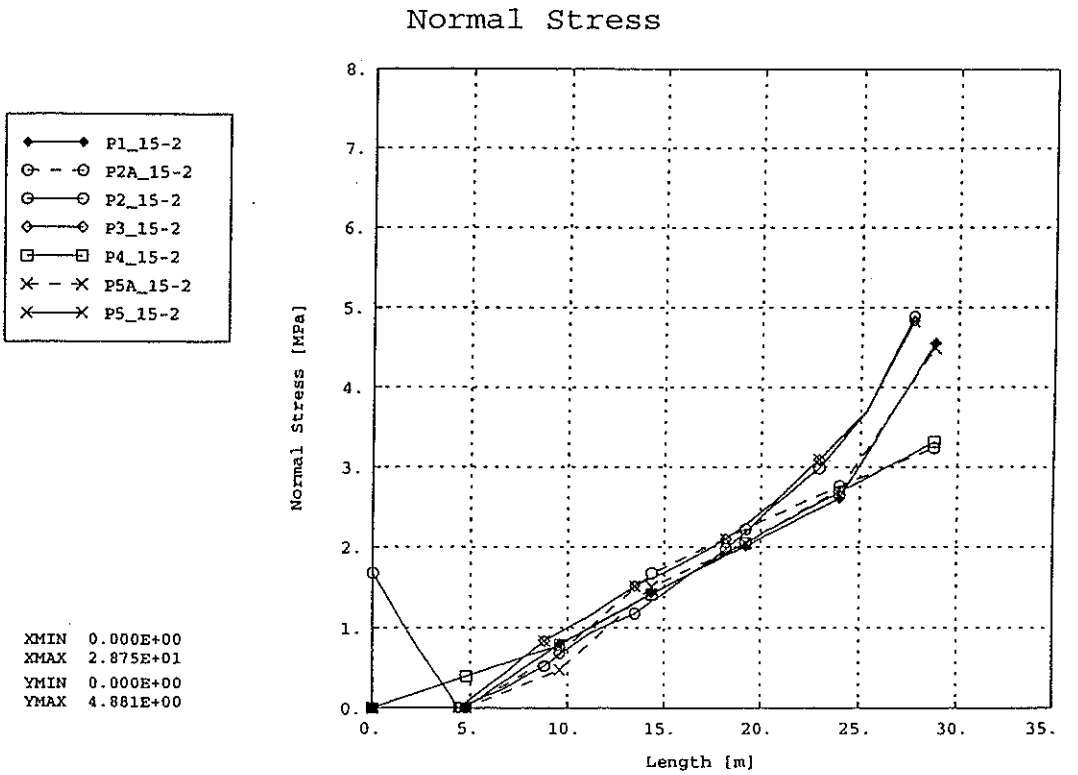

Figure 9: DEAD WEIGHT, WATER LOAD - Opening & Normal Stress: Block 15

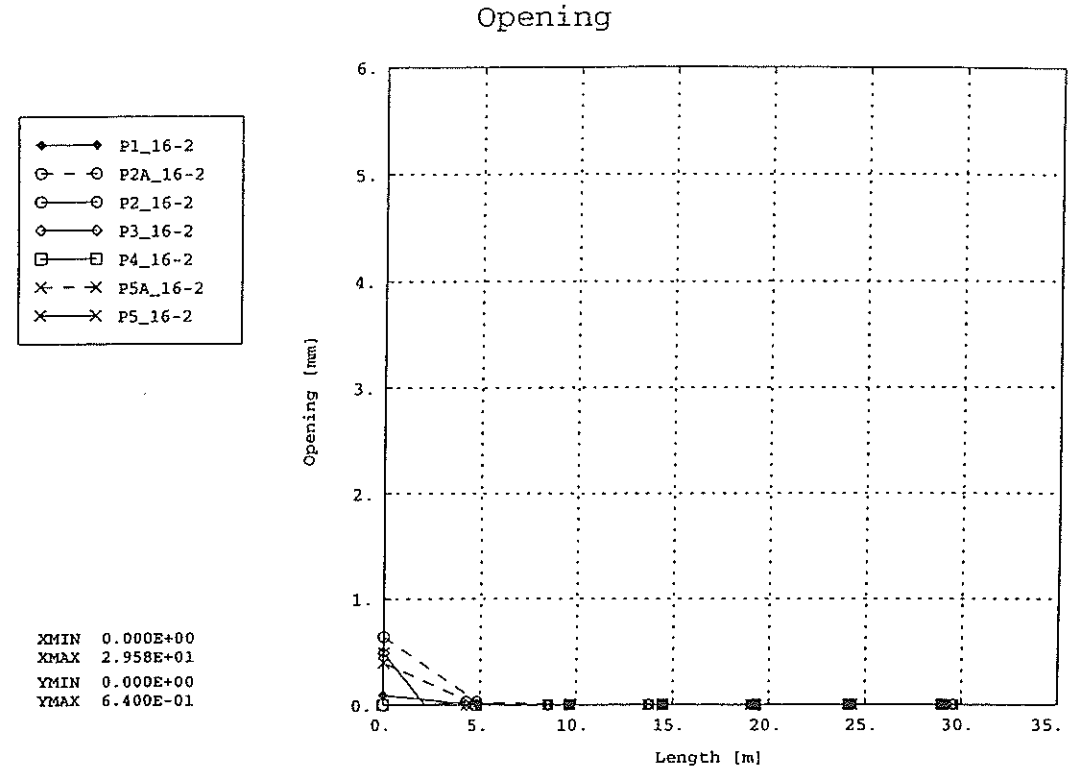

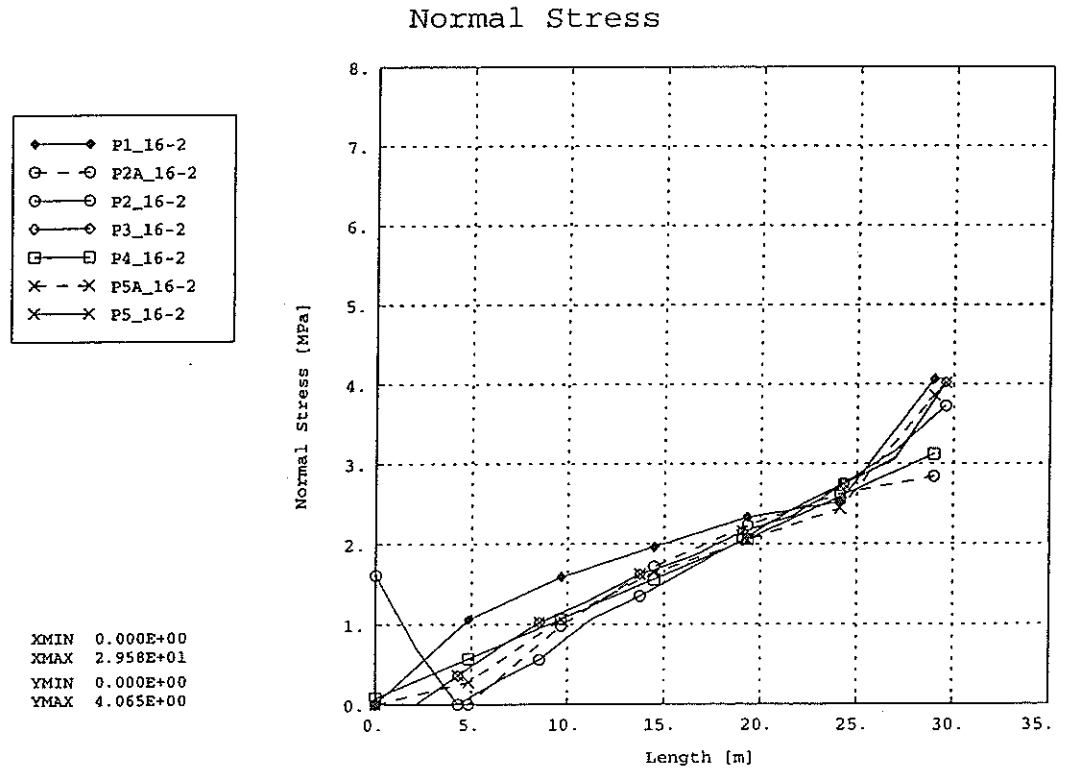

Figure 10: DEAD WEIGHT, WATER LOAD - Opening & Normal Stress: Block 16

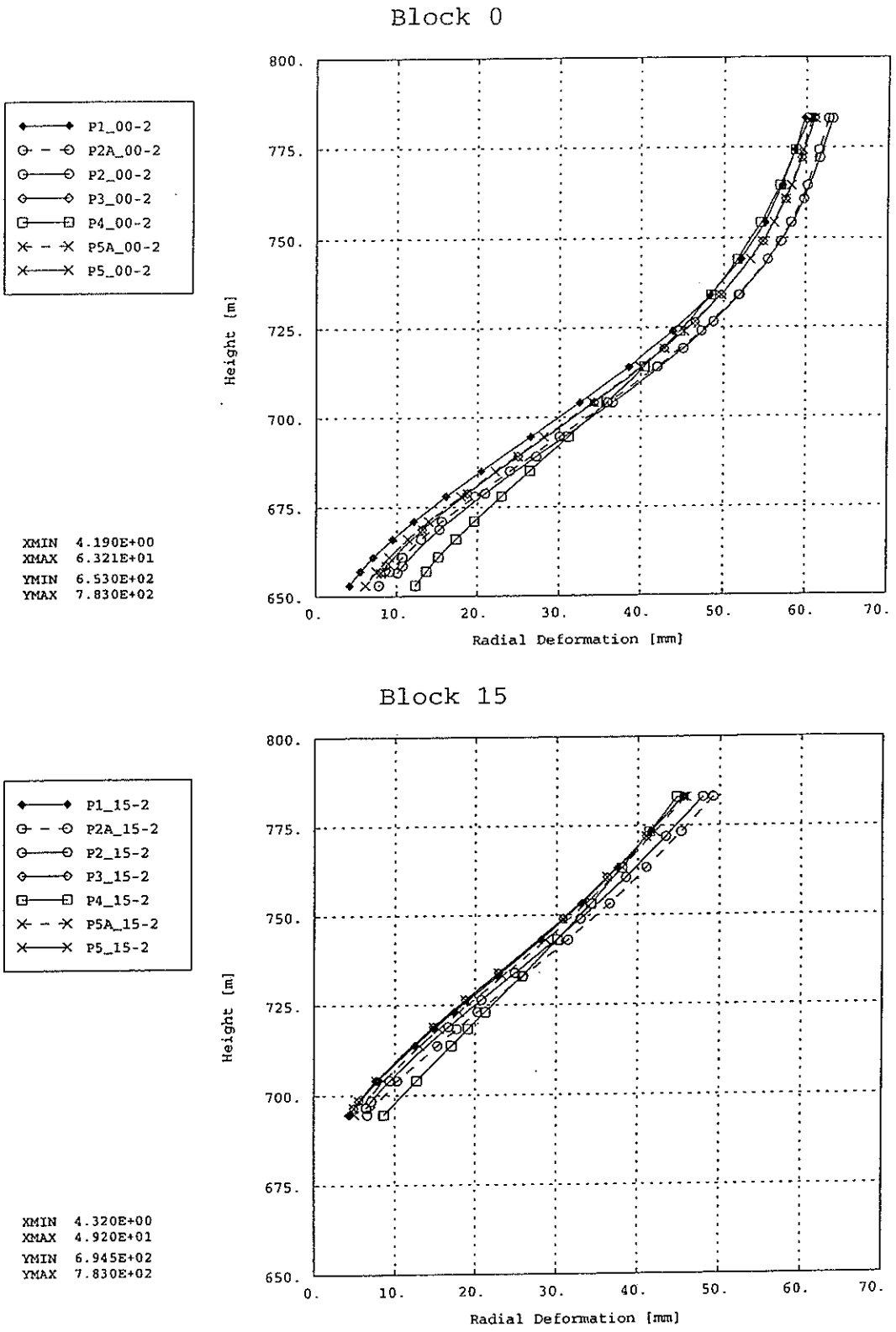

Figure 11: DEAD WEIGHT, WATER LOAD - Radial Deformation: Block 0, Block 15

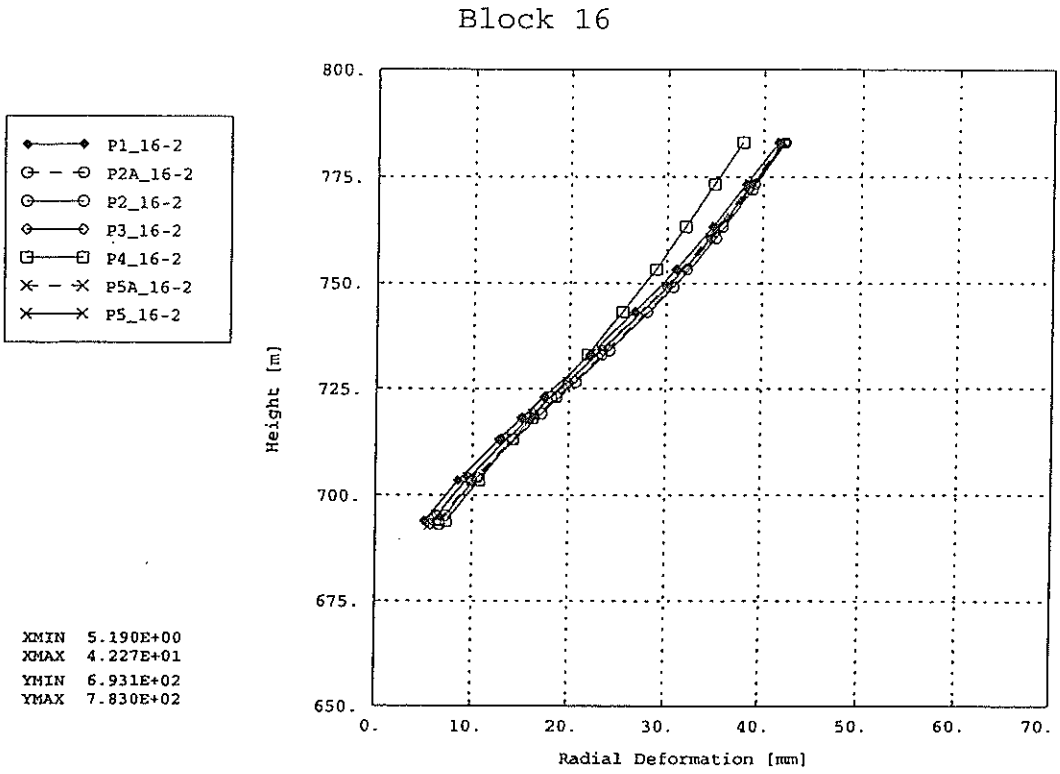

Figure 12: DEAD WEIGHT, WATER LOAD - Radial Deformation: Block 16

DEAD WEIGHT, WATER LOADING, TEMPERATURE Step 3		
Block 0	Minimum Principle Stress	
	Upstream	Downstream
Block 0	Middle Principle Stress	
	Upstream	Downstream
Block 0	Opening - Normal Stress	
Block 15	Opening - Normal Stress	
Block 16	Opening - Normal Stress	
Block 0	Radial Deformation	
Block 15	Radial Deformation	
Block 16	Radial Deformation	

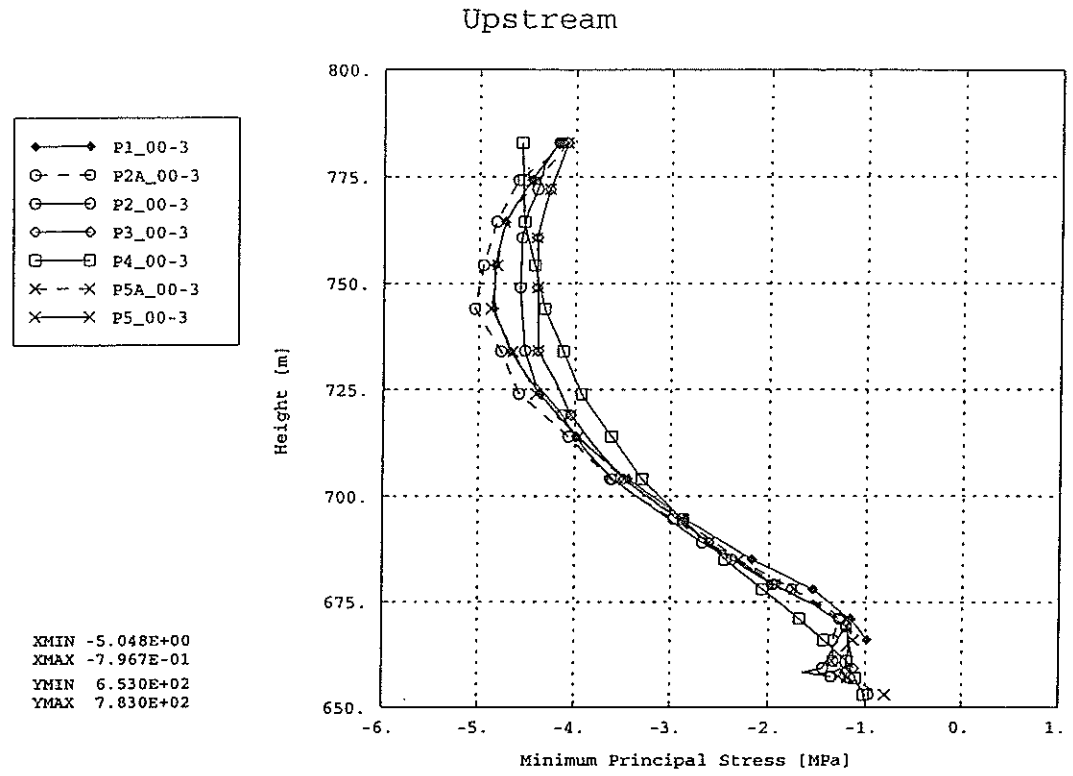

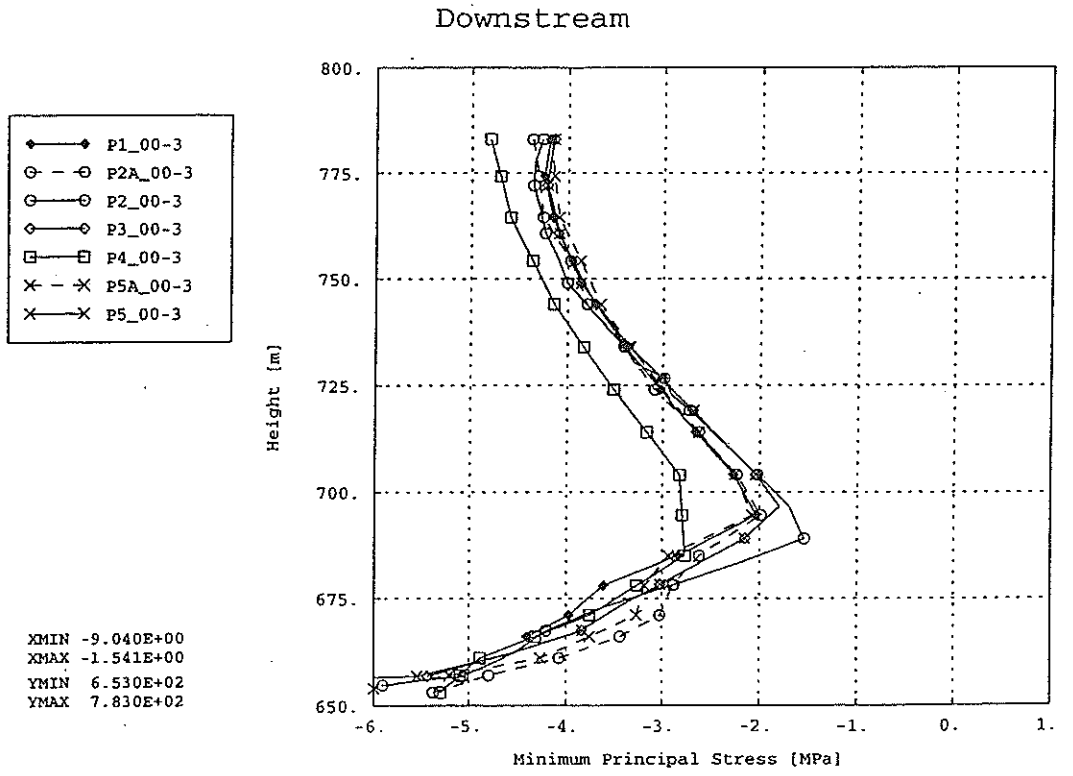

Figure 13: DEAD WEIGHT, WATER LOAD, TEMP - Minimum Principle Stress: Block 0

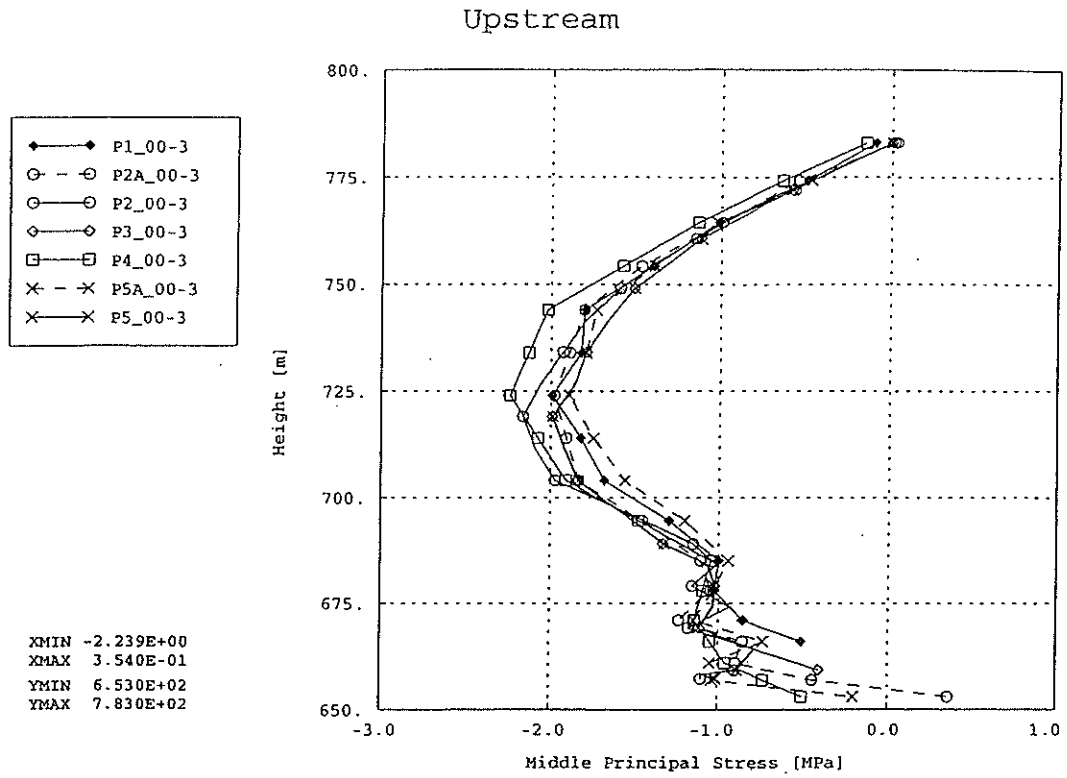

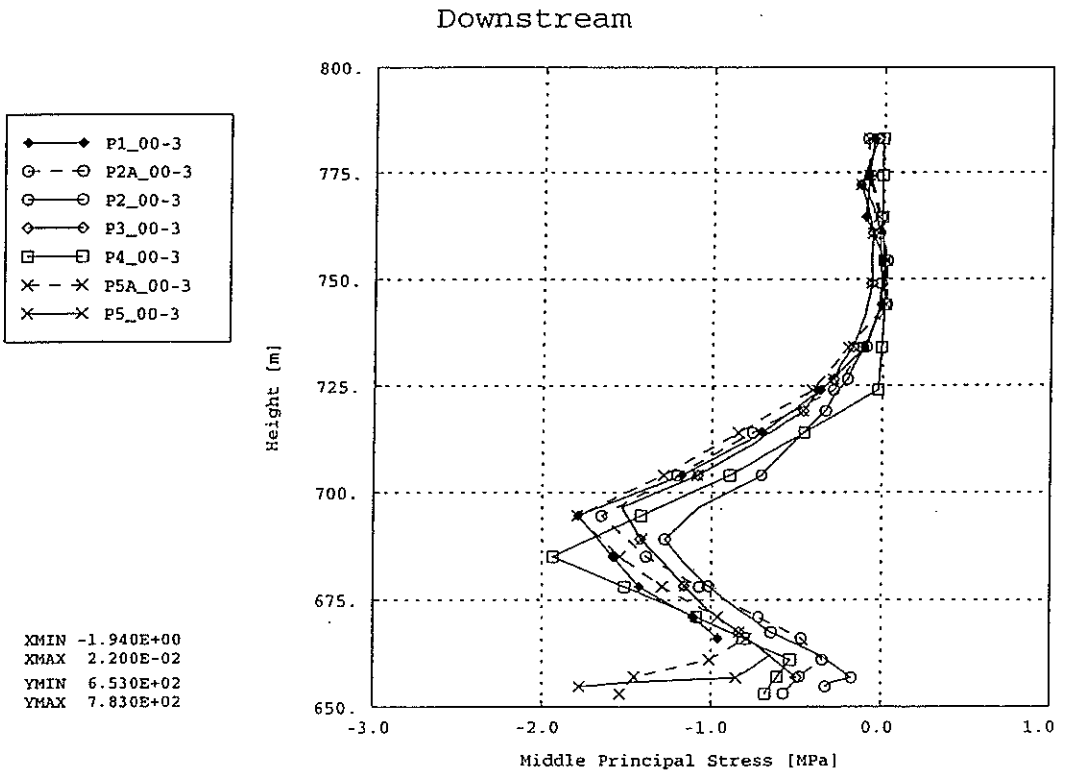

Figure 14: DEAD WEIGHT, WATER LOAD, TEMP - Middle Principle Stress: Block 0

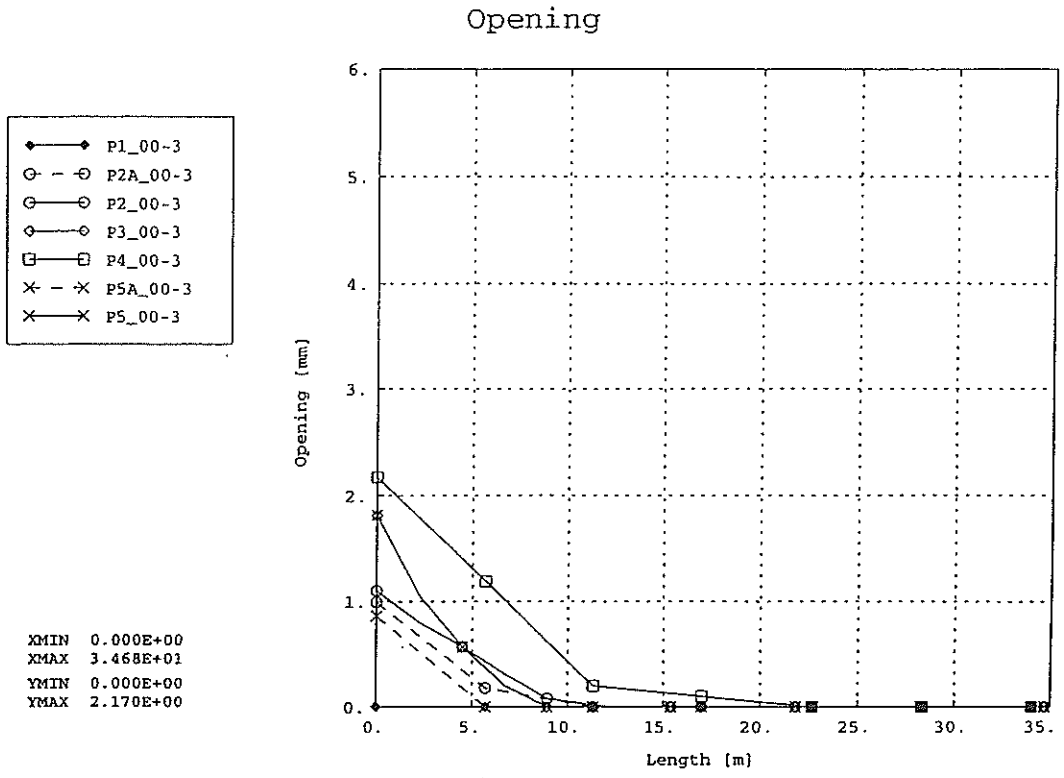

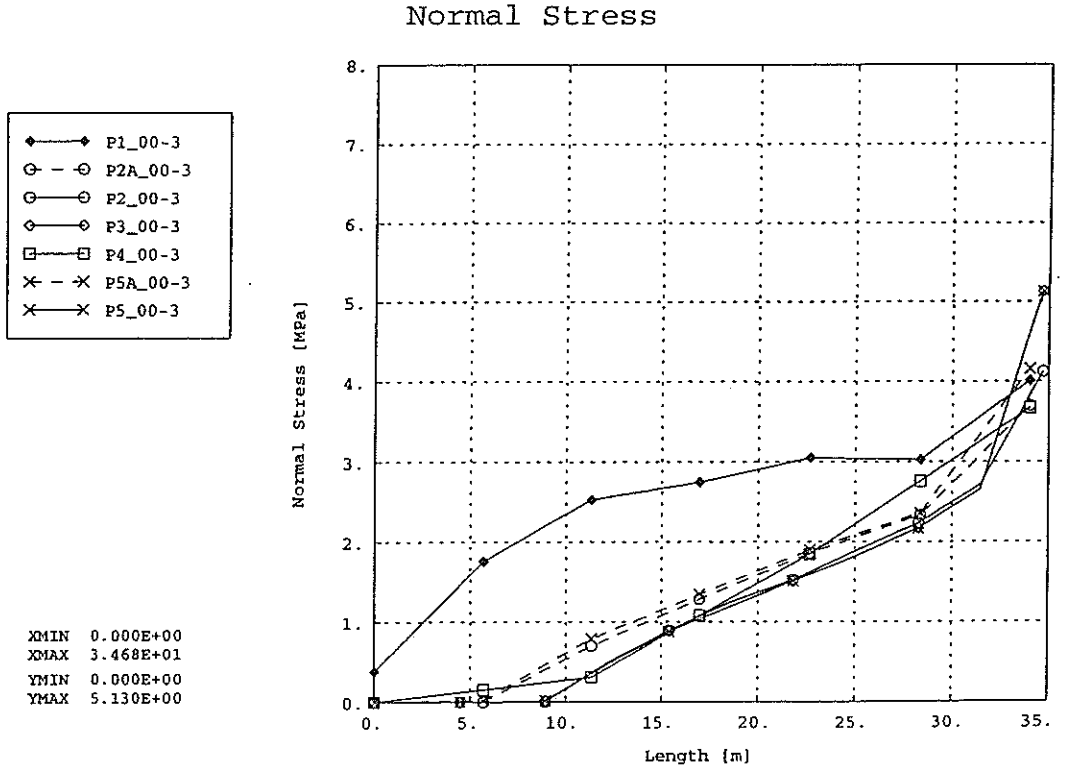

Figure 15: DEAD WEIGHT, WATER LOAD, TEMP. - Opening & Normal Stress: Block 0

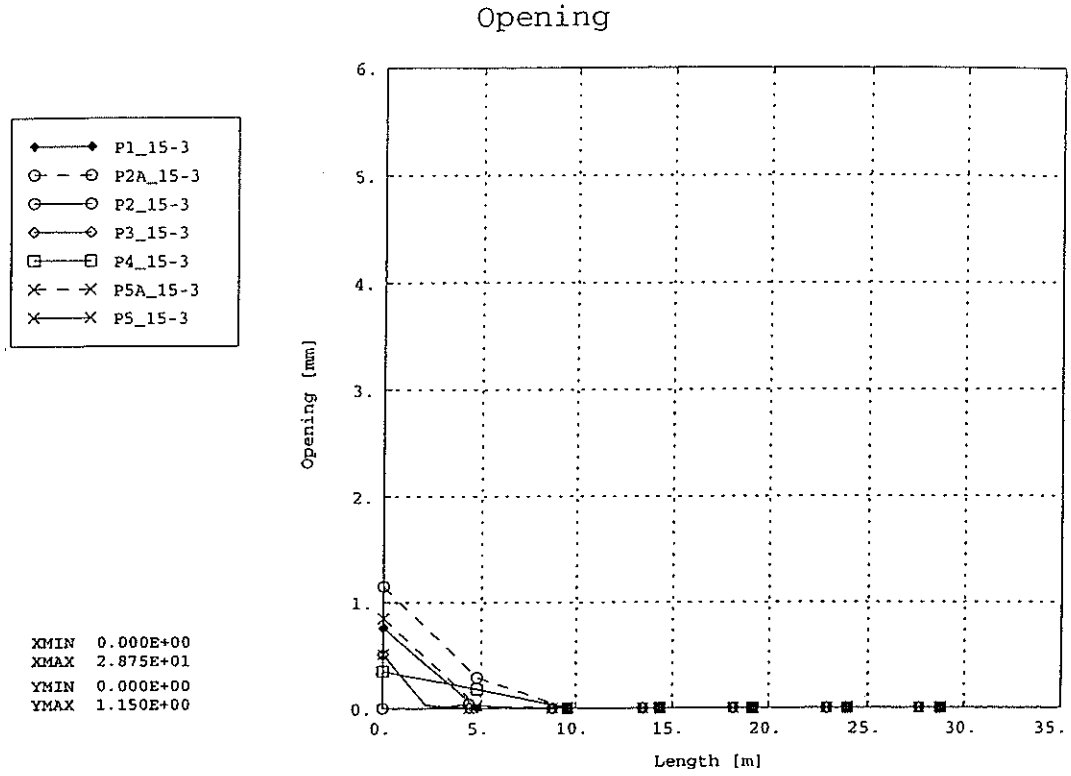

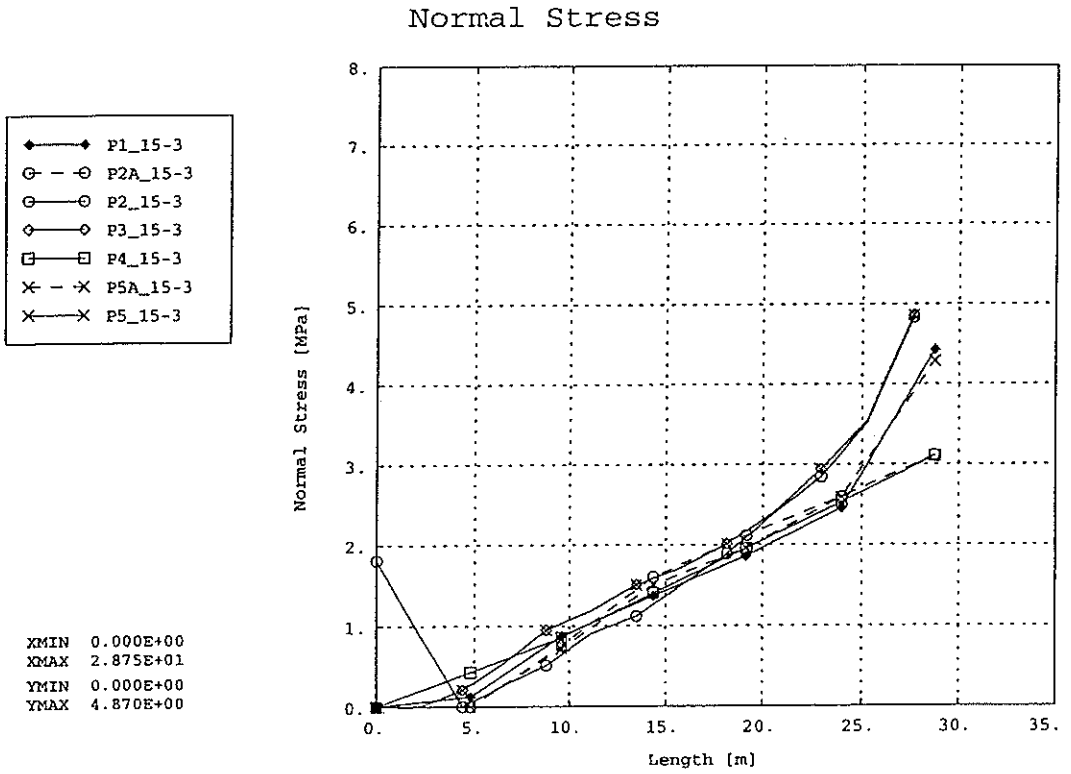

Figure 16: DEAD WEIGHT, WATER LOAD, TEMP. - Opening & Normal Stress: Block 15

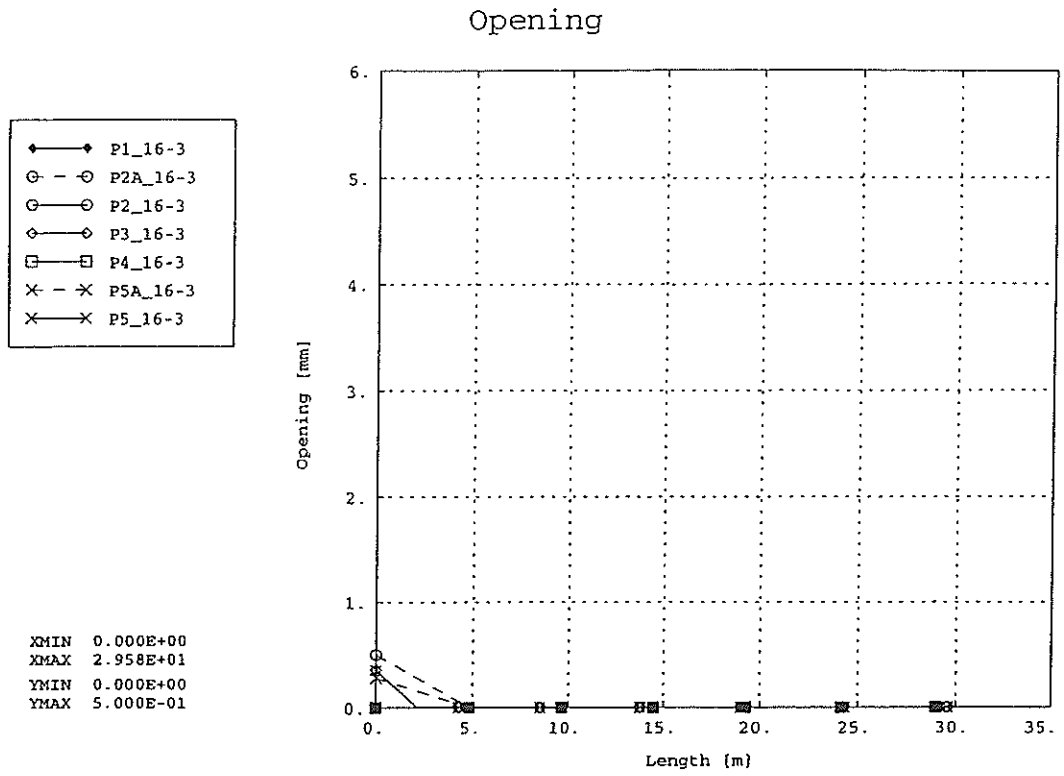

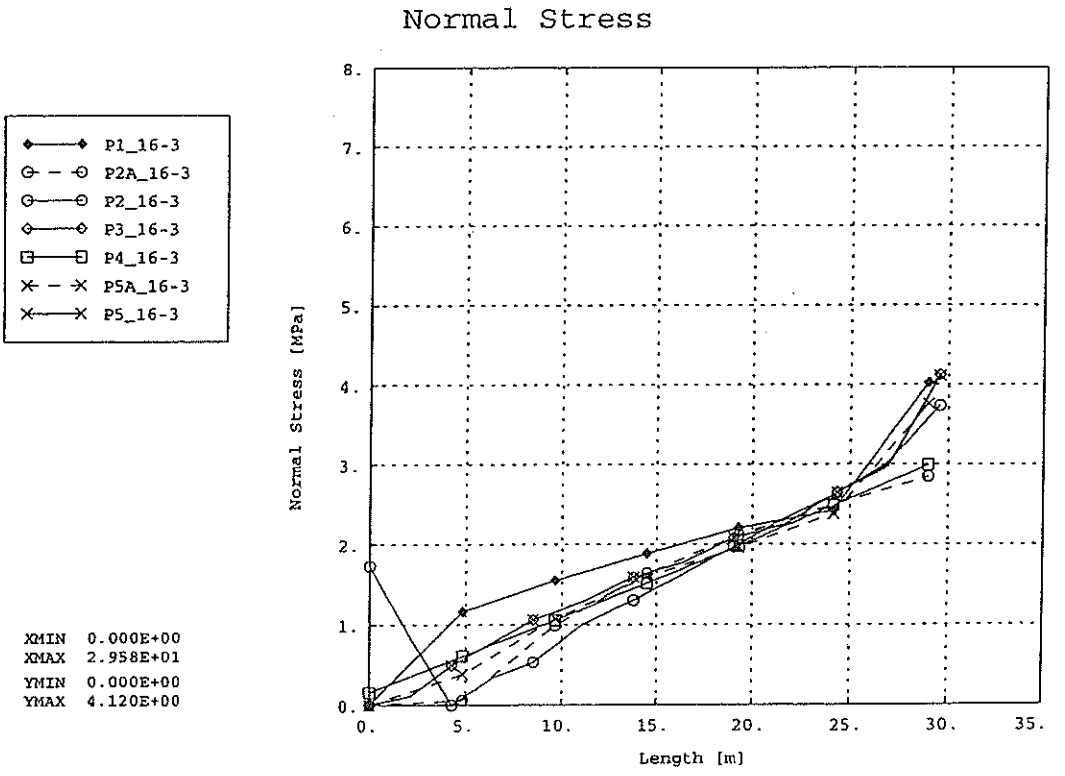

Figure 17: DEAD WEIGHT, WATER LOAD, TEMP. - Opening & Normal Stress: Block 16

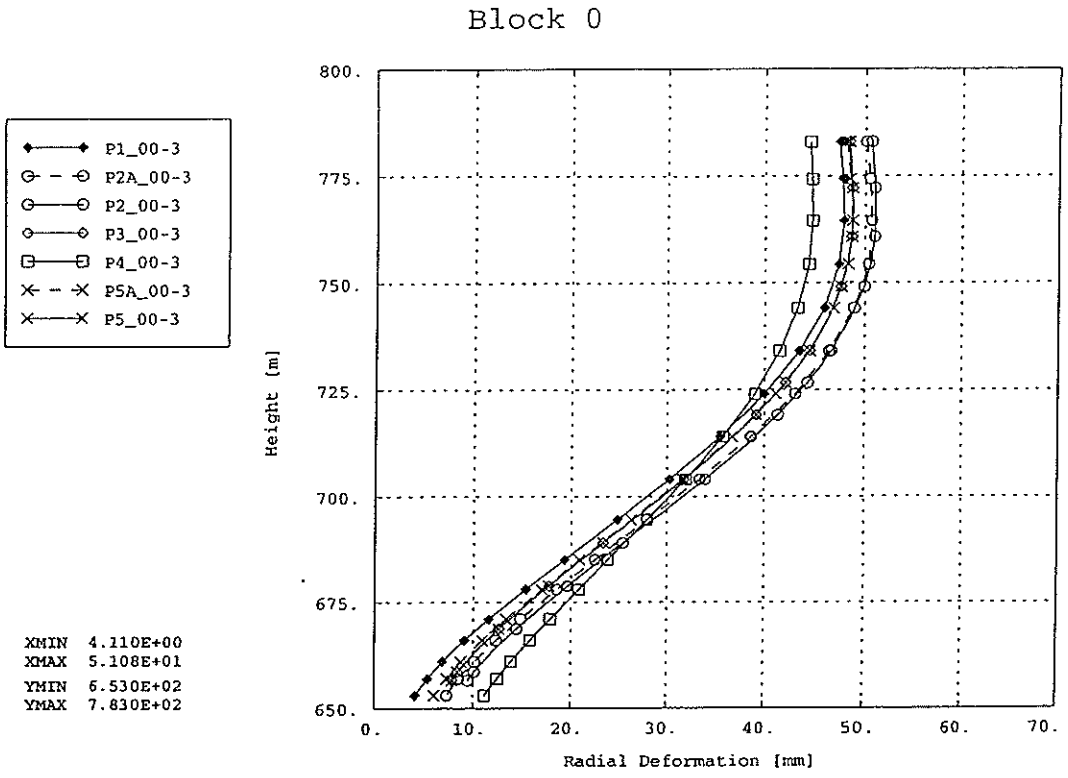

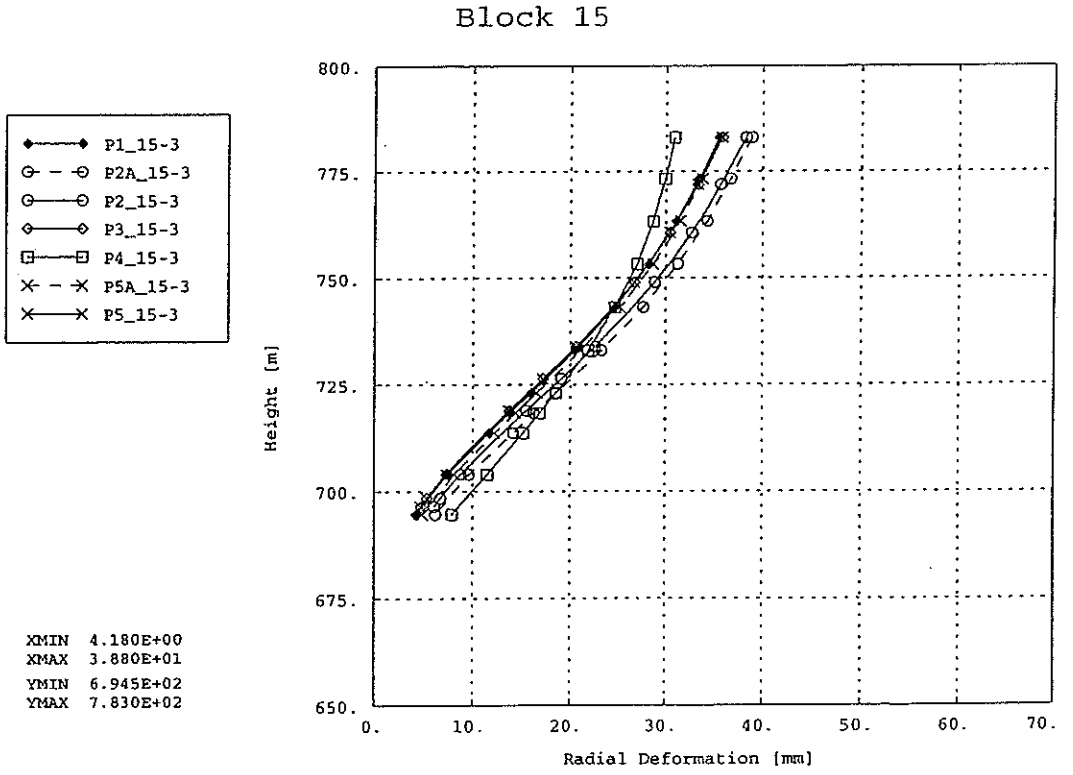

Figure 18: DEAD WEIGHT, WATER LOAD, TEMP - Radial Deformation: Block 0, Block 15

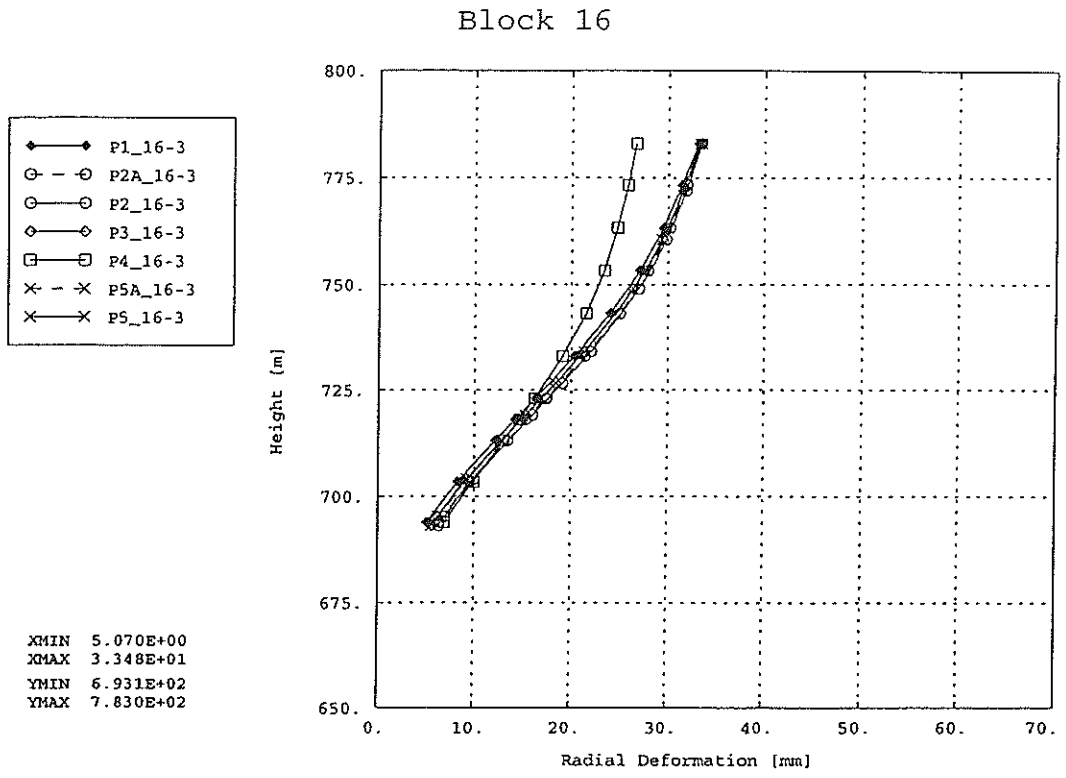

Figure 19: DEAD WEIGHT, WATER LOAD, TEMP - Radial Deformation: Block 16

FULL LOADING CONDITION - Step 4		
Block 0	Minimum Principle Stress	
	Upstream	Downstream
Block 0	Middle Principle Stress	
	Upstream	Downstream
Block 0	Opening - Normal Stress	
Block 15	Opening - Normal Stress	
Block 16	Opening - Normal Stress	
Block 0	Radial Deformation	
Block 15	Radial Deformation	
Block 16	Radial Deformation	

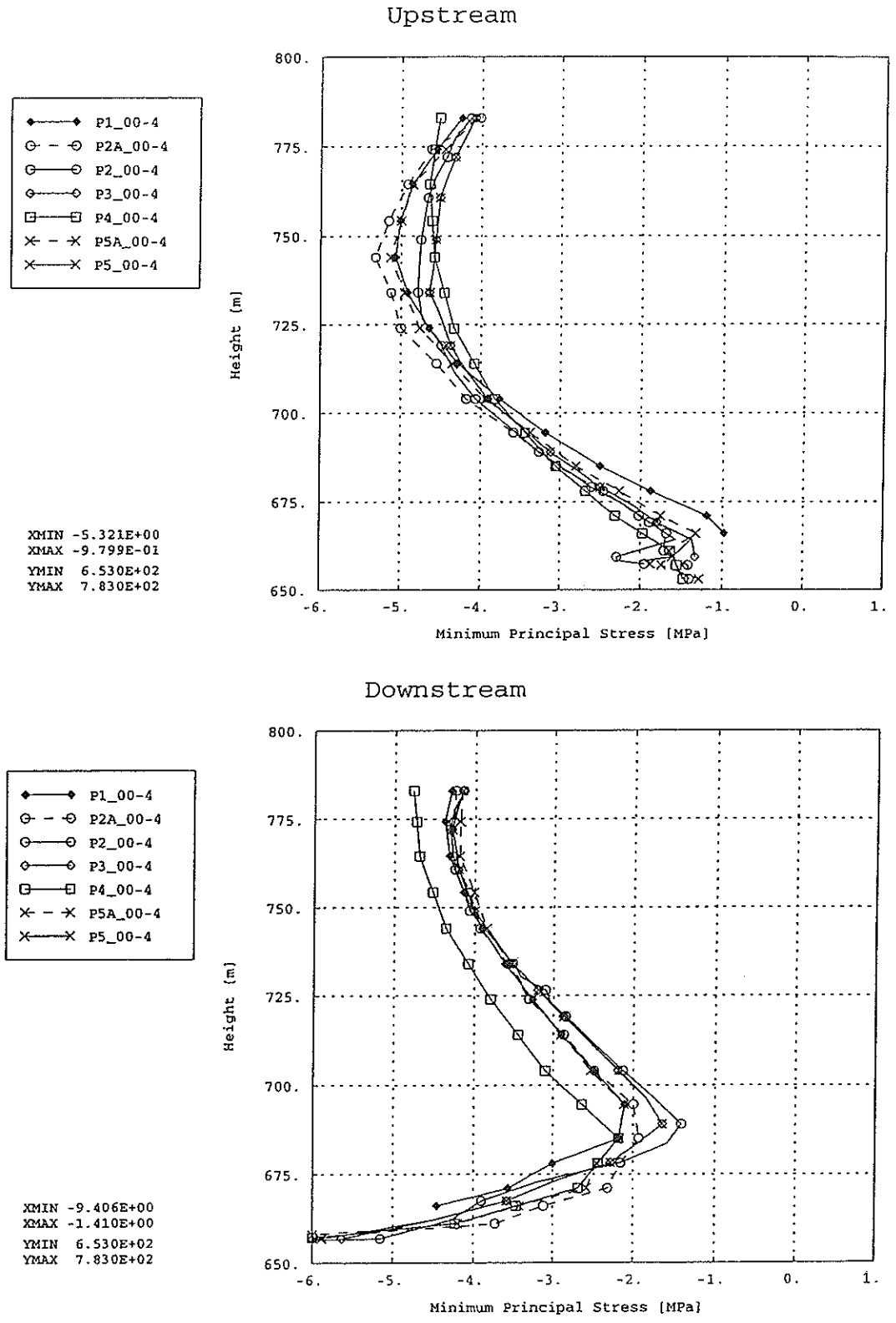

Figure 20: DEAD W., WATER L., TEMP., UPLIFT - Minimum Principle Stress: Block 0

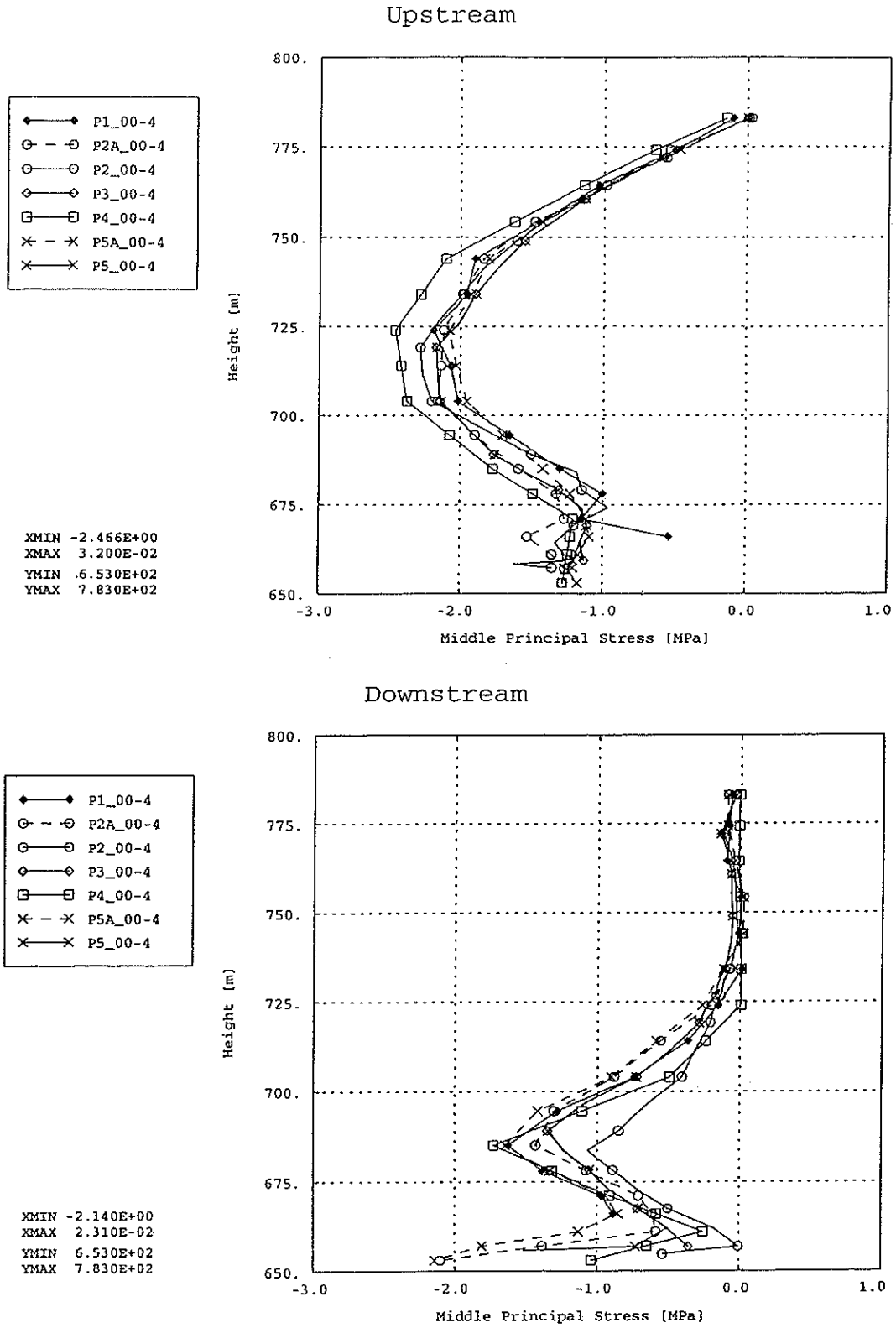

Figure 21: DEAD W., WATER L., TEMP., UPLIFT - Middle Principle Stress: Block 0

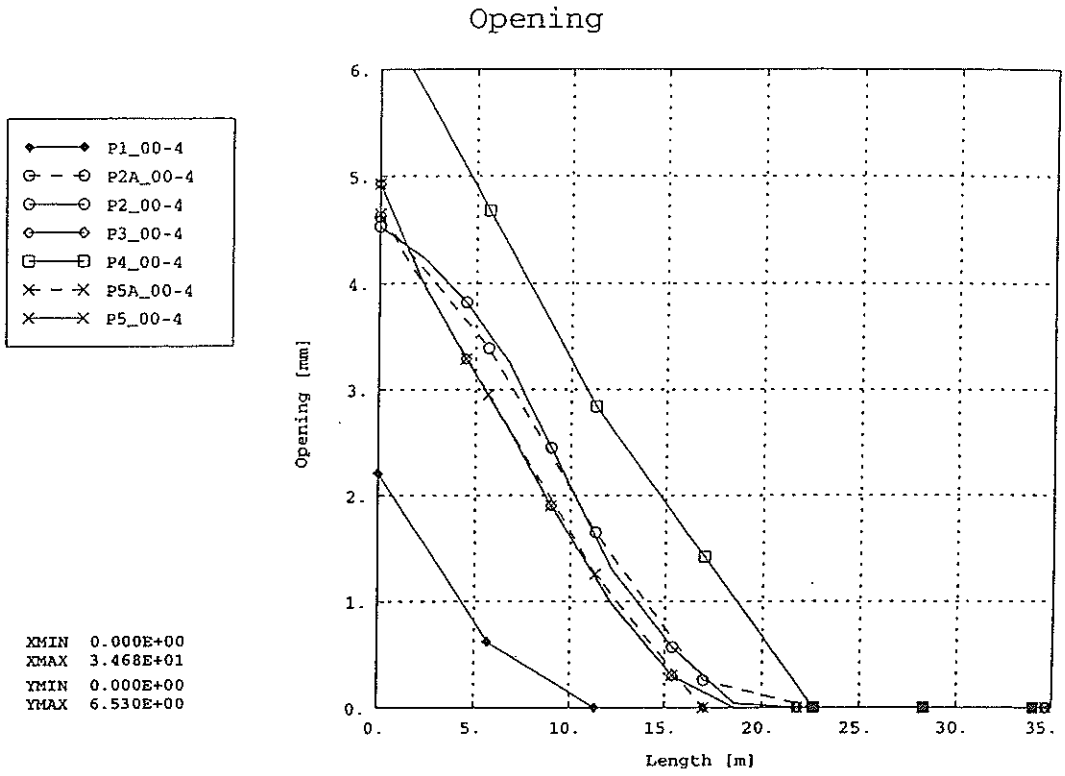

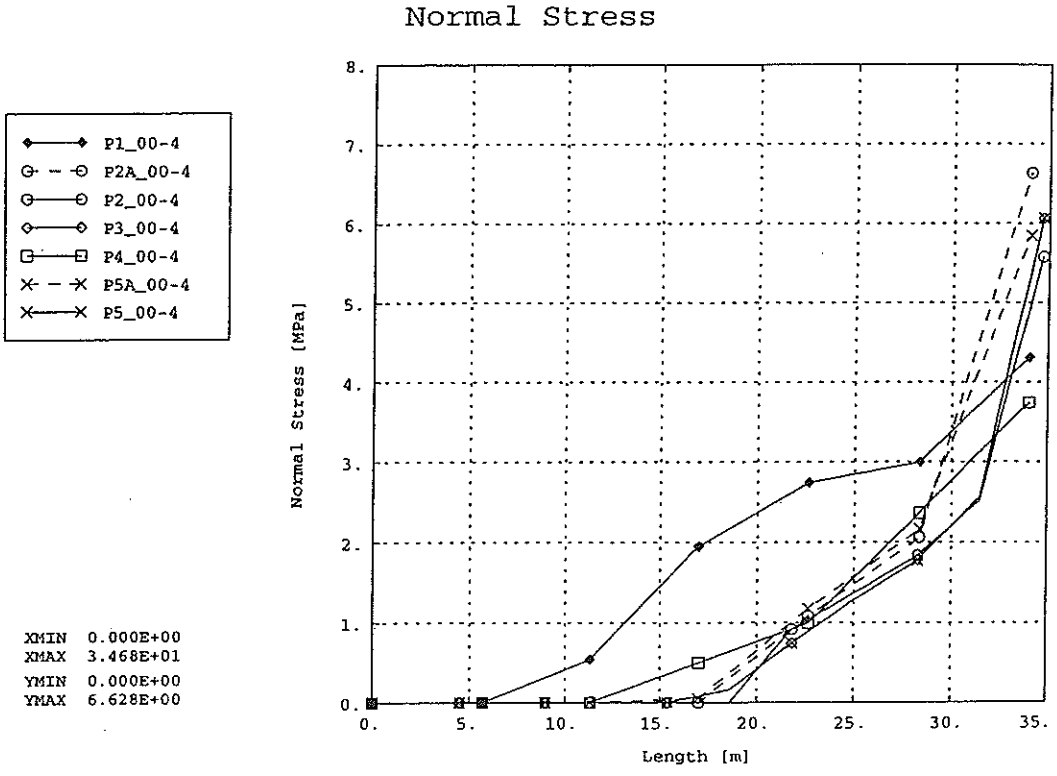

Figure 22: DEAD W., WATER L., TEMP., UPLIFT - Opening & Normal Stress: Block 0

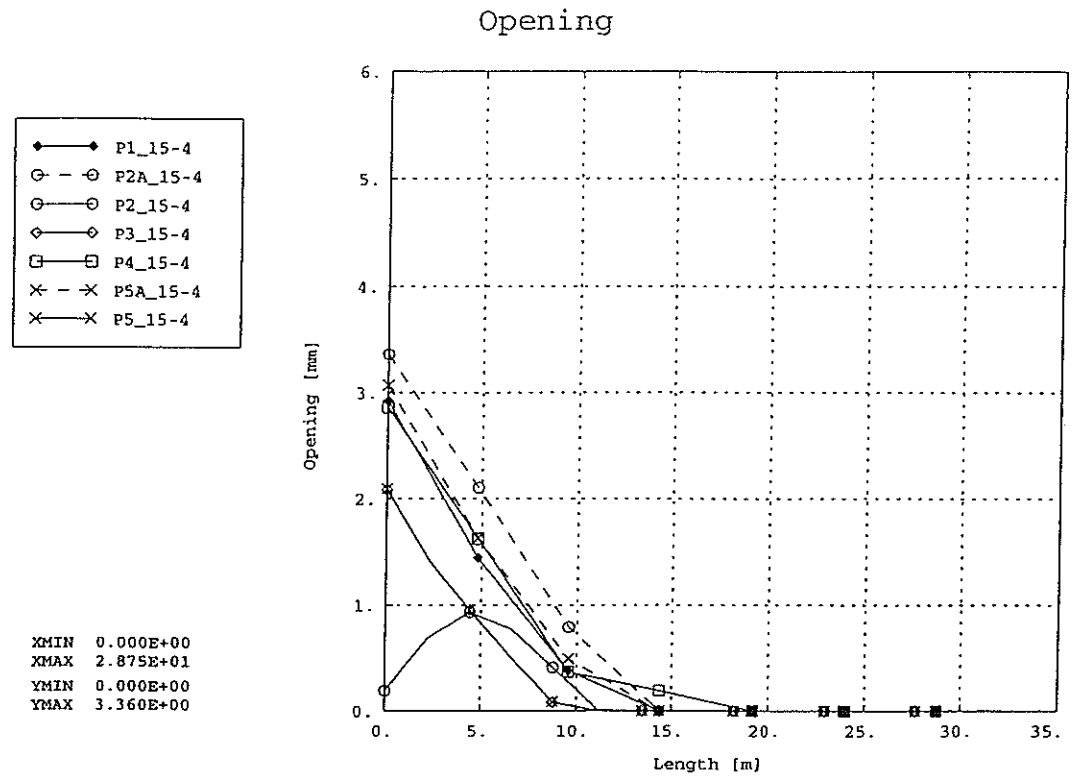

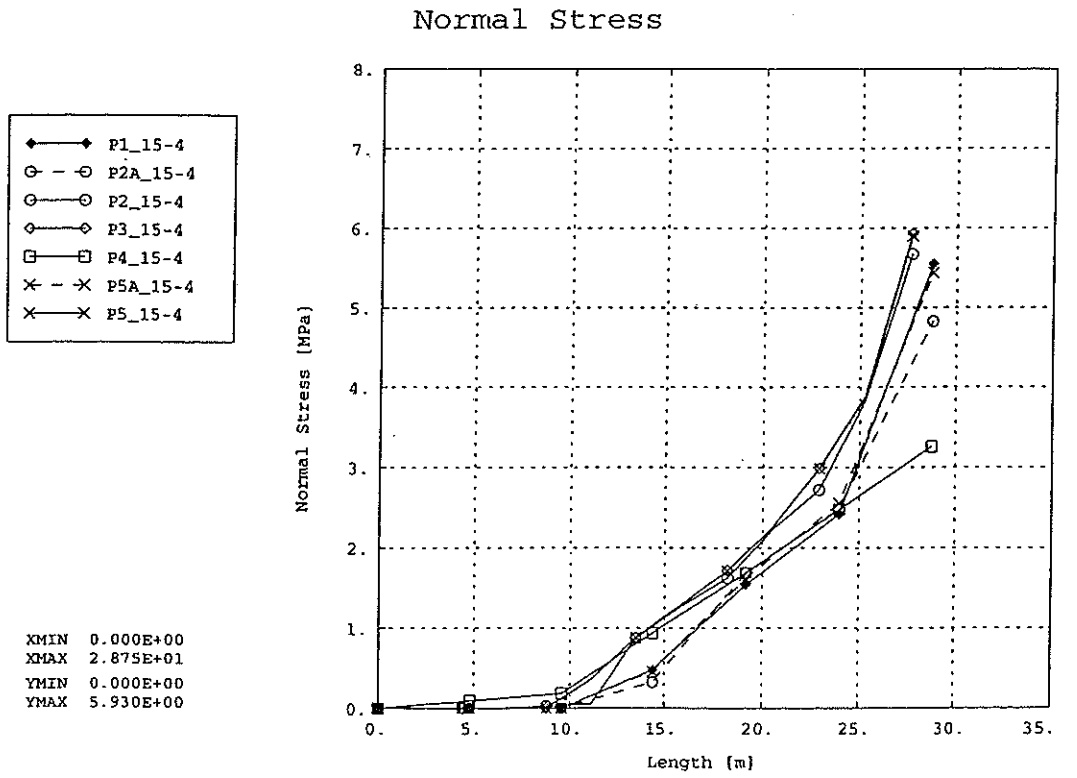

Figure 23: DEAD W., WATER L., TEMP., UPLIFT - Opening & Normal Stress: Block 15

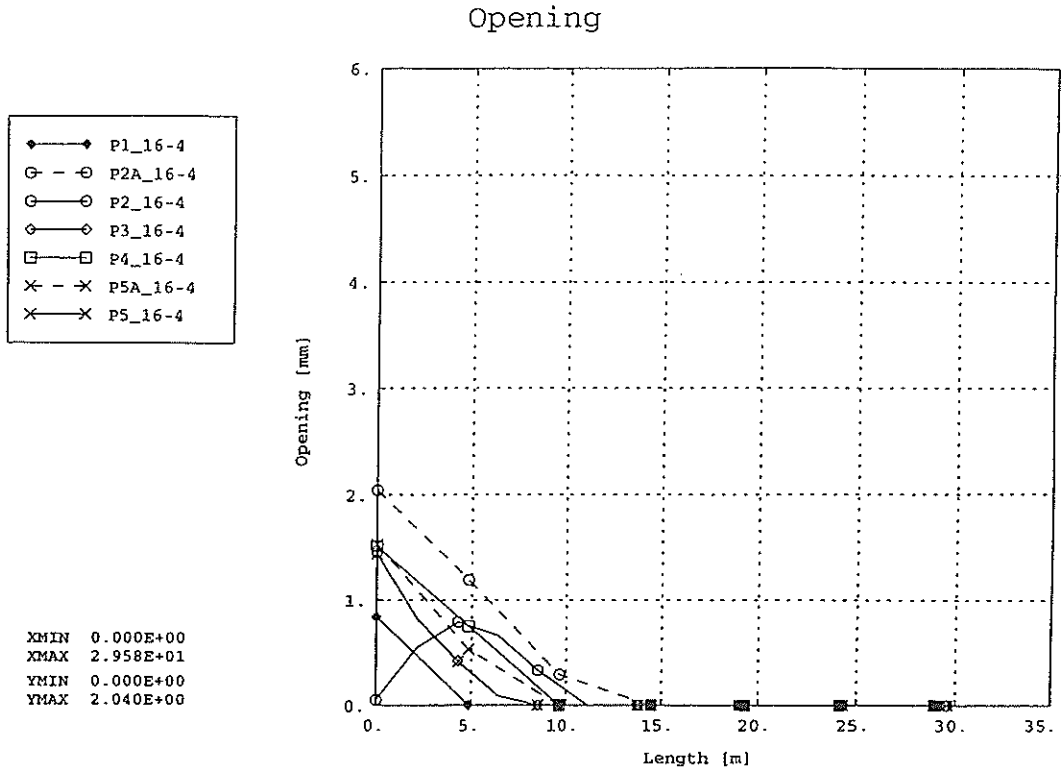

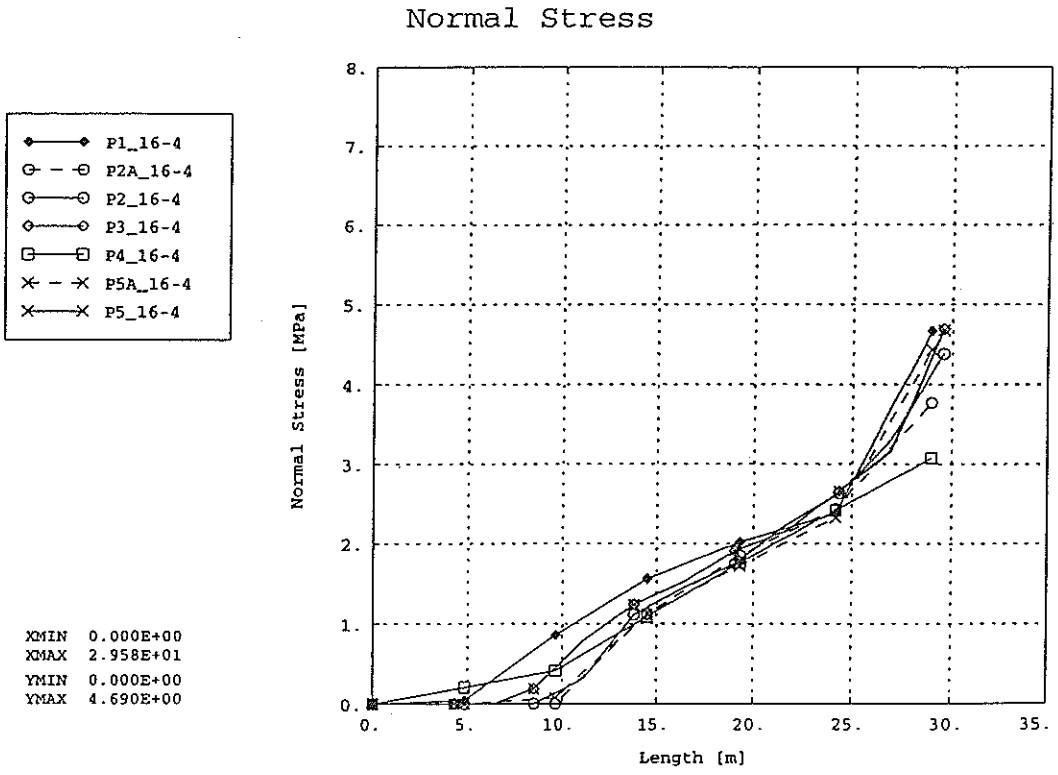

Figure 24: DEAD W., WATER L., TEMP., UPLIFT - Opening & Normal Stress: Block 16

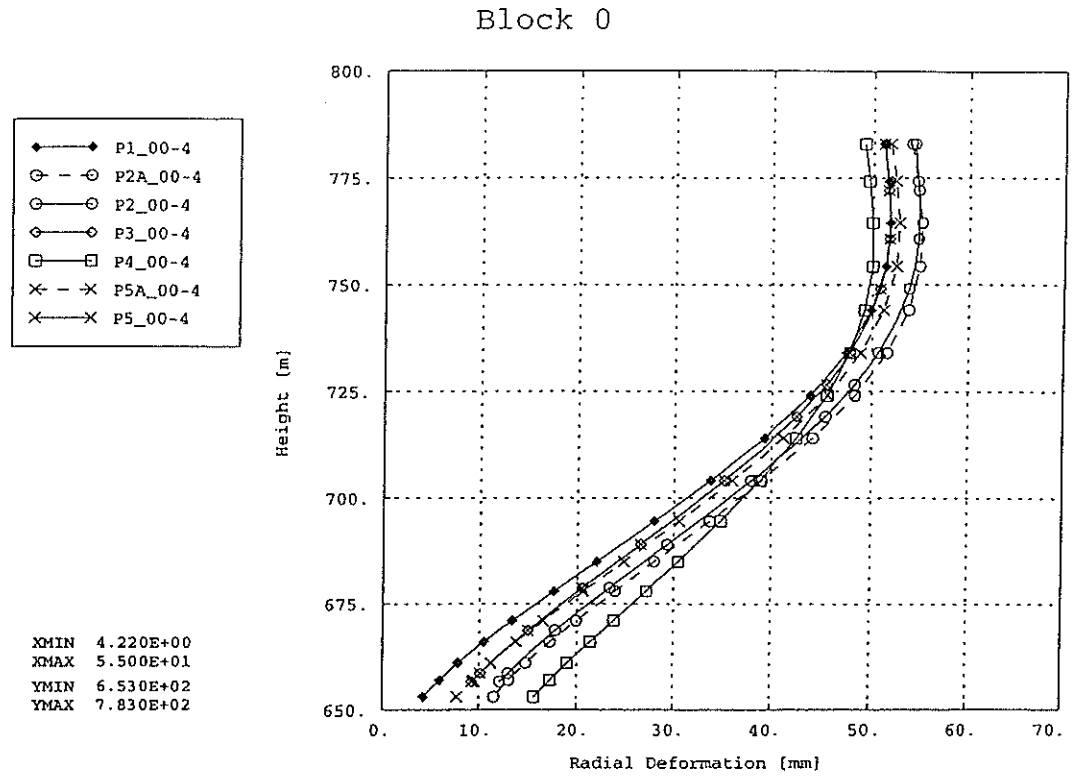

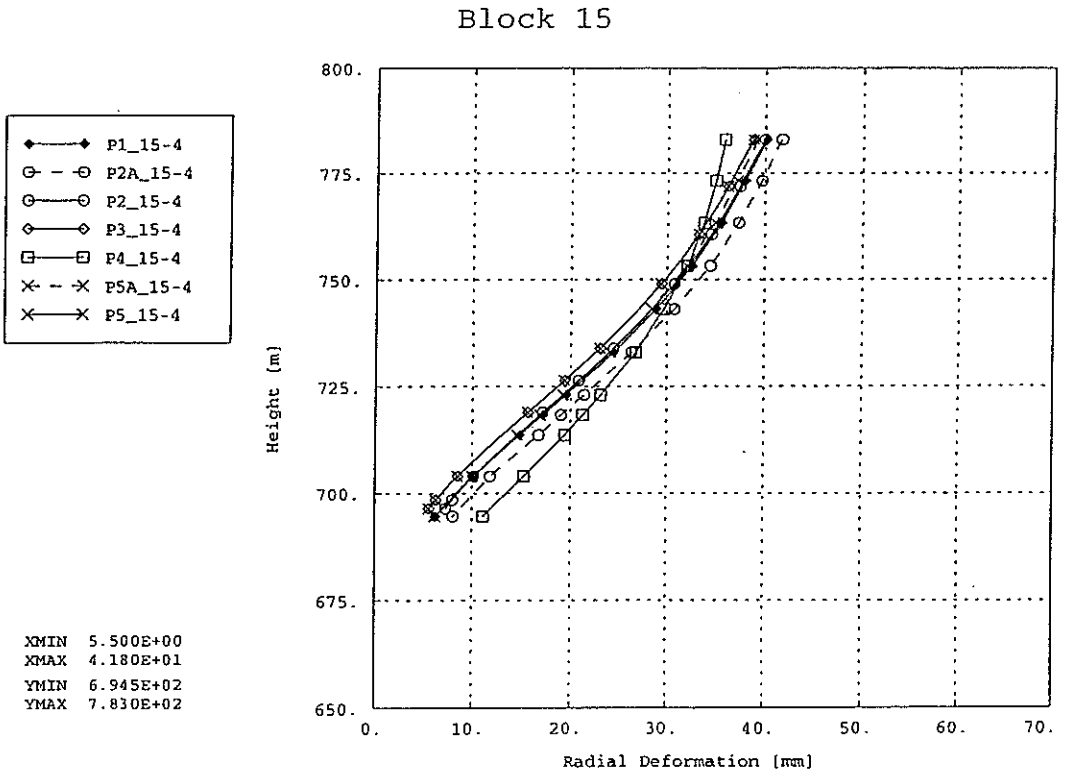

Figure 25: DEAD W., WATER L., TEMP., UPLIFT - Radial Deformation: Block 0, Block 15

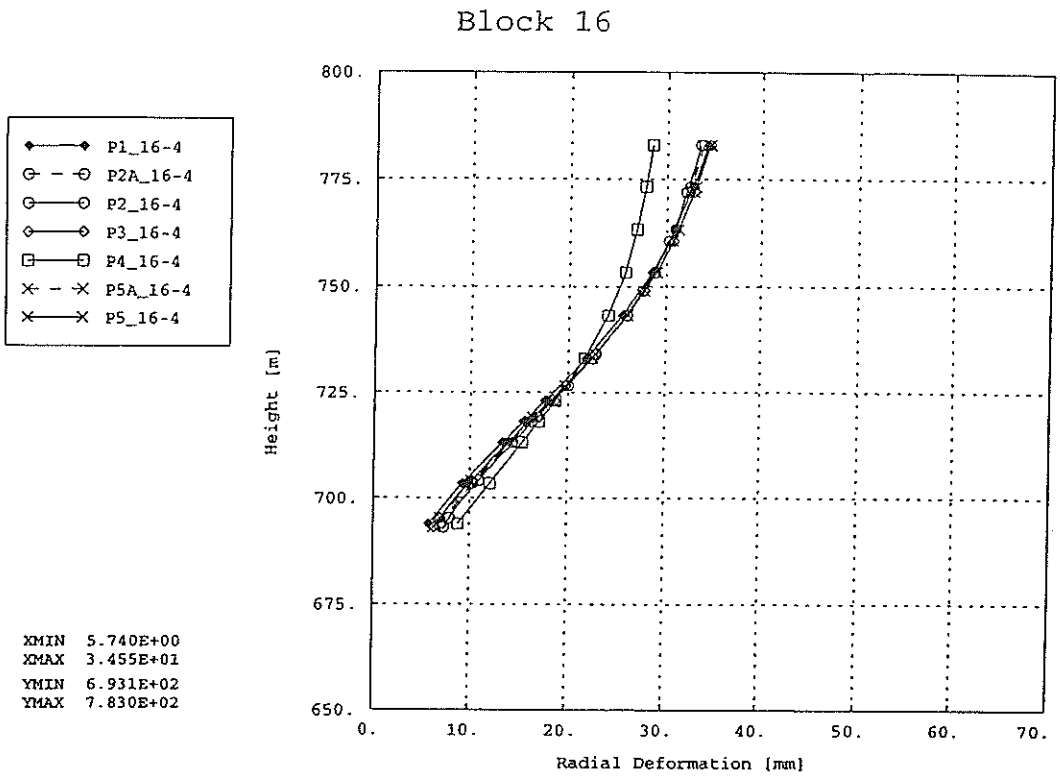

Figure 26: DEAD W., WATER L., TEMP., UPLIFT - Radial Deformation: Block 16

FULL LOADING CONDITION with and without UPLIFT	
Block 0	Normal Stress - Shear Stress

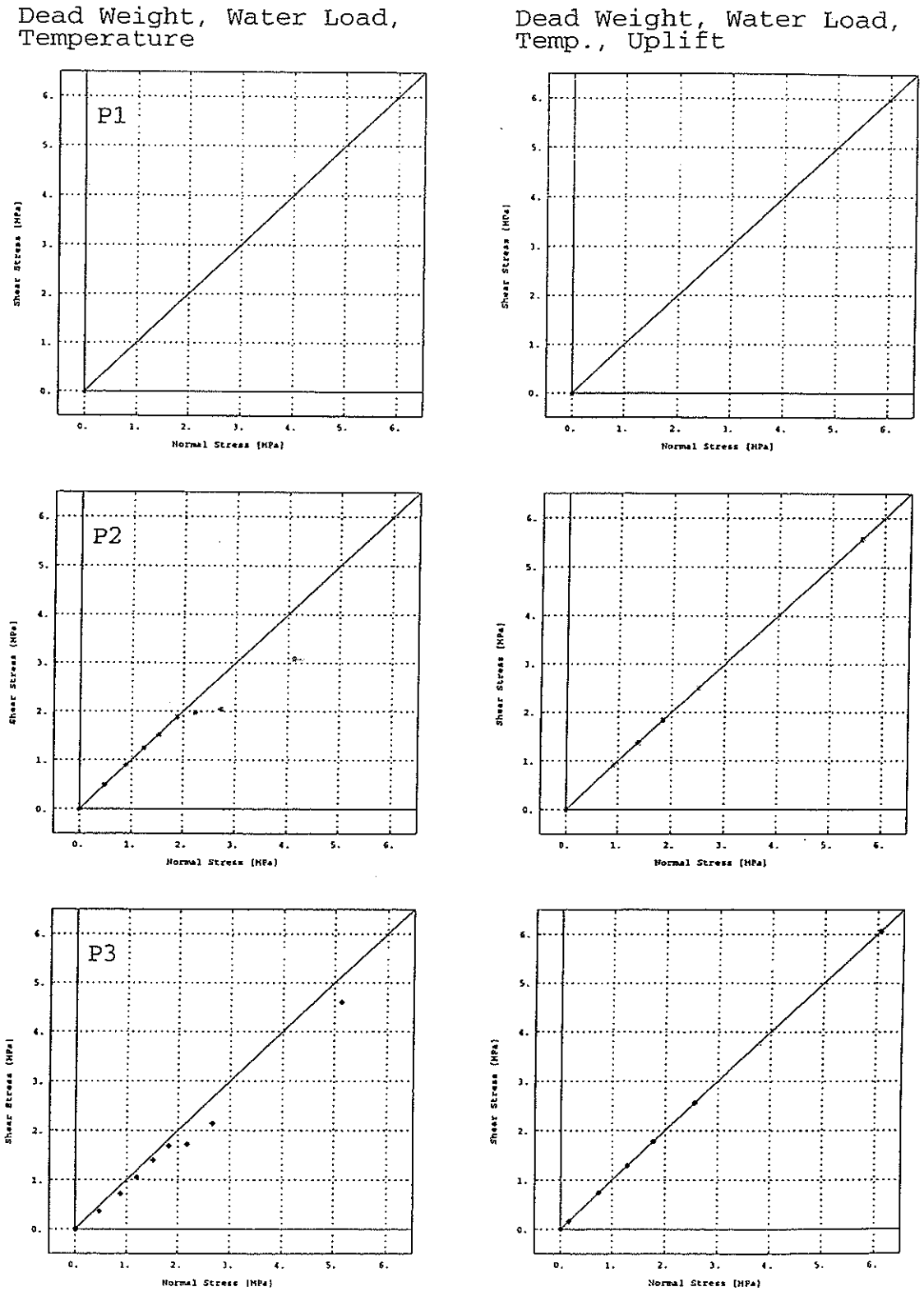

Figure 27: Normal Stress - Shear Stress: Block 0

Dead Weight, Water Load, Temperature

Dead Weight, Water Load, Temp., Uplift

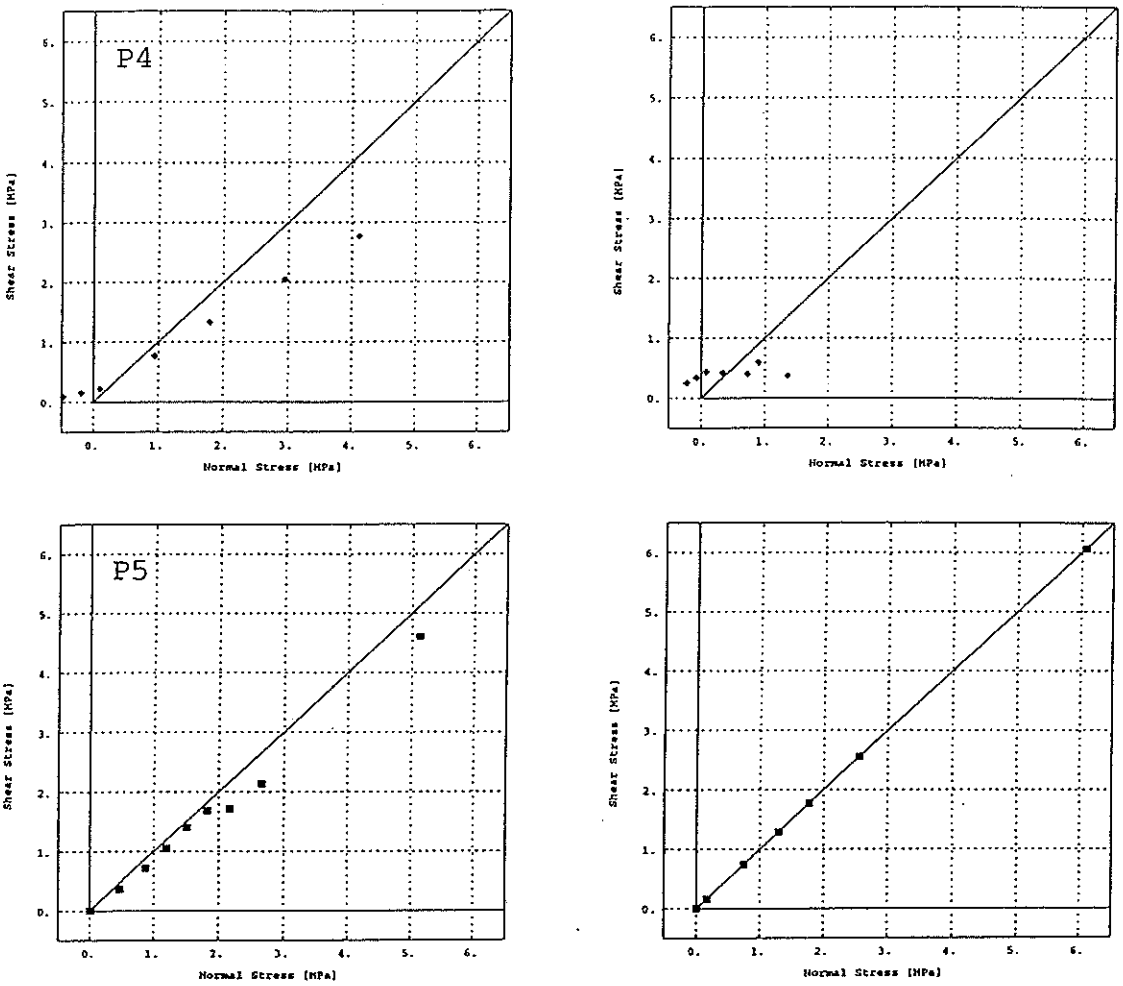

Figure 28: Normal Stress - Shear Stress: Block 0

LINEAR AND NON-LINEAR STATIC ANALYSIS OF AN ARCH DAM

Q. CAI [1], J.H. DURIEUX[2]

ABSTRACT

A contact analysis of the Schlegeis Arch Dam in Austria was performed to investigate the overall contact behaviour of the structure and to compare the results at the 5th international ICOLD benchmark workshop on numerical analysis of dams. The finite element code – ABAQUS was used for this task and the contact surface between the concrete wall and rock foundation was modeled by the contact elements in the program. The calculated results of linear and non-linear analyses are discussed.

INTRODUCTION

The use of contacting components, such as the analytical simulation of a cracked dam or rock - structure interaction, is very common in the design of structures and also very important in evaluating structural safety such as stability of arch dams. Problems are naturally non-linear and therefore generally difficult to solve analytically. Numerical solutions using the finite element method seem to be an attractive alternative. ABAQUS has various interface surfaces and elements to model contact and friction conditions.

This is the first benchmark analysis on contact problems undertaken at Department of Water Affairs & Forestry in South Africa to evaluate the accuracy and versatility of the ABAQUS program which has been used for the contact related analysis of the dam structures in South Africa. Previously we used our own in-house developed program JNT ARCH.

The analysis was carried out on a SUN ULTRA 5 workstation using SPARC 300 MHz processor and Solaris 2.6 operating system.

The Schlegeis arch dam which was built between 1969 and 1971, is the main structure of the Zemm power plant in Austria. The main geometric data of the dam is as follows:

1) Deputy Chief Engineer, Department of Water Affairs, South Africa

2) Chief Engineer, Department of Water Affairs, South Africa

- Height of concrete wall 131 m
- Crest length 725 m
- Crest / height ratio 5.5 m
- Thickness of ãrest 9.0 m
- Thickness at base 34.0 m

The dam consists of 43 blocks each 17 m wide. Grouting of the joints was undertaken after construction.

The foundation of the dam is composed of fairly uniform gneiss. It has schistosity planes which are approximately parallel to the right bank abutment and has a very steep dip towards downstream.

THE FINITE ELEMENT MODEL

The suggested finite element model was provided by the formulator of the problem – Verbundplan Consulting Engineers, Austria.

The element types used in the analysis are 3 –D second order brick and wedge elements. Contact element type (INTER9) are used to simulate the interface between dam and foundation. The basic data of the finite element mesh are shown in the following table 1:

Table 1: Basic Data – Finite Element Mesh

	Elements	Nodes
Dam	246	1477
Rock	896	4821
Interface	54	

MATERIAL PROPERTIES

The material behavior of the concrete was assumed to be orthotropic for the gravity loading (step1) in order to simulate the construction of the dam. An isotropic concrete model was assumed for the subsequent loading cases (step 2~4). The rock foundation was modeled as an orthotropic material according to the direction of the schistosity.

The following material properties were used in the analysis:

Table 2: Basic Data – Material Parameters

	Rock	Concrete
Young's modulus E [GPa] (for rock E_{II})	30	25
Young's modulus E [GPa] (for rock $E_{\perp}$)	10	
Poisson ratio ν	0.17	0.17
Density [kg/m^3]		2400
Thermal expansion coefficient α_T		$8x10^{-6}$

The contact behavior of the interface between dam and foundation was modeled with an isotropic Coulomb friction model with a friction angle of $\varphi = 45°$.

LOADS

The following load cases as required were considered in the analysis:

LOAD CASE 1 (linear static)

Step 1: Gravity - with independent columns

Step 2: Step 1 (results) + hydrostatic loading

Step 3: Step 2 (results) + temperature loading

Step 4: Step 3 (results) + uplift pressure loading

LOAD CASE 2 (non-linear static, with the joint interface between the concrete wall and rock foundation included)

Step 1: Gravity - with independent columns

Step 2: Step 1 (results) + hydrostatic loading

Step 3: Step 2 (results) + temperature loading

Step 4: Step 3 (results) + uplift pressure loading

The hydrostatic pressure and the uplift pressure were applied as shown in fig. 1.

For the temperature loading condition, the distribution of a measured summer-temperature field relative to the joint closing temperature supplied by the formulator was used.

LOADING SEQUENCE

Step 1 (dead weight loading) was the first analysis run with a dam material of only significant vertical stiffness and very low tangential and radial stiffness. The stress state due to dead weight was recorded on a result file and re-read into the second analysis (step 2, 3 and 4) as initial stress state. The following graph shows the sequence of analyses.

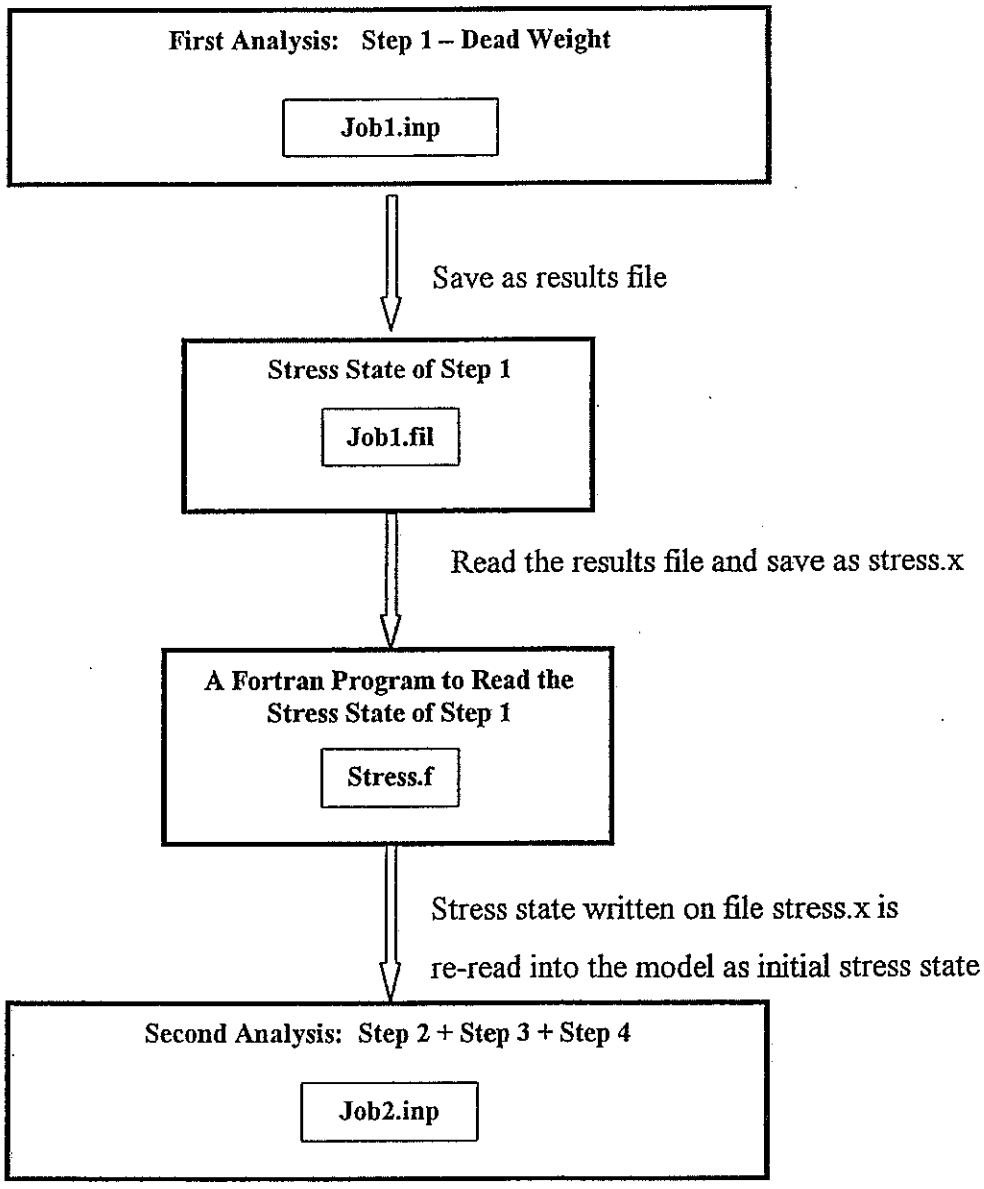

RESULTS

The output results are processed in the form of stress and displacement contours.

CASE 1 - linear model (without base joint)

The dead weight loading (step 1) is done for the purpose of simulating the construction procedure. The minimum principal stresses (SP1) show a maximum compressive stress of approximately 8 MPa at the heel of the dam. Along the toe of the dam the maximum principal stresses (SP3) (tensile stresses) are between 0 MPa to 0.8 MPa for most of the surface. For a small portion in the vicinity of the right abutment, the tensile stresses reach a value of up to 1.3 MPa (refer to fig.3, 4 ,5 and 6).

For the full loading case (step 4), the minimum principal stresses (SP1) along the most of heel decrease to about 0.7 MPa and are even in tension of 0,6 MPa in a small area of the centre heel. The maximum value of compressive stresses are in the region of 8 MPa at the toe. The maximum tensile stresses at the heel of the dam are approximately 5.8 MPa (refer to fig. 7, 8, 9 and 10).

The maximum radial deflection under full loading condition is 48 mm which occurs at the top in the centre of the dam. (refer to fig. 11)

CASE 2 - non-linear model (with base joint)

The dead weight loading (step1) has the same stress pattern as load case 1.

Under full loading conditions, the base joint opens to a certain extent and the results obtained are discussed below:

In general, compared to the linear model, an increase in the compressive stress occurs at the toe of the dam. The tensile stresses along the heel decrease dramatically from the maximum value of 5.8 MPa in load case 1, to below 0.7 MPa in case 2 (refer to fig. 12 to 15).

The opening of the base joint along the entire dam is shown in fig. 17. The heel in the middle part of the dam is open to some extent on the base joint (refer to fig. 18).

The calculated maximum radial displacements are approximately 52 mm for the block 0.

The horizontal displacement at the crest for the load case 1 and 2 is shown in fig. 19. The minimum and maximum principal stresses along the crown cantilever for the four steps in load case 2 are shown in figures 20 and 21 respectively.

The displacements in the radial direction for block 0, 15 and 16 in the four loading steps are shown in the following four tables.

1. DEAD WEIGHT			
Node	Def-x (m)	Def-y (m)	Def-radial(m)
BLOCK 0			
407	-4.2020E-04	4.4220E-05	-4.2020E-04
412	-4.8499E-04	4.7424E-05	-4.8499E-04
422	-5.5250E-04	4.9355E-05	-5.5250E-04
427	-6.1298E-04	5.0370E-05	-6.1298E-04
437	-6.5658E-04	5.0662E-05	-6.5658E-04
442	-6.7793E-04	5.0205E-05	-6.7793E-04
452	-6.7704E-04	4.9252E-05	-6.7704E-04
457	-6.5232E-04	4.7506E-05	-6.5232E-04
467	-6.0443E-04	4.5452E-05	-6.0443E-04
472	-5.3700E-04	4.3586E-05	-5.3700E-04
482	-4.5095E-04	4.1231E-05	-4.5095E-04
491	-3.7414E-04	3.9217E-05	-3.7414E-04
508	-2.8673E-04	3.8204E-05	-2.8673E-04
1362	-2.1800E-04	3.8139E-05	-2.1800E-04
1080	-1.3885E-04	3.6897E-05	-1.3885E-04
1081	-6.9232E-05	3.4640E-05	-6.9232E-05
1082	-1.0034E-05	3.1440E-05	-1.0034E-05
BLOCK 15			
622	-1.3523E-03	7.7519E-04	-1.5441E-03
635	-1.2607E-03	6.9200E-04	-1.4208E-03
6µ2	-1.1647E-03	6.1301E-04	-1.2966E-03
665	-1.0612E-03	5.3490E-04	-1.1669E-03
682	-9.5241E-04	4.5512E-04	-1.0320E-03
695	-8.3590E-04	3.6725E-04	-8.8608E-04
716	-7.0018E-04	2.6994E-04	-7.1911E-04
1359	-6.2734E-04	2.2152E-04	-6.3194E-04
1063	-5.6011E-04	1.5680E-04	-5.3910E-04
1064	-3.6573E-04	-7.7869E-06	-3.6224E-04
1065	-1.6763E-04	-1.7992E-04	-2.2734E-05
BLOCK 16			
105	-1.4615E-03	-5.8186E-04	-1.5371E-03
121	-1.3534E-03	-4.9713E-04	-1.4000E-03
135	-1.2379E-03	-4.1941E-04	-1.3019E-03
151	-1.1142E-03	-3.4563E-04	-1.2041E-03
165	-9.8946E-04	-2.7391E-04	-9.7347E-04
185	-8.6041E-04	-1.9774E-04	-8.3049E-04
206	-7.1592E-04	-1.1927E-04	-7.0040E-04
1367	-6.3736E-04	-8.0126E-05	-6.1234E-04
1303	-5.6451E-04	-2.9095E-05	-5.3517E-04
1263	-3.7290E-04	9.7253E-05	-2.5476E-04
1204	-1.8150E-04	2.2848E-04	-2.2706E-05

2. DEAD WEIGHT + WATER LOAD			
Node	Def-x (m)	Def-y (m)	Def-radial(m)
BLOCK 0			
407	5.9600E-02	-1.9611E-04	5.9600E-02
412	5.8341E-02	-6.6665E-05	5.8431E-02
422	5.6796E-02	6.9997E-05	5.6796E-02
427	5.4655E-02	2.0526E-04	5.4655E-02
437	5.1699E-02	3.3233E-04	5.1699E-02
442	4.7954E-02	4.4785E-04	4.7954E-02
452	4.3378E-02	5.5001E-04	4.3378E-02
457	3.8039E-02	6.4598E-04	3.8039E-02
467	3.2103E-02	7.2734E-04	3.2103E-02
472	2.6138E-02	7.9812E-04	2.6138E-02
482	2.0139E-02	8.5597E-04	2.0139E-02
491	1.5886E-02	8.8198E-04	1.5886E-02
508	1.1924E-02	9.0270E-04	1.1924E-02
1362	9.3479E-03	9.1354E-04	9.3479E-03
1080	7.0565E-03	9.1532E-04	7.0565E-03
1081	5.5460E-03	9.0450E-04	5.5460E-03
1082	4.2690E-03	8.7514E-04	4.2690E-03
BLOCK 15			
622	4.1063E-02	-1.8646E-02	4.3898E-02
635	3.7519E-02	-1.7185E-02	4.0200E-02
652	3.3830E-02	-1.5547E-02	3.6279E-02
665	2.9852E-02	-1.3607E-02	3.1945E-02
682	2.5550E-02	-1.1313E-02	2.7138E-02
695	2.0975E-02	-8.7201E-03	2.1931E-02
716	1.6393E-02	-5.9870E-03	1.6634E-02
1359	1.4333E-02	-4.7027E-03	1.4219E-02
1063	1.2329E-02	-3.4880E-03	1.1891E-02
1064	8.6480E-03	-1.1839E-03	7.5688E-03
1065	5.8033E-03	4.8623E-04	4.2964E-03
BLOCK 16			
105	3.8847E-02	1.3892E-02	3.9974E-02
121	3.5499E-02	1.3293E-02	3.6863E-02
135	3.2062E-02	1.2475E-02	3.3557E-02
151	2.8393E-02	1.1342E-02	2.9882E-02
165	2.4449E-02	9.8564E-03	2.5683E-02
185	2.0260E-02	8.0703E-03	2.1309E-02
206	1.6045E-02	6.1054E-03	1.6716E-02
1367	1.4011E-02	5.0919E-03	1.4463E-02
1303	1.2028E-02	4.1265E-03	1.2279E-02
1263	8.4828E-03	2.3137E-03	8.3264E-03
1204	5.5818E-03	9.6191E-04	5.1654E-03

3. DEAD WEIGHT + WATER LOAD + TEMP.			
Node	Def-x (m)	Def-y (m)	Def-radial(m)
BLOCK 0			
407	4.7277E-02	9.3030E-06	4.7277E-02
412	4.7524E-02	1.1007E-04	4.7524E-02
422	4.7615E-02	2.1838E-04	4.7615E-02
427	4.7082E-02	3.2704E-04	4.7082E-02
437	4.5565E-02	4.3038E-04	4.5565E-02
442	4.3038E-02	5.2410E-04	4.3038E-02
452	3.9508E-02	6.0762E-04	3.9508E-02
457	3.5052E-02	6.8610E-04	3.5052E-02
467	2.9861E-02	7.5241E-04	2.9861E-02
472	2.4493E-02	8.1000E-04	2.4493E-02
482	1.9000E-02	8.5659E-04	1.9000E-02
491	1.5074E-02	8.7698E-04	1.5074E-02
508	1.1389E-02	8.9304E-04	1.1389E-02
1362	8.9781E-03	9.0140E-04	8.9781E-03
1080	6.8203E-03	9.0079E-04	6.8203E-03
1081	5.3954E-03	8.8992E-04	5.3954E-03
1082	4.1795E-03	8.5899E-04	4.1795E-03
BLOCK 15			
622	3.2636E-02	-1.3291E-02	3.3955E-02
635	3.0586E-02	-1.2821E-02	3.2045E-02
652	2.8352E-02	-1.2152E-02	2.9868E-02
665	2.5711E-02	-1.1108E-02	2.7140E-02
682	2.2561E-02	-9.5911E-03	2.3719E-02
695	1.8928E-02	-7.6304E-03	1.9645E-02
716	1.5071E-02	-5.3766E-03	1.5215E-02
1359	1.3277E-02	-4.2657E-03	1.3116E-02
1063	1.1506E-02	-3.1934E-03	1.1059E-02
1064	8.1853E-03	-1.1144E-03	7.1600E-03
1065	5.5813E-03	4.2997E-04	4.1551E-03
BLOCK 16			
105	3.1300E-02	9.9977E-03	3.1540E-02
121	2.9354E-02	1.0132E-02	3.0001E-02
135	2.7278E-02	1.0043E-02	2.8230E-02
151	2.4844E-02	9.5866E-03	2.5957E-02
165	2.1942E-02	8.6814E-03	2.3045E-02
185	1.8581E-02	7.3553E-03	1.9517E-02
206	1.4984E-02	5.7235E-03	1.5623E-02
1367	1.3181E-02	4.8315E-03	1.3630E-02
1303	1.1396E-02	3.9602E-03	1.1662E-02
1263	8.1361E-03	2.2787E-03	8.0194E-03
1204	5.4178E-03	9.8926E-04	5.0448E-03

4. DEAD WEIGHT + WATER LOAD + TEMP. + UPLIFT			
Node	Def-x (m)	Def-y (m)	Def-radial(m)
BLOCK 0			
407	5.0854E-02	-5.3134E-04	5.0854E-02
412	5.1182E-02	-3.1183E-04	5.1182E-02
422	5.1359E-02	-9.2831E-05	5.1359E-02
427	5.0905E-02	1.1751E-04	5.0905E-02
437	4.9441E-02	3.1152E-04	4.9441E-02
442	4.6926E-02	4.8377E-04	4.6926E-02
452	4.3353E-02	6.3589E-04	4.3353E-02
457	3.8777E-02	7.7365E-04	3.8777E-02
467	3.3365E-02	8.8971E-04	3.3365E-02
472	2.7664E-02	9.8704E-04	2.7664E-02
482	2.1703E-02	1.0637E-03	2.1703E-02
491	1.7338E-02	1.0953E-03	1.7338E-02
508	1.3145E-02	1.1157E-03	1.3145E-02
1362	1.0345E-02	1.1226E-03	1.0345E-02
1080	7.7773E-03	1.1183E-03	7.7773E-03
1081	5.9428E-03	1.0827E-03	5.9428E-03
1082	4.3117E-03	1.0196E-03	4.3117E-03
BLOCK 15			
622	3.7576E-02	-1.4562E-02	3.8643E-02
635	3.5338E-02	-1.4160E-02	3.6626E-02
652	3.2929E-02	-1.3534E-02	3.4336E-02
665	3.0111E-02	-1.2504E-02	3.1476E-02
682	2.6763E-02	-1.0959E-02	2.7881E-02
695	2.2899E-02	-8.9174E-03	2.3575E-02
716	1.8742E-02	-6.5052E-03	1.8811E-02
1359	1.6778E-02	-5.2895E-03	1.6513E-02
1063	1.4828E-02	-4.0888E-03	1.4235E-02
1064	1.1055E-02	-1.6732E-03	9.7731E-03
1065	8.0790E-03	4.1997E-04	6.1382E-03
BLOCK 16			
105	3.3062E-02	9.5767E-03	3.2765E-02
121	3.1095E-02	9.8991E-03	3.1315E-02
135	2.9001E-02	9.9825E-03	2.9624E-02
151	2.6542E-02	9.6785E-03	2.7417E-02
165	2.3591E-02	8.8975E-03	2.4533E-02
185	2.0148E-02	7.6625E-03	2.0988E-02
206	1.6420E-02	6.0712E-03	1.7008E-02
1367	1.4535E-02	5.1757E-03	1.4944E-02
1303	1.2649E-02	4.2868E-03	1.2884E-02
1263	9.1475E-03	2.5363E-03	9.0019E-03
1204	6.1364E-03	1.1299E-03	5.7192E-03

CONCLUSIONS

The results of this static analysis show that the compressive stresses are relatively low and within the allowable limits. The maximum compressive stress is approximately 11.3 MPa which occurs in load case 2.

In the linear elastic case (load case 1), the tensile stresses along the heel, especially in the river section, are higher than the allowable tensile strength of the concrete with a maximum value of 5.8 MPa.

When comparing load case 1, the stress re-distribution process caused by the base contact model was significant. A reduction in the maximum tensile stresses of up to approximately 88% was encountered as well as an increase in the compressive stresses of up to 41% and 8% in horizontal displacement at the crest.

In the base joint included case (load case 2) under the full loading (step 4), the base joint is open to approximately one third of the base thickness mainly in the river section on the upstream side. The maximum opening at the upstream heel is approximately 6 mm.

REFERENCES

1. S.C. Shyu, T.Y. Chang and A.F. Saleeb, "Friction - Contact Analysis Using a Mixed Finite Element Method", Computer and Structures, 32 (1989) 223 - 242.

2. W.H. Chen and J.T. Yeh, "Three - Dimensional Finite Element Analysis of Static and Dynamic Contact Problems with Friction", Computer and Structure, 35 (1990) 541 - 552.

3. H.S. Jing and M.L. Liao, "An Improved Finite Element Scheme for Elastic Contact Problems with Friction", Computer and Structure 35 (1990) 571 - 578.

4. ABAQUS Program Release 5.7 User's Manuals.

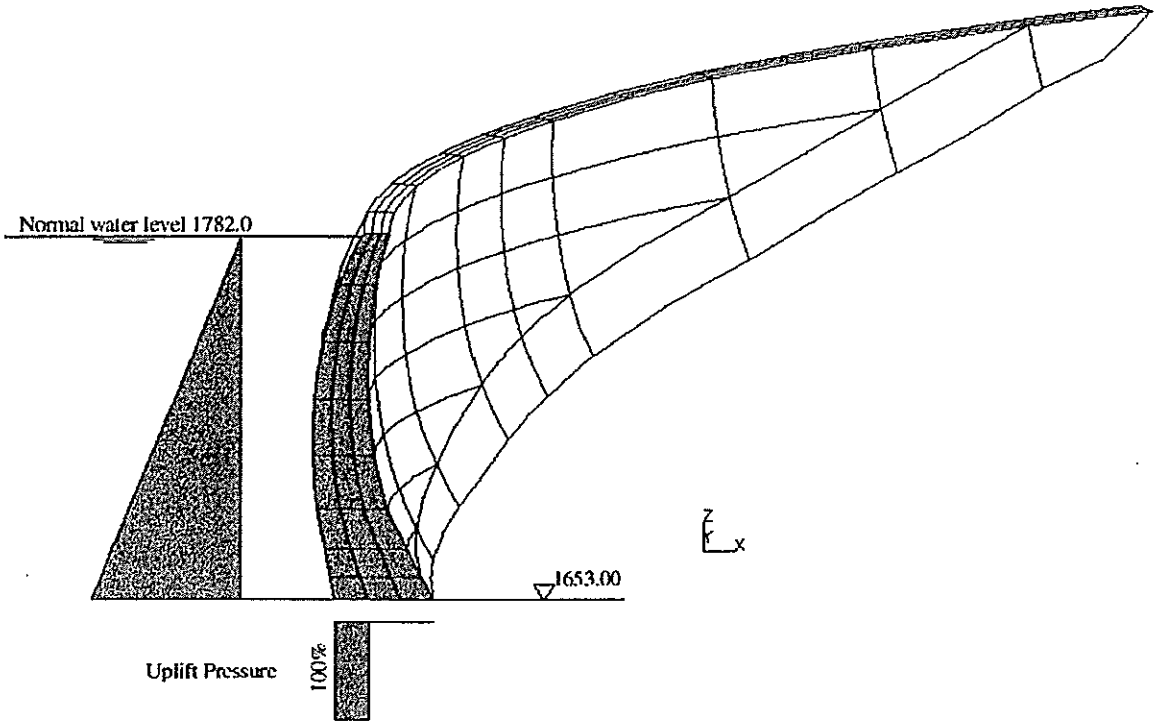

Fig. 1 Finite Element Mesh; Water and Uplift Loading

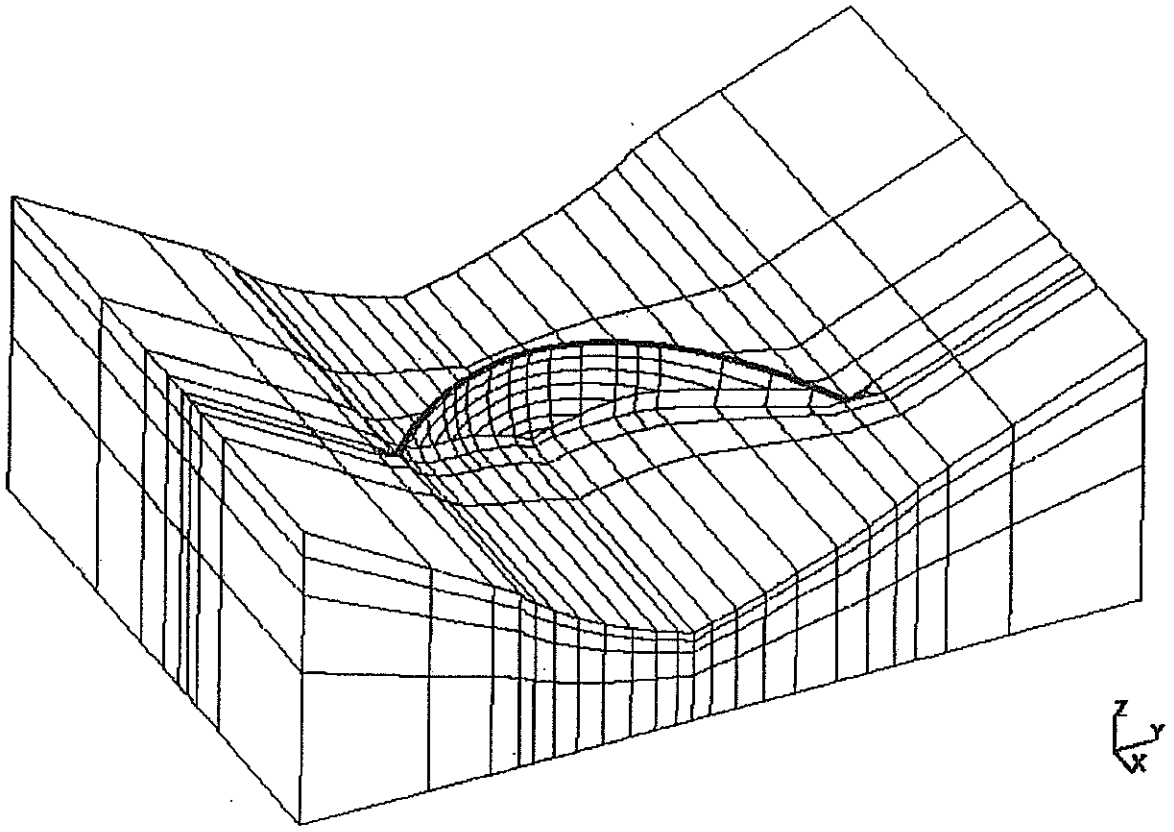

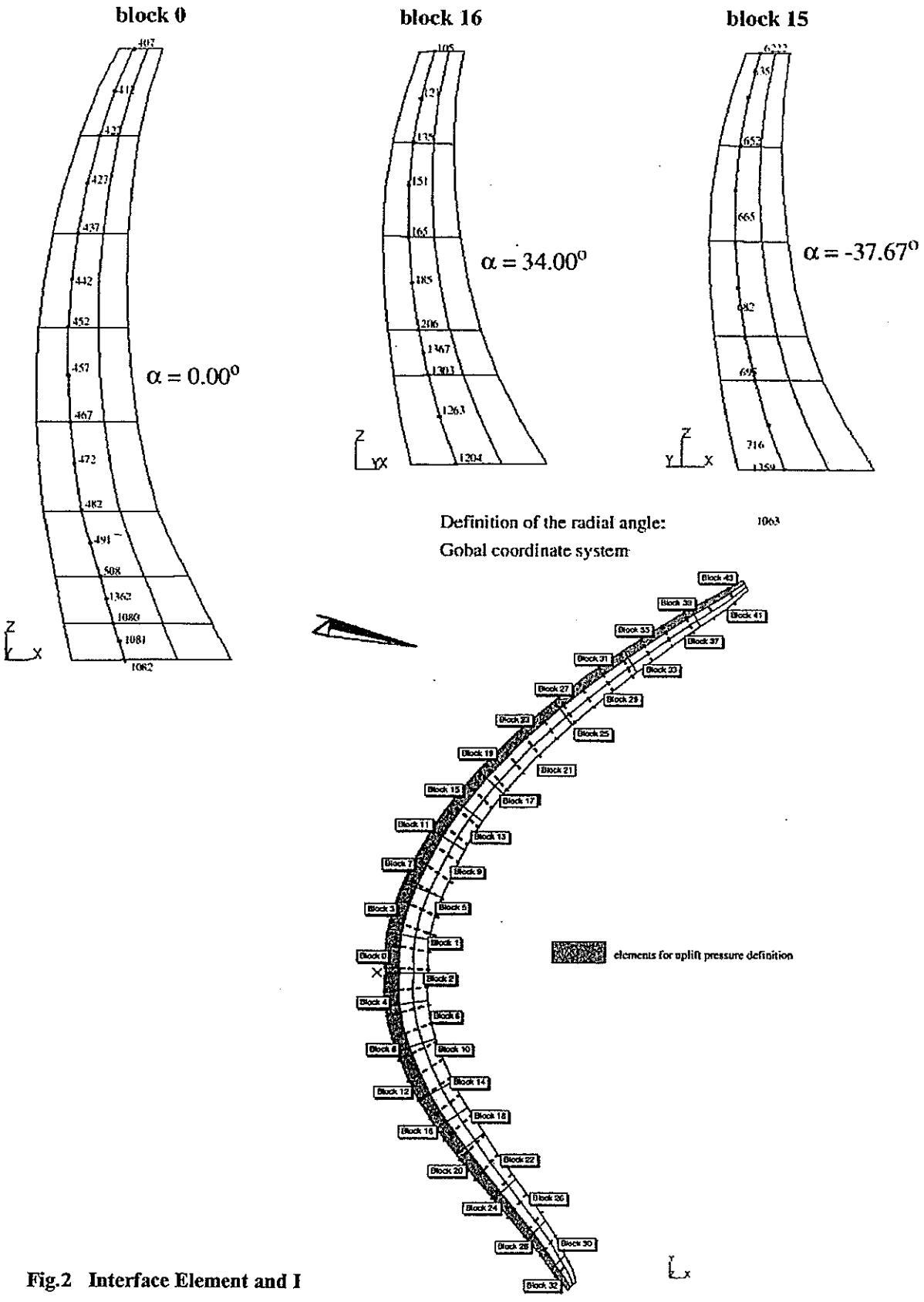

Fig.2 Interface Element and I

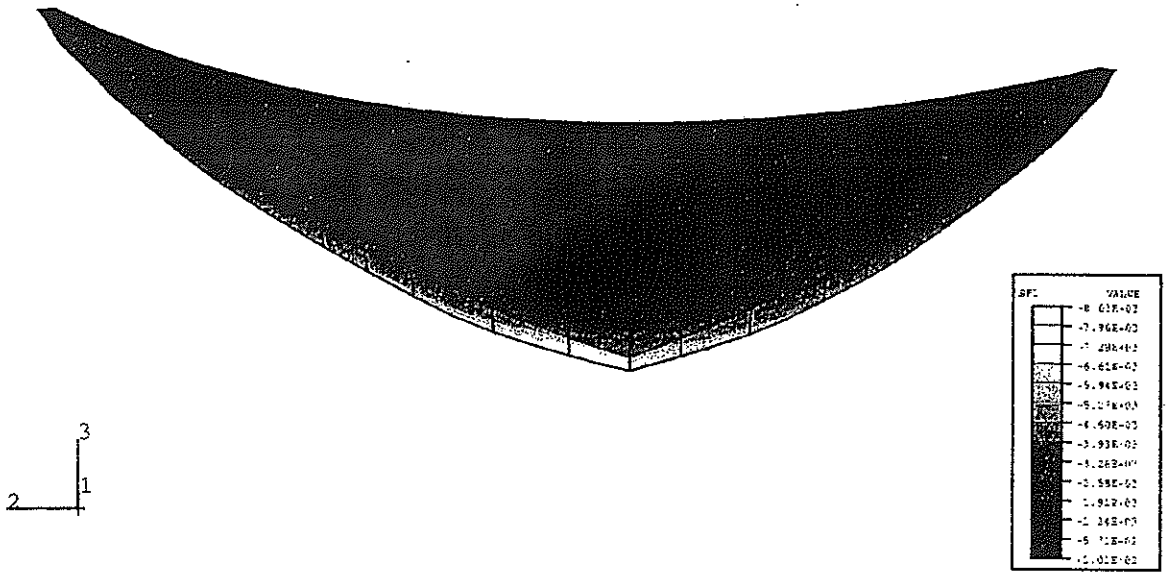

Fig. 3 CASE1: Minimum (SP1) Principal Stresses – Step 1 (Dead Weight) Upstream

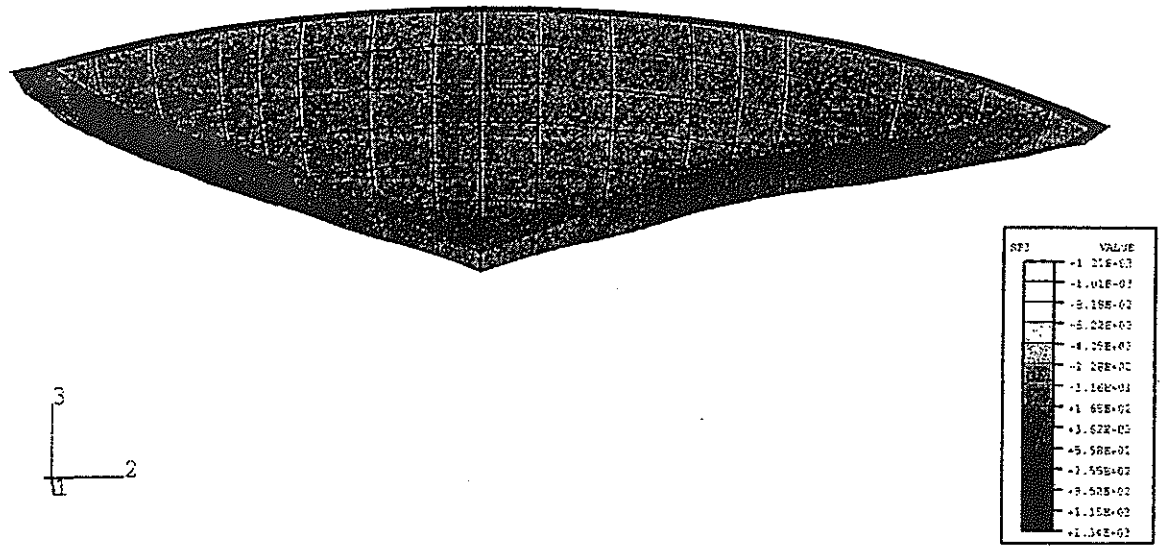

Fig. 4 CASE1: Maximum (SP3) Principal Stresses – Step 1 (Dead Weight) Downstream

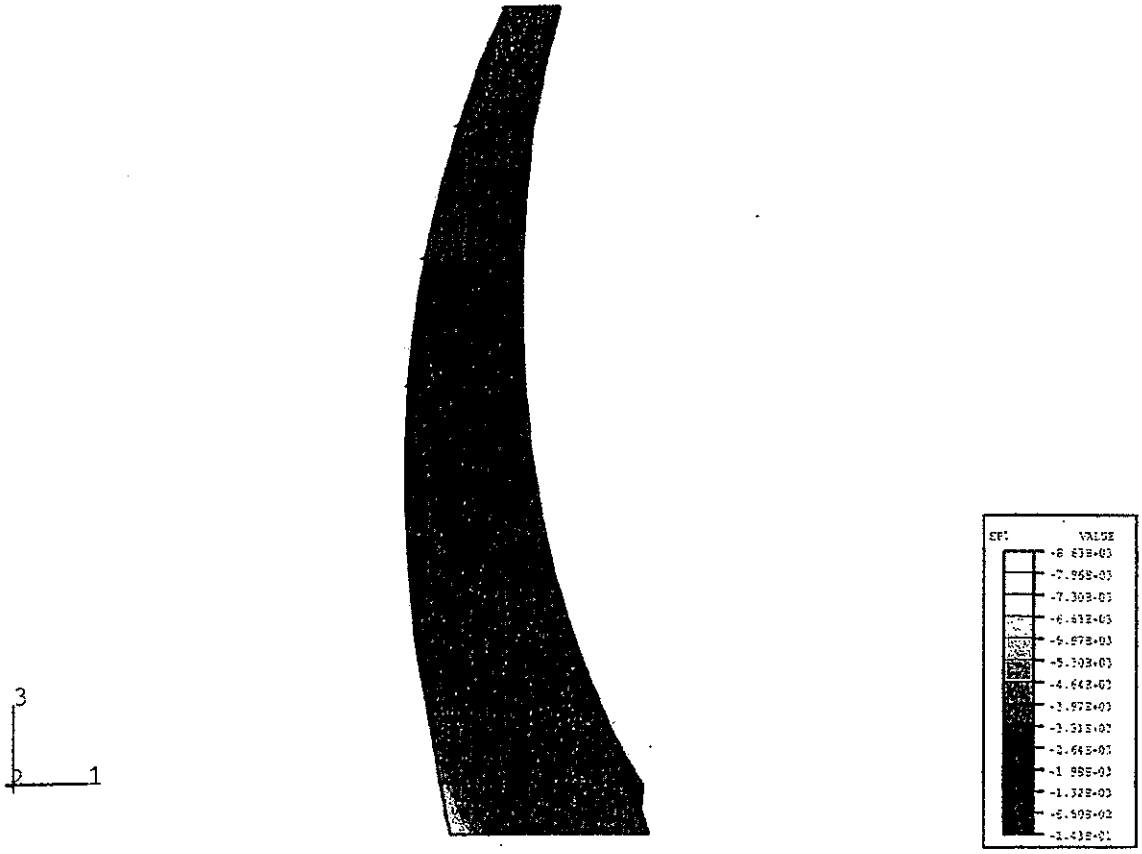

Fig. 5 CASE1: Minimum (SP1) Principal Stresses – Step 1 (Dead Weight) Block 0

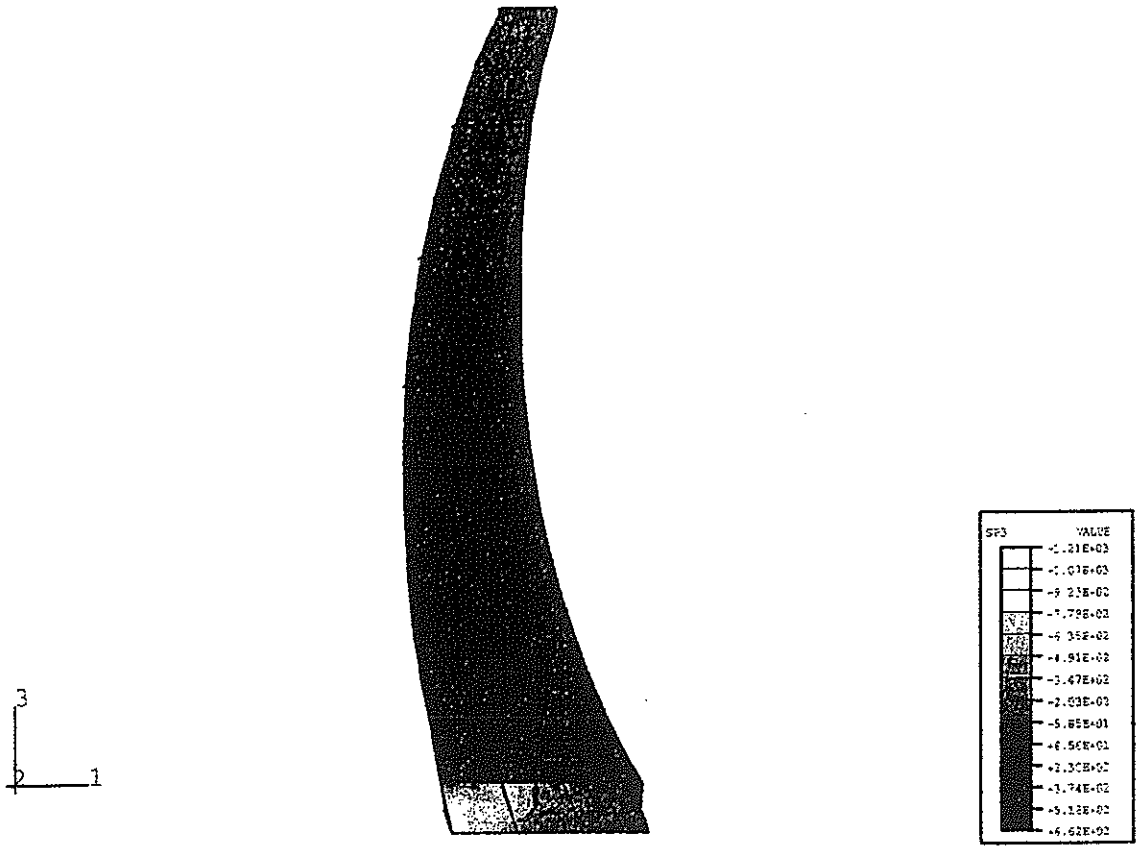

Fig. 6 CASE1: Maximum (SP3) Principal Stresses – Step 1 (Dead Weight) Block 0

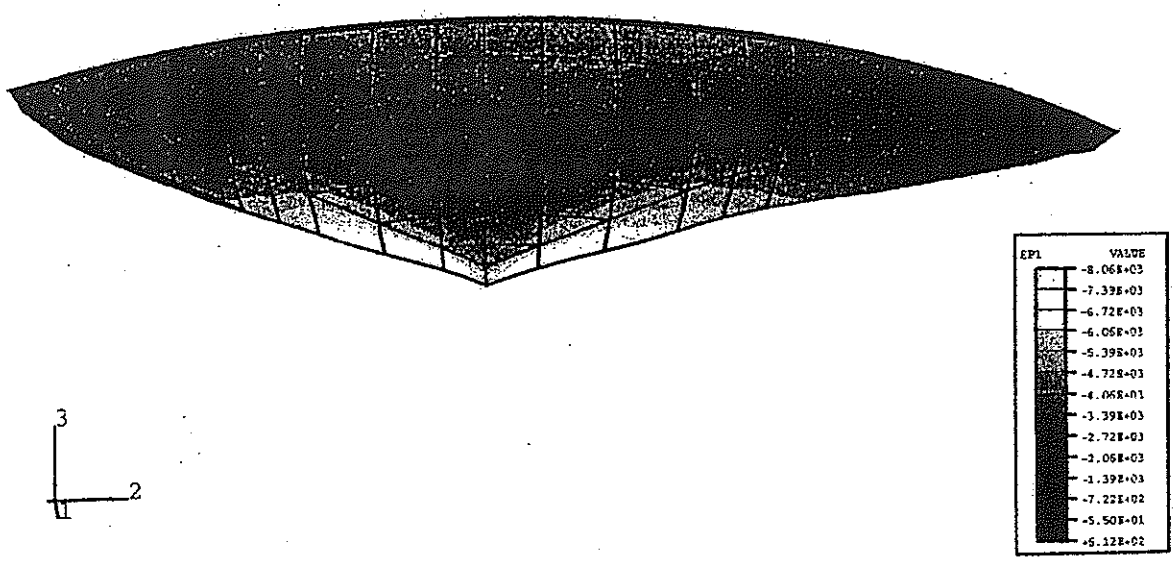

Fig. 7 CASE1: Minimum (SP1) Principal Stresses – Step 4 (Full Loading) Downstream

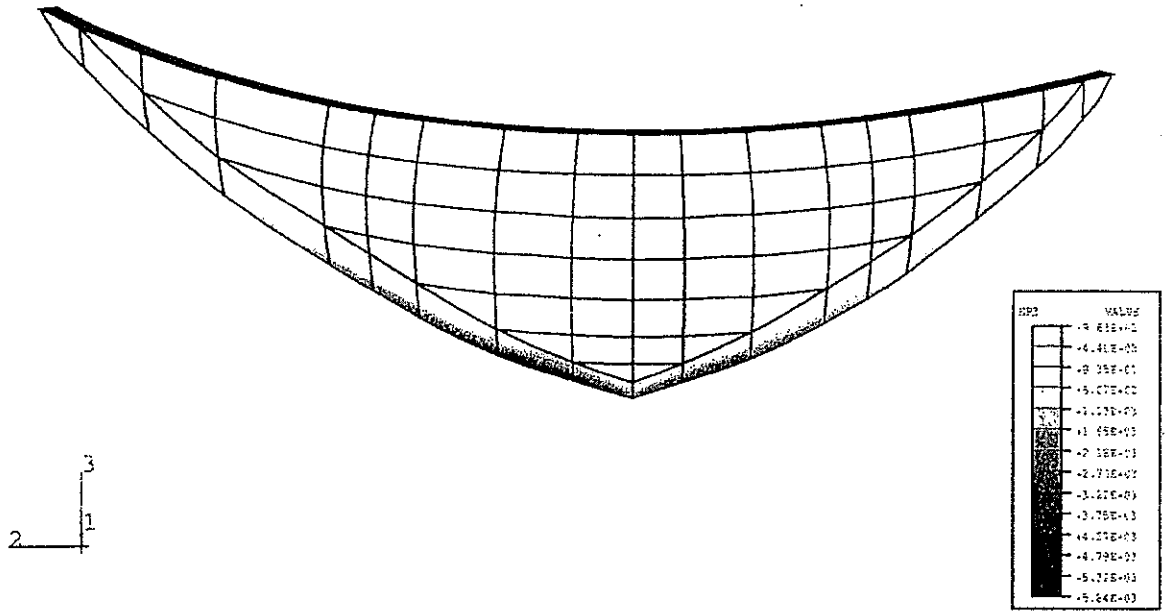

Fig. 8 CASE1: Maximum (SP3) Principal Stresses – Step 4 (Full Loading) Upstream

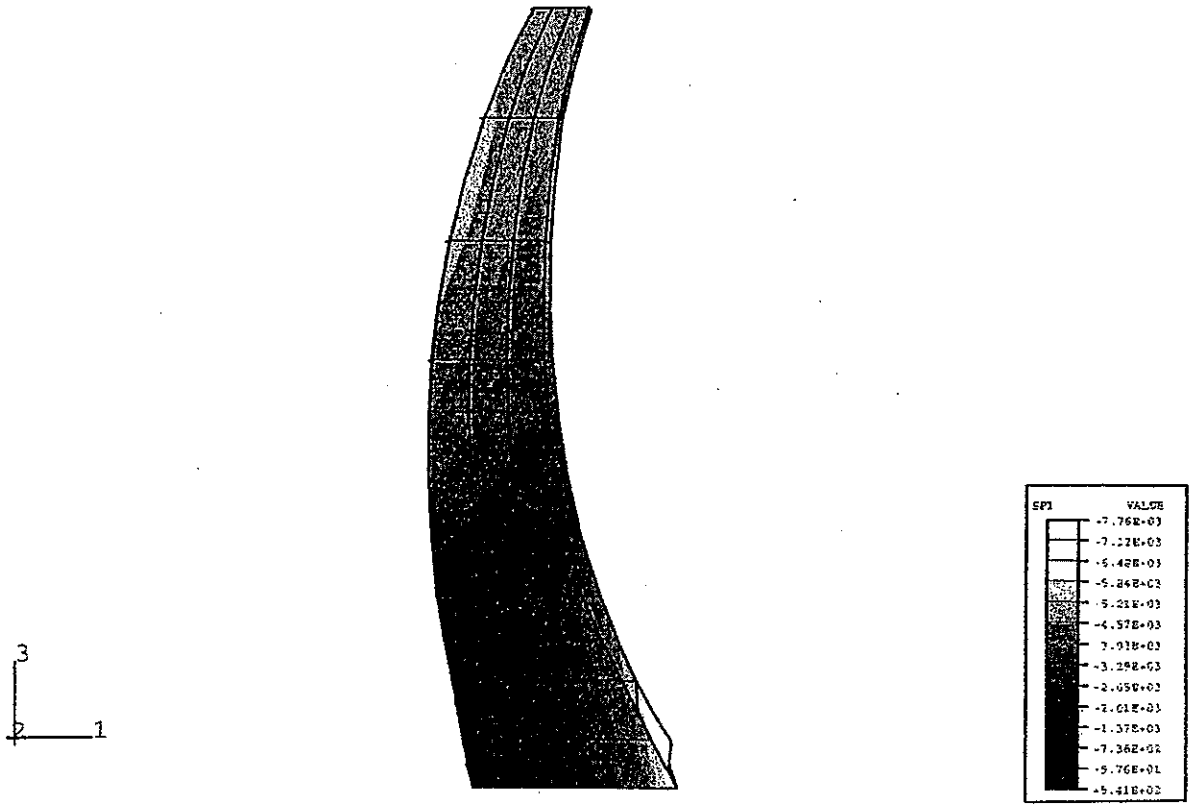

Fig. 9 CASE1: Minimum (SP1) Principal Stresses – Step 4 (Full Loading) Block 0

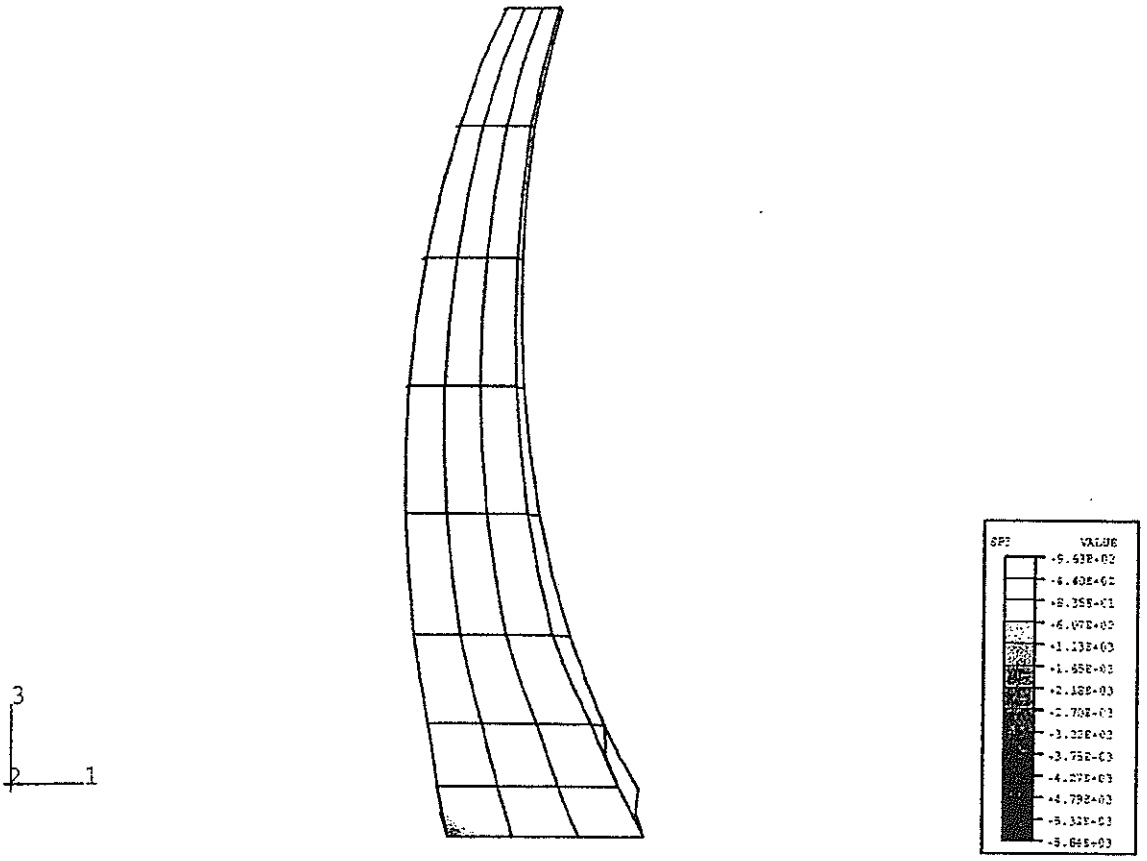

Fig. 10 CASE1: Maximum (SP3) Principal Stresses – Step 4 (Full Loading) Block 0

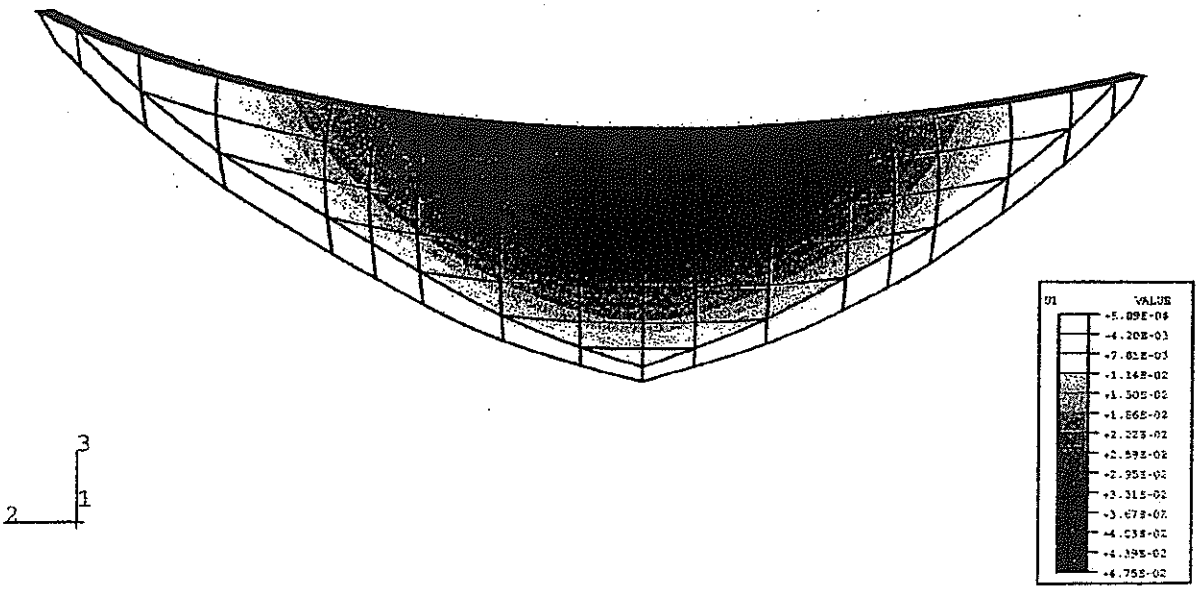

Fig. 11 CASE1: Horizontal Displacement (U1) – Step 4 (Full Loading)

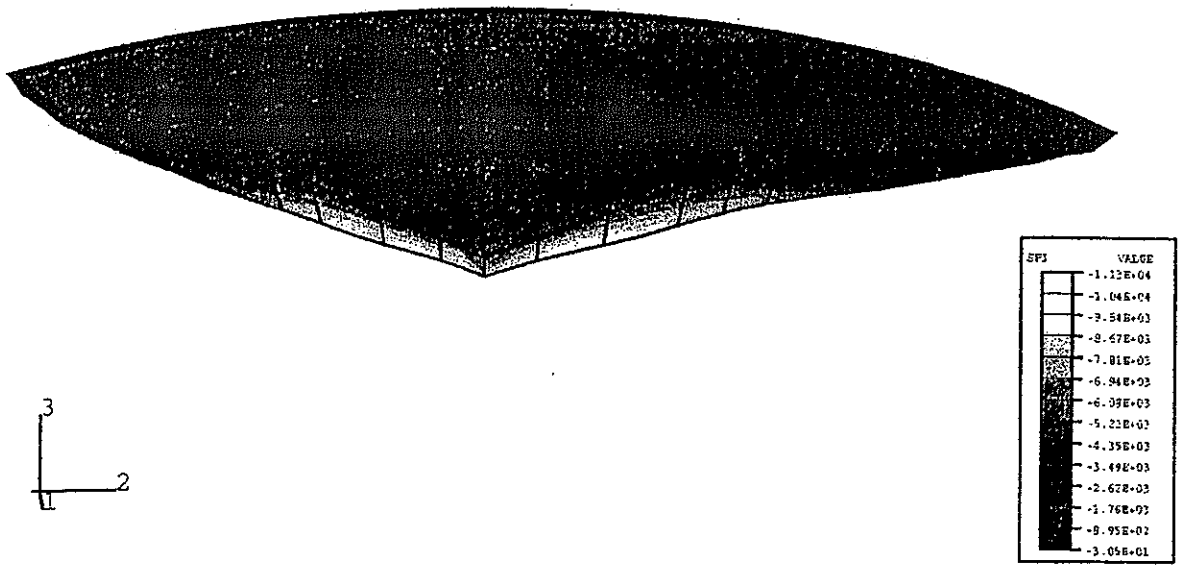

Fig. 12 CASE2: Minimum (SP1) Principal Stresses – Step 4 (Full Loading) Downstream

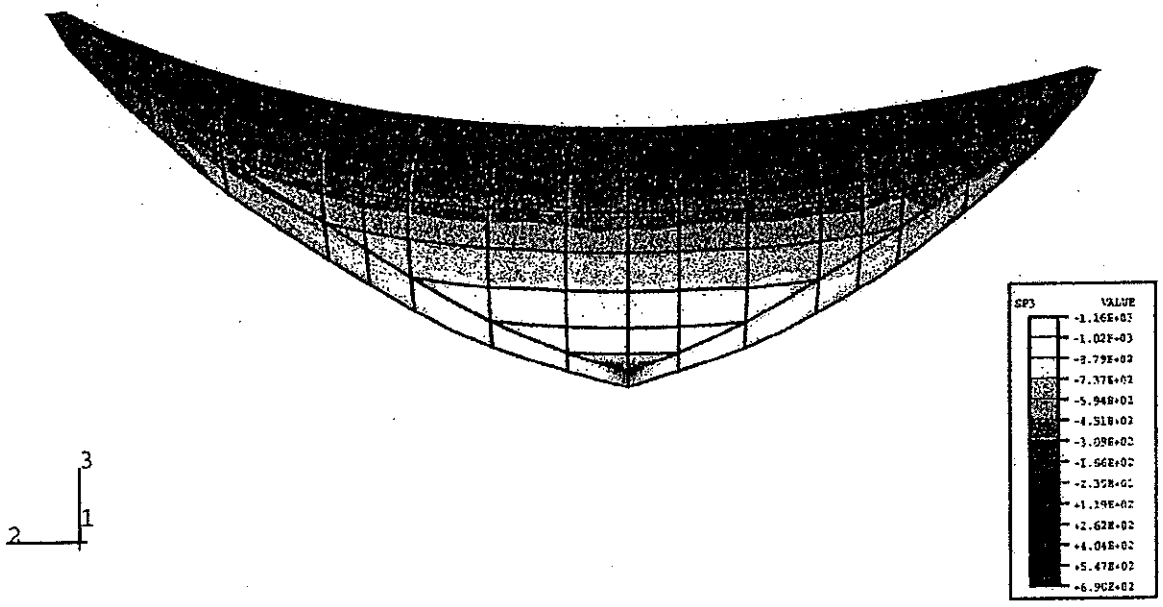

Fig. 13 CASE2: Maximum (SP3) Principal Stresses – Step 4 (Full Loading) Upstream

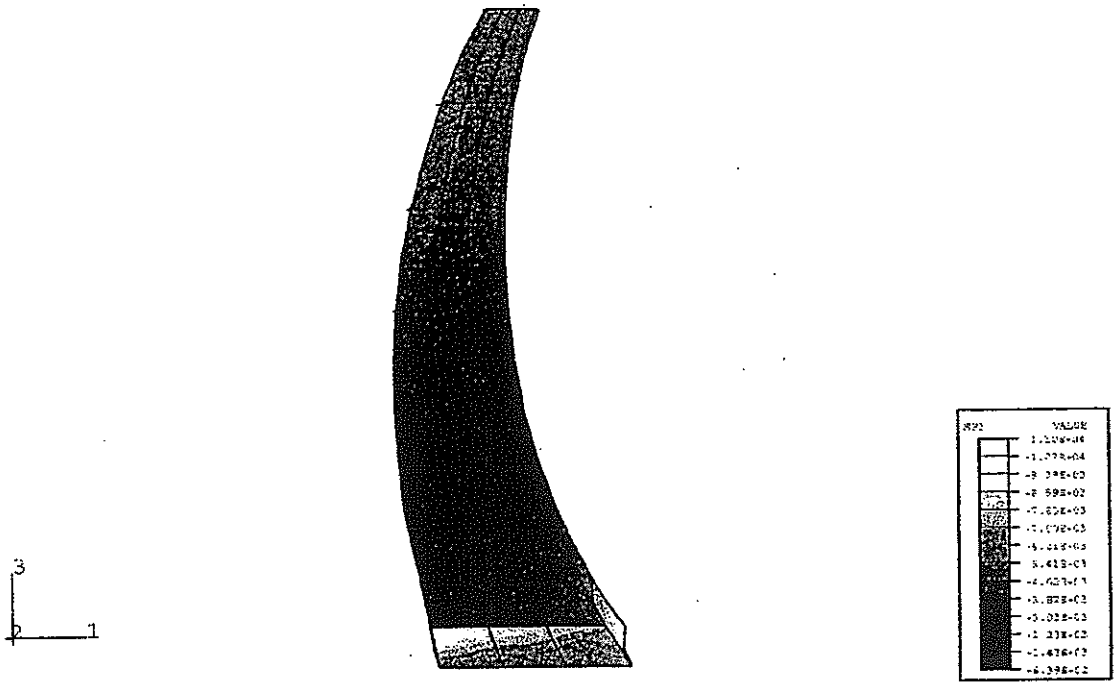

Fig. 14 CASE2: Minimum (SP1) Principal Stresses – Step 4 (Full Loading) Block 0

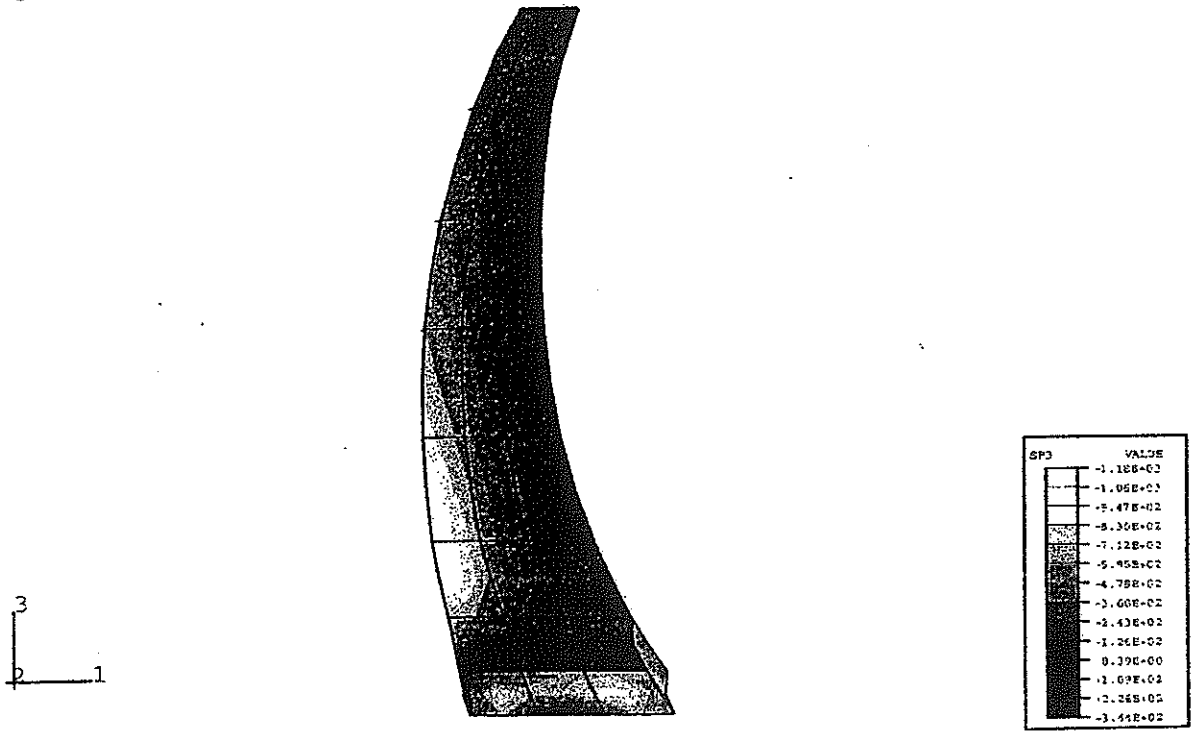

Fig. 15 CASE2: Maximum (SP3) Principal Stresses – Step 4 (Full Loading) Block 0

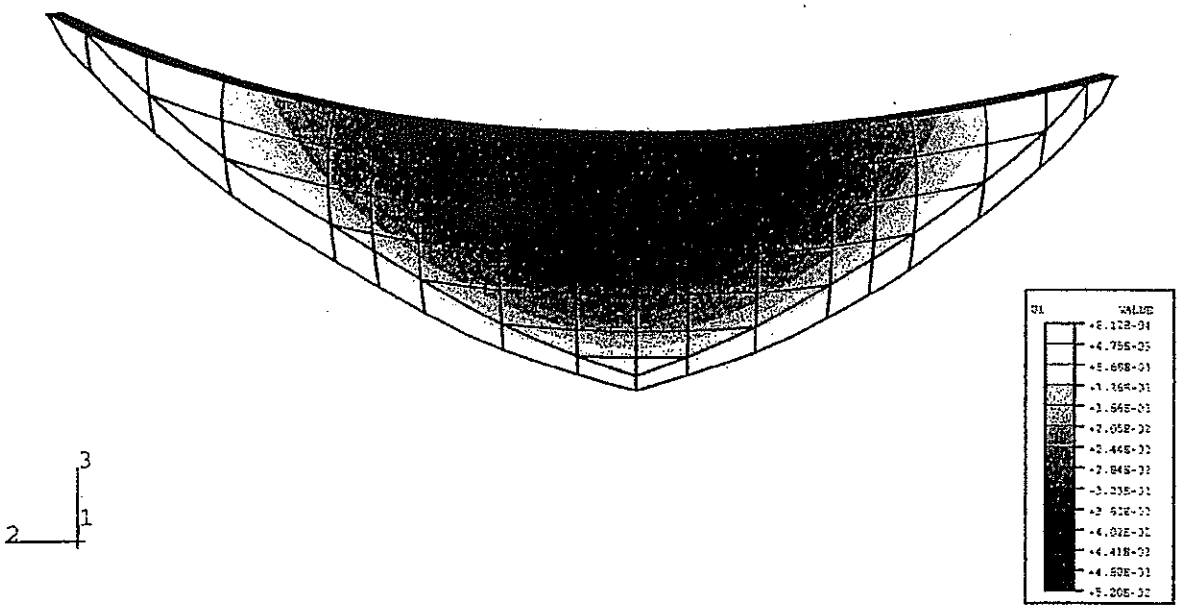

Fig. 16 CASE2: Horizontal Displacement (U1) – Step 4 (Full Loading)

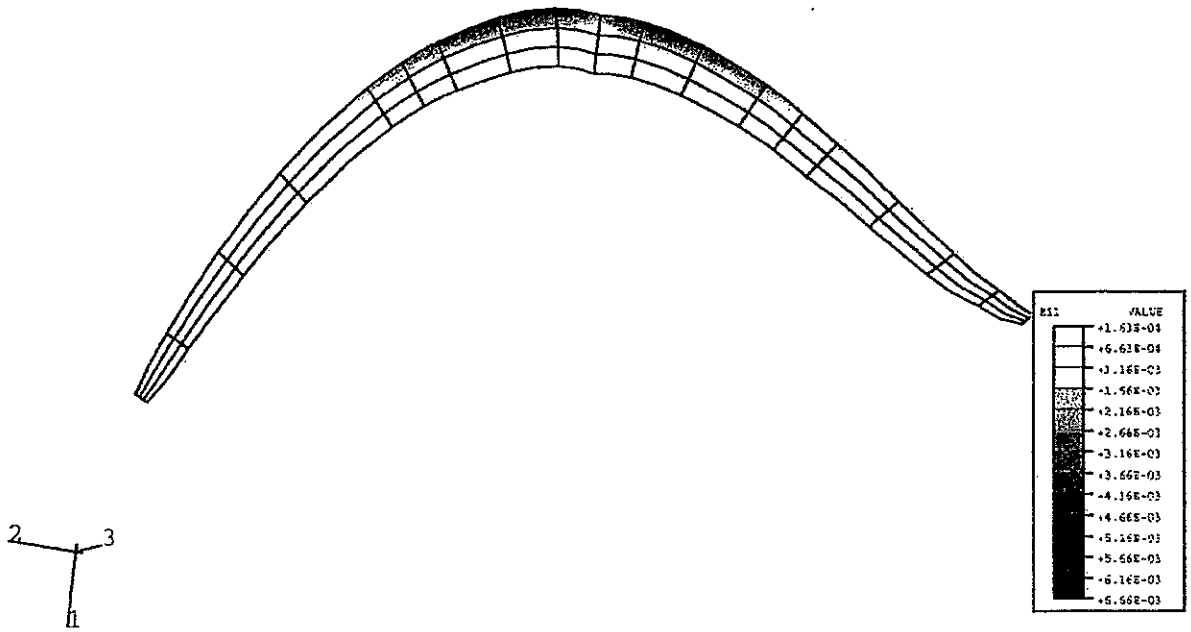

Fig. 17 CASE2: Contact Openings Contour – Step 4 (Full Loading)

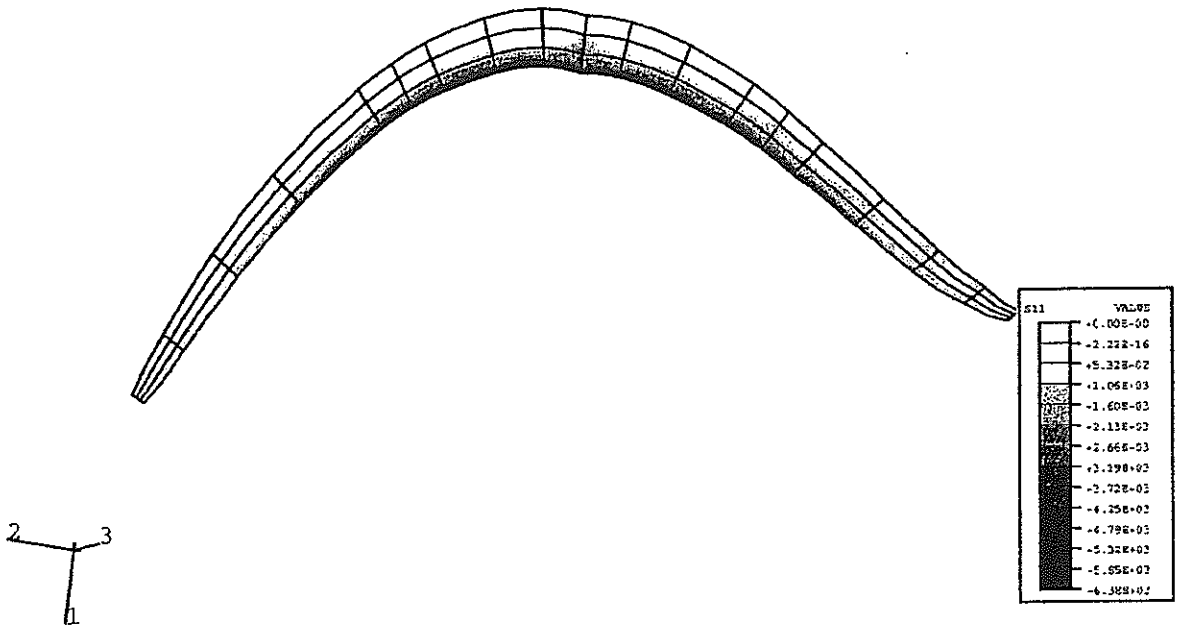

Fig. 18 CASE2: Contact Pressure Contour – Step 4 (Full Loading)

Fig. 19 CASE 1 AND 2: Horizontal Displacement at Crest Level

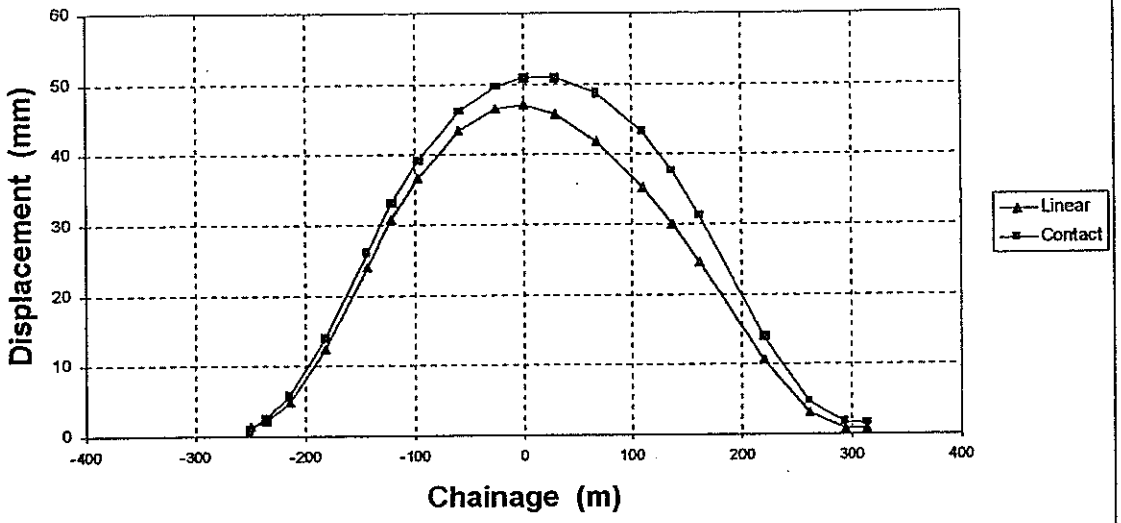

Fig. 20 CASE2: Minimum Principal Stresses Along Crown Cantilever

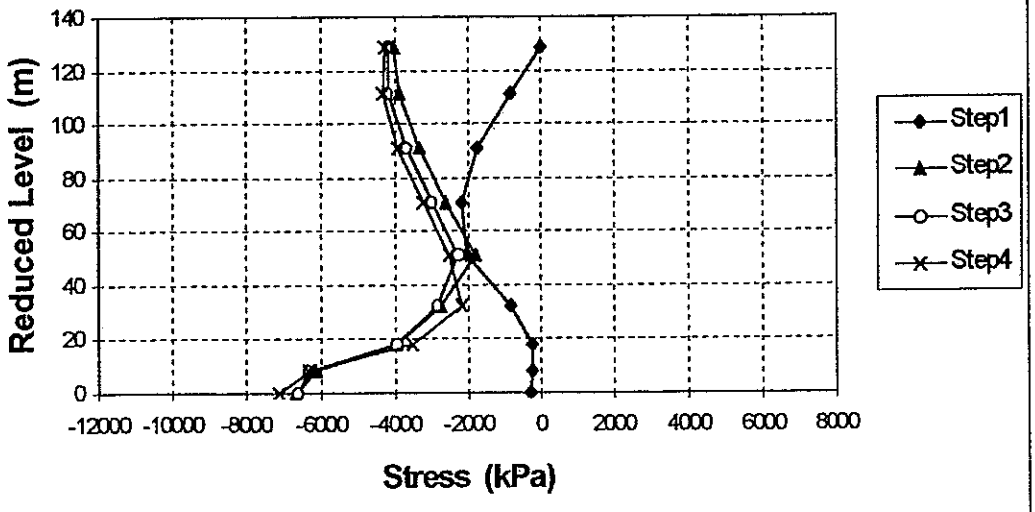

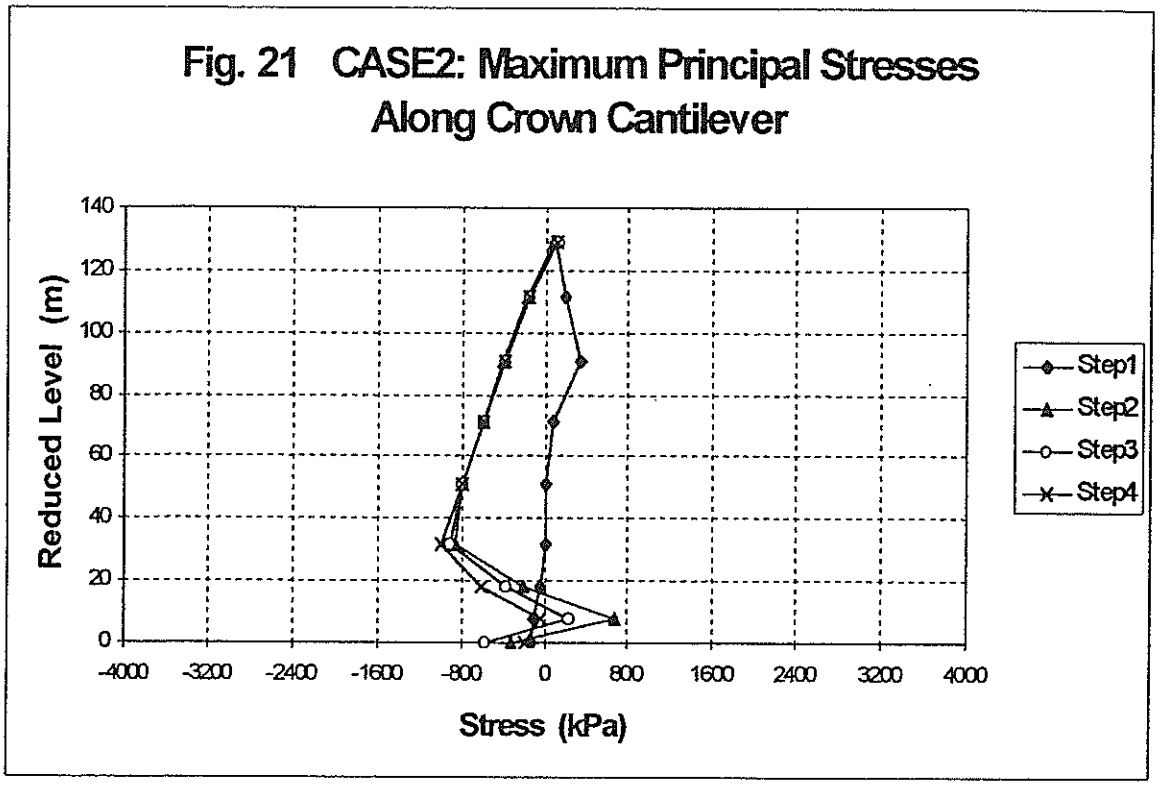
Fig. 21 CASE2: Maximum Principal Stresses Along Crown Cantilever
Reduced Level (m)
140
120
100
80
60
40
20
0
-4000
-3200
-2400
-1600
-800
0
800
1600
2400
3200
4000
Stress (kPa)
Step1
Step2
Step3
Step4

DESIGN AND ANALYSIS OF ARCH DAMS - EFFECTS OF BLOCK JOINTS NON-LINEAR BEHAVIOUR AND PROPAGATION OF THE UPLIFT PRESSURE.

Patrick DIVOUX *

INTRODUCTION

The behaviour of concrete dams is greatly influenced by the non-linear behaviour of discontinuities, i.e. block joints, concrete lift joints and dam-foundation contact.
Concrete dam stability or design analysis are performed using interface elements to model the behaviour of the dam-foundation contact and the block joints. Considering the proposed method, effects of dam construction scenario, thermal shrinkage, joint grouting scenario, as well as effects of water level and concrete temperature variations can be estimated. Openings, stresses and uplift pressures propagation at the dam-foundation contact are directly computed.
The rock foundation matrix and the dam's concrete are materials that are first assumed to be elastic. Structure's non-linearities are mainly concentrated at the block joints and the concrete-rock contact, and follow a non linear hydromechanical constitutive law.
In the case of the Schlegeis arch dam, four computations have been performed with the software GEFDYN in order to estimate the effects of the non-linear behaviour of the dam-foundation contact and the effects of three different numerical methods used to model the construction of the dam.

*Electricité de France
Centre National d'Equipement Hydraulique
Savoie Technolac
73373 Le Bourget du Lac cédex
France

MATERIAL BEHAVIOUR

Foundation behaviour

The foundation is modelled with volume elements separated into two parts :

- the layer of elements in contact with the dam-foundation interface is called material F1
- the other elements are called material F2.

Behaviour of material F1 :

It follows an isotropic linear elastic law :

- E = 30 GPa Young modulus
- ν = 0.17 Poisson's ratio

Behaviour of material F2 :

It follows an orthotropic elastic law (figure 1).
The direction of the plane of shistosity is constant and given by the following angles :

- a=150.1° angle of strike with respect to y axis
- b=75° angle of dip

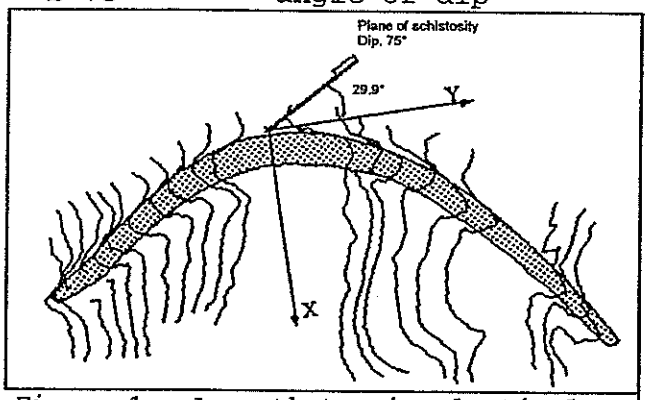

Figure 1 - An orthotropic elastic law to model a plane of schistosity

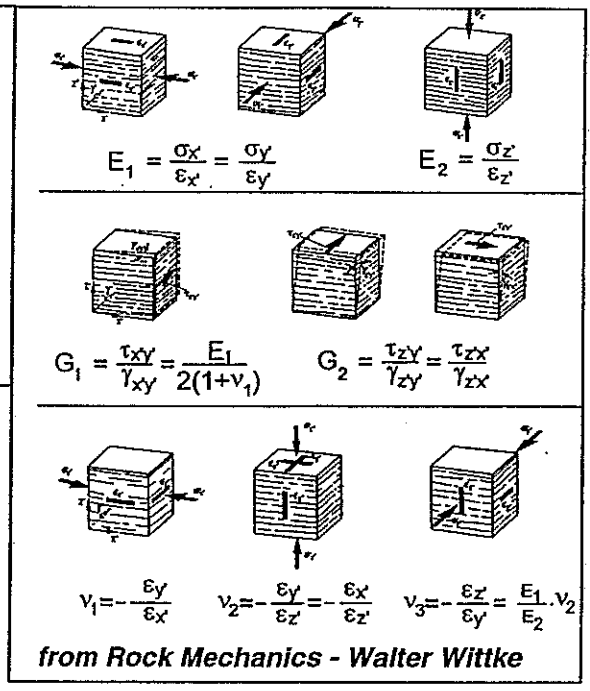

The five parameters of this law are :

- E_1=30 GPa Young modulus for the direction parallel to the plane of schistosity
- ν_1=0.17 Poisson's ratio for the direction parallel to the plane of schistosity
- $G_1=E_1/2(1+\nu_1)$ Shearing modulus for shear loading in the plane of schistosity
- E_2=10 GPa Young modulus for the direction perpendicular to the plane of schistosity
- ν_2=0.04 Poisson's ratio in the direction perpendicular to the plane of schistosity
- $G_2 = E2/2(1+\nu_2) = 0.4808$ Pa Shearing modulus for shear loading in planes perpendicular to the plan of schistosity

Dam-foundation contact behaviour

The dam foundation contact is modelled with quadratic interface elements.

These elements follow a five parameters Mohr-Coulomb elastoplatic law (figure 2). The parameters are :

- k_n = 10 GPa/m Normal stiffness
- k_s = 10 GPa/m Shear stiffness
- c = 0 Cohesion
- φ = 45° Friction angle
- ψ = 0° Dilatancy angle

The dilatancy and the cohesion are nil in order to follow the prescribed behaviour.

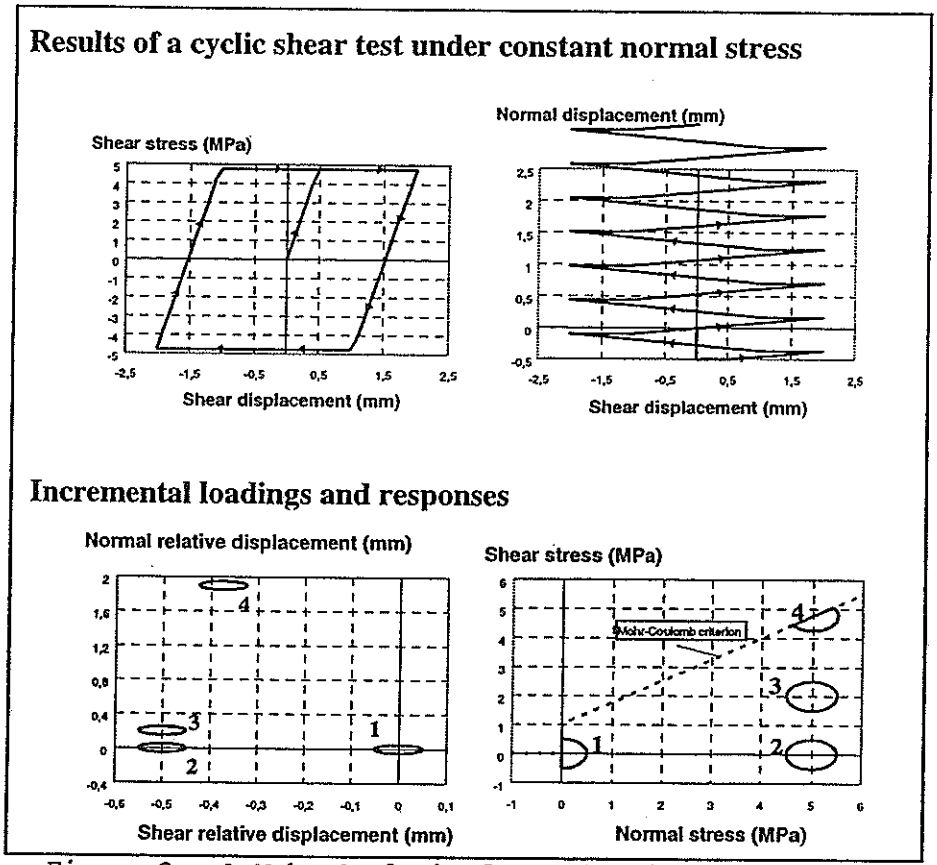

Figure 2 - A Mohr-Coulomb elastoplastic law to model the dam foundation contact behaviour

Dam : Behaviour 1

The dam is modelled with volume elements separated into two parts :

- the layer of element in contact with the dam-foundation is called material D1
- the other elements are called material D2.

The dam density is 2.4.

Behaviour of material D1 :

The concrete D1 follows an isotropic linear elastic law :

- E = 25 GPa Young modulus
- ν = 0.17 Poisson's ratio

Behaviour of material D2 :

During construction (dead weight), the concrete D2 follows an orthotropic elastic law.

At a point located inside the dam volume, the radial direction is given by the subroutine ORIENT.f. The local axes (1,2,3) are defined as following :

- axe 1 : vertical equal to z
- axe 2 : horizontal and in the radial direction
- axe 3 : horizontal and in the tangential direction

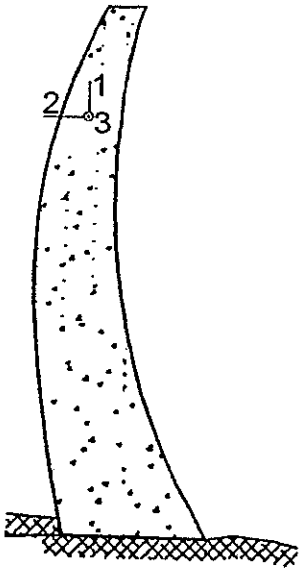

The plane (1,2) is vertical and oriented in the dam radial direction. The behaviour law is a function of the position of the integration point considered.

The five parameters of this law are :

- E_1=25 GPa Young modulus for the direction parallel to plane (1,2)
- ν_1=0.17 Poisson's ratio for the direction parallel to plane (1,2)
- G_1=E1/2(1+ν_1) Shearing modulus for shear loading in plane (1,2)
- E_2=10^5 Pa Young modulus for the direction perpendicular to plane (1,2)
- ν_2=0.0 Poisson's ratio in the direction perpendicular to plane (1,2)
- G_2=10^5 Pa Shearing modulus for shear loading in planes perpendicular to plan (1,2)

After construction (hydrostatic load, thermal load, uplift pressure), the concrete D2 follows an isotropic elastic law :

- E = 25 GPa Young modulus
- ν = 0.17 Poisson's ratio

Dam : Behaviour 2

During construction (dead weight), the dam concrete follows a no-tension law.
The radial direction of a point located into the dam is given by the subroutine ORIENT.f. The local axes (1,2,3) are defined as before :

- axe 1 : vertical equal to z
- axe 2 : horizontal and in the radial direction
- axe 3 : horizontal and in the tangential direction

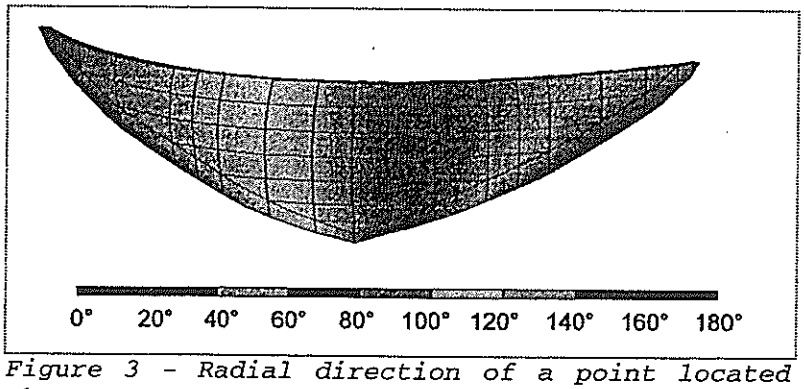

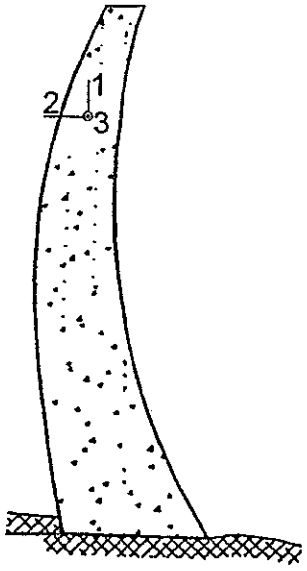

Figure 3 - Radial direction of a point located on the upstream face of the dam

At every integration point, a linear elastic stress state (S_{xx}, S_{yy}, S_{zz}, S_{xy}, S_{yz}, S_{zx}) is computed. A rotation of the stress tensor from (x,y,z) axes to (1,2,3) axes is performed to obtain the following stress tensor (S_{11}, S_{22}, S_{33}, S_{12}, S_{23}, S_{31}).
Then, the stress tensor is modified in order to apply the no-tension law :

- if $S_{33}>0$ (tension) then $S_{33} = 0$
- $S_{23} = S_{31} = 0$

From the modified stress tensor, the inverse rotation gives the modified (S_{xx}, S_{yy}, S_{zz}, S_{xy}, S_{yz}, S_{zx}) stress tensor.

The two parameters of this law are :

- E = 25 GPa Young modulus
- ν = 0.17 Poisson's ratio

After construction (hydrostatic load, thermal load, uplift pressure), the dam follows an isotropic elastic law :

- E = 25 GPa Young modulus
- ν = 0.17 Poisson's ratio

Dam : Behaviour 3

The dam is modelled with volume elements (material DV) and vertical interface elements (figure 4, material DJ) which separate every column of volume elements.

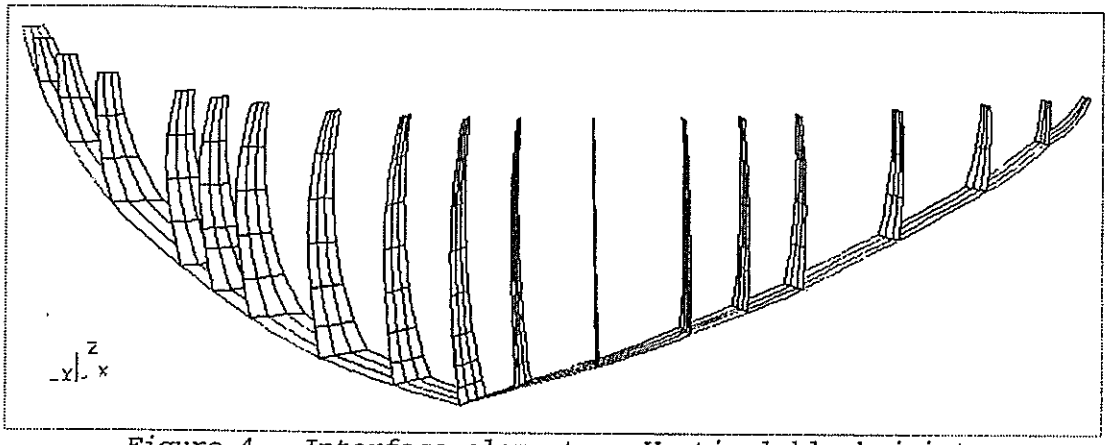

Figure 4 - Interface elements - Vertical block joints and dam-foundation contact

Behaviour of the dam concrete (volume elements DV)
The concrete DV follows an isotropic elastic law for every types of loading.

- E = 25 GPa Young modulus :
- ν = 0.17 Poisson's ratio :

Behaviour of the vertical block joints (interface elements DJ)
Block joints are modelled with a no-tension Mohr-Coulomb elastoplastic law. The relative normal displacement of the joint at closure (δ_{nf}) has to be taken into account as a state variable in order to model joint grouting.

During construction, the following parameters have been considered :

- k_n = 10 GPa Compressive joint stiffness (= 0 in tension)
- k_s = 0 GPa Shear stiffness
- c and φ has no influence as k_s = 0
- ψ = 0° Dilatancy angle
- δ_{nf} = 0 at every integration points

During joint grouting :

- k_n = 10 GPa Compressive joint stiffness (= 0 in tension)
- k_s = 0 GPa Shear stiffness
- c and φ has no influence as k_s = 0
- ψ = 0° Dilatancy angle
- δ_{nf} = δ_n for opened integration points, = 0 if closed

During the next loading (hydrostatic load, thermal load, uplift pressure), the following set of parameters was considered :

- k_n = 10 GPa Compressive joint stiffness (= 0 in tension)
- k_s = 10 GPa Shear stiffness
- c =0 Cohesion
- φ = 45° Friction angle
- ψ = 0° Dilatancy angle
- δ_{nf} is unchanged

NUMERICAL HYPOTHESES

Numerical integration

Results (especially stresses) obtained from finite element computations with interfaces often show some numerical oscillations caused by the interpolation functions in the element. To solve this numerical problem, it is possible to reduce the stress gradient by refining the mesh but this operation is difficult in 3D.
Another possible method is to use 18 node interface elements with a Newton-Cotes numerical integration order 3. Integration points are located on the element nodes and no interpolation is needed in the element.
At the present time, 18 node interface elements as well as 27 node volume hexahedron are not implemented in GEFDYN software. Computations were done with 16 node interface elements and a Gauss numerical integration order 3.

Evaluation method and convergence criteria

The modified Newton-Raphson method was used to perform all the calculations whose results are presented in this paper. This algorithm seems to be very robust, although not very effective. As few calculation stages are necessary to perform quasi-static calculations, this algorithm is sufficient to model the non-linear behaviour of joints.

Convergence is reached if the two criteria for strength and displacement are complied with.

Relative residual strength : $\dfrac{\|\underline{\mathbf{F}}_i - \underline{\mathbf{F}}_0\|}{\|\underline{\mathbf{F}}_0\|} < 1\%$

Relative residual displacement : $\dfrac{\|\underline{\mathbf{U}}_i - \underline{\mathbf{U}}_{i-1}\|}{\|\underline{\mathbf{U}}_1 - \underline{\mathbf{U}}_0\|} < 0{,}1\%$

DESCRIPTION OF THE MODELS

Table 5 presents the different computations performed considering different behaviours for the dam and the dam-foundation contact.

	F. E. model	*Dam behaviour*	*Contact behaviour*
Small model 1	Small	**Behaviour 1 : Orthotropic law**	**Elastic**
Small model 2	Small	**Behaviour 1 : Orthotropic law**	Elasto-plastic
Big model 2	**Big**	**Behaviour 1 : Orthotropic law**	Elasto-plastic
Small model 3	Small	**Behaviour 2 : No-tension law**	Elasto-plastic
Small model 4	Small	**Behaviour 3 : Block joints elements**	Elasto-plastic

Table 5 - Computation performed, hypotheses

A comparative analysis of the results is performed to understand the effects of the hypotheses chosen on the dam behaviour.
The following points are studied :

- the mesh refinement,
- the non-linear behaviour of the dam-foundation contact,
- the method used to model the dam construction.

REMARKS AND ANALYSIS

Remarks on model 1

All the elements of the model (dam concrete, foundation rock and dam-foundation contact) have a linear behaviour. Each computation step needs only one equilibrium iteration.

Dam construction :
The stress state obtained at the end of the construction steps shows no tangential stresses in the dam in order to reproduce the construction scenario of dam (step by step). It seems that tension stresses in the dam-foundation contact are very low and that the stress state computed is in good agreement with the real one.

However, as the Young modulus in the tangential direction is very low compared to the usual concrete modulus, we observed important and unrealistic tangential deformations of the dam. Thus, the strain state of the dam after the construction step is difficult to analyse.

Hydrostatic and thermal loading :
At the end of the impounding of the reservoir, high tension stresses are computed in the upstream part of the dam-foundation contact. These results have no physical reality.

Remarks on model 2

The only difference between models 1 and 2 is the behaviour of the dam-foundation contact. The interface law is elastic in model 1 and elastoplastic with a Mohr-Coulomb criteria in model 2.
Considering the model 2 hypotheses, computations have been performed on the small and on the big model. Results are not significantly different but the most refined mesh gives most accurate values along the dam-foundation contact.

As for model 1, there are no tangential stresses in the dam at the end of the construction step (figure 6). At the end of impounding there is no tension stresses at the toe (figure 7) because the dam-foundation contact is partly opened.

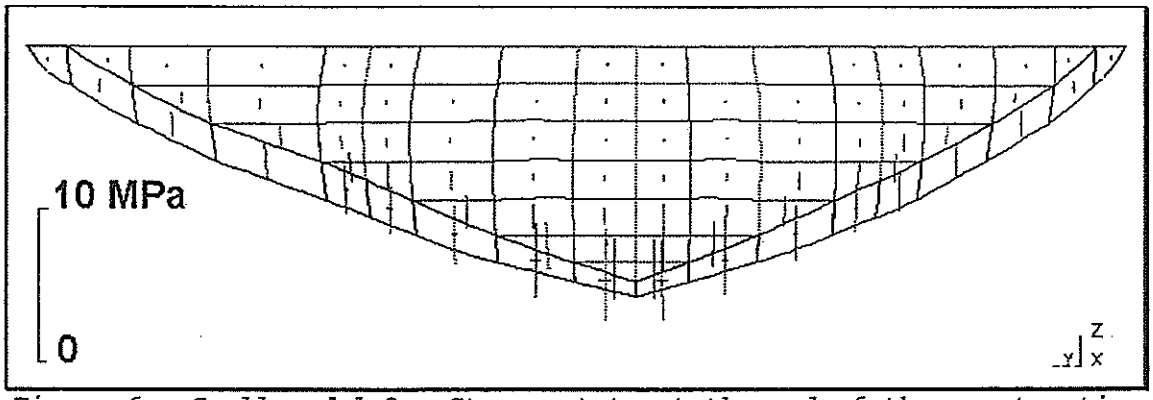

Figure 6 - Small model 2 - Stress state at the end of the construction step

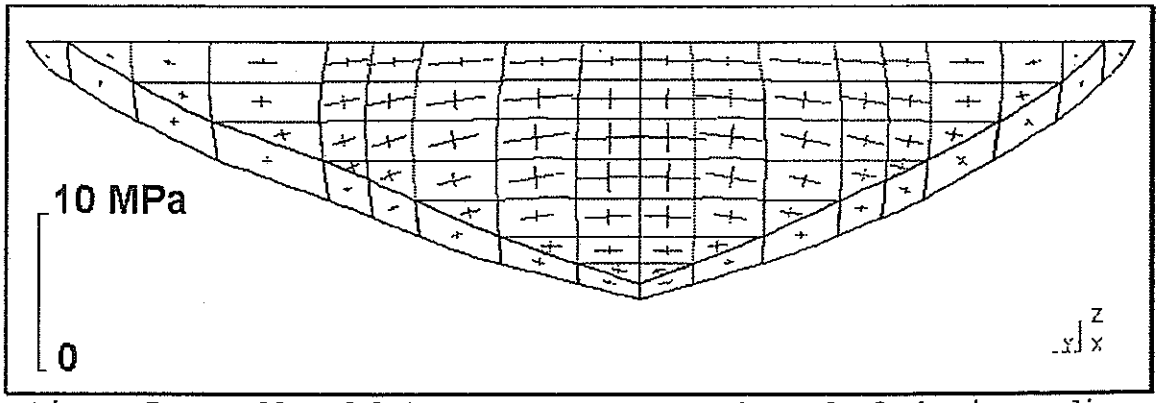

Figure 7 - Small model 2 - Stress state at the end of the impounding step (dead weight + hydrostatic load)

Figures 8 and 9 show the significant effect of the uplift pressure on the opening at the dam-foundation contact. The thermal load leads to an increase of the temperature in the dam. Effects are the dilatation of the concrete and the reduction of the opening of the dam-foundation contact.

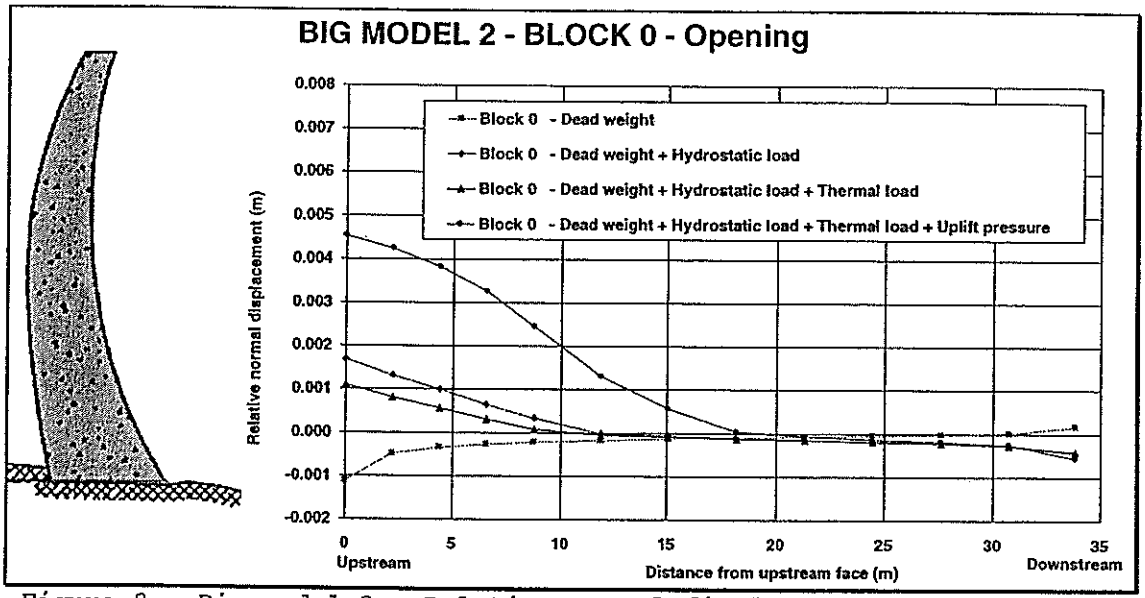

Figure 8 - Big model 2 - Relative normal displacement along the dam-foundation contact of the central cantilever

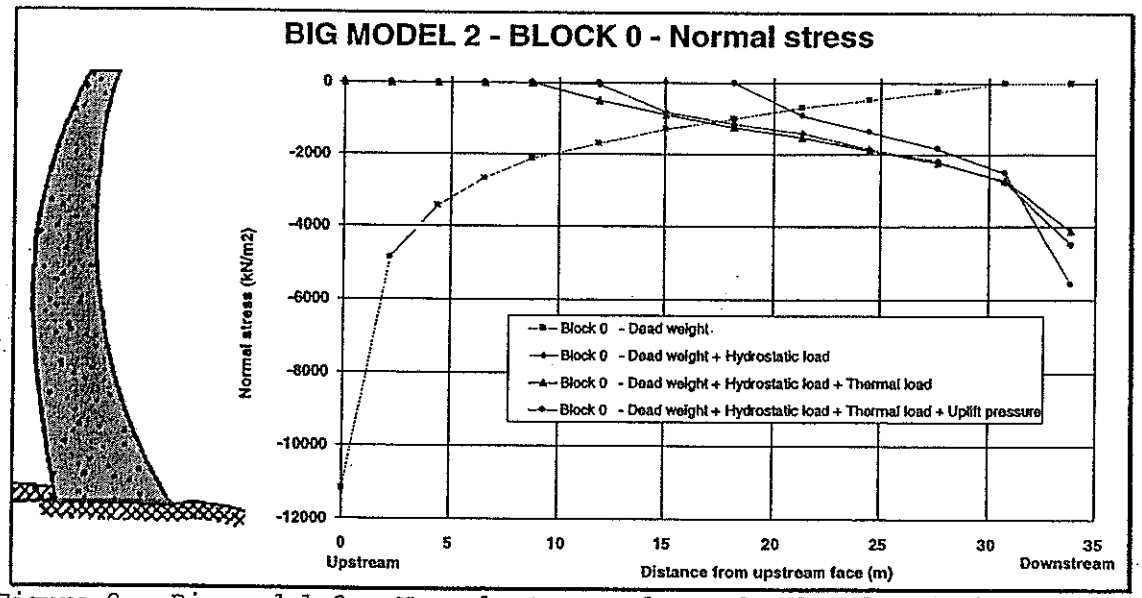

Figure 9 - Big model 2 - Normal stress along the dam-foundation contact of the central cantilever

Figure 10 shows that the radial displacement at the dam for different loadings. The thermal load have a significant effect on the displacements at the crest. When the uplift pressure is applied, a 4 mm sliding of the central cantilever was computed in the upstream-downstream direction. Direct pendulum located in the dam can't measure such deformation.

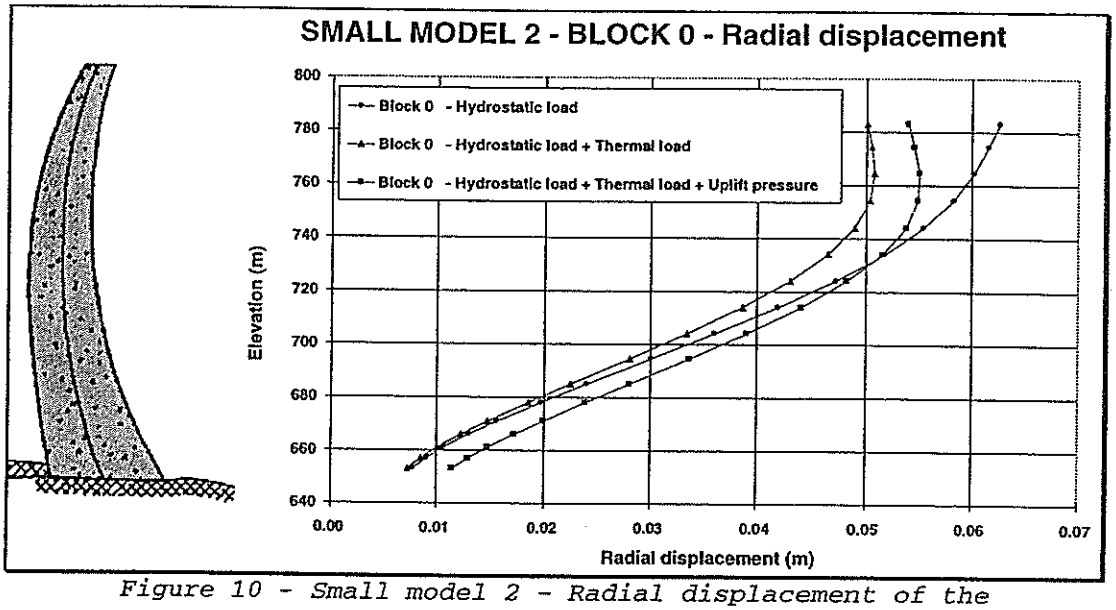

Figure 10 - Small model 2 - Radial displacement of the central cantilever

Remarks on model 3

Dam construction :
The main differences between the results of models 2 and 3 are observed after the dam construction. In the dam, compressive tangential stresses are not equal to zero with model 3 because of the Poisson's ratio effect. The compression at the toe (figure 11) and the radial displacement at the crest in the upstream direction are higher with model 3 than with model 2.
The thermal shrinkage of the concrete leads to the partial opening of the block joints. At the end of the construction, tangential compressive stresses in the dam are not equal to zero with model 3 whereas they are equal to zero with model 2. However, the tangential displacements and the strain state of the dam obtained with model 3 are more realistic than those obtained with model 2.

Hydrostatic and thermal loading :
Results with model 2 and 3 are very similar. The compressive stress computed at the toe at the end of the construction is higher with model 3 than with model 2 and the opening of the dam-foundation contact at the end of the impounding is lower (figure 12).

The no-tension law used to model the dam behaviour during construction could have been used during the impounding of the reservoir to simulate the opening of the vertical block joints (if tension).

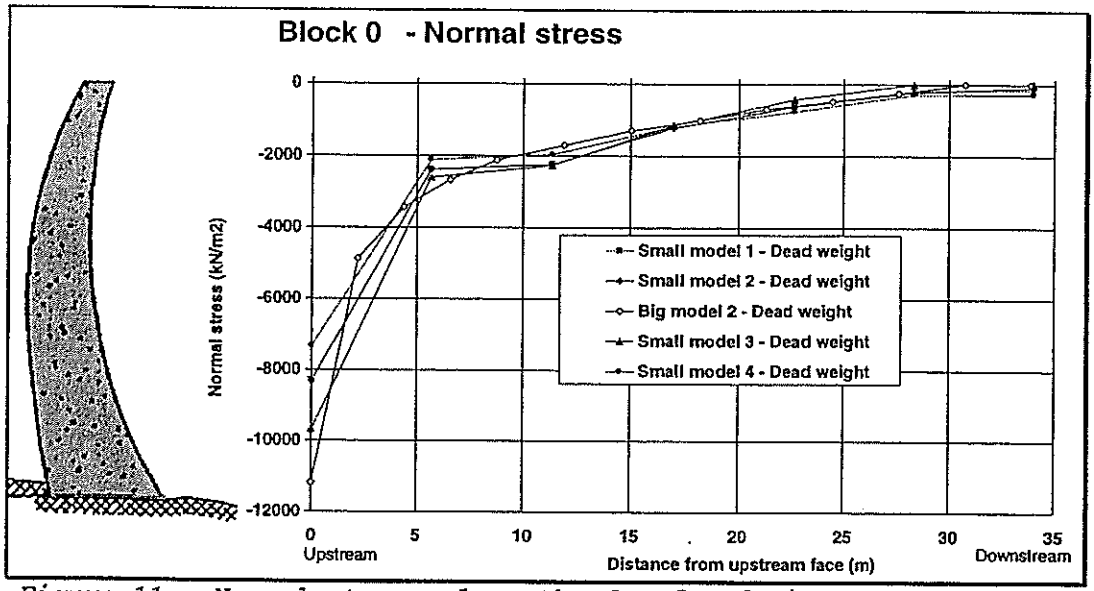

Figure 11 - Normal stress along the dam-foundation contact of the central cantilever - Comparison of the results obtained with models 1, 2, 3 and 4
Loading : Dead weight

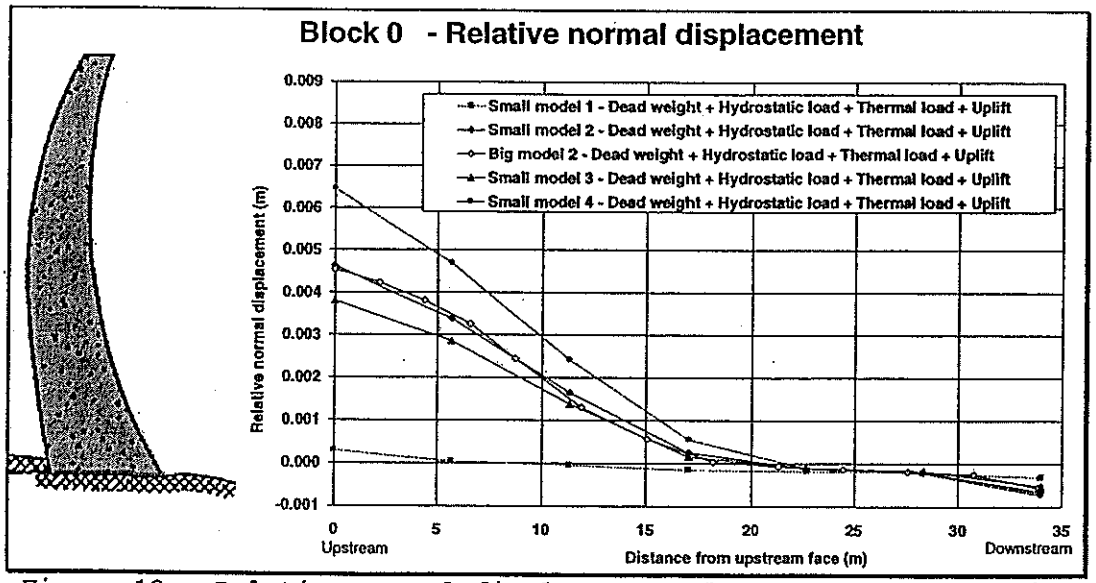

Figure 12 - Relative normal displacement along the dam-foundation contact of the central cantilever Comparison of the results obtained with models 1, 2, 3 and 4
Loading : Dead weight+Hydrostatic load+Thermal load+Uplift pressure

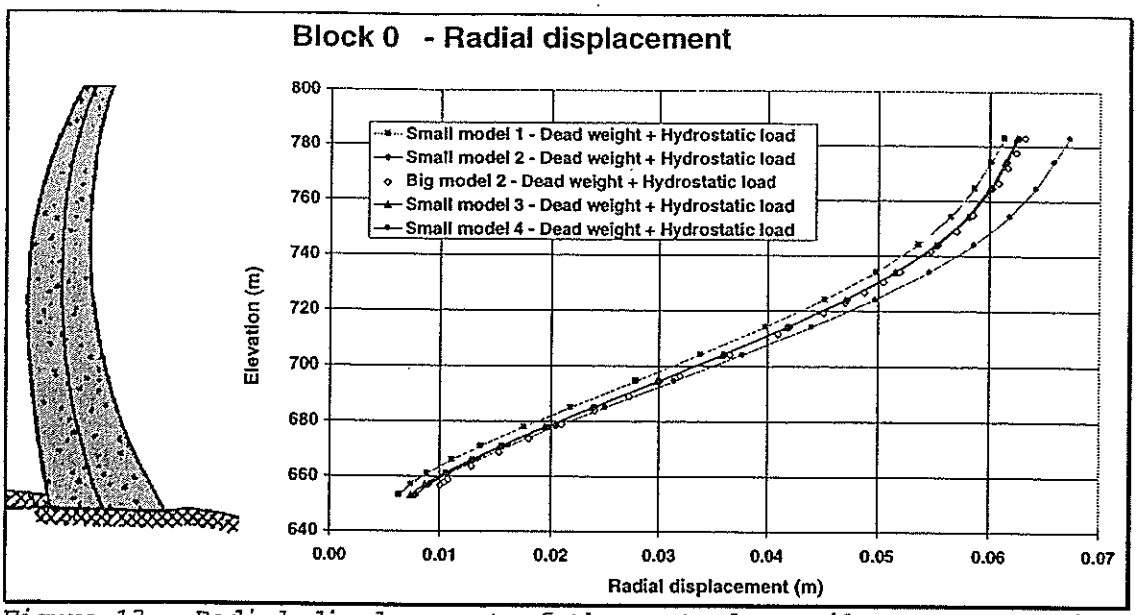

Figure 13 - Radial displacement of the central cantilever - Comparison of the results obtained with models 1, 2, 3 and 4
Loading : Dead weight + Hydrostatic load

Remarks on model 4

Compare to model 2 and 3, it is not necessary to have the radial direction of a point into the dam to model its behaviour during construction.

Dam construction :
The use of vertical block joints allows to take into account and to analyse the effects of thermal shrinkage and joint grouting on the mechanical behaviour of the dam. Thermal shrinkage clearly shows the discontinuities on the stress state along the dam-foundation contact at the intersection between block joints. Joint grouting under high pressures (0.5 to 1 MPa) can lead to a significant increase of the compression at the toe.
Another advantage of this method is the possibility to model accurately and easily the dam construction steps and the joint grouting scenario.

Hydrostatic and thermal loading :
Radial displacements obtained with model 4 (figure 13) are slightly greater than the ones obtained with model 2 and 3 because :

- the behaviour of the dam remains non-linear during these loadings (no-tension in the joint).
- under high compression, the normal compressive stiffness of the block joints allows some deformations. The normal stiffness of the vertical joints or the Young modulus of the concrete have

to be estimated in order to adjust the computed and the measured displacements of the dam.

In model 4, the thermal shrinkage has not been taken into account and a zero joint grouting pressure is considered in order to compare the results of the different models.

CONCLUSION

The behaviour of Schlegeis arch dam have been computed for different types of loading.
The GEFDYN software was used taking into account recent developments especially on the interface elements.

Three methods were used to model the dam construction with independent columns. Two of them are based on the knowledge of the radial direction of the points located into the dam, the third takes into account the non-linear behaviour of the vertical block joints.
Results obtained are in good agreement. However, the third method allows to model the joint grouting and the thermal shrinkage of the dam.

REFERENCES

GEFDYN, 1991, « Notice d'utilisation. », EDF/CNEH, Coyne&Bellier, Ecole Centrale de Paris, France

DIVOUX P., BOURDAROT E., BOULON M., 1997, « Use of joint elements in the behaviour analysis of arch dams. », Numerical Models in Geomechanics, NUMOG VI, Montreal, Canada

DIVOUX P., 1997, « Modélisation du comportement hydro-mécanique des discontinuités dans les structures et les fondations rocheuses. Application aux barrages en béton. », Thèse de l'Université Joseph Fourier, Grenoble, France

STATIC ANALYSIS OF SCHLEGEIS DAM INCLUDING THE EFFECTS OF CONCRETE-TO-ROCK AND VERTICAL JOINTS

V.Rebecchi[1], P.Palumbo[2]
G.Mazzà[3]

ABSTRACT

Schlegeis dam has been analysed using finite element method both neglecting and considering the joint located at the rock to concrete contact. The effect of such a joint has been pointed out through the evaluation of stresses in the body of the dam and joint openings for different loading conditions.

INTRODUCTION

The non-linear behaviour of an arch dam was the subject of Theme A1 during the Third Benchmark Workshops (see Ref.[1]). At that time an effort was made to analyse the static behaviour of the dam taking into consideration the presence of structural discontinuities represented by 4 large vertical joints.
Results obtained by different authors were substantially in agreement with each other, whence it was possible to draw a positive conclusion about the reliability of finite element codes used, at least for what concerned the kind of analysis carried out.
The verification of results, in compliance with the CICG ICOLD Bulletin 94 (see Ref. [2]), is defined "validation" and represents the first aim in the development of the Benchmark Workshops activities devoted to enable the dam engineering community to set up reliable computational tools for the numerical analyses of dams.
The further phase (the "justification", see Ref.[2]) should now be faced. The A1 theme of the present Fifth B.W. is a step in this direction, since the matching of numerical analysis and observed behaviour is attempted for the first time. The Schlegeis dam has been selected by the formulator for the analysis. The dam is provided with a perimeter base joint which separates the dam from rock foundation. By

[1] ISMES S.p.A., Seriate (Italy)
[2] ISMES S.p.A., Seriate (Italy)
[3] ENEL S.p.A.-Polo Idraulico Strutturale, Milano (Italy)

comparing analytical results with experimental data collected during the first life phases of the dam it will be possible to acquire a deeper knowledge about the ability of numerical procedures in reproducing observed behaviour.

1.0 MODELS, MATERIALS AND LOADS

To run the proposed analyses, the refined finite element model suggested in the Specifications was adopted (about 150.000 d.o.f.). In the following, all data about modelling choices and loading conditions will be outlined.
The suggested geometry, including a large rock foundation volume, is reported in Fig.1.

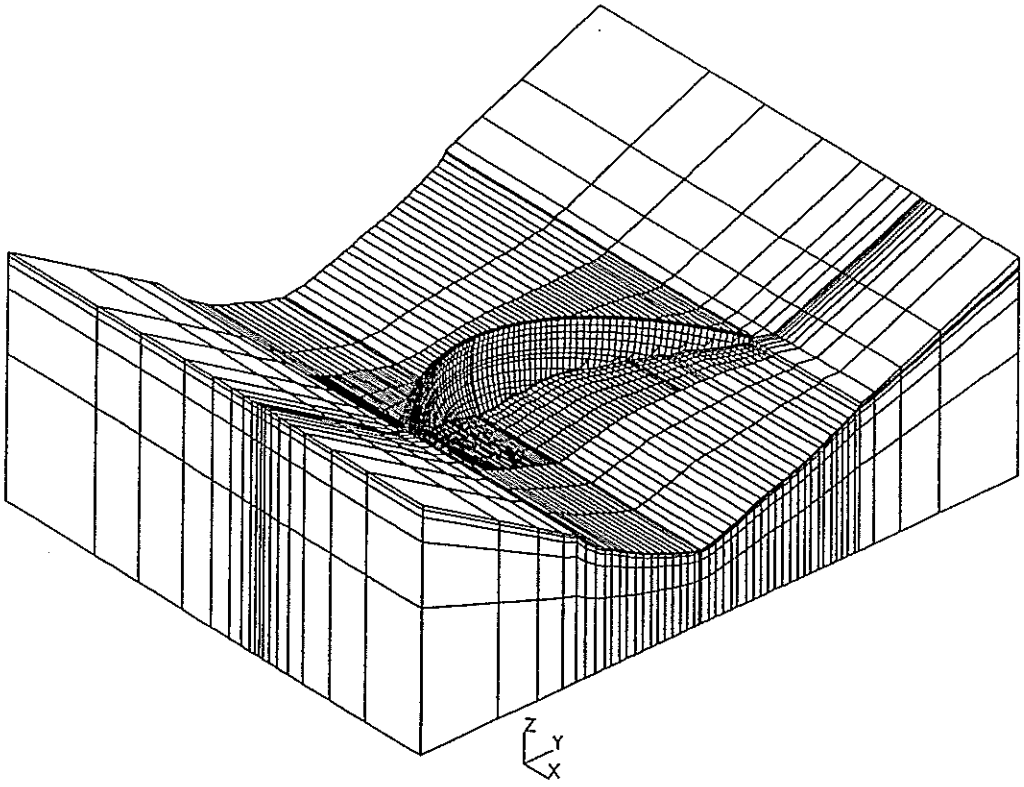

Figure 1. F.E. model with foundation rock

The whole model is formed by 20 nodes hexahedron and 15 nodes pentahedron elements. Two different models were set up to run the analyses: a linear monolithic model without perimeter joint and a non-linear model including the perimeter joint.
Both the analyses were carried out using the F.E. code ABAQUS version 5.8.

Rock foundation

According to B.W. specifications, rock foundation has an orthotropic stiffness matrix (except for the first row of elements below the dam), with the orthotropy axes oriented like the schistosity plane. The Young moduli parallel and normal to the schistosity plane are equal to 30 and 10 GPa respectively. Poisson ratio has been assumed equal to 0.17. Rock foundation has been assumed massless.

Dam body

The dam body is modelled using 6 elements through the thickness at the base and 3 at the top. The Young Modulus of concrete has been assumed equal to 25 GPa, with a 0.17 Poisson ratio and a concrete density equal to 2400 kg/m^3.
The thermal expansion coefficient has been assumed equal to 8 10^{-6}.

Perimeter joint

The perimeter base joint has been modelled using 18 node contact elements. A "softened" behaviour was chosen to allow for a faster convergence, with a "zero pressure clearance" c=1 mm and a "pressure at zero clearance" p0=10 kN (see Fig.2).

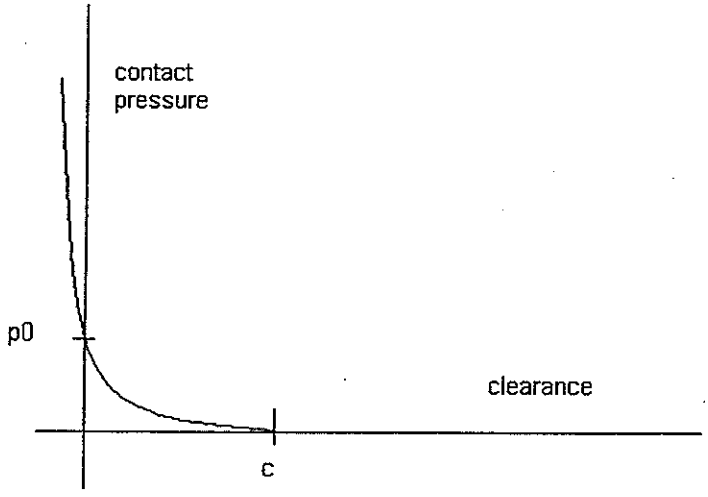

Fig.2 Normal pressure-clearance relationship

A "penalty function" formulation was adopted for the sliding behaviour. An "elastic slip" of 1 mm is allowed before real sliding can take place. For displacements lying

in the joint plane smaller than 1 mm an elastic behaviour is considered. For displacements greater than 1 mm a Coulomb friction coefficient equal to 1 is adopted.

Loading phases

Four consecutive loading phases were considered:
1. Dead weight
2. Hydrostatic pressure for the top reservoir level (1782 m a.s.l.)
3. Temperature loading assuming node temperatures as reported in specification file
4. Uplift pressure, assuming 100% of hydrostatic pressure under the first two upstream rows of finite elements. This load condition was not applied to the monolithic dam.

2.0 ANALYSES

The effects of the construction phase have been taken into account using a dedicated finite element model of the dam body characterised by an orthotropic stiffness matrix with a very low Young modulus in the arch direction. The low module in the arch direction makes the different vertical blocks of the dam work almost independently, avoiding the development of arch stresses. Dam stresses for the selfweight load computed with this model have been then applied to the isotropic model of the dam to complete the loading phases.
A monolithic linear model has also been set up to check the influence of the base perimeter joint on the structural behaviour of the dam. Results in terms of displacements and stresses relevant to both models (monolithic and with joint) are reported in the following.

Displacements comparison

Deformed configuration for the monolithic dam under the final loading condition (selfweight + hydrostatic pressure +thermal loading) is shown in Fig.3. The maximum upstream-downstream displacement is equal to 49.1 mm.

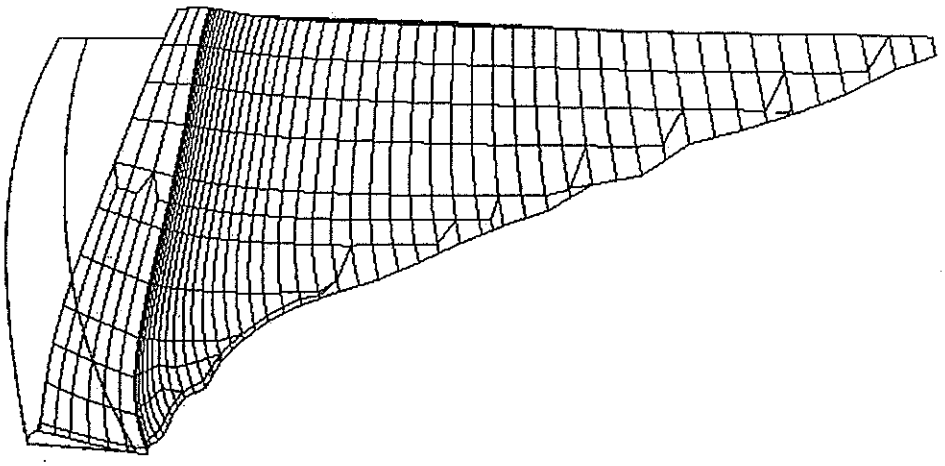

Fig.3 Total displacements for monolithic dam

Displacements under the same loading conditions (plus the uplift pressures acting along the base joint) are reported in Fig.4; maximum upstream-downstream displacement is equal to 53.1 mm.

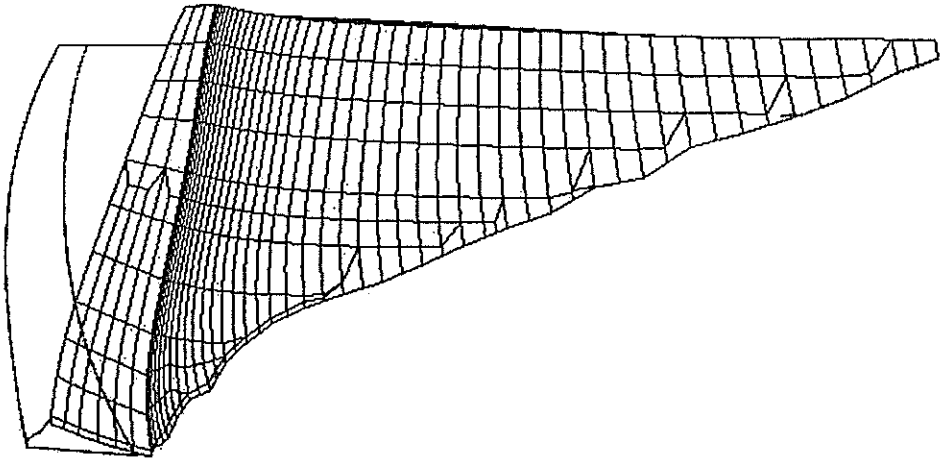

Fig.4 Total displacements for dam with perimeter joint

The direct comparison between Fig.3 and 4 shows that the principal effect of base joint is the increased upstream-downstream rotation of the dam base. The magnitude of displacements shows just small changes. Radial displacements along the height of central cantilever for the non-linear model are reported in Fig.5a for the selfweight and in Fig.5b for the remaining loading conditions.

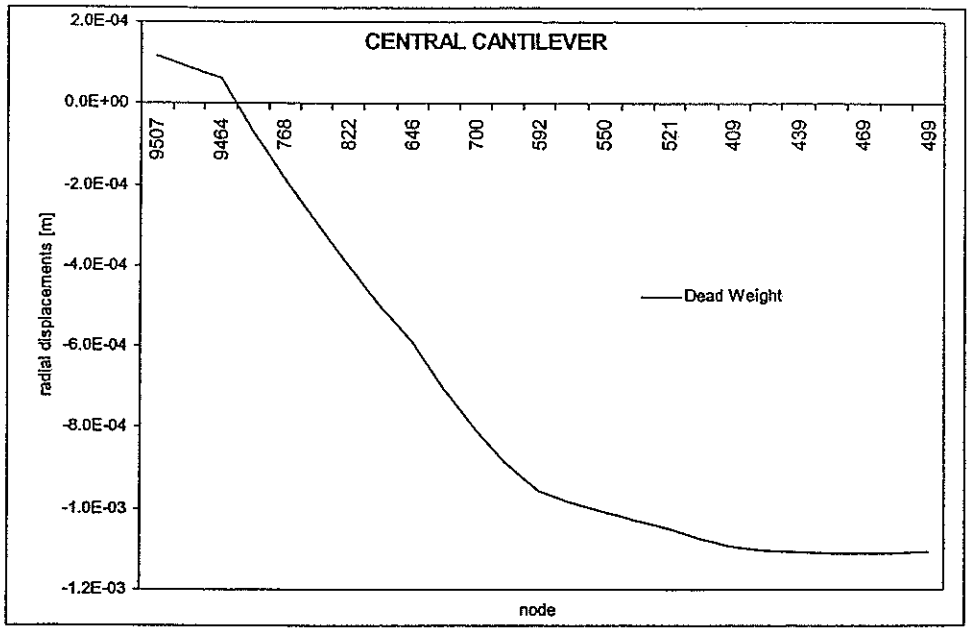

Fig.5a radial displacements on central cantilever

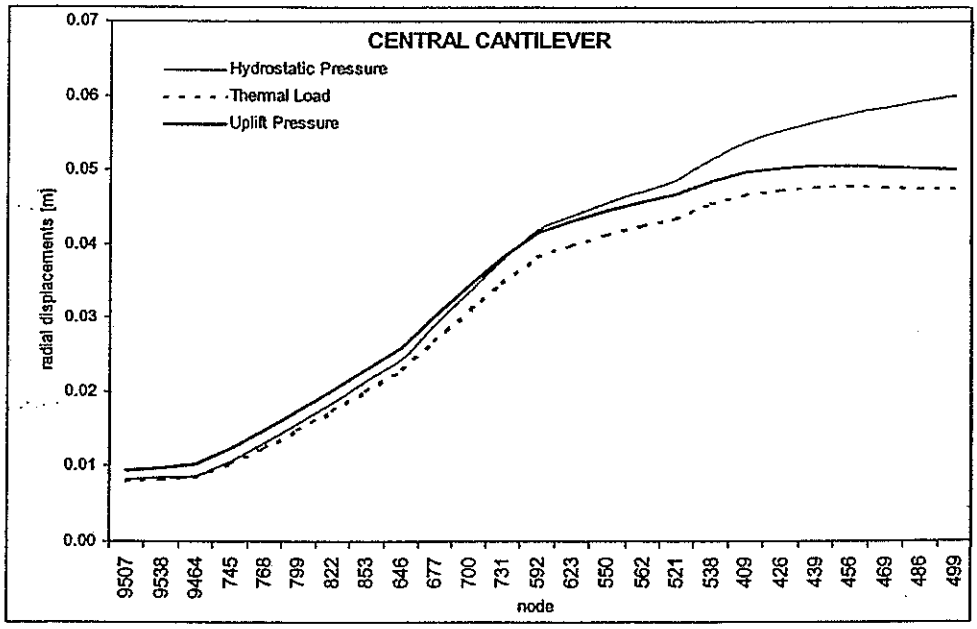

Fig.5b radial displacements on central cantilever

As it can be noted, maximum radial displacements due to selfweight are about 1 mm upstream, while the hydrostatic pressure brings the maximum radial displacement at 60 mm downstream on the crest (node 499) and about 8 mm downstream at the dam base (node 9507). subsequent thermal load reduces radial displacements in the central-upper part of the dam, while the uplift pressure adds 1-2 mm downstream.

Stress comparison

For a basic understanding of the influence that the perimeter joint has on the static response of the dam, a direct comparison between maximum principal stresses computed using the linear model on the one hand and the non-linear model of Schleigeis dam on the other has been carried out. The presence of perimeter joint can play a fundamental role in defining the stress state, reducing cantilever tensile stresses that can be developed near the dam-rock interface. While dam displacements relevant to the selfweight loading condition show an upstream component (which can cause cantilever tensile stresses on downstream face), the hydrostatic loading activates the arch mechanism of the dam which tends to make both upstream and downstream faces of the dam work in a compressive stress state. Figures 6a and 6b show the comparison between maximum principal stresses at the upstream face for the monolithic model of the dam and for the non-linear one respectively under self weight plus hydrostatic load.

Line number:	**1**	**2**	**3**	**4**	**5**	**6**	**7**
Stress [MPa]:	-1.0	-0.8	-0.5	-0.3	-0.1	0.0	0.1

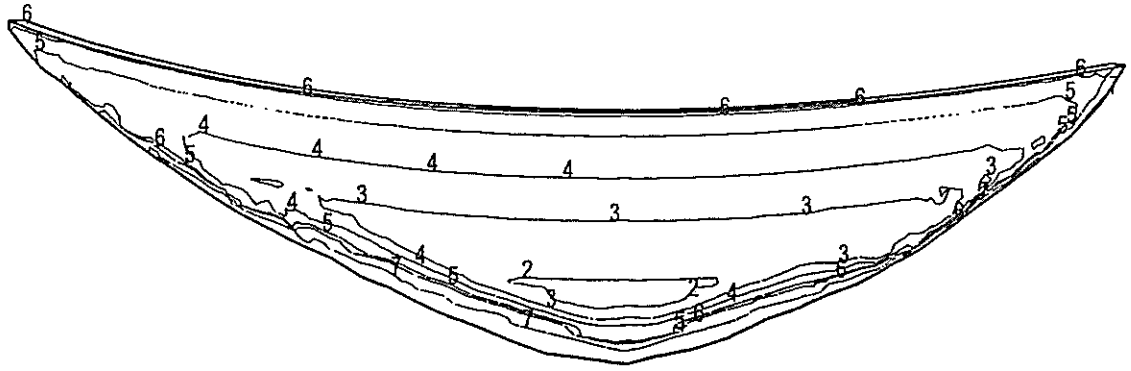

Fig.6a Upstream max princ. stress on for monolithic dam (selfweight+hydrostatic load)

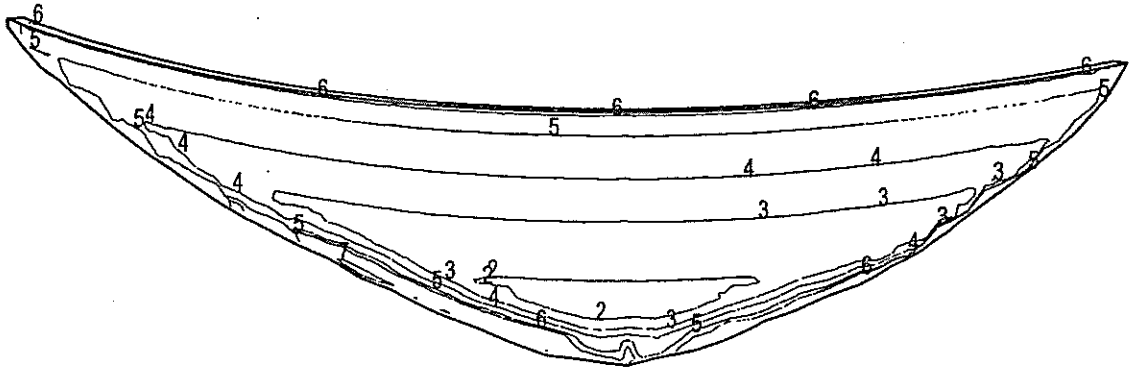

Fig.6b Upstream max princ. stress on for dam with joint (selfweight+hydrostatic load)

The only significant differences between the two models are located at the dam base, while in the dam body the effect of perimeter joint seems to be negligible.
A similar conclusion can be drawn also for the downstream face of the dam. Figures 7a and 7b show maximum principal stresses for the two F.E. models; a general agreement with just a slight increase of tensile stresses for the model with the perimeter joint is highlighted. The spotted appearance of stress contours is due to the fact that computed stress values are near to zero.

Maximum principal stresses scale

Line number:	1	2	3	4	5	6	7
Stress [MPa]:	-1.0	-0.8	-0.5	-0.3	-0.1	0.0	0.1

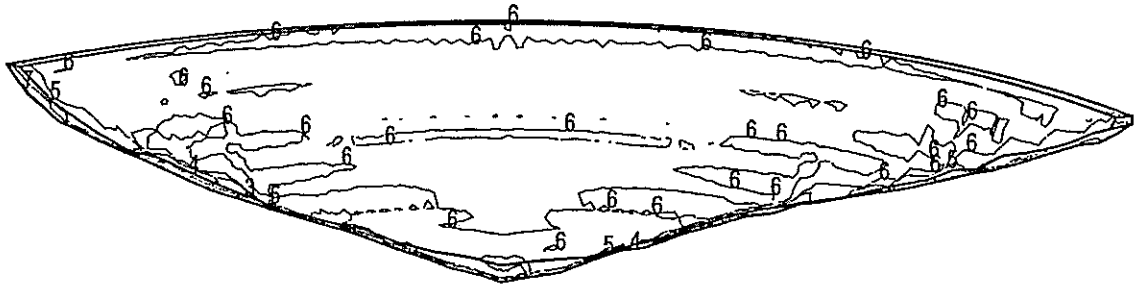

Fig.7a Downstream max princ. stress for monolithic dam (selfweight+hydrostatic load)

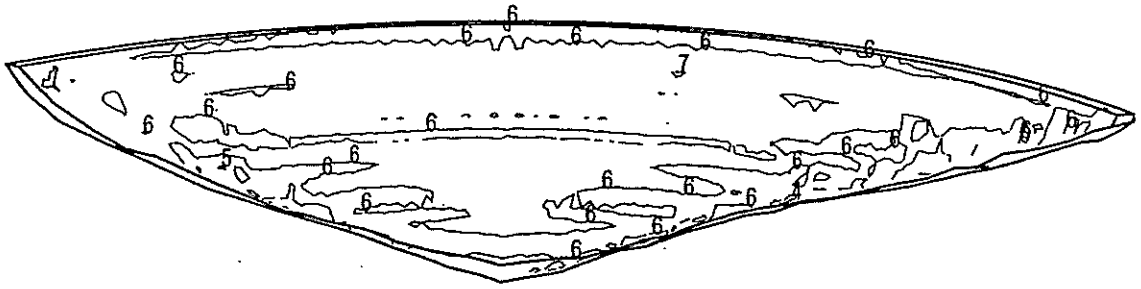

Fig.7b Downstream max princ. stress for dam with joint (selfweight+hydrostatic load)

As a final result, with regard to the stress state in the dam body, Figures 8 and 9 show the contours of maximum and minimum principal stresses at upstream and downstream faces of the model with perimeter joint under the complete load sequence. Maximum tensile stresses in the dam body are located at the downstream face (Fig.8b) where a quite large area shows values beyond 0.1 MPa. No remarkable tensile values are located at the upstream face.

Maximum principal stresses scale

Line number:	1	2	3	4	5	6	7
Stress [MPa]:	-1.0	-0.8	-0.5	-0.3	-0.1	0.0	0.1

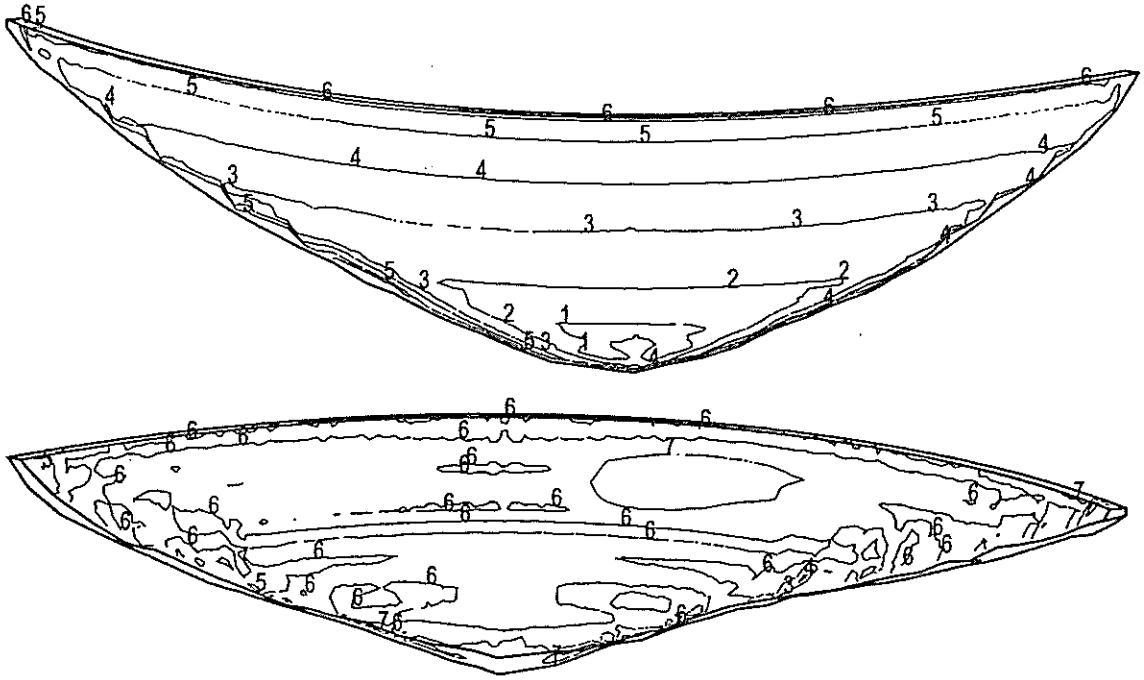

Figg.8a,b Max princ. stress for dam with joint
(selfweight+hydrostatic load+thermal load+uplift)

Minimum principal stresses scale

Line number:	1	2	3	4	5	6	7	8	9
Stress [MPa]:	-4.5	-3.5	-3.0	-2.5	-2.0	-1.5	-1.0	-0.5	0.5

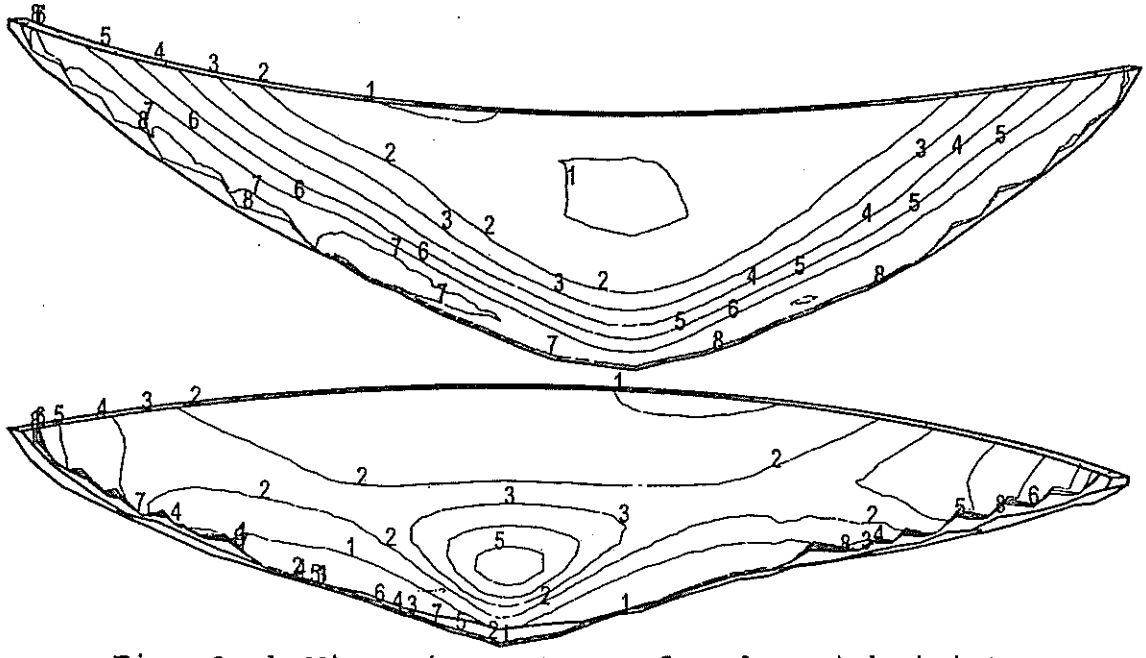

Figg.9a,b Min princ. stress for dam with joint
(selfweight+hydrostatic load+thermal load+uplift)

Compressive stresses beyond 3.5 MPa are located both at upstream and downstream faces (Fig.9a and 9b) where wide zones of the dam undergo compressive stresses greater than 3.5 MPa (contour line 2).

Joint openings, sliding and stresses

Line contours of openings of the perimeter joint have been drawn for each loading condition to investigate the behaviour of perimeter joint. Since a "softened" contact behaviour has been implemented for the joint (see Chap.1), these contours should be viewed as a qualitative indication about distribution of openings and not as a precise evaluation of punctual openings values.

Scale for joint openings

Line number:	1	2	3	4	5	6	7	8
opening [mm]:	0.25	0.5	0.75	1.0	2.0	3.0	4.0	5.0

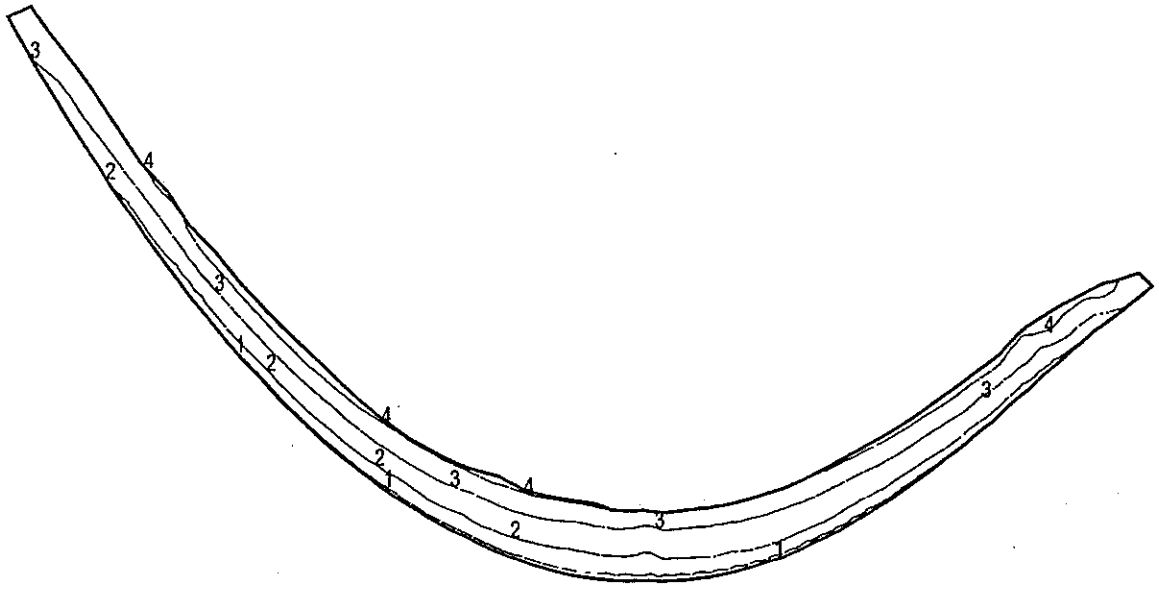

Fig.11 joint opening under selfweight

For the selfweight loading condition the largest openings are located downstream (Fig.11), while under the selfweight plus hydrostatic load the maximum openings are located at the upstream and reach a value of about 4 mm near the central cantilever (Fig.12).

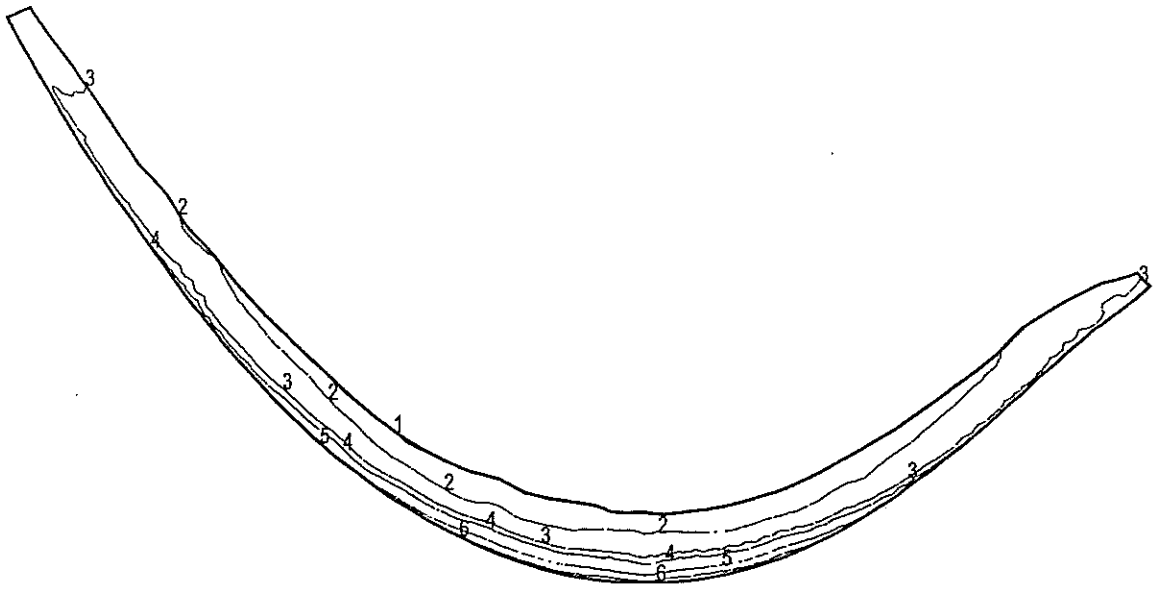

Fig.12 joint opening under selfweight+hydrostatic load

The subsequent application of thermal load (Fig.13) tends to reduce the upstream maximum openings without changing the general deformed shape too much. With the application of uplift pressures (Fig.14) the upstream openings increase remarkably, attaining the value of 6 mm.

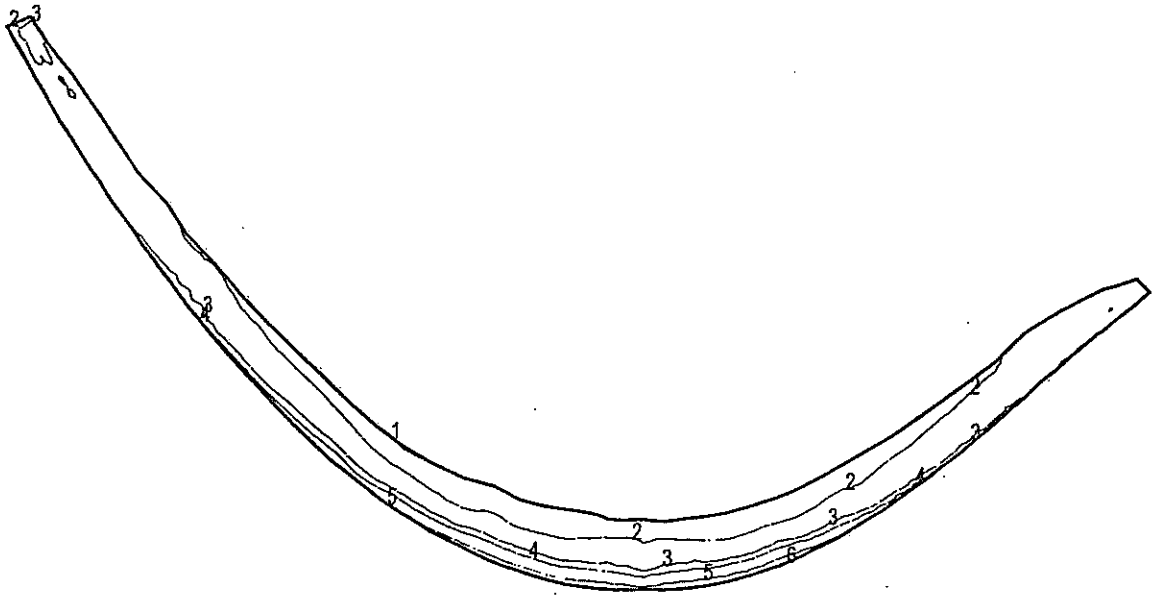

Fig.13 joint opening under selfweight+hydrostatic load+thermal load

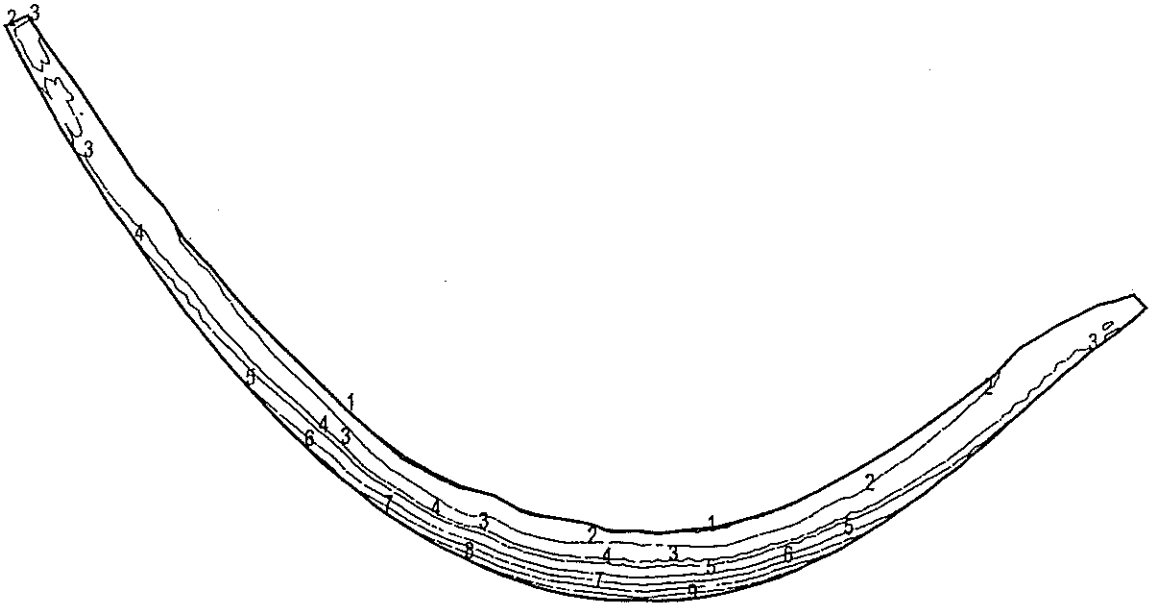

Fig.14 joint opening under selfweight+hydrostatic load+thermal load+uplift

3.0 CONCLUSIONS

Linear and non linear finite element analyses have been carried out to analyse the static behaviour of Schlegeis arch dam. Results indicate that the effect of perimeter joint dominates the stress state near the dam base, but has little influence on maximum and minimum principal stresses developed in the central part of the dam.
Computed openings of perimeter joint reach their maximum value near the upstream of central cantilever.
Direct comparison of these results with experimental data collected during the first life phases of the dam will make it possible to have a measure about the adequacy of such an analysis to provide reliable information on the static behaviour of the dam.

4.0 REFERENCES

[1] Proceedings of the "Third Benchmark Workshop on Numerical Analysis of Dams"; Paris (France), September 29-30 1994.

[2] Computer Software for Dams. Validation. Comments and Proposal. CICG ICOLD Bullettin 94; 1994.

STATIC ANALYSIS OF AN ARCH DAM-FOUNDATION SYSTEM TAKING INTO ACCOUNT UPLIFT PRESSURE

Adrian Popovici*, Lucian Lefter**, Radu Sârghiuta*,
Constantin Vacarescu*

1. INTRODUCTION

The paper aims to investigate the performance of the Schlegeis arch dam from Austria, which is a wide spanned arch dam. The main geometric data of this dam (fig. 1) are the followings:

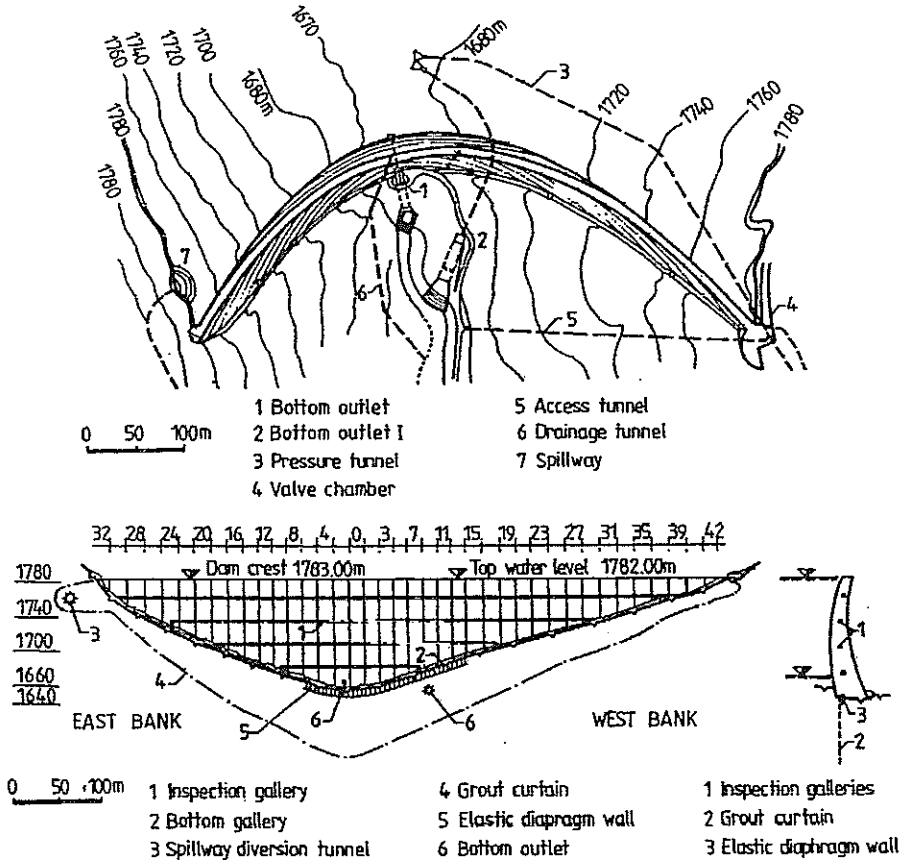

Figure 1. Schlegeis dam: a - layout, b - central and longitudinal sections.

* Technical University of Civil Engineering - Bucharest
** Studies and Consulting Institute for Energetics - Bucharest

- dam height 131 m
- crest length 725 m
- crest/height ratio 5.5
- crest thickness 9 m
- base thickness 34 m

The dam consists of 43 blocks, each of them having 17 m wide. Some incidents have appeared during dam's operation. In 1973, when the reservoir reached maximum level, the seepage flow measured in the base gallery from the dam upstream toe was 200 l/s. This water seepage was provoked by cracking of the dam-foundation contact in the dam upstream toe. In order to reduce the water seepage a cut off wall was carried out in a total of eleven blocks from the dam's central zone. After this remedial work, the maximum seepage flow corresponding to maximum level in reservoir has not exceeded 25 l/s.

A dam-foundation standard and respectively, small finite element model with contact elements in the interface between dam and foundation was proposed by the formulator of the problem - Verbundplan Gm b H Salzburg, Austria - in order to simulate the behaviour of the Schlegeis dam. In the present paper, the small finite element model was considered. It consisted of 6080 nodes and 1142 bricks and wedges elements with 20 and respectively 15 nodes per element.

The analysis was performed with well-known commercial computer code ANSYS 5.5. (Swanson Analysis System, Inc. 1998). The computer code was run on a PC PENTIUM MMX 200 MHz.

2. MATHEMATICAL MODEL

The dam body were discretized with the SOLID95 element type, brick and wedge with 20 and respectively 15 nodes per element. The foundation were discretized with the SOLID45 element type, brick with 8 nodes. A number of 246 bricks (wedges) elements were used to discretize dam body and respectively 896 elements for foundation discretizing. Three rows of elements were considered on dam's, thickness from top to bottom. Also, 18 rows of element blocks were considered in the dam longitudinal profile. The formulator proposed bricks with curved sides to discretize dam body, but some of them were not accepted by ANSYS because of their shape (distorsion degree). Consequently, the curved bricks were equivalated by bricks with linear sides, and

the coordinates of the middle side nodes were computed again averaging the coordinates of the corresponding corner nodes. However, the middle side nodes from the dam and foundation elements adjacent to contact zone were eliminated in order to save the computer time.

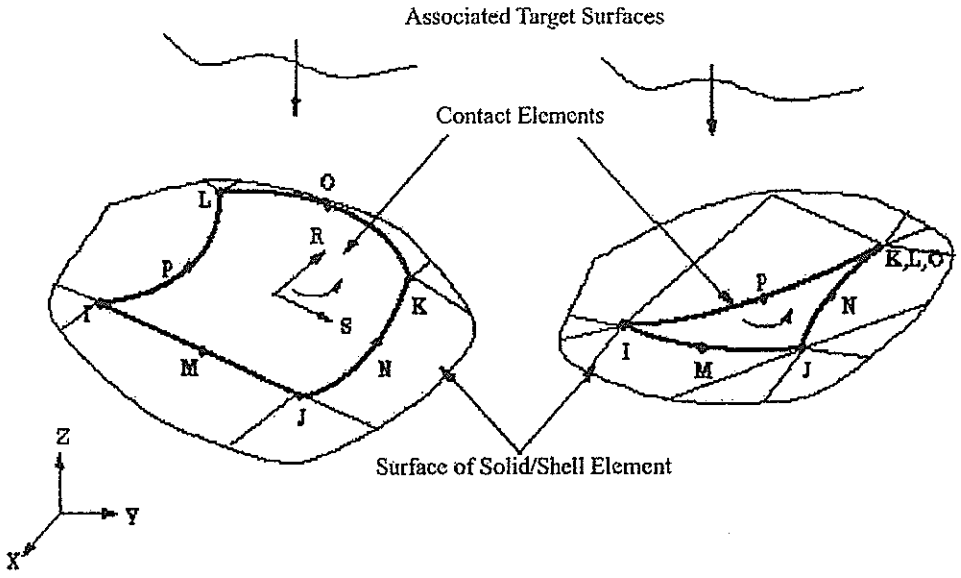

Figure 2. CONTAC173 3-D Surface-to-Surface Contact Element (4 nodes) (ANSYS 5.5. computer code).

The contact dam-foundation was modeled with CONTA173 3-D Surface-to-Surface Contact Element (fig. 2). This element is used to represent contact, gap and sliding between 3-D "target" surfaces (TARGE170) and a deformable surface, defined by this element. It is located on the surfaces of 3-D solid or shell elements, and it has three degrees of freedom at each from its corner nodes: translations in the nodal x, y, and z directions. The element has the same geometric characteristics as the solid or shell element face with which it is connected. Contact occurs when the element surface penetrates one of the target segment elements, on a specified target surface. Coulomb and shear stress friction is allowed.
TARGE170 is used to represent various 3-D "target" surfaces for the associated contact elements. The target surface is discretized by a set of target segment elements (TARGE170) and is paired with its associated contact surface via a shared real constant set. Any translation or rotation displacement, also forces and moments can be imposed on the

target segment element. The target surfaces can be rigid or flexible. For flexible targets, the target segment elements will overlay the solid elements describing the boundary of the deformable target body.
In the present model the contact elements were connected to the faces of the dam body brick elements adjacents to the dam-foundation interface. The corresponding targets overlay the face of the foundation brick elements adjacents to the dam-foundation interface. Consequently, the dam-foundation interface was modeled as flexible-flexible contact surfaces.

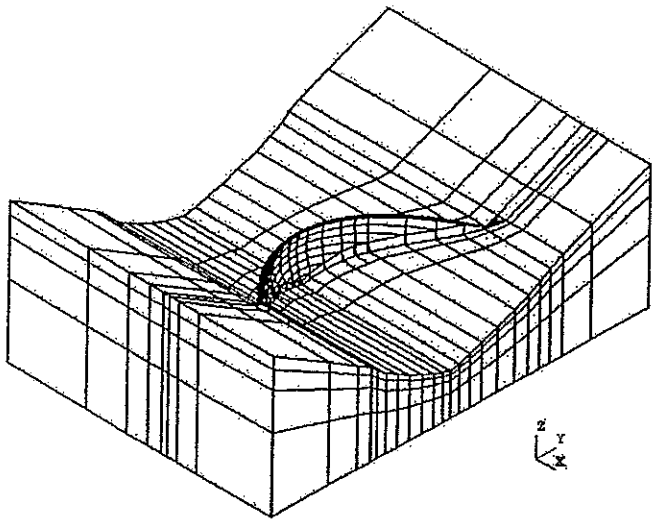

Figure 3. General view of the finite element mesh - small model.

A total number of 54 contact elements, respectively 54 "target" surfaces were used to model dam-foundation interface. The interface coefficient of friction, $\mu = 1.00$ was considered for Coulomb friction and no tensile stresses are allowed on normal directions to dam-foundation interface.
Also an aditional condition concerning $\tau_{limit\ sliding} \leq 100$ MPa, was imposed in order to have sticking contact between contact element and its "target" surface.
In the figure 3 can be seen a general view of the finite element mesh for the small model case, which was adopted in the present analysis.

3. INPUT DATA

The formulator of the problem gave the input data. The rock foundation was assumed with orthotropic behaviour. In the

table 1 are presented the main material parameters considered in analysis.

Table 1

Parameter	Material type	
	Rock	Concrete
Young's Modulus E [GPa] (for rock EII)	30	25
Young's Modulus E [GPa] (for rock E⊥)	10	
Poisson ratio ν	0.17	0.17
Density [Kg/m^3]		2400

The following four load hypotheses were analysed:

1. Dead weight
2. Dead weight + Hydrostatic load
3. Dead weight + Hydrostatic load + Thermal load
4. Dead weight + Hydrostatic load + Thermal load + Uplift pressure.

4. TECHNICAL ASPECTS

The analysis was performed using a PC PENTIUM MMX (200 MHz, 32 Mb RAM).
The computation time for a load hypothesis varied between 5900 ... 6600 seconds.
The contact element (CONTA173 3-D Surface to Surface) used in the analysis being nonlinear, it requires an iterative solution. Some input data concerning the characteristics of the contact elements respectively, $\mu = 0.75$ and $\tau_{\text{limit sliding}} = 20$ MPa which were used in an initial stage of the analysis provoked problems of convergence of solutions.
It can be remarked, in the preliminary stage of the analysis, the dam-foundation interface was modeled with threedimensional point to point contact elements (spring) named CONTAC52-3D, existent also in ANSYS elements library. This three-dimensional interface element represents two surfaces which may maintain or break physical contact and may slide relative to each other. However, this model was abandonded because of low rate of convergence of solutions and numerical instabilities.

5. RESULTS OF THE ANALYSIS

The results are provided according to formulator instructions. A linear analysis free of contact elements on the dam-foundation interface was performed in order to

emphasize the effects of nonlinear analysis versus a standard solution.

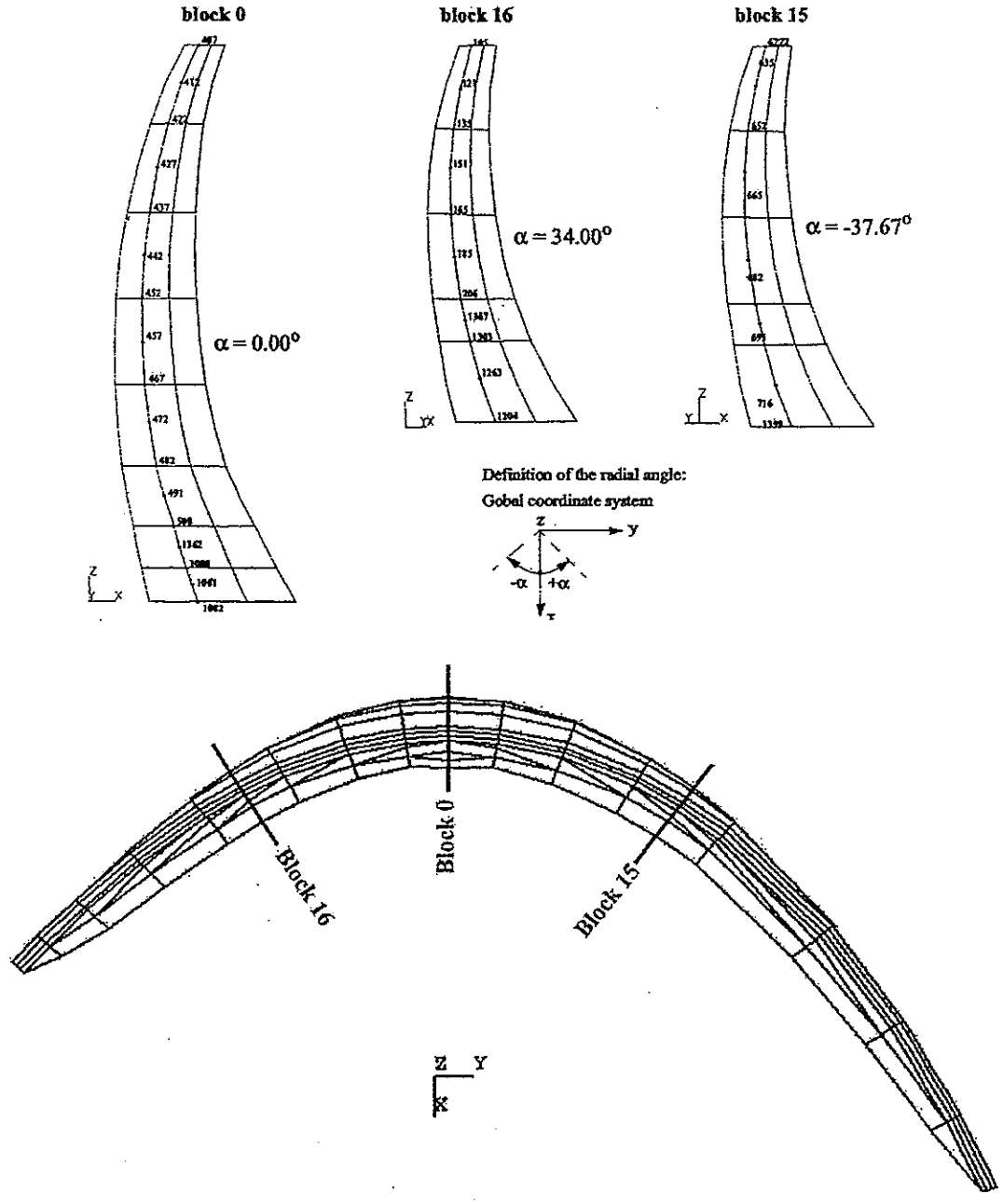

Figure 4. Characteristic sections through finite element mesh:
a - radial sections, blocks number 0, 16 and 15;
b - dam-foundation interface section.

In the figure 4 are illustrated some sections through finite element mesh corresponding to radial sections,

blocks number 0, 16 and 15 and respectively dam-foundation interface section.

Some output results (contours of horizontal radial displacements, contours of principal stresses, stress diagrams) are presented in Figure 5...9.

The openings of the base joint in those four load hypotheses examined are presented in Figure 10.

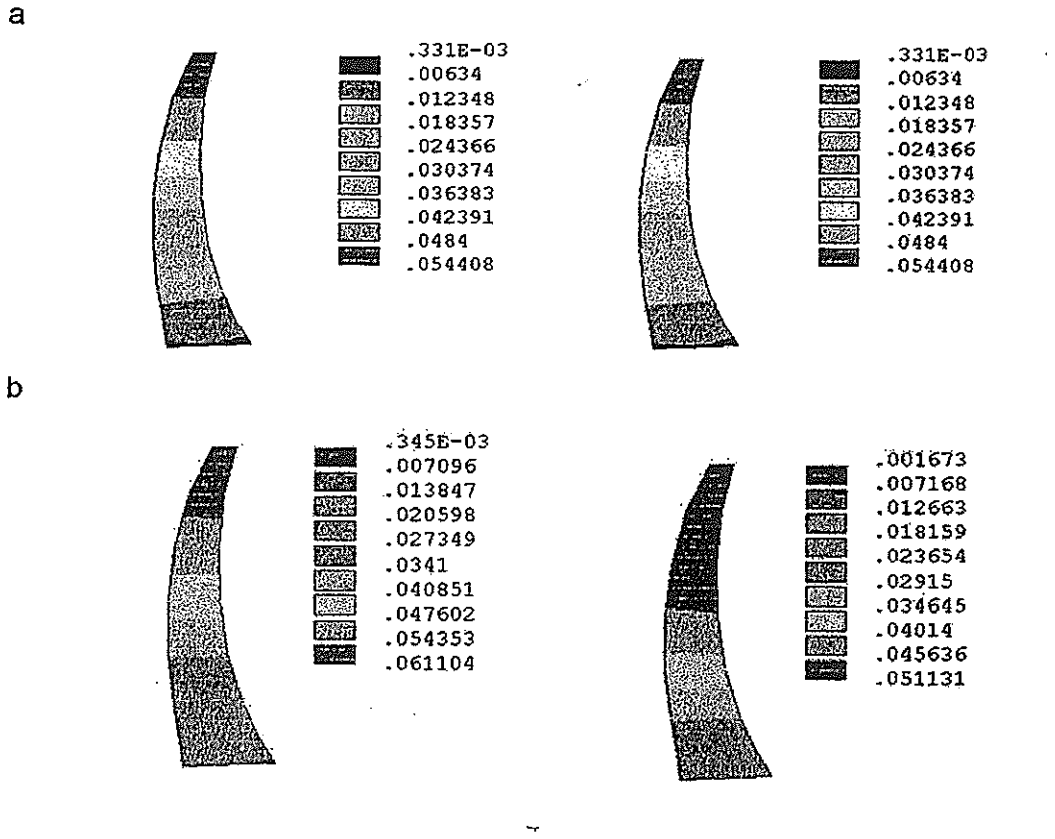

Figure 5. Contours of the horizontal radial displacements in the dam central section (block 0) [m] in the load hypotheses No.2 and No. 4, linear and nonlinear analyses [m].

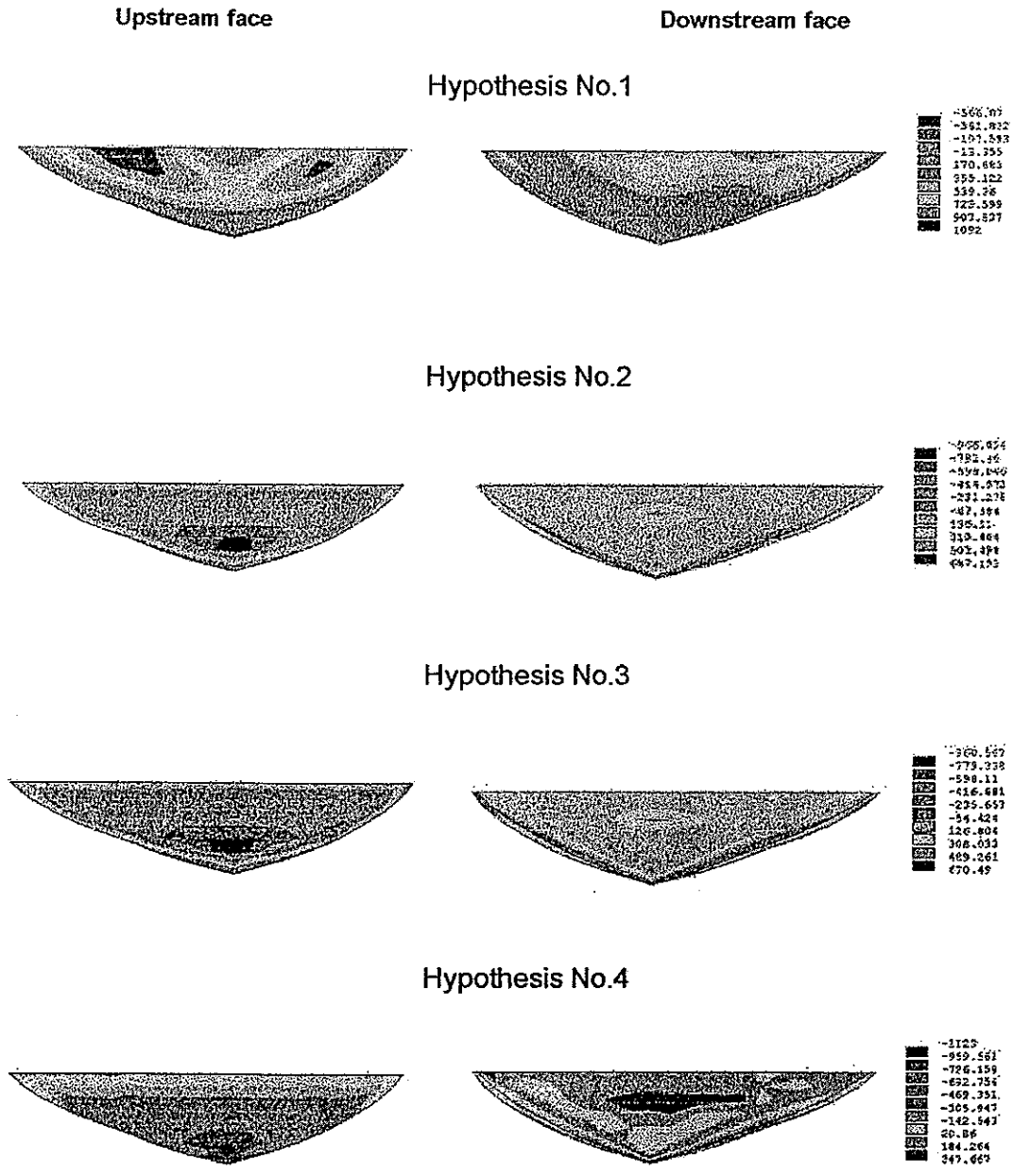

Figure 6. Contours of the maximum principal stress (σ_1) in the nonlinear analysis and different load hypotheses [kPa].

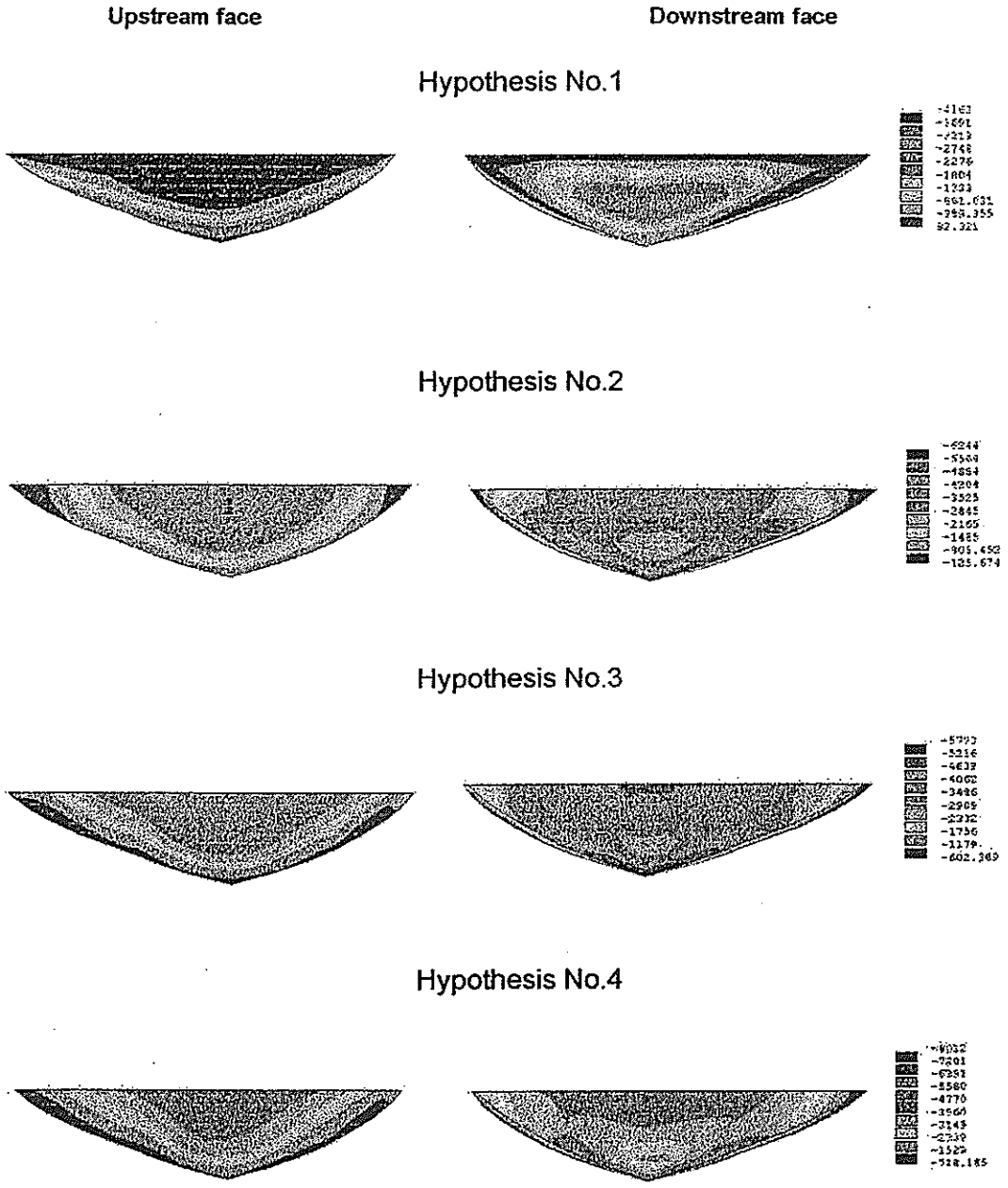

Figure 7. Contours of the minimum principal stress (σ_3) in the nonlinear analysis and different load hypotheses [kPa].

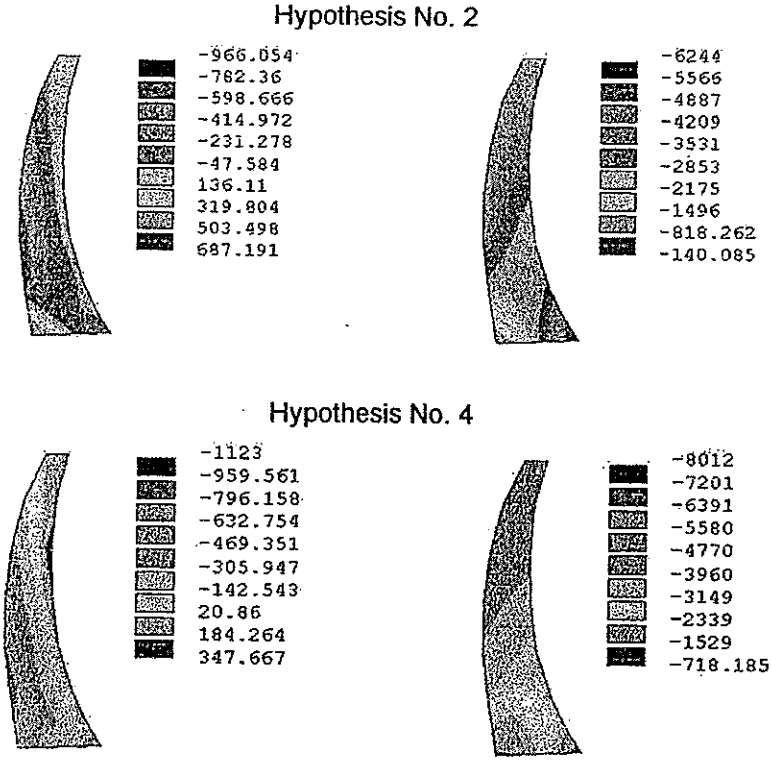

Figure 8. Contours of the maximum and minimum principal stresses in the dam section (block 0) nonlinear analysis and load hypotheses No. 2 and No. 4 [kPa].

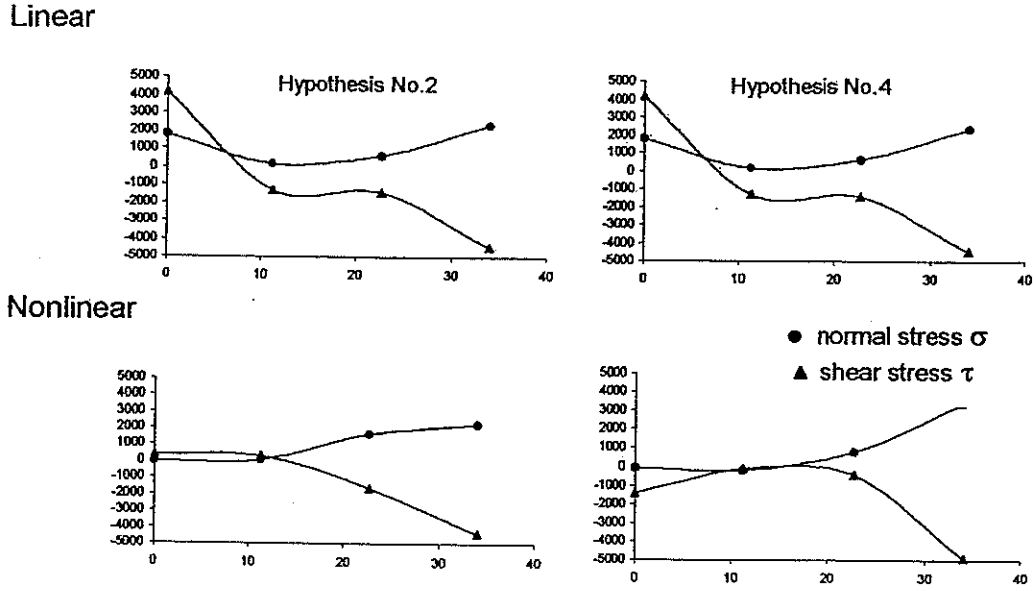

Figure 9. Normal (σ_z) and shear (τ_{xz}) stresses in the central section (block 0) along a radial line of the dam-foundation interface [kPa].

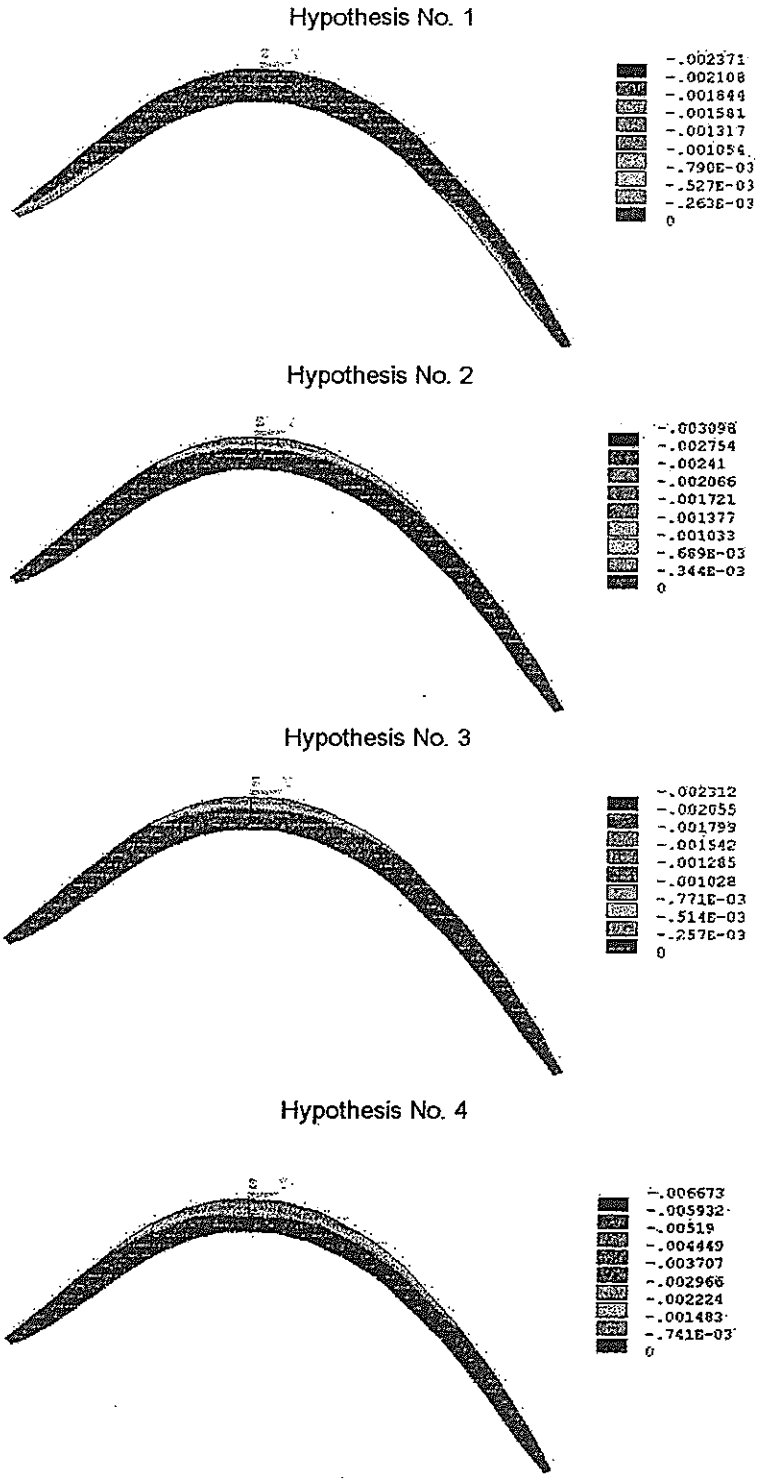

Figure 10. The openings of the base joint in different load hypotheses

6. CONCLUDING REMARKS

The small model used in the present analysis had the advantage of smaller computer resource consumption. The results obtained can be considered as satisfactory for the point of view of the model ability to simulate the real behaviour of the Schlegeis dam (Popovici, Popescu, 1992).
The linear analysis for the dam foundation monolithic system, pointed out the highest risk for cracking of the dam-foundation contact in the central upstream toe dam zone because of excessive vertical tensile stresses. (Popovici et al, 1992).
The nonlinear analysis using contact elements to model the dam-foundation interface has offered the possibility to evaluate the opening of a predefined joint between concrete dam and rock foundation.
Some relevant comments may be done about the results of the nonlinear analysis, as follows:

- Applying the dead weight on monolithic dam finite element mesh with contact elements on dam-foundation interface, some openings appeared in the abutments downstream toe zone of the dam (fig. 10, hypothesis No. 1). As a matter of fact, due to large span of the dam site, the stress state loading dead weight on dam's independent columns could not differ significantly versus loading dead weight on monolithic structure.
- The impounding of the Schlegeis dam reservoir conducted to some opening of the contact dam-foundation at the upstream toe zone, central blocks number 0, 1 and 2; The maximum opening reached 3.09 mm.
- The temperature field of the dam body given by formulator had generally little influence on strain and stress state of the dam.
- The uplift pressure applied on the one third of the dam-foundation surface from its upstream zone conducted to increase of the area from the dam upstream toe zone presenting openings of the contact dam-foundation. The maximum opening of the dam-foundation contact from central zone reached in this fourth hypothesis 6.67 mm.
- The uplift pressures diminished the global normal loads acting on dam foundation, but the contact remained closed on the large area in the downstream

zone. The maximum radial displacements on the contact dam-foundation area reached 49 mm.

- Finally, it may be remarked that results performed by mathematical model used in this analysis are compatible with physical real behaviour of the dam.

REFERENCES

1. *** ANSYS *Element Reference*. Tenth Edition. SAS IP, Inc®, 1998.
2. Popovici, A., Toma, I., Sârghiuta, R. *Comments on static and dynamic analysis of two large dams*. Proceedings International Symposium on Arch Dams, Nanjing-China, 1992.
3. Popovici, A., Popescu, C. *Dams for water storage* (in Romanian). Editura Tehnica, Bucharest, 1992.
4. Popovici, A., Toma, I., Sârghiuta, R., Abdulamit, A. *Earthquake analysis of an arch dam*. Proceedings 4th ICOLD Benchmark Workshop on Numerical Analysis of Dams, Madrid, 1996.
5. Sârghiuta, R., Abdulamit, A. *Nonlinear analysis of joint behaviour under thermal and hydrostatic loads for an arch dam*. Proceedings 3 rd ICOLD Benchmark Workshop on Numerical Analysis of Dams, Paris, 1994.

ARCH DAM ANALYSIS WITH BASE JOINT OPENING

Gerald Zenz*, Ernst Aigner*, Franz Perner*

1. ABSTRACT

The Schlegeis Arch Dam was designed as double-curvature arch-gravity dam in a wide spanned valley. The design and safety analyses were carried out with linear numerical models. As it is shown, the linear analysis provides an appropriate representation of the overall bearing behavior of the structure. Since the first impounding the dam is operated under planned conditions.
However, during the first filling of the reservoir unexpected high seepage into the bottom gallery was monitored. This was explained by local deformations at the dam's upstream heel. The construction of an elastic cut off wall solved the seepage problem.
To find an appropriate model for the interpretation of measured data and to derive an answer for the structural safety and integrity - considering this local phenomena - a detailed finite element model was developed. The linear analysis results show tensile stresses at the upstream heel of the dam. Paying attention to the geological site condition the model was updated with a perimetral base joint at the abutment, to allow the separation of the dam from the rock. To reduce the computational effort afterwards a coarse model was discretized.

This contribution deals with the numerical model assumptions and discussion of results gained with a continuous base joint over the entire dam abutment. The results show an opening of the base joint. The arch dam bearing behavior enables a safe redistribution of stresses. The results of these investigations are intended for further discussions in the community of Dam Engineers.

Keywords: Arch Dam Analysis, Base Joint Opening,
Stress Analysis, Dam Safety Assessment

* Verbundplan Consulting Engineers, Austria

2. DESCRIPTION OF SCHLEGEIS DAM

The Schlegeis arch dam is the main structure of the Zemm power plant in Austria. The dam was concreted between 1969 and 1971. The first filling was commenced in 1970 and full storage level was reached 1973.
The main data of the dam are as follows:

- Height 131m
- Crest length 725m
- Crest width 9m
- Maximum dam thickness 34m
- Total Concrete Volume 960000m^3
- Live Storage 127 Mill.m^3

The foundation of the dam consists of fairly uniform gneiss. It's schistosity plane strikes approximately parallel to the right bank abutment and has a very steep dip towards downstream. The intercalation of soft biotite schists in the schistosity plane of the gneiss has a thickness of up to several decimeters.
The grout curtain was built vertical at a distance of about 4m off the upstream dam toe. Due to the grout curtain a permeability of 1 Lugeon was achieved. About 3m off the grout curtain an inspection gallery which is open towards the rock was located directly on the surface of the foundation rock. Drainages were drilled from this gallery and from downstream to relieve the pressures in the lower part of the dam foundation.

Behavior of the Dam

The dam is installed with different kind of instrumentation system as these are:

- Plumb lines down to 80 m depth into the foundation
- Extensometers and Piezometers
- Uplift pressure cells embedded on the dam foundation.

The readings taken during the first filling confirm the behavior of the dam predicted by computations. However for the dam foundation a different behavior was envisaged.

During the first filling of the reservoir, a maximum rate of seepage of about 250 l/sec were encountered. The extensometer readings suggested a clear relationship between the width of rock joints beneath the upstream toe of the dam and the seepage flow.

Measurements of uplift pressure showed values of about 100% of the reservoir head upstream the inspection gallery, whereas downstream of the gallery the uplift pressure was reduced to 10% of the reservoir head in maximum.

Measures taken to improve the situation

Based on extensometer readings it could be elaborated, that high strains occur in the uppermost part of the foundation rock (of about 5m in depth) in a close vicinity to the upstream dam base. These led to the opening of cracks into the grout curtain and resulted in high seepage inflow into the gallery. Due to the presence of the gallery the uplift pressure could be reduced significantly.
To prevent this water seeping into the gallery an elastic cut off wall was constructed with 6 m into the rock and made by boreholes of 128mm in diameter. The upper part of the cut off wall is integrated into a reinforced concrete vault sealing the inspection gallery towards downstream.
After completion of the grouting works a drainage curtain inclining towards downstream was drilled.
After completion of the works the amount of seepage were reduced to 25 l/sec without increasing the uplift pressure which impairs the stability of the dams.

3. SYSTEM DESCRIPTION

Finite Element Mesh

The Finite-Elemente discretization for the dam and a sufficient portion of the foundation is made on the basis of quadratic, isoparametric 20 and 15 node volume elements. For the fine mesh 6 elements are foreseen in radial direction at the base of the highest blocks and three at the crest. The dam has 2553 elements and the foundation 8170 (see fig. 1). The coarse mesh has three elements in radial direction over the whole dam with 246 elements for the dam and 896 elements for the foundation. In both cases contact elements are introduced between the dam and the foundation.

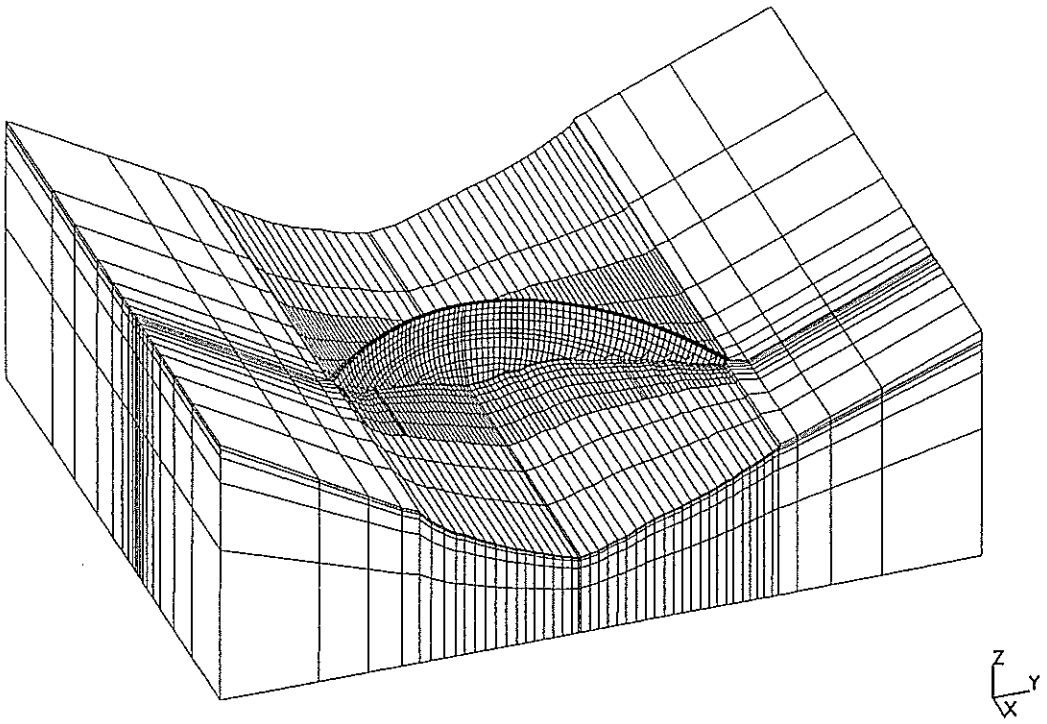

Figure 1: Downstream View of the Fine Finite Element Mesh

Material Behavior

The material behavior for the concrete is anisotropic for the loading dead weight to simulate the construction of the dam. For the subsequent loading cases an elastic material behavior is assumed. The rock foundation is modeled with an orthotropic material law according to the direction of the schistosity.
The material behavior are given in the following table:

	Rock	Concrete
Young's modulus E [GPa] (for rock E_{II})	30	25
Young's modulus E [GPa] (for rock E⊥)	10	
Poisson ratio ν	0.17	0.17
Density [kg/m^3]		2400
α_T		8.10^{-6}

The joint behavior of the interface between dam and rock foundation is modeled with isotropic Coulomb friction. The friction angle is $\varphi=45^\circ$ and no tensile stresses are allowed for being transmitted across the surface.

Applied Loading

For the investigation of the behavior of this arch dam two different analyses were carried out - first a linear analysis with a closed base joint and second a non-linear one with the possibility of opening of the base joint.

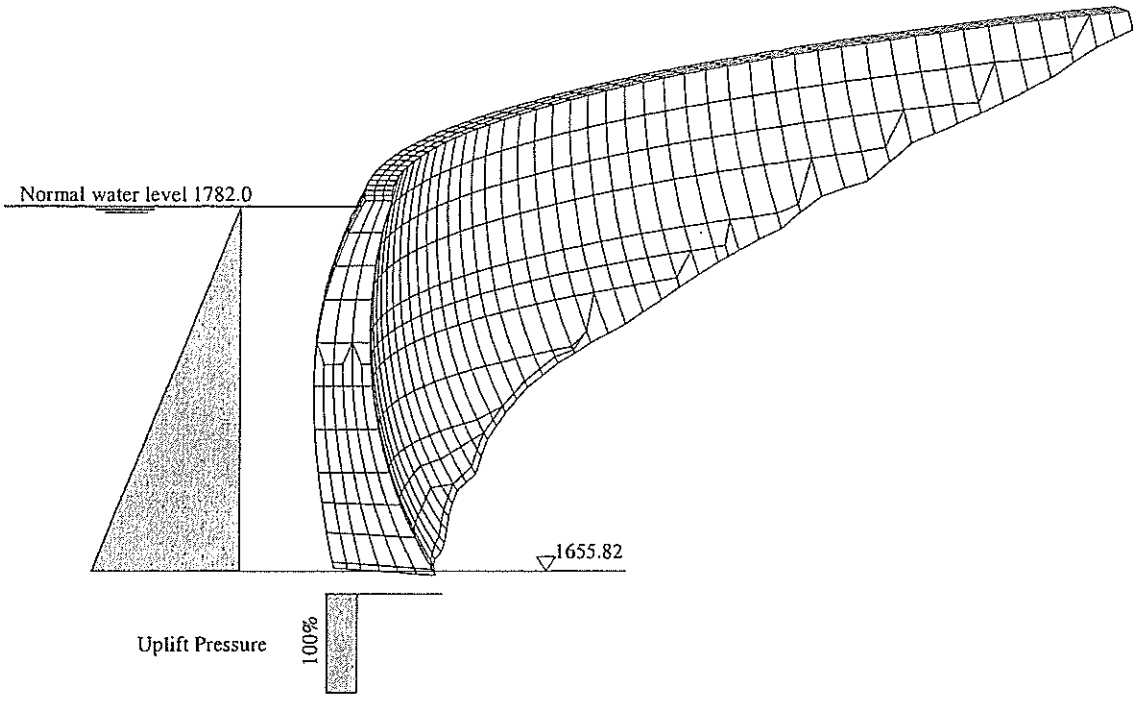

Figure 2: Dam Model, Water and Uplift Loading

The assumed loading conditions for each case is as following:

- dead weight loading - with independent columns
- water loading
- temperature loading
- and uplift pressure loading.

The water loading acts at the upstream face of the dam. The uplift pressure is included in about one third of the radial direction with 100% of the related water level height. The water loading and uplift pressure assumptions are shown in fig. 4.
For the loading case temperature the distribution of a measured summer-temperature field relative to the joint closing temperature is used.

4. NUMERICAL PROCEDURE

Contact Algorithm

The contact procedure required accounts for opening, closing and for frictional behavior in the defined interface. Numerical investigations are used to verify the numerical performance during static and dynamic analysis of joint elements (ICOLD benchmark, 1994 and 1996). Within the IVth benchmark the evaluated results by nonlinear block joint behavior during earthquake excitation with different finite element codes were compared against each other.

The contact condition together with the defined numerical parameters for contact formulation are displayed in fig. 3. Isotropic Coulomb model with a friction angle of $\varphi = 45°$ is used. The allowable shear stress transmitted within the contact surface is calculated with $\tau_{max} < \mu^*p$ for sticking state; the surfaces are glued to each other. If the current shear stress τ equals τ_{max}, the sticking state changes to sliding. This sliding is controlled in the program by $\gamma_{elastic}$ value, which is an allowed "sliding deformation" prior τ_{slide} is reached.

The contact algorithm itself is realized by a so called softened contact condition. This needs the definition of a contact pressure p_0 at the status closed. At a relative deformation between the two contact surfaces of c_0 zero pressure is transmitted in this contact zone. The pressure clearance relationship itself is an exponential function, resulting in a penetration of two bodies if the contact pressure is above p_0.

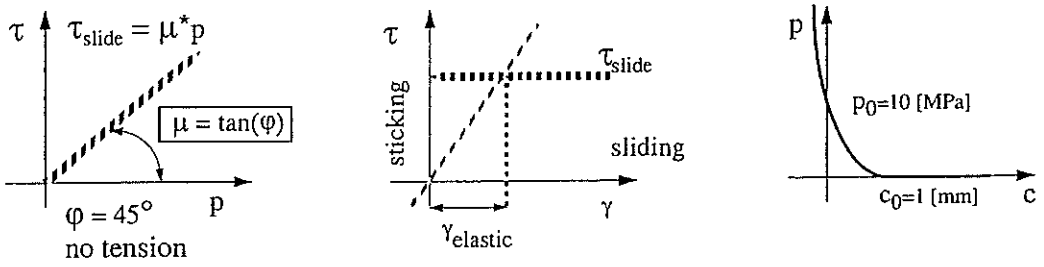

Figure 3: Coulomb friction with softened contact condition

5. LOADING SEQUENCE

The dead weight loading case is modeled taking the construction procedure into account. The concrete blocks are constructed as columns separated by vertical block joints. After completion of construction the block joints are grouted at a specific temperature. After the block joint grouting the arch dam supporting behavior is enabled for further loading cases. In this analysis the dead weight is applied for the entire dam structure with a material model with only significant vertical stiffness but reduced tangential and radial stiffness.
In the context of the used finite element code the change of material parameter - as this is necessary from dead weight application to water loading - would lead to a stress redistribution in subsequent loading cases. Therefore the stress state due to dead weight is written on file and reread into the model as initial stress state by applying dead weight loading. The equilibrium iteration carried out gives none deformations, but a changed structural behavior for the subsequent loading cases as these are water, temperature and uplift pressure loading.

6. ALLOCATED COMPUTER RESOURCES - PROGRAM USED

The computations are carried out on a Silicon Graphics Origin 200 Computer with 2 CPU's. The computer runs Irix 6.5 operating system and has 1024 MB memory installed. The finite elemente code used is Abaqus 5.8.

	Fine Model	Coarse Model
Scratch file	3.7 GB	255 MB
Result file	100 MB	100 MB
CPU Time all loading cases	42 h	43 min

7. PRESENTATION OF RESULTS

For reference purpose the results of a linear model are presented in terms of minimum principle stress and middle principle stress. The minimum principle stress represent for dead weight the vertical stress and for further loading hoop stress in the dam body. The middle principle stress represents the vertical stress component in the dam body. In the vicinity of the abutment the direction of the principle stresses have no specific orientation. The nonlinear model - with the proposed base joint - is presented for fine and coarse discretization.

Linear Model - Closed Base Joint

The presented dead weight loading is the first reference step for further calculations. This loading shows minimum principal stresses at the upstream heel of the dam at about 6MPa. At the downstream face of the dam the maximum principle stresses are between 0 to 0.5MPa for most of the surface and for a small portion in the vicinity of the abutment this tensile stresses reach values up to 0.8MPa (fig. 4 and fig. 5).

For the full loading case (Dead Weight, Water, Temperature and Uplift) under the assumption of a closed base joint the minimum principle stresses at upstream face of the dam body are hoop stresses at about 4 to 5MPa. The maximum tensile stresses at the heel of the dam are higher than 2MPa.

At the downstream face of the dam the minimum principle stresses in the dam body are hoop stresses and are between 4 to 5MPa. At the abutment the compressive stresses are higher than 6MPa. The maximum principle stresses are small and are less than 0.5MPa (fig. 6, fig. 7 and fig. 8).

The maximum radial deflection under full loading condition is 48mm. The deformation at the highest concrete block at the interface level concrete to rock and in radial direction is 6mm (see fig. 9).

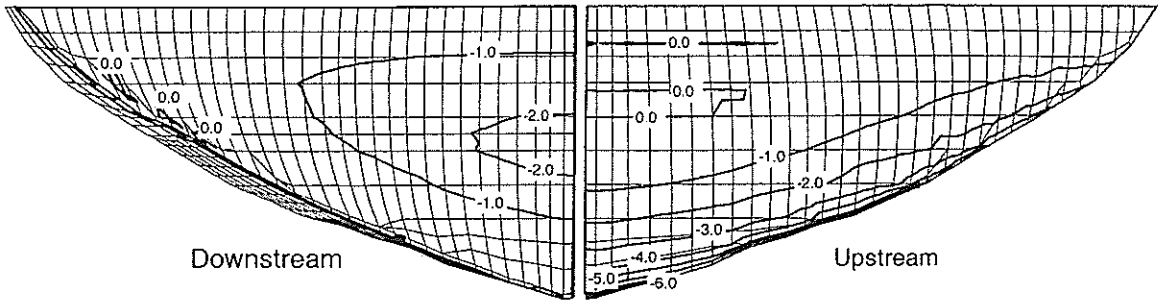

Figure 4: Dead Weight - Minimum Principle Stress

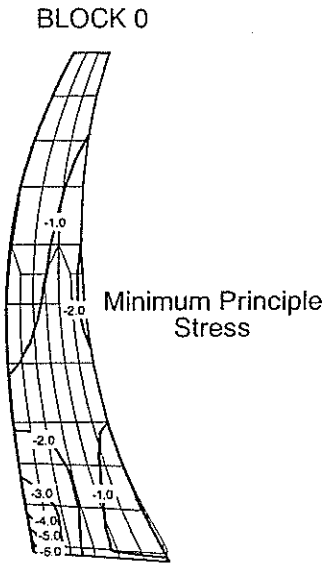

Figure 5: Dead Weight - Minimum Principle Stress - Cantilever

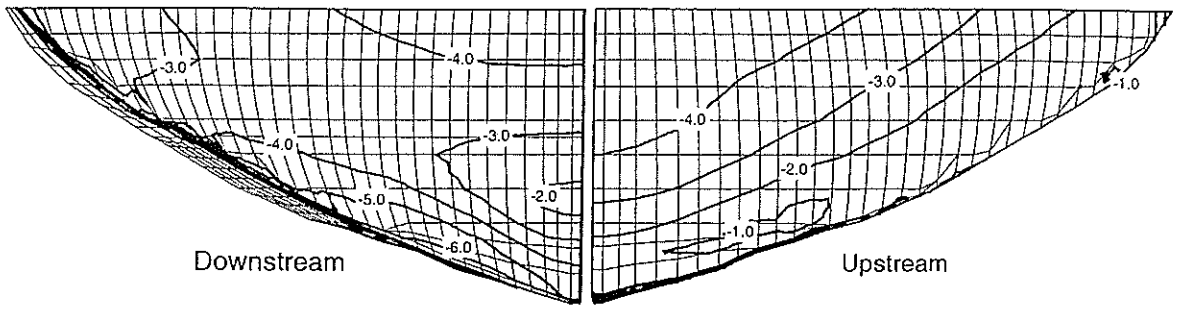

Figure 6: Full Loading - Closed - Min. Prin. Stress

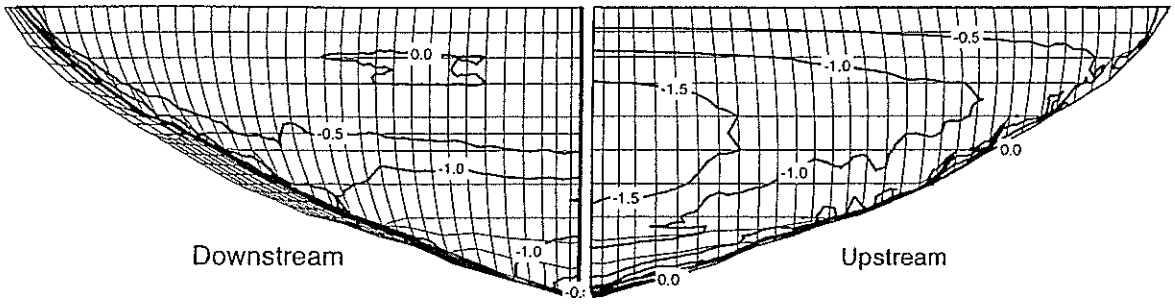

Figure 7: Full Loading - Closed - Middle Prin. Stress

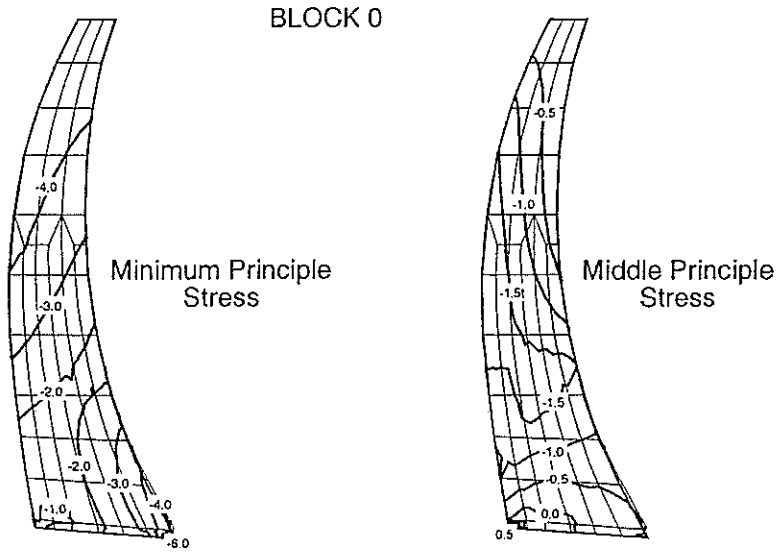

Figure 8: Full Loading - Closed - Cantilever

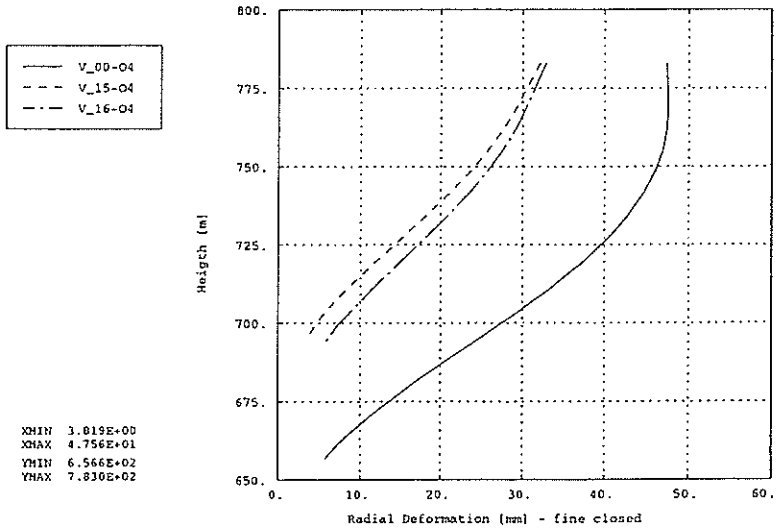

Figure 9: Full Loading - Closed - Radial Disp. Block 0, 15, 16

Nonlinear Model with base joint

The stress distribution for dead weight loading is equivalent to the results calculated with the help of the closed model. Under full loading conditions the base joint opens to a certain extent and the gained results are discussed.

In total two geometrically different discretized models are investigated. These are the so called fine model and the coarse model.

Results of the "Fine Model"

Compared to the linear model, in general an increase in compressive stress occurs for hoop stresses at the upstream face of the dam. This can also be seen for compression stress at the downstream abutment (fig. 10, fig. 11 and fig. 12). Due to the presence of uplift pressure the upstream heel of the dam is still under compression, though the dam itself has separated from the rock.

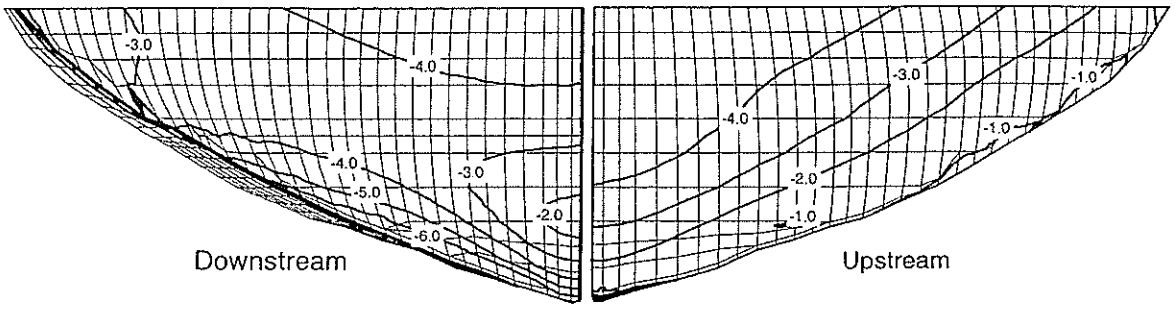

Figure 10: Full Loading - Open - Min. Principle Stress

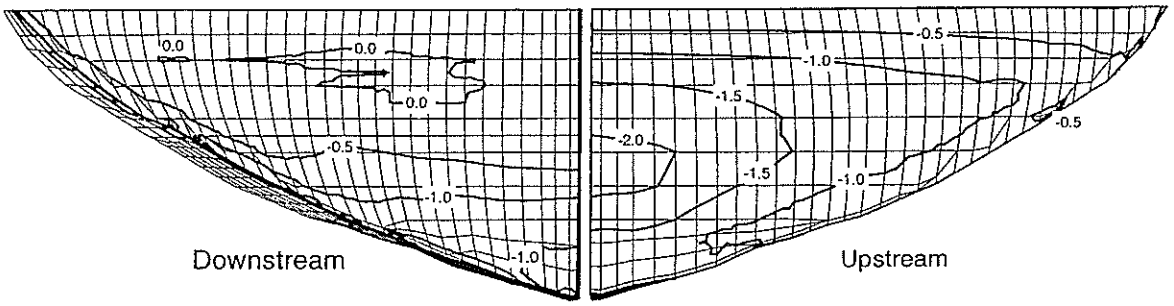

Figure 11: Full Loading - Open - Middle Principle Stress

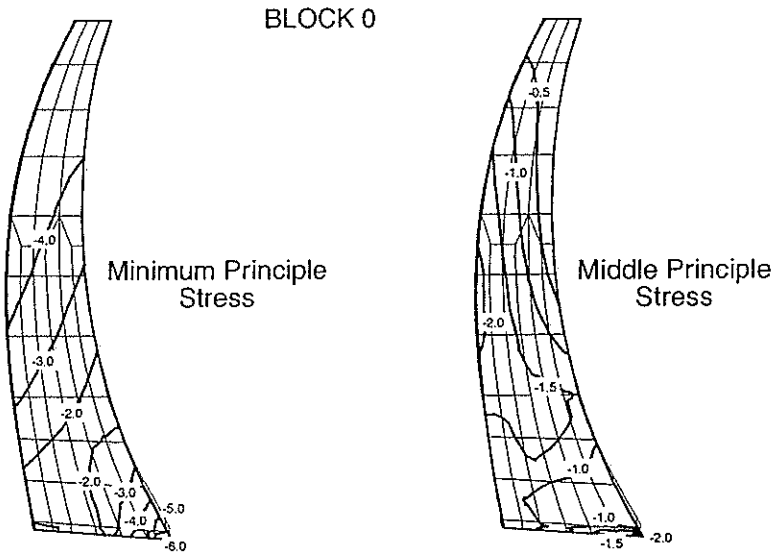

Figure 12: Full Loading - Open - Cantilever

The opening of the base joint along the entire dam abutment is shown in fig. 13. To a relative large extent the dam's base joint is open. (The displayed values are corrected against c_0, which is a numerical value of 1 mm). Within the base joint under compression, the resultant forces have to be transmitted.

The calculated radial displacements are at about 52mm for the block 0, and reduce to 34mm for block 16 and 39mm for block 15 (fig. 14).

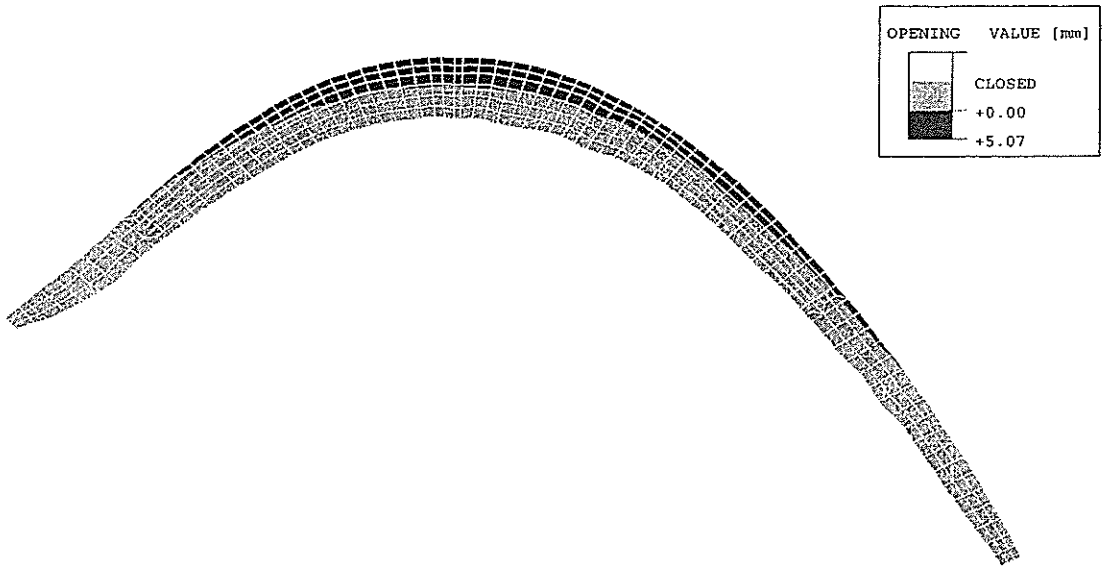

Figure 13: Full Loading - Opening Base Joint

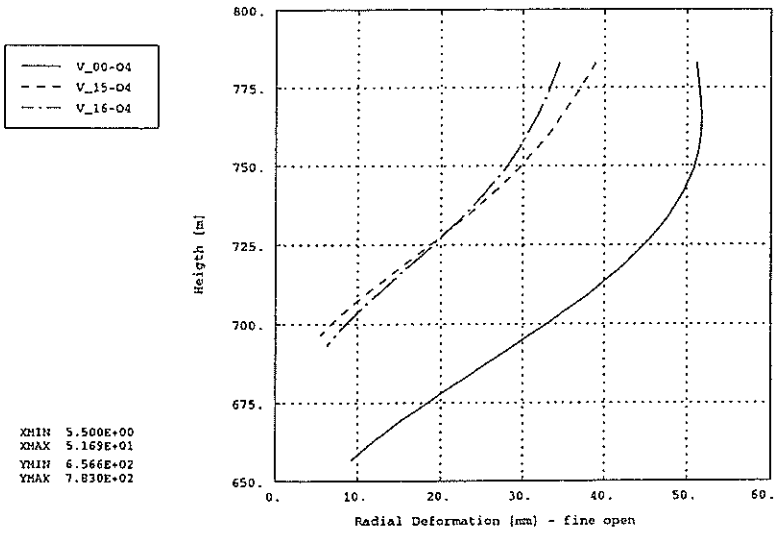

Figure 14: Full Load - Open - Radial Disp. for Block 0, 15, 16

The stress distribution along a radial line is shown on fig. 17. For the highest concrete blocks the diagram shows a base joint opening of about 42%. Nearly within the entire remaining cross section the contact failure condition is reached and sliding occurs.
Within blocks 15/16 the joint opens to an amount of 30% and 22% respectively. As it can be seen, sliding is only within the first 10m of the joint significant.

Results of the Coarse Model

The coarse model gives in general the same stress distribution along the entire dam as it can be calculated with the fine model. Due to the different discretization with the same element family, the stresses as well as the deformations gradients are less for the coarse model.
From the subsequent figures (15,16,18) it can be seen, that the stress distribution is in line with Fig. 10, 11 and 12 of the fine model.
The differences between the fine and the coarse model in terms of normal stress and base joint opening are shown on fig. 19.

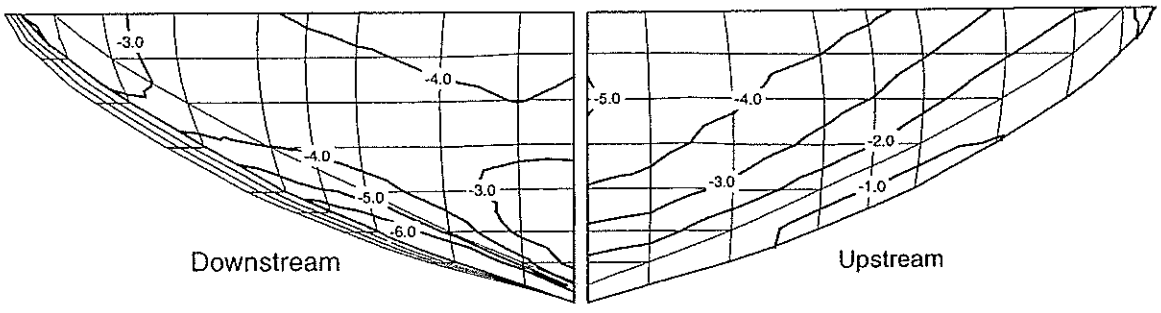

Figure 15: Full Loading - Minimum Principle Stress - Surface

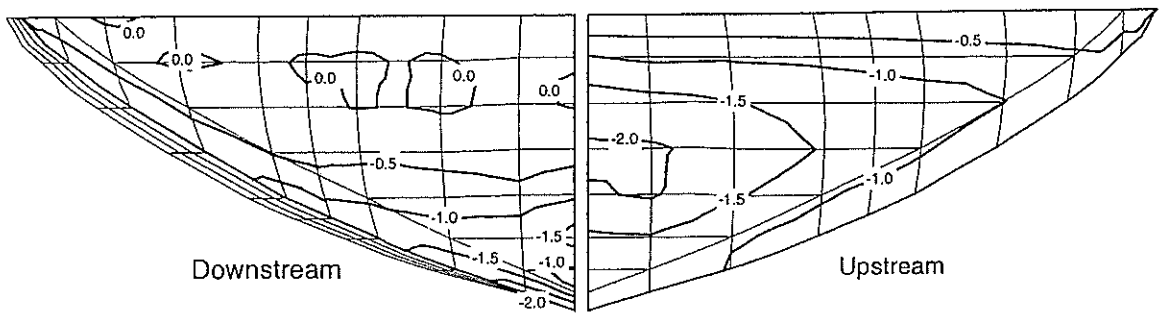

Figure 16: Full Loading - Middle Principle Stress - Surface

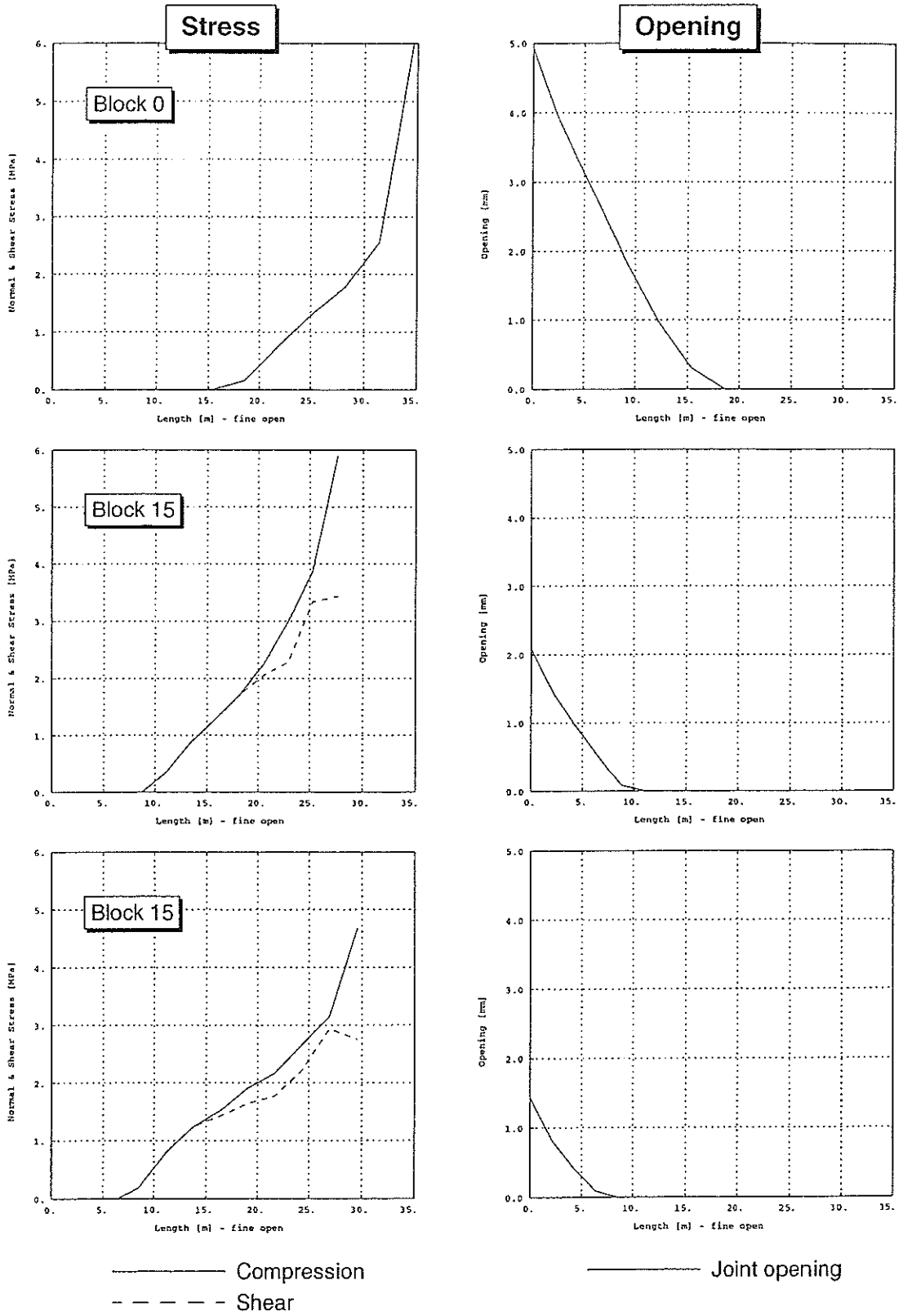

Figure 17: Full Loading - Compressive Stress - Joint Opening

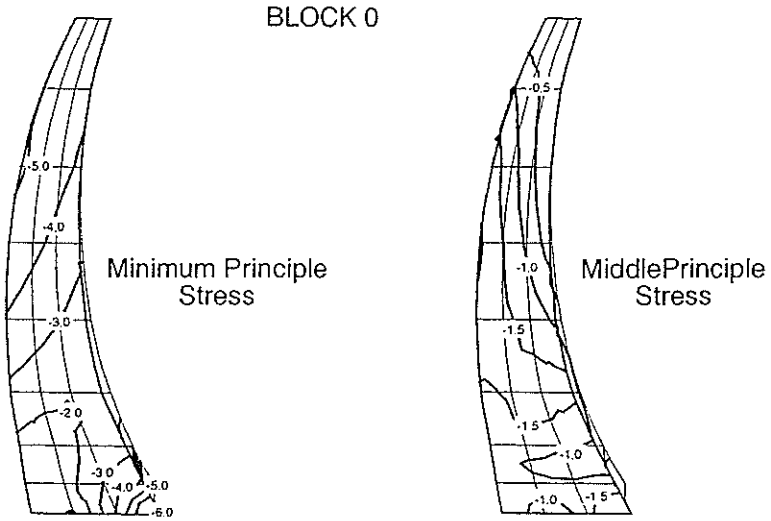

Figure 18: Full Loading - Cantilever

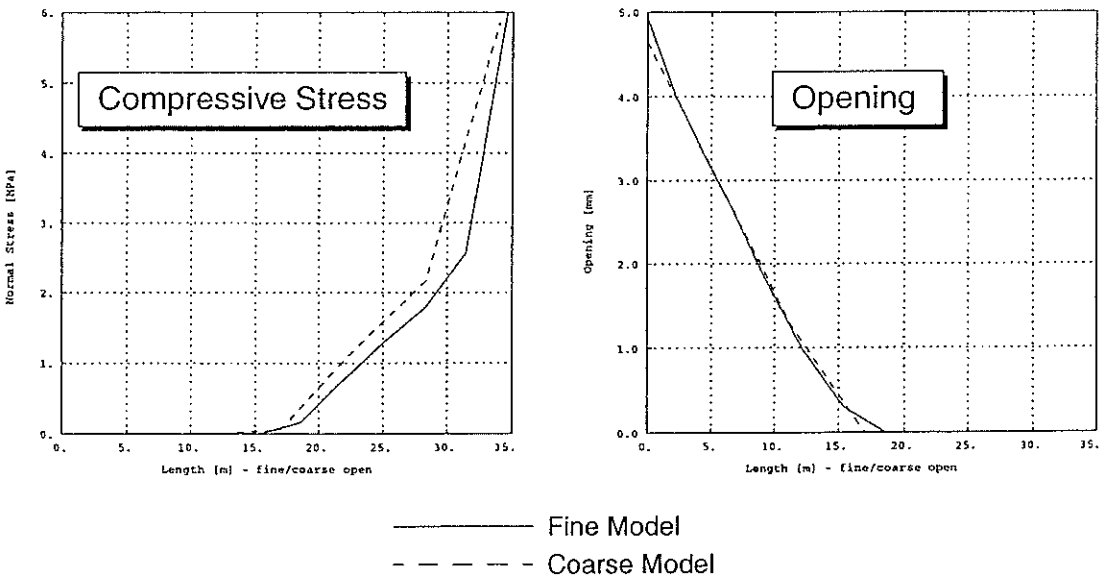

Figure 19: Comparison Fine - Coarse Model

8. SLIDING STABILITY

Displayed on the level of stresses in the interface the friction criteria is processed for block 0, 15 and 16 for full loading condition. The applied Coulomb failure criteria - residual friction angle of $\varphi = 45°$ only - is reached nearly all over the entire cross section for block 0 (see fig. 20).

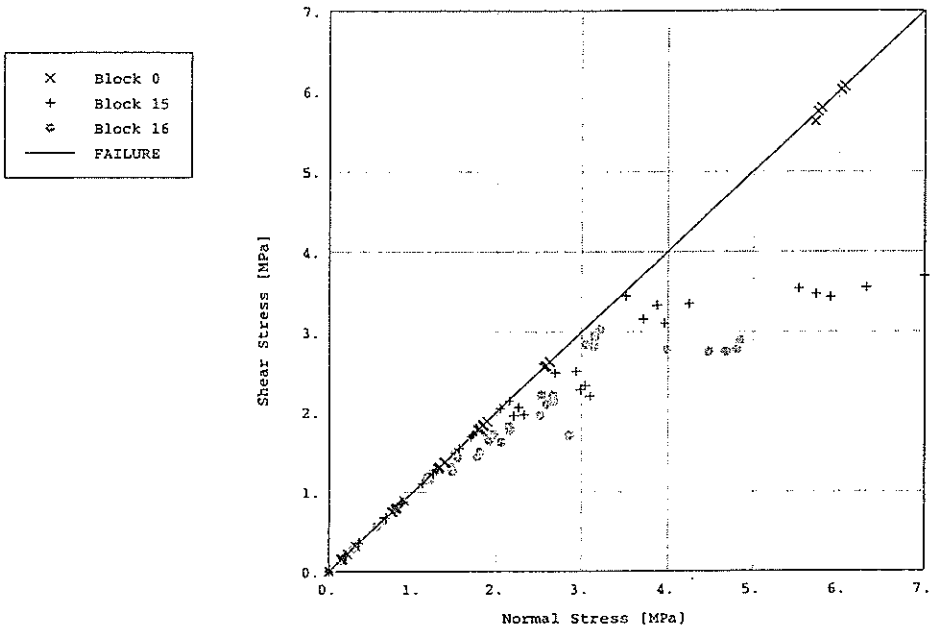

Figure 20: Coulomb Failure Criteria for Block 0, 15, 16

However, for the sliding safety assessment of the structure the shear strength, found by material tests, is $\tau_{max} = 4.0 + 0{,}75\ \sigma_N$.

The sliding deformations are of about 5.2 mm.

The distribution of the vertical reaction force along the projection of the crown axis at the abutment is shown on fig. 21. The reaction force per m in MN for dead weight, dead weight and water loading and under full loading conditions is displayed. It can be seen, that the water loading and water loading together with the applied uplift pressure results in a significant vertical unloading of the dam.

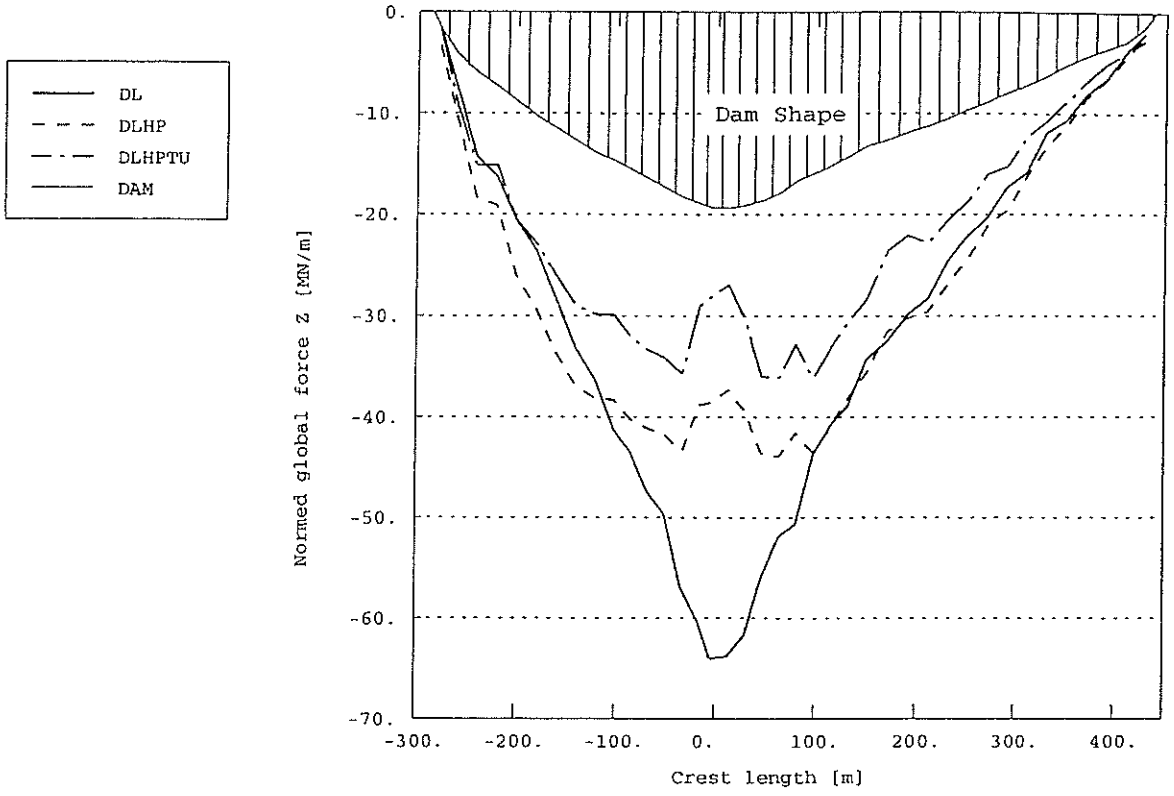

Figure 21: Normed vertical global force along the Crown Axis

9. CONCLUSIONS

Under a given model assumption the numerical analysis for Schlegeis Arch Dam is carried out. Respectively dead weight, water, temperature and uplift pressure loading are investigated.
For these loading cases the first analysis run was a standard finite element analysis with a linear model. The evaluated results show tensile stresses at the upstream heel of the dam.

Additionally to the linear analysis a model is employed, which gives the dam the possibility to separate from the foundation rock. For the entire dam in general the results calculated show compressive stresses slightly higher than for the linear model. Under full loading condition the upstream heel of the dam separates for an amount of 5mm from it's rock foundation. Due to the uplift pressure acting in

the base joint no tensile stress is apparently in the dam abutment.
Due to the nonlinear analysis a more favorable stress state in the dam structure can be evaluated. The hoop stresses in the dam increase slightly and the tensile stresses at the abutment decrease. Additionally to this investigation the sliding stability considerations at the dam abutment needs a reevaluation.

Based on the nonlinear analysis it is shown that the compressive stress level increases slightly in the dam body. Compared to the linear model a safe redistribution of stress occurs, due to the base joint opening.

REFERENCES

Abaqus, 1998: Theory and User's Guide, Hibbit, Karlsson&Sorensen, Inc., Version 5.8-1.

Dams in Austria, Schlegeis Arch Dam, Austrian National Committee on Large Dams, Vienna 1991.

Flögl H., Stäuble H.: Experience with the supplementary installation of an elastic diaphragm in the rock of Schlegeis arch dam, ICOLD, Vienna, Q.66, R.41, 1991.

R. Widmann, M. Eiselmayr: Analysis of an arch dam using the loading distribution method, Int. Symp. for Numerical Analysis of Dam, Swansea 1975.

G. Zenz, P. Obernhuber & F. Perner: Static arch dam analysis considering nonlinear block joint behavior, in IIIth International Benchmark Workshop on Numerical Analysis of Dams, Paris, France 1994.

G. Zenz, E. Aigner & P. Obernhuber: Dynamic arch dam analysis considering nonlinear block joint behavior, in IVth International Benchmark Workshop on Numerical Analysis of Dams, Madrid, Spain 1996.

5th INTERNATIONAL BENCHMARKWORKSHOP
ON NUMERICAL ANALYSIS OF DAMS

THEME A2

IMMINENT FAILURE FLOOD FOR A CONCRETE GRAVITY DAM

DENVER, COLORADO JUNE 2-5, 1999

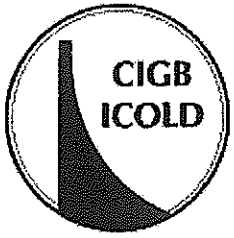

1. Introduction

Imminent failure flood (IFF) of a concrete dam is an important parameter in dam safety assessment which should be compared with the probable maximum flood (PMF). Failure of concrete dams may occur by overturning or sliding. In either cases, the analyst must not only consider the horizontal hydrostatic forces, but also the vertical uplift ones (with due account for the efficiency of the drains). Failure tends to initiate at the rock/concrete interface which is the weakest part of the structure and, depending on the rock/concrete bond, may progress along the joint or into the rock.

The objective of this Theme A2 problem is thus to determine the IFF for a concrete gravity dam under specified conditions.

2. Analysis Data

- Geometry of the main section is provided in fig. 1.
- Rock and concrete are homogeneous, isotropic, impervious and are characterised by (see also fig. 2):

Material parameters	Rock	Concrete
Density [kg/m^3]	2,700	2,400
Uniaxial compressive strength σ_c [MPa]	40.0	24.0
Uniaxial tensile ultimate strength σ_u [MPa]	2.6	1.3
Ultimate tensile strain ε_u	0.63×10^{-4}	0.54×10^{-4}
Fracture strain ε_f	6.00×10^{-4}	5.00×10^{-4}
Softening law for tensile strength	Linear	Linear
Young's modulus E [MPa]	41,000	24,000
Poisson ratio ν	0.10	0.15
Specific mode I fracture energy G_f^I [N/m]	200	150

- The rock-concrete interface is pervious and is characterised[1] by (see figg. 3a, b):

Material parameters	Mean values
Shear stiffness K_s [MPa/mm]	20
Peak cohesion [MPa]	0.7
Residual cohesion [MPa]	0.0
Tensile strength [Mpa]	0.0
Friction angle [deg.]	30
Dilatancy angle [deg.]	10
Softening module H [MPa/mm]	-0.7

[1] For explanation of parameters see the Appendix and fig. 3

- Uplift Pressure depends on drain efficiency as shown in fig. 4.

- Loads: dead load and then hydrostatic load (including uplift) by increasing the water elevation until it reaches the IFF level. Neglect rock self weight.

3. Requested results

The participants have to determine:
1. The IFF level and the corresponding failure modes;
2. Load versus crest displacement curves for the incremental analyses;
3. Stresses distributions along the closed rock-concrete interface for a water elevation equal to 0.8 IFF;
4. Crack opening displacements for a water elevation equal to 0.8 IFF;

in the following cases:
1. Neglecting uplift pressures;
2. Uplift pressure with 100% efficiency of the drain (see fig. 4 - case 2);
3. Uplift pressure with zero drain efficiency (see fig. 4 - case 3).

Notes:

1. In all cases, the participant should determine if the crack propagates along the joint or may branch into the rock. In the case of uplift pressure and kinked crack, the uplift pressure should be assumed to be present up to the crack tip in the rock.

2. Participant can select any post-elastic model they deem appropriate.

3. In order to facilitate comparison of results, it is strongly recommended that all participants analyse the following simple test problem.
   Given the sliding-mass system reproduced in fig. 5, let the horizontal forces increase progressively. Provide the shear stress versus horizontal displacement diagram for point G.

Appendix A: Joint at the Concrete-to-Rock contact

Direct shear strength data from tests performed on core samples including concrete-to-rock contacts provide experimental results that are in good agreement with the classical idealisation represented in fig. 3a. Following the figure, for low values of strain, the joint presents a purely elastic deformation which is linearly related to the stress by the following incremental law:

(1) $$d\gamma = d\tau / Ks$$

where γ represents the tangential relative shift occurring in the joint between concrete and rock, Ks the tangential stiffness of the joint, τ the shear stress acting over the joint surfaces. When the peak shear strength, τ_p, is reached, the joint enters the softening state, characterized by a fall of resistance that follows the law:

(2) $$d\gamma = d\tau / H_a$$

where H_a is a negative parameter with the dimension of a stiffness that can be considered a phenomenological softening module.

In this phase the shear displacement can be splitted into two contributions:

(3) $$d\gamma = d\gamma_{el} + d\gamma_{pl}$$

where $d\gamma_{el}$ and $d\gamma_p$ are, respectively, the elastic and plastic component of the shear strain given by:

(4) $$d\gamma_{el} = d\tau / K_s$$

(5) $$d\gamma_{pl} = d\tau / H$$

In eq. (5) H represents the actual softening module. By inserting expressions (2), (4), (5) in equations (3) one obtains H_a in terms of H and K_s :

(6) $$Ha = (H \times K_s) / (K_s + H)$$

During softening, shear strength decreases linearly up to a residual value equal to τ_r .From this point on, the behaviour is perfectly plastic.

In addition to the tangential shift γ, a normal relative displacement, v, can be frequently observed between contact faces; the total relative displacement is therefore inclined of an angle ψ (dilatancy angle) with respect to the contact surface given by:

(7) $$\psi = \text{atan}(v/\gamma)$$

With reference to a Mohr-Coulomb failure model, the Mohr envelopes of peak and residual strengths are indicated in fig. 3b.

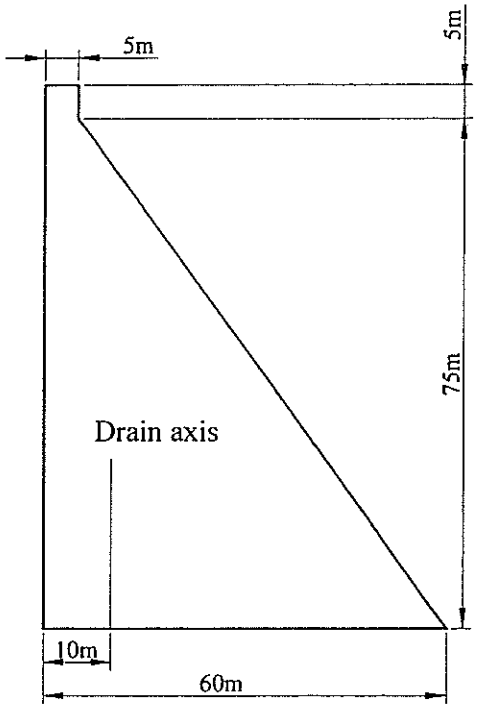
5m
5m
75m
Drain axis
10m
60m

Fig. 1

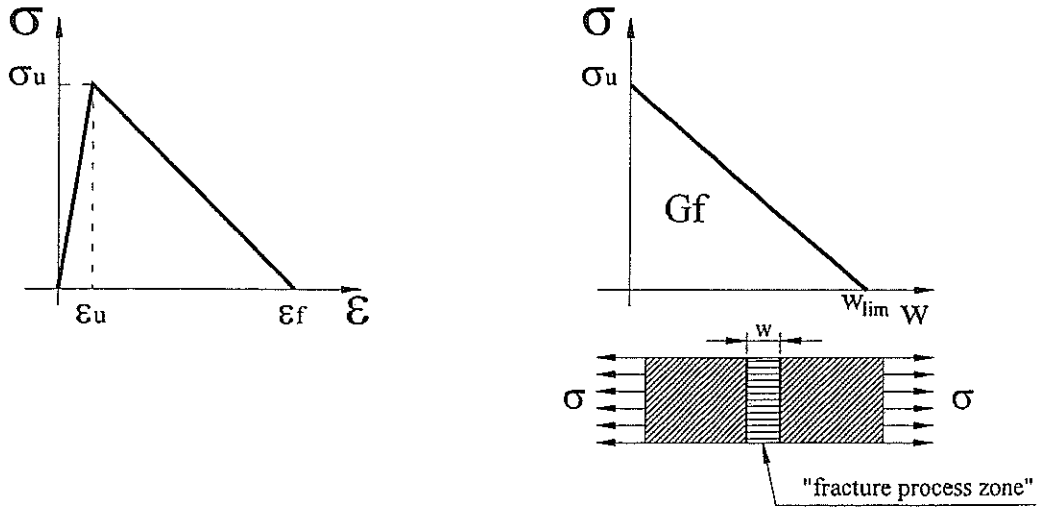
σ
σu
εu
εf
ε
σ
σu
Gf
Wlim W
w
σ
σ
"fracture process zone"

Fig. 2

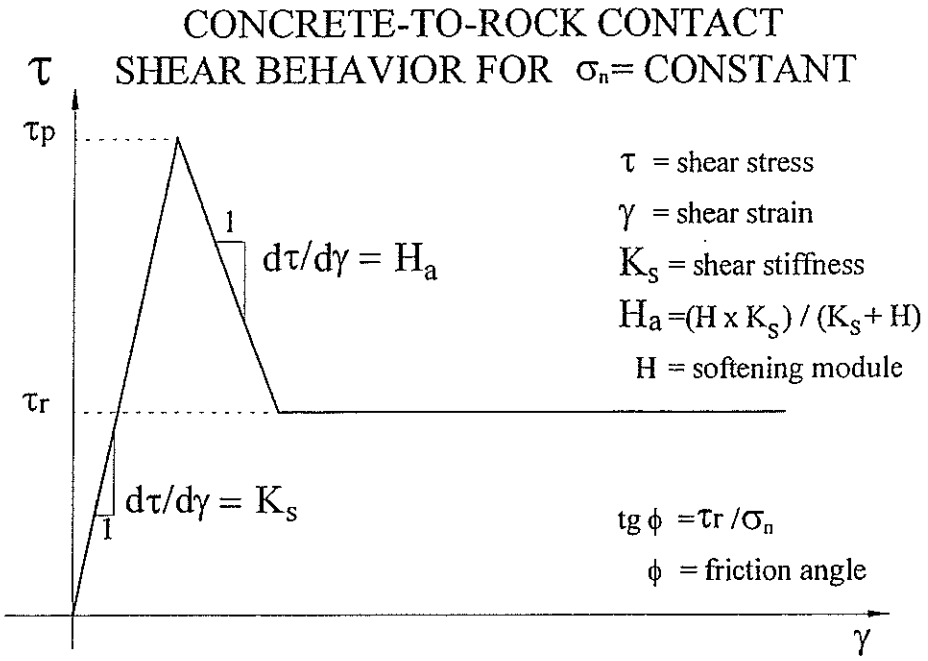
CONCRETE-TO-ROCK CONTACT
SHEAR BEHAVIOR FOR σn= CONSTANT
τ
τp
τr
1
dτ/dγ = Ha
1
dτ/dγ = Ks
τ = shear stress
γ = shear strain
Ks = shear stiffness
Ha =(H x Ks) / (Ks+ H)
H = softening module
tg ϕ =τr /σn
ϕ = friction angle
γ

Fig. 3a

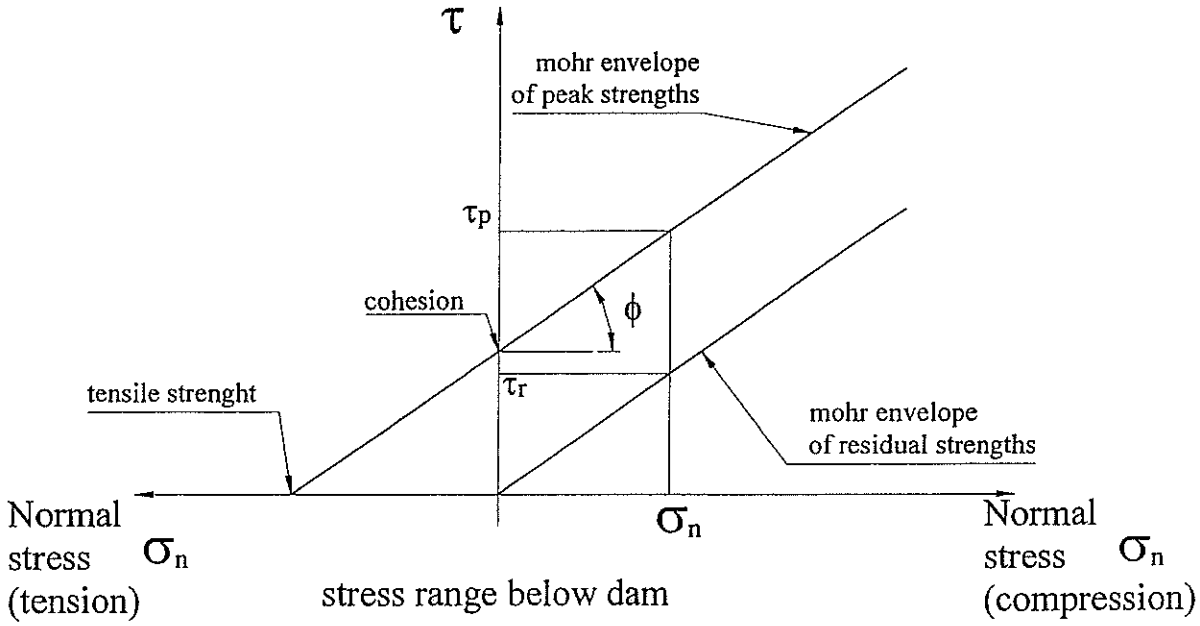
τ
mohr envelope
of peak strengths
τp
cohesion
ϕ
τr
tensile strenght
mohr envelope
of residual strengths
Normal
stress σn
(tension)
σn
Normal
stress σn
(compression)
stress range below dam

Fig. 3b

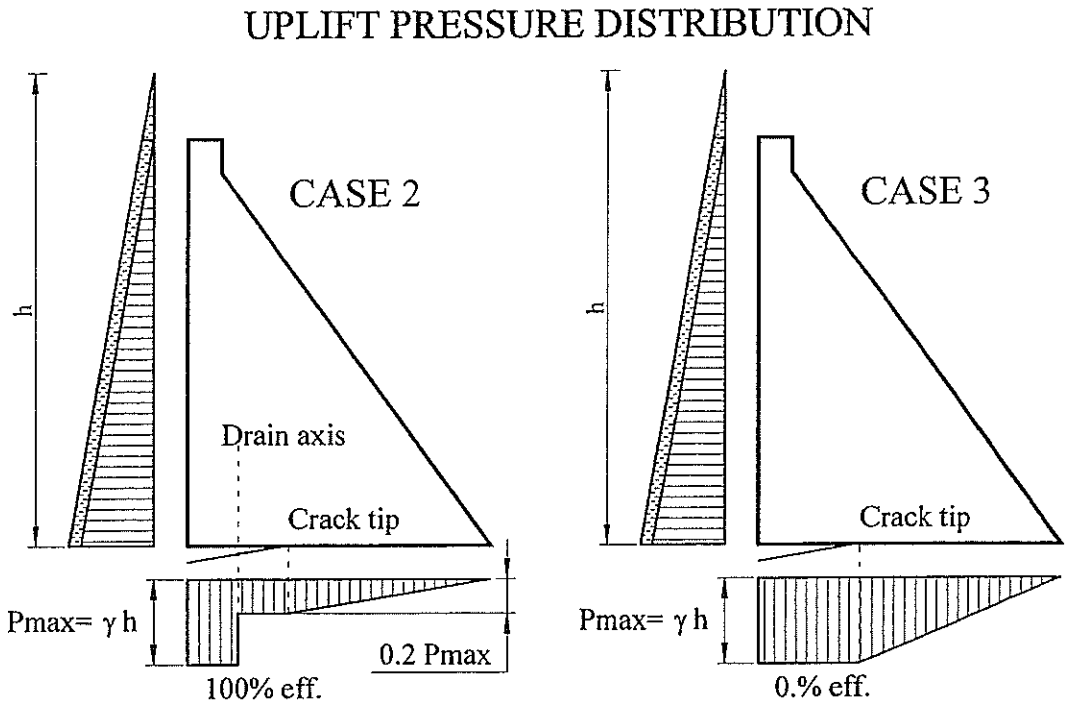
UPLIFT PRESSURE DISTRIBUTION
CASE 2
CASE 3
h
h
Drain axis
Crack tip
Crack tip
Pmax= γ h
Pmax= γ h
0.2 Pmax
100% eff.
0.% eff.

Fig. 4

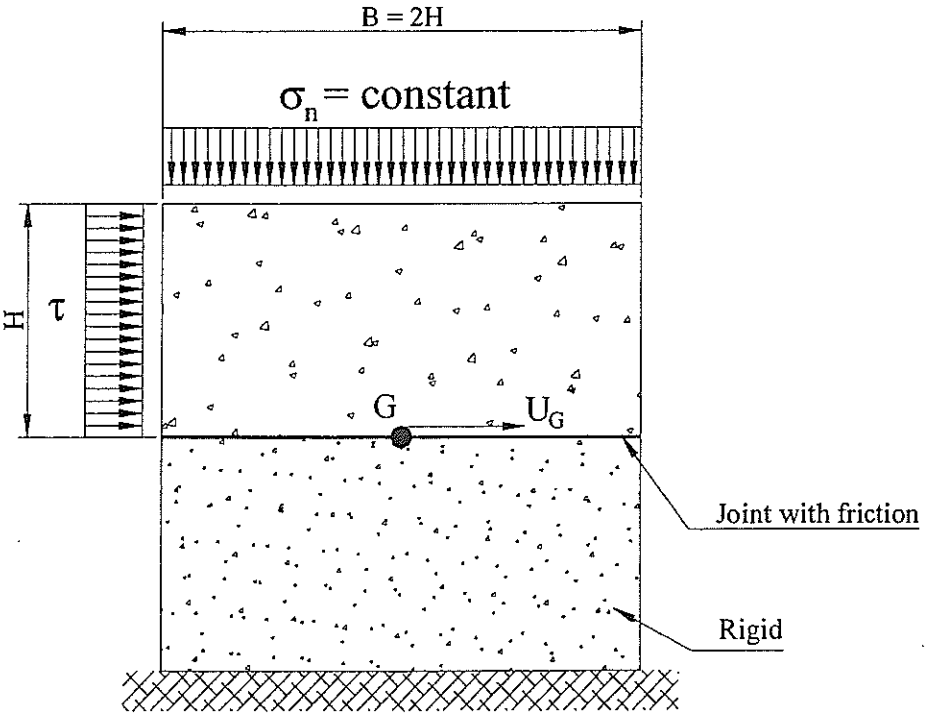
B = 2H
σn = constant
H
τ
G
UG
Joint with friction
Rigid

Fig.5

Fifth Benchmark Workshop on
Numerical Analysis of Dams
June 2-5, 1999
Denver, Colorado U.S.A.
Theme A - Concrete Dams
Problem A2

Synthesis of Methods and Analyses

P. Palumbo

CONTRIBUTIONS

Six contributions were foreseen in the final program of the Fifth B.W. for problem A2. In the end we have only three papers to compare (see Tab. 1).
Most likely the reason of this quantitatively scarce participation is related to the complexity of the problem that was underestimated during the definition phase.
We have further to recognise that this remarkable burden cannot be easily sustained without any kind of financial support. In this regard, I wish to thank Prof. Linsbauer and my friends at ENEL for their collaboration thanks to which the proposed problem of the failure of gravity dams didn't collapse under its own weight.

FINITE ELEMENT SOFTWARE

Tab. 2 provides the short list of computer codes used by the participants. P1 used FRAC_DAM that is a dedicated software. Then we have ABAQUS, a commercial software, in which P2 has implemented an "ad hoc" user subroutine to reproduce the Mohr Coulomb Yield criterion with cohesion softening. Last we have the DIANA code used by P3 in its standard version.

SHEAR TESTS

As you know, a shear test to check the capability of reproducing joint properties was requested in the specifications. In this test an increasing displacement is imposed on the upper block to activate all resisting resources of the joint. Fig.1 shows results obtained by

participants. In all cases the slopes of elastic range and softening branch are in practice coincident. We can observe that:

- P1 has not extended the test up to the attainment of the pure frictional behaviour;
- P2 has carried out a complete set of tests with loading-unloading cycles with different amplitudes;
- P3 has carried out only a monotonic test.

METHODS AND ANALYSES

Although few authors provided their contribution, several approaches have been adopted. It is worth summarising the main features of the analyses in the following.

P1: Linsbauer, Bhattacharjee

Smeared Crack Concept and a Thin-Layer-Formulation for the joint element have been used. The interface is replaced by an equivalent solid continuum with a finite thickness. Not in compliance with the instructions of the workshop, the authors have assumed a non zero tensile strength (0.35 MPa) at the rock to concrete contact.
With regard to the loading sequence, an initial analysis has been conducted for self-weight, initial reservoir elevation and associated uplift pressure.
Subsequently, the reservoir elevation is increased to the IFF level which may or may not overtop the dam. The uplift pressure is always proportional to the latest reservoir elevation.
In the paper it is not specified if uplift pressure acts on both dam and rock sides and in which way uplift is made consistent with the crack length. All cases requested have been considered.

P2: Manfredini, Chillè and Meghella

First L.E.F.M. with J-integral approach is adopted for case 1 only. The critical J value has been assumed equal to the energy dissipated during a shear test reported in the literature (Jc = 300 N/m - Energy for mode two, G_{II}).
The assumed value is about equal to the value that one can derive by the cohesion linear softening law provided by the instructions for the workshop.

This approach is not in compliance with the specifications because the joint is not modelled explicitly. Results depend on the value assumed for fracture energy in the joint and this parameter was not explicitly provided. Therefore direct comparisons of results obtained from LEFM with results from other analyses are not meaningful. Nevertheless the proposed solution represent an effective contribution in highlighting LEFM ability to treat failure problems in gravity dams.
Then a N.L.F.M. approach with three models has been used.
In all cases non linear behaviour has been restricted at the rock to concrete interface.

- Model 1 considers mode I fracture with a low value of tensile fracture energy Gf (GI= 40 N/m); therefore a non zero tensile strength is assumed (0.28 MPa). Sliding is suppressed by geometrical constraint.
- Model 2 considers a Mohr-Coulomb yield criterion without softening and with zero tensile strength; two analyses with different values of cohesion are considered:
  - c=0
  - c=0.7 MPa
- Model 3 considers a Mohr-Coulomb yield criterion with cohesion softening, and no tensile strength. All parameters are in compliance with the specifications.

Therefore only model 3 complies with the instructions provided for the workshop. The joint has been reproduced in this model as it was in the shear test. Only Case 1 has been solved with this model. With regard to loading sequence, non proportional loading has been considered with uplift increasing simultaneously with water level.

P3: Palumbo, Pellegrini, Giuseppetti

First the rigid block method has been used.
Then the NLFM approach has been adopted. The Rankine/Von Mises multi surface yield criterion with tensile strength softening has been used for concrete and rock whereas Coulomb friction and cohesion softening at rock-concrete interface.
Three finite element models with different levels of global and local refinement of the meshes have been considered in solving case 1.
With regard to loading sequence, P3 has examined two cases. The first considers proportional incremental loading and can be considered representative of an ideal very fast filling

of the reservoir whereas the second considers non proportional increment of loading and could be assumed to reproduce a slow filling. In both cases (proportional and non proportional loading) uplift has been applied simultaneously with hydrostatic loads. Possible paths in loading sequence are indicated in the fig. 2. In the analyses path n.2 (dashed blue line) has been adopted but other paths have been also tested finding that the results depend remarkably on the sequence considered.

DIVERGING CHOICES INVOLVED IN THE ANALYSES

The main diverging features involved in the analyses carried out by participants may be summarised in the following items:

- Concrete and rock modelling: plasticity and smeared cracking or damage modelling and smeared cracking.
- Strength criteria (Mohr/Coulomb, Rankine/Von Mises) with or without softening;
- Peak values of cohesion and tensile strength;
- Interface elements with zero thickness and Coulomb friction or thin continuous elements with smeared crack;
- Levels of mesh refinement;
- Loading distributions and sequences;
- Non linear system solution procedures.

These factors may affect the results in such a way as to make quantitative comparisons impossible. Therefore in most cases only qualitative considerations can be outlined.

MAIN QUANTITATIVE COMPARISONS

With regard to quantitative comparisons, first let's compare in fig. 3 horizontal displacements of the dam crest for **case 1** (no uplift). Lines with belong to P3, lines with × to P2 and the very small black stretch to P1.
The full line with is relevant to the refined mesh whereas the dashed line with refers to the locally extra refined model. Comparing these two curves we can note that the locally extra refined model is stiffer than the refined one.
The × and black continuous stretches result very close to lines with in their own displacement ranges. We will look at a zoom of these parts of the diagram later.

Still in fig. 3 the dashed lines with × refer to plastic models without softening. It is interesting to note that the plastic model with non zero cohesion reaches the same limit level obtained from models with softening, even if this happens for a remarkably greater displacement.
Last comment, it would have been good to receive data letting us examine the whole curves to establish if they start from different initial conditions after the weight loading has been completed.
Zooming the diagram around the short stretches we can better appreciate some features (fig. 4). First we can note that the solution of P2 (the line with ×) arrives at a certain point and then undergoes a strange snap back. It is strange because the return path is higher than the preceding branch. It is reasonable to think that here the algorithm fails.
The derivative of the curves, that is the tangent stiffness of the model condensed at the crest horizontal displacement, deserves a further comment. We can observe the both the black stretch and the line with × have a slightly lower slope with respect to the line with ; this indicates that the model of P3 is stiffer probably due to the lower level of mesh refinement.
In case 2 we have only results from P1 and P3 (fig.5). The closeness of the results is no longer maintained most likely as a consequence of different paths in loading sequence.
For case 3 we can compare again three solutions (fig. 6). I remind you that P2 has used here a model not in compliance with the instructions since it assumes a tensile fracture energy for the joint; in addition in this model sliding at rock to concrete interface was geometrically constrained.
The comparison would not be meaningful; nevertheless it is worth noting that the red curve has a starting point remarkably different with respect to the green line. Since at the end of weight loading the structure is still linear, all starting points should be practically coincident unless additional constraints are imposed on the model.
Looking at the small black stretch provided by P1 we observe that it is located slightly below the crown level at 80 m. and that its derivative is practically zero; on the other hand the line with proceeds onward up to the level of 92 m. We can further observe (fig. 7) that this line presents a little "snap back" around the crown level. This indicates a certain difficulty encountered by the algorithm in overcoming this level.

STRESSES FOR CASE 1

Comparison of stresses relevant to the water level equal to the 80% of the limit value can only be performed between P1 and P3 for case 1.
Vertical stresses along the dam base are shown in fig. 8. We note a general agreement with the exception of some divergence located upstream and downstream. These are most likely attributable to:

- the tensile strength greater than zero assumed by P1;
- the lower level of mesh refinement adopted by P3;

The same observations hold for shear stresses shown in fig. 9.

GENERAL SUMMARY OF FUNDAMENTAL RESULTS

Let's now summarise the main results looking at tab. 3.
Case 1 : a good agreement can be observed between P1 and P3 when the refined and extra refined meshes are considered. The convergence is attained even if P1 assumed a non zero tensile strength for concrete to rock joint.
This parameter seems not to affect the failure level significantly when both shear and tensile strength are considered, at least in absence of uplift. A quite good agreement can be also observed between:

- the result that P2 obtained using the model which adopted the Mohr Coulomb criterion without cohesion softening and with zero tensile strength
- and the result of P1.

Case 2: The agreement observed between P1 and P3 is lost in this case. The divergence should not be ascribed to the tensile strength assumed by P1 because the lower water level is attained in the analysis where the tensile strength is considered. The difference in this case might be ascribed to loading sequence or distribution.
Case 3: The same considerations as for case 2 are still valid. However a perfect agreement between the rigid block method and the result of P1 must be underlined.
Last, looking at results obtained considering proportional loading, we can observe a remarkable overestimation of the limit water level with respect to any other solution.

CONCLUDING REMARKS

- The stability failure of the gravity dam has been analysed by means of several approaches; in spite of the differences in modelling choices, a certain degree of convergence among results can be recognised, at least in absence of uplift.

- However the results have pointed out some aspects of the problem which deserve further study for better understanding.

- Numerical experimentation is necessary to gain greater confidence about the robustness of algorithms in non linear solution procedures especially when a fast softening post peak behaviour is expected.

- Only parameters that are actually significant in the characterisation of the real scale physical phenomenon should be used. In this regard analysts need more certain knowledge of the parameters with respect to which the collapse limit is more sensitive (cohesion, tensile strength, fracture energy, softening laws etc).

- The realistic hydraulic filtration rate and reservoir filling velocity should be duly considered.

Contributions

P1
Linsbauer, Bhattacharjee
(University of Technology Vienna)

P2
Manfredini, Chillè, Meghella
(ENEL PIS Milano)

P3
Palumbo, Pellegrini, Giuseppetti
(ENEL ISMES Bergamo)

Tab.1

Finite element software

P1:	FRAC_DAM	Dedicated software
P2:	ABAQUS	Commercial software; a special subroutine for cohesion softening has been developed
P3:	DIANA	Commercial software; only library elements have been used

Tab.2

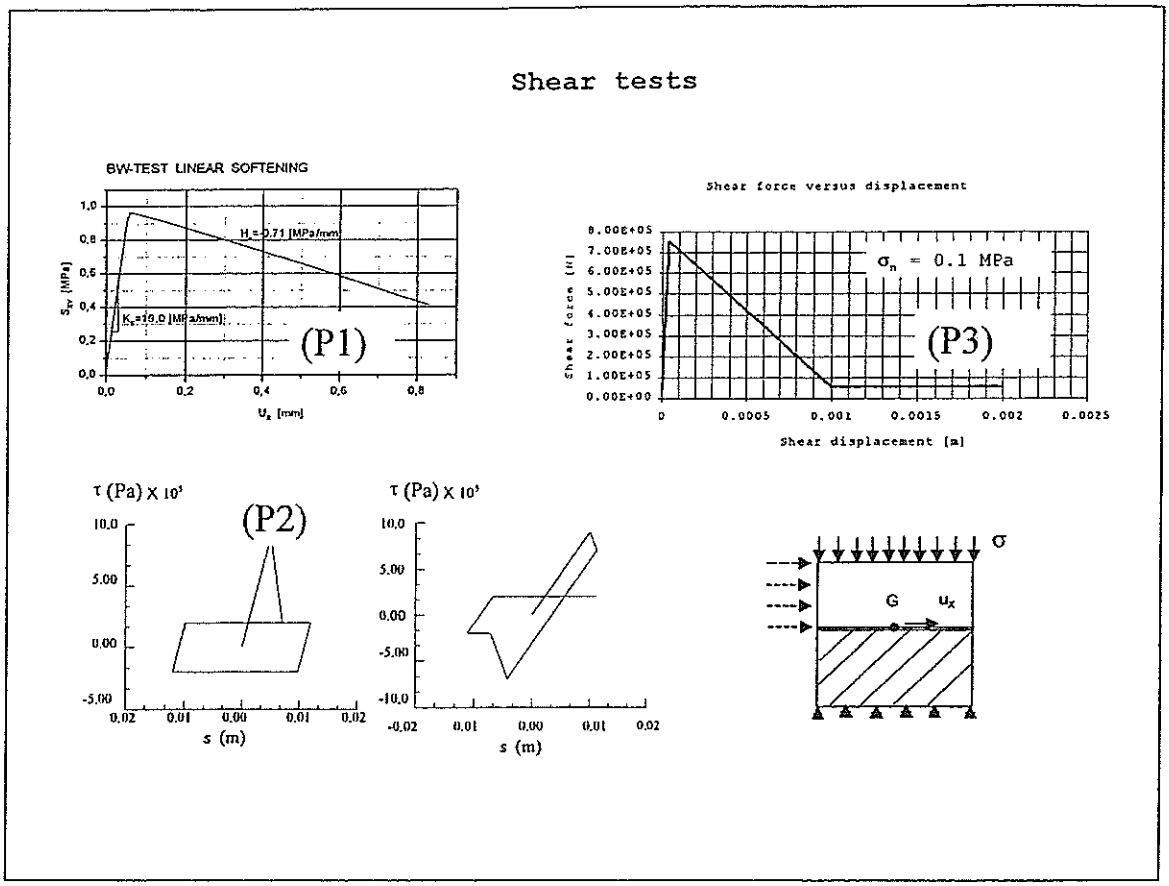
Shear tests
BW-TEST LINEAR SOFTENING
H=-0.71 [MPa/mm]
K0=10.0 [MPa/mm]
(P1)
Shear force versus displacement
σn = 0.1 MPa
(P3)
Shear displacement [m]
τ (Pa) X 10⁵
(P2)
s (m)
σ
G
ux

Fig. 1

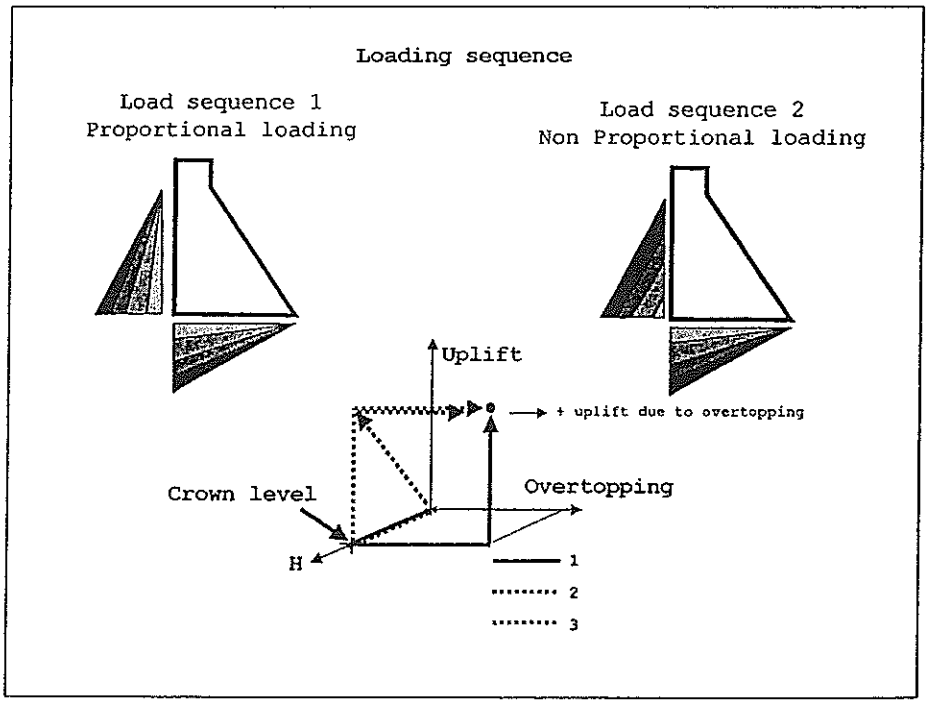
Loading sequence
Load sequence 1
Proportional loading
Load sequence 2
Non Proportional loading
Uplift
+ uplift due to overtopping
Crown level
Overtopping
H
1
2
3

Fig. 2

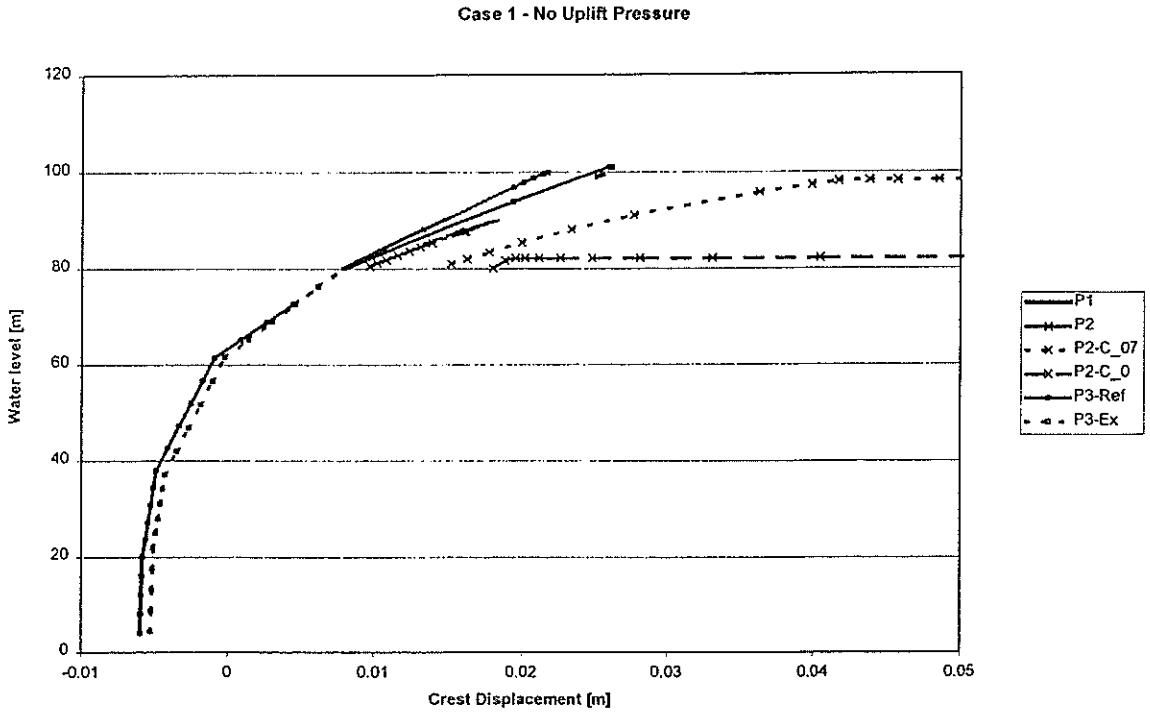
Case 1 - No Uplift Pressure
Water level [m]
Crest Displacement [m]
120
100
80
60
40
20
0
-0.01
0
0.01
0.02
0.03
0.04
0.05
P1
P2
P2-C_07
P2-C_0
P3-Ref
P3-Ex

Fig. 3

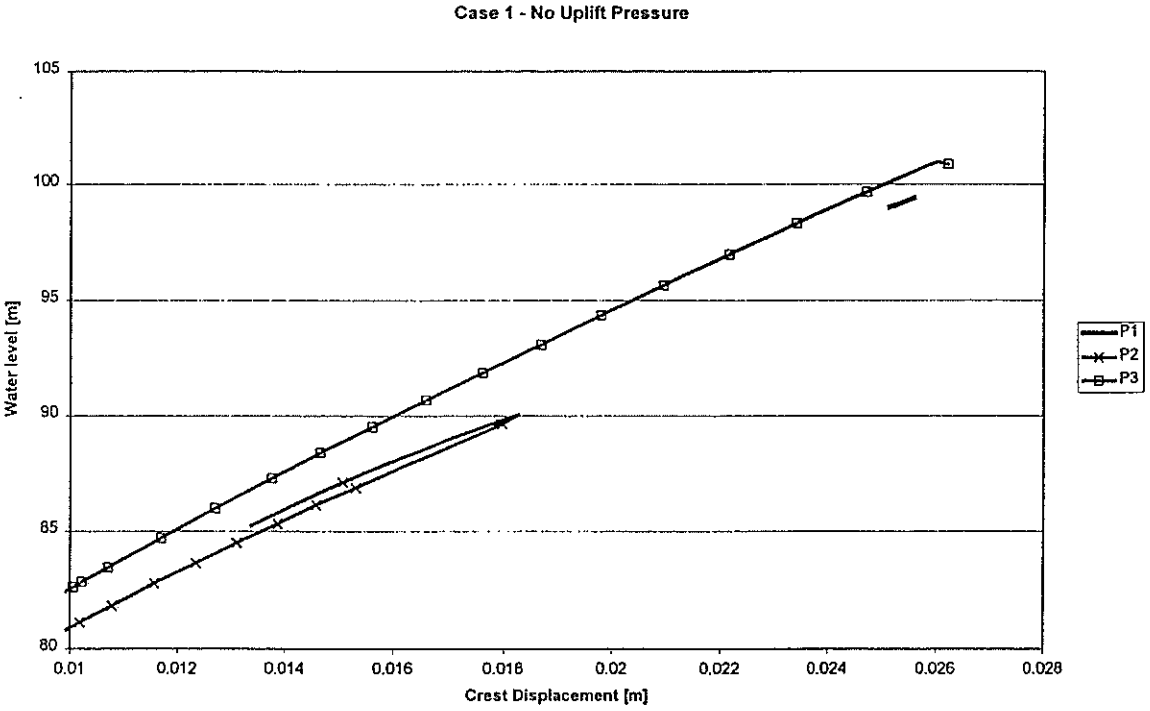
Case 1 - No Uplift Pressure
Water level [m]
Crest Displacement [m]
105
100
95
90
85
80
0.01
0.012
0.014
0.016
0.018
0.02
0.022
0.024
0.026
0.028
P1
P2
P3

Fig. 4

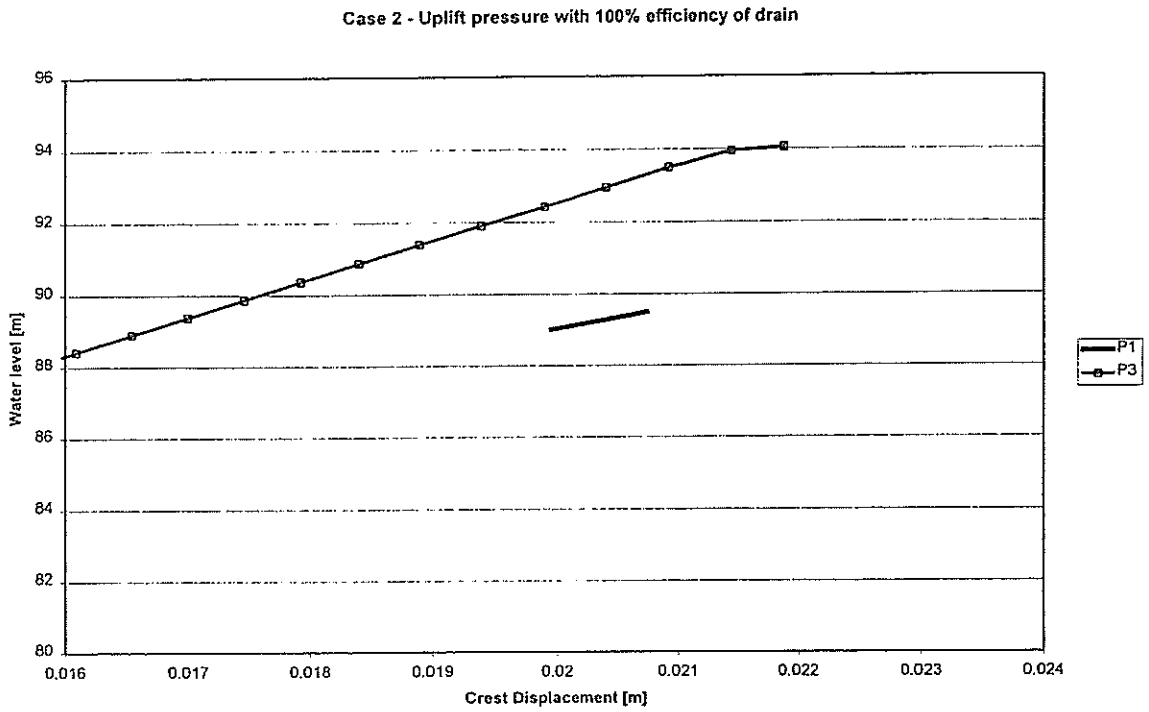
Case 2 - Uplift pressure with 100% efficiency of drain
Water level [m]
96
94
92
90
88
86
84
82
80
0.016
0.017
0.018
0.019
0.02
0.021
0.022
0.023
0.024
Crest Displacement [m]
P1
P3

Fig.5

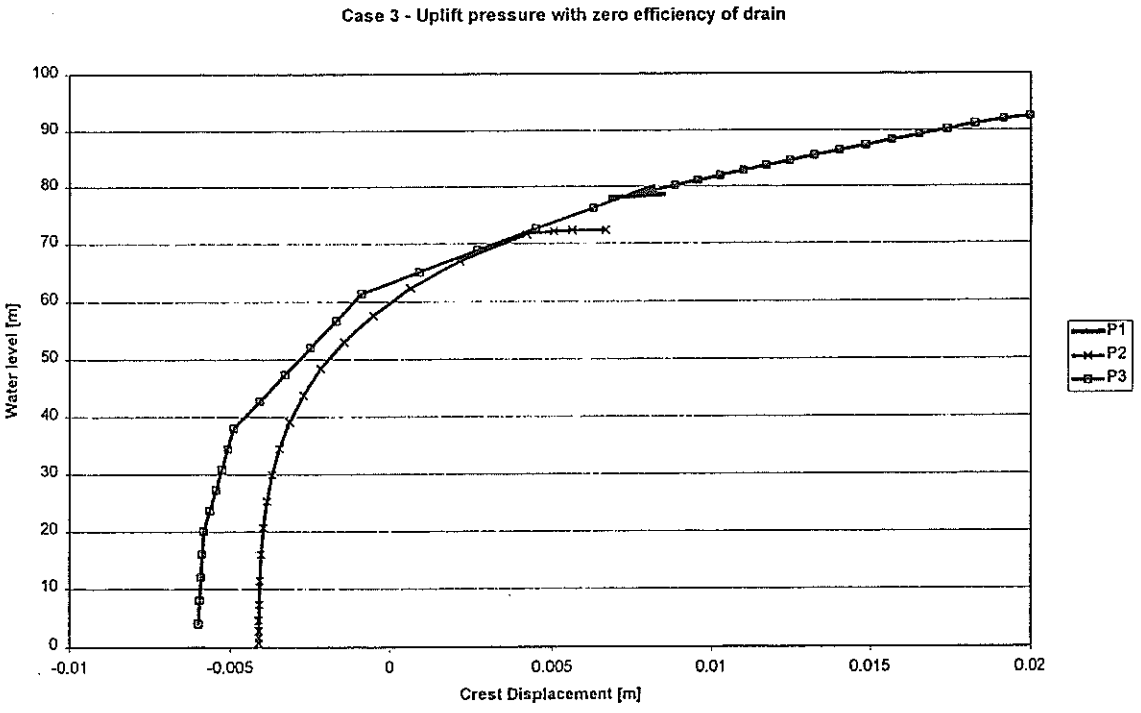
Case 3 - Uplift pressure with zero efficiency of drain
Water level [m]
100
90
80
70
60
50
40
30
20
10
0
-0.01
-0.005
0
0.005
0.01
0.015
0.02
Crest Displacement [m]
P1
P2
P3

Fig.6

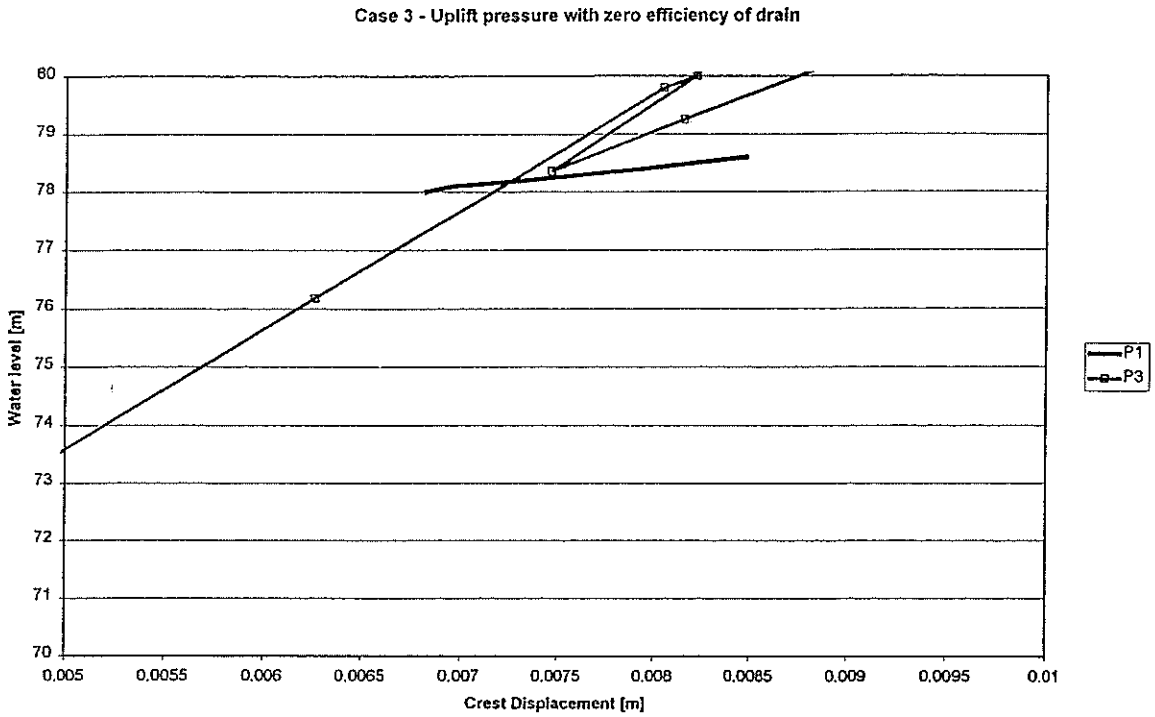
Case 3 - Uplift pressure with zero efficiency of drain
Water level [m]
80
79
78
77
76
75
74
73
72
71
70
0.005
0.0055
0.006
0.0065
0.007
0.0075
0.008
0.0085
0.009
0.0095
0.01
Crest Displacement [m]
P1
P3

Fig. 7

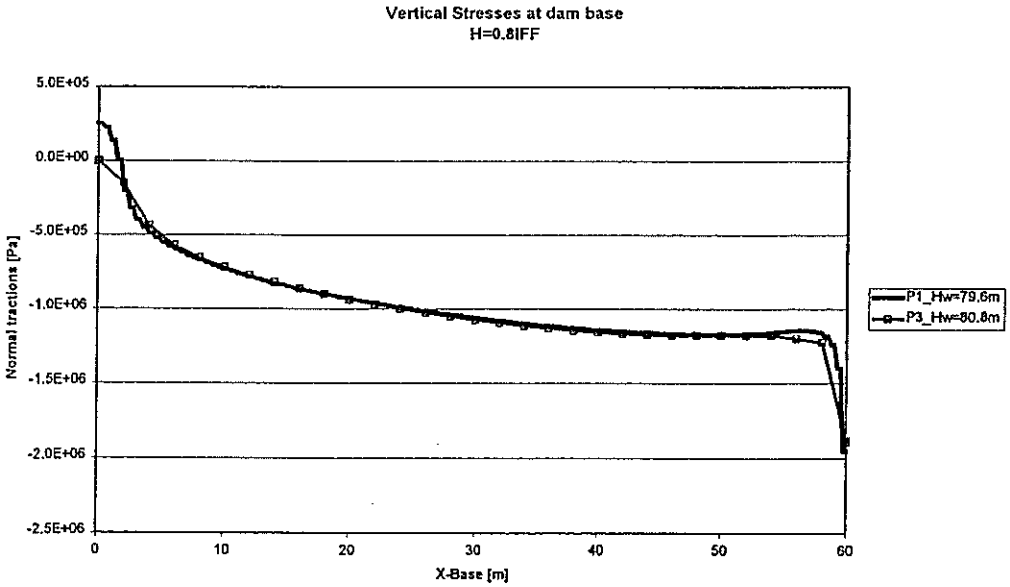
Vertical Stresses at dam base
H=0.8IFF
Normal tractions [Pa]
5.0E+05
0.0E+00
-5.0E+05
-1.0E+06
-1.5E+06
-2.0E+06
-2.5E+06
0
10
20
30
40
50
60
X-Base [m]
P1_Hw=79.6m
P3_Hw=80.8m

Fig. 8

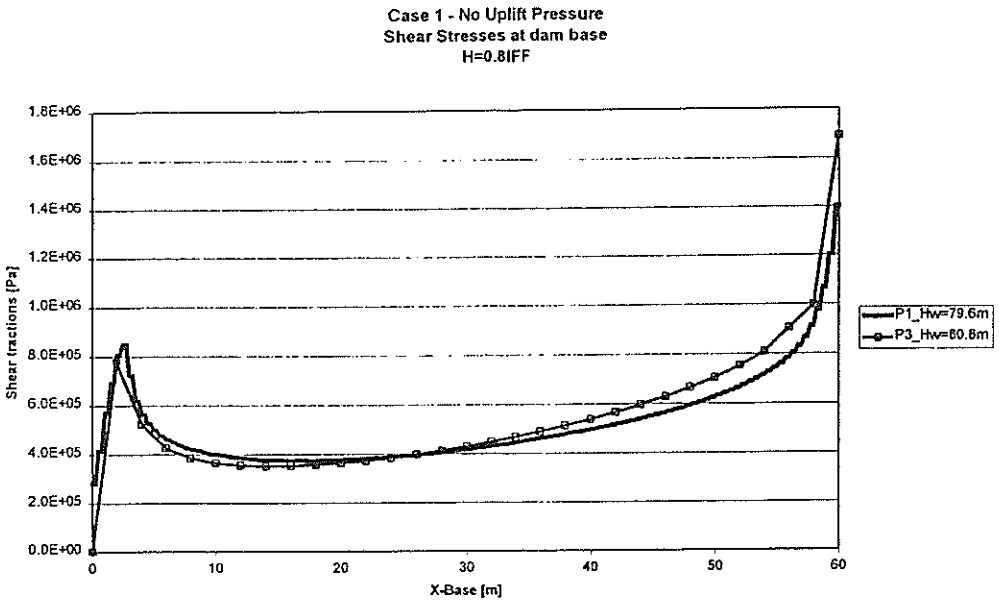

Fig. 9

General summary of main results

IFF

Analysis	IFF (m) Case 1		Case 2		Case 3	
[illegible]		79 [illegible]		[illegible]		78.7
P2_LEFM_II		~140		-		~120
P2_NLFM_I		~125		-		72.0
P2_MC_C0		82		-		-
[illegible]		[illegible]		-		-
P2_MC_CS		90		-		-
P3_R_BLOCK		109		-		79.3
P3_RANVMI_1	109	105				
[illegible]	112.0	[illegible]	112.5	[illegible]	107	92.0
P3_RANVMI_3	111	[illegible]				
	Loa_s1	Loa_s2	Loa_s1	Loa_s2	Loa_s1	Loa_s2

Tab. 3

DAM SAFETY ASSESSMENT DUE TO UPLIFT PRESSURE ACTION IN A DAM-FOUNDATION INTERFACE CRACK.

Herbert N. Linsbauer*
Sudip Bhattacharjee**

INTRODUCTION

In traditional practices, the rigid-body equilibrium approach of structural mechanics is used to study the dam-foundation interface behavior under uplift pressure effects. The relevant assumption that a crack would extend along the interface up to the point of equilibrium between the force of the water acting inside and the compressive forces generated in the dam, naturally, casts doubt on the reliability of such results. The recent technological development in the field of fracture mechanics of cementitious materials, in terms of material characterization and analytical/numerical simulation, offers the possibility of undertaking a realistic investigation of the water pressure effects at the dam-foundation interface cracks. The objective of this paper is to assess the inflow flood resistance of a concrete gravity dam, for various conditions of uplift pressure distribution, by using a damage mechanics based finite element formulation of the dam-foundation interface.

Interface Cracks

Interface cracks always have been a subject of intensive investigation, especially, because of the oscillatory behavior of the stress and displacement fields, in the vicinity of the crack tip, under the assumption of an elastic characteristic of the dissimilar media. This behavior is associated with an inter-penetration of the

*Vienna University of Technology
Karlsplatz 13, A-1040 Wien,Austria

**University of Windsor
Windsor, Ontario, Canada, N9B 3P4

crack surfaces, which has no physical significance. A multitude of models has been developed, to overcome this problem, varying from a homogeneous thin layer idealization to an extended model with continuously varying material behavior between the two adjacent structural sub-domains. Specific to cementitious composite interfaces, the energy release rate concept has been used under the considerations of kinking out and trapping mechanisms. A comprehensive treatise of the behavior and the modeling of (interface) joints is given by Tinawi et al. (1998). The current investigation, involving uplift pressure effects on inflow flood resistance of dam-foundation system, utilizes a thin layer interface joint model developed by the same authors (Tinawi et al. 1998).

GENERAL CONSIDERATIONS

In view of fracture mechanics of cementitious materials, it seems necessary to add some comments concerning the validity of the material parameters, especially, in the case of mass concrete with aggregate sizes up to 100 mm and more. The testing of representative samples, with characteristic sizes of 1.5 m and more, generally, is difficult to carry out. Size-effect models, based on the testing of smaller samples, have been developed (Sajna and Linsbauer 1998). However, a certain scattering range should be considered in the design and analysis. Moreover, the determination of fracture mechanics characteristics of the interface material has to be seen as a very complicated matter, particularly, for the mixed-mode deformation state.

BENCHMARK PROBLEMS

Problem descriptions and specified material characteristics are summarized in the following:

Shear Element

This test problem is a quadratic cube with an embedded interface. The analysis objective is to predict the shear behavior (shear stress versus horizontal displacement response) at the center point of the interface. A graphical sketch of the problem is shown with the results in Fig. 4.

Gravity Dam

This is a 80 m high concrete gravity dam with a flexible foundation support. The analysis objectives are as follows:

- Determination of the IFF (Imminent Failure Flood) level, including the load versus crest displacement response curve.
- Stress distribution along the intact interface for a water elevation equal to 0.8 IFF and the associated crack opening displacement.

Three load cases are considered to study the effects of assumptions related to the uplift pressure distribution at the dam-foundation interface:

Case 1: Dead Load + Upstream Water Pressure (no Uplift Pressure at the dam-foundation interface)

Cases 2 & 3: Dead Load + Upstream Water Pressure + Uplift Pressure as shown in the following:

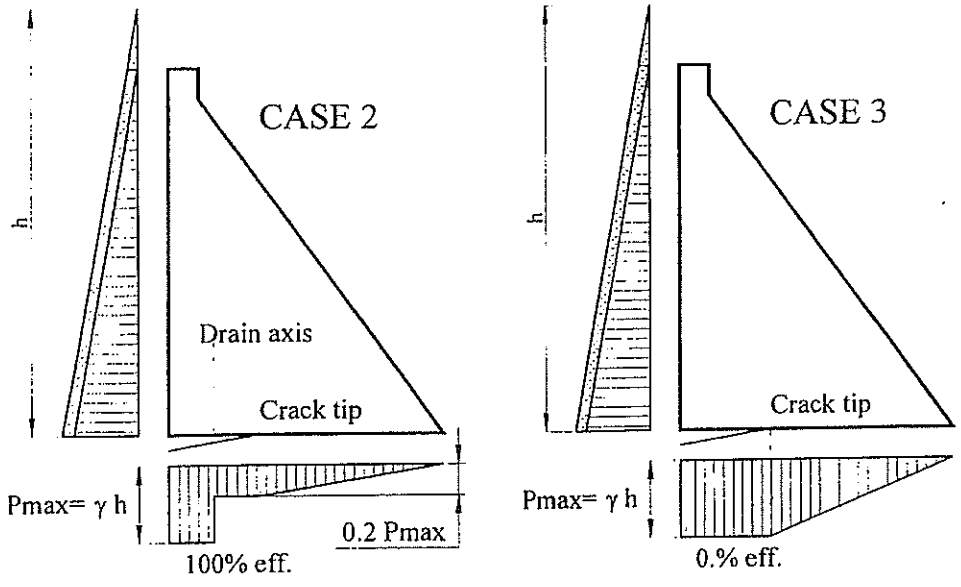

MATERIAL PARAMETERS

Table 1: Properties of dam and rock materials

Materialpar.	Rock	Concr.
Compr. Strength (MPa)	40.0	24.0
Tensile Strength (MPa)	2.6	1.3
Ultimate Tensile Strain	$0.63 \cdot 10^{-4}$	$0.54 \cdot 10^{-4}$
Fracture Strain	$6.0 \cdot 10^{-4}$	$5.0 \cdot 10^{-4}$
Young's Modulus (MPa)	41000	24000
Poisson Ratio	0.1	0.15
Spec. Fracture En. (N/m)	200	150

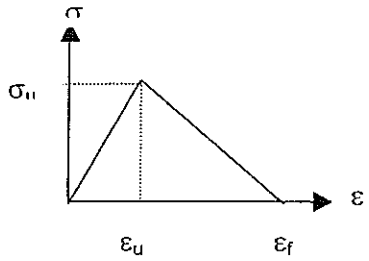

Element size due to the conservation of fracture energy:

$$w_c = \frac{2 \cdot G_f}{\sigma_u \cdot (\varepsilon_f - \varepsilon_u)} \cong 0.50\,\text{m}$$

Table 2: Joint at the Concrete-to-Rock contact (requested characteristic):

Materialpar.	Values
K_S Mpa/mm	20.0
C MPa	0.7
C_{Res}	0.0
Tens. Strength MPa	0.35*
Friction Angle	30°
(Dilat. Angel)	(10°)
H_a Mpa/mm	-0.7

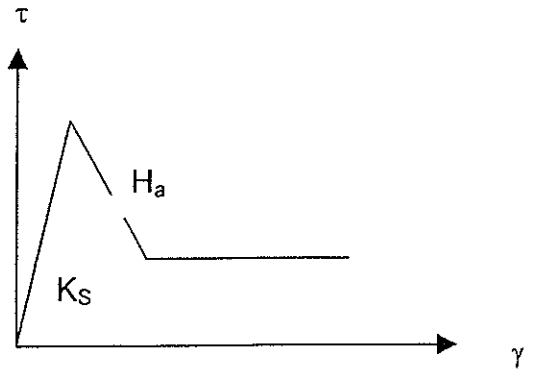

* Changed from 0.00 to 0.35

METHODOLOGY OF THE ANALYSIS

The analysis was carried out with FRAC_DAM, a Finite Element computer program to predict the fracture and damage response of concrete structures under static and dynamic (seismic) loads (Bhattacharjee 1999).

The methodology used in the program is based on Smeared Crack and Damage Mechanics Concepts.

Interfaces or joints are represented by thin layer finite elements (with a small thickness t). Principal characteristics of the joint element are summarized in Figs. 1 and 2.

The failure criterion is based on a modified Mohr-Coulomb yield surface with a special tension cut-off branch (Fig.1).

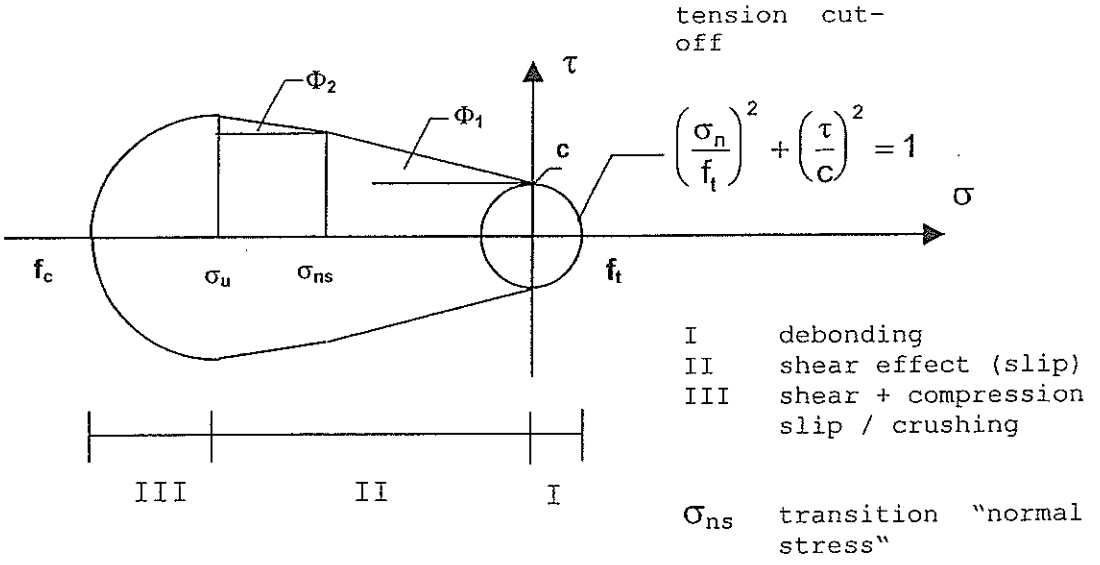

Fig.1 Thin Layer Joint Element
Modified Mohr-Coulomb criterion (Tinawi et al. 1998)

The simulation of the *post-peak* strength and stiffness degradation is performed via a damage mechanics concept

under consideration of a final residual state of the joint behavior. The damage procedure is associated with the principle of conservation of fracture energy, which defines the evolution of damage in a one-dimensional characteristic strain field. The characteristic strain definition includes both opening and sliding mode deformations of the joint. Special strain-displacement interpolation functions are used to eliminate artificial restraints on the joint deformation modes. Detail descriptions on the joint element formulation are available in Tinawi et al. (1998).

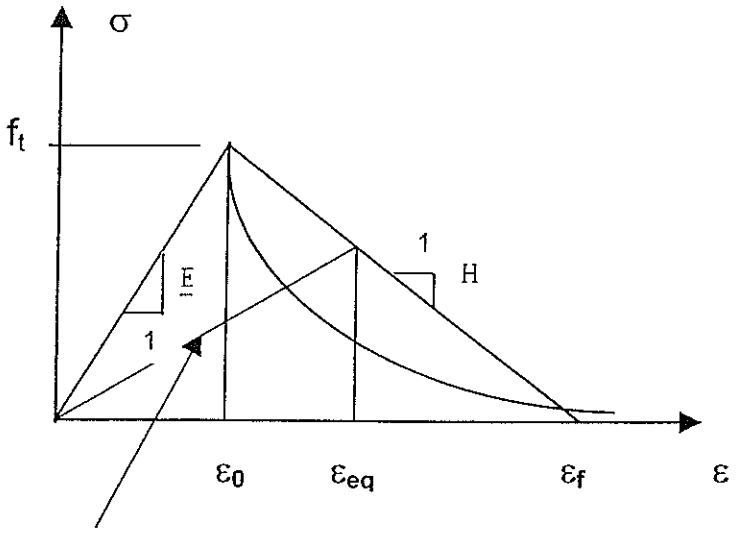

Fig. 2 Thin Layer Joint Element
Damage evaluation with fracture energy conservation principle (Tinawi et al. 1998)

MESH CONFIGURATION

Element sizes in the crack-prone zone of the dam-foundation system are restricted to the limit imposed by the principle of conservation of fracture energy; that are approximately 0.5m quadratic dimension for the dam and 0.05x0.5m for the joint elements. Figure 3 shows the finite element model.

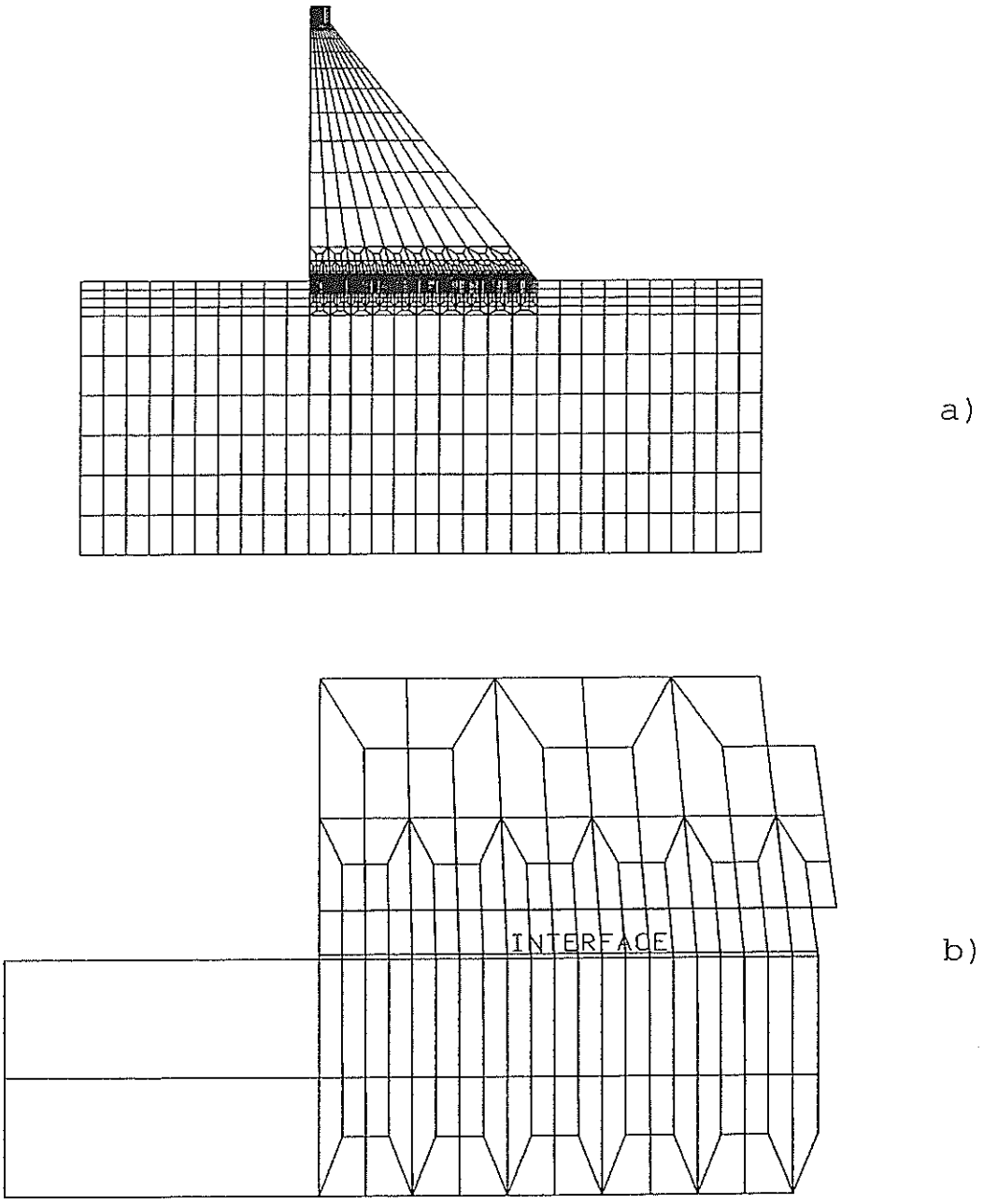

Fig. 3 Mesh configuration: a) Full mesh
b) Upstream dam toe area

Shear Element

Figure 4 provides a schematic description of the shear element as well as the stress-displacement response at the control point G.

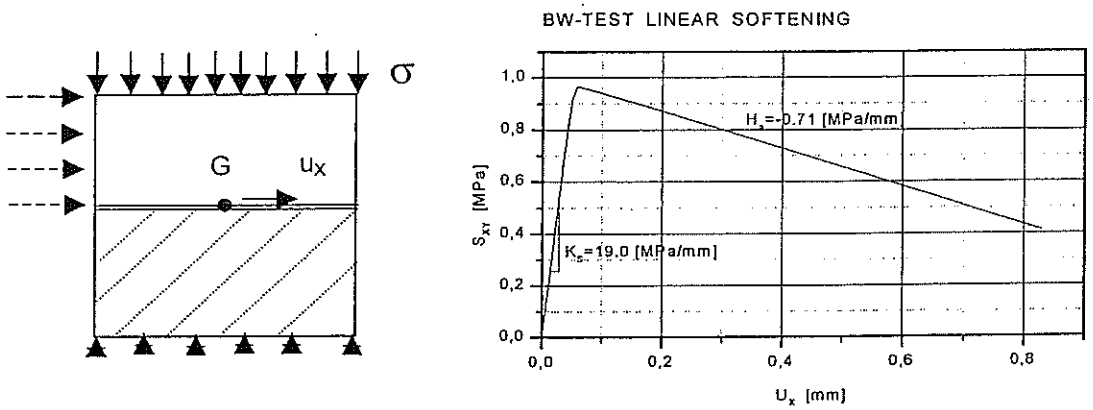

a) b)

Fig.4 Test Analysis of Shear Element
a) Geometry and loading description
b) Shear stress versus u_{xg} displacement of point G for monotonic (horizontal) loading condition

The results of this elementary test analysis, shown in Fig.4b, correspond quite well with the values of K_S and H_a listed in Table 2.

Analysis of Dam-Foundation System

The dam-foundation system, subjected to 3 loading cases described earlier, has been analyzed to determine the IFF level, the damage situation at the ultimate level, the crown displacement during the incremental analysis and the stress distribution in the interface at a 0.8*IFF water level.

The IFF-level, the damage situation and the uplift pressure distribution at the ultimate water level are shown in the following tables:

Interface - Damage Pattern and Uplift Distribution

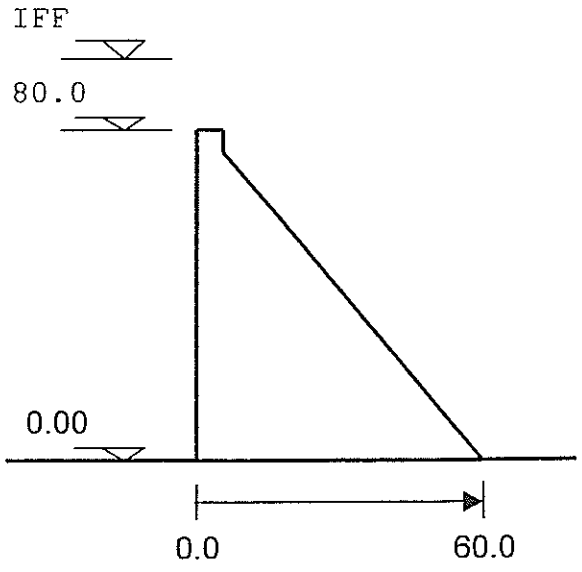

DAMAGE PATTERN

0	undamaged
4	cracked
2	partially cracked
-2	partially damaged under compression and shear

Damage pattern

4	2	-2

Uplift distribution

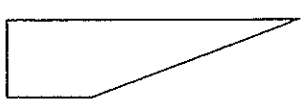

Case	IFF	Ultimate	Damage Pattern				
1	99.5 m	99.4 m	0-20 m	20-24 m	24-36 m	36-58 m	58-60 m
			4	2	-2	0	-2
2	89.6 m	89.5 m	0-25 m	25-30 m	30-42 m	42-59 m	59-60 m
			4	2	-2	0	-2
3	78.7 m	78.6 m	0-16 m	16-31 m	31-39 m	39-60 m	
			4	2	-2	0	

Case	IFF	Ultimate	Uplift Distribution (WC)		
2	89.6 m	89.5 m	0-10 m	10-42 m	42-60 m
			89.6	17.92	LIN→0
3	78.7 m	78.6 m	0-39 m	39-60 m	
			78.60	LIN→0	

Figure 5 shows the deformed configuration of the dam for Case 3 (representative also for Case 1 and Case 2) at the impending failure state.

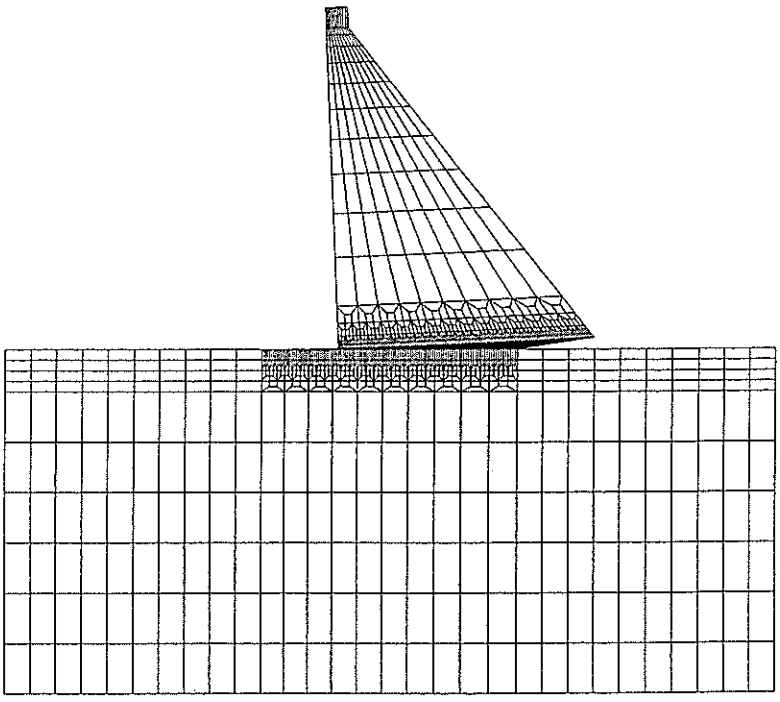

Fig. 5 Deformation of the dam for Case 3 (failure level)

Crown Displacement

The crown displacement responses with increasing reservoir elevation, for three load cases, are shown in Fig.6

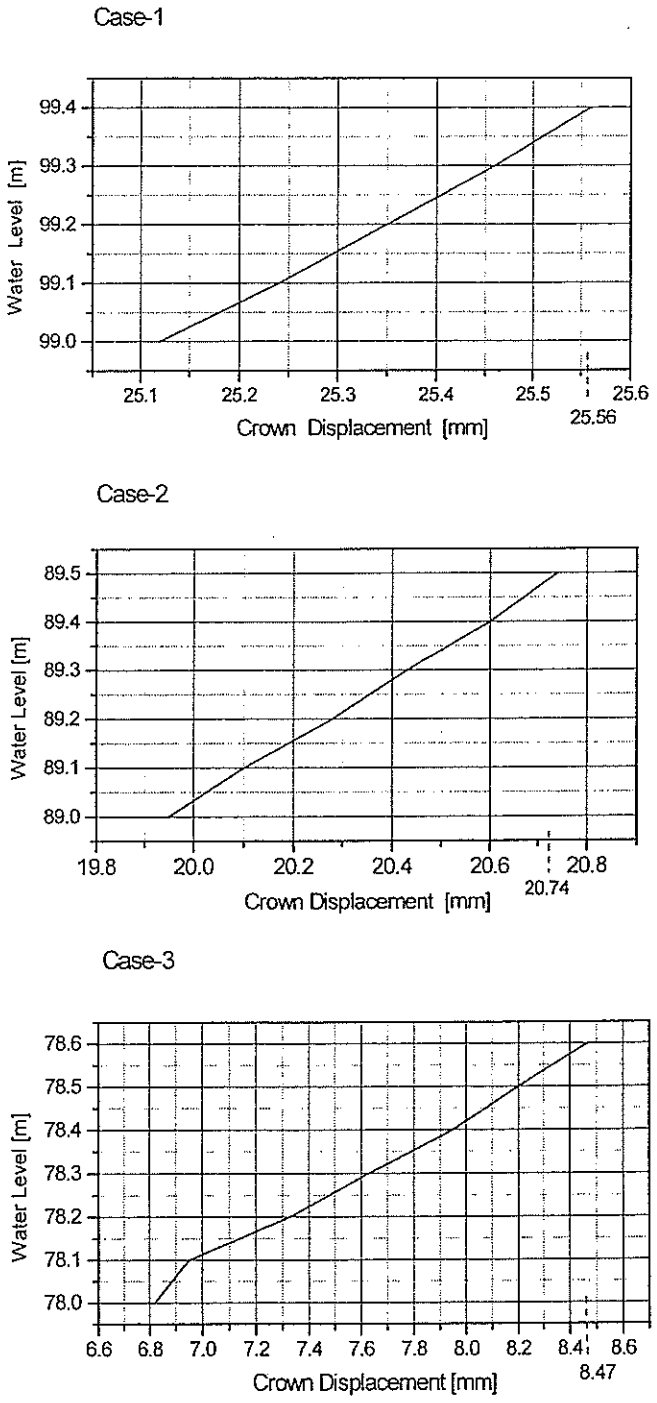

Fig.6 Crown displacement Case-1, Case-2 and Case-3

Stress Distribution

Stress distributions in the intact interface area, corresponding to a water level of 0.8*IFF, for the three load cases are presented in Fig.7a and Fig.7b.

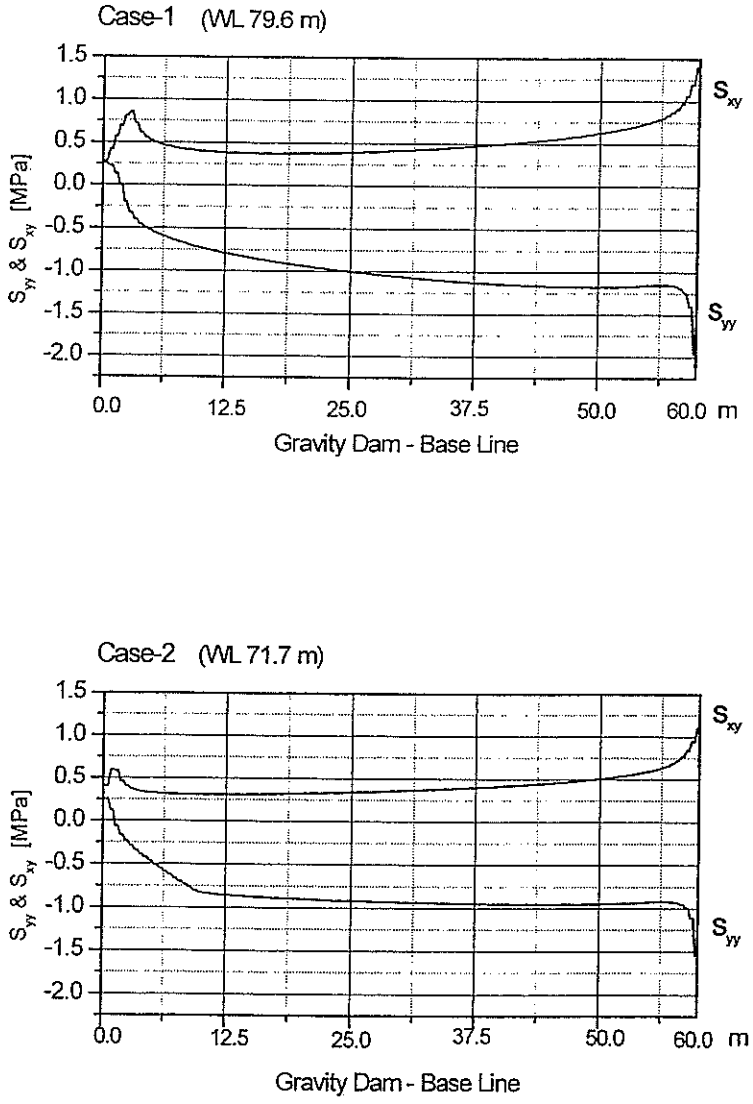

Fig.7a Normal and shear stress distributions along the interface for Case-1 and Case-2

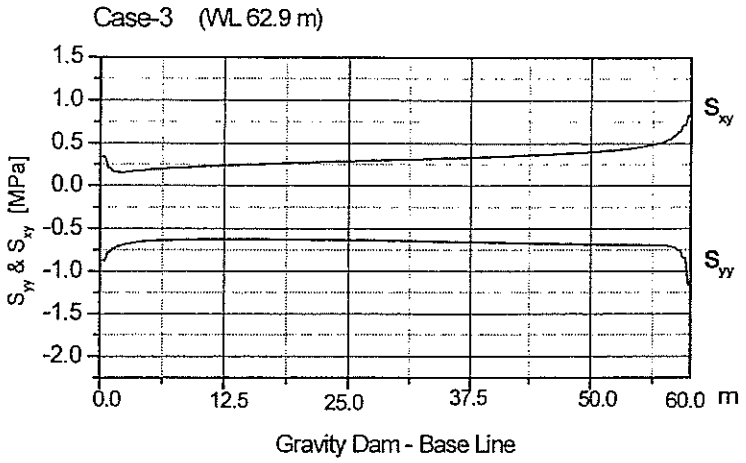

Fig.7b Normal and shear stress distributions along the interface for Case-3

The tensile stresses on the upstream side result due to a certain amount of tensile strength which was necessary according to the thin layer joint element formulation. On the other side this also meets the reality because materials with cohesion usually also have some tensile strength.

CONCLUSION

The Benchmark Workshop Problem dealt with here may be seen as a challenge for the researchers as well as for practitioners. In the present investigation, a finite element, dedicated to dam safety analysis, had to be adapted to meet the special requirements - uplift penetration during crack propagation associated with a grout curtain plus drainage as a special exercise.

ACKNOWLEDGMENT

The authors would like to express their thanks to Mr. A. Hochrainer for support concerning the mesh generation of the problem.

REFERENCES

Bhattacharjee,S.: FRAC_DAM Manual, A Finite Element Analysis Computer Program to Predict the Fracture and damage Response of Concrete Structures, Upgrade 99-09, University of Windsor, Ontario, Canada,1999.

Sajna,A. and Linsbauer,H.: Fracture Mechanics of Mass Concrete- Wet Screening Procedure, in: Fracture Mechanics of Concrete Structures, Vol.1, AEDIFICATIO Publ.,Freiburg, Germany, 1998

Tinawi,R., Leger,P., Ghrib,F., Bhattacharjee,S. and Leclerc,M.: Structural Safety of Existing Concrete Dams - Influence of Construction Joints. Vol.B. Report for the Canadian Electricity Association, CEA No.9032 G 905, 1998

Fifth Benchmark Workshop on Numerical Analysis of Dams

June 2-5, 1999-05-06 Denver, Colorado U.S.A.

Theme A - Concrete Dams

Problem A2 - Imminent Failure Flood Level Evaluation for a Gravity Dam with Interface Crack and Varying Uplift Pressures

Fracture Mechanics Analysis of a Gravity Dam

Manfredini P.,* Chillé F.** and Meghella M.**[1]

Abstract

In this paper the proposed A2 Problem of the Fifth ICOLD BW on Numerical Analysis of Dams is solved by the Finite Element Method. The numerical analyses have been performed by means of a commercial code (ABAQUS). The effect of the uplift pressure in the fracture is considered. The objectives of the study are: (1) to evaluate the imminent failure flood level for the concrete gravity dam; (2) to investigate the mixed-mode fracture propagation in dam/foundation interface; (3) to evaluate both advantages and disadvantages in using a general-purpose finite element code for fracture mechanics analysis of large dams.

1. Introduction

Cracks may occur on the upstream face of a dam, due to thermal loads, shrinkage during dam construction, hydrostatic load cycling, irregular foundation settlements

* Consultant Engineer, Doctoral Student, Technical University, Milan, Italy

**ENEL RICERCA Polo Idraulico Strutturale, Milan, Italy

Water may penetrate these cracks; water pressure represents an additional load on the crack faces and fracture propagation may occur. It is therefore essential to investigate the fluid/fracture interaction and its effect on the safety of large concrete dams (Brühwiller, E. Saouma V. E., 1995a,b).
The methods commonly used for the safety assessment of concrete gravity dams are based on rigid body equilibrium. However, these approaches do not take into account the stress distribution around the crack tip, providing in general a too conservative value of the safety factor with respect to fracture mechanics analysis.
In the proposed Problem A2 the stability condition of a concrete dam subjected to water pressure load on the upstream face and within the crack has to be determined. The crack propagation along the dam-foundation interface is analysed by using both linear and non-linear fracture mechanics. All the data referred to the gravity dam cross section geometry and the concrete and rock mechanical parameters are defined in the proposed Problem A2.

2. Linear elastic fracture mechanics

In gravity dams the length of the zone where the fracture processes take place around the crack tip is small in comparison with all the characteristic dimensions of the structure. Nevertheless this condition is not satisfied in the early stage of crack propagation, when the crack size is small. Therefore, LEFM represents an effective approach for the study of large dams which are already cracked (see Gàlvez et al.; 1996); worse results may be expected for the detection of crack initiation. LEFM approach is anyhow attractive due to the simplicity of the numerical analyses and the relatively small effort required for the calculations.
In this paper, a J integral LEFM approach is firstly used to solve the proposed problem. The structural problem is linear for a given crack length; this permits to calculate the value of total J using linear superposition, by evaluating the contributions of the four different loads separately, J^{Hp} J^{Fp} from water pressure on the upstream surface and within the crack respectively, J^{OT} from overtopping load, J^{G} from dam dead weight. A critical J criterion is then assumed to define the crack propagation condition through the relation:

$$J = J^{Hp} - J^{G} + \lambda \left(J^{Fp} + J^{OT} \right) = J_c \quad (0)$$

where J is the total J-integral at the crack tip, J_c is the J critical value at propagation and λ is the current overtopping load multiplier. For each crack tip position along the dam-foundation interface the four contributions have been calculated by means of a linear elastic finite element analysis; then equation (0) is solved with respect to λ in order to calculate the overtopping load multiplier for the current crack length.
The critical value J_c is assumed to be equal to the energy dissipated during a shear test with high confinement normal stress G_{II}^{a}=300 N/m (Slowik *et al.*, 1998).
The model used for the dam and foundation is shown in figure 1. Six and eight-node parabolic isoparametric plane strain elements were used in the discretization. In order to reduce the computational cost a static condensation is applied by defining two *superelements* (ABAQUS) for the dam body and the foundation, as shown in the same figure. For each crack length four separate analyses are performed in order to evaluate J^{Hp}, J^{G}, J^{Fp}, J^{OT}.

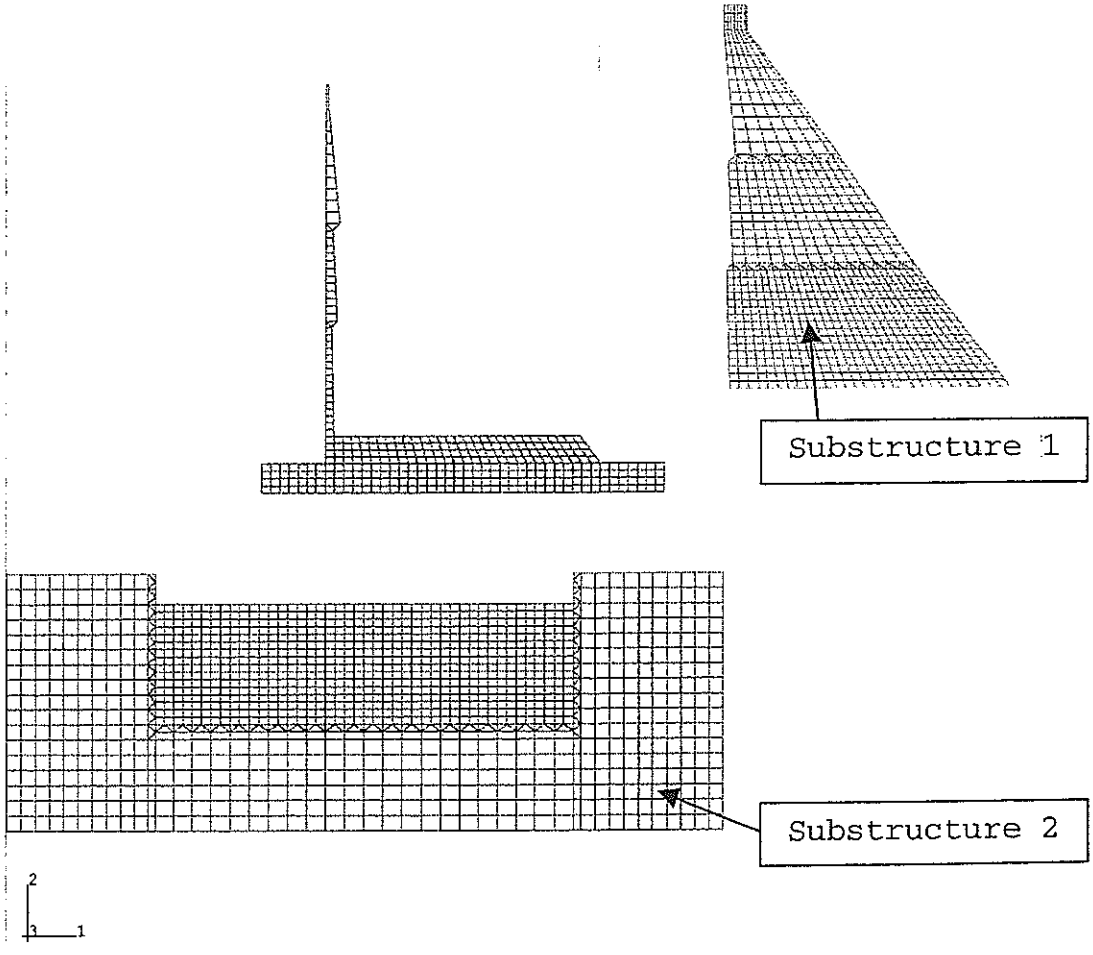

Figure 1. Mesh for linear analyses

In figure 2 the contours of vertical stress component due to hydrostatic pressure inside the crack for a given crack length are reported, on the amplified deformed mesh.

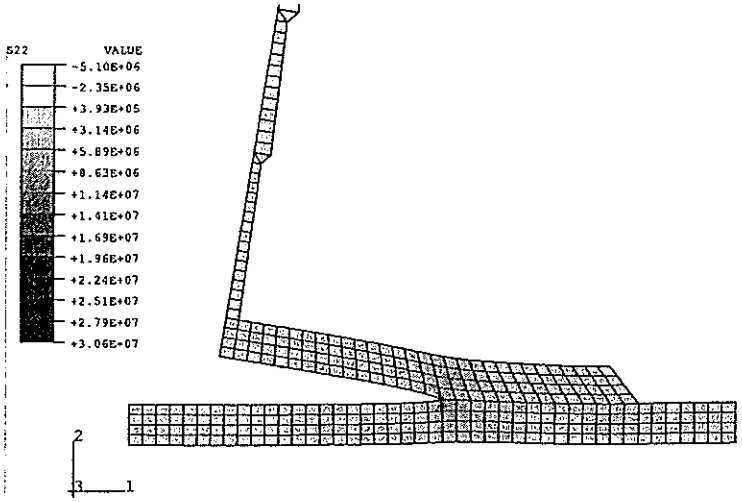

Figure 2. LEFM: Vertical stress contours due to hydrostatic pressure inside the crack for a given crack length

Values of the J-integral for different loading conditions (pressurized or no pressurized crack, assuming overtopping equal to 20m) and different crack lengths are plotted in figure 3. In figure 4 overtopping load factor (water level measured from dam crest) versus crest displacement plots are shown, obtained both considering and neglecting the uplift pressure effects. Figure 4 shows that peak load is significantly reduced when uplift pressure effect is considered.

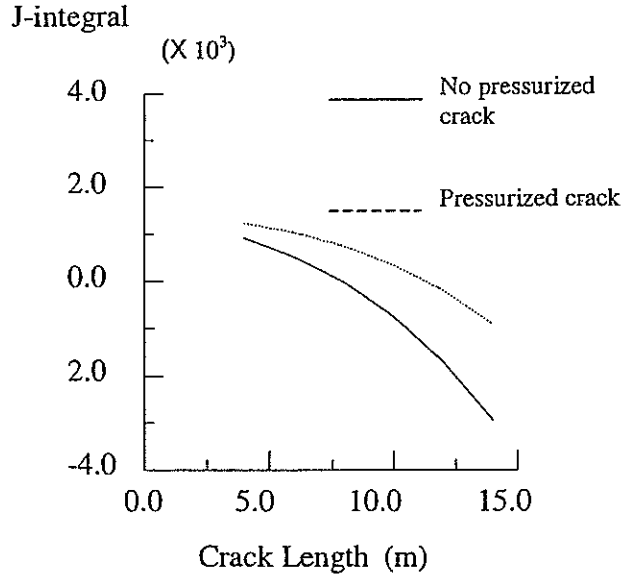

Figure 3. J-Integral versus crack lengths (overtopping equal to 20m)

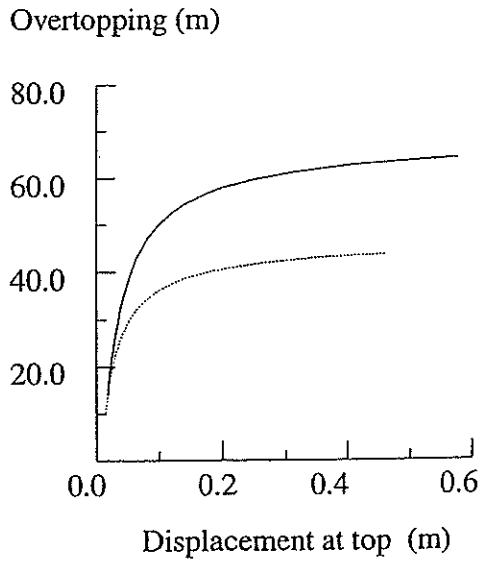

Figure 4. overtopping load factor versus crest displacement

3. Non linear fracture mechanics

In this paper the crack is assumed to propagate along the interface of concrete dam and rock foundation, so that the crack itinerary is a priori known.
In accordance with Cervenka (1994), for incremental non linear analysis of dams it is necessary to consider the non-proportionality of load application (increasing of the pressure both on the upstream face of the gravity dam and within the crack). In fact, the traditional non-linear techniques based on the arc-length method is not applicable until the water elevation in the reservoir reaches the crest of the dam. Furthermore, in order to apply this technique, the pressure rise of the fluid inside the crack due to the overtopping load should be applied by imposing suitable tractions along the bottom edge of the dam.
In the numerical simulations the water elevation is gradually increased up to the top of the dam. Then the arc-length algorithm (ABAQUS) is used to determine the peak load carrying capacity and the post peak response.
In the present work, the effect of water pressure inside the crack is taken into account by applying a suitable load on the slave and master contact surfaces nodes in which the fluid pressure is greater than a predefined threshold value. The pressure of the fluid inside the crack is applied normally to the contact surface, based on the contact pressure at the beginning of each increment. The pressure of the fluid is applied when the contact is lost (zero contact pressure).
Three numerical models have been set up using different assumptions on shear stress transfer and tensile strength of the interface:

Model 1) the cohesive crack model (Hillerborg) governs the relations between the opening displacement and the normal traction, while the displacement discontinuities in the direction tangential to the crack profile are ruled out: unlimited transfer of shear traction is admitted across the whole discontinuity line (see Bolzon et al., 1994);

Model 2) the transmission of the shear stress across the crack face is governed by the Mohr-Coulomb criterion and no tensile strength of the interface is considered (no-tension);

Model 3) the softening law in the Mohr-Coulomb criterion is introduced, as described in Appendix A.

In Model 1, in accordance with Cervenka (1994), the fracture energy GI_f is assumed 40 N/m and the tensile

strength σ_u = 2.83 10^5 N/m^2, the contact surface slave and master are introduced along the fracture path and double nodes are connected by non-linear springs normal to the crack itinerary. The role of this springs is to transmit the nodal forces equivalent to the cohesive normal tractions prescribed by the adopted cohesive model (Bolzon et al., 1994; Gàlvez J. C. et al., 1999; Gàlvez J. C. et al., 1998).

The material properties of the interface are: c = cohesion = 0.7 10^6 N/m^2, the softening modulus H = 0.7 N/m^3, the friction angle ϕ = 30°. The interface tensile strength σ_t is assumed to be zero in accordance with the theme A2.
The non-linear behaviour is assumed to be concentrated at the interface elements; therefore a static condensation algorithm is adopted, as done for the LEFM analyses, in order to reduce the problem size by retaining only the nodes related to the contact elements. The static condensation greatly reduces the computational effort for non linear analyses.
The use of a cohesive crack model in a finite element problem can introduce significant errors when the discretization of the cohesive zone is coarse (Cervenka, 1994). Both the meshes are composed by three and four nodes linear isoparametric elements.

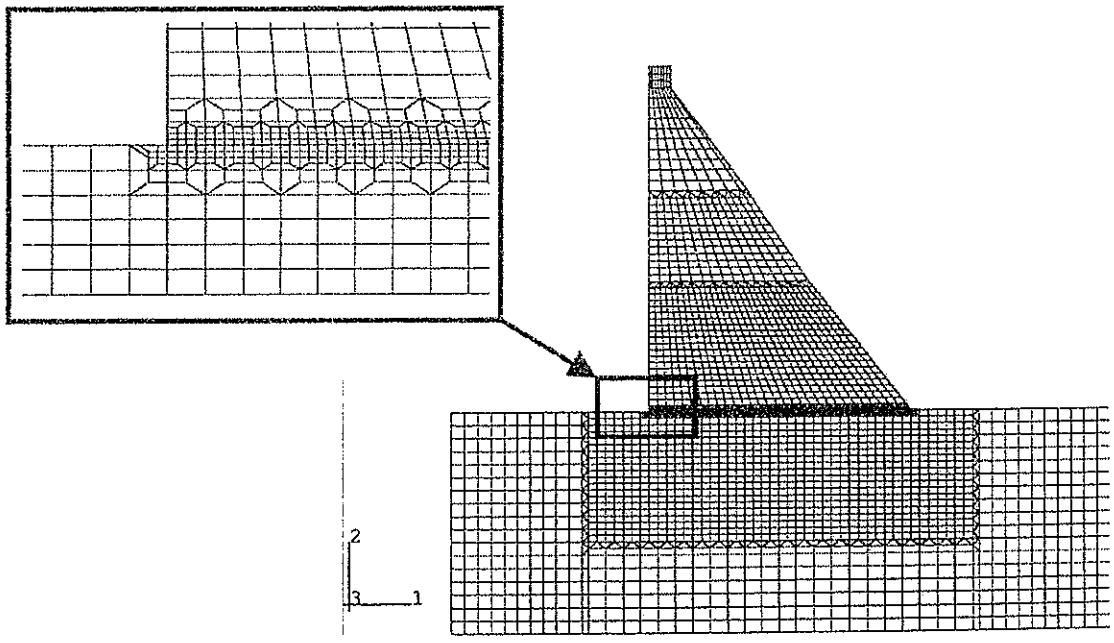

Figure 5. Mesh for non-linear analyses

4. Results

Figure 6 shows the vertical stress component contour plots obtained with model 1 (continuity of tangential displacement) when neglecting uplift pressures.

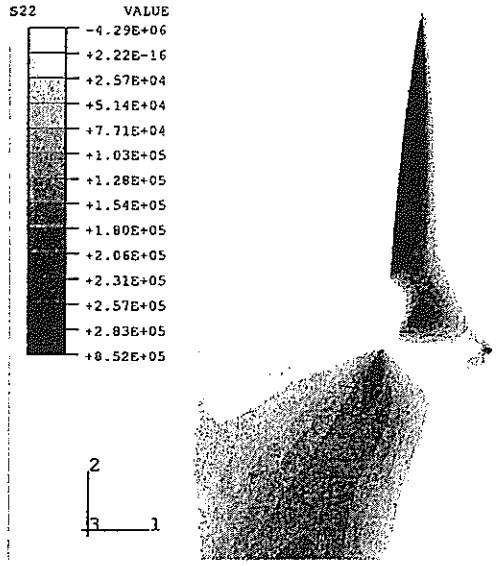

Figure 6. Model 1: Vertical stress component contour plots without uplift pressures

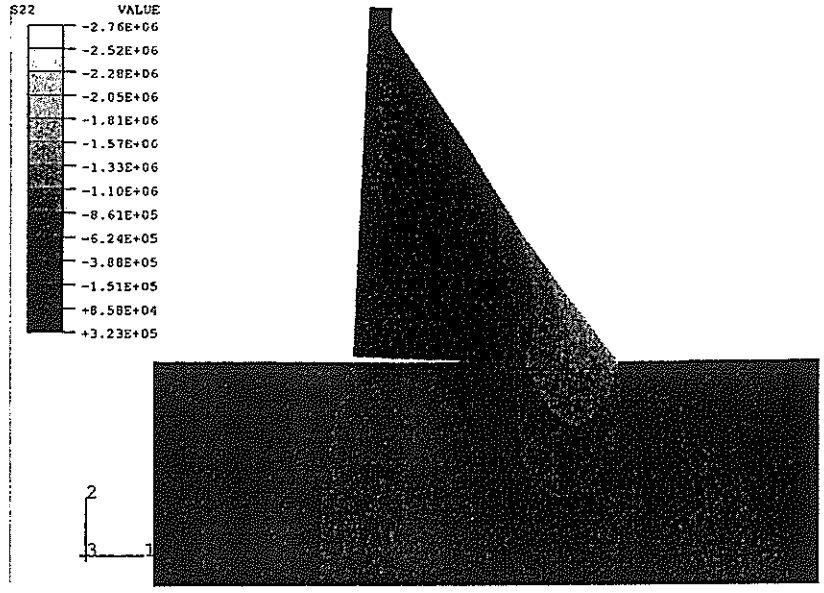

Figure 7. Model 1: Vertical stress component contour plots with uplift pressures

In figure 7 the same stress component contours are reported referring to the case including uplift pressure effects. Figure 8 shows a typical shear stress distribution obtained for the model 3 (Mohr-Coulomb with softening). In this case, it is interesting to note that the process zone of the shear stresses (mode II sliding) precedes the opening of the crack.

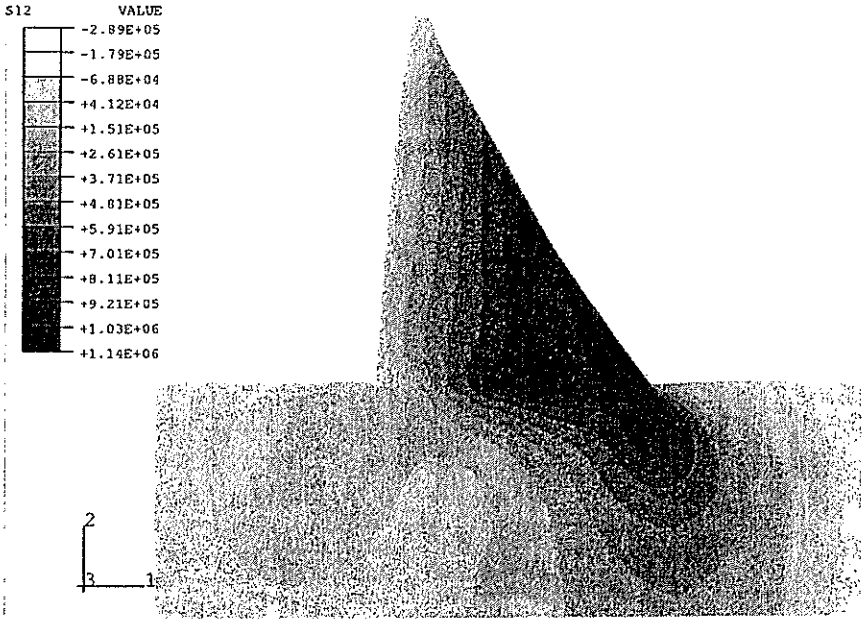

Figure 8. Model 3: Shear stress contours

The figure 9 shows the plastic sliding along the interface for the model 3. The cracks propagate from both upstream and downstream heels. In this figure, s_{cr} is the critical sliding corresponding to zero cohesion.

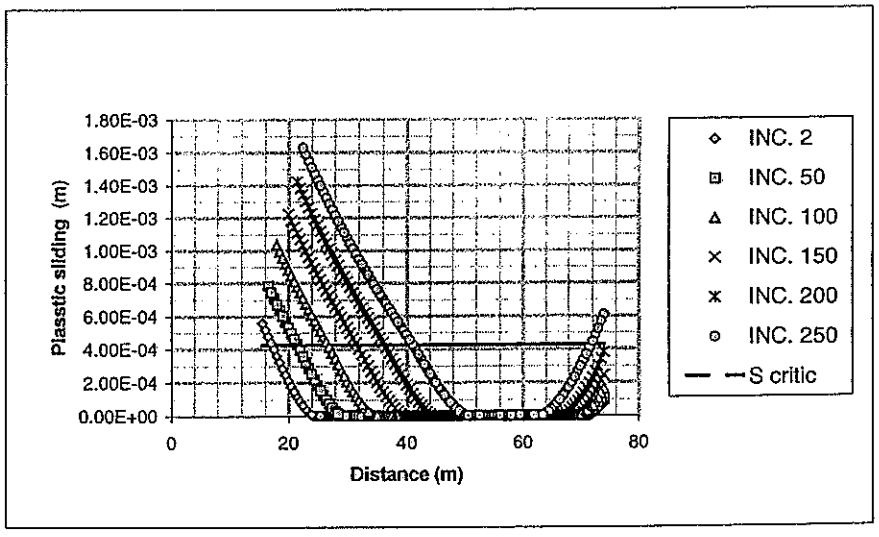

Figure 9. Plastic sliding along the dam foundation for different increments when the overtopping load is applied.

Overtopping load (water level measured from dam crest) versus crest displacement plots obtained with the three different nonlinear models neglecting uplift pressures are reported in figure 10a, together with LEFM results. Two cases have been analysed with Model 2, related to cohesion values respectively equal to 0.0 and 0.7MPa. A detail of the curves related to Models 2 and 3 is shown in figure 10b.

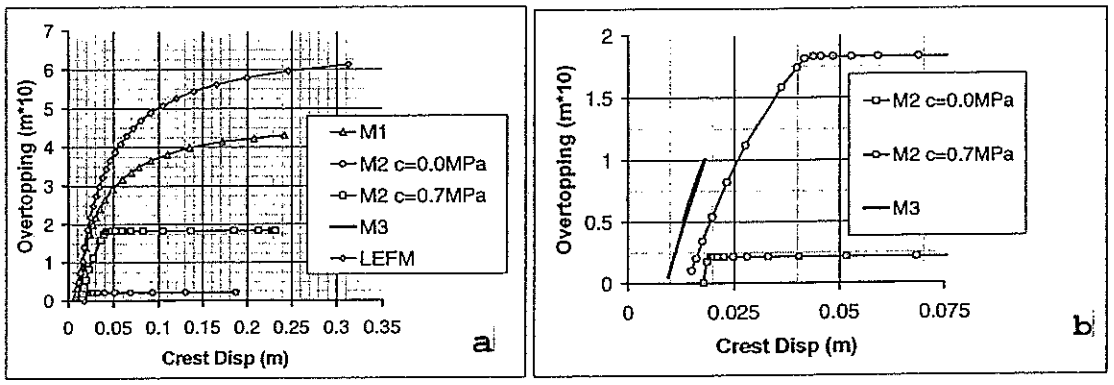

Figure 10. Overtopping load versus crest displacement (no uplift pressures)

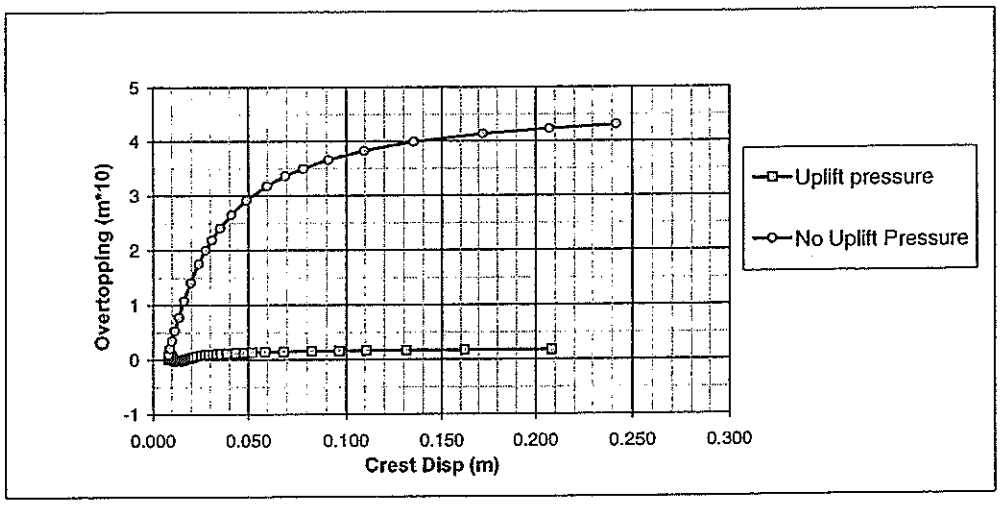

Figure 11. Hydrostatic load versus crest displacement (with and without uplift pressures)

In figure 11 the load/displacement curves obtained with model 1 respectively considering and neglecting the uplift pressures are reported; the failure overtopping load is considerably lower in the former case.

5. Comparative remarks

Figure 10 shows that modelling of shear behaviour strongly affects the structural response: this is due to the fact that the proposed theme refers to a shear failure mechanism. For such a problem it is important to include mode II (i.e. sliding) in the interface crack model in order to be able to model non uniform shear and normal stress distribution along the interface.
Numerical results show significant difference between NLFM and LEFM structural response. This can be explained by observing the difference in the crack length values obtained with the two approaches (see figure 12). This difference is less significant when the model 1 is considered, where the continuity of the tangential displacements is imposed.
When uplift pressure is introduced the peak load obtained by LEFM is significantly greater than the one obtained by NLFM. This is due to the different crack length and to the non uniform distribution of the normal stress along the interface.

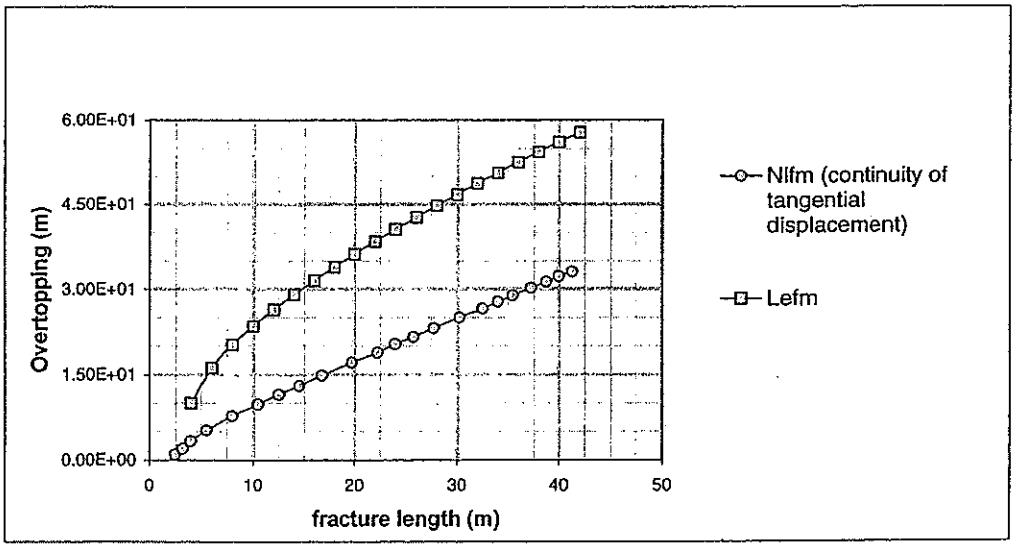

Figure 12. Overtopping load versus fracture length for LEFM and NLFM (no uplift pressures)

Furthermore, when the pressurized crack is considered in order to obtain a realistic value of the peak load, it is necessary to use a refined mesh along the interface and a very small time increment must be introduced.

6. Conclusions

In this paper linear and non-linear fracture mechanics analyses of a gravity dam are presented.
Remarkable differences between NLFM and LEFM response have been found, due to different crack length and stress distribution along the interface.
More important differences have been found for different hypotheses on shear behaviour. Peak loads obtained by various frictional laws (Model 2 and Model 3) are considerably smaller than the one obtained by imposing the continuity of tangential displacement along the interface. This difference can be attributed, in accordance with Cervenka (1994), to the non uniform distribution of shear and normal stresses along the interface.
In fact, it is interesting to notice that highest shear stresses are concentrated not only in the areas close to the upstream heel but also at the downstream heel. Mode II cracks propagate from both upstream and downstream heels.
Bifurcation of solution is an important feature of cohesive crack analysis that can be unambiguously predicted only by the formulation of the fracture process as a linear complementary problem either in finite increments or in rates (Bolzon *et al.*, 1997).
Uplift pressure significantly reduces the actual load-carrying capacity (see figure 11). Thus the effect of the pressurized fluid inside the crack must be taken into account in dam design and safety assessment.
A substantially different alternative to FEM, recently developed, is represented by the application of the symmetric Galerkin method (SGBEM) to the cohesive fracture mechanics (Maier and Frangi, 1997; 1998). This approach leads to a drastic reduction of computational effort in terms of both problem size and remeshing burden cost.

7. REFERENCES

ABAQUS Manuals - V. 5.8 (1999), Hibbitt, Karlsson & Sorensen.

Camacho, G. T. and Ortiz, M. (1996) Computational modelling of impact demage in brittle materials. *Int. J. Solids Structures* 33, 2899-2938.

Bazant Z. P. (1990) A critical appraisal of 'no-tension' dam design: a fracture mechanics viewpoint. *Dam Engineering* 1, 237-246.

Gioia, G., Bazant, Z. P. ,Pohl, B. P. (1992) Is no-tension dam design always safe? A numerical study. *Dam Engineering* 1, 23-29.

Bolzon, G., Cocchetti G., Maier G., Novati G., and Giuseppetti G. (1994) Boundary Element and finite element fracture analysis of dams by the cohesive crack model: a comparative study, in "Dam Fracture and Damage", Bourdarot E., Mazars J., Saouma V. (Eds.), A.A. Balkema, Rotterdam, 69-78.

Bolzon, G., Maier G., Tin-Loi F., (1997) On multiplicity of solutions in quasi-brittle fracture computations. *Computational Mechanics* 19 511-516.

Brühwiller, E. Saouma V. E. (1995) "Water Fracture Interaction in Concrete - Part I: Fracture properties", *ACI Materials Journal.* 92, 296-303.

Brühwiller, E. Saouma V. E. (1995) "Water Fracture Interaction in Concrete - Part II: Hydrostatic Pressure in Cracks", *ACI Materials Journal* 92, 383-389.

Cervenka, J, (1994) "Discrete crack modeling in concrete structures" *Ph. D. Thesis*, Boulder University.

Gàlvez J. C., Cendón D. A., Planas J., Guinea G.V. and Elices M., (1998) "Fracture of concrete under mixed loading. Experimental results and numerical prediction", in Fracture Mechanics of Concrete Structures Proceedings FRAMCOS-3 AEDIFICATIO Publishers, D-79104 Freiburg, Germany.

Gàlvez J. C., Elices M., Guinea G.V., and J. Planas, (1999) "Mixed mode fracture of concrete under proportional and non proportional loading". *Int. J. of Fracture*, to appear.

Gàlvez J., Llorca J.L. and M. Elices (1996) "Fracture mechanics analysis of crack stability in concrete gravity dams". *Dam Engineering* 7, 35-63.

Giannakopoulos, A. E. (1989), "The return mapping method for the integration of friction constitutive relations ", Computers & Structures 32, 155-167.

Lofti, H. (1992) "Finite element analysis of fracture of concrete and masorny structures" *PhD thesis*, University of Colorado, Boulder (1992).

Lofti, H. and Shing, P. (1994) "Interface model applied to fracture of masorny structures", *J. Struct. Engng.*, ASCE, 120, 63-80

Maier, G., Frangi A., (1997) "Quasi brittle fracture analysis by a symmetric Galerkin boundary element method". Invited lecture at 9th International Conference on Fracture, Sydney, April 1997. In: Advances in Fracture Research. Eds.

Karihaloo B. L., Mai Y. W., Ripley M. I., Ritchie R. O., Pergamon Press, Oxford, Vol. 4, 1837-1848, 1997.

Maier, G., Frangi, A., (1998) "Symmetric boundary element method for discrete crack modelling of Fracture Processes", *Computer Assisted Mech. and Engng. Sciences*, 5, 201-226.

Oden, J. T. and Pires, E.B. (1983) "Non local and nonlinear friction laws and variationals principles for contact problems in elasticity", *Journal of Applied Mechanics*, 50, 67-76.

Salvadori A., Benson Shing P. (1999), "An elastic plastic cohesive interface model for fracture of quasi brittle material", in preparation.

Salvadori A., (1999) Private communication.

Slowik, V., Chandra Kishen J. M., Saouma V. E. (1998) "Mixed mode fracture of cementitious bimaterial interfaces; part II: numerical simulation" *Engng. Fracture Mechanics* 60, 95-107.

Swoboda G. and Lei X. Y. (1994) "Simulation of arch dam-foundation interaction with a new friction interface element". *Int. J. Num. Analytic. Meth. Geomech*, 8, 19-43.

Zhong, H. Z. (1993) "Finite element procedures for contact-impact problems, Oxford University Press, Oxford.

Appendix A

A1. Introduction

Sliding (rather than overturning) along the uncracked ligament is the primary mode of failure in a gravity dam. Hence the evaluation of shear friction safety factor of the dam is commonly required. In addition, all the analyses for design and safety assessment of dams usually assume that crack propagates along the weak interface between dam and foundation. Recently, the crack kinking into the rock due to the presence of large shear stresses along the interface has been considered by Chandra Kishen (1996), and Cervenka (1994).
Contact/friction algorithms (see e.g. Giannakopoulos, 1989) have been used in order to study rock-concrete interaction (see: Chandra Kishen, 1996, Swoboda and Lei, 1994) and to model the fracture in brittle materials (Camacho and Ortiz, 1996).
The simplified model herein proposed to represent the behaviour of rock-concrete interaction is based on the modified Mohr-Coulomb criterion, in which the tensile yield limit is set to zero ('no-tension', see Gioia et.al., 1992, Bazant, 1990)).

A2. Frictional Interface Model

In the proposed model the strength of the interface law is described by a failure function (see figure a1):

$$|\tau| - \sigma \tan(\Phi) - c\left(s^{*}_{pl}\right) = 0 \tag{1}$$

$$s^{*}_{pl} = s^{+}_{pl} - s^{-}_{pl} \qquad s_{pl} = s^{+}_{pl} + s^{-}_{pl} \qquad s^{+}_{pl} \geq 0 \qquad s^{-}_{pl} \leq 0 \tag{2}$$

$$\begin{cases} c\left(s^{*}_{pl}\right) = c_0\left(1 - \dfrac{s^{*}_{pl}}{s_{cr}}\right) & s^{*}_{pl} < s_{cr} \\ 0 & s^{*}_{pl} \geq s_{cr} \end{cases} \tag{3}$$

where s_{pl} is the plastic sliding of the joint (positive in the x-direction), σ is the normal compression stress, φ is the friction angle, c is the cohesion. The equation (3) governs the softening evolution of failure function by a

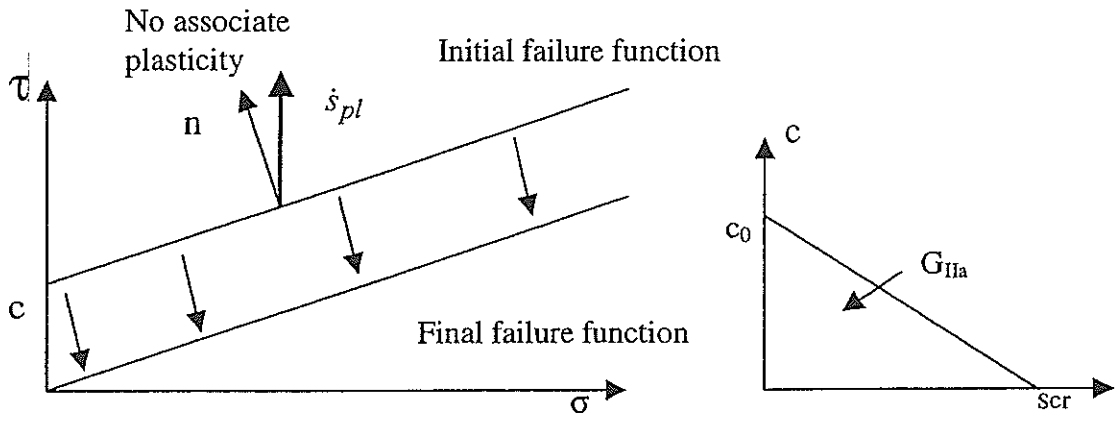

Figure a1. a) Failure function; b) Cohesive law

softening parameter s^*_{pl} which represents the cumulated plastic sliding. The critical sliding corresponding to zero cohesion is denoted by s_{cr} and it is obtained by imposing the area under the linear softening law to be equal to G_F^{IIa}.
A "master-slave" contact algorithm is adopted to handle the dam-foundation interface interaction.
Plasticity theory is used to define the constitutive driver for the interface crack model. In order to obtain a more realistic friction model a non-local friction law should be introduced (see Oden and Pires, 1983). Contact friction algorithms are extensively dealt with in the comprehensive book by Zhong (1993).
The increment tangent stiffness matrix is obtained by imposing the condition $\Delta\Phi = 0$ (see Eq. 2) and the incremental constitutive equation (see Eq. 3):

$$d\varphi \equiv \frac{\partial \varphi}{\partial \sigma} d\sigma + \frac{\partial \varphi}{\partial s} ds + \frac{\partial \varphi}{\partial s^+_{pl}} ds^+_{pl} + \frac{\partial \varphi}{\partial s^-_{pl}} ds^-_{pl} = 0 \qquad (2)$$

$$d\tau = K_\tau \left(ds - ds^\pm_{pl} \right) \qquad (3)$$

If $ds^+_{pl} \neq 0 \quad ds^-_{pl} = 0$

$$ds^+_{pl} \equiv -\left(\frac{\partial \varphi}{\partial s^+_{pl}} \right)^{-1} \left[\frac{\partial \varphi}{\partial \sigma} d\sigma + \frac{\partial \varphi}{\partial s} ds \right] \qquad (4)$$

If $ds_{pl}^{+}=0 \quad ds_{pl}^{-}\neq 0$

$$ds_{pl}^{-} \equiv -\left(\frac{\partial\varphi}{\partial s_{pl}^{-}}\right)^{-1}\left[\frac{\partial\varphi}{\partial\sigma_n}d\sigma_n+\frac{\partial\varphi}{\partial s}ds\right] \tag{5}$$

where $\dfrac{\partial\varphi}{\partial\sigma}=-\tan(\varphi) \quad \dfrac{\partial\varphi}{\partial s}=K_\tau\dfrac{|s_{el}|}{s_{el}}$

$$\frac{\partial\varphi}{\partial s_{pl}^{+}}=-K_\tau\frac{|s_{el}|}{s_{el}}+\frac{c_0}{s_{cr}} \qquad \frac{\partial\varphi}{\partial s_{pl}^{-}}=-K_\tau\frac{|s_{el}|}{s_{el}}-\frac{c_0}{s_{cr}} \tag{6}$$

$$d\tau=K_\tau\left\{ds+\left(\frac{\partial\varphi}{\partial s_{pl}^{\pm}}\right)^{-1}\left[\frac{\partial\varphi}{\partial\sigma}d\sigma+\frac{\partial\varphi}{\partial s}ds\right]\right\} \tag{7}$$

The incremental tangent matrix reads:

$$\frac{\partial\tau}{\partial s}=K_\tau\left\{1+\left(\frac{\partial\varphi}{\partial s_{pl}^{\pm}}\right)^{-1}\frac{\partial\varphi}{\partial s}\right\}; \quad \frac{\partial\tau}{\partial\sigma}=-K_\tau\left\{1+\left(\frac{\partial\varphi}{\partial s_{pl}^{\pm}}\right)^{-1}\right\}\tan(\varphi) \tag{8}$$

The interface finite element developed by Cervenka (1994), Lofti (1992), Lofti and Shing (1994) exhibit a very large initial stiffness (Cervenka, 1994). Thus, in accordance with Chandra Kishen (1996), the implementation of the interface law in an appropriate contact algorithm permits to reproduce the realistic frictional behaviour of the interface.

A3. Incremental formulation

For a given stress state $(\sigma_n;\tau_n)$ on the yield surface, softening parameter $s^{*}_{pl_n}$ and total sliding increment Δs_{n+1}. In the state n+1 the failure function must be satisfied condition, so that:

$$\Phi\left(\sigma_{n+1};\tau_{n+1};s^{*}_{pl_{n+1}}\right)=0 \tag{1.a}$$

The elastic predictor is $\tau_e^{pr}=K_\tau\left(s_n^{el}+\Delta s_{n+1}\right)$; the plastic correction is $\tau_{n+1}=\tau_e^{pr}-K_\tau\,\Delta s_{pl_{n+1}}$.

$$K_\tau\left|s_n^{el}+\Delta s_{n+1}-\Delta s_{pl_{n+1}}\right|+C\left|\Delta s_{pl_{n+1}}\right|=\sigma_{n+1}\tan(\phi)+C\left(1-\frac{s^{*}_{pl_n}}{s_{cr}}\right) \tag{2.a}$$

if $s^*_{pl_n} + \left|\Delta s_{pl_{n+1}}\right| < s_{cr} \Rightarrow C = c_0 ; s^*_{pl_n} + \left|\Delta s_{pl_{n+1}}\right| \geq s_{cr} \Rightarrow C = 0$.

The increment of the plastic sliding $\Delta s_{pl_{n+1}}$ of the joint is obtained by solving the equation (2.a). The root of this equation is obtained by consider four different cases (Salvadori, 1999)

i) if $s^{el}_n + \Delta s_{n+1} - \Delta s_{pl_{n+1}} > 0$ and $\Delta s_{pl_{n+1}} > 0 \Rightarrow \Delta s_{pl_{n+1}} = \dfrac{p - K_\tau \left(s^{el}_n + \Delta s_{n+1}\right)}{c_0 / s_{cr} - K_\tau}$

ii) if $s^{el}_n + \Delta s_{n+1} - \Delta s_{pl_{n+1}} < 0$ and $\Delta s_{pl_{n+1}} < 0 \Rightarrow \Delta s_{pl_{n+1}} = \dfrac{p + K_\tau \left(s^{el}_n + \Delta s_{n+1}\right)}{K_\tau - c_0 / s_{cr}}$

iii) if $s^{el}_n + \Delta s_{n+1} - \Delta s_{pl_{n+1}} > 0$ and $\Delta s_{pl_{n+1}} < 0 \Rightarrow \Delta s_{pl_{n+1}} = \dfrac{p - K_\tau \left(s^{el}_n + \Delta s_{n+1}\right)}{-K_\tau - c_0 / s_{cr}}$

iv) if $s^{el}_n + \Delta s_{n+1} - \Delta s_{pl_{n+1}} < 0$ and $\Delta s_{pl_{n+1}} > 0 \Rightarrow \Delta s_{pl_{n+1}} = \dfrac{p + K_\tau \left(s^{el}_n + \Delta s_{n+1}\right)}{K_\tau + c_0 / s_{cr}}$

where $p = \sigma_{n+1} \tan(\phi) + c_0 \left(1 - \dfrac{s^*_{pl_n}}{s_{cr}}\right)$, and $c_0 = 0$ if $s^*_{pl_n} + \left|\Delta s_{pl_{n+1}}\right| \geq s_{cr}$, thus an implicit procedure is used in order to solve the Eq. 2.

A4. Direct shear test

The frictional interface assigned in Problem A2 (Appendix A) has been implemented in the commercial finite element code ABAQUS by means of a suitable "user subroutine". In order to check the validity of the implemented algorithm some examples with known analytical or numerical solutions are analysed. The numerical simulation of a cyclic direct shear test with different values of the displacement imposed has been carried out. An elastic slab lying on a flat rigid foundation has been considered. Friction is supposed to exist between the bottom surface of the elastic slab and the foundation and the slab is subjected to a downward uniformly distributed force on the top surface. The friction coefficient between the bottom surface of the rigid slab and the rigid foundation is 0.577. A uniform traction of $3.46 \cdot 10^5$ N/m^2 is applied in the downward direction on the slab. The peak cohesion is $0.7 \cdot 10^6$ N/m^2 and the softening module which represents the slope of the softening branch in the plane τ-σ is Ha = $-7.25 \cdot 10^8$. N/m^3 The slab is subjected to a cyclic displacement (see figure a2).

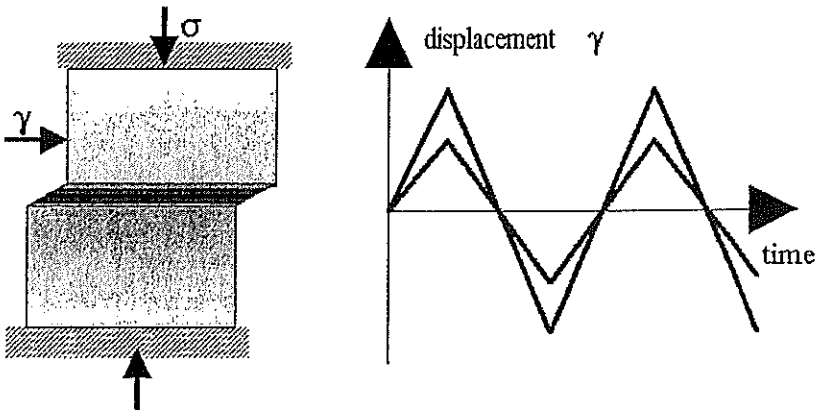

Figure a2. Direct shear test setup.

The finite element model consists of four-node linear quadrilateral plane strain elements. The interface problem is solved using a "master and slave" contact algorithm. The obtained results in terms of tangential stress cycles are represented in figure a3.

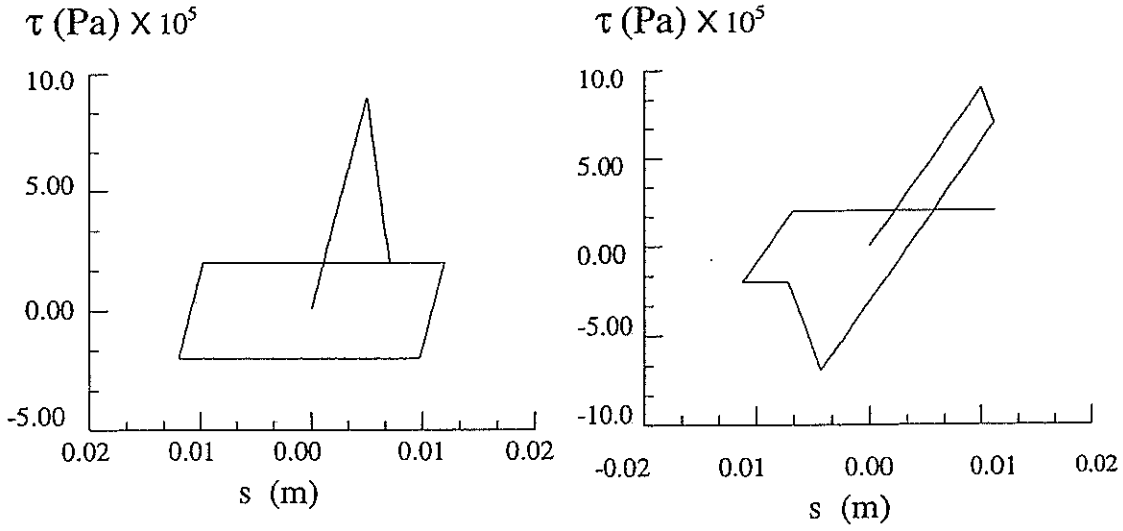

Figure a3: Direct shear test for different values of the maximum displacement amplitude.

Authors's response

Manfredini P.,* Chillé F.** and Meghella M.**

*Graduate School in Structural Engineering, Technical University (Politecnico),Milan, Italy
**ENEL RICERCA Polo Idraulico Strutturale, Milan, Italy

In the frictional model of the dam/rock interface highest shear stresses are concentrated not only in the areas close to the upstream hell but also at the downstream heel. Mode II cracks propagate from both upstream and downstream heels. In this case the iteration process may diverge.
In fact, the figure 1b shows that during fracture propagation the elastic region of the joint becomes very small. Finally, the shear fracture passes through nearly completely the dam foundation interface. In this figure, s_{cr} is the critical sliding corresponding to zero cohesion.

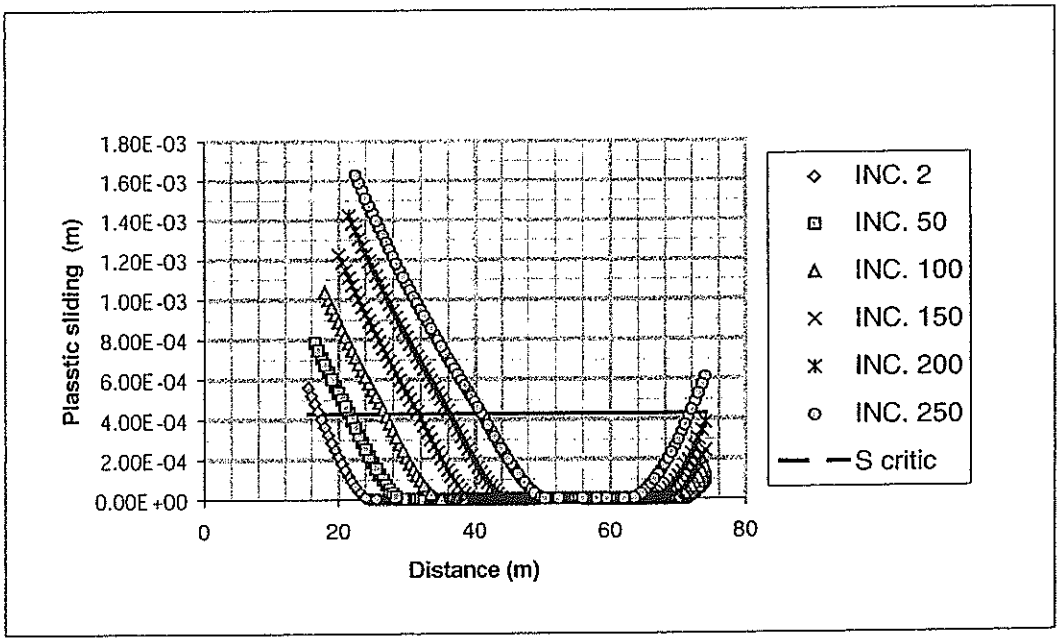

Figure 1b. Plastic sliding along the dam foundation for different increments when the overtopping load is applied.

During the analysis, excessive interface sliding may occur. The return-mapping algorithm proposed for friction law with softening fails to map the elastic predictor. In fact, the root of the equation 2a can not exist when the sliding of

the joint is excessive Δs_{n+1}. If we suppose to consider the case i).with $s_n^{el} + \Delta s_{n+1} - \Delta s_{pl_{n+1}} > 0$ and $\Delta s_{pl_{n+1}} > 0$

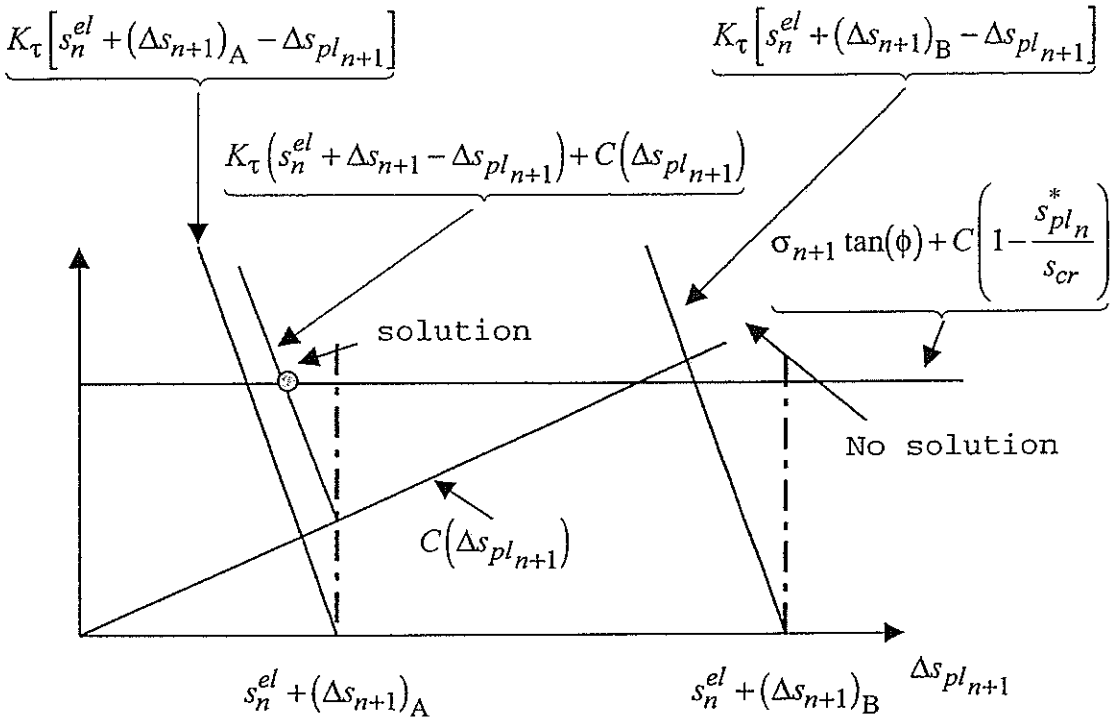

Figure 2b. Representation of the solution of the equation (2.a).

If $(\Delta s_{n+1})_B >> (\Delta s_{n+1})_A$ the solution of the equation (2,a) does not exist (see figure 2b). This problem should be solved by introducing an automatic control of the increment. However, in this case the computational cost increases.
Finally, the stabilisation algorithm for the contact problem could not be used since negative values or unrealistic values of the contact pressure are introduced in the friction contact algorithm. In this case the solution provided by the algorithm can be wrong.

STABILITY OF OVERTOPPED GRAVITY DAMS NUMERICAL IDENTIFICATION OF THE FAILURE MODE

P.Palumbo[1], R.Pellegrini[2]
G.Giuseppetti[3]

ABSTRACT

The stability failure of a gravity dam subjected to an increasing level of water even beyond the crest level is numerically estimated. Two methods are exploited, namely the rigid block approach and the finite element method. In the latter case the sensitivity of results on three different options for the mesh is investigated.

INTRODUCTION

To assess the safety of a dam, the detection of the modes of static stability failure may be necessary. The numerical identification of the failure mode due to overtopping in gravity dams is attained addressing appropriate considerations to internal stresses and sliding stability.
In practice, the rigid block method of analysis is considered sufficient in most cases. Using this method and the elementary beam theory, the stresses in the cross sections of the dam and the extent of cracking can be estimated. The latter is obtained establishing the allowable tensile stress that can be developed in horizontal sections and then using static equilibrium procedures which properly consider all forces, including uplift, to determine a base pressure distribution that satisfies both stress and equilibrium requirements. A section is considered cracked when the tensile stress exceeds the allowable threshold limit. The tensile strength is generally assumed to be zero ("no-tension" approach).
A more refined version of the no-tension approach than the rigid block method is based on elastic/perfectly plastic limit analysis in which a yield condition characterised by a zero value for tensile strength is assumed. This hypothesis is a consequence of the belief, never justified theoretically, that failure load obtained by no-tension analysis is lower than that obtained by an analysis in

[1] ISMES S.p.A., Seriate (Italy)
[2] ISMES S.p.A., Seriate (Italy)
[3] ENEL Research - Polo Idraulico strutturale, Milano (Italy)

which the tensile strength is taken into account. But, in this case, one couldn't state that no-tension analysis is certainly safe. In fact concrete is not actually a plastic material and under tension it exhibits post peak softening. Therefore, to obtain a realistic representation of the structural behaviour, the finite not zero tensile strength and the post peak properties of the material should be taken into account.
To assess the stability condition of a gravity dam it is also necessary to consider the properties of the joint at the concrete to rock interface. In this regard experimental data on rock-concrete interface show that the decrease in shear strength is not abrupt, but is rather gradual. Further related observable phenomena are:

- shear strength depends on the normal stress;
- softening is present both in shear and tension;
- there is a residual shear strength due to the friction along the interface, which depends on the compressive normal stress;
- irreversible relative displacements are caused by broken segments of the interface material and by friction between the two crack surfaces;
- roughness of the interface causes opening displacements (i.e. dilatancy) when subjected to sliding displacements.

To reproduce this behaviour, a model whose parameters can be easily derived from laboratory tests must be used.
The problem A2 proposed for Theme A of the Fifth Benchmark Workshop on numerical analysis of dams provides a good opportunity to test and discuss the current methods for gravity dams failure mode estimation.
This paper describes the analyses carried out using the rigid block method and the non-linear finite element analysis with a smeared-fracture model for concrete dam and rock foundation. On the other hand the concrete to rock contact has been idealised as an interface between two dissimilar materials with zero thickness using a discrete crack approach. The relationships between normal and tangential stresses with opening and sliding displacements have been derived from data contained in the specifications of the problem.

1.0 SIMPLIFIED ANALYSIS: RIGID BLOCK METHOD

Problem A2 is first solved evaluating the sliding stability of the dam by means of the rigid block method [1]. This

method assumes a linear stress distribution on the potential sliding plane. The sliding plane taken into consideration is the concrete to rock contact surface.
The uncracked section is determined computing internal stresses by means of a simplified analysis in which the distribution of the compressive normal stresses throughout the cross sections is linear and no tensile stresses are allowed at the concrete to rock contact. According to this analysis procedure, the cross section of the dam is idealised as a cantilever beam. When at the upstream end of a horizontal plane the predicted compressive stress due to body forces and applied lateral loads disappears as an effect of the increasing level of water, the propagation of a horizontal crack is simulated by reducing the effective area that provides resistance to overturning moments and shear forces. With reference to Figure 1, where M represents the summation of moments of all forces about the centre of gravity of the base, the following equations hold:

Case 1: in absence of uplift pressure

Assuming e = M/N

When e<B/6:
   Be=B
   scmin=N/B-6*M/B^2 (minimum compressive stress)
   scmax=N/B+6*M/B^2 (maximum compressive stress)

When B/6<e<B/2:
   u=B/2-e
   Be=3*u
   scmin=0
   scmax=2*N/(3*u)

Case 3: in presence of uplift pressure

$$B_e = 3 \cdot \left(\frac{B}{2} - \frac{M}{N - p_1 B} \right)$$

$$p_2 = \frac{2 \cdot (N - p_1 B)}{B_e} + p_1$$

Figure 2 shows the results in terms of stresses at the base section obtained, respectively, with uplift pressure absent (Case 1) and present (Case 3). The stresses, expressed in

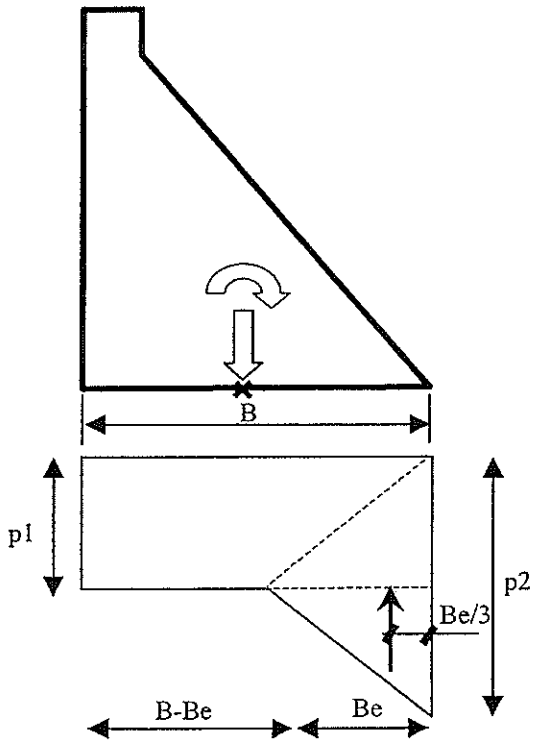

Figure 1. Compression diagram at the concrete to rock contact for cracked section in presence of uplift pressure (U.S. BUREC [1])

N/m², are plotted against the water elevation measured from the base of the dam.

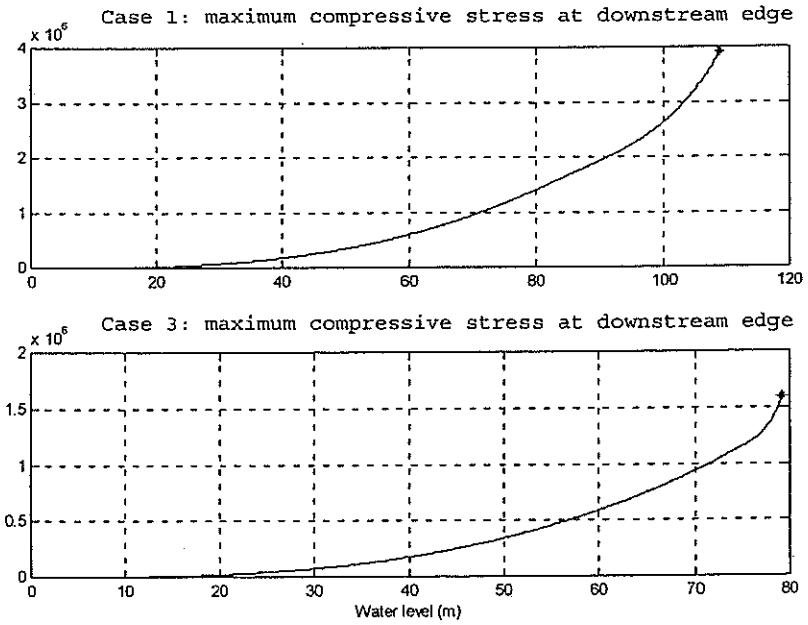

Figure 2. Maximum compressive stress (N/m²) at downstream edge. In Case 1 uplift pressure is not considered. In Case 3 uplift pressure is considered.

The IFF (Imminent Failure Flood) requested for the solution of the problem A2 is the level of overflow at which the failure occurs. Under the above specified assumptions, it is determined by solving the equation:

(1) $S\_OT + S\_I = f*(N-UP) + c*Be$

where the balance of driving forces (first member) and resisting forces (second member) is expressed.

In this equation:

S_OT = horizontal force determined by the height of overtopping corresponding to IFF;
S_I = horizontal force due to water at crown level;
f = friction factor;
N = summation of normal forces;
UP = summation of uplift forces;
c = unit cohesion;
Be = width of the uncracked portion of the section.

Figure 3 highlights the solution of equation (1) carried out to identify the limit condition in case 1. In the upper part of the figure, two curves are plotted representing, respectively, the resisting forces, expressed in N, decreasing when water level increases, and the driving forces, increasing with water level; their common point determines the solution of the equation. Figure 4 provides the same information of Figure 3 for case 2.

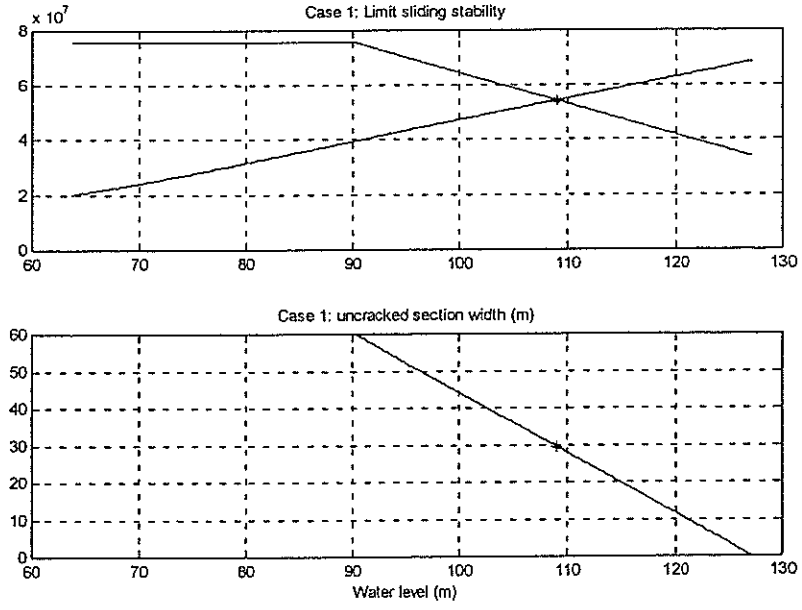

Figure 3

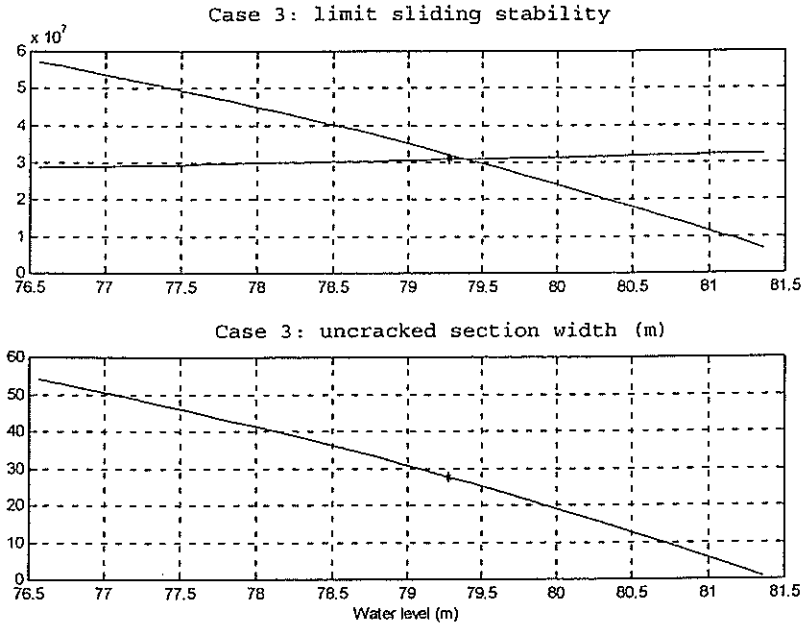

Figure 4

In conclusion, results are summarised in the following points:

- Case 1
  Maximum allowable water level: 109.0 m;
  Uncracked portion of the base section: 29.5 m;
  Maximum compressive stress at downstream edge: 3.92 MPa.
- Case 3
  Maximum allowable water level: 79.3 m;
  Uncracked portion of the base section: 27.8 m;
  Maximum compressive stress at downstream edge: 1.59 MPa.

2.0 NON-LINEAR FINITE ELEMENT APPROACH

When the dam-foundation system subjected to extreme loading conditions and the risk of cracks propagation are taken into account by the Finite Element Method, two cases can be distinguished:

- the crack path is known, as it is often assumed at the rock to concrete contact or in the rock joints;
- the path is not a priori known, as it is in the body of the dam or in the intact rock.

Dealing with the first case, a discrete crack approach can be effectively adopted. In the second case, the pursuit of the crack path would imply repeated re-meshing at the crack tip, a task that can only be performed efficiently by means of a sophisticated computational tool. In the present

context the adoption of the smeared crack technique has been judged more practical. Furthermore, since the magnitude of the uplift loading in case 2 and 3 depends on the length of the crack, the determination of the water level which causes the failure requires the repetition of analyses according to the flow chart reported in figure 5.

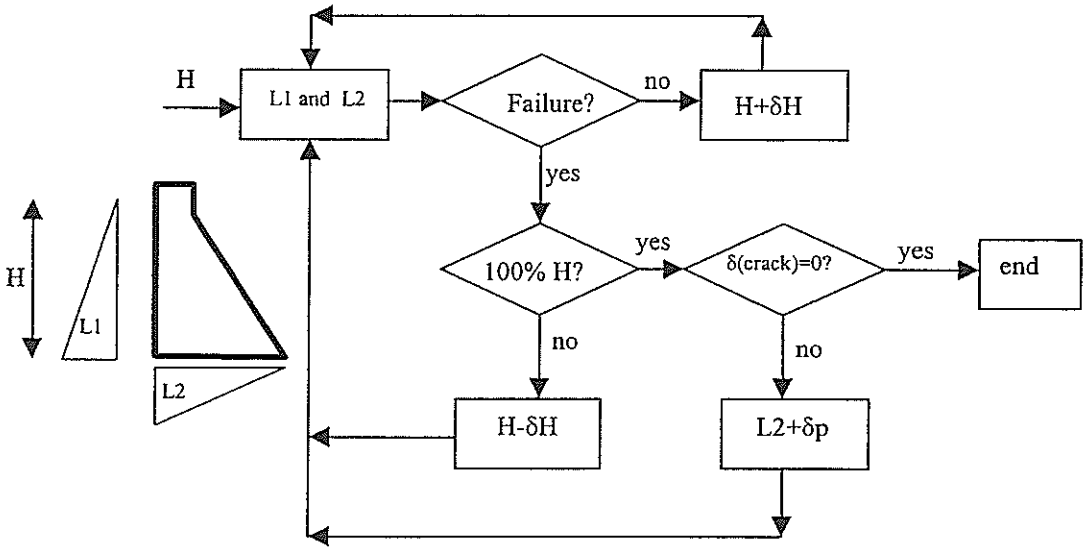

Figure 5

In particular, when the loading incremental procedure for a given level of water H is completed, one has to check if the a priori assumed uplift distribution is consistent with the actual opening of the crack.
All the analyses have been carried out using DIANA code [8]. Three finite element models at different degrees of mesh local refinement have been considered; the first one is denoted in the following as "coarse model" the second as "refined model" the third as "extra-refined model" (Fig. 10). For the "coarse" mesh, four nodes linear elements have been used; for the "refined" mesh eight-node isoparametric elements; for the "extra-refined" mesh three nodes linear elements. Plane strain is assumed in all cases.
Since the attainment of a limit state has to be simulated in the analyses, an incremental procedure where the external loads are increased with fixed load increments can cause very large predictions for displacements. The problem can be solved by means of an indirect displacement control using the "arc-length" method which enables the analyst to constrain the norm of a selected vector of incremental displacements to a prescribed value.

2.1 Model for the rock concrete interface.

The constitutive model was calibrated to follow the specified properties of the joint. Material constants are summarised in the following.
Coulomb friction for interface elements has been specified. The parameters to be defined for this kind of model are: the peak cohesion (coh), the friction angle (φ), the dilatancy angle (ψ). Furthermore the cohesion softening diagram must be defined versus the corresponding equivalent plastic relative displacements. In compliance with the specifications for problem A2 a linear softening has been assumed and:

coh	=	0.7 MPa
φ	=	30 degrees
ψ	=	10 degrees
H	=	-0.7 MPa/mm

Fig. 6 gives the shear force - shear displacement obtained in a displacement controlled shearing test carried out with DIANA and the above material parameters.

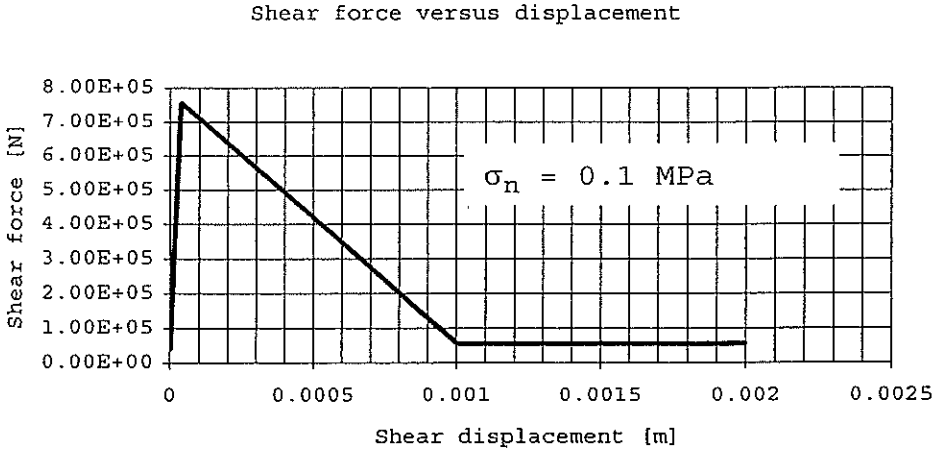

Figure 6

Joint behaviour described in the specifications of the benchmark is a piece-wise linear representation of the actual behaviour of concrete-rock interfaces observed in different laboratory and in situ tests [6,9,10]. For example, Fig. 7,8 show measured values of shear stress vs.

shear displacement for tests run at ISMES [6,10] on some concrete-rock interfaces.

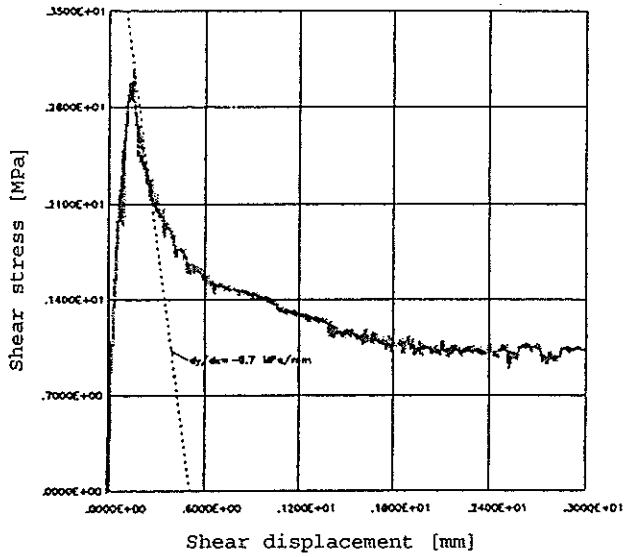

Figure 7. Shear test on a rock-concrete interface: shear stress vs. shear displacement (detail)

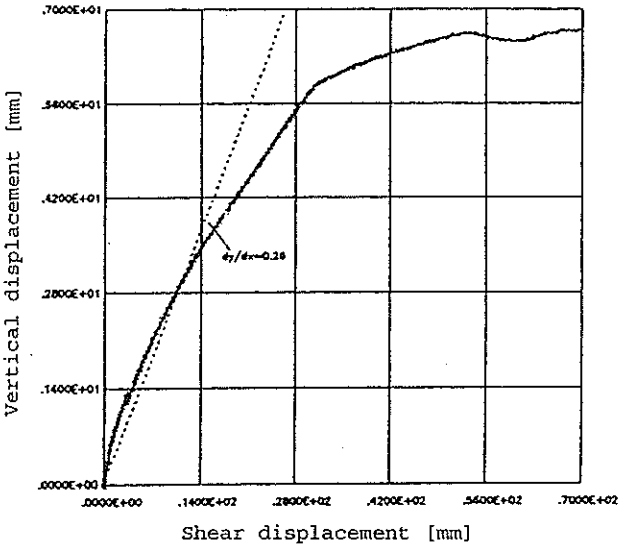

Figure 8. Shear test on a rock-concrete interface: vertical displacement vs. shear displacement

The nominal contact area of the specimen is 0.5 m^2 (Fig. 9). Tests were run under an applied vertical pressure exerted by a servo-controlled flat jack. Nominal applied pressure values (0.5, 1.0, 1.5 MPa) were selected as representative of typical normal stresses acting on a dam-foundation

interface. According to this layout, the joint is free to displace upwards during shearing.
Shearing was applied by hydraulic servo-controlled actuators until a nominal shear displacement of 10% of the contact length (0.7m) was attained. The shearing rate was kept low at low displacement values (1μm/s), where severe peak conditions were expected, and increased thereafter (10μm/s).

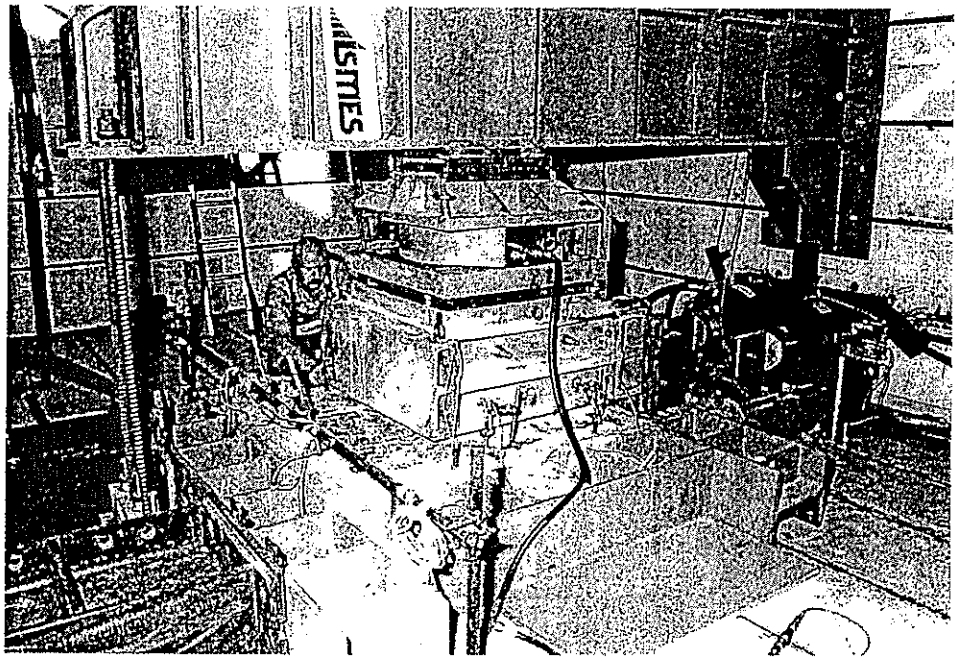

Figure 9. Shear tests on concrete-rock interfaces: layout of the testing apparatus set up at ISMES laboratories.

Shear response is characterised by neat peak stress occurring at very small shear displacements (0.02% of the contact length), followed by a sharp decrease of shear load carrying capacity (softening) accompanied by dilatancy increase(Fig. 8). A clear final stage is observed at a relative displacement of about 2% (residual condition) where the capability of further sustaining shear stress reaches a minimum and where vertical relative displacements stop increasing (Fig. 8). Small variations are then mainly due to non-planar conditions of the average plan of the joint.
In these tests sharp peak conditions are attributed to a very effective locking of rock to concrete enhanced by the interposition of a cement milk, as it was customary in dam construction. Much lower peak strengths are obtained by

avoiding such films of adhesive material [10]. Indeed, whatever the conditions of the contact, a representation of the interface response to shear loads characterised by a peak and a residual stage is considered adequate for the purposes of the exercise.

2.2 Smeared crack model for concrete and rock

The commonly used material model for the behaviour of concrete combines a smeared cracking model for tension with a plasticity model for compression. In analyses where tension and compression arise simultaneously in one particular stress point, these models may lead to numerical oscillation. The code DIANA offers a combined yield criterion to describe both the tensile and compressive regime that is treated as a multi-surface plasticity model [8]. By the Rankine/Von Mises criterion the bi-axial stress state in the material can be modelled by a combination of the yield conditions of Rankine and Von Mises. The first to describe the tensile regime, the latter to describe the compressive regime. Parameters to be defined for this kind of model are: the Rankine yield stress (*fct*), the Von Mises yield stress (*fcc*), the softening diagram with the selected softening hypothesis (strain or work hardening), the fracture energy (*Gf*) and the ultimate softening parameter. The latter depends on the "crack band width" of the element, for which DIANA assumes by default a value related to the square root of the area of the element. In compliance with the specifications for problem A2 it has been assumed:

for concrete
fct = 1.3 MPa
fcc = 24.0 MPa
Gf = 150 N/m
linear softening; internal state variable: equivalent strain.

for rock
fct = 2.6 MPa
fcc = 40.0 MPa
Gf = 200 N/m
linear softening; internal state variable: equivalent strain.

2.3 Case 1 (no uplift pressure)

Results may be summarised as follows (marks (1), (2), (3) are referred to the coarse, refined and locally extra refined meshes respectively).

- Maximum allowable water level:
  - 107 m (1); 101 m (2); 100 m (3).
  Uncracked portion of the base section:
  - 43 m (1); 43 m (2); 45 m (3).
  Maximum compressive stress (downstream toe):
  - 5.78 MPa (1); 6.42 MPa (2); 6.49 MPa (3).
- Diagrams showing displacement δu_x at the crest level versus loading increments: figure C1.1;
- Diagrams showing displacement δu_y at the upstream toe versus loading increments: figure C1.2;
- Diagrams showing normal compressive stresses along the dam base: figure C1.3;
- Diagrams showing shear stresses along the dam base: figure C1.4;
- Deformed shapes preceding failure: figures C1.5.

2.4 Case 2 (uplift pressure with full efficiency of drain)

Main results are:

- Maximum allowable water level: 94 m (2);
  Uncracked portion of the base section: 41 (2)m;
  Maximum compressive stress (downstream): 5.83 MPa (2).
- Diagram showing displacement δu_x at the crest level versus loading increments: figure C2.1.
- Diagram showing displacement δu_y at the upstream toe versus loading increments: figure C2.2.
- Diagram showing normal compressive stresses along the dam base: figure C2.3.
- Diagram showing shear stresses along the dam base: figure C2.4.
- Deformed shapes preceding failure: figure C2.5.

2.5 Case 3 (uplift pressure with zero efficiency of drain)

Main results are:

- Maximum allowable water level: 92 m (2);
  Uncracked portion of the base section: 32 m (2);
  Maximum compressive stress (downstream): 5.63 MPa (2).
- Diagram showing displacement δu_x at the crest level versus loading increments: figure C3.1.
- Diagram showing displacement δu_y at the upstream toe versus loading increments: figure C3.2.
- Diagram showing normal compressive stresses along the dam base: figure C3.3.
- Diagram showing shear stresses along the dam base: figure C3.4.
- Deformed shapes preceding failure: figure C3.5.

2.6 General summary of results

Main results obtained from different analyses are summarised in the following table.

		Mesh	H m	B_e m	σ_{min} MPa	UB_x mm	UA_y mm	σ_n MPa	τ MPa
Rigid block	Case 1	-	109	29	-	-	-	3.9	2.9
	Case 3	-	79	28	-	-	-	1.6	1.6
Finite element	Case 1	(1)	107	43	5.78	33.8	3.80	2.78	1.61
		(2)	101	43	6.42	26.2	1.65	3.13	2.46
		(3)	100	45	6.49	21.7	1.12	3.20	2.52
	Case 2	(2)	94	41	5.83	21.9	1.87	2.88	2.34
	Case 3	(2)	92	32	5.63	20.0	1.33	2.78	2.29

The column containing "Mesh" at the heading indicates the refinement of the finite element discretisation, i.e. "coarse", "refined" and "extra-refined" for (1), (2) and (3) respectively. Furthermore: H, B_e, σ_{min}, UB_x, UA_y, σ_n, and τ stand for maximum allowable water level, uncracked portion of the base section, minimum principal stress at downstream toe, maximum horizontal displacement at the crown level, maximum vertical displacement at the upstream toe, maximum vertical compressive stress at downstream toe and maximum shear stress along the rock-concrete interface respectively.
We can compare results derived from the rigid block and finite element methods with each other as well as results obtained from the different finite element models used in case 1. Looking at maximum allowable water level H

determined in absence of uplift (case 1) we can observe a satisfactory agreement between the rigid block and the coarse finite element model whereas significant discrepancies appear among the results derived from the three finite element models. The observed agreement on the water height between rigid block and coarse finite element models is lost when we look at the extension of the uncracked section Be. With the rigid block method we have a value of 28 m whereas with f.e. models we have 43, 43, 45 m for coarse, refined and locally extra refined models respectively. The divergences revealed by the f.e. models, although present, can be considered negligible.
When we consider the minimum principal stress at downstream edge of the dam, the result derived from the refined f.e. model matches quite well the one derived from the extra refined f.e. model; on the other hand both these results are rather different with respect to the value obtained from the coarse mesh.
Last, if we, always for case 1, consider displacements, we can again note rather significant discrepancies: for instance the extra refined model provides the lowest value of horizontal displacement at crown level (i.e. 21.7 mm for a water level equal to 100 m) whereas the almost equal water level attained by the refined model (101 m) causes a displacement remarkably greater (26.2 mm). This result can be explained considering that the extra refined mesh has very small elements at the bottom of the dam but the element's size increases rapidly along the height of the dam. This fact causes a higher average stiffness of the dam and, in addition, makes inaccurate the reproduction of stresses at the mid height of the dam.
For case 3, looking at the maximum water level, we can note a big discrepancy between the result derived from rigid block (i.e. 79 m) and finite element (i.e. 92 m).

3.0 CONCLUDING REMARKS

The stability of an overtopped gravity dam has been analysed into two different frameworks, namely the rigid block method, widely used in the engineering practice, and the non linear fracture mechanics approach implemented in the finite element method.
The results obtained have pointed out some features of these analytical tools which deserve further effort to allow for a more certain approach to the problem.

To enhance modelling capabilities, numerical and experimental investigations should be strengthened.
Numerical experimentation is necessary to gain more confidence about the robustness of algorithms in non linear solution procedures especially when a fast softening post peak behaviour is expected; in this study it has been proved that different load histories can cause the incapacity of finding static equilibrium, most likely as a consequence of purely numerical divergence. A further need really felt in practice consists in the detection of clear rules which enable the analyst to select appropriate levels of discretisation in finite element modelling. With regard to experimentation, data on uplift pressure and drain efficiency and complete case histories should be collected and used to validate predictive numerical models.

4.0 REFERENCE

[1] U.S. Department of Interior - Bureau of Reclamation, "Design of small dams", A Water Resources Technical Publication, 1987

[2] Z.P.Bazant, "A critical appraisal of no-tension dam design: a fracture mechanics viewpoint", Dam Engineering, Vol.I Issue 4, October 1990

[3] V.E.Saouma, D.Milner, "On why fracture mechanics should be adopted for dam safety investigation", Dam Engineering, Vol.VII Issue 3, October 1996

[4] H.N.Linsbauer, "Fracture mechanics models for characterising crack behaviour in gravity dams, 15th ICOLD Lausanne, Vol.2, pp.279-291, 1985

[5] S.Bhattacharjee, P.Leger, "Fracture response of gravity dams due to rise of reservoir elevation", ASCE Journal of Structural Engineering, Vol.121, No.9,September 1995

[6] D'Andrea L. and Imperato L., "Valutazione e previsioni delle proprietà delle discontinuità strutturali in opere di sbarramento in calcestruzzo", ISMES Report for ENEL PIS (in Italian) RAT-STR-2658/97, 1997

[7] E.Hinton, R.Owen, "Computational modelling of reinforced concrete structure", Chap.2, R.DeBorst, "Computational aspects of smeared crack analysis", Pineridge Press Limited, Swansea U.K., 1986

[8] DIANA Finite Element Analysis, User's Manual, "Non linear analysis" Release 6.1, TNO Building and Construction Research

[9] EPRI TR-100345, Uplift Pressures, Shear Strengths and Tensile Strengths for Stability Analysis of Concrete Gravity Dams, Volume 1, Final Report - August 1992
[10] Lozza S. Attività sperimentale di novembre-dicembre 1998 su modelli fisici di beola e calcestruzzo senza interposizione di latte di cemento. ISMES Report for ENEL PIS (in italian) RAT-STR-2223/98, 1998.

ACKNOWLEDGEMENT

Authors wish to thank Mr. A. Bariletti for his smart collaboration in running analyses and editing figures.

Coarse Model - ndof = 3301
Refined Model - ndof = 9722

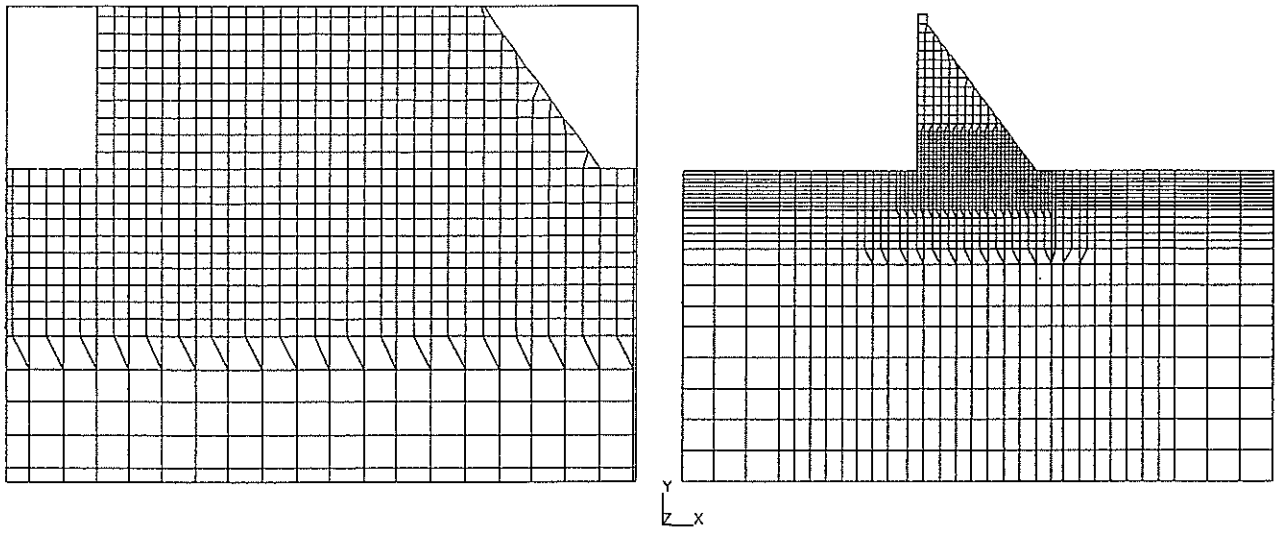

Locally Extra Refined Model - ndof = 6650

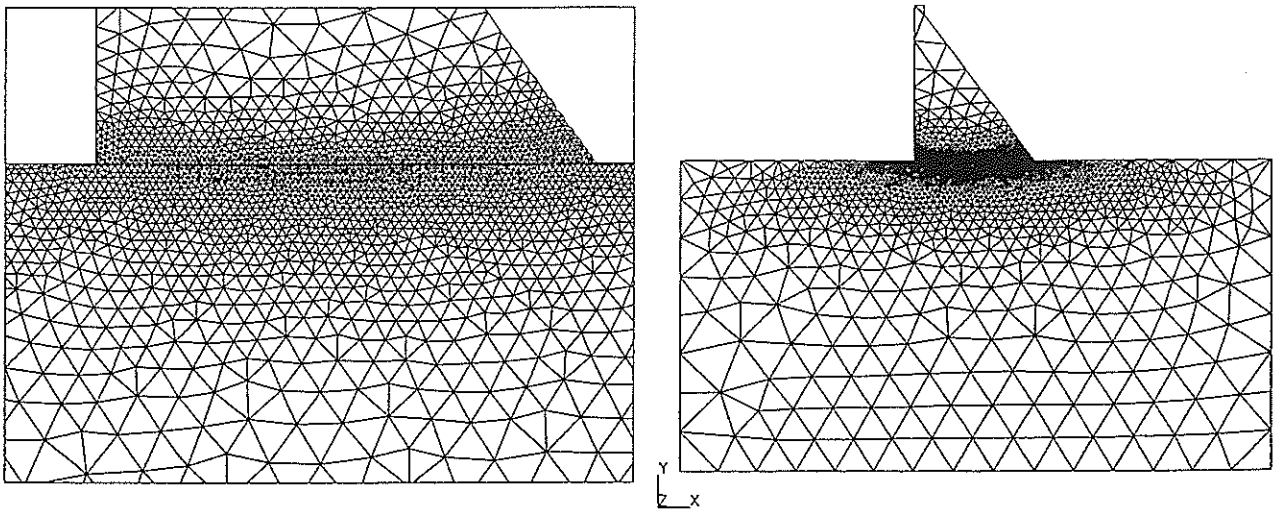

Figure 10

(1) Coarse Model - Horizontal displacement point B

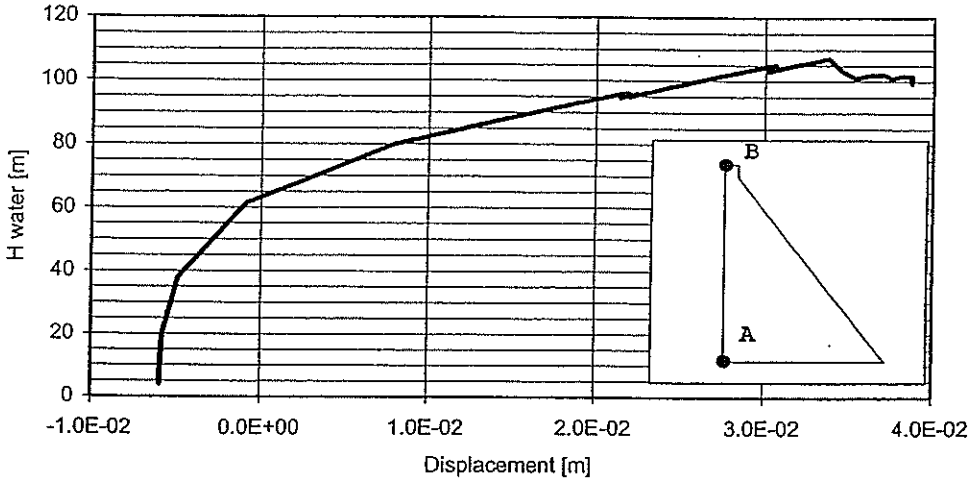

(2) Refined Model - Horizontal displacement point B

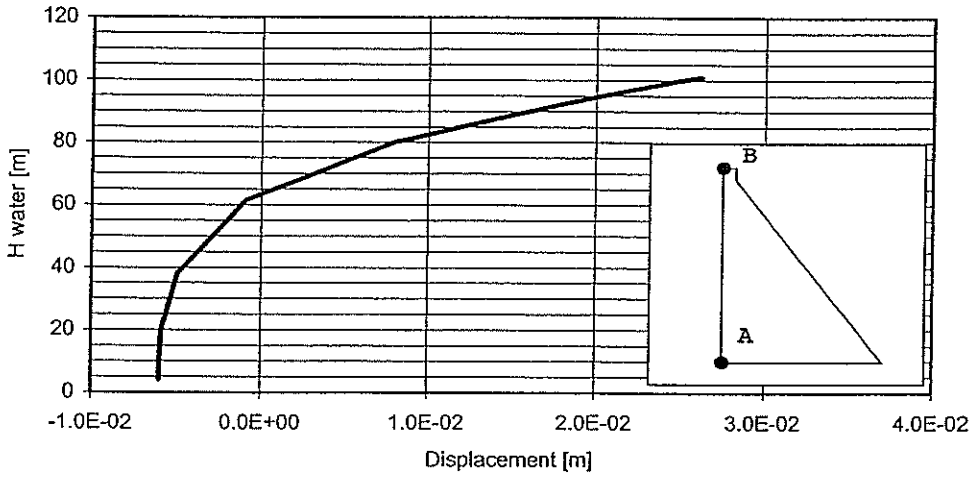

(3) Extra Refined Model - Horizontal displacement point B

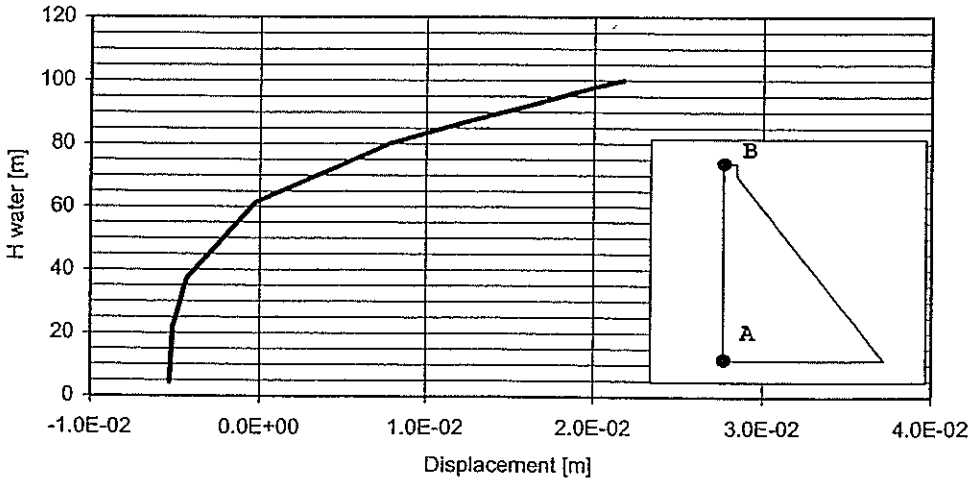

Figure C1.1 - Case 1 - No uplift pressure

(1) Coarse Model - Vertical displacement point A

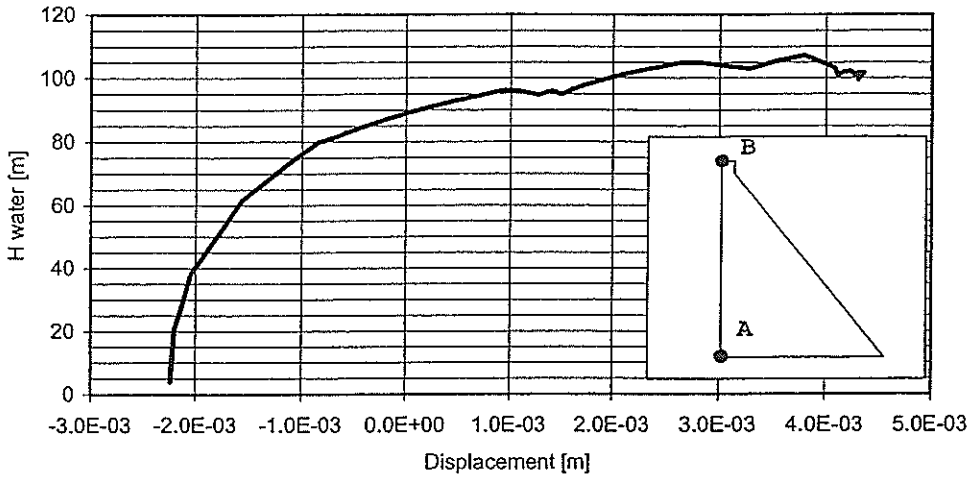

(2) Refined Model - Vertical displacement point A

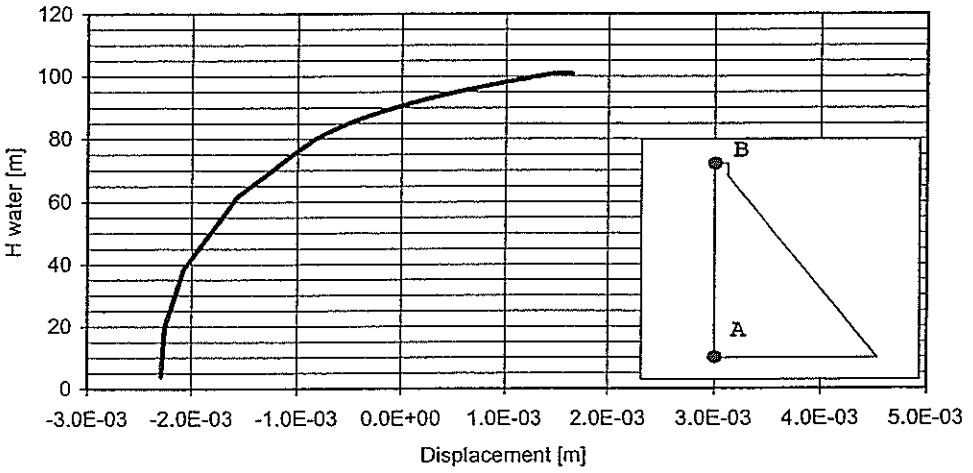

(3) Extra Refined Model - Vertical displacement point A

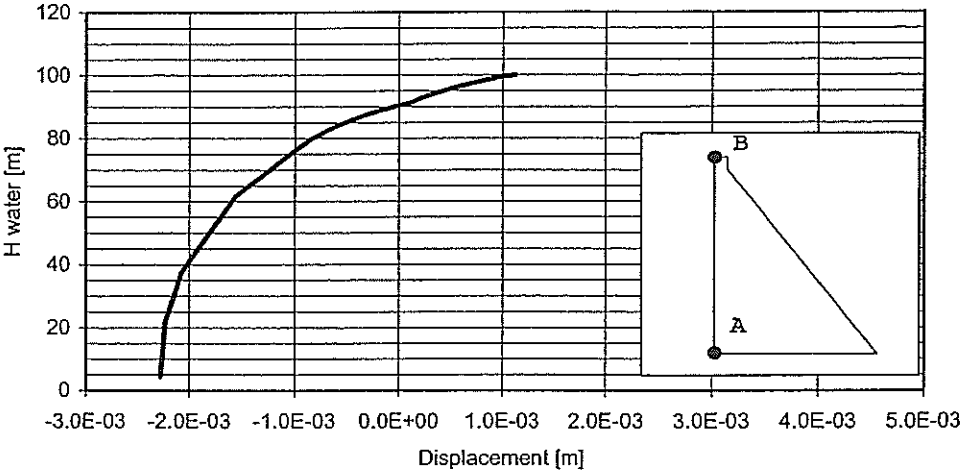

Figure C1.2 - Case 1 - No uplift pressure

(1) Coarse Model - Normal Tractions along the dam base [Pa]

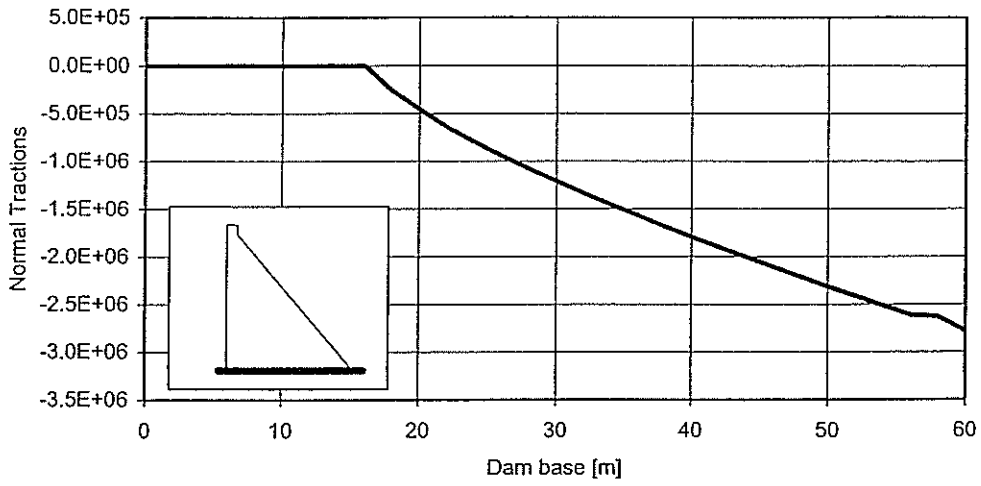

(2) Refined Model - Normal Tractions along the dam base [Pa]

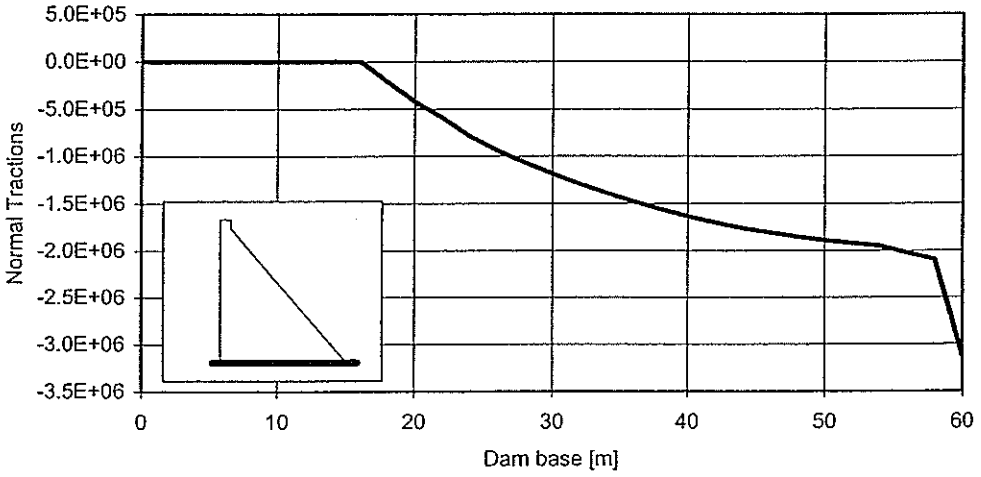

(3) Extra Refined Model - Normal Tractions along the dam base [Pa]

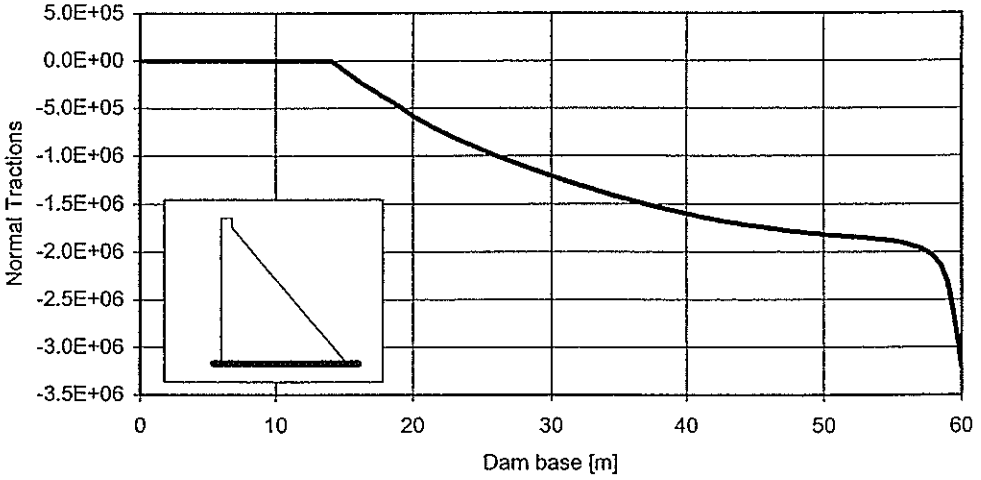

Figure C1.3 - Case 1 - No uplift pressure

(1) Coarse Model - Shear Tractions along the dam base [Pa]

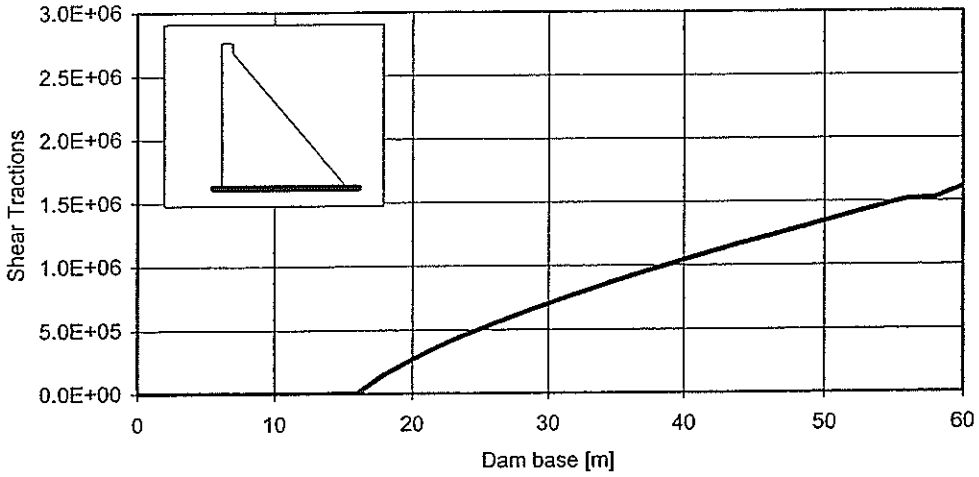

(2) Refined Model - Shear Tractions along the dam base [Pa]

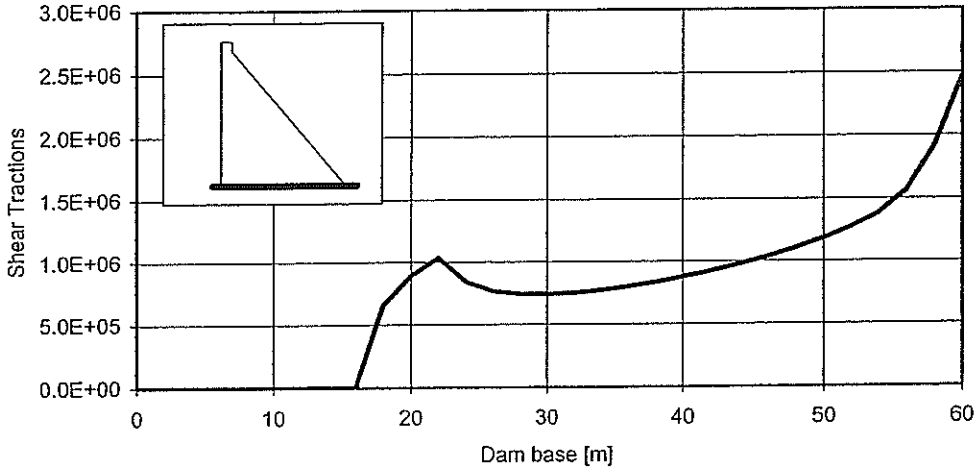

(3) Extra Refined Model - Shear Tractions along the dam base [Pa]

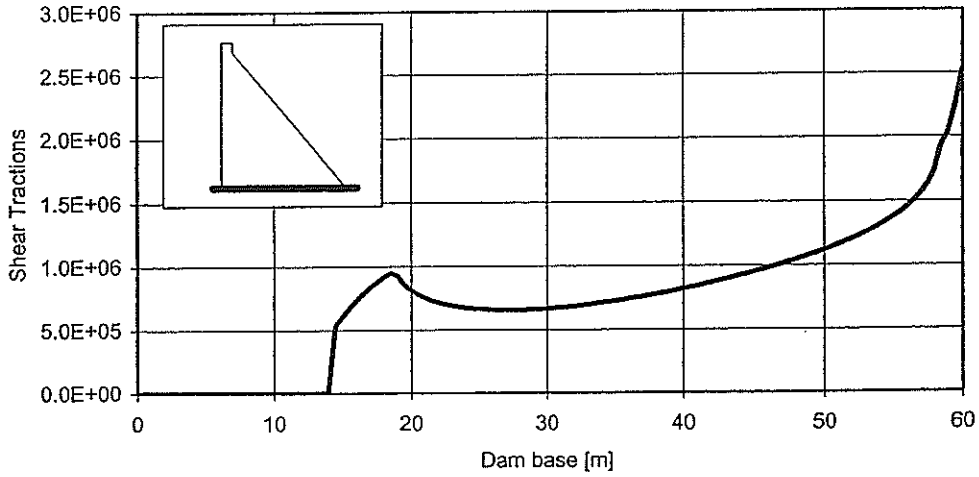

Figure C1.4 - Case 1 - No uplift pressure

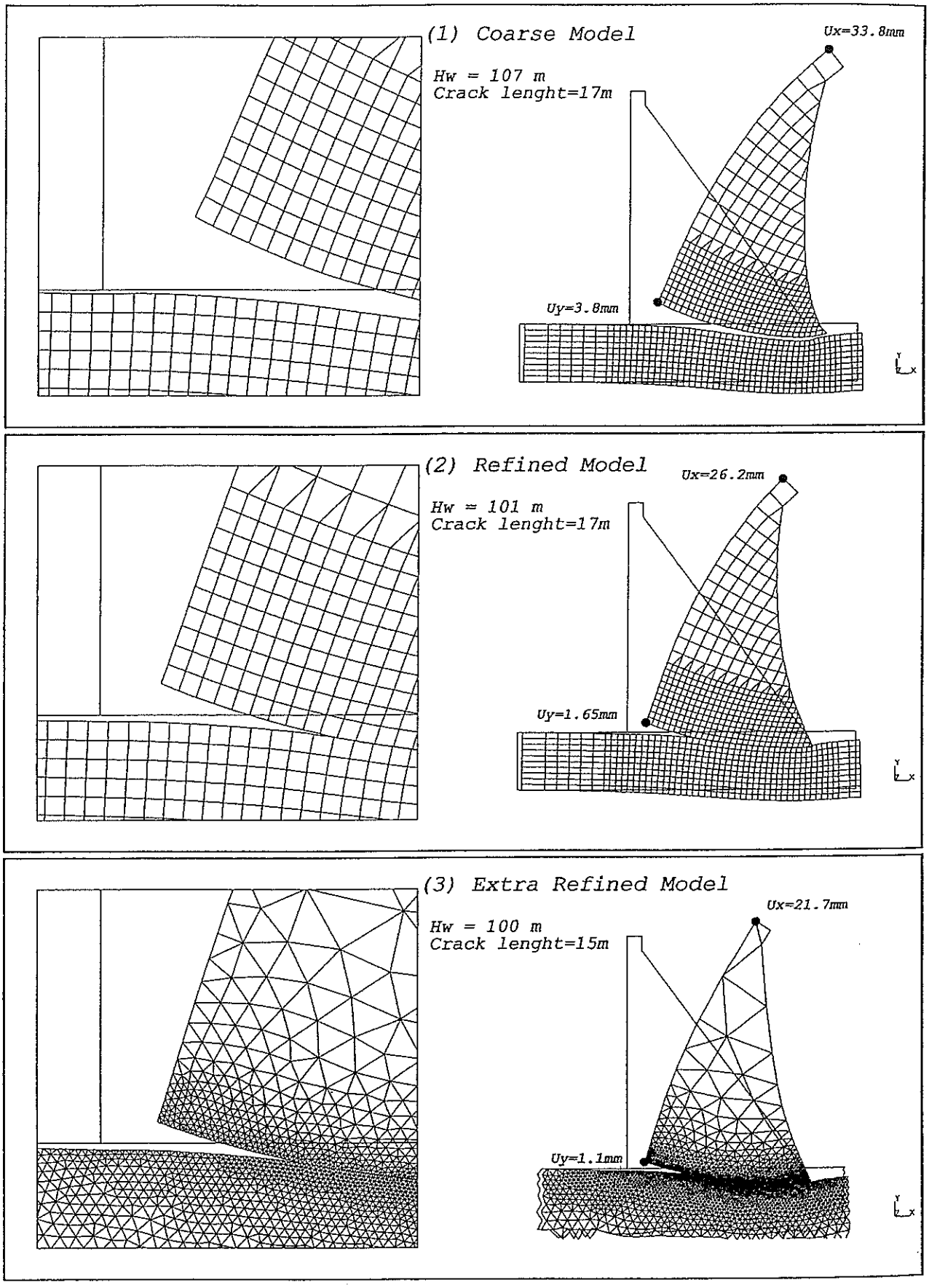

Figure C1.5 - Case 1 - No uplift pressure

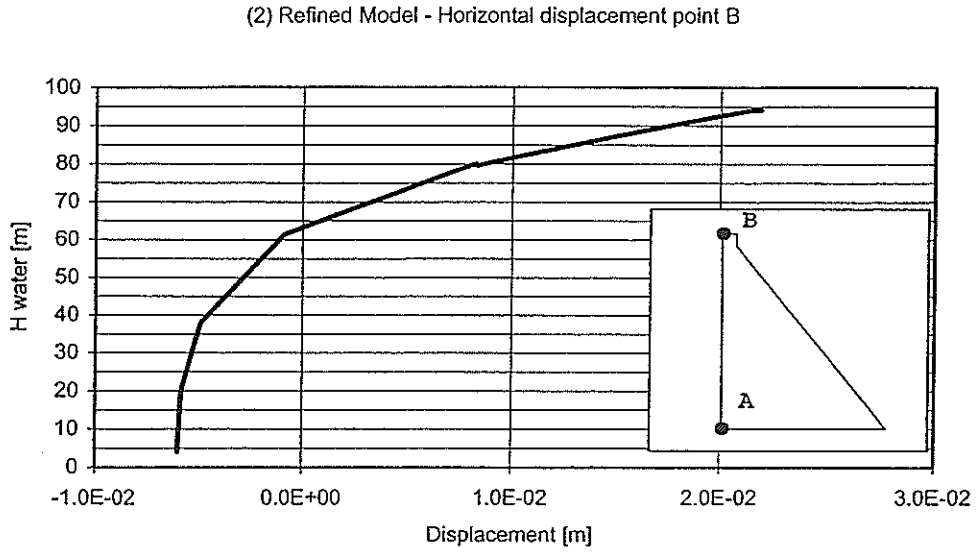

Figure C2.1 - Case 2 - Uplift pressure with 100% efficency of drain

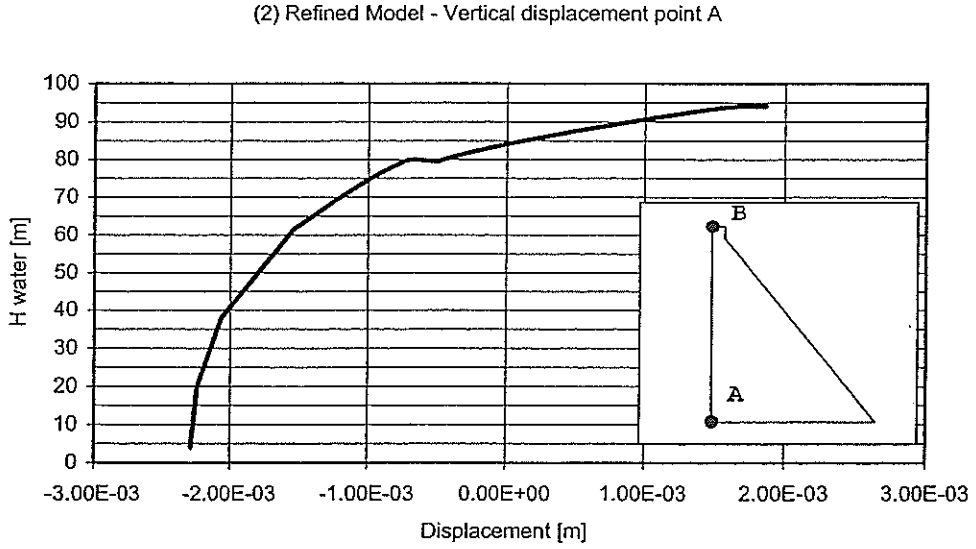

Figure C2.2 - Case 2 - Uplift pressure with 100% efficency of drain

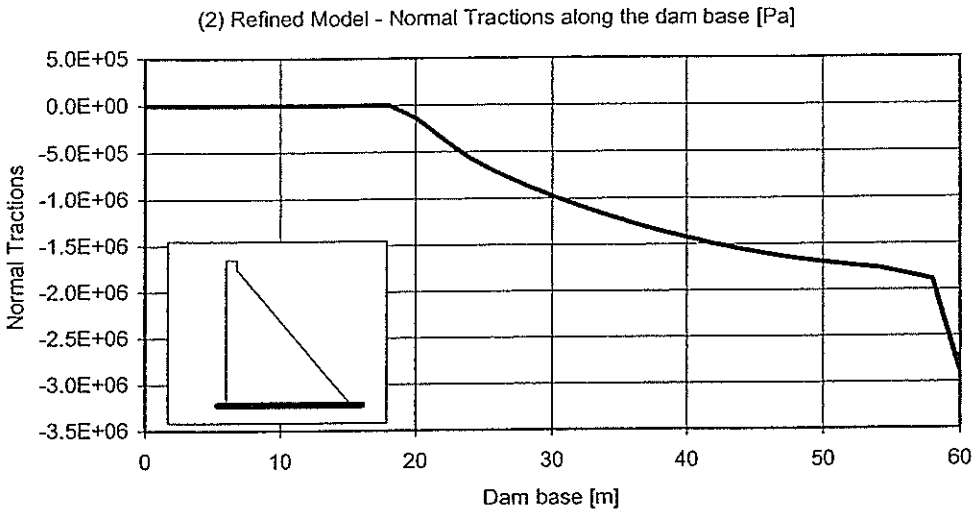

Figure C2.3 - Case 2 - Uplift pressure with 100% efficency of drain

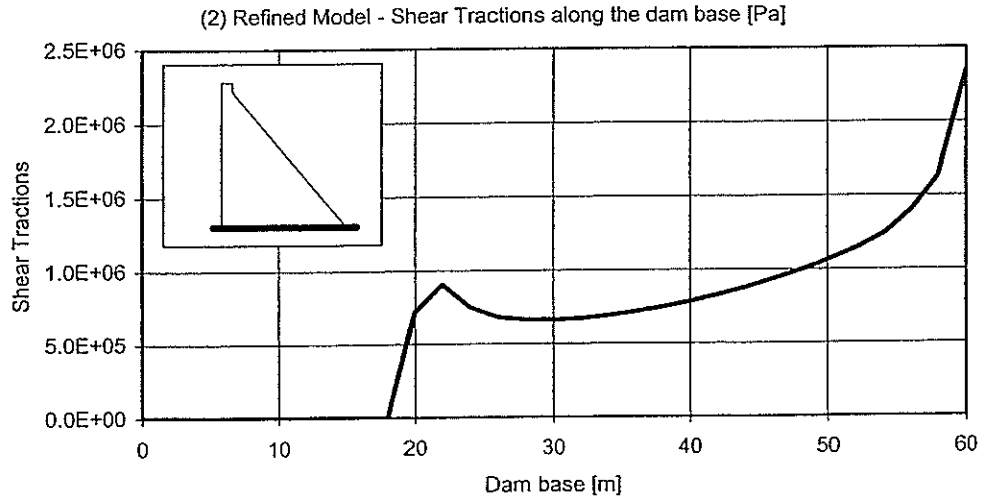

Figure C2.4 - Case 2 - Uplift pressure with 100% efficency of drain

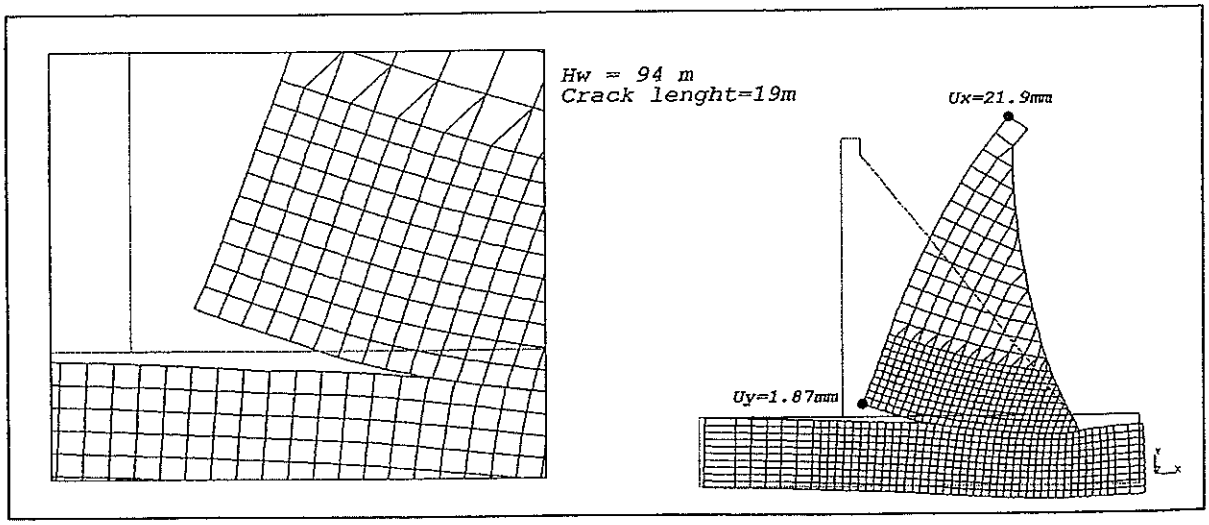

Figure C2.5 - Case 2 - Uplift pressure with 100% efficency of drain

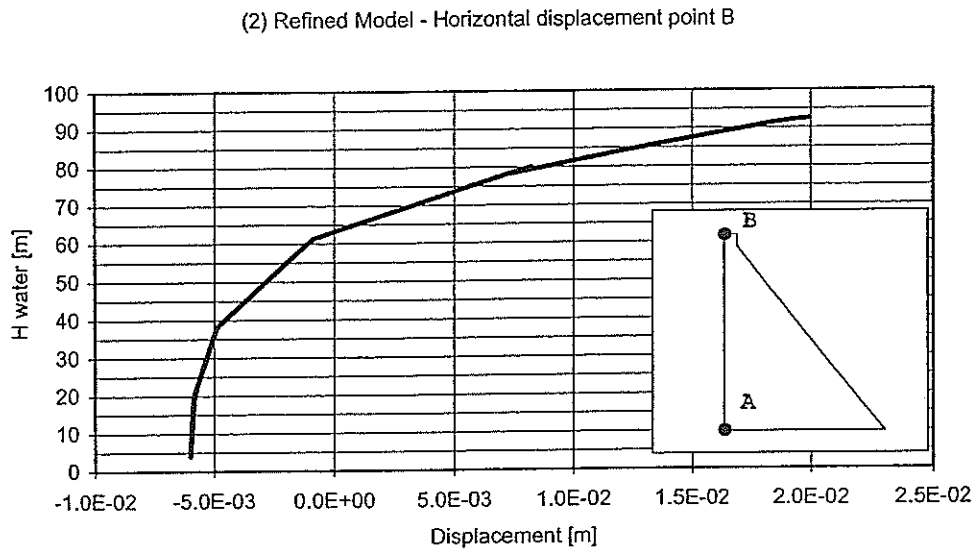

Figure C3.1 - Case 3 - Uplift pressure with zero efficency of drain

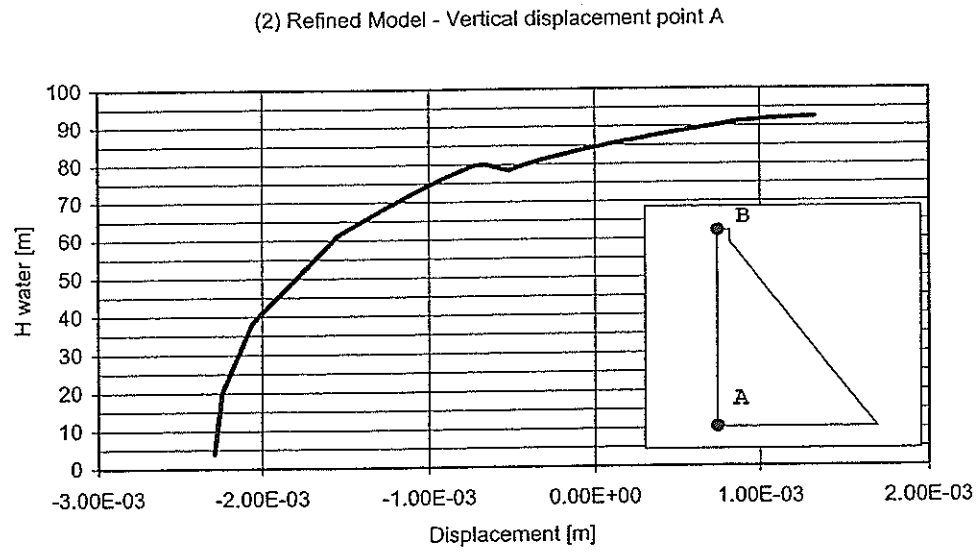

Figure C3.2 - Case 3 - Uplift pressure with zero efficency of drain

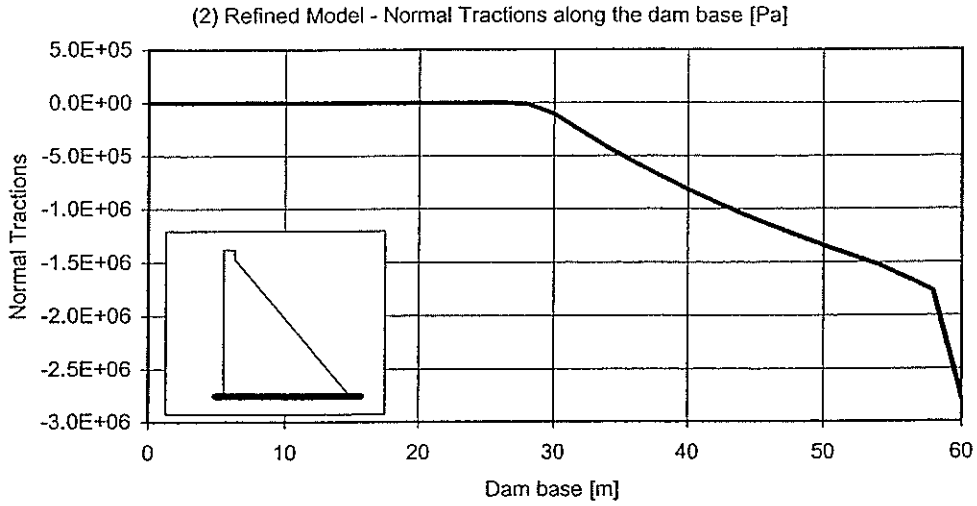

Figure C3.3 - Case 3 - Uplift pressure with zero efficency of drain

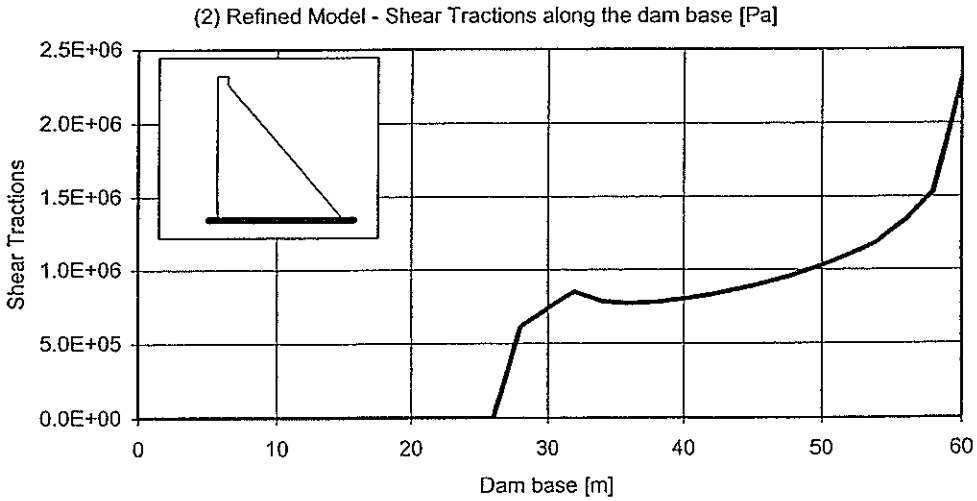

Figure C3.4 - Case 3 - Uplift pressure with zero efficency of drain

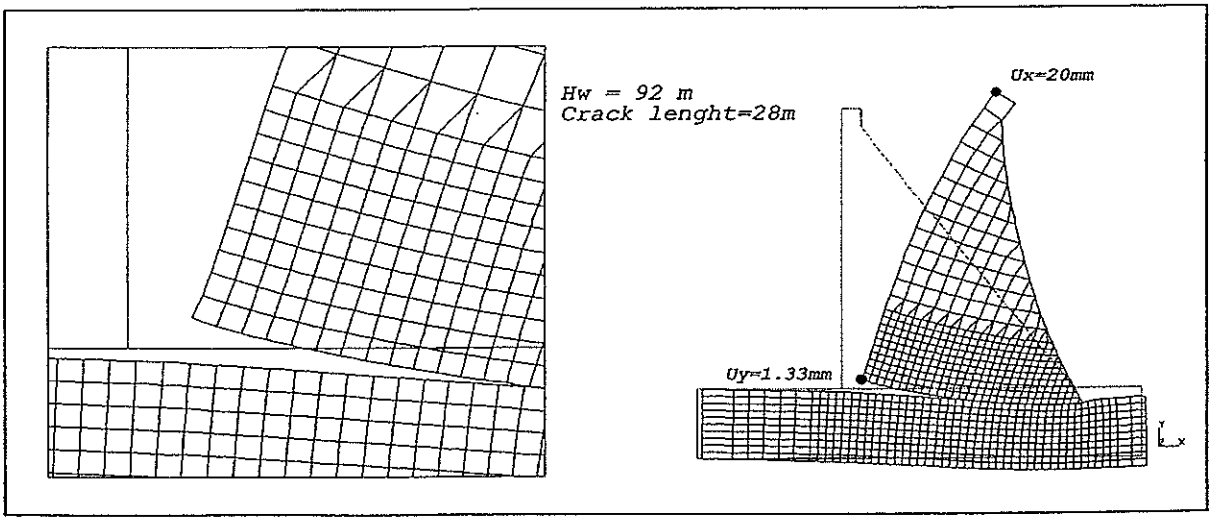

Figure C3.5 - Case 3 - Uplift pressure with zero efficency of drain

Fifth Benchmark Workshop on

Numerical Analysis of Dams

Theme B1 - Stability analysis of a homogeneous embankment dam

1 INTRODUCTION - SCOPE OF THEME B1

During the IVth Benchmark Workshop held in Madrid in September 1996, the need was identified for setting up bridges between, on a one hand, conventional stability analyses which use forces and provide safety factors and, on the other one, rheological models whose basic variables are displacements, stresses and materials states.

The purpose of this Theme B1 is to provide a common frame for several types of methods to be performed and finally compared, from the FELLENIUS circular stability method to the most advanced models using coupled constitutive laws for soils. The only common aspects are that all analyses are 2-D, and they should be carried out in effective stresses. The range of methods being used is quite open, although the same sets of data should be used, and a minimum set of key results should be provided in all cases.

In order to avoid further discrepancies between results, the subject for Theme B1 has been kept rather simple. It takes inspiration from the history of a small homogeneous earthfill dam which was built in Southern France in the early eighties, which has shown some evidence of unstability during the first drawdown of its reservoir. Pore pressure, influenced by a high initial degree of saturation, appeared to be the critical factor. However it must be pointed out that the conditions proposed below for the simulation have substantially been altered from those observed on the prototype, in order to make the analyses more attractive.

The proposed simulations consist in calculating safety factors prevailing at the upstream shell : A) at the end of construction, B) in normal operation conditions, at the end of impounding, and C) after a rapid drawdown. The pore pressure field relative to these three conditions should be taken into account.

The pore pressure field should preferably be determined through a coupled (mechanical/hydraulical) analysis, and enough experimental data are provided for such analyses to be carried out. However, for those who would like to carry out stability analyses only, information is provided to estimate pore pressure through simplified methods of their choice.

The stability of the upstream shell of the dam shall be estimated through determination of safety factors. The calculations shall be carried out in effective stresses, using the corresponding pore pressure fields for the three conditions.

The determination of safety factors should be carried out by one of the following ways:

i) using conventional stability methods : in this case, safety factors will be calculated according to their definition in the method being referred to (i.e. derived from the equilibrium of forces, momentums, etc.) ; at least FELLENIUS and BISHOP results shall be provided along a specified circular failure line; other results obtained with other methods and/or other worse failure lines may also be given;

ii) using rheological models (finite elements or others) : in this case, the behaviour of the fill will be calculated, in terms of (elastic and plastic) displacements, effective stresses etc., with different sets of strength properties, and the safety factor will be defined as the reducing factor which, applied to the strength parameters, produce the failure of the system[1].

Each participant is requested to produce his results in a paper which should not exceed 14 pages, and should include:

- the methodology used for the analyses,
- the selected computation method(s),
- the main assumptions for the numerical model adopted, if not widely used,
- the software used,
- the results, in specified formats (result sheets B1-A, B1-B and B1-C) for purpose of comparison,
- any additional useful result or information.

2 INPUT DATA

2.1 Geometrical definition

This prototype dam has been built in 1979-1980 with a purpose of irrigation; it creates a small reservoir of 4 million cubic metres which is filled each year in spring, water being released during the summer. The cross section of the dam is shown in Figure 1 and its main characteristics are given in Table 1.

1 *From numerical point of view the failure is reached when the tangent stiffness matrix reaches a singularity. In practice this state can be considered to be attained when the order of magnitude of the maximum displacement is changed.*

Table 1: Characteristics of the dam	
Maximum height above foundation	24 m.
Crest length	100 m.
Volume of fill	140 000 m^3
Crest elevation	384.70 masl
Crest width	5.00 m.
Slope of upstream face	3H / 1V
Slope of downstream face	2.5H / 1V
Nature of fill	clay and clayey loam
Nature of foundation	rock
Internal drainage	vertical + horizontal

The suggested simplified section for computation purposes is defined in Figure 2 and Table 2.

Table 2: Geometrical definition of the cross section			
Point	**Description**	**Y**	**Z**
a	base of U/S face	-76.60	362.00
b	U/S face	-35.50	375.70
c	U/S face	-29.50	375.70
d	Crest	-2.50	384.70
e	Crest	+2.50	384.70
f	D/S face	+56.75	363.00
g	base of D/S face	+59.25	362.00
h	base of vertical drain	-0.50	362.00
i	top of drain	-0.50	381.80
j	top of drain	+0.50	381.80
k	base of vertical drain	+0.50	363.00
l	upper limit of material 1 (U/S)	-52.60	370.00
m	upper limit of material 1 (drain)	-0.50	370.00
n	upper limit of material 1 (drain)	+0.50	370.00
o	upper limit of material 1 (D/S)	+39.25	370.00
p	upper limit of material 2 (drain)	-0.50	375.70
q	upper limit of material 2 (drain)	+0.50	375.70
r	upper limit of material 2 (D/S)	+25.00	375.70

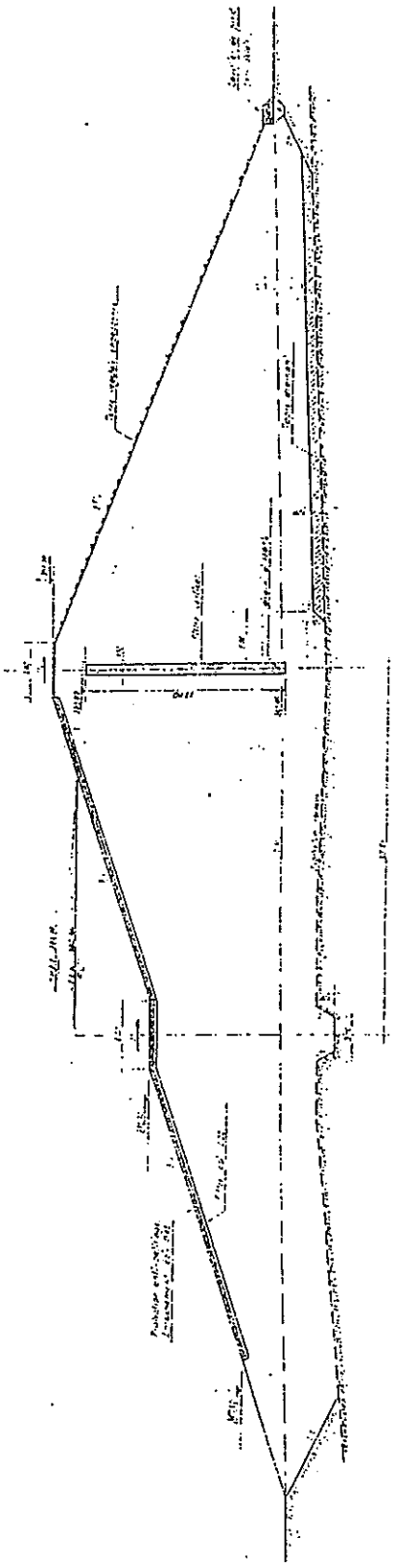

Figure 1: Cross section of the prototype dam

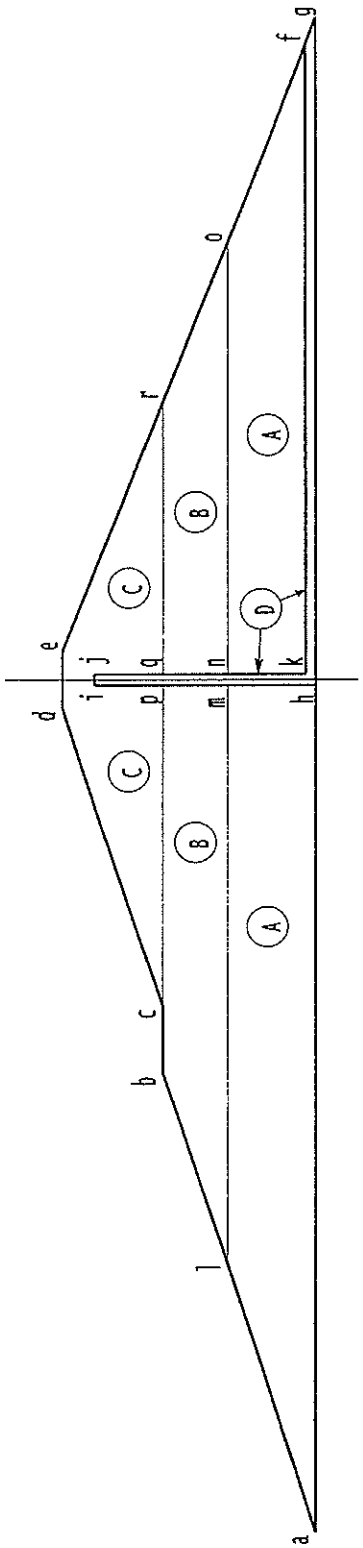

Figure 2: Simplifies cross cection for analysis

2.2 Material properties

The characteristics of the materials are given in Table 3. Their numbers correspond to their location also shown on Figure 2.

Table 3: Properties and initial conditions of materials in the fill

Materials :			Clayey loam	Clay		Drain
Characteristics	**Name**	**Unit**	**A**	**B**	**C**	**D**
Specific weight of grains	**G**	kN/m³	27.3	27.3		-
Young's modulus	E_y	MPa	8	5		80
Poisson's ratio	ν		0.3	0.3		0.3
Effective shear angle	Φ'	°	32	26		36
Effective cohesion	**C'**	kPa	10	18		0
Dilatancy angle	ψ (1)	°	5	5		5
Vertical permeability	K_v	m/s	4.0×10^{-9}	1.0×10^{-9}		1×10^{-3}
Horizontal permeability	K_h	m/s	16.0×10^{-9}	4.0×10^{-9}		1×10^{-3}
Proctor Opt. water content	W_{opt}	%	14.5	18.5		-
Proctor Opt. dry density	$\gamma_{d.opt}$	kN/m³	18.0	17.2		-
Properties at time of placement						
Water content	W_i	%	16.5	20.7	21.2	8
Saturation ratio	***Sr***	%	95.1	94.7	95.5	
Dry density	γ_d	kN/m³	18.0	17.1	17.0	18.6
Measured ratio $u/\gamma.h$	r_u	-	0.45	0.70	0.45	0
Properties in operation						
Skempton coefficient	**B**		0.90	0.80	0.80	1.0

Note (1) : dilatancy angle ψ is required only with a Mohr-Coulomb model with a non-associated flow rule; otherwise $\psi = \Phi$.

The foundation below el. 362 is supposed to be infinitely rigid and watertight rock.

3 ANALYSES TO BE CARRIED OUT

3.1 History and load cases

The simplified history proposed for simulation is given in Table 4 below together with the different conditions for analysis A, B and C. These correspond to the end of construction, the end of the first impounding, and the end of the first drawdown. Only the stability of the upstream shell of the dam will be analysed.

Table 4: Summarised time-history for analyses		
Period	**From start of Month n°**	**To end of Month n°**
Construction	1	12
Analysis A		***12***
First impounding	13	18
Analysis B		***18***
First drawdown	19	22
Analysis C		***22***

3.2 Stability condition A : End of construction

Construction shall be supposed to have occurred during 12 months at a constant rate of elevation from 362 to 384.70. The dam condition at the end of Month n°12 will be analysed as condition A.

3.2.1 Pore pressure field

The pore pressure field shall be determined either by a coupled (mechanical/hydraulical) analysis of construction and consolidation, or by simplified methods, or by a combination of simplified methods and seepage analyses.

Results shall be provided on the upper part of Result sheet B1-A and shall include:

- pore pressure at specified points P1, P2 and P3,
- graph of pore pressure map with iso-contours at 2 metres intervals.

3.2.2 Safety factors

The stability analyses at the end of construction shall be carried out with the pore pressure field obtained as explained above.

The conventional stability analyses shall include the circular failure line C1 defined on Figure 3.

Whatever the method being used, results will be given on the lower part of Result sheet B1-A and shall include:

- Safety factor along circle C1 with the FELLENIUS method,
- Safety factor along circle C1 with the BISHOP method.

Safety factors obtained along other more critical failure lines may optionally be added; in this case the failure line(s) will be indicated on the graph. Methods of analysis different from the two specified will be explained in the text.

If rheological models are used to determine safety factor, the safety factor obtained will be reported in the last column of the result sheet, and the curve giving the displacement at crest level (point P4) Vs reducing factor should be given. If the failure line is determined (e.g. as the line with maximum displacement gradients), the map of incremental displacements and/or plastic strains will be given on the graph, and the method used will be explained in the text.

3.3 Stability condition B : End of first impounding

The reservoir impounding shall be supposed to have occurred during 6 months from the beginning of Month 13 to the end of Month 18, at a constant rate of elevation from 362 to 381.30. The dam condition at the end of Month n°18 will be analysed as condition B.

Results of the pore pressure determination and stability analyses shall be provided on Result sheet B1-B and shall include the same elements as for condition A.

Specified points for pore pressure
P1: Y=-20.00 Z=372.00
P2: Y=-14.00 Z=376.00
P3: Y=-8.00 Z=380.00

Specified points for displacements
P4: Y=-29.50 Z=375.70
P5: Y= -2.50 Z=384.70

Specified failure line C1
Circle center: Yc=-20.00 Zc=392.00
Circle radius R=20.00 m.

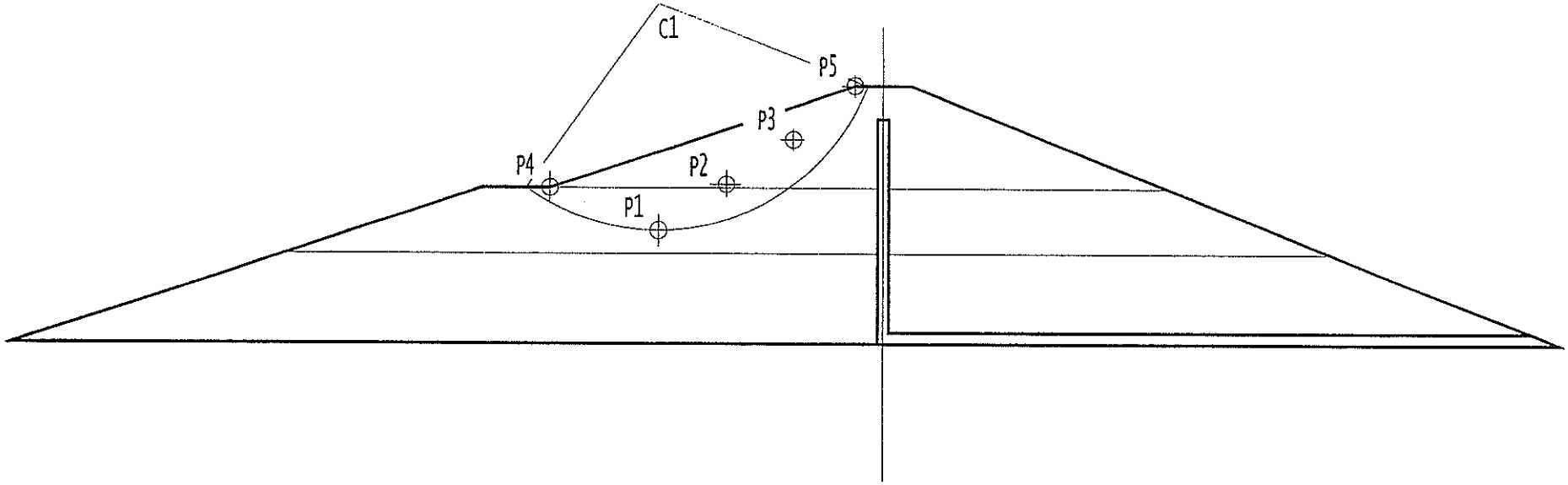

Figure 3 : Specified results

3.4 Stability condition C : End of first drawdown

The lowering of the reservoir shall be supposed to have been done at a constant rate from el. 381.30 at the beginning of Month 19, to el. 362 at the end of Month 22.

The dam condition at the end of Month n°22 shall be analysed as condition C.

Results of the pore pressure determination and stability analyses shall be provided on Result sheet B1-C and shall include the same elements as for conditions A and B.

Result sheet B1-A: End of Construction

1 - Pore pressure

Point	P1	P2	P3
Pressure (kPa)			
Head (m)			

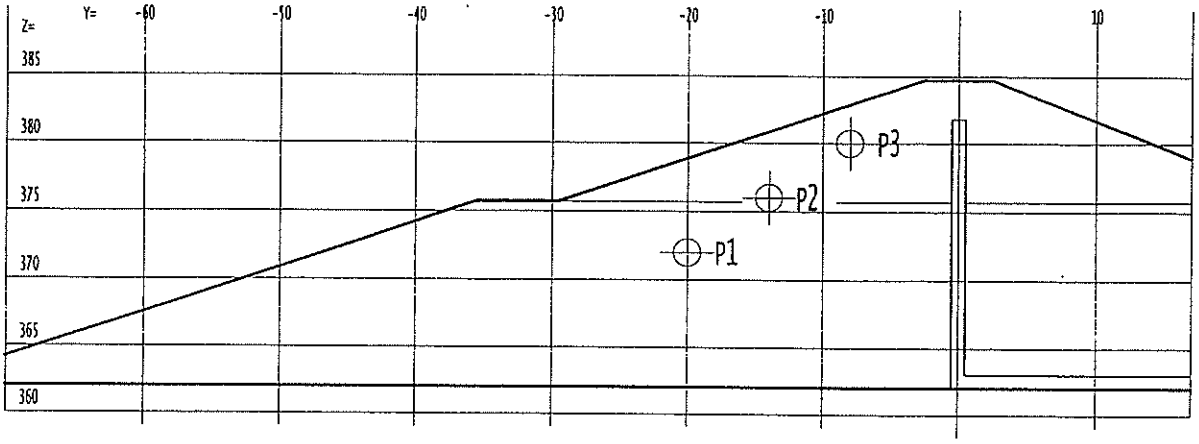

2 - Stability - Factors of safety

Failure line	Circle C1	Critical line
SF (Fellenius)		
SF (Bishop)		
SF (other)		

F factor	Displacement P4 (cm)		Displacement P5 (cm)	
	dY	dZ	dY	dZ

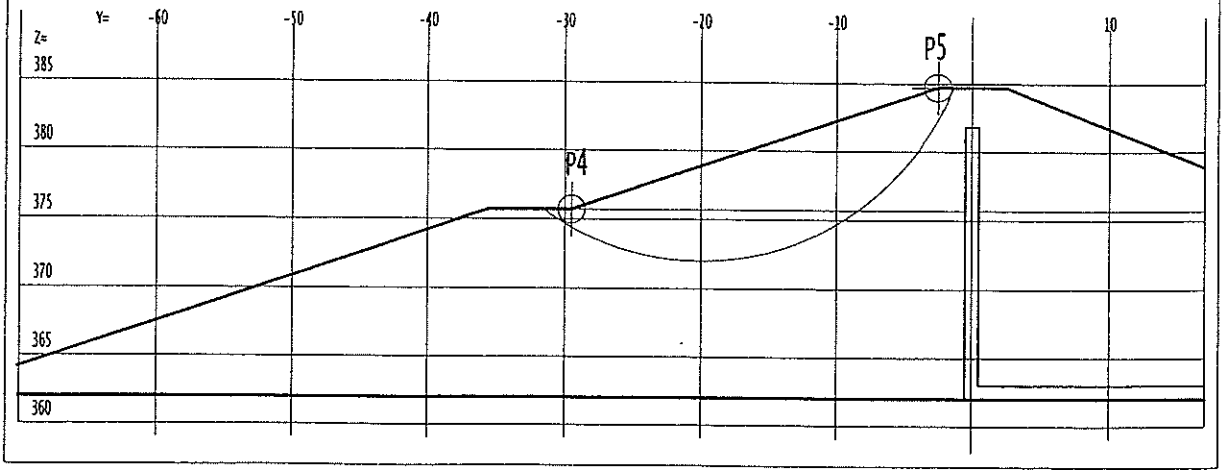

Result sheet B1-B: End of Impounding

1 - Pore pressure

Point	P1	P2	P3
Pressure (kPa)			
Head (m)			

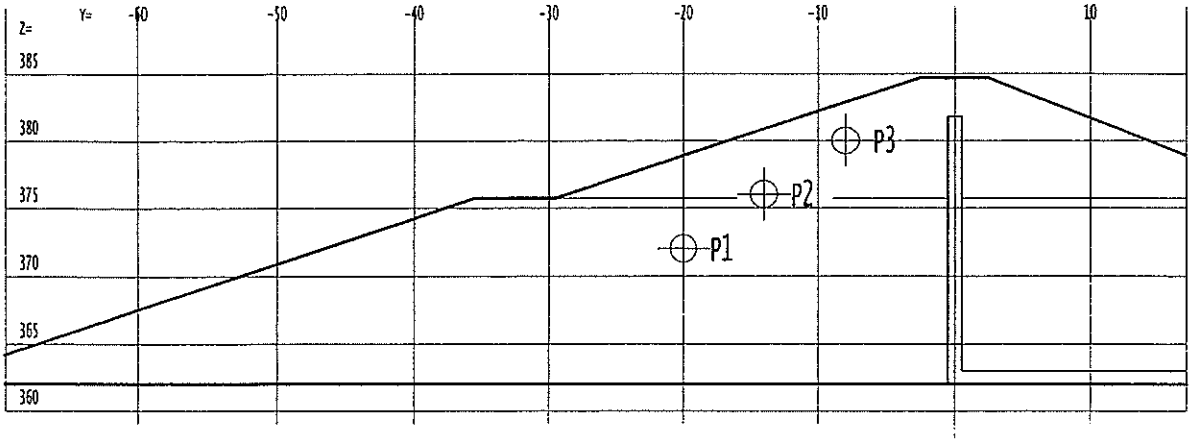

2 - Stability - Factors of safety

Failure line	Circle C1	Critical line
SF (Fellenius)		
SF (Bishop)		
SF (other)		

F factor	Displacement P4 (cm)		Displacement P5 (cm)	
	dY	dZ	dY	dZ

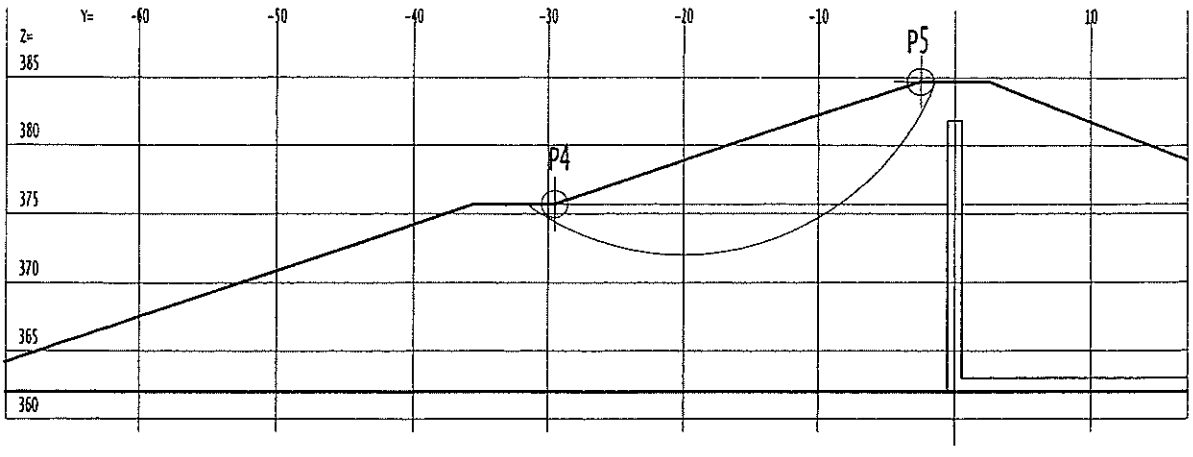

Result sheet B1-C: Rapid Drawdown

1 - Pore pressure

Point	P1	P2	P3
Pressure (kPa)			
Head (m)			

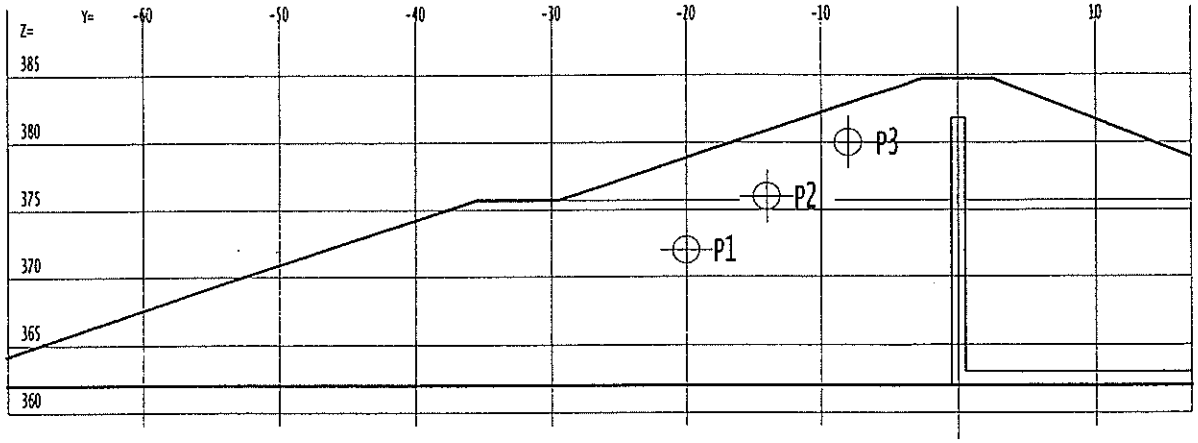

2 - Stability - Factors of safety

Failure line	Circle C1	Critical line
SF (Fellenius)		
SF (Bishop)		
SF (other)		

F factor	Displacement P4 (cm)		Displacement P5 (cm)	
	dY	dZ	dY	dZ

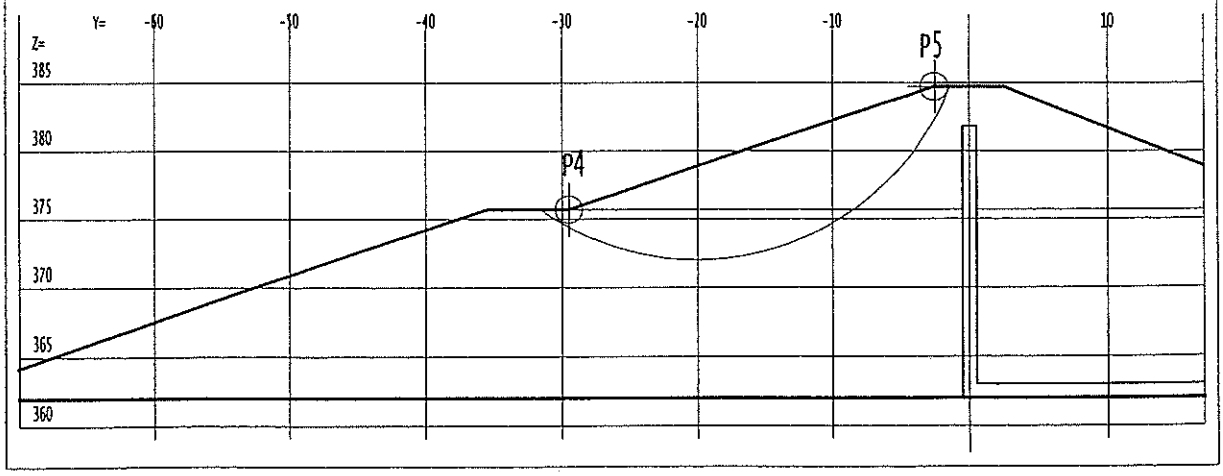

FIFTH INTERNATIONAL BENCHMARK WORKSHOP
ON NUMERICAL ANALYSIS OF DAMS
DENVER, CO, USA, JUNE 2-5 1999

THEME B1
EMBANKMENT DAMS
STABILITY ANALYSIS OF A HOMOGENEOUS EMBANKMENT DAM

SYNTHESIS - COMPARISON OF NUMERICAL RESULTS

FINAL REPORT - SEPTEMBER 1999

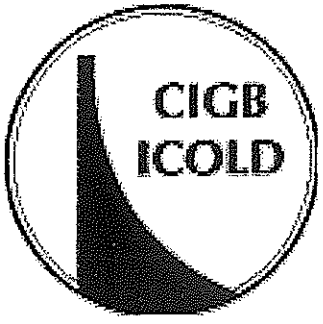

DENVER, CO, USA, JUNE 2-5 1999

This report was prepared by the formulator of Theme B1 :

Alain J. CARRERE, Coyne et Bellier,
Gennevilliers, France

in collaboration with the participants to theme B1 of the Benchmark Workshop :

Participant #1 (P1): C. Brunet, J.J Fry (France)

Participant #2 (P2) : La Barbera, A. Bani and G. Mazza (Italy)

Participant #3 (P3) : D.V. Griffiths, R.L. Torres, P.A. Lane (U.S.A.)

.0 INTRODUCTION TO THE PROBLEM OF THEME B1

)uring the IVth Benchmark Workshop held in Madrid in September 1996, the need was identified ɔr setting up bridges between, on a one hand, conventional stability analyses which use forces .nd provide safety factors and, on the other one, rheological models whose basic variables are lisplacements, stresses and materials states.

'he purpose of this Theme B1 was to provide a common frame for several types of methods to ıe performed and finally compared, from the FELLENIUS circular stability method to the most ıdvanced models using coupled constitutive laws for soils. The only common aspects are that .ll analyses are 2-D, and they should be carried out in effective stresses. The range of methods ıeing used was quite open, although the same sets of data should be used, and a minimum set ıf key results should be provided in all cases.

ı order to avoid further discrepancies between results, the subject for Theme B1 has been kept ather simple. It takes inspiration from the history of the MONDELY dam, a small homogeneous ıarthfill dam which was built in Southern France in the early eighties, which has shown some ıvidence of unstability during the first drawdown of its reservoir. Pore pressure, influenced by a ıigh initial degree of saturation, appeared to be the critical factor. However it must be pointed ıut that the conditions proposed for the simulation have substantially been altered from those ıbserved on the prototype, in order to make the analyses more attractive.

'he databook for Theme B1 contains all details on the dam geometry, mechanical properties of ıe materials as well as conditions for their placement, time history of construction, impounding ıd beginning of operation of the reservoir.

'he proposed simulations consisted in calculating safety factors prevailing at the upstream hell: A) at the end of construction, B) in normal operation conditions, at the end of impounding, .nd C) after a rapid drawdown.

'or each of the three conditions to be analysed, the pore pressure field should first be ıvaluated, then the safety factor against failure should be provided.

ı order to allow comparisons between analyses from different contributions, the pore pressure ıad to be indicated at 3 points close to the top of the upstream face, and the local safety factor ıad to be given along a determined circular slip surface; these points and this surface had been hosen according to the behaviour of the prototype.

2.0 DESCRIPTION OF CONTRIBUTIONS

Three participants presented a communication to this 5th Benchmark Workshop. They are :

- P1: EDF – CNEH (Chambéry, France),
- P2: Ismes and Enel (Seriate, Milano, Italy),
- P3: Colorado School of Mines (Golden), with USBR (Denver) and UMIST (Manchester, UK).

2.1 CONTRIBUTION OF PARTICIPANT P1

Participant P1 has used limit equilibrium methods (TALREN3 software), finite elements (GEFDYN) and finite differences (FLAC).

For limit equilibrium methods, pore pressure has been evaluated using Bishop's approximation, applying provided coefficients Ru (construction and impounding) and B (drawdown). Analyses through flow nets have also been carried out. Safety factors have been calculated following Fellenius, Bishop, and the 'perturbation method', close to Bishop's. Two slip surfaces have been assumed, the circle determined in the databook at the top of the upstream face, plus a second larger circle along the whole upstream face.

Finite elements methods implemented in GEFDYN have been used with a fully coupled model, with the compressibility of the fluid being adjusted in order to meet the provided value of the B coefficient. The mechanical behaviour of the fill has been represented with an elasto-plastic Mohr-Coulomb model with a non-associated flow rule. The stability has been assessed along the same pre-determined slip surfaces as for the equilibrium methods, the safety factor being calculated by integration of local safety factors (distance of the stress circle to the Mohr-Coulomb criterion).

Assumptions for finite difference method are globally similar to those for finite element ones.

2.2 CONTRIBUTION OF PARTICIPANT P2

Participant P2 has used limit equilibrium methods (FELLENIUS and PENDII software), and finite elements (OMEGA).

For limit equilibrium methods, pore pressure has been evaluated using Bishop's approximation, applying provided Ru coefficients Ru. Pore pressures calculated by the coupled FEM analyses have also been used at this level. Several slip surfaces have been analysed including automatic determination of the most critical one.

For finite elements analyses, a coupled 2-phase model ECAM (extended from Cam-Clay) using both Drücker-Präger and Mohr-Coulomb failure criteria. Construction has been simulated in 10

stages with a coupled approach. Impounding and drawdown have been calculated uncoupled, the pore pressure variation being analysed separately. Safety factors have been determined by decreasing resistance parameters until the displacements are significantly increased.

2.3 CONTRIBUTION OF PARTICIPANT P3

Participant P3 has used finite element method, together with a Mohr-Coulomb failure criterion. Pore pressure has been evaluated using Bishop's approximation, applying provided coefficients Ru and B. Safety factors have been determined by decreasing resistance parameters until the displacements are significantly increased.

Table 1 gives a general view of the methods and assumptions used by different contributors.

Table 1 – Methods and assumptions used by Contributors

			A : End of construction	B : End of impounding	C : Rapid drawdown
Pore pressure determination					
P1	From Ru		+		
	Approx. Bishop			+	+
	Seepage analysis			+	+
P2	Seepage analysis		+	+	+
P3	Approx. Bishop		+		
Determination of factors of safety					
P1	Equilibrium	Fellenius	+	+	+
		Bishop	+	+	+
		Perturbations	+	+	+
	Finite elem.	Local S.F.	+	+	+
	Finite Diff.		+	+	+
P2	Equilibrium	Fellenius	+	+	+
		Bishop	+	+	+
		Janbu	+	+	+
		Spencer	+	+	+
	Finite elem.	Global S.F.	+	+	+
P3	Finite elem.	Global S.F.	+	+	+

3.0 PRESENTATION AND DISCUSSION OF RESULTS

3.1 PORE PRESSURE

Pore pressure at determined points P1, P2 and P3, provided by the different Contributors, are given in following Tables 2 to 4, expressed in kPa.

Table 2 – Pore pressure – A End of construction

Contributor	Method	P1	P2	P3	Observations
P1	Ru	96	69	26	Calculated from Ru provided
P1	FEM	91	69	24	Coupled analysis, uncompressible water, unsaturated (Bishop)
P1	FDM	98	55	22	Coupled analysis, compressible water, saturated (Bishop)
P2	FEM	103	73	36	Coupled analysis, ECAM

Table 3 – Pore pressure – B End of impounding

Contributor	Method	P1	P2	P3	Observations
P1	Seepage	74	60	19	Uncoupled seepage analysis
P1	Bishop	117	74	26	Bishop approximation
P1	FEM	86	57	11	Coupled analysis, uncompressible water, unsaturated (Bishop)
P1	FDM	111	55	16	Coupled analysis, compressible water, saturated (Bishop)
P2	FEM	41	27	-20	Coupled analysis, ECAM

Table 4 – Pore pressure – C Rapid drawdown

Contributor	Method	P1	P2	P3	Observations
P1	Seepage	62	52	14	Uncoupled seepage analysis
P1	Bishop	94	68	26	Bishop approximation
P1	FEM	47	27	1	Coupled analysis, uncompressible water, unsaturated (Bishop)
P1	FDM	86	41	10	Coupled analysis, compressible water, saturated (Bishop)
P2	FEM	23	4	-52	Coupled analysis, ECAM

Figure 1 below also shows the different results obtained by the different methods used.

It can be seen that the pore pressure given at the end of construction is roughly consistent between each other. This can be seen as the result of adopting the Ru coefficient given in the databook, either directly, or indirectly through seepage analyses aiming to fitting the given value.

At the end of impounding, values provided are less consistent between each other, probably due to the variety of determination methods used. This is still truer after the drawdown has been simulated, with a total bandwidth of 14 metres of water head.

Figure 1 : Pore pressure calculated at fixed points

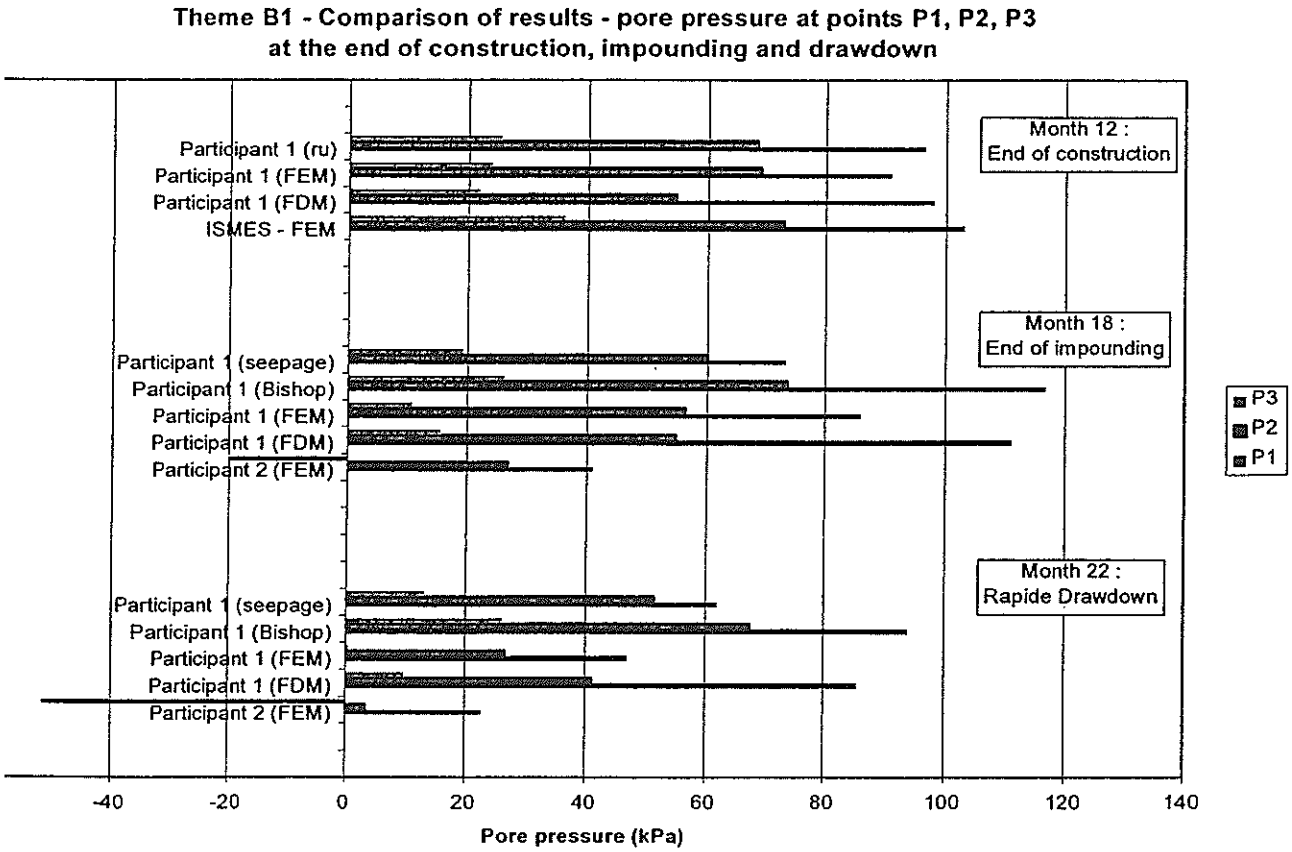

3.2 FACTORS OF SAFETY

Pore pressure at determined points P1, P2 and P3, provided by the different Contributors, are given in following tables (expressed in kPa).

Table 5 – Factors of safety – A End of construction

Contributor	Method	Circle C1	Critical S.F.	Critical line	Observations
P1	Fellenius	1.11	1.37	Large U/S	Pore pressure from Ru provided
P1	Bishop	1.40	1.44	Large U/S	Pore pressure from Ru provided
P1	Perturb.	1.40	1.45	Large U/S	Pore pressure from Ru provided
P1	FEM	1.44	1.18		Pore pressure from Ru provided, critical circle selected similar to eq. Methods
P1	FDM	1.52	1.09		
P2	Fellenius	1.30			
P2	Bishop	1.46	1.43	Large U/S & D/S	
P2	Janbu	1.29			
P2	Spencer	1.44			
P2	FEM		1.70	Large U/S & D/S	Coupled analysis, ECAM, displacement 0.78 cm
P3	FEM		2.00	D/S	No uplift

For this loading, all methods in which an automatic determination of the critical slip surface have found that it was located on the D/S face which is steeper. The prototype actually showed some unstability at the end of construction, due to especially wet weather conditions that led to increased water contents of the fill. The rest of the structure appeared to keep stable at this stage, despite the fact that construction rates were much higher than stipulated for the exercise. Values given at the end of construction are shown on Figure 2.

Figure 2 : Factors of safety at the end of construction

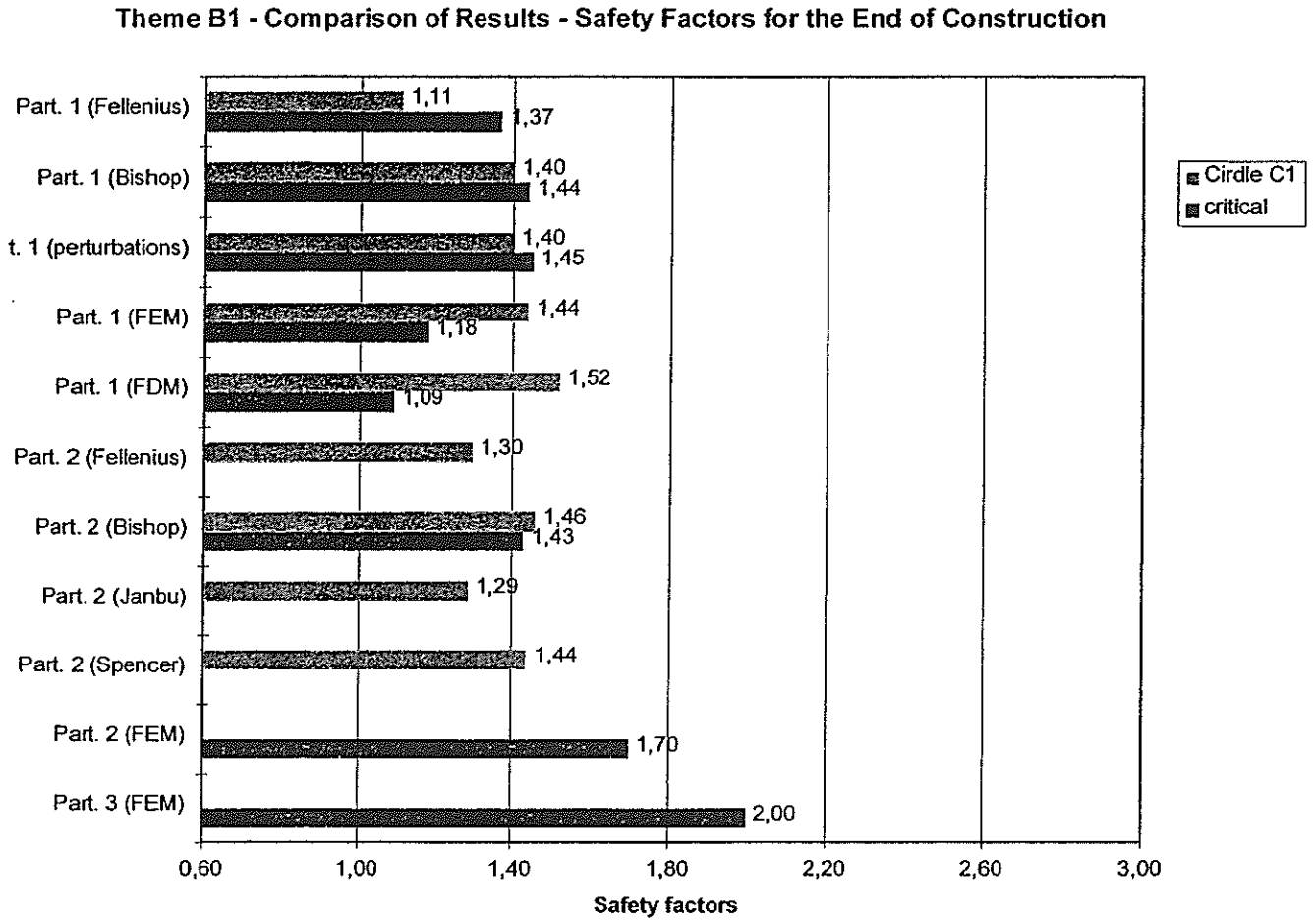

Table 6 – Factors of safety – B End of impounding

Contributor	Method	Circle C1	Critical S.F.	Critical line	Observations
P1	Fellenius	2.73		Large U/S	Pore pressure from seepage analysis
P1	Fellenius	1.80		Large U/S	Pore pressure from Bishop approx.
P1	Bishop	3.28		Large U/S	Pore pressure from seepage analysis
P1	Bishop	2.35		Large U/S	Pore pressure from Bishop approx.
P1	Perturb.	3.22		Large U/S	Pore pressure from seepage analysis
P1	Perturb.	2.29		Large U/S	Pore pressure from Bishop approx.
P1	FEM	3.29	2.79		Coupled analysis, uncompressible water, unsaturated (Bishop)
P1	FDM	4.69	3.52		Coupled analysis, compressible water, saturated (Bishop)
P2	Fellenius	2.60			
P2	Bishop	3.30	2.86	Large U/S & D/S	
P2	Janbu	2.88			
P2	Spencer	3.57			
P2	FEM		2.17	Large U/S & D/S	
P3	FEM		2.00	D/S	

All methods give high safety factors, whatever the method being used. In fact, the prototype on which the exercise is based showed no abnormal behaviour during the impoundment of its reservoir, which occurred within a couple of months.

However the wide variation between results is to be noticed, which is due to the discrepancies between pore pressure values as already stated. Of special interest are results provided by Participant P1 who carried out pairs of analyses with the same methods, the only difference being is the determination of pore pressure: if using Bishop's approximation, factors of safety are approximately 30 percent lower than with a seepage flow analysis (the six first lines of Table 6).

Figure 3 : Factors of safety at the end of impounding

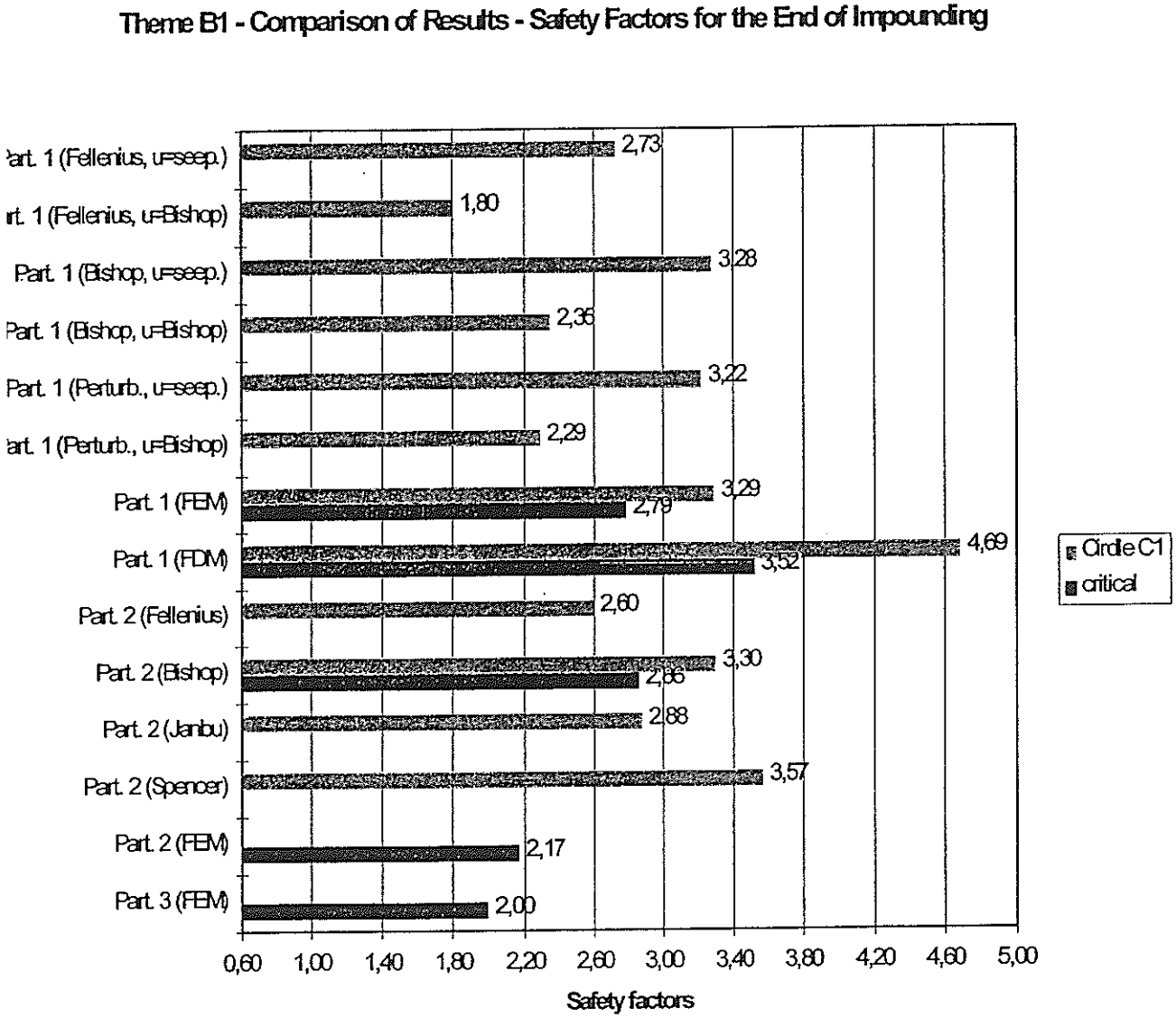

Table 7 – Factors of safety – C Rapid drawdown

Contributor	Method	Circle C1	Critical S.F.	Critical line	Observations
P1	Fellenius	1.75	1.34	Large U/S	Pore pressure from seepage analysis
P1	Fellenius	1.14	1.90	Large U/S	Pore pressure from Bishop approx.
P1	Bishop	2.02	1.38	Large U/S	Pore pressure from seepage analysis
P1	Bishop	1.45	2.00	Large U/S	Pore pressure from Bishop approx.
P1	Perturb.	2.01	1.38	Large U/S	Pore pressure from seepage analysis
P1	Perturb.	1.44	2.01	Large U/S	Pore pressure from Bishop approx.
P1	FEM	2.24	1.60		Coupled analysis, uncompressible water, unsaturated (Bishop)
P1	FDM	1.89	1.32		Coupled analysis, compressible water, saturated (Bishop)
P2	Fellenius	2.00			
P2	Bishop	2.36	1.59	Lower U/S	
P2	Janbu	2.01			
P2	Spencer	2.33			
P2	FEM		1.50	Lower U/S	
P3	FEM		1.55	U/S	

The same remarks already done for the previous load step are still valid, with inverted results according to the slip surface assumed by Participant P1: the large upstream circle appears more stable if pore pressure is calculated than with Bishop's approximation. It has to be recalled that the 'critical circle' for this participant has not been determined by each method, but fixed for all different methods, with the purpose of making comparisons easier.

From Table 7 above, most participants seem to converge to saying that the most critical slip surface is a large upstream circle. However the prototype showed a failure surface, with a slip of several decimetres, at the top of the upstream face. This occurred shortly after a nearly complete drawdown of the lake, in less than 2 months of time. The main reason for this type of failure has been attributed to the use of slightly more plastic materials at the top, and to higher water contents, which did the zoning provided in the databook incompletely represent.

Figure 4 : Factors of safety at rapid drawdown

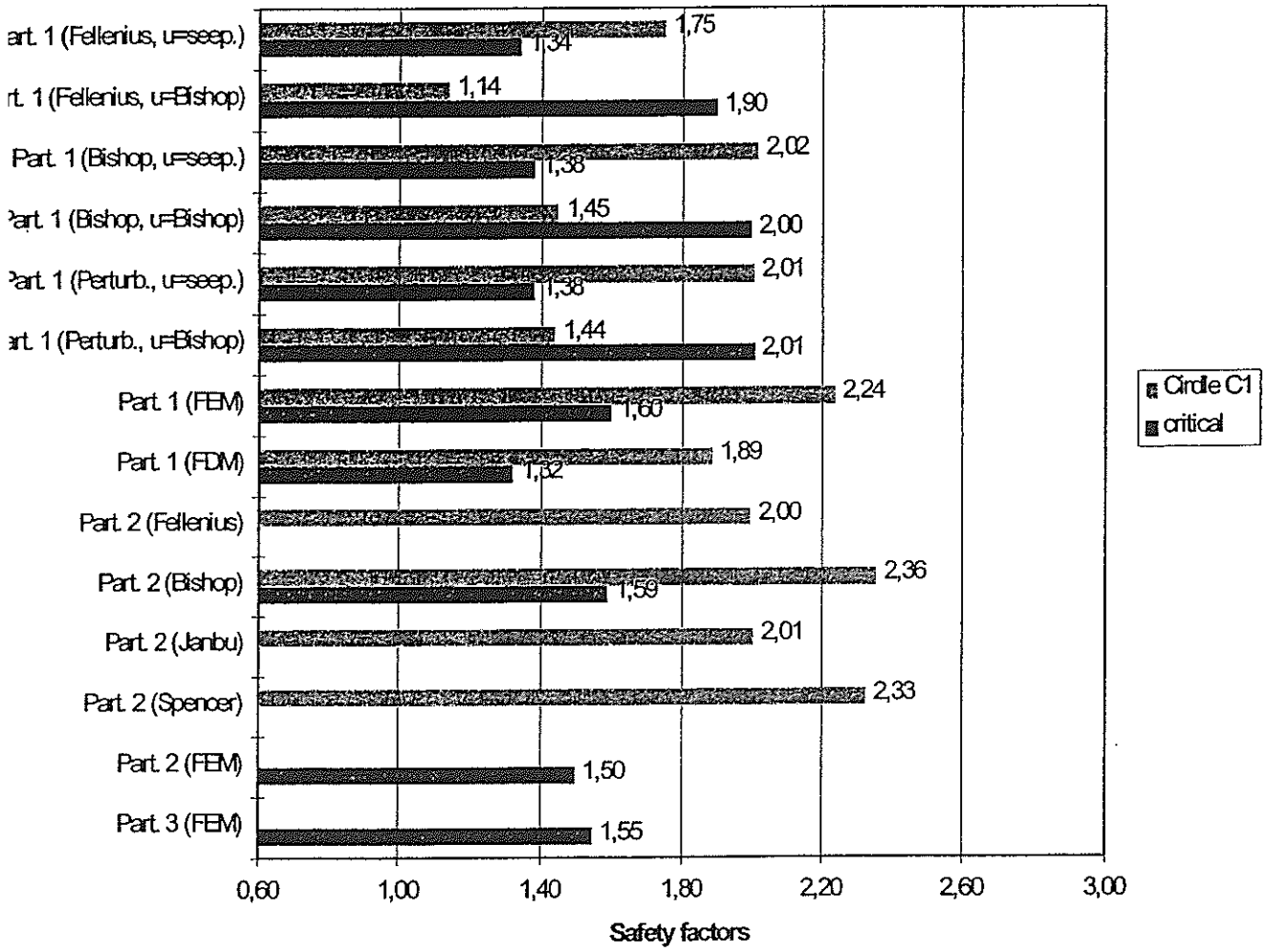

4.0 CONCLUSIONS

Safety factors provided by different participants using different methods of analysis cover wide ranges, especially load cases B and C. It is possible to investigate on reasons for such discrepancies, thanks to the number of different methods used by several participants.

Differences between equilibrium methods are small and consistent : for example, safety factors coming from Fellenius method are in average 14 percent less than if given by Bishop method (11 pairs of values coming from the same participant); in the same way, results from Janbu method are comparable to Fellenius' (3 pairs), and on the other side the Spencer and perturbations methods are consistent to Bishop (6 and 3 pairs respectively). These relations are already known.

When comparing results provided by different participants using the same equilibrium method (Bishop), results become more scattered: from 1.40 to 1.46 at the end of construction, but from 1.80 to 3.30 at the end of impounding, and from 1.45 to 2.36 at the end of drawdown. This clearly indicates the pore pressure field as the main responsible for discrepancies observed, which affects results not only of equilibrium methods, but also FE methods.

Another reasons for differences in FE results is the mean of calculating safety factors:

- participant P2 followed the suggestion to compute it as the reducing factor applied on all soil resistance parameters for which the displacement is strongly increased,
- participant P1 first calculated a local safety factor at each point as a distance of Mohr circles to the yield curve, then integrated them along assumed lines.

Altogether, participants were unable to detect the failure that actually affected the upper part of the upstream face of the prototype at drawdown, and gave for this event safety factors ranging from 1.14 to 2.36 for the actual failure surface. On the opposite, they found the critical surface as a large U/S circle with safety factors between 1.34 and 2.01, with an average at 1.5 similar to predictions by the designer of the prototype.

This fact is likely to be due to the simplified materials properties provided, which did not represent the full reality. It is also likely that the redundancy between intrinsic parameters (compressibility, permeability) and the placement parameters measured (Ru, B) were not fully consistent between each them. Actually the sliding of the upper zone of the U/S face was attributed to high local increase of pore pressure which did not dissipate even after a long time, for reasons which are not yet completely clarified.

If pore pressure had been discarded from the exercise, or if its determination method had been fully imposed, it is likely that results would have kept within a reasonable narrow range of variation. By leaving freedom in pore pressure determination way, participants were in fact put in conditions similar to that of the designer of a new dam, who has only uncompleted or inaccurate data to work out his project.

The conclusion of the exercise may seem obvious, but it still needs to be recalled: pore pressure in impervious materials is strongly influenced not only by intrinsic properties of these materials, but also and mainly by conditions of placement: saturation ratio, compaction energy, speed of raising of the fill. These parameters are badly known at the time of design, if fill tests are not carried out, which is the general case for small dams. The only practical way for the designer is therefore to make reasonable assumptions based on experience, then to follow construction through appropriate monitoring during construction, and to permanently adjust placement conditions as required.

Lessons for the future benchmark subjects can also be drawn from this :

- The main difficulty of the present exercise was clearly identified, since results in terms of pore pressure were required. But the second aspect, the purely 'mechanical' one, could not be judged independently from the other. An intermediate step, e.g. by asking a stability analysis based on total stresses, would have been profitable for this purpose,

- Extracting data from a real problem is very delicate, because the necessary simplification of data provided to participants may affect their influence on the results, which in turn makes the comparison with the prototype meaningless ; a similar observation had already been done during the previous benchmark workshop in Madrid. It is therefore maybe wiser to limit subjects to purely academic ones, or to refer only to very simple historical cases.

ACKNOWLEDGEMENTS

The formulator of theme B1 of the 5th Benchmark Workshop expresses his thanks to the Compagnie d'Aménagement des Coteaux de Gascogne (Tarbes, France) for the information they provided on the MONDELY dam, from which the academic subject of the workshop was derived.

REFERENCES

Databook prepared by the Formulator

Alain J. Carrère, 1999. Theme B1. Embankment dams – Stability analysis of a homogeneous embankment – Coyne et Bellier.

Paper Contributions to the 5th Benchmark Workshop :

C. Brunet, J.J. Fry, 1999. Comparison of classical and elasto-plastic methods for the evaluation of safety factor against failure of an embankment dam.
Electricité de France, Centre National d'Etudes Hydrauliques, Chambéry, France.

G.La Barbera[1], A.Bani[1], G.Mazzà[2] , 1999. Numerical Evaluation of Global Factors of Safety against Failure of an homogeneous embankment dam.
1 ISMES S.p.A. – Seriate (Italy), 2 ENEL S.p.A. Research – Milano (Italy).

D.V. Griffiths[1], R.L. Torres[2], P.A. Lane[3] , 1999. Embankment stability analysis by elasto-plastic finite elements.
1 Colorado School of Mines, Golden CO (USA), 2 US Bureau of Reclamation, Denver CO (USA), 3 UMIST, Manchester (UK).

Figure 1 below also shows the different results obtained by the different methods used.

It can be seen that the pore pressure given at the end of construction is roughly consistent between each other. This can be seen as the result of adopting the Ru coefficient given in the databook, either directly, or indirectly through seepage analyses aiming to fitting the given value.

At the end of impounding, values provided are less consistent between each other, probably due to the variety of determination methods used. This is still truer after the drawdown has been simulated, with a total bandwidth of 14 metres of water head.

Figure 1 : Pore pressure calculated at fixed points

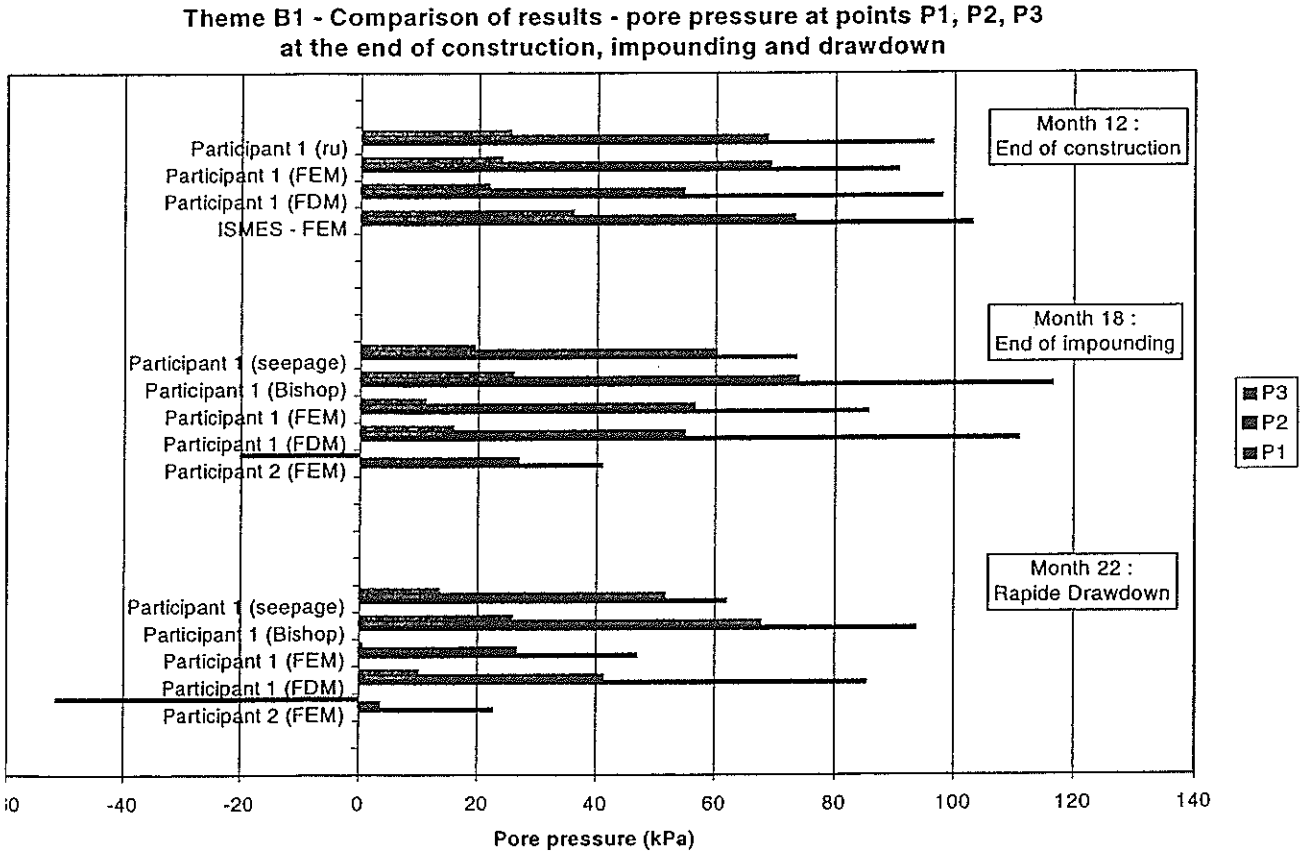

Figure 2 : Factors of safety at the end of construction

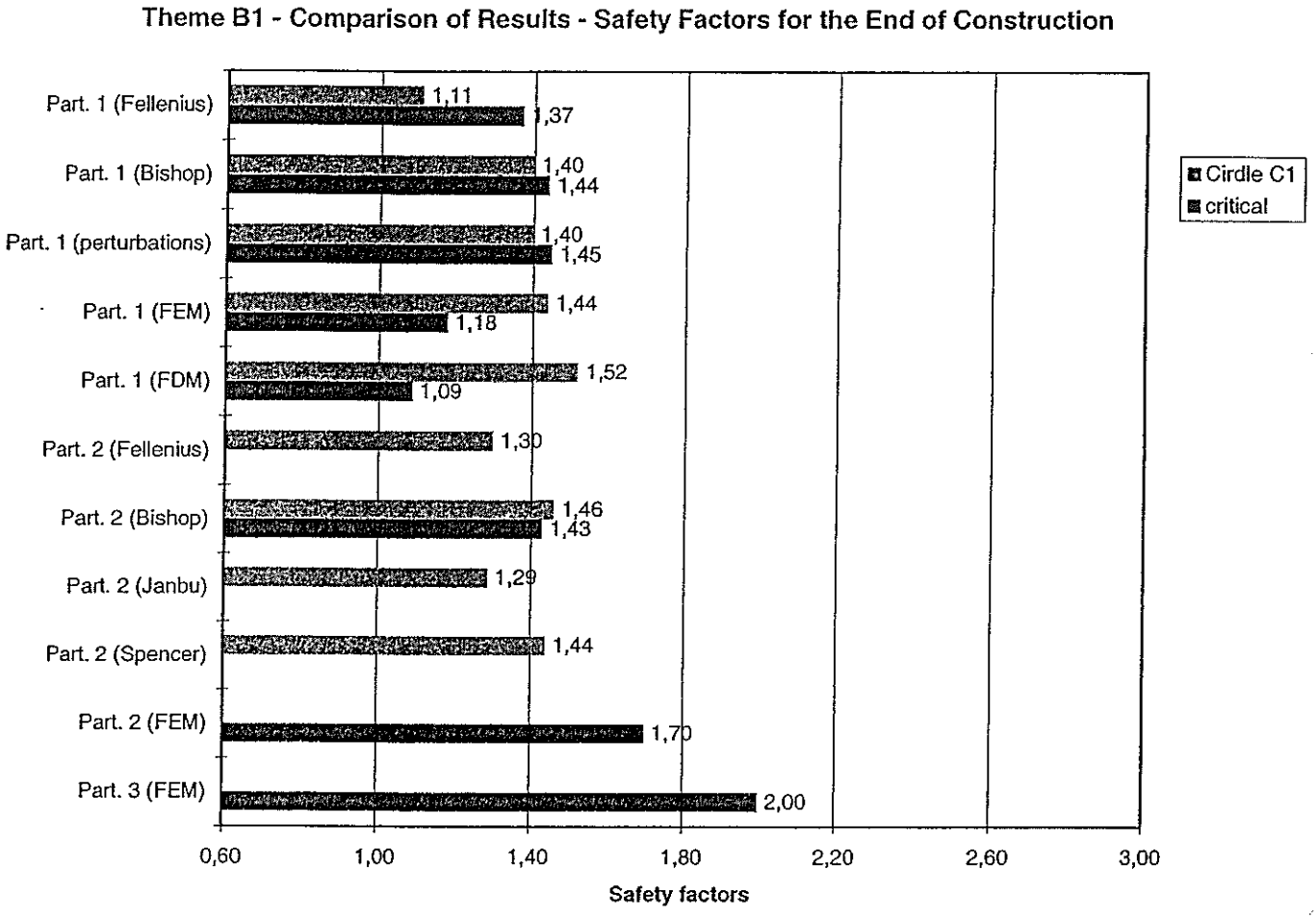

Figure 3 : Factors of safety at the end of impounding

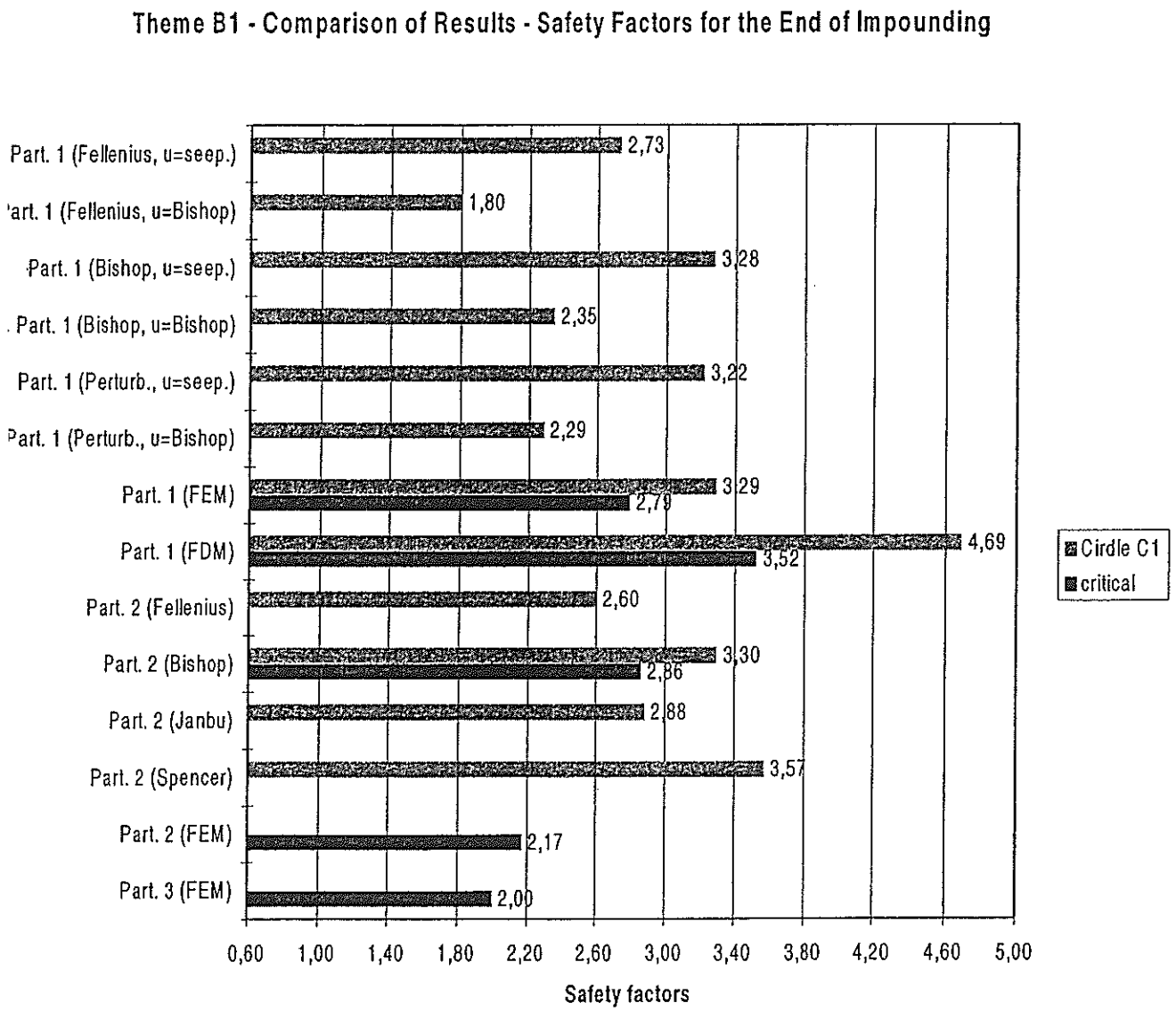

Figure 4 : Factors of safety at rapid drawdown

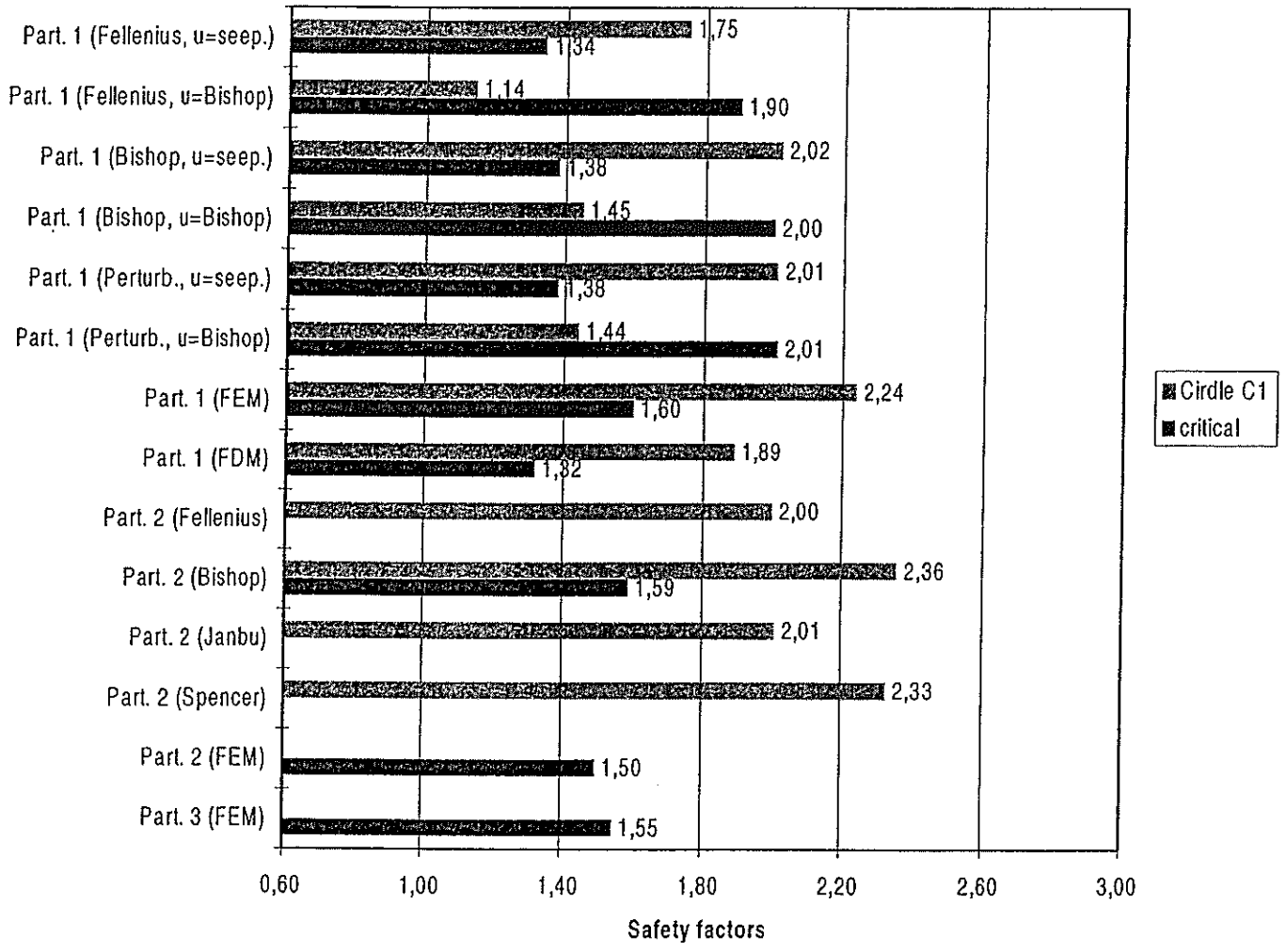

COMPARISON OF CLASSICAL AND ELASTO-PLASTICS METHOS FOR THE EVALUATION OF SAFETY FACTOR AGAINST FAILURE OF AN EMBANKMENT DAM

Claude Brunet and Jean Jacques Fry *

Electricité de France - Centre National d'Equipement Hydraulique
Savoie technolac 73373 LE BOURGET DU LAC
Tél : 004 79 60 60 94 fax 004 79 60 61 78

1 INTRODUCTION

Theme B1 of the fifth benchmark workshop on numerical analysis of dams is the stability analysis of an homogeneous embankment dam. The geometrical definition of the dam and the material properties are given by the formulator. These characteristics are reminded below.

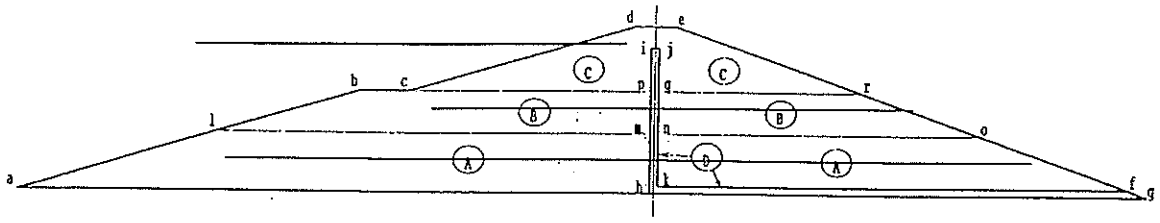

Table 3: Properties and initial conditions of materials in the fill						
	Materials :		Clayey loam	Clay		Drain
Characteristics	Name	Unit	A	B	C	D
Specific weight of grains	G	kN/m³	27.3	27.3		-
Young's modulus	E_y	MPa	8	5		80
Poisson's ratio	ν		0.3	0.3		0.3
Effective shear angle	Φ'	°	32	26		36
Effective cohesion	C'	kPa	10	18		0
Dilatancy angle	$\psi_{(1)}$	°	5	5		5
Vertical permeability	K_v	m/s	4.0×10^{-9}	1.0×10^{-9}		1×10^{-3}
Horizontal permeability	K_h	m/s	16.0×10^{-9}	4.0×10^{-9}		1×10^{-3}
Proctor Opt. water content	W_{opt}	%	14.5	18.5		-
Proctor Opt. dry density	$\gamma_{d.opt}$	kN/m³	18.0	17.2		-
Properties at time of placement						
Water content	W_i	%	16.5	20.7	21.2	8
Saturation ratio	*Sr*	%	95.1	94.7	95.5	
Dry density	γ_d	kN/m³	18.0	17.1	17.0	18.6
Measured ratio u/γ.h	r_u	-	0.45	0.70	0.45	0
Properties in operation						
Skempton coefficient	$\bar{B}$		0.90	0.80	0.80	1.0

Three approaches have been developped to analyse the stability :

- the first one is the limit équilibrium methods assessing the slope stability of the upstream face. The pore pressure field in the embankment computed by the flow net NS2D software is implemented in TALREN3 software to analyse the safety factor by the method of slices.
- the second one is an elasto-plastic model with the Mohr Coulomb constitutive equations for the soil. The problem is solved by a Finite Element Method. GEFDYN software is used for this computation. This software have been developped by Electricite De France, Coyne et Bellier and Ecole Centrale de Paris for geotechnicals applications and specially for the computation of dams.
- the third one is also an elasto-plastic model with the mohr coulomb constitutive equations, but the integration is solved by a finite difference method. FLAC software is used in this case.

In this study, the pore pressure field have an over-riding influence in the computation of safety factor, when the shear parameters (cohesion and friction angle) are known.
The assumptions of the pore pressure computations of each approach are given in chapter 2. The assumptions of stability analysis in chapter 3.
Both results of pore pressure and stability factor are presented in chapter 4.
Conclusions of this survey are given in chapter 5.

2 PORE PRESSURE COMPUTATION

2.1 Limit equilibrium method

For limit equilibrium method, the pore pressure field has to be computed regardless of the stability analysis. Two types of uncoupled approach are used :

1. the undrained method related to Bishop assumption: This method doesn't take into account the seepage into the embankment and the pore pressure is only due to a load. The pore pressure u is generated by the overburden above the considered point with the following relationship :

$$u = u_0 + \alpha.\gamma.H$$

- u_0 is the pore pressure following compaction during construction, during the impounding u_0 is the pore pressure at the end of the construction and during

the drawdown the pore pressure at the end of the impounding.
- a is a multiplicative coefficient. For the construction and the impounding this factor is the pore pressure ratio r_u. For the drawdown, it is the pore pressure coefficient B.
- *g.H* is the overburden above the considered point. During the construction, *g.H* is the total vertical stress created by the vertical colum of placed material. During the impounding and the drawdown, it is the vertical stress below the vertical column of water (fig 2.1).

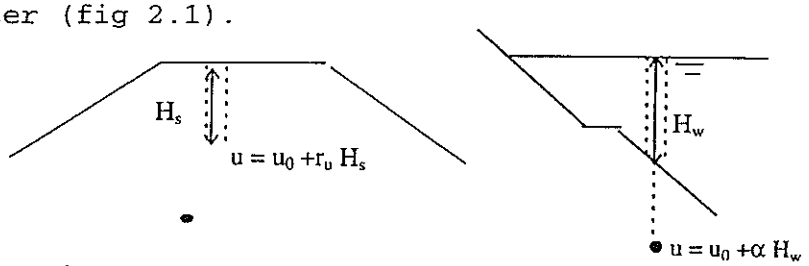

Figure 2.1 : overburden in undrained method

2. Analysis of the seepage and flow net through the embankment from Finite Element Method. The permeability is constant in the saturated media and function of the saturation for the unsaturated media. The seepage analysis start at the beginning of the impounding with the pore pressure field achieved during construction with the undrained method. For this computation some assumptions on the material properties are required. The soil water characteristic curves in the unsatured area, are achieved with correlations based on the index of plasticity (I_p). From I_p, we can have the a and n parameters of Van Genuchten model [ref 1, 2, 3, 4]. For the clayed loam, Ip is supposed to be 15 and 25 for the clay (fig 2.2). two relations are used : the relation beetween the negative pore pressure and the water content and the permeability versus the water content.

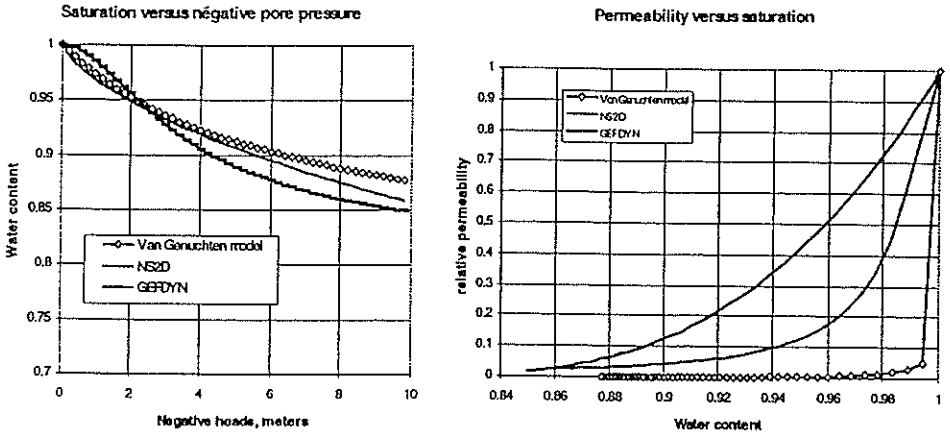

Figure 2.2 soil water characteristic curve for the clay

The influence of the compressibility of the satured soil, under the pore pressure change is taken into assuming the total stress constant and founded on the Young modulus of the soil.

2.2 Finite element analysis

With the finite element analysis, the pore pressure is compute directly by the fully coupled model. As in the seepage computation for limit equilibrium method, two relations are used : the relation beetween the negative pore pressure and the water content and the permeability versus the water content. The model of Van Genuchten is also used in this case, with the same parameters given above (fig 2.2).
Because of the degree of saturation after compaction (95%) during placement, the initial pore pressure of the layer is negative at the value of -2 meters. This value can be red on the curve water content versus negative pore pressure (fig 2.2) and is automatically computed by GEFDYN software.
The change in boundary conditions which occurs on potential seepage surfaces is taken into account in this analysis. It is necessary to have a real unsatured media and special interface element is required on the boundary of this model (ref 5).

With the finite element method, two analysis have been done :
- for the first one, the fluid is supposed to be uncompressible,
- for the second, the fluid compressibility is get from the Skempton pore pressure ratio B. The relation ship beetween B and water compressibility is given below.

$$B = 1 - \frac{1}{1 + \frac{K_w}{n * K_s}}$$

Kw : bulk fluid modulus,
Ks : bulk soil modulus
n : porosity

2.3 Finite difference analysis

The finite difference analysis assumed a saturated media with compressible fluid. The value of the compressibility of the fluid depend on the material, and it have been fitted with the pore pressure ratio B in each material with the same relation ship used with the finite element model.
For this model, the pressure in the drain is nil. The pore pressure is also fixed at zero on the upstream and downstream faces. This boundary condition have an important influence in pore pressure generation as we can see on the results (chapter 4.1).

3 STABILITY ANALYSIS

3.1 Limit equilibrium method :

Three methods of slices have been used to compute the limit equilibrium :

- Fellenius,
- Bishop,
- Method of perturbations.

Two slip surfaces have been tested (fig 3.1) :

- the first one is shaped by the circle C1 (center coordinates : -20,39, radius : 20 meters)
- the other is the circle C2 (center coordinates : -52,43, radius : 133 meters). The circle C2 intersects the upstream toe and the crest of the dam. In a view of comparing more accuratly the results, that critical line given by the method of slices and the elasto plastics method are compared on. This circle is close to the critical surface given by the finite difference model (see chapter 4).

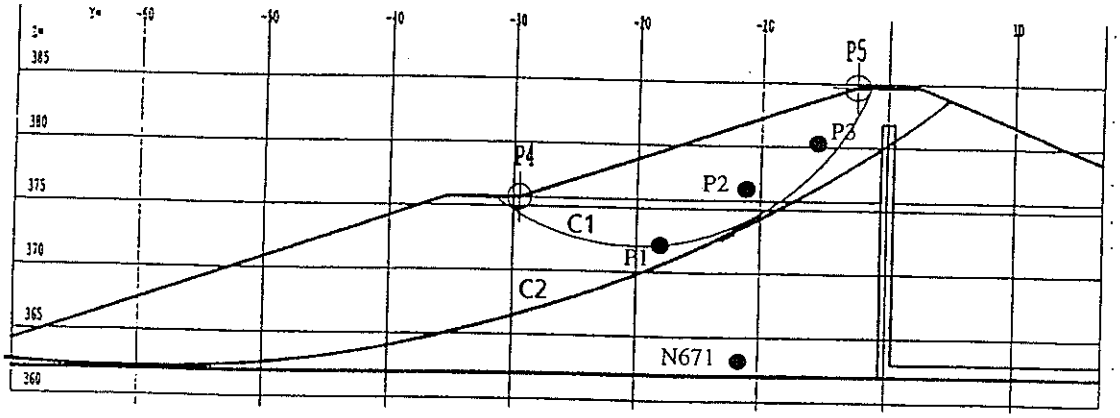

Figure 3.1 : slip surfaces and position of the comparison points

The limit equilibrium method of Fellenius and Bishop are well known and are not described in this paper. The method of perturbations is a global method : the three equations of the static equilibrium are established. The assumption of the method of perturbations is to take the initial stress given by the Fellenius method and to multiplicate it by a factor of perturbation depending on two unknowns : l and m .

$$\sigma_n = \sigma_0 * (\lambda + \mu * \mathrm{tg}(\alpha))$$

$$F = \frac{(\sigma_n - u) * tg\Phi' + c'}{F_0 \tau}$$

The three static equilibrium équations with the three unknowns l, m,and F are solved.

3.2 Elasto plastic model :

According to the shortcomings of the method of slices the elasto-plastics models are used with previous hypothesis. The finite elements mesh has 1644 elements and the finite difference mesh 1628. Both have 23 layers which are placed successively during the 23 construction steps. The reservoir is impounded in 28 steps and the drawdown in 12 steps for the finite element method. 70 steps are used for the impounding and the drawdown for the finite difference method. Note that the number of steps in the finite difference method is depending upon the mesh.
GEFDYN software is used for the finite element analysis and FLAC for the finite difference analysis.
The elasto-plastic Mohr-Coulomb constitutive model is used in both with a non-associated flow rule. So the dilatancy angle given in the general hypothesis is taken into account. The Mohr Coulomb model is not very accurate for the behaviour of clays, and more realistics laws which include multimecanism of yield (isotrope and shear plasticity) and strain hardening could be used. Unfortunately the experimental data are required to calibrate multimechanism elastoplastic model.
The generalized effective stress principle of Terzaghi is justified in the unsatured media used with the finite element computation according to the high degree of saturation leading to the continuity of liquid phase in the clay and the discontinuity of the air phase.

The stability is assessed with a local safety factor as defined hereunder:

$$f_g = \frac{\frac{\sigma_1^{max}}{\sigma_3} - 1}{\left(\frac{\sigma_1}{\sigma_3}\right) - 1}$$

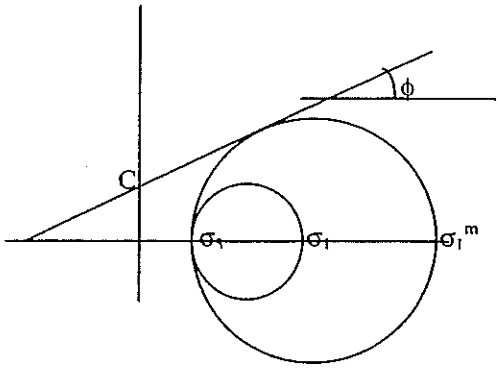

The local safety factor is calculated for each element and the global safety factor is an average of the whole local safety factor except the section of the circle on the upstream side of the drain for the circle C2.

$$F_g = \frac{1}{L_t}\sum(f_g * l_i)$$

f_g : local safety factor
l_i : element lenght along the circle
L_t : lenght of the slip surface

4 RESULTS

4.1 Pore pressure

At the end of the construction, the maximum of pore pressure is located at the foundation contact at the bottom of the mesh. The pore pressure computed analytically with the pore pressure ratio r_u for the limit equilibrium method is 200 KPa, whereas the pore pressure from the elasto-plastic model is greater with the finite difference model (220 KPa) and lower with the finite element model (170 KPa). The effect of the seepage and the nearness of the drain explain the difference beetween these results. For the limit equilibrium method, the seepage isn't take into account to achieve the pore pressure and the maximum is near the drain. Even thought it is an important short-coming of this method, it could be quite satisfactory because this result is beetween the results get with and without compressible fluid. For the finite element method the fluid is uncompressible making the seepage faster and the pressure lower whereas for the finite difference method the pore pressure is greater and nearer the drain because of the compressibility of the fluid.

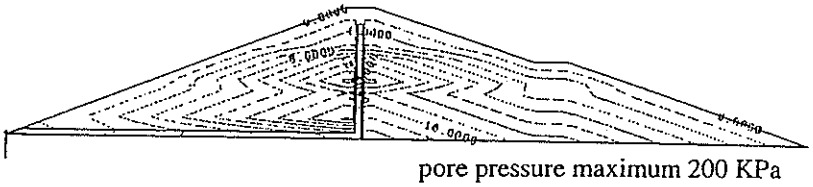

pore pressure maximum 200 KPa

pore pressure for the limit equilibrium method

pore pressure maximum220 KPa

pore pressure for the finite element method

pore pressure maximum 170 KPa

pore pressure for the finit difference method

Figure 4.1 : Pore pressure at the end of the construction for the analical and elasto plastic model

As we can see in figure 4.2, the maximum of the pore pressure is risen before the end of the construction at the bottom of the model near the foundation.
Whereas the pore pressure build-up is bigger with the uncompressible water model, the dissipation of the pore pressure is faster. For point 1, the difference is around 2 metres at the end of the construction whereas it is only 1 meter at the end of the impounding. After all, at the end of the construction, the pore pressure, calculated with the finite difference model is close to the pore pressure calculated with the finite element model.

The value of the compressibility of the fluid have a over-riding influence on the pore pressure build up. the difficulty for the computation is to know as accuratly as possible the distribution of pore pressure so the distribution of coefficient B in the embankment. The nearness of the drain changes the value of the compressibility of the fluid depending on the pore pressure itself. The best solution to have the more accurate behaviour, would be to fit some triaxial isotropic test of the material with B varying in order to located much better the increase in pore pressure in the soft clay area.

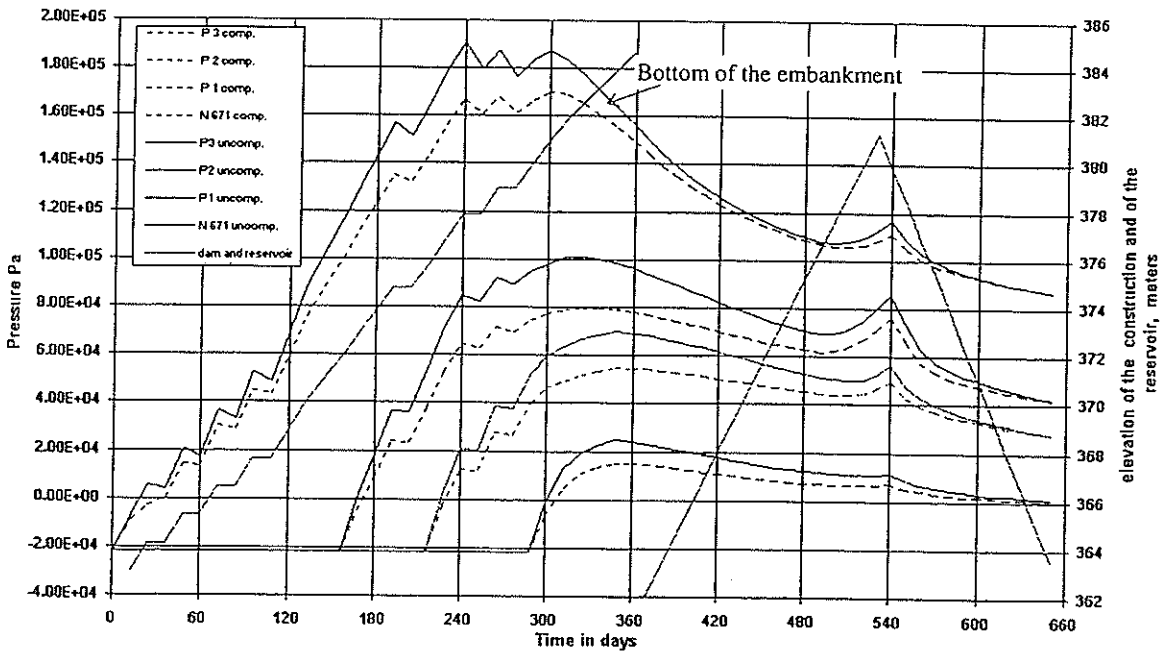

Figure 4.2 : Comparison beetween pore pressure get with the uncompressible and compressible model for the construction, the impounding and the drawdown.

During the construction, the pore pressure stay negative until the overburden reaches about 30 KPa. This corresponds to the vertical stress under the next 2 layers placed .

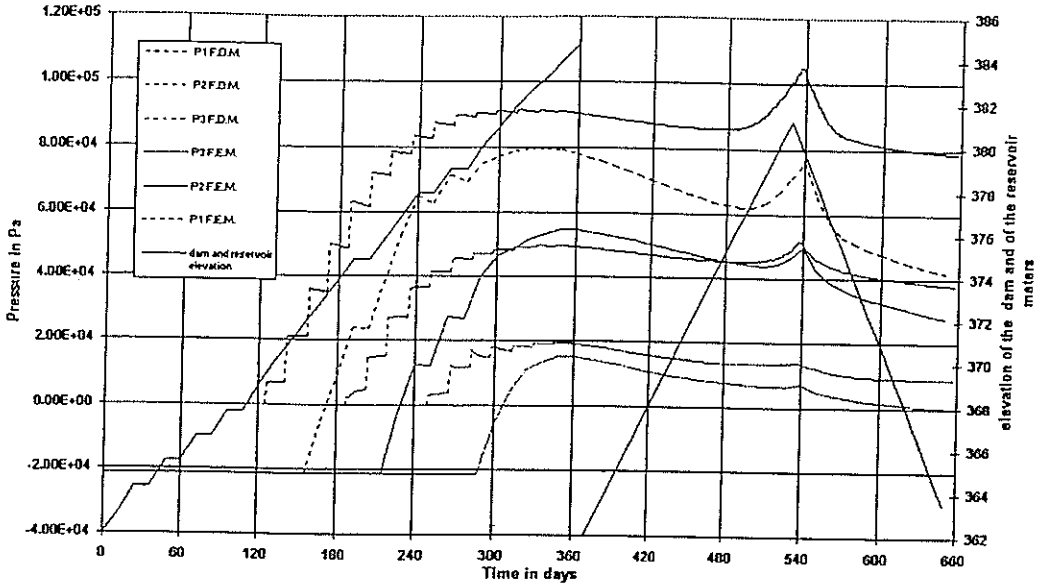

Figure 4.3 : Comparison beetween pore pressure obtained with Finite Element Method and Finite Difference Method during the construction, the impounding and the drawdown

For the Finite Element Model, a potential seepage surface is taken into account whereas the pressure on the upstream and downsream faces of the finite difference model are fixed at zero. In the first case negative pore pressure is allowed and there is a computation of the seepage in the unsatured area whereas the model stay satured in the second case. Pore pressure is more important with the Finite Difference Model, wich can be easy see at the end of the drawdown for points 1, 2 and 3 of the figure 4.3.

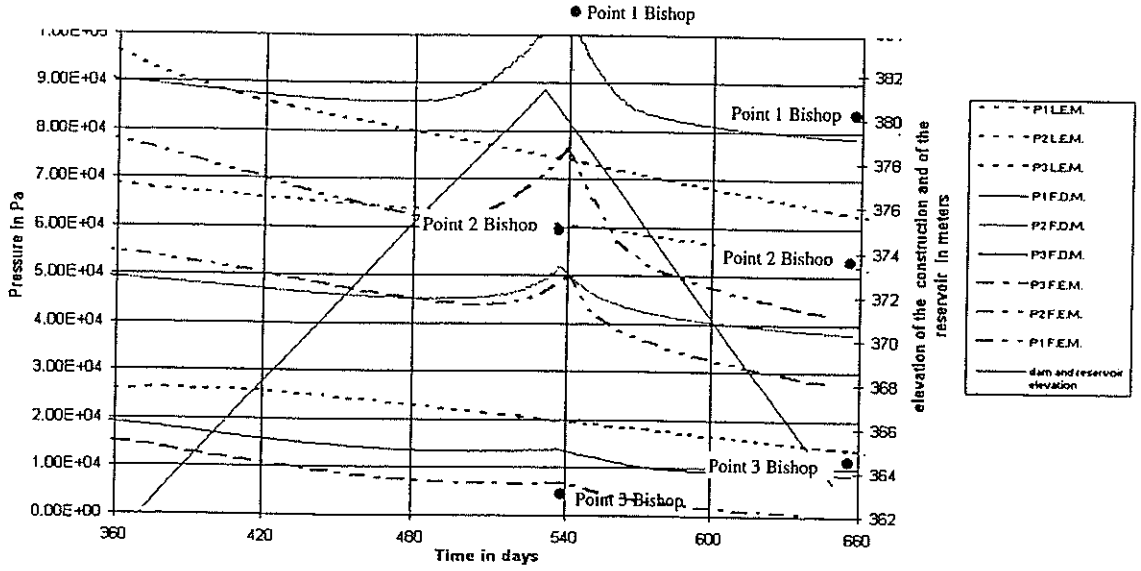

Figure 4.4 : comparison beetween pore pressure get with uncoupled and coupled method

At the end of impounding the higher pore pressure is achieved by the Bishop method, that leads naturally to the lowest global safety factor for the upstream part of the dam and circle C1. For the drawdown, same type of results is found.
The permeability of the clay make the pressure very low, and the impounding have nearly no influence on the seepage computed for the limit equilibrium method. This computation is only a computation of the seepage without taking into account the overburden of the water weight. The increase of pore pressure during the impounding, due to this overburden, is brought to the fore with the elastoplastic method.
The elastoplastic method give intermediate resultsbeetween the pressure achieved with hydraulic computation and the pressure get with the undrained method.

4.2.1 Local safety factor

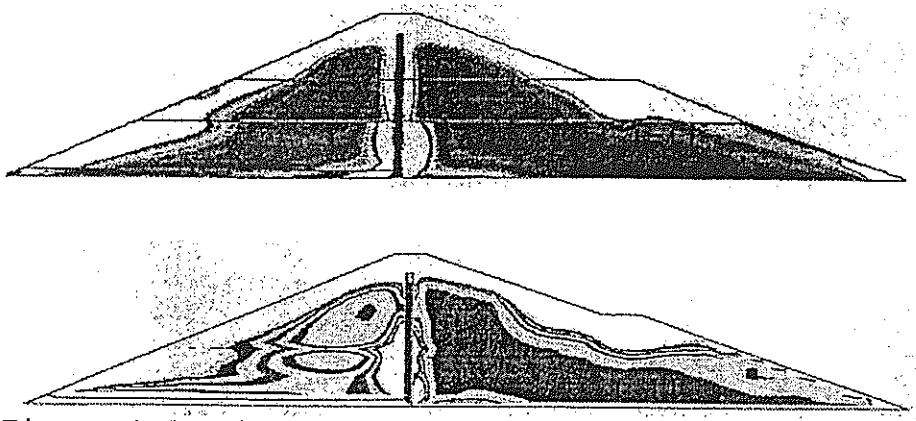

Figure 4.5 : iso contours of the local safety factor for the finite element model and for the finite difference model at the end of the construction

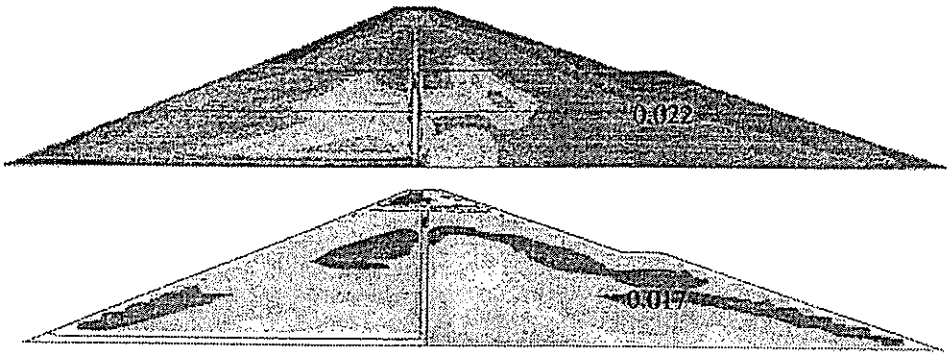

Figure 4.6 : iso contours of the shear deformation for the finite element model and for the finite difference model at the end of the construction

The local safety factor and the shear displacement give an idea of the yield area in our example. It is the area B, at the end of

the construction. The distribution of the local safety factor can draw the slip surface. The maximum of shear displacement (approximatly 0.02) is achieved in the same area of the maximum of maximum local safety factor.approximatly.

4.2.2 Global safety factor

Failure line	circle C1	circle C2
SF (Fellenius)	1.11	1.37
SF (Bishop)	1.4	1.44
SF (Perturbations)	1.4	1.45
SF finite element method	1.44	1.18
SF finite difference method	1.52	1.09

Table 4.1 : safety factor at the end of the construction

- At the end of the construction, the lowest safety factor is 1.09 for circle C2, given by the Finite Difference Method (table 4 .1). The important pore pressure calculated at the bottom of the dam is the reason of this result. Safety factors obtained with the limit equilibrium method are more important because of the less pore pressure calculated even with the Bishop method. For Circle C1, Fellenius method of slices gives the lowest value whereas over methods give the same value, arround 1.4.

methods	Point	P1	P2	P3
limite equil. : seepage computation	pressure (kPa)	73.6	60.2	19.4
limite equil. : Bishop method	pressure (kPa)	116.7	73.8	26.1
finite element method	pressure (kPa)	85.9	56.5	11.1
finite difference method	pressure (kPa)	111.1	54.9	15.8
limite equil. : seepage computation	Head (m)	7.51	6.14	1.98
limite equil. :bishop method	Head (m)	11.6	7.53	2.66
finite element method	Head (m)	8.75	5.76	1.13
finite difference method	Head (m)	11.32	5.59	1.6

Table 4.2 : safety factor at the end of the imponding

- At the end of impounding, the lowest safety factor is calculated on the downstream face of the dam, for the first impounding (table 4.2). The lowest global safety factor of the upstream face is given by the Bishop limit equilibrium method because the pore pressure are the highest in that case.

Failure line	circle C1	circle C
SF (Fellenius) seepage comput.	1.75	1.34
SF (Fellenius) bishop method	1.14	1.9
SF (Bishop) seepage comput	2.02	1.38
SF (Bishop) bishop method	1.45	2.0
SF (Perturbations) seepage comput.	2.01	1.38
SF (Perturbations) bishop method	1.44	2.01
SF finite element method	2.24	1.6
SF finite difference method	1.89	1.32

Table 4.3 : safety factor at the end of the drawdown

- At the end of the drawdown, we find again the lowest safety factor with finite difference method for circle C2 (table 4.3). For circle C1, Bishop method of pore pressure computation assiociated with Fellenius method of slices give the lowest safety factor.

4.2.3 Slip surface given by the finite difference method

The shear parameters, cohesion and tangent of friction angle, have been divided by an increasing factor b up to obtaining uncalculable displacements. The dilatancy angle, for this computation is egual to 0, imposed by the search of yield.

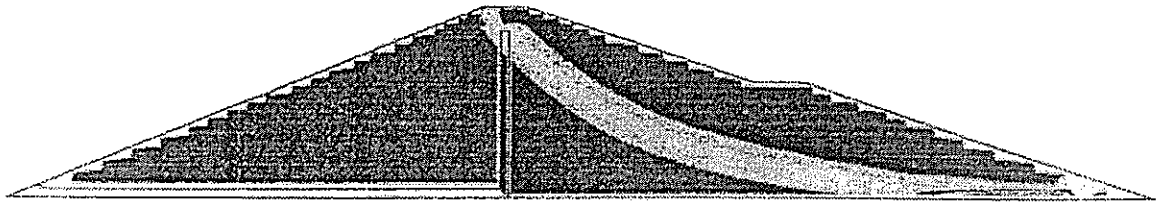

Figure 4.7 : Slip surface given by finite difference method

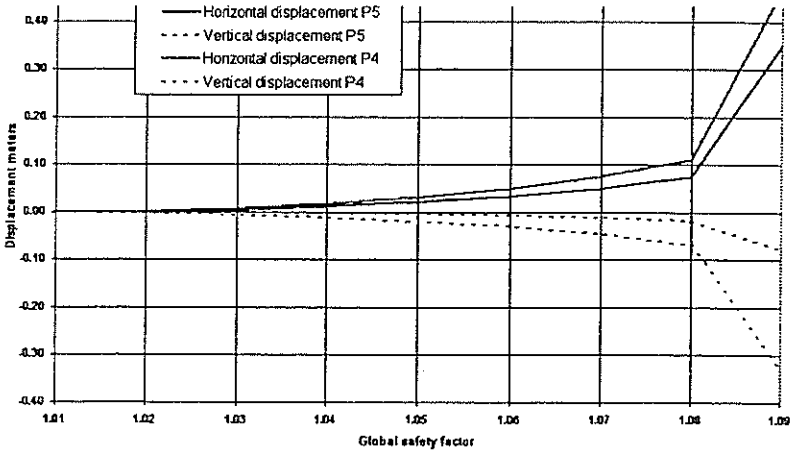

Fig 4.8 : Displacement at point 5 versus the global safety factor for the finite difference model

The shear parameters can be divided by a factor of 1.09 to have a displacement which an important value, and cannot be divided by 1.1, corresponding to the yield of the upstream face is achieved

5 CONCLUSIONS

Differences beetween the safety factors come mainly from the differences beetwen the method of pore pressure computation. Among the assumptions of the computation, the value of the compressibility of the fluid is over-riding, during the construction or drawdown.
A potential seepage surface on the upstream and downstream faces of the dam is neccessary to have a unsatured media. Without this surface, the pore pressure at the end of the drawdown seem to be very important and lead to low safety factor.
The mechanical behaviour of the dam is mainly dependant upon the pore pressure generation and decrease. To have an accurate hydraulic behaviour, isotrope triaxial tests are required to improve the pore pressure build-up parameters, in particular near the drain which have a big importance . In this case, parameters known do not lead to have circle C1 as the critical slip surface.

References

ref 1: Soil water characteristic curves for compacted clays, J.Tinjum, journal of geotechnical and geoenvironmental engineering november 1997.

ref 2: Simulation d'un écoulement polyphasique compositionnel hermique dans un milieux poreux, C.Serra, Ph D EDF/CNEH dcemder 1998

ref 3 : Les calculs d'écoulement transitoire dans les sols : à la recherche d'une méthodologie. technical reppport J.J. Fry. EDF/CNEH may 1990

ref 4 : a closed form equation for predicting the hydraulic conductivity of unsatured soils. Van Genuchten journal of the american society of soils science. vol 4 1980.

ref 5 : modelisation numerique des sols elastoplastiques non saturées applications aux barrages en remblai. Odile OZZANAM 1988. Ph D thesis of Ecole Centrale De Paris..

Result sheet B1-A: End of construction

1 - Pore pressure

methods	Point	P1	P2	P3
limite equilibrium method	pressure (kPa)	96.4	68.6	25.5
finite element method	pressure (kPa)	91	69.2	24.1
finite difference method	pressure (kPa)	98.1	54.7	21.9
classical method	Head (m)	9.83	7.0	2.6
finite element method	Head (m)	9.27	7.05	2.46
finite difference method	Head (m)	9.99	5.57	2.23

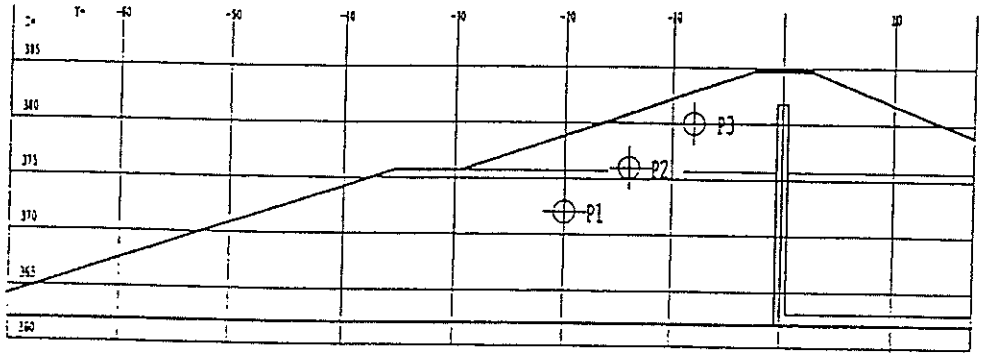

2 - Stability - factors of safety

Failure line	circle C1	circle C2
SF (Fellenius)	1.11	1.37
SF (Bishop)	1.4	1.44
SF (Perturbations)	1.4	1.45
SF finite element method	1.44	1.18
SF finite difference method	1.52	1.09

	Settlement P4 (cm)		Settlement P5 (cm)	
	dy	dz	dy	dz
finite element method	-7.03	-0.44	0.56	-2.72
finite difference method	-11.95	0.17	0.33	-2.09

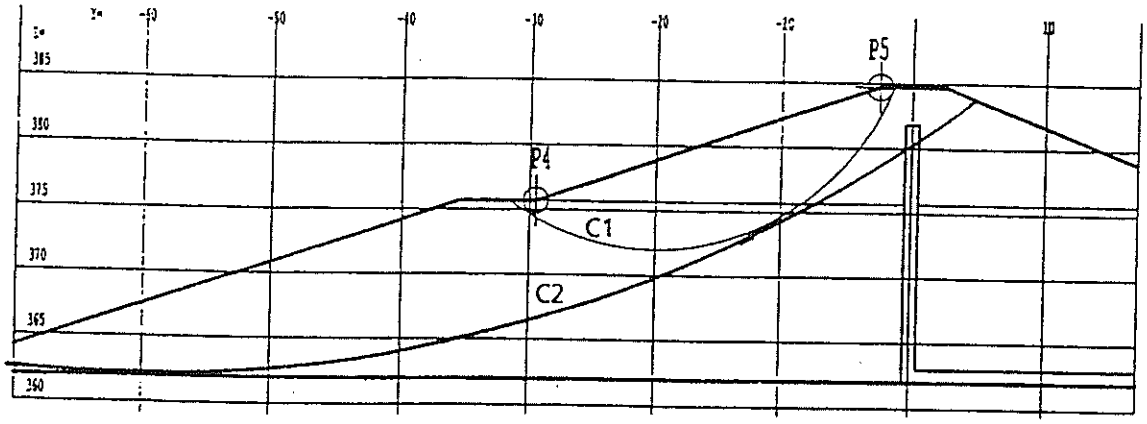

Result sheet B1-B: End of impounding

1 - Pore pressure

methods	Point	P1	P2	P3
limite equil. : seepage computation	pressure (kPa)	73.6	60.2	19.4
limite equil. : Bishop method	pressure (kPa)	116.7	73.8	26.1
finite element method	pressure (kPa)	85.9	56.5	11.1
finite difference method	pressure (kPa)	111.1	54.9	15.8
limite equil. : seepage computation	Head (m)	7.51	6.14	1.98
limite equil. :bishop method	Head (m)	11.6	7.53	2.66
finite element method	Head (m)	8.75	5.76	1.13
finite difference method	Head (m)	11.32	5.59	1.6

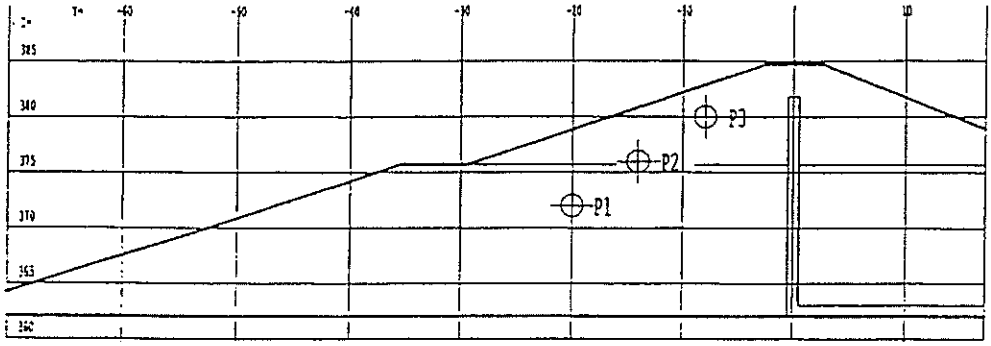

2 - Stability - factors of safety

Failure line	circle C1	circle C2
SF (Fellenius) seepage comput.	2.73	
SF (Fellenius) bishop method	1.8	
SF (Bishop) seepage comput	3.28	
SF (Bishop) bishop method	2.35	
SF (Perturbations) seepage comput.	3.22	
SF (Perturbations) bishop method	2.29	
SF finite element method	3.29	2.79
SF finite difference method	4.69	3.52

	Displacement P4 (cm)		Displacement P5 (cm)	
	dy	dz	dy	dz
finite element method	8.51	-4.39	4.34	-6.68
finite difference method	6.57	-2.85	4.76	-3.02

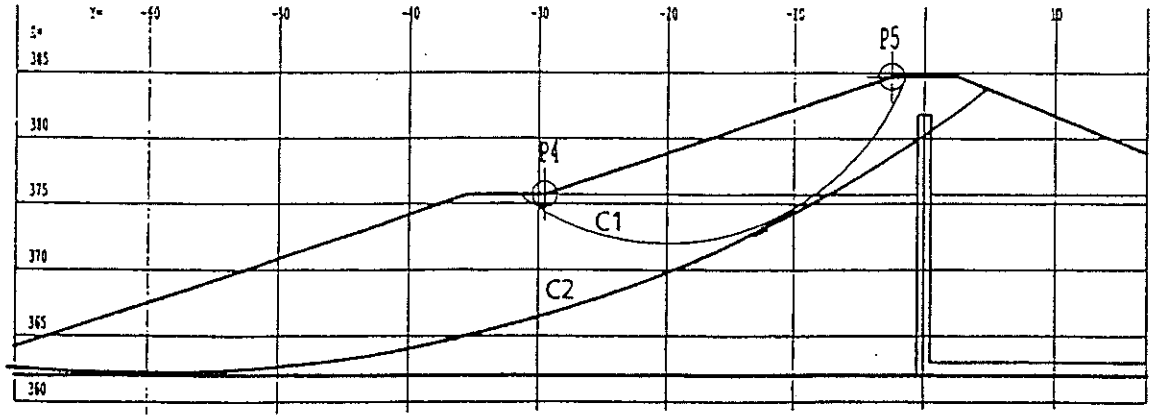

Result sheet B1 - End of drawdown

1 - Pore pressure

methods	Point	P1	P2	P3
limite equil. : seepage computation	pressure (kPa)	62.1	51.6	13.5
limite equil. : Bishop method	pressure (kPa)	94.0	67.7	26.1
finite element method	pressure (kPa)	47	26.6	0.6
finite difference method	pressure (kPa)	85.6	41.2	10.1
limite equil. : seepage computation	Head (m)	6.33	5.26	1.38
limite equil. :bishop method	Head (m)	9.58	6.9	2.66
finite element method	Head (m)	4.79	2.71	0.06
finite difference method	Head (m)	8.72	4.2	1.03

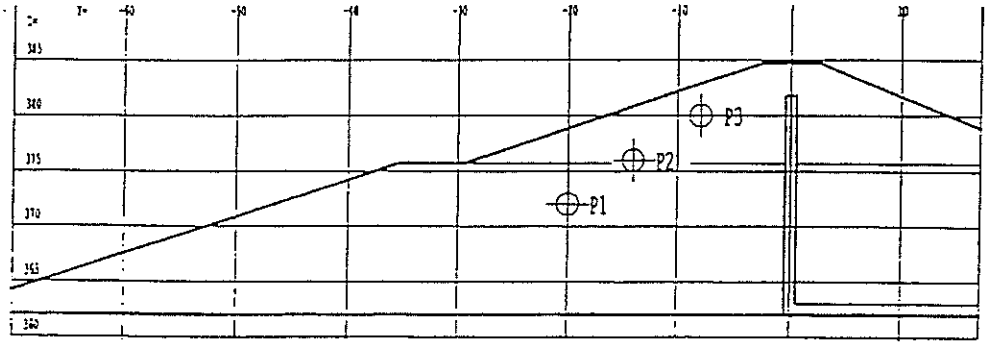

2 - Stability - factors of safety

Failure line	circle C1	circle C2
SF (Fellenius) seepage comput.	1.75	1.34
SF (Fellenius) bishop method	1.14	1.9
SF (Bishop) seepage comput	2.02	1.38
SF (Bishop) bishop method	1.45	2.0
SF (Perturbations) seepage comput.	2.01	1.38
SF (Perturbations) bishop method	1.44	2.01
SF finite element method	2.24	1.6
SF finite difference method	1.89	1.32

	Displacement P4 (cm)		Displacement P5 (cm)	
	dy	dz	dy	dz
finite element method	-5.86	-1.29	-4.12	-4.31
finite difference method	-5.05	-1.64	-3.62	-2.86

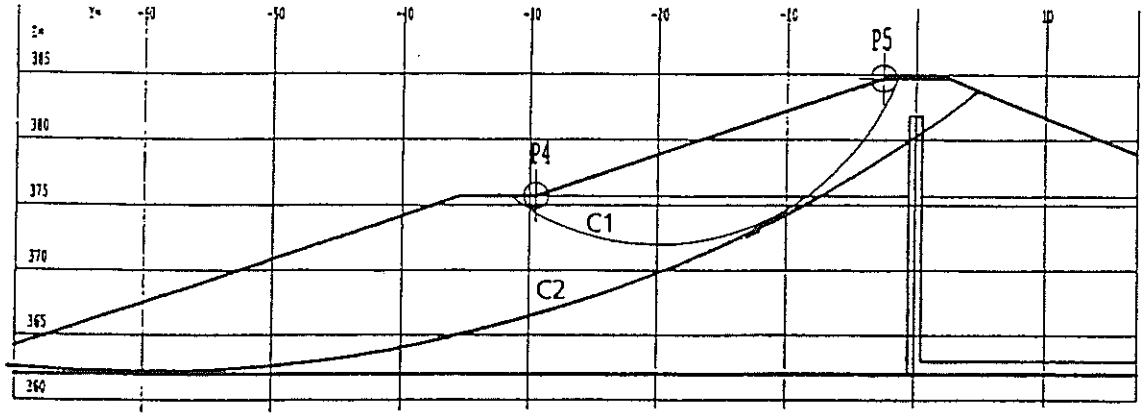

FIFTH ICOLD BENCHMARK WORKSHOP ON NUMERICAL ANALYSIS OF DAMS
DENVER (COLORADO U.S.A.), JUNE 2-5, 1999

THEME B1

NUMERICAL EVALUATION OF GLOBAL FACTORS OF SAFETY AGAINST FAILURE OF AN HOMOGENEOUS EMBANKMENT DAM

G.LA BARBERA*, A.BANI*, G.MAZZÀ**

ABSTRACT

Shells stability of an homogeneous earth dam, through factors of safety determination, have been evaluated. Limiting equilibrium and rheological methods have been adopted. Conventional stability analyses have been performed with FELLENIUS and PENDII codes, adopting different methods (Janbu, Fellenius, Bishop, Spencer) for the required loads conditions: end of construction, end of first impounding, end of first drawdown. The prescribed shear surface C1 has been considered, but also a random automatic search of the shear surfaces in the worst stability conditions has been carried out.
The simulation of the time-history of the dam and some failure analyses have been performed with the OMEGA finite element code. Three different constitutive models have been considered considered: the modified Cam-Clay (ECAM extended Cam Clay model), the Drucker-Prager and Mohr-Coulomb.
The results (position of critical shear surfaces and factor of safety) obtained through the two considered approaches were in quite good agreement.

1. INTRODUCTION

The paper presents the results of the analyses which have been carried out for the stability evaluation of the shells of a small homogeneous earthfill dam built in Southern France in the early eighties. Both conventional stability and rheological methods have been considered, as proposed by the Benchmark programme.
Three computer codes have been used for running the analyses: *OMEGA*, a 2D and 3D F.E.M. code for the numerical solution of non-linear problems. The code allows to treat both one phase medium(solid or fluid) and two-phases solid and fluid medium under static and dynamic load conditions. This code has been developed by ISMES S.p.A. on the basis of

* ISMES S.p.A. - Seriate (Italy)
** ENEL S.p.A. Research - Milano (Italy)

the theoretical formulation presented in [5], [6], [7], [8]; *FELLENIUS* code, for the evaluation of factor of safety along a defined sliding surface with Fellenius method; and *PENDII* code(whose core is PCSTABL5 code [11]),for the evaluation of factor of safety along potential sliding surfaces randomly generated. The shape of the generated potential shear surfaces can be defined as, circular, irregular or block shaped; Bishop, Janbu or Spencer methods can be used. These codes have been developed by ISMES S.p.A. (Bergamo, Italy).

The numerical computations have been carried out on a Personal Computer (486 or more) in Windows environment and on HP 9000 computer at the ISMES computer facilities in Bergamo (F.E.M.analyses).

2. FACTOR OF SAFETY DEFINITION

The definition of a factor of safety (Fs) is generally the main basic assumption underlying the formulation of limiting equilibrium methodology. Factor of safety is usually defined as the ratio of the available shear strength to the mobilised shear strength along an investigated shear surface. Such models implicitly assumes that the shear strength is constant along the whole shear surface, stress concentrations are not taken into account.
As the factor of safety equals 1 on a prescribed shear surface, we state that the shear surface is in a critical conditions (critical surface.)

Rheological models allow to simulate the general stress-strain behaviour of a structure, but they do not permit a factor of safety definition. The only way to compare results from the two mentioned approaches is to reach, with the rheological model, a failure condition. At failure we can state that for both approaches the factor of safety is equal to 1 (Fs =1)
From a numerical point of view, for the rheological model, the failure condition is reached when the tangent global stiffness matrix reaches a singularity. In practice it is impossible to model numerically this state but it is only possible to try to approximate it.
Failure state can be reached in two different ways: by increasing the applied loads, or by reducing the strength parameters. Starting from such considerations the factor of safety can be defined as the reducing factor which, applied to the strength parameters, generate the failure of the system (in agreement with Theme B1 requirements).

Factors of safety defined for limiting equilibrium methods and for rheological models are conceptually different and they can not be directly compared.

3. BRIEF DESCRIPTION OF THE ADOPTED SOLUTION ALGORITHMS

3.1 Limiting equilibrium methods

The general approach , originating earlier with Coulomb (1776), considers the assessment of the stability of the material above an assumed potential shear surface. The equilibrium of the material above such surface is examined by assuming enough shear strength is mobilised to maintain the slope at incipient failure condition (limit condition). A large number of potential shear surfaces (randomly generated) are analysed in order to determine the critical one.

The most commonly used procedure for slope stability analysis are the so called methods of slices. These methods divide the mass above an assumed shear surface into slices, so that the base of each slices is characterised by a single set of shear strength parameters. Factor of safety is considered constant along the whole shear surface.
In general, the limiting equilibrium approach is statically undetermined. The number of available equation is less than the unknowns. It is then necessary to introduce new hypothesis to increase equation number, commonly n-2, where n is the slices number. Different methods have been developed considering different hypothesis. In the present analyses Fellenius, Janbu and Bishop (simplified version), and Spencer methods have been considered.

PENDII code can automatically generate potential shear surfaces. A circular shaped surface is composed of a series of straight line segments of equal length (user's specified). The shear surface initiates from a point on the ground surface, within a specified zone (downstream). The first line segments direction is chosen randomly between two limit values. Subsequent segments direction is obtained changing the previous direction of a constant angle until the exit upstream zone specified by the users is reached.

3.2 Finite Element model

Both one phase solid and coupled two phase solid-fluid formulation together with an incremental elasto-plastic deformation theory have been adopted. A plane strain hypothesis has also been considered.

The following constitutive models have been considered:

(ECAM) Extended Cam-Clay model

The following hypothesis underlay ECAM model:

- isotropic material;
- linear elasticity inside the yield surface;
- associative flow rule G ≡ F;
- strain hardening;
- yield function F(p,q,θ,k)=0 of the type shown in Fig.1.

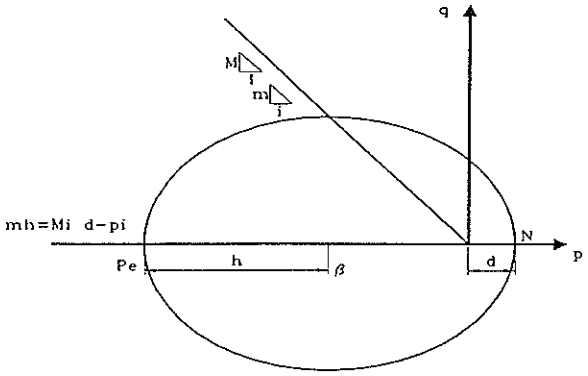

Figure 1

ECAM model requires the definition of the following material parameters:

E	Young modulus;
ν	Poisson coefficient;
c	cohesion;
ϕ	friction angle;
$\overline{V}$	specific volume;
λ	slope of virgin line;
χ	slope of swelling line;
OCR	over consolidation ratio;
r	ECAM yield parameter.

The critical state function results:

$f = q + M \cdot p - N \qquad (q = -Mp + N)$

The mathematical formulations for M and N parameters differ according to the adopted failure criteria, namely:

for Drucker-Prager failure criteria:

$$M = \frac{6\sin\phi}{3-\sin\phi}$$

$$N = \frac{6c\cos\phi}{3-\sin\phi}$$

for Mohr-Coulomb failure criteria:

$$M = \frac{3\sin\phi}{\sqrt{3}\cos\theta - \sin\theta\sin\phi}$$

$$N = \frac{3c\cos\phi}{\sqrt{3}\cos\theta - \sin\theta\sin\phi}$$

The yield function formula is the following:

$$F = (p-\beta)^2 + \frac{q^2}{m^2} - h^2$$

where:

$\beta = d - r \cdot h$

$d = c \cdot \tan^{-1}\phi$

$m = r \cdot M$ where r is a given constant value defined as:

$$r = \frac{m(\theta=30°)}{M(\theta=30°)}$$

Drucker_Prager failure criteria has been adopted in the coupled analysis. Mohr-Coulomb failure criteria has been adopted for failure analyses.

Drucker-Prager and Mohr-Coulomb models

The elastic-perfectly plastic Drucker-Prager constitutive model inscribed to the Mohr-Coulomb was adopted (Fig. 2-3). Plastic deformations were calculated considering an associated flow rule.
The failure criteria formulations are the same as those explained for ECAM model.

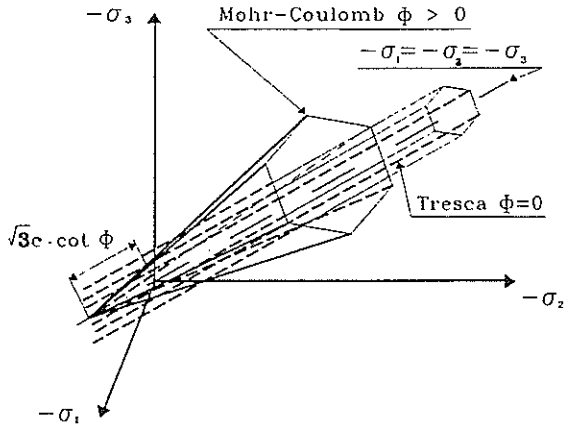

Figure 2

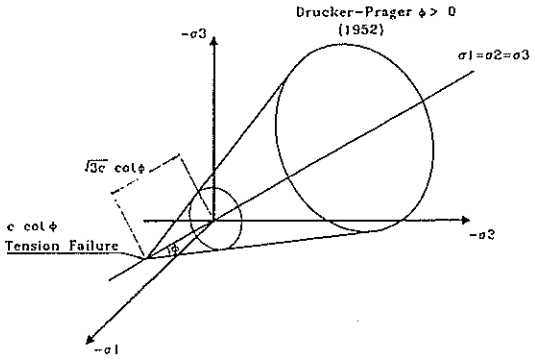

Figure 3

4. GEOMETRICAL DEFINITIONS

The cross section of the dam adopted in all the performed analyses (Fig. 4) is the same as that proposed in Theme B1 requirements.

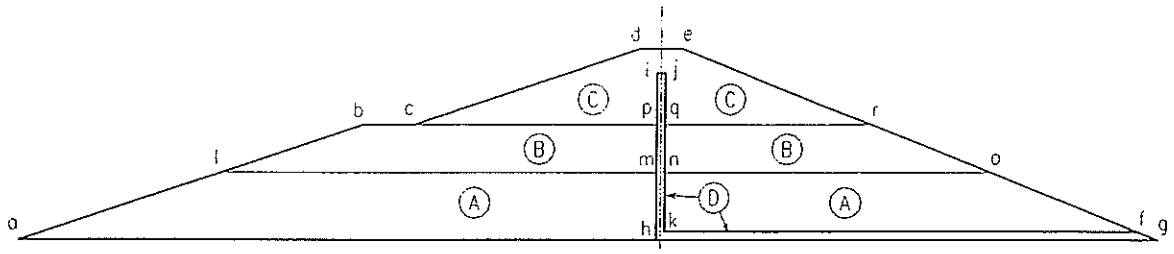

Fig. 4 - Simplified cross section for analyses

5. MATERIAL PARAMETERS

Four material zones have been considered (Fig.4):

- A - Clayey loam
- B - Clay (lower part of embankment- thickness of 5.7 m)
- C - Clay (upper part of embankment- thickness of 9 m)
- D - horizontal and vertical drain

The reference values of material parameters are the same as those proposed in Theme B1 requirements. Some other parameters requested by the adopted models have been estimated from usual geothecnical relationships and/or from empirical correlations.
Tables 1 reports material parameters input values adopted for limiting equilibrium analyses; Table 2 those adopted for the Finite Element analyses (Ecam and Drucker_Prager models); Table 3 the specific storage coefficients values used in seepage analysis.

Limiting equilibrium methods

	Mat.A Clayey loam	*Mat.B Clay*	*Mat.C Clay*	*Mat.D Drain*
Saturated unit weight (kN/m^3)	21.3	20.6	20.6	20.
Moist unit weight (kN/m^3)	20.9	20.6	20.6	20
Cohesion (kPa)	10	18	10	0
φ (^{o})	32	26	26	36

Table 1

Finite Elements Models

	Mat.A Clayey loam	*Mat.B Clay*	*Mat.C Clay*	*Mat.D Drain*
Moist unit weight (kN/m^3)	21.3	20.6	20.6	20.
Cohesion (kPa)	6.63	12.08	12.08	0
φ^* (^{o})	22.509	19.136	19.136	24.538
ν	0.3	0.3	0.3	0.3
E (Kpa)	8000	5000	5000	80000
λ	0.05	0.06	0.065	-
K	0.01	0.01	0.01	-
Vs_{tot}	1.52	1.6	1.6	-
OCR	5.0	5.0	5.0	-
Kh (m/s)	16.0e-9	4.0e-9	4.0e-9	1.0e-3
Kv (m/s)	4.0e-9	1.0e-9	1.0e-9	1.0e-3

*) Equivalent friction angle φ^e for Drucker_Prager failure criteria

Table 2

Specific storage coefficients (Seepage analysis)

	Mat.A Clayey loam	*Mat.B Clay*	*Mat.C Clay*	*Mat.D Drain*
Ss (1/m)	9.0E-04	1.5E-03	1.5E-03	1.E-04

Table 3

6. F.E.M. ANALYSES

Adopted mesh

A mesh composed by 659 8-node quadrangular parabolic elements and 2080 nodes has been adopted. The same mesh has been used for both structural and seepage analyses (Fig.5).

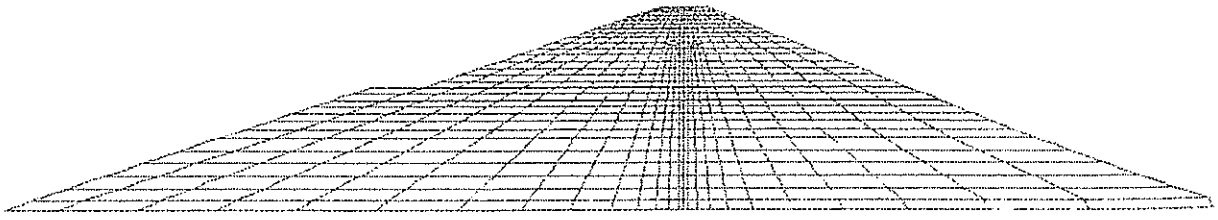

Fig. 5 - Adopted mesh in F.E.M. analyses

Boundary conditions

Structural analyses
Null horizontal and vertical displacements at the base. Null excess pore water pressure on lateral and upper boundaries of the core in the coupled analyses.

Seepage analysis
Upstream dam face below water level: imposed hydraulic head equal to water table level (381.3 m a.s.l.); base impervious (no flow conditions); downstream face considered as a seepage surface.

Initial conditions

In order to simulate the over-consolidation due to material compaction, an initial stress state of 20 kPa has been considered in the whole domain for the all performed analyses.

In seepage analysis an initial pore pressure distribution equal to the excess pore water pressure distribution evaluated at the end of construction was assumed.

Performed analyses

The following analyses have been carried out:

1 - *dam history simulation*, in order to evaluate the evolution of the pore water pressure distribution in the dam body. A coupled analysis adopting ECAM model for cohesive materials and Mohr-Coulomb model for drains have been adopted. The following history-phases have been considered:

- construction: ten phases (one layer each) in twelve months;
- first impounding: three phases (reservoir level increase 6.4 m each) in six months;
- first drawdown: two phases (reservoir level decrease 9.5 m each) in four months.

Seepage phenomena during first impounding and drawdown have been modelled with an independent analysis.

2 -*failure analyses*
An uncoupled approach has been adopted. Acting loads have been simultaneously applied. They are: gravity load, surface load on the wet upstream side of the dam, hydraulic load (pore water pressures evaluated in the previous analysis at end of construction, end of first impounding, end of first drawdown). The following cases have been considered:

- ✓ end of construction - two analyses performed: in the first one ECAM model for cohesive material and D.P. model for drain, in the second one D.P. model for all materials have been adopted.
- ✓ end of first impounding - one analysis performed: D.P. model for all materials have been adopted.
- ✓ end of first drawdown - one analysis performed: D.P. model for all material have been adopted.

Main remarks on the obtained results

The main results of the performed analyses are plotted as following.
Pore water pressure contours,pore water pressure and total hydraulic head vs. time at requested points P1, P2, P3, evaluated with coupled analysis are reported in Figures 6-7. Displacements vectors at failure state are shown in Figure 8. Horizontal and vertical displacements vs. load factor at some selected points of dam faces are reported in Figures 9-10.

Factors of safety evaluated with the failure analyses are reported in the following table:

Load condition	*Fs*
End of construction->failure	1.7-1.8
End of impounding ->failure	2.17
End of first drawdown ->failure	1.50

The maximum pore pressure values (about 125 kPa)have been calculated in upstream zone of the dam, close to the dam-foundation interface. At the end of impounding, pore pressures in downstream zone are close to zero and they are about 40-60 kPa in the central zone.

At the end of first drawdown, saturation line (u=0) exit is close to the upstream berm (Fig.6-7).

The critical shear surfaces obtained with the failure analyses are well defined for all the examined load conditions. Displacements evaluated with Drucker-Prager models show a sudden increase close to failure; Those obtained with ECAM models show a smoothed increase (Fig.8-10).

7. LIMITING EQUILIBRIUM ANALYSES

Fellenius, simplified Bishop, simplified Janbu (not considering empirical corrective coefficient) and Spencer methods have been considered in the analyses.

Performed analyses

Stability analyses have been carried out according to Theme B1 requirements, namely:

Case 1A - End of construction - Defined surface C1
Case 1B - End of first impounding - Defined surface C1
Case 1C - End of first drawdown - Defined surface C1

Further, considering the simplified Bishop method only, an automatic search of the surfaces in worst conditions (supposed of circular shape) has been made for the same loads conditions for both upstream and downstream shell.

The Following analyses have been performed:
Case 2A End of construction - surface in worst conditions in upstream shell;
Case 2B End of first impounding - surface in worst conditions surface in upstream shell
Case 2C End of first drawdown - surface in worst conditions in upstream shell
Case 3A End of construction - surface in worst conditions in downstream shell
Case 3B End of first impounding - surface in worst conditions in downstream shell

For downstream shell, End of first impounding and End of first drawdown condition can be considered the same.

Automatic search conditions

Starting and exit zone of the examined potential shear surfaces for the examined cases are reported in the following table:

Case	*Coord. x starting zone (m) (*)*	*Coord. x exit zone (m) (*)*
Case 2a	23 - 70	75-100
Case 2b	23 - 70	75-105
Case 2c	23 -30	70-100
Case 3a	40 -60	70-105
Case 3b	40 -60	70-105

(*) Reference system is the same as that assumed in the Theme b1 result sheets.

For each analysis 1000 surfaces have been examined.

Pore pressure evaluation

Pore pressure input data have been defined as following:

- definition of a phreatic surface within the dam body. Fellenius code computes piezometric heads as the distance from the base of the slice to the phreatic surface immediately above; PENDII code as the average between previous methods and the distance from the base of the slice perpendicular to the line through the piezometric surface bounding the top of that slice.
- definition of r_u parameter (pore pressure v.s. overburden pressure ratio) for each material. Such a parameter have been evaluated considering F.E.M. analysis results, averaged in the zone near the most probable position of the critical surface.
- definition of pore pressures along a defined shear surface.

The values adopted in the analyses are summarised in the following table:

Case	*r_u parameter*	*Phreatic surface*
Case 1a Case 2a	Mat. A 0.45 Mat. B 0.70 Mat. C 0.45	case 1a with Fellenius method (Fig.11)
Case 1b Case 2b	-	Surf.1 (Fig.11)
Case 1c Case 2c	-	Surf. 2 (Fig.11)
Case 3a	Mat. A 0.1 Mat. B 0.5 Mat. C 0.45	-
Case 3b	-	-

Main remarks on the obtained results

The main results of the performed analyses are plotted according to the required result sheets. They are reported in Figures 12-14.

The critical surfaces automatically evaluated in general do not match with the prescribed C1 surface.

The worst condition is at the end of construction. Minimum factor of safety is about 1.3 (Fellenius and Janbu methods), for surface C1.

Evaluated factors of safety are reported in the following tables:

Factors of safety calculated for the prescribed surface C1

Load condition	*Methods*			
	Fellenius	Bishop	Janbu	Spencer
End of construction	1.30 (r_u) 1.31 (phreatic sur.)	1.46	1.29	1.44
End of impounding	2.60	3.30	2.88	3.57
End of first drawdown	2.00	2.36	2.01	2.33

Minimum factors of safety (for surfaces in worst conditions)

Load condition	Methods
Upstream shell	Bishop
End of construction	1.43
End of first impounding	2.86
End of first drawdown	1.59
Downstream shell	
End of construction	1.41
End of first impounding/drawdown	1.96

8. REQUIRED COMPUTATION TIME

Coupled analyses required a CPU time of about 15 minutes.

Failure analyses required a CPU time varying from about 1 min. to 10 min each.

9. CONCLUDING REMARKS

The whole set of results obtained from the carried out analyses for the Fifth Benchmark Workshop are presented and discussed in this paper.

Both limiting equilibrium and rheological methods have been considered. The first approach have been used in order to evaluate the factor of safety for the prescribed surface C1 with different methods (Janbu, Fellenius, Bishop, Spencer). The sliding surfaces in worst conditions have also been determined by means of a random search technique.
Analysed load conditions were: end of construction, end of first impounding, end of first drawdown.
F.E.M. model has been used to simulate the time-history of the dam and to perform the failure analyses.

Fellenius method resulted the most conservative. Average differences between the considered limiting equilibrium methods are about 10-20%.

Position of critical surfaces evaluated with the two approach is generally similar. At the end of construction downstream shell is in the worst condition (Fs=1.7-1.8 obtained from F.E.M. model; Fs=1.4-1.5 from limiting equilibrium method).
At the end of first impounding calculated factors of safety are higher. The worst situation is again in the downstream shell(Fs=2.2 obtained from F.E.M. model; Fs=2.0 from limiting equilibrium method).
At the end of first drawdown the critical surface is located in the lower part of upstream shell (Fs=1.5 obtained from F.E.M. model; Fs=1.6 from limiting equilibrium method, not considering seepage forces).

10. REFERENCES

[1] Biot M.A. (1941). General theory of three dimensional consolidation J Appl. Phis.

[2] Biot M.A. (1956). The theory of propagations of elastic waves in a fluid saturated porous solid. J. Acou.Soc.Am., 168 191.

[5] Fusco A. (1985). Continuum mechanics and finite element numerical solutions in geomechanics. Ph. D. Thesis, University of Ottawa.

[6] Fusco A. (1993). Numerical analysis for engineers. Monograph CIMNE, N.19

[7] Fusco A. (1993). The Continuum Mechanics Theory for engineers. Monograph CIMNE, N.20

[8] Fusco A. (1993).The Finite Element Method for engineers. Monograph CIMNE, N.21

[9] Fusco A., Cervera M.(1993).Coupled solid-pore fluid problems solved by Finite Elements. Monograph CIMNE, N.22

[10] La Barbera G., Bani A., Mazzà G. (1994), Evaluation of pore pressure and settlements of an embankment dam under static loading"
Third Icold Benchmark Workshop on Numerical Analysis of Dams, Paris 1994

[11] ISMES,S.p.A. " Codici APPLIGEO", User and Theoretical manuals - Ver. 1.2 December 1996

Pore Water Pressure

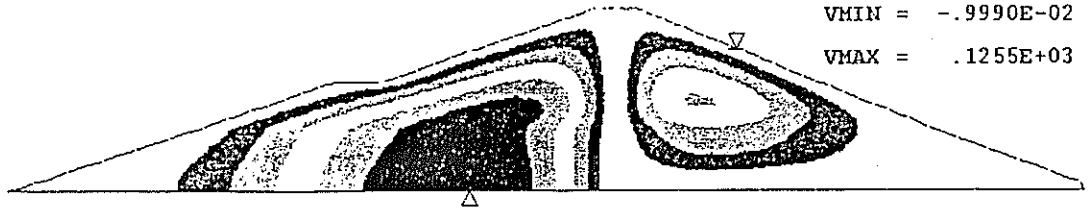

End construction

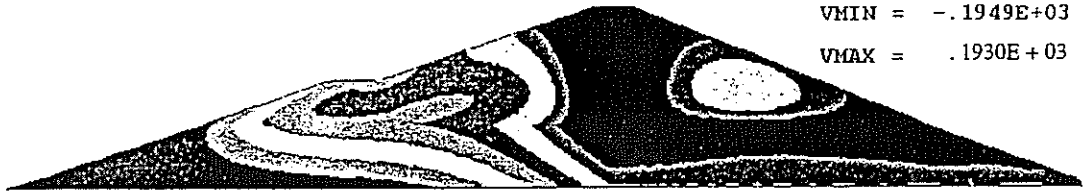

End of first impounding

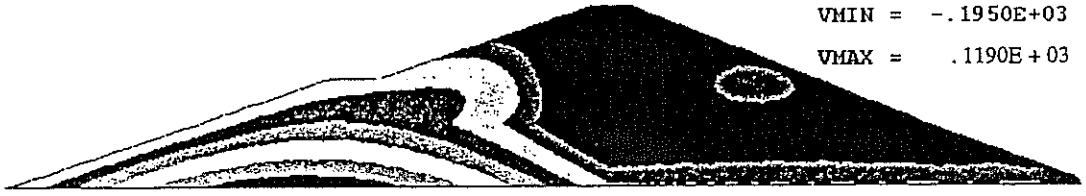

End of first drawdown

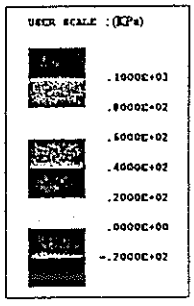

Fig. 6

Pore pressure vs. time at nodes P1 P2 P3

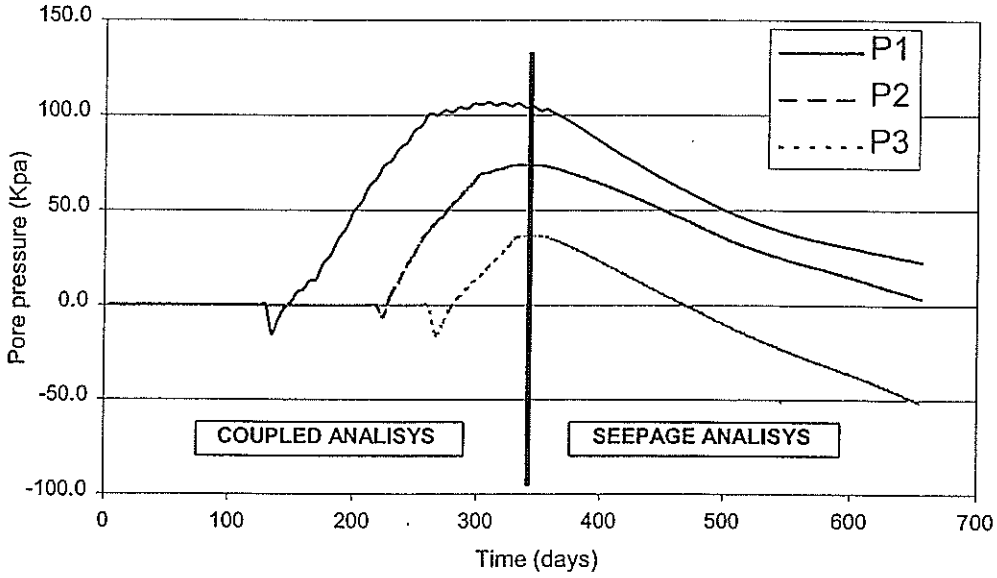

Total hydraulic head vs. time at nodes P1 P2 P3

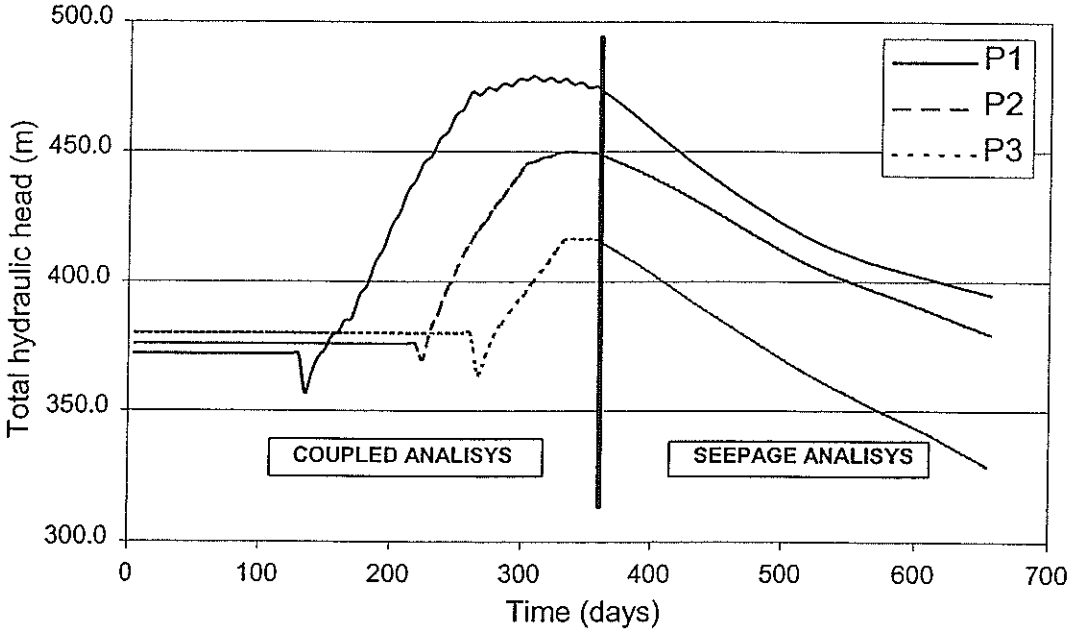

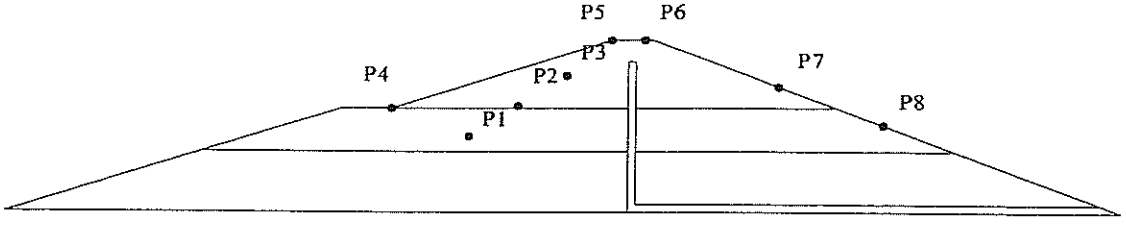

Fig. 7

5th ICOLD Benchmark Workshop - Theme B1

Analyses at Failure State - Displacement vectors at failure state

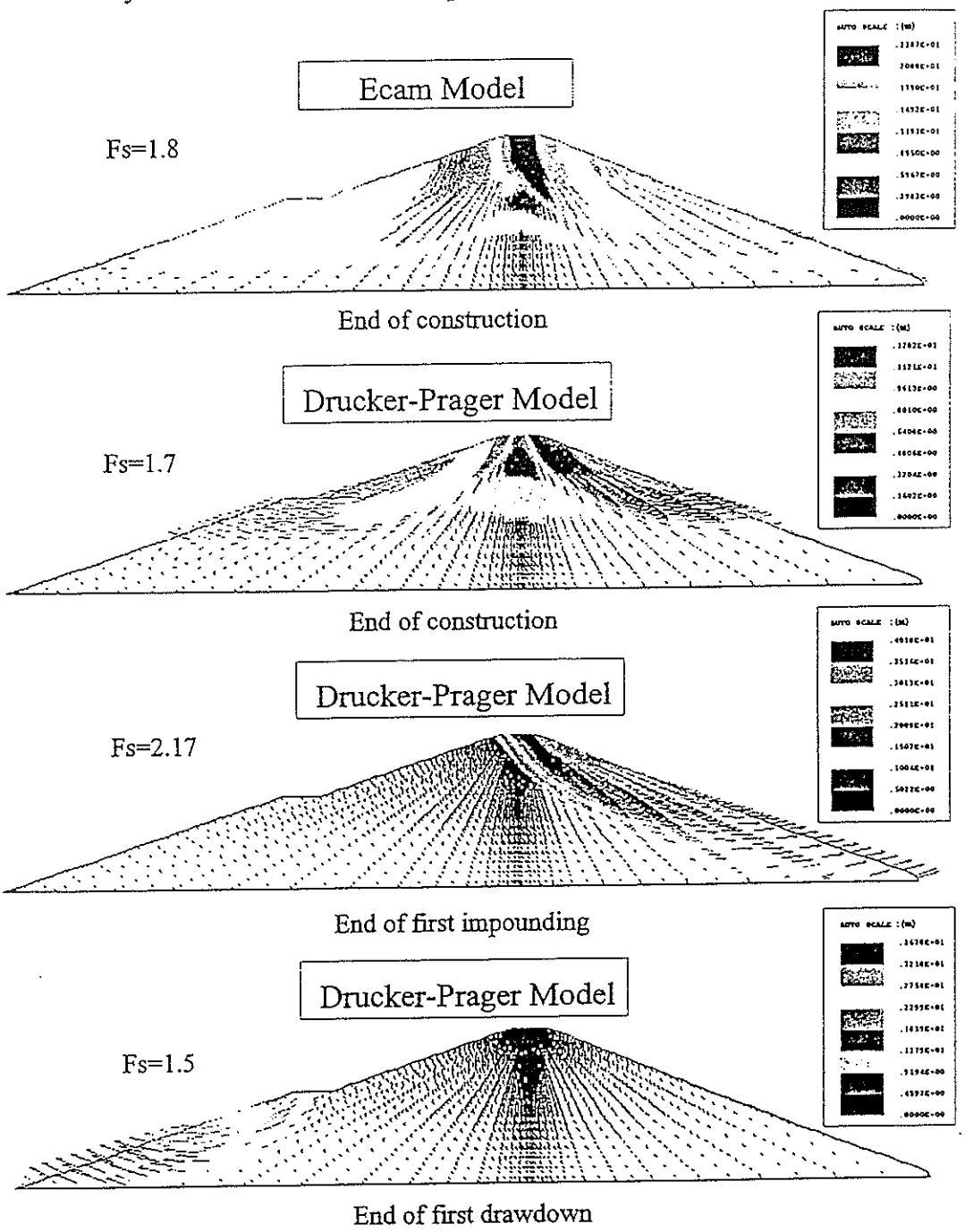

Fig. 8

5th ICOLD Benckmark Workshop - Theme B1

Ecam Model

Horizontal displacements at the end of costruction

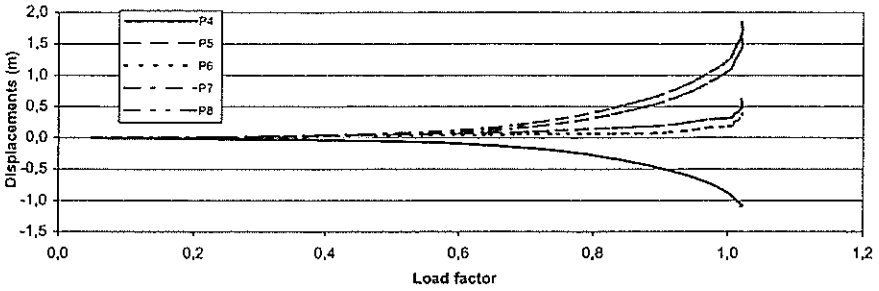

Vertical displacements at the end of costruction

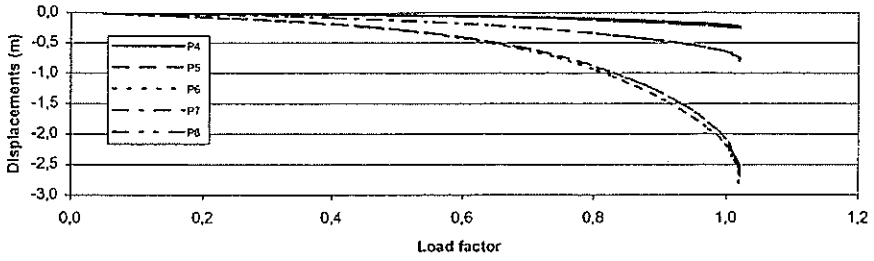

Drucker-Prager Model

Horizontal displacements at the end of costruction

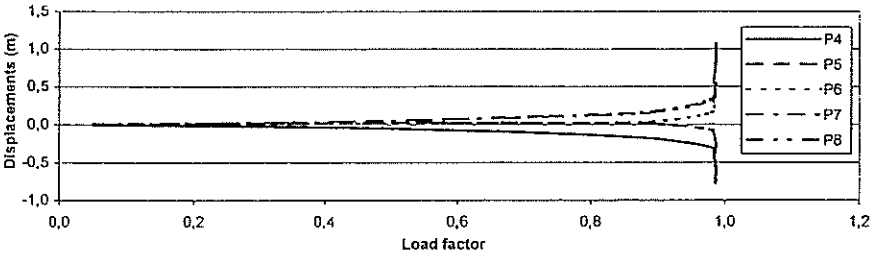

Vertical displacements at the end of costruction

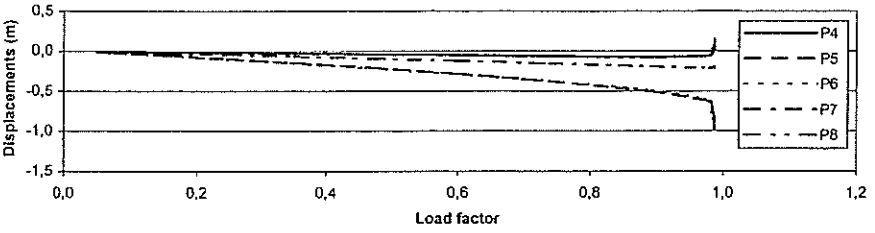

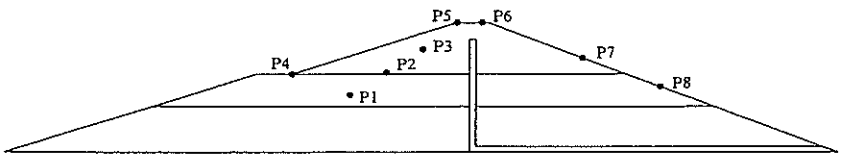

Fig. 9

5th ICOLD Benckmark Workshop - Theme B1
Drucker-Prager Model

Horizontal displacements at the end of first impunding

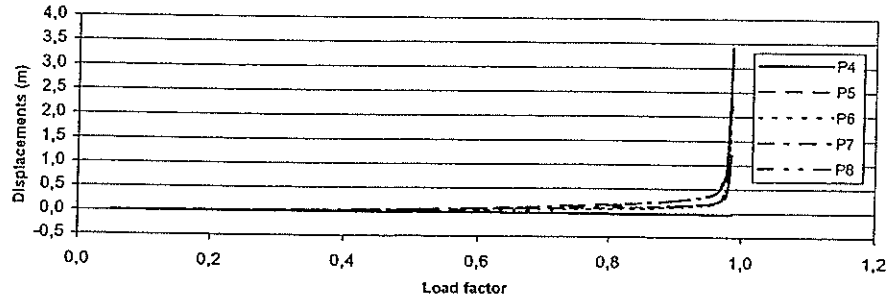

Vertical displacements at the end of first impunding

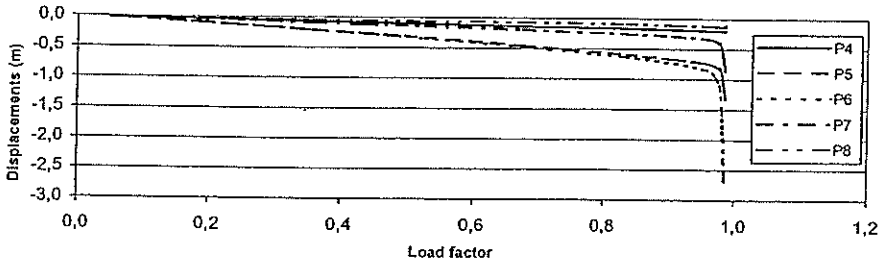

Horizontal displacements at the end of first drawdown

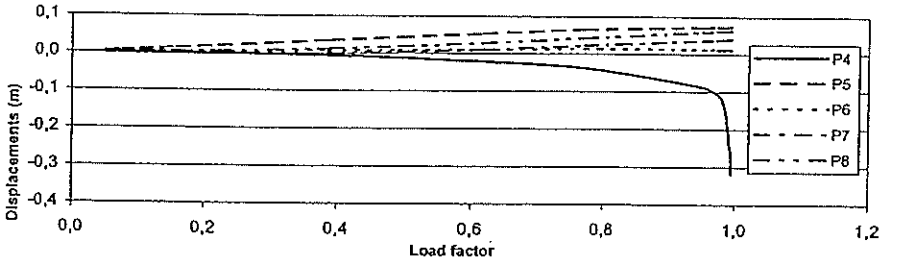

Vertical displacements at the end of first drawdown

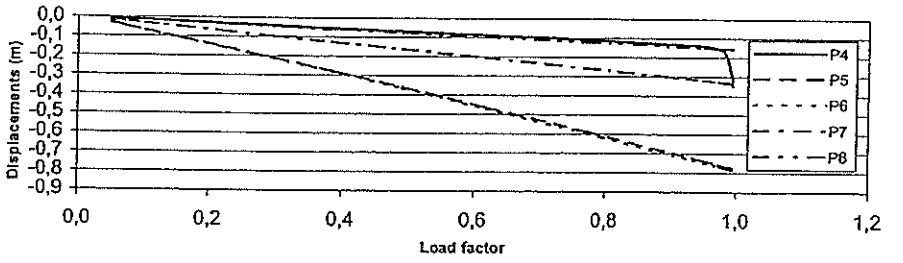

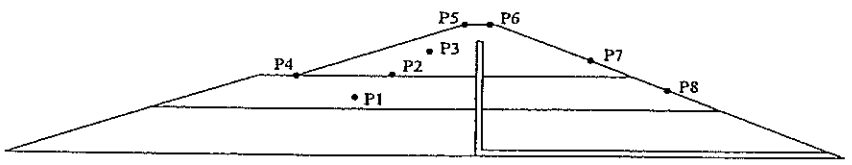

Fig. 10

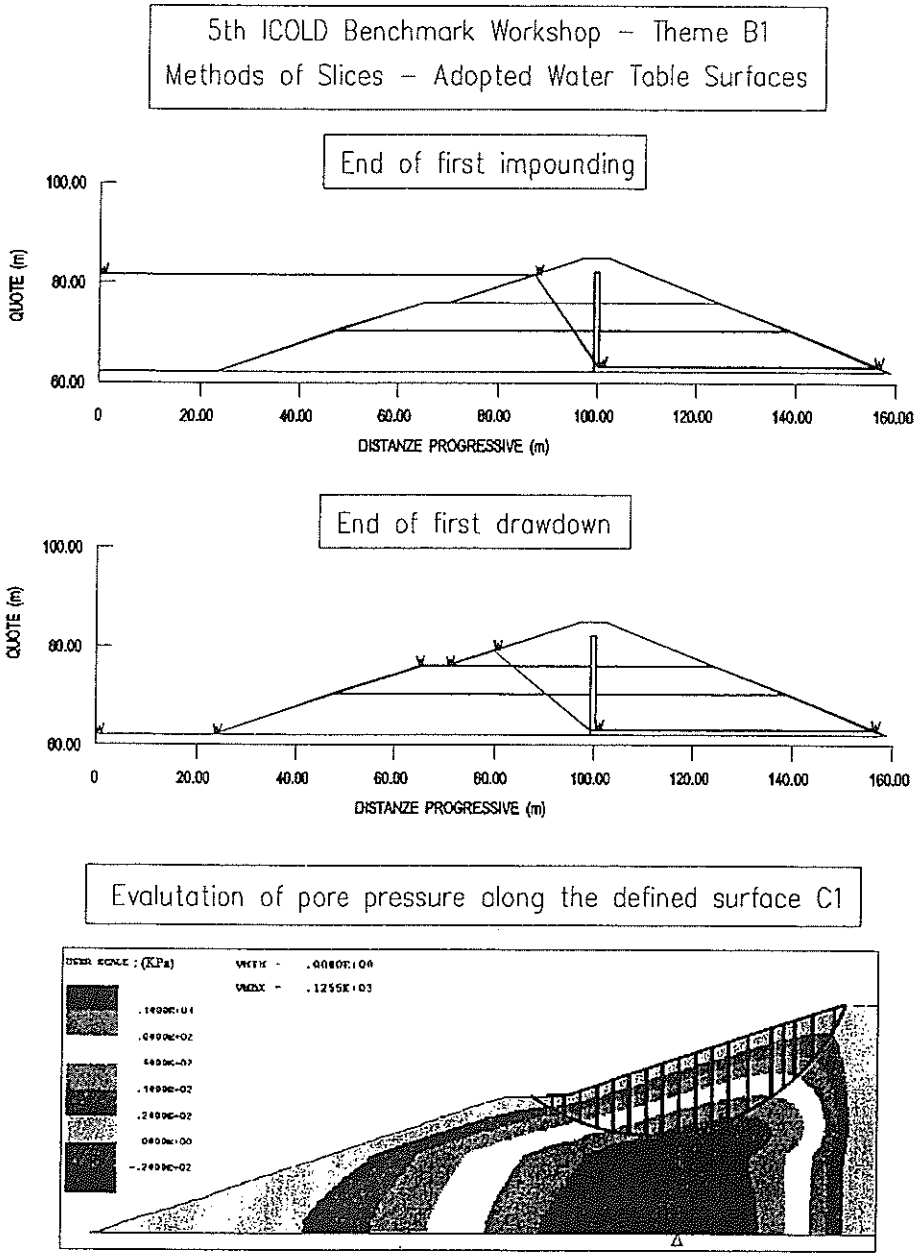
5th ICOLD Benchmark Workshop – Theme B1
Methods of Slices – Adopted Water Table Surfaces
End of first impounding
QUOTE (m)
100.00
80.00
60.00
0
20.00
40.00
60.00
80.00
100.00
120.00
140.00
160.00
DISTANZE PROGRESSIVE (m)
End of first drawdown
QUOTE (m)
100.00
80.00
60.00
0
20.00
40.00
60.00
80.00
100.00
120.00
140.00
160.00
DISTANZE PROGRESSIVE (m)
Evalutation of pore pressure along the defined surface C1

Fig. 11

5th ICOLD Benchmark Workshop – Theme B1
Result sheet B1–A: End of Construction

1 – Pore pressure

Point	P1	P2	P3
Pressure (kPa)	103.14	73.17	36.19
Head (m)	475.15	449.17	416.19

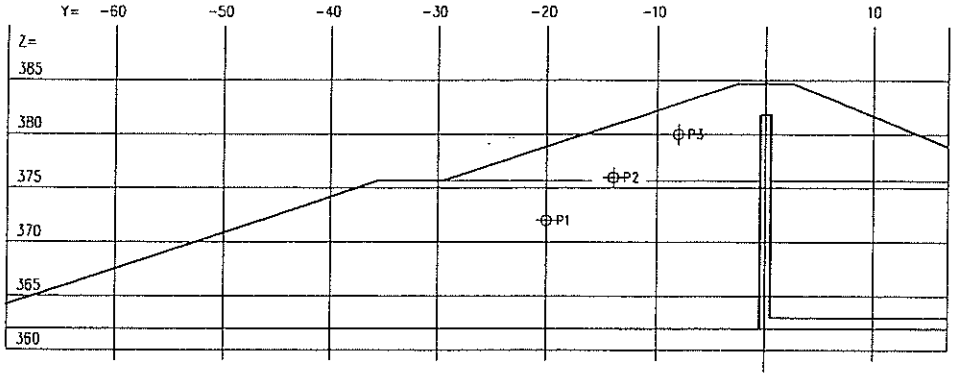

2 – Stability – Factors of safety

Failure line	Circle C1	Critical line
SF (Fellenius)	1.30	–
SF (Bishop)	1.46	1.43
SF (Jambu)	1.29	–
SF (Spencer)	1.44	–

F.E.M. ANALYSIS – D.P. MODEL				
F factor	Displacement P4 (cm)		Displacement P5 (cm)	
	dY	dZ	dY	dZ
1.7	-78.0	6.0	-38.0	-93.0
Critical line				

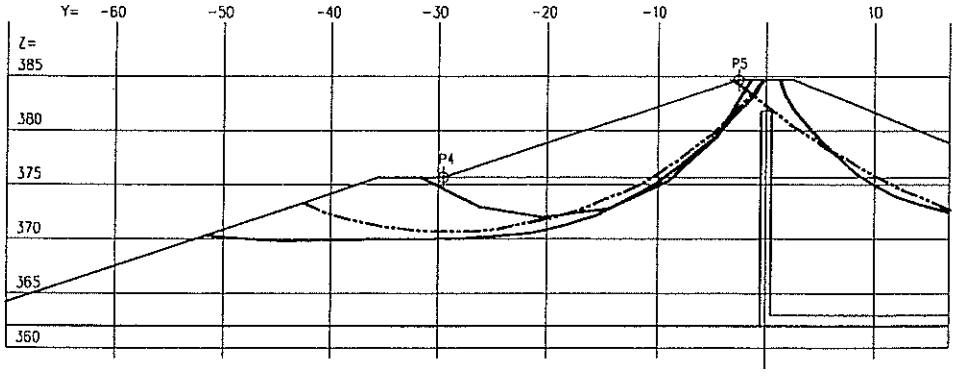

Fig. 12

5th ICOLD Benchmark Workshop - Theme B1
Result sheet B1-6: End of Impounding

1 - Pore pressure

Point	P1	P2	P3
Pressure (kPa)	41.06	26.84	-20.27
Head (m)	413.06	402.84	359.73

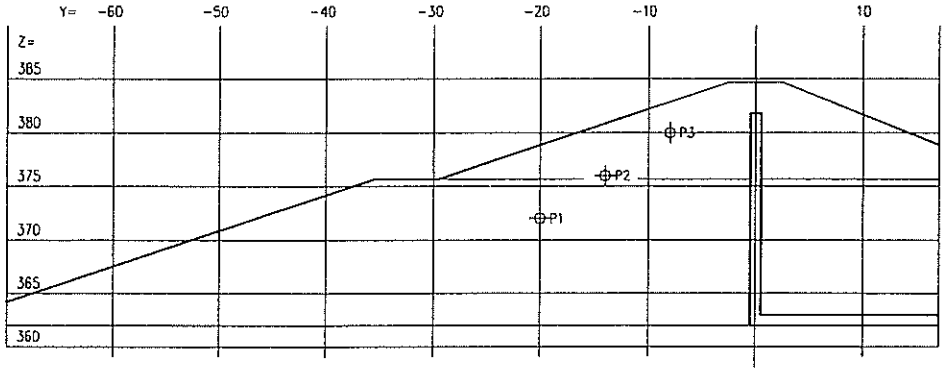

2 - Stability - Factors of safety

Failure line	Circle C1	Critical line
	———	- - - -
SF (Fellenius)	2.60	-
SF (Bishop)	3.30	2.86
SF (Jambu)	2.88	-
SF (Spencer)	3.57	-

F.E.M. ANALYSIS - D.P. MODEL				
F factor	Displacement P4 (cm)		Displacement P5 (cm)	
	dY	dZ	dY	dZ
2.17	-3.0	-20.0	121.0	-133.0
Critical line ———				

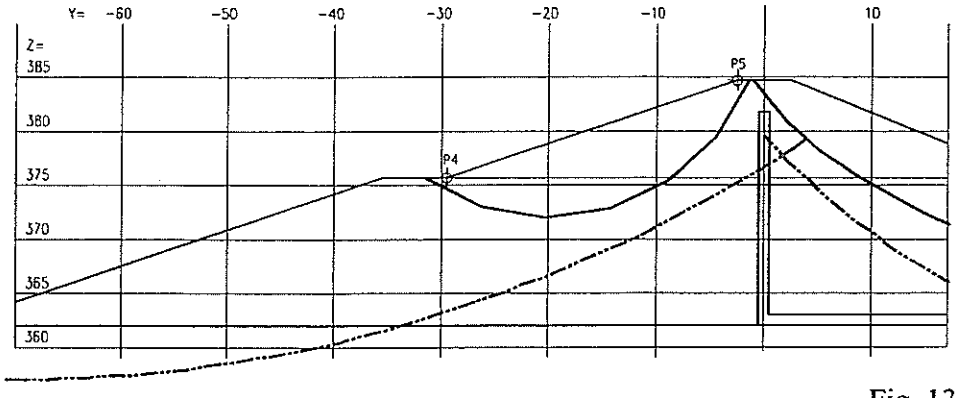

Fig. 13

5th ICOLD Benchmark Workshop – Theme B1
Result sheet B1–C Rapid Drawdown

1 – Pore pressure

Point	P1	P2	P3
Pressure (kPa)	22.81	3.53	–51.63
Head (m)	394.81	379.53	328.37

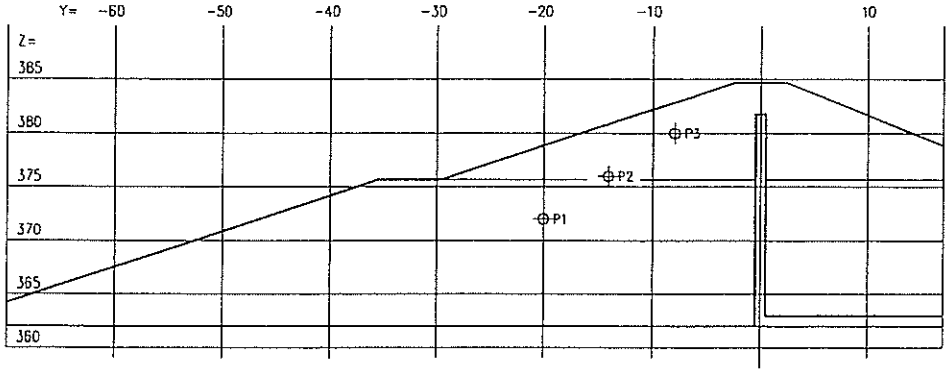

2 – Stability – Factors of safety

Failure line	Circle C1 ———	Critical line – – –
SF (Fellenius)	2.00	–
SF (Bishop)	2.36	1.59
SF (Jambu)	2.01	–
SF (Spencer)	2.33	–

F.E.M. ANALYSIS – D.P. MODEL				
F factor	Displacement P4 (cm)		Displacement P5 (cm)	
	dY	dZ	dY	dZ
1.5	–32.0	–35.0	7.0	–78.0
Critical line ———				

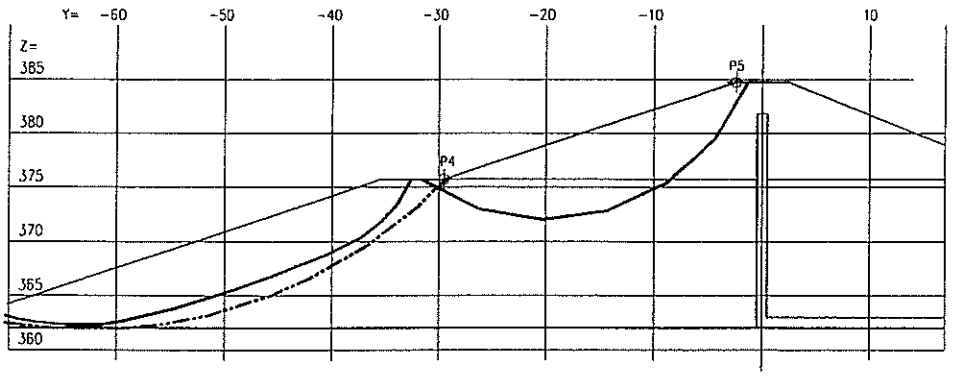

Fig. 14

Embankment stability analysis by elasto-plastic finite elements

D. V. Griffiths [1], R.L. Torres [2], and P.A. Lane [3]

ABSTRACT:

This paper describes the stability analysis of an embankment problem using the finite element method. The method of analysis uses an effective stress approach and assumes elastic-perfectly plastic (Mohr-Coulomb) behavior implemented using a visco-plastic algorithm. The analyses use a gravity 'turn-on' procedure. The method easily incorporates different soil property groups and water table conditions, and if presented with reasonable soil compressibility data, will also give information about deformations at working stress levels. The main objective of the present work however, is to compute the factor of safety of a particular earth dam under various construction, impoundment and drawdown conditions.

The extremes of such conditions were examined and the analysis shows that the dam presented is highly vulnerable to changes in construction timetable and sensitive to small changes in data. This vulnerability is confirmed by the collapse of the actual structure on first drawdown. For comparison a number of the cases considered are also analyzed using the traditional limit state method incorporating material properties given and pore water pressures appropriate to each case.

INTRODUCTION

The finite element method is a powerful technique for estimating the factor of safety of soil slopes (Griffiths and Lane 1999) . The advantages of the method relative to traditional limit equilibrium methods can be summarized as follows:

1. No assumption needs to be made in advance about the shape or location of the failure surface. Failure occurs 'naturally' through the weakest zones within the soil mass.

2. Since there is no concept of "slices" in the finite element approach there is no need for assumptions about slice side forces. The method preserves local and global equilibrium to within tight tolerances at all times.

3. If realistic soil compressibility data is available, the finite element solutions will give information about deformations at working stress levels.

4. The method is able to monitor progressive failure of the slope up to and including overall shear failure.

[1]Colorado School of Mines, Golden CO
[2]US Bureau of Reclamation, Denver, CO
[3]UMIST, Manchester, UK

The program used in this study are based closely on Program 6.2 in the text by Smith and Griffiths (1997)–the main difference being the ability to model more realistic geometries with better graphical output facilities. The programs are for 2-d analysis of elastic-perfectly plastic soils with a Mohr-Coulomb failure criterion. The programs use 8-node quadrilateral elements with reduced integration (4 Gauss-points per element) in both the stiffness and stress redistribution phases of the algorithm. A gravity 'turn-on' procedure generates nodal forces which act in the vertical direction at all nodes. These loads are applied in a single increment and generate normal and shear stresses at all the Gauss-points within the mesh. These stresses are then compared with the Mohr-Coulomb failure criterion. If the stresses at a particular Gauss-point lie within the Mohr-Coulomb failure envelope then that location is assumed to remain elastic. If the stresses lie on or outside the failure envelope, then that location is assumed to be yielding. Overall shear failure occurs when a sufficient number of Gauss-points have yielded to allow a mechanism to develop.

The analysis is based on an iterative Modified Newton-Raphson method called the Visco-plastic algorithm (Zienkiewicz *et al* 1975). If a particular zone within the soil mass is yielding as indicated by a stress level that lies outside the Mohr-Coulomb failure envelope, the algorithm attempts to redistribute those excess stresses by sharing them with neighboring regions that still have reserves of strength. The redistribution process is achieved by the algorithm generating self-equilibrating nodal forces (or body forces) which act on each element that contains stresses that are violating the failure criterion. These forces, being self-equilibrating, do not alter the overall gravity loading on the finite element mesh, but do influence the stresses in the regions where they are applied. In reducing excess stresses in one part of the mesh however, other parts of the mesh that were initially 'safe' may now start to violate the failure criterion themselves necessitating another iteration of the redistribution process. The algorithm will continue to iterate until both equilibrium and the failure criterion at all points within the soil mass are satisfied within quite strict tolerances.

If the algorithm is unable to satisfy these criteria at all yielding points within the soil mass, 'failure' is said to have occurred. Failure of the slope and numerical non-convergence occur together, and are usually accompanied by a dramatic increase in the nodal displacements. Within the data, the user is asked to provide an iteration ceiling beyond which the algorithm will stop trying to redistribute the stresses. Failure to converge implies that a mechanism has developed and the algorithm is unable to simultaneously satisfy both the failure criterion (Mohr-Coulomb) and global equilibrium.

SOIL MODEL

The soil model used in this study consists of seven parameters as shown in Table 1.

Table 1: Seven-parameter model

ϕ'	Friction angle
c'	Cohesion
ψ	Dilation angle
E	Young's modulus
ν	Poisson's ratio
γ	Total unit weight
r_u	Pore pressure ratio

In terms of principal stresses and assuming a compression-negative sign convention, the Mohr-Coulomb criterion can be written as follows:

$$F = \frac{\sigma_1' + \sigma_3'}{2} \sin\phi' - \frac{\sigma_1' - \sigma_3'}{2} - c' \cos\phi' \tag{1}$$

where σ_1' and σ_3' the major and minor principal effective stresses at the point under consideration. The failure function F can be interpreted as follows:

$F < 0$	stresses lie inside the failure envelope (elastic)
$F = 0$	stresses lie on the failure envelope (yielding)
$F > 0$	stresses lie outside the failure envelope (yielding) and must be redistributed

GRAVITY LOADING

The forces generated by the self weight of the soil are computed using a gravity 'turn-on' procedure involving integrals over each element of the form:

$$\mathrm{p}^{(e)} = \gamma \int_{V^e} \mathrm{N}^T \, \mathrm{d(vol)} \tag{2}$$

where the N terms are the shape functions of the 8-node element and the superscript e refers to the element number. These element forces are assembled into a global gravity force vector that is applied to the finite element mesh at the first iteration.

DETERMINATION OF THE FACTOR OF SAFETY

The Factor of Safety of a soil slope is defined as that factor by which the original shear strength parameters must be reduced in order to bring the slope to the point of failure. The analyses therefore use the factored shear strength parameters c_f' and ϕ_f', where:

$$c_f' = c'/FOS \tag{3}$$

$$\phi_f' = \arctan\left(\frac{\tan\phi'}{FOS}\right) \tag{4}$$

To find the 'true' Factor of Safety, it is necessary to search for the value of FOS that will just cause the slope to fail. This requires analysis of a sequence of FOS values on a trial and error basis. Usually the range of FOS values in which to search will be quite narrow based on experience of similar geometries. The following comments give some guidance as to the logic of choosing a sequence of FOS:

- The chosen FOS value results in rapid convergence (one or two iterations)–This implies that the slope is still elastic and probably no yield has occurred at any of the Gauss points. Repeat the analysis with a significantly higher value of FOS.
- The chosen FOS value results in convergence in a reasonable number of iterations (well below the iteration ceiling)–This implies that some Gauss points have yielded and stress redistribution has taken place comfortably. Repeat the analysis with a moderately higher value of FOS.
- The chosen FOS value results in convergence in a considerable number of iterations (quite close to the iteration ceiling)–This implies that quite a lot of Gauss points have yielded and the algorithm has had to work hard to achieve the necessary stress redistribution. Repeat the analysis with a slightly higher value of FOS.
- The chosen FOS value does not converge (the iteration ceiling has been reached)–This implies that the slope has failed and enough Gauss points have yielded to allow the formation of a mechanism. Repeat the analysis with a slightly lower value of FOS.

The true Factor of Safety of the slope will lie between the highest value of FOS for which convergence was achieved and the lowest value of FOS for which convergence was not achieved.

Lack of convergence is a good guide to failure, however it is also recommended that the user plots a graph of FOS vs. δ_{max} (the maximum nodal displacement in the mesh at convergence). Such graphs are shown in the validation section of this report and indicate that the FOS value that corresponds to failure also usually results in a significant increase in the nodal displacements in the mesh.

INCORPORATION OF PORE PRESSURES

The effective stress analyses described in this paper take into account pore pressures at the Gauss points. These pore pressures can be generated using a pore pressure ratio r_u, as in:

$$\begin{aligned} u &= \gamma h r_u \\ &= \sigma_v r_u \end{aligned} \tag{5}$$

where σ_v is the total vertical stress at that point.

Alternatively, a free-surface can be defined as shown in Figure 1. In this case, pore pressures are set equal to the depth of each Gauss point beneath the free surface multiplied by the unit weight of water. Free standing water in the reservoir is modeled as a pressure loading against the submerged upstream side of the embankment.

Finally, nodal head data derived from a the sequence of construction, impounding and drawdown of the dam was incorporated into the analysis. The package Seep W was used to track the development of pore pressures at the end of construction, the advancing front during impounding and finally the retreat on drawdown. Where the seepage analysis produced pore suctions these were neglected in the analysis as a conservative assumption.

Figure 2a shows the saturation front of the ground water in the embankment for the end of construction, impounding and drawdown. Observe that the variations of the saturation front for each case are not significantly different from one another. Figure 2b shows an enlarged portion of Figure 2a. The end of construction values were obtained assuming that the pore pressures had dissipated to some extent from the values computed using r_u. These pore pressures were then used as initial condition for the impounding process. Impounding went on for six months and was followed by a drawdown of 3 months. To show what might happen with a much more permeable embankment, the analysis were repeated with permeabilities all increased by a factor of 1000. In this case (Figure 2c) the saturation fronts for each case are significantly different.

This range of pore pressure conditions plots the envelope of possible Factors of Safety of the structure under the full range of operating conditions and the results confirmed the dependence of the structure on the rate of construction and subsequent impounding and drawdown.

Drawdown

Conditions of drawdown are modeled in two ways. Firstly by assuming that the upstream reservoir has been removed, with the new free surface coinciding with the upstream slope of the embankment as shown in Figure 6b. This approach implies an equal change in pore pressure and total stress, thus no change in effective stress within the upstream embankment soils. The stabilizing effect of the reservoir water however, has been removed.

Secondly, the seepage analysis allowed the consideration of transient pore pressure conditions, both allowing for construction pore pressures and neglecting them.

STABILITY ANALYSIS OF AN EMBANKMENT DAM

Introduction

The geometry and material properties of the dam to be analyzed are fully described under "Theme B1" in the hand-out to participants of the workshop. The embankment shown in Figure 3a has a height of 22.7m and a crest width of 5m. The upstream slope has a gradient of 3:1 (horizontal:vertical) and includes a horizontal terrace of width 6m,

8m below the crest. The downstream slope gradient is 2.5:1 and continuous. The total width of the embankment is thus 135.85m. The embankment consists of three main horizontal soil layers with a thin vertical chimney drain (type D) at the centerline. The chimney drain is not shown in the figure. The soil properties are given in Table 2.

Table 2: Soil properties

Soil	ϕ'	c' kN/m^2	ψ'	E kN/m^2	ν	γ kN/m^3	r_u
A	32°	10	5°	8000	0.3	21.0	0.45
B	26°	18	5°	5000	0.3	20.6	0.70
C	26°	18	5°	5000	0.3	20.6	0.45
D	36°	0	5°	80000	0.3	20.1	0.0

The finite element discretization of the dam is shown in Figure 3b and consists of 224, 8-node plane strain quadrilateral elements. Although the mesh design can account for the chimney drain, its shear strength has not been included in the present study.

Results of Stability Analyses

After construction

Two analyses under two assumptions on pore water pressure were conducted to assess the embankment stability after construction and prior to impoundment. In one case zero construction pore pressures were assumed and in the other the r_u values from Table 2 were used. The results from the finite element analysis, assuming zero pore pressures, are presented in Figure 4 in the form of a trial factor of safety (FOS) vs. δ_{max}. The trial factor of safety is gradually increased until there is a sudden increase in nodal displacements and the algorithm fails to converge. This occurred at a FOS of 1.95. Figure 5 shows the displacement vectors at failure for this case indicating a quite shallow downstream failure mechanism. Limit analysis using the Fellinius method gave a comparable FOS of 1.91 for an upstream circle similar to that identified in the finite element analysis.

It is a feature of the finite element approach that the method will always identify the most critical condition. By contrast the limit analysis method can be used for any (usually circular) specified slip. Hence, the Fellenius solution for circle C1 gave a FOS of 2.58 assuming full dissipation or zero construction pore pressures.

When r_u values were included, an inconclusive result was obtained for the finite element method in which the algorithm required many iterations, even at low FOS values. Furthermore as indicated in Figure 4, case b0, no clear break in the displacements was observed. This result implies that the embankment is potentially unstable depending on the rate of construction. The limit state approach suggested a FOS of less than 1.0 for both slopes with a minimum of around 0.8 on the downstream side and so is consistent with the finite element outcome. These results are summarized in Table 3. Other methods of limit state analysis were also employed such as Bishop's and Janbu's methods.

Results from these are summarised in the Result sheets B1-A to B1-C. In general Janbu gives the lowest predictions of FOS which Bishops lie below but closer to the Finite Element results.

Table 3: End of Construction

	Utilising r_u	Assuming full dissipation
Finite element model	< 1.0 downstream	1.95 upstream
Slope program Fellinius	0.96 (u/s) 0.8 (d/s)	1.91 (u/s) 2.58 (circle C1)

After impoundment

The actual location of the free surface within the embankment requires transient analyses but again the two extreme conditions can be used to bound the likely solution. A stability analysis corresponding to steady seepage conditions assuming a free surface as shown in Figure 6 was performed using both the finite element method and limit state stability. The results obtained for the stability of the embankment under steady seepage conditions and following complete drawdown from the steady seepage condition are shown in Figure 7 for the finite element method.

The results indicate a clear factor of safety of $FOS \approx 2.0$ for steady seepage. The mechanisms of failure indicated by the finite element analyses for this case is shown in Figure 8a. These results are comparable with those obtained using limit state analysis where FOS of 1.93 was obtained for the downstream slope. If construction pore pressures are included based on the values of r_u given then the FOS is around 1.8 on impounding. This compares to a value of around 1.0 at the end of construction and indicates the stabilizing effect of the impounding on the upstream face. Figure 9 shows the deep base slip that would be the most critical in these circumstances.

The steady state mechanism (Figure 8a) and Factor of Safety (Figure 7, case a)) are similar to those given in case a) in Figure 4 and Figure 5 following construction assuming no pore pressures. This is perhaps to be expected since the location of the steady state free surface is confined to the upstream side, and will therefore not have much influence on downstream stability. Although Figure 8a for steady seepage indicates that the critical mechanism will lie on the downstream side, the presence of more displacement vector activity on the upstream side as compared with Figure 5 confirms that the free surface does have an effect on the upstream slope.

Under drawdown condition the FOS falls to 1.5 assuming a steady state starting condition and around 1.4 assuming maximum pore pressures from construction have not fully dissipated. The drawdown mechanism (Figure 8b) clearly indicates that the upstream slope has now become the most critical but for a deep slip. For comparison, circle C1 analyzed by the limit state method gives a FOS of 2.2. This implies that there must

be an intermediate drawdown height at which the critical mechanism transitions from downstream to upstream but again that circle C is not the most critical.

If the transient pore pressures derived from the Seep/W program are used then some degree of dissipation of the construction pore pressures is assumed and in all cases the downstream slope is most critical with an FOS of around 1.9. The following section on the impact of pore pressure estimates demonstrates this.

A summary of results obtained is given in Table 4.

Table 4: Impounding and Drawdown

	Steady State	r_u or Transient
First Impounding		
FE Method	2.0 (d/s)	1.8 (u/s)
Limit state	1.93 (d/s)	1.96 (d/s)
Drawdown		
FE Method	1.5 (deep slip)	1.9 (d/s)
Limit state	1.54 (u/s lower face)	1.37 (u/s upper face)
(Bishop)	2.2 (Circle C1)	1.45 (Circle C1)

IMPACT OF PORE PRESSURE ESTIMATES

Values of pore pressure at the end of the construction phase have been assumed to be zero (or fully dissipated) or are derived from the value of r_u given in each material. In the subsequent stages pore pressures are derived either from a steady state seepage condition or a transient analysis using the Seep / W program starting from either the zero or r_u values. This allows the full possible range of values to be included in the analysis to illustrate the sensitivity of the structure to construction time and method. Values presented on sheets B1-A to B1-C are those from the transient analysis unless otherwise stated except that pore suctions have been neglected for stability analyses.

Illustrations of the advancing front of pore pressures on impounding and then the retreat on drawdown derived from Seep /W are given in Figures 10a and 10b to highlight the pore pressure variation on these later stages by neglecting the construction pore pressures. It is interesting to note that the effects of impounding never penetrate the central area in material B of the upstream face because of the short time before drawdown for the given permeabilities. Hence, a true steady state is never reached for seepage appropriate to the full impounding height. Thus it would be expected that the steady state case shown in Figure 6 is an extreme case and is not reached in practice. This was verified by the results from the Seep/W program where the FOS values were higher than those from the steady state analysis.

Figure 11 shows the Factor of Safety limits reached in both impounding (a) and drawdown (b) assuming a transient pore pressure distribution derived from the Seep/W program. In both cases the FOS is around 1.9 with a major slip surface on the downstream

face and the drawdown case actually gives a slightly higher FOS because of the extra time available for dissipation of the construction pore pressures - the dominant factor in this system. Figure 12 illustrates the dominance of the downstream slope stability for (a) impounding and (b) drawdown although in the case of drawdown there are also developments on the upstream face as would be expected.

CONCLUDING REMARKS

This paper has described a finite element methodology for estimating the stability of slopes. The technique has been applied to an embankment problem provided as part of the Fifth Benchmark Workshop on Numerical Analysis of Dams to be held in Denver, Colorado in June, 1999. A number of stability analyses have been presented including post-construction conditions, steady state and transient seepage conditions, and full drawdown conditions. In general the analyses, except the drawdown analysis, indicated that the steeper downstream embankment slope was most critical.

While well defined Factors of Safety were obtained in the majority of cases, an inconclusive result for observed for the embankment post-construction stability analysis when including the full r_u values. This suggested inherent instability in the design which is critically dependent on the rate of construction. The actual structure experienced first a delay and then a catch-up in placing of material which threatened its immediate stability and also created the start of conditions leading to its eventual failure.

The impounding of the dam tended to assist its stability on the upstream side and as the pore pressure front did not reach the more susceptible downstream face did not significantly affect that. The drawdown reduced the overall stability of the dam but the limiting condition appeared to be a deeper slip than the circle C identified. In the timescales given in this problem, a year for construction, six months impounding and three months for drawdown, the degree of dissipation of the construction pore pressures is just sufficient to allow the dam to stabilize between stages. However, if construction, impounding and then drawdown took place over too short a time to allow significant dissipation of the high levels of pore pressures generated on construction, instability will result. It was this set up of excess pore pressures during the actual shortened contruction phase of the upper layers that set up the conditions that would induce failure on the first drawdown.

In summary the design of the dam is flawed because of its over sensitivity to time constraints and it would have benefited from careful on-site control or it should have been reviewed to a more robust design. The bounds of stability of this dam have been identified together with a reasonable estimate of likely interim conditions with finite element and limit state analyses giving consistent results.

References

[1] D.V. Griffiths and P.A. Lane. Slope stability analysis by finite elements. *Géotechnique*, 49(4), 1999. To appear.

[2] I.M. Smith and D.V. Griffiths. *Programming the Finite Element Method.* John Wiley and Sons, Chichester, New York, 3rd edition, 1997.

[3] O.C. Zienkiewicz, C. Humpheson, and R.W. Lewis. Associated and non-associated viscoplasticity and plasticity in soil mechanics. *Géotechnique*, 25:671–689, 1975.

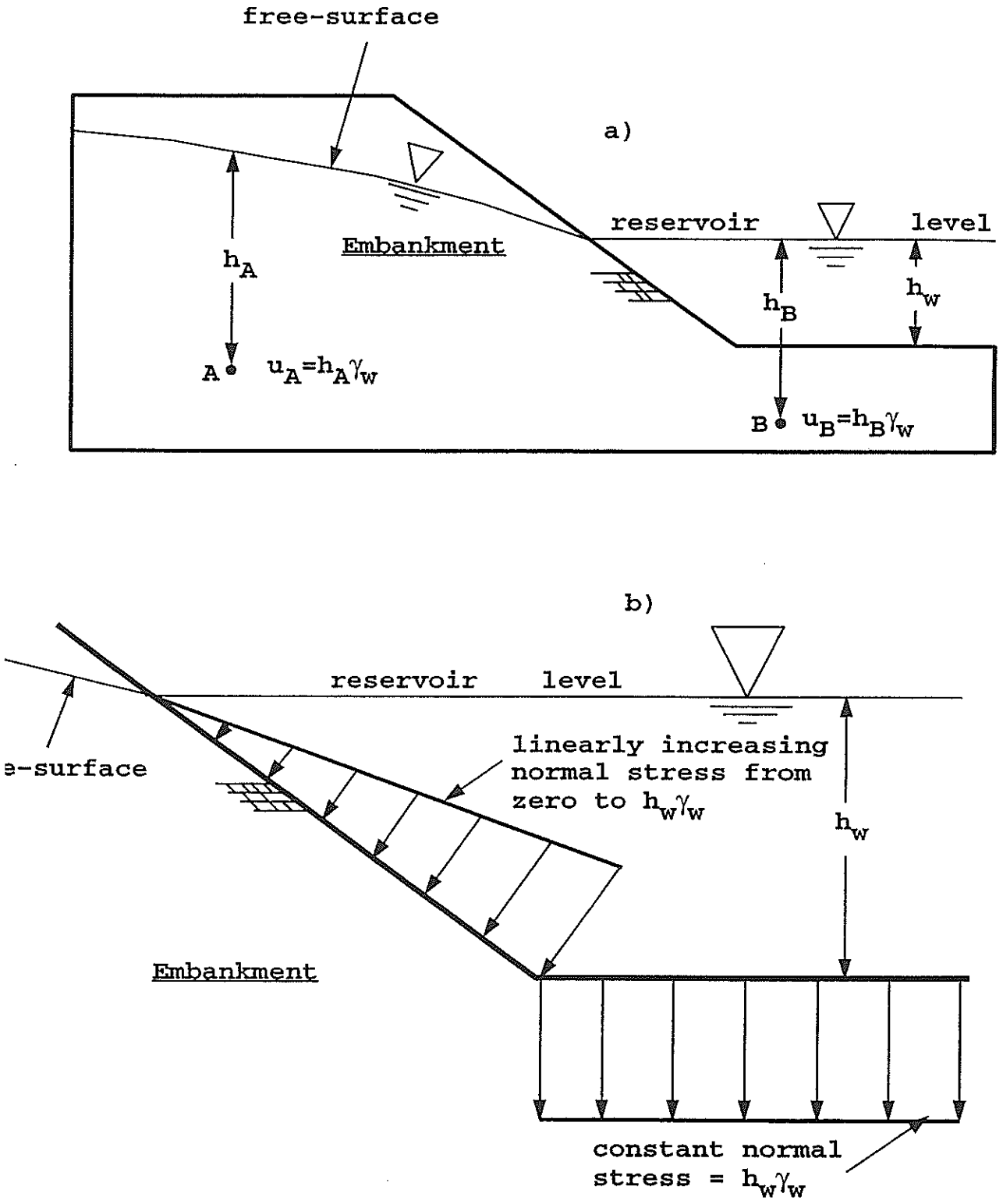

Fig. 1. a) Slope with free-surface and reservoir loading. b) Detail of submerged area of slope beneath free-standing reservoir water showing stresses to be applied to the surface of the mesh as equivalent nodal loads.

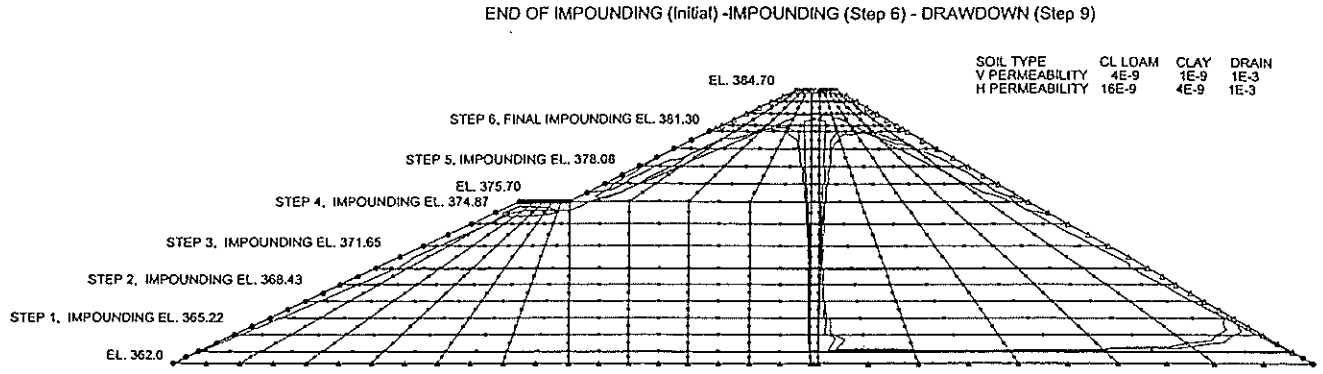

a)

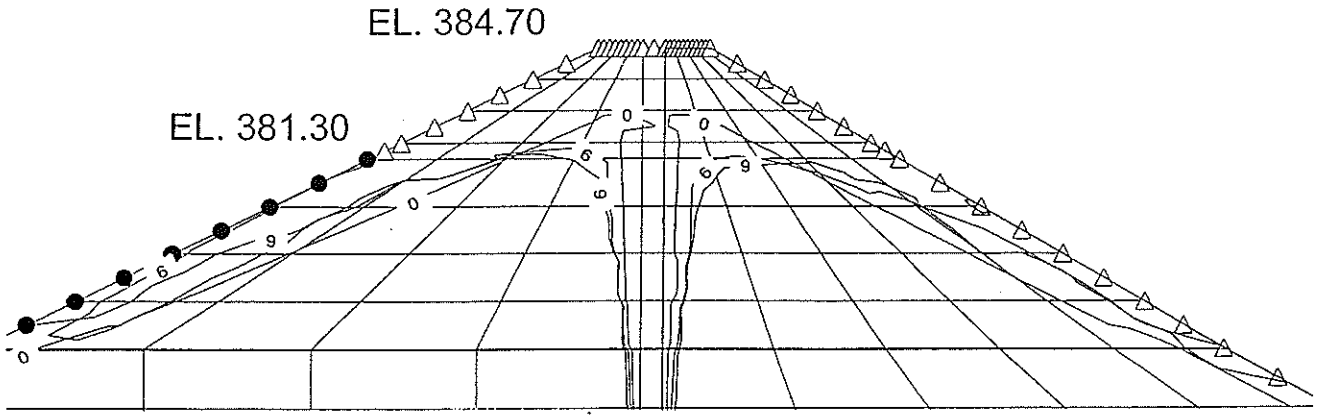

b)

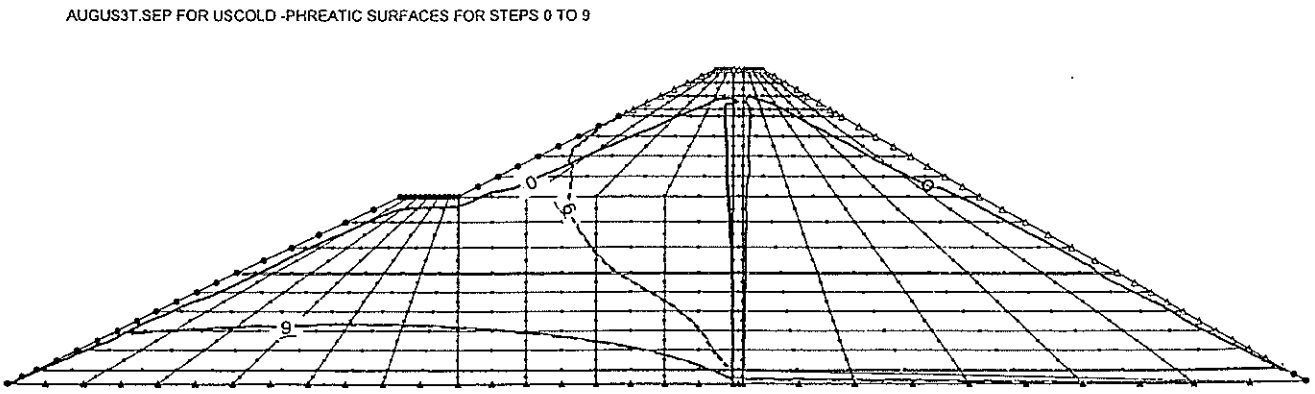

c)

Fig. 2. Saturation front process. a) Using given k-properties, b) detail of a), c) using increased k-values to illustrate the different fronts that could occur.

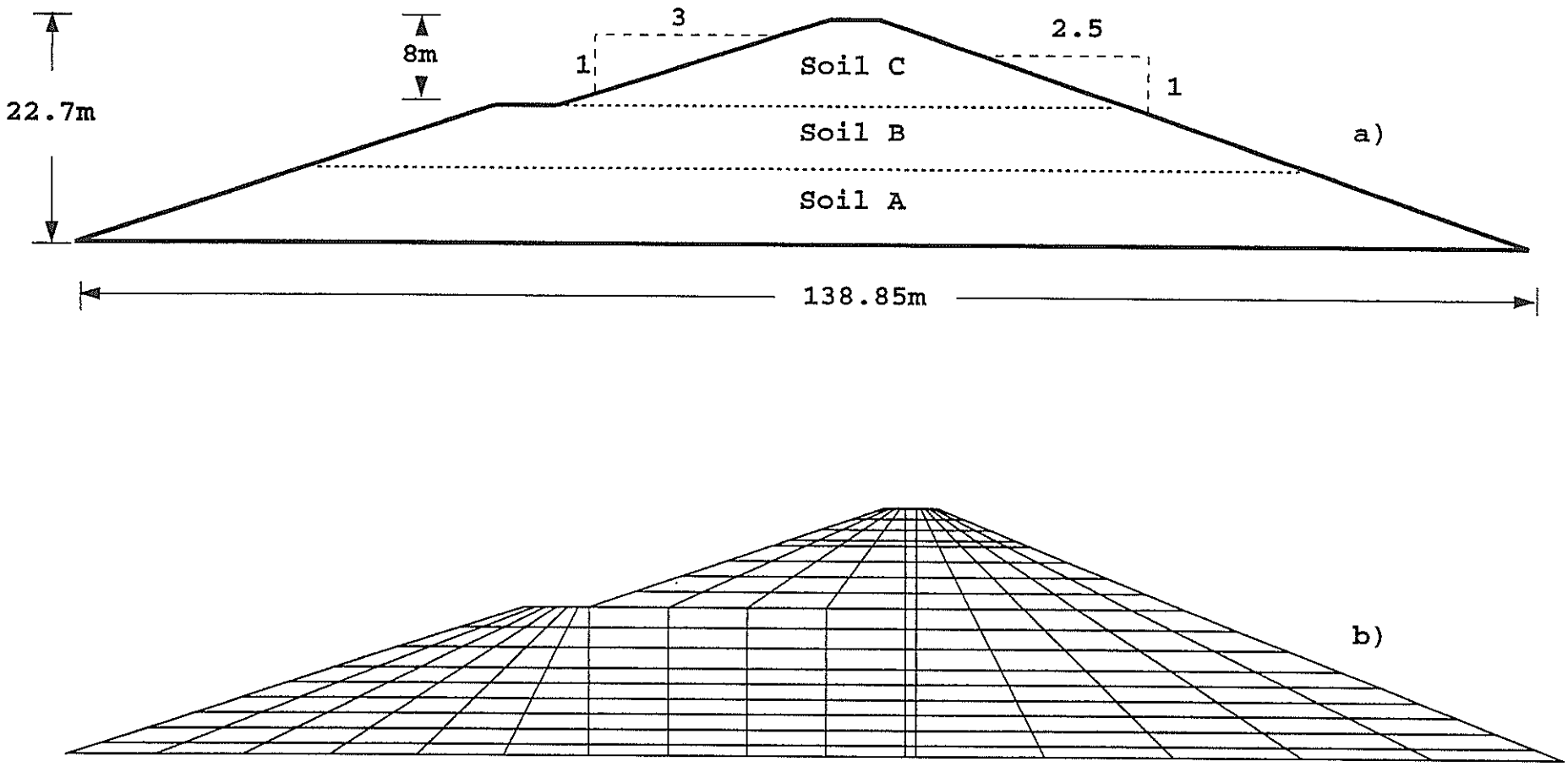

Fig. 3. a) Embankment dimensions and zoning
b) Finite element discretization.

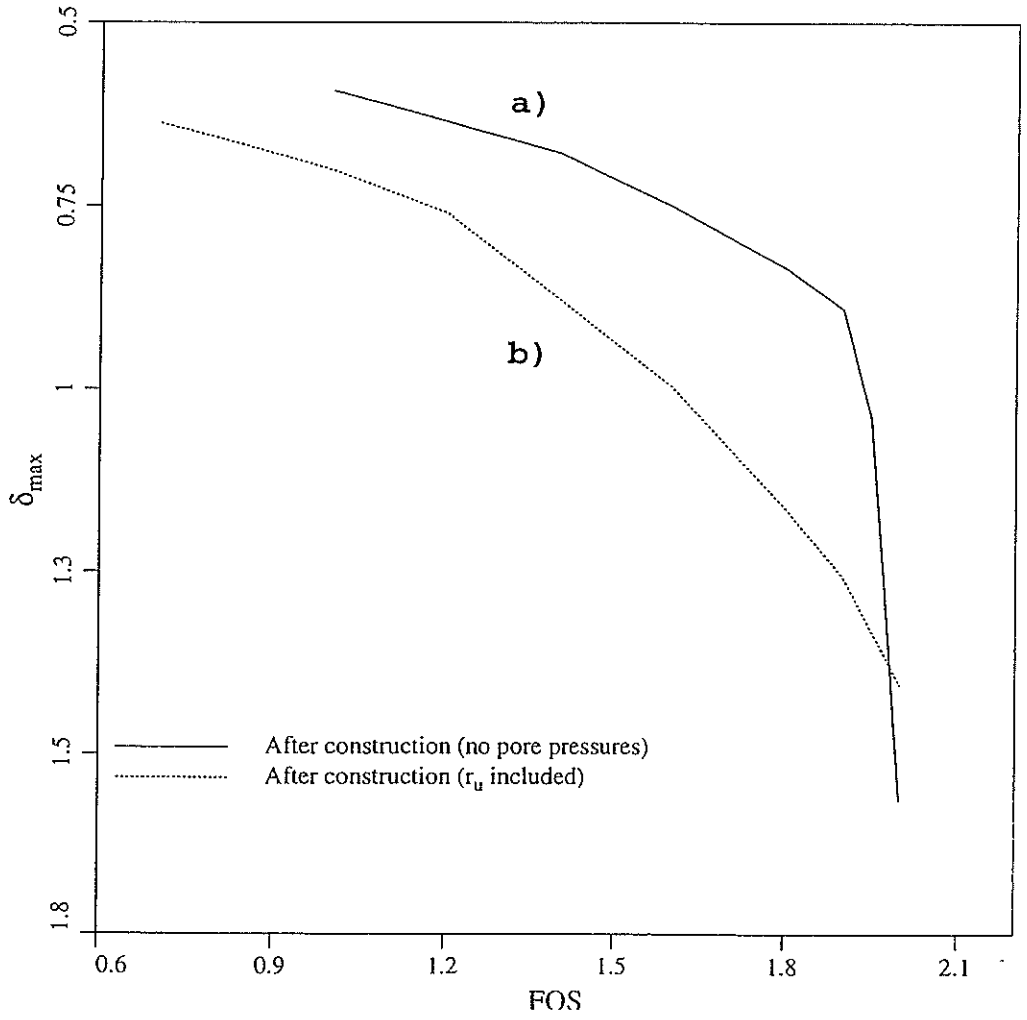

Fig. 4. FOS vs. δ_{max} for stability after construction for cases assuming a) no pore pressures and b) r_u values from Table 2.

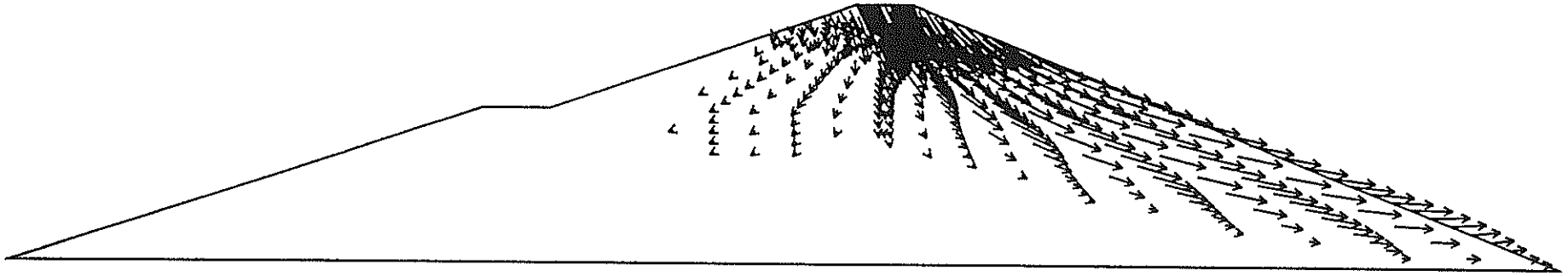

Fig. 5. Displacement vectors at failure for embankment after construction assuming no pore-pressures.

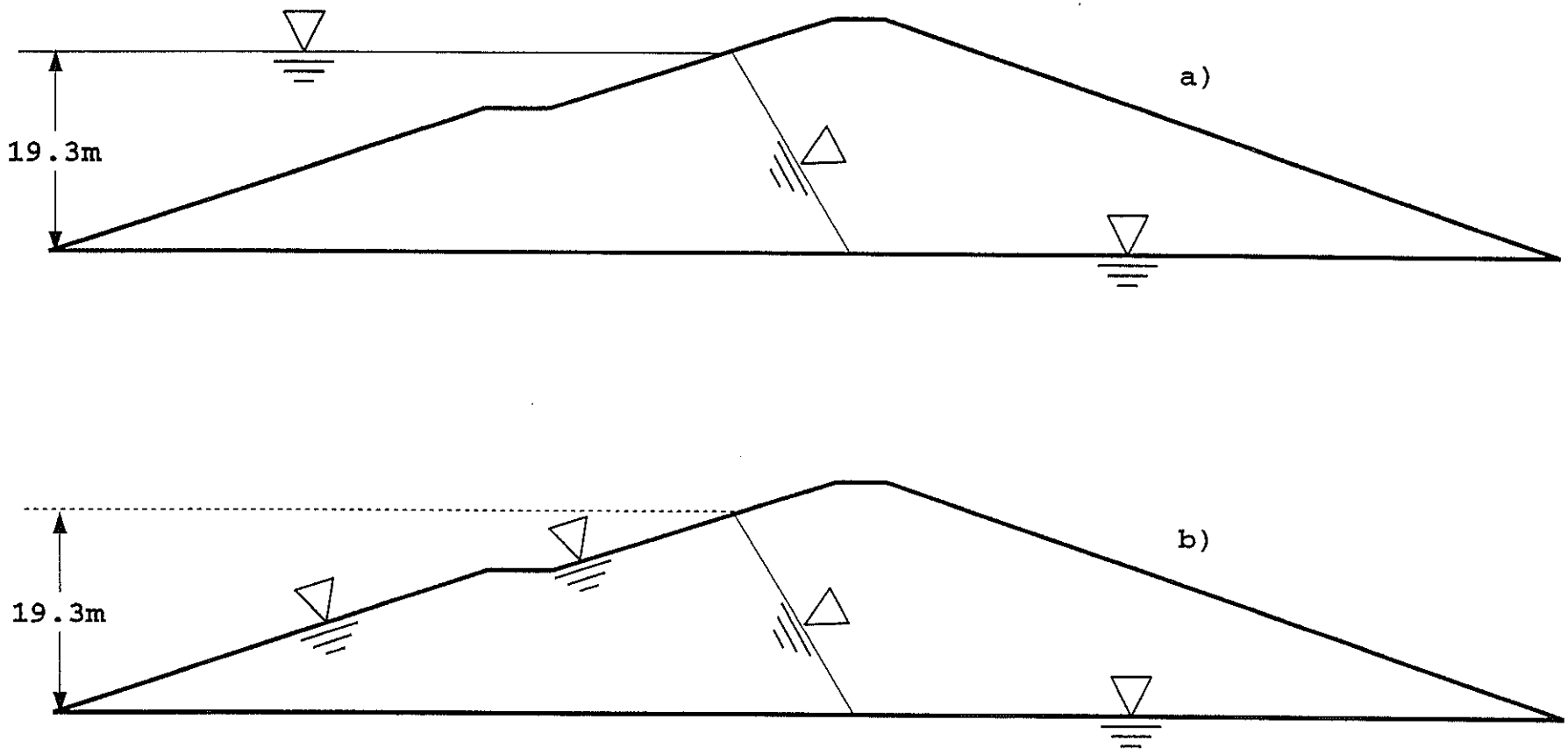

Fig. 6.Location of free surface for a) steady seepage and b) following complete drawdown.

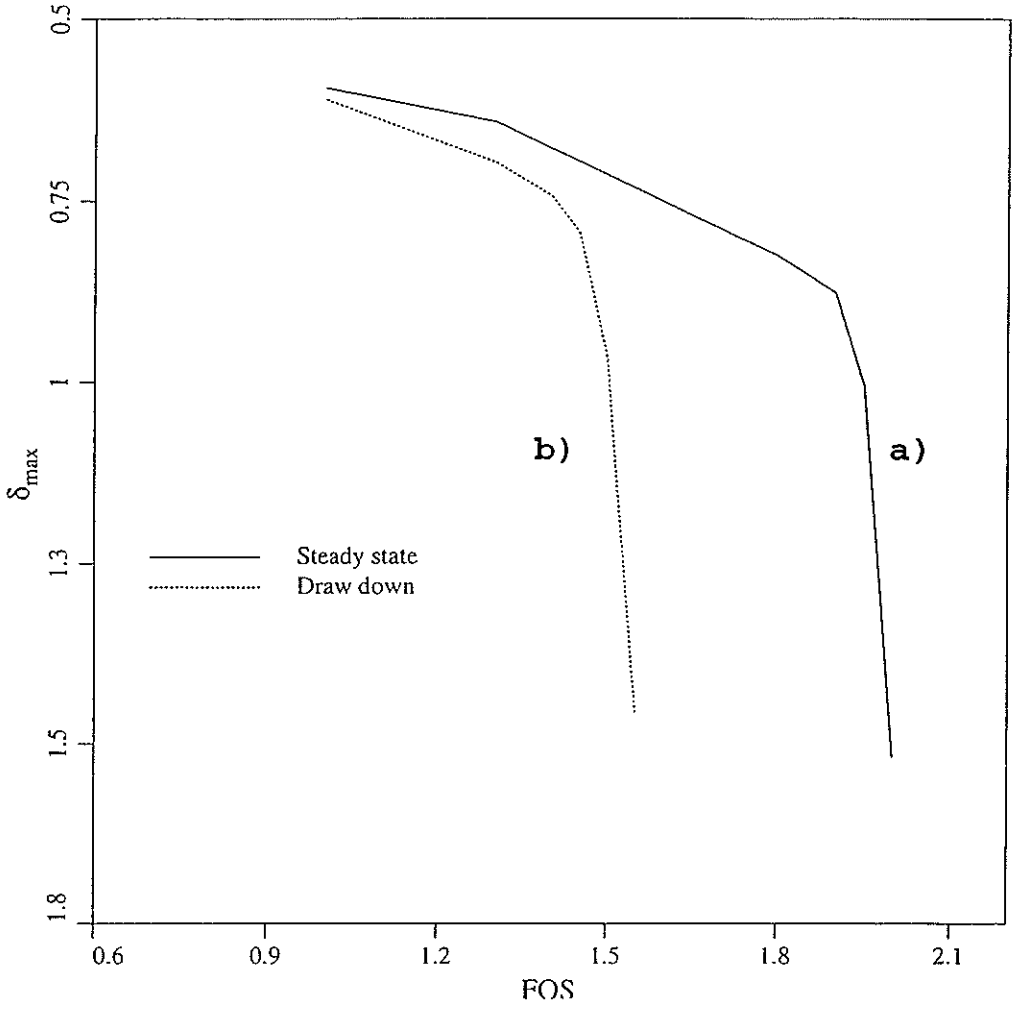

Fig. 7. FOS vs. δ_{max} for stability a) during steady seepage and b) following complete drawdown.

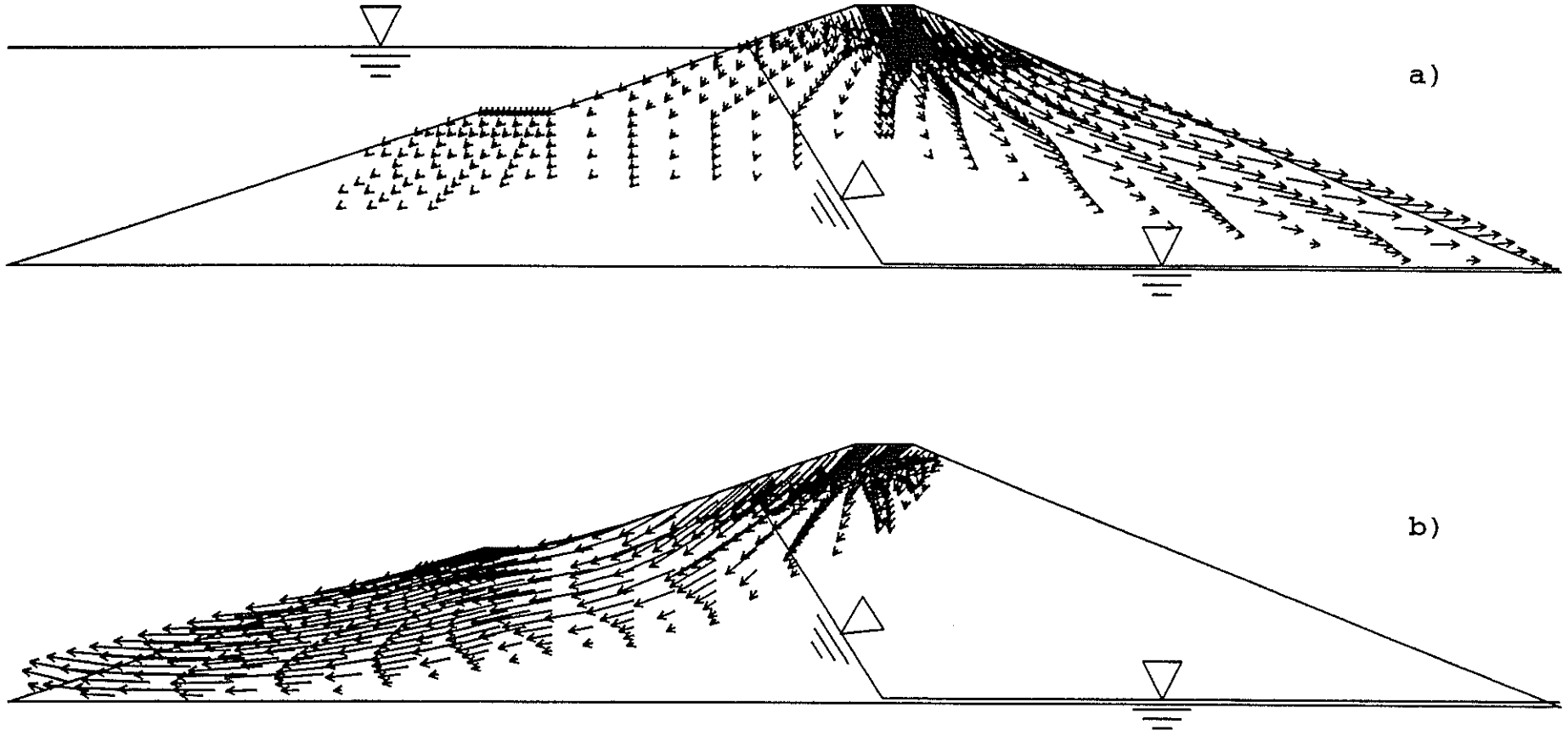

Fig. 8. Displacement vectors at failure for embankment:
a) during steady seepage and b) following complete drawdown.

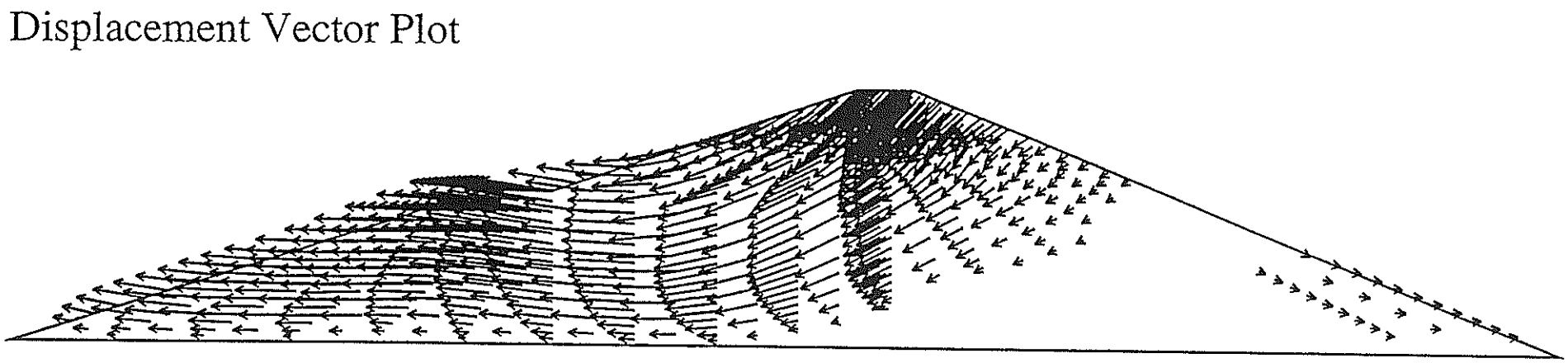

Fig. 9. Displacement vectors for impounding assuming pore pressures from r_u values. FOS=1.8

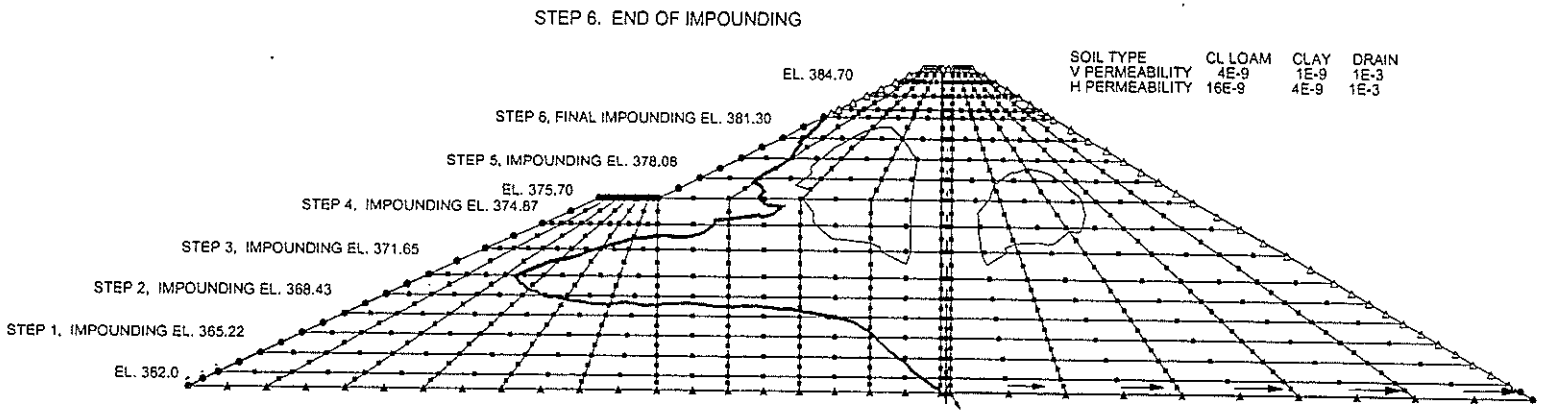

a)

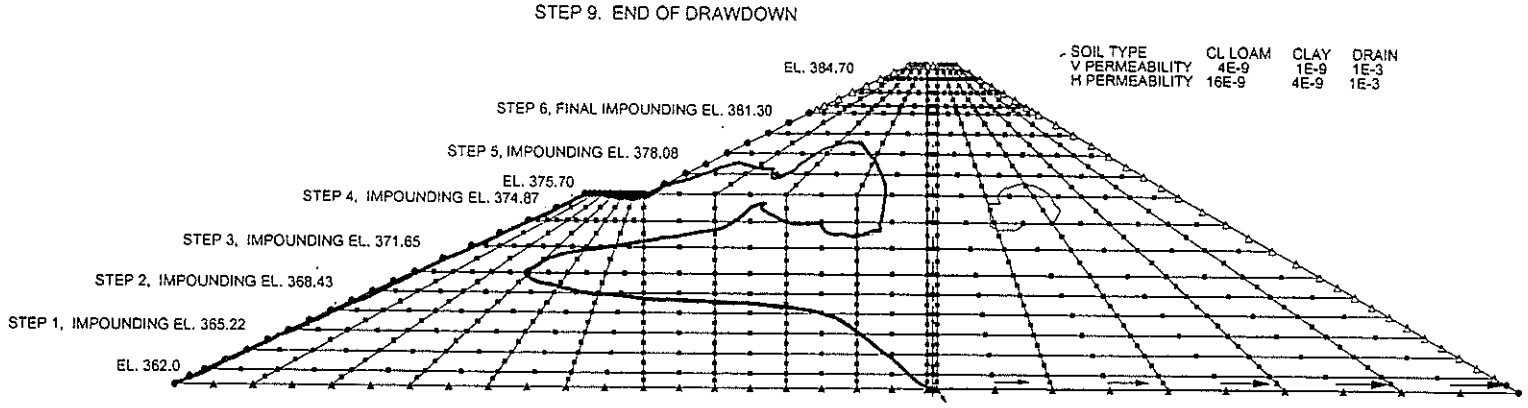

b)

Fig. 10. Saturation front process neglecting construction pore pressures: a) for impounding and b) for drawdown

Factors of Safety with Iterations to Convergence
a) after impounding
b) after drawdown

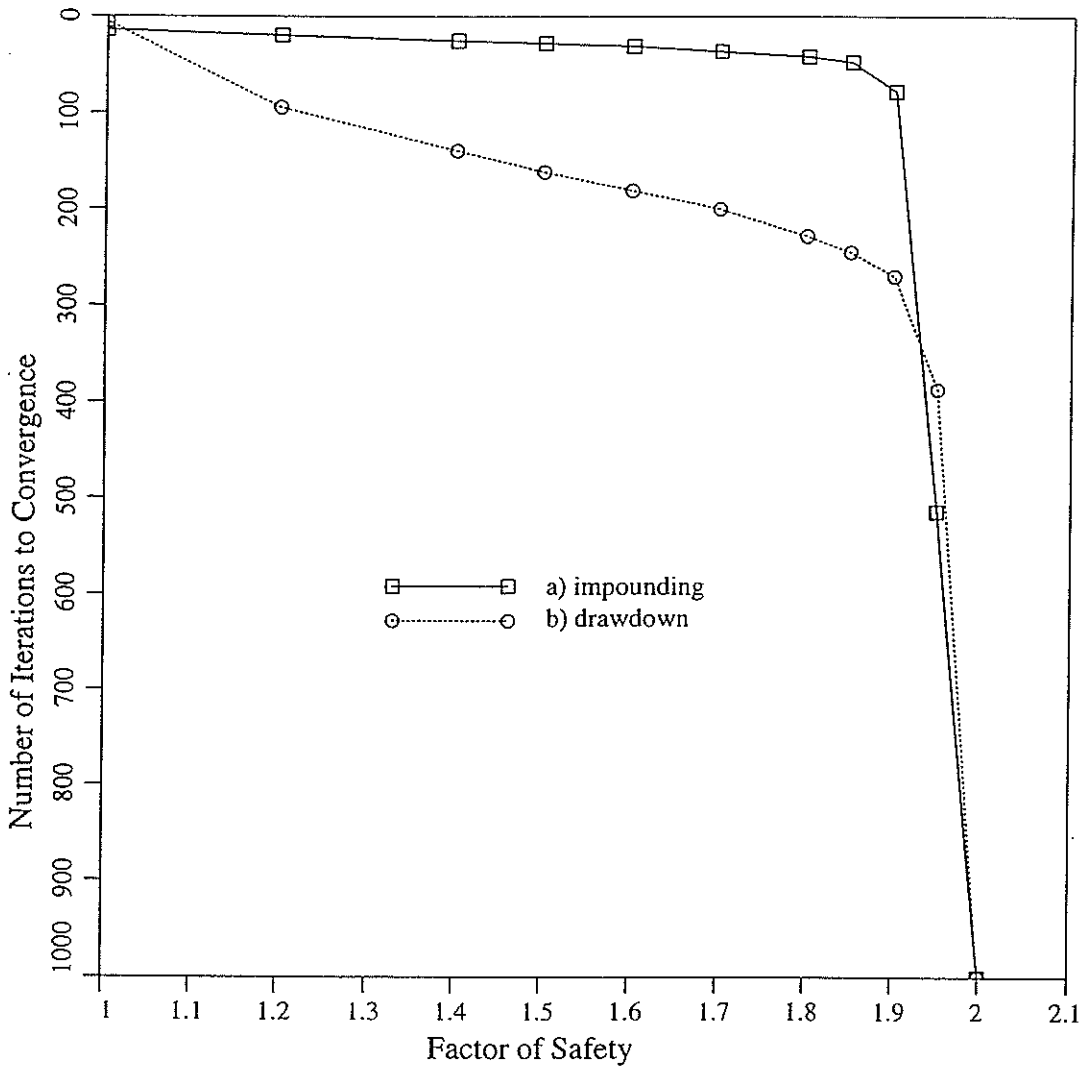

Fig. 11. Factor of safety limits reached: a) for impounding and b) for drawdown.

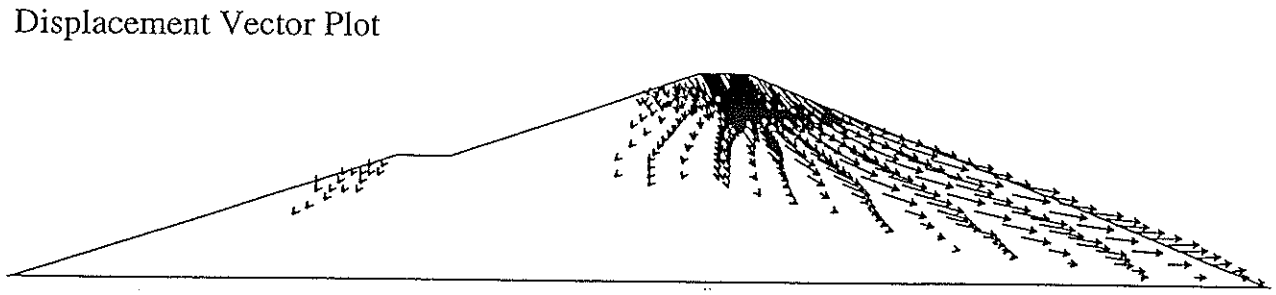

a)

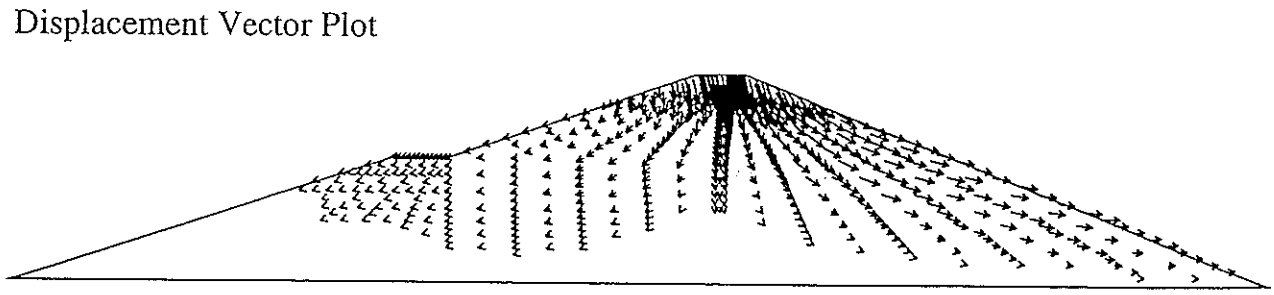

b)

Fig. 12. Dominance of the downstream slope stability: a) for impounding and b) for drawdown.

Result sheet B1-A: End of Construction

1 - Pore pressure

Point	P1	P2	P3
Pressure (kPa)			
Head (m)	470.0	405.3	384.5

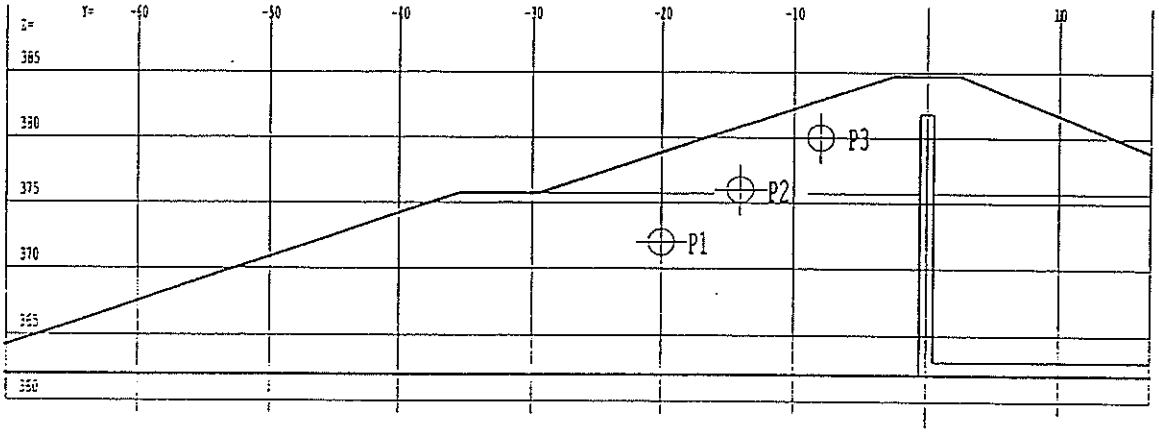

2 - Stability - Factors of safety

Failure line	Circle C1		Circle C2	
p.w.p (assumption)	0	ru	0	ru
SF (Fellenius)	2.58	0.96	1.91	0.8
SF(Bishop)	2.75	1.44	1.96	1.07
SF (Jambu)	2.52	1.22	1.88	0.95
SF (FE)			1.95	< 1.0

F	Displacement P4 (cm)		Displacement P5 (cm)	
factor	dY	dZ	dY	dZ
1.0	-3.41	-20.6	1.00	-58.6
1.2	-3.45	-20.6	1.08	-58.8
1.4	-3.51	-20.6	1.21	-59.2
1.6	-3.53	-20.6	1.46	-59.7
1.8	-3.55	-20.6	1.77	-60.2
1.9	-3.56	-20.6	1.93	-60.4

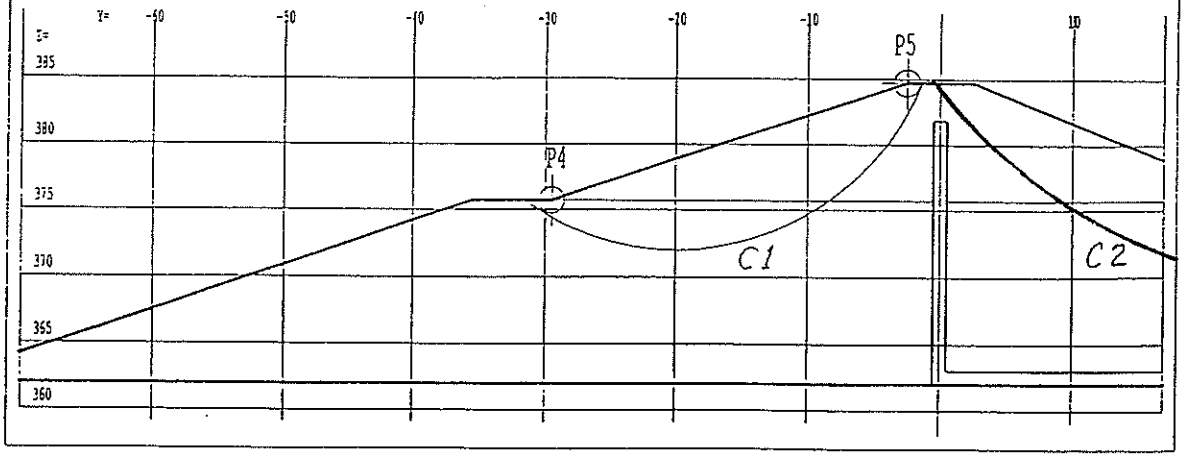

Result sheet B1-B: End of Impounding

1 - Pore pressure

Point	P1	P2	P3
Pressure (kPa)			
Head (m)	373.2	372.8	374.0

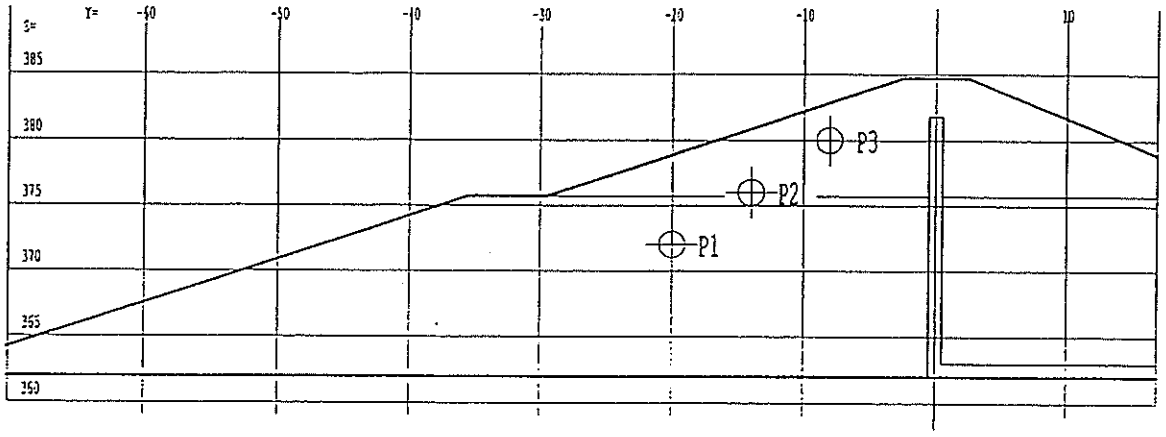

2 - Stability - Factors of safety

Failure line	Circle C1			Circle C2
p.w.p (assumption)	1	2	3	2
SF (Fellenius)				
SF(Bishop)	3.2	2.6	4.7	
SF (Jambu)		2.1	2.2	
SF (FE)				1.8

1 = Steady state seepage
2 = End of construction, p.w.p. from ru / or transient if greater
3 = Transient p.w.p. from SEEP/W

Most critical case for FE is still downstream slip

F	Displacement P4 (cm)		Displacement P5 (cm)	
factor	dY	dZ	dY	dZ
1	0.978	-29.3	2.56	-58.1
1.5	-0.939	-31.4	4.20	-67.0
1.7	-2.12	-32.2	5.77	-73.5
1.9	-3.28	-33.1	9.06	-81.4
1.95	-3.49	-33.2	16.4	-87.7

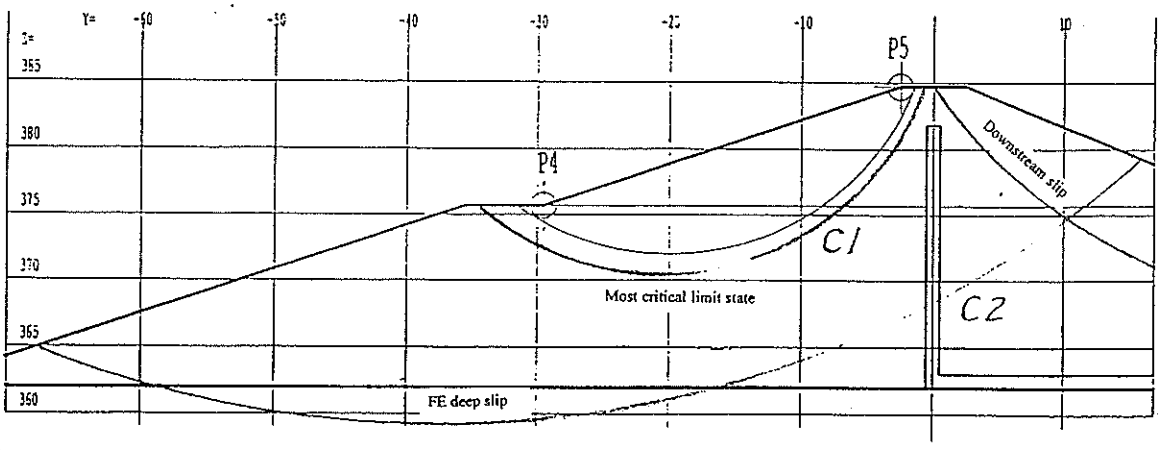

Result sheet B1-C: Rapid Drawdown

1 - Pore pressure

Point	P1	P2	P3
Pressure (kPa)			
Head (m)	367.5	371.1	374.0

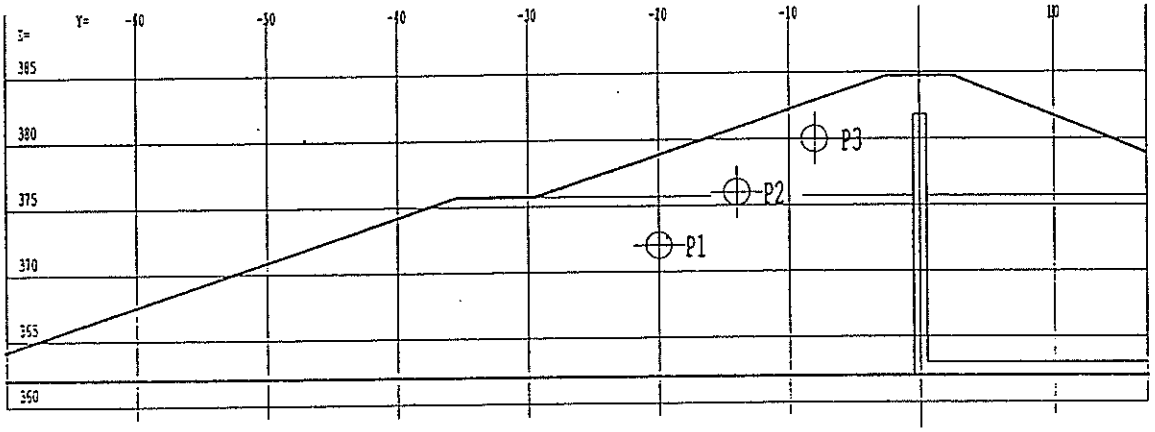

2 - Stability - Factors of safety

Failure line	Circle C1		Circle C2		Circle C3
p.w.p (assumption)	1	2	1	2	1
SF (Fellenius)					
SF(Bishop)	2.2	1.5	1.5	1.4	
SF (Jambu)	2	1.3	1.5	1.3	
SF (FE)					1.6

1 = Steady state seepage
2 = Transient / ru condition immediately prior to drawdown

Most critical case for FE is still downstream slip

F	Displacement P4 (cm)		Displacement P5 (cm)	
factor	dY	dZ	dY	dZ
1.0	-3.42	-20.6	0.987	-58.6
1.2	-3.88	-20.6	1.36	-60.9
1.4	-5.22	-20.7	1.85	-66.3
1.6	-7.05	-20.9	2.56	-73.3
1.8	-9.10	-21.0	3.71	-81.3
1.9	-10.2	-21.4	4.89	-86.0
2.0	-11.4	-21.7	9.56	-94.0

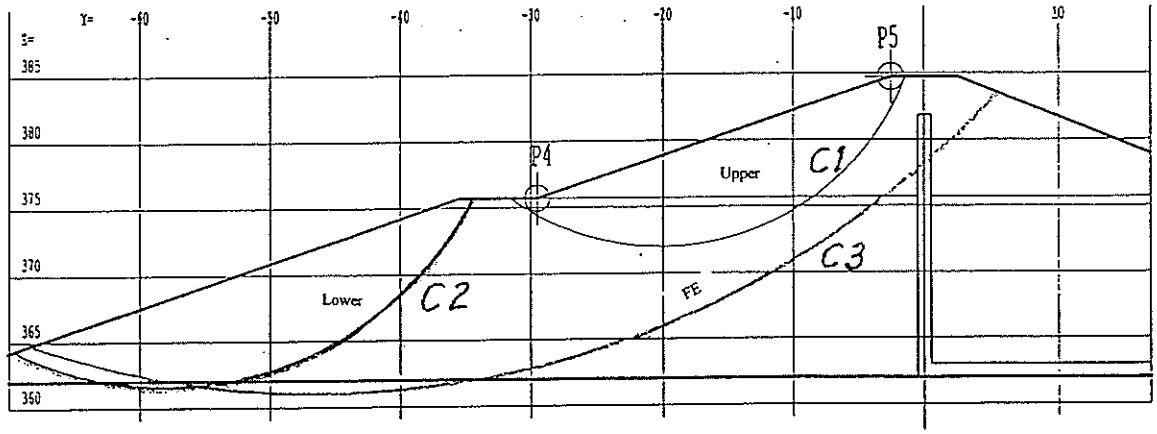

FIFTH INTERNATIONAL BENCHMARK WORKSHOP
ON NUMERICAL ANALYSIS OF DAMS
DENVER, CO, USA, JUNE 2-5 1999

THEME B2
EMBANKMENT DAMS
FIRST FILL OF A ROCKFILL DAM : A CASE STUDY

LG-2 ROCKFILL DAM

COMPARISON OF NUMERICAL RESULTS AND SOME IN-SITU MEASUREMENTS

FINAL REPORT - SEPTEMBER 1999

Hydro Québec

CIGB ICOLD

DENVER, CO, USA, JUNE 2-5 1999

This report was prepared by the formulator of Theme B2 :

Bachir N. Touileb, Hydro-Québec, QC, Canada

in collaboration with the participants to theme B2 of the Benchmark Workshop :

Participant #1 (P1): G. La Barbera, A. Bani and G. Mazza (Italy)

Participant #2 (P2) : L. Pagano, A. Desideri, F. Vinale, F. Sorvillo (Italy)

Participant #3 (P3) : P. Anthiniac, S. Bonnelli, A. Carrère, O. Débordes (France)

1.0 EXECUTIVE SUMMARY

Two main targets were followed by the 5th Icold Benchmark Workshop :

- The behavior (collapse) of the upstream rockfill under the wetting and the reservoir filling
- The piezometric response of the impervious material of the core.

Three participants presented a communication to this 5th Benchmark Workshop. They are :

- Ismes and Enel from Italy,
- University of Napoli from Italy,
- Cemagref, Coyne et Bellier and EM2/IMT from France.

One of the main shortcoming associated with an excessive deformation of the upstream rockfill is the combination of two opposite trends that could lead to the opening of a crack :

- The collapsible rockfill tends to move the filter towards the upstream
- The water forces that are acting on the upstream face of the core tend to move the filter towards the downstream.

Regarding the first target - collapse of the upstream rockfill -, Ismes-Enel aw well as Cemagref et al. pointed out the main features of the behavior, despite some differences in the calculated values.

In the case of the second target of the proposed theme - piezometric response of the core material - an important (but universal) discrepancy between the calculated and measured piezometric levels was noticed. In fact, it is found that the calculated piezometric levels are lower than the measured piezometric levels, particularly near the downstream part of the core, where a higher amount of pore pressure seams to dissipate. The actual question is a fundamental problem that need further research and discussions. In the opinion of the formulator, the 5th Icold Benchmark Workshop was in fact as a great opportunity to raise « the problem of the transient seepage and the high pore pressures in the core of dams » to the specialists and to the ad-hoc committee. To explain such a discrepancy, several arguments and explanations were proposed in the literature, but none of these was retained as the unique cause of the difficulty to predict the piezometric levels properly. A promising explanation, that needs further research and consolidation, could be related to the real behavior of the gaz phase of the till of the core.

The excessive deformation - crack - that appeared near the crest, in the upstream part of the dam, when the reservoir level reached 75% of the maximum level, were not predicted properly by the available results. The actual observed behavior could be related to the combination of an excessive settlement of the upstream rockfill and the horizontal movement towards downstream that is imposed by the reservoir. Both opposite movements are conducting to a lack of confinement leading to the potential opening of a crack along the upstream transition zone.

2.0 MAIN FEATURES AND CHARACTERISTICS OF THE DAM

2.1 GENERAL DESCRIPTION OF THE LG2 DEVELOPMENT

The LG2 development is part of the Phase One of the La Grande Rivière Complex, which also includes the LG3 and LG4 hydroelectric projects.

The LG2 hydroelectrical development comprises an underground powerhouse, with an installed capacity of *5 328* MW, a *162* m high main dam, a spillway with a maximum discharge capacity of *16 280* m^3/s *at the maximum operation level*, as well as a chain of some *30* dikes required to close the reservoir rim.

2.2 MAIN DAM GEOMETRY

The LG-2 dam which is the object of this case study is a zoned earth and rockfill embankment having a maximum height of 155,5 m (510 ft) - (the 1,5 m (5 ft) thick camber added to the crest is not considered herein) - . The dam cross section shown in figure 1 is located at chainage 52+50 (PM 1600). The total length of the structure is *2 836* m. The dam construction required a total volume of 23 millions m^3, 20% of which is the moraine of the impervious core. The cross section of the rockfill structure has a slightly inclined upstream central core, made out of compacted moraine. Upstream and downstream, the fine material of the core is protected by filter and transition zones. The dam shells are made of rockfill.

2.3 CONSTRUCTION SCHEDULE

Before beginning construction of the main dam it was necessary to divert the river and to dewater the central excavation area. The dam construction as such took over 2 years, i.e. from July 1976 to November 1978.

The impounding of LG2 reservoir started on November 27th, 1978, following closure of the diversion tunnel.

The following table shows the 9 steps considered for the particular case of the LG-2 rockfill dam.

Table 1 Construction Steps

Main construction steps	Date	Note	Crest elevation at the center line of the dam	
			(ft)	(m)
10	November 78	End of construction	590,0	179,8
9	August 78		564,13	171,9
8	July 78		512,07	156,1
7	June 78		486,2	148,2
6	November 77	end of 2nd season	420,7	128,2
5	August 77		362,06	110,35
4	June 77		300,0	91,44
3	May 77		234,1	71,35
2	October 76	end of 1st season	193,1	58,85
1	July 76		150,0	45,72

Table 2 LG-2 dam. Main dates and events

Construction of the main dam	From : October 1974	To : November 1978
Reservoir impoundment	From : 27 November 1978	To : December 13th, 1979 (174,86 m)
Cracks observed at the upstream edge of the crest (5 cm wide)	September, 1979	Reservoir level at 2/3 from maximum: 140,0 m

3.0 MAIN CONCLUSIONS AS PRESENTED BY THE PARTICIPANTS

It is interesting to recall the main conclusions obtained by the the participants :

3.1 ISMES-ENEL :

The solution with Duncan Chang model presented some numerical difficulties and some doubt arose about the strong differential settlement calculated at contact zone between upstream filter and core.

The wetting collapse phenomena has been simulated by mean of an empirical procedure, which main steps consist in a series of simplified and subsequent analyses. The obtained results are in agreement with the measurements taken on other dams of similar typology and dimension to LG-2 dam (i.e. El Infernillo dam).

3.2 UNIVERSITY OF NAPOLI :

The reservoir filling case was not treated.

3.3 CEMAGREF, COYNE ET BELLIER AND EM2/IMT

The authors raised some questions regarding the parameters that were proposed in theme B2, since they were based on the hyperbolic Duncan and Chang model. In particular, the authors raised the question of the determination of parameters of the rockfill. This issue was not addressed in explicitly in the proposed paper.

A fully coupled analysis of construction and impounding phase of LG2-Dam has been realized. The hydro-plastic model used (elasto-plastic model including water effects) seems to give acceptable results in terms of stresses and displacements, especially in the upstream shoulder during impoundment : large settlements are obtained. A transverse displacement of the core during impoundment is observed : first an upstream movement, then downstream as the reservoir reaches maximum water level.

Large settlements occur in the upstream shell during impounding phase (up to 0.5m). In the same phase, vertical displacements in the core are very close to zero. This discontinuity is support mainly by the upstream filter. About horizontal displacements, an upstream movement is observed in the upstream shoulder during the impounding phase (-0.1m), while the core moves downstream (+0.2m). We can ask questions about potential crack appearance in filters near the top of the dam, because of the filter thickness.

The differential displacements occurred between upstream shoulder and core are able to cause cracks in upstream filter, especially in the upper part of the dam, where the filter thickness is thin.

4.0 DISCUSSION OF THE CONTRIBUTIONS BY THE FORMULATOR

4.1 ISMES-ENEL :

The use of three different models led to major differences in the results. However, the first model (MOD-1, based on Duncan and Chang formulation) gives the most appropriate results since it coincides with the model used to give the data as presented in the data-book of theme B2. The results deduced from models other than the Duncan and Chang model seems to under-estimate both deformations and displacements, in general. In dam engineering practice, such an approach in which more than one model is used are encouraged in order to evaluate the sensitivity and the robustness of the solution.

4.2 UNIVERSITY OF NAPOLI :

In this particular case, the problem was simplified since the determination of the parameters was not based on the parameters that were given in the databook. Moreover the reservoir filling phase was not tackeled by in the paper. Consequently, the results of the university of Napoli are compared to the other results just in the case of the « dam construction phase ».

4.3 CEMAGREF, COYNE ET BELLIER, ESM2/IMT :

The hydroplastic model appear to be a robust and a promising one whose parameters differ from the Duncan and Chang model parameters. The link between both sets are not explicitly shown in the actual contribution.

Table 3 models, software and hardware used by the participants to theme b2

				Models				
Participant	**Authors**	**Ref**	**Color**	**Dam Construction**	**Reservoir Filling**	**Software**	**Hardware**	**RUN TIME**
								MOD1: 15 min. CPU
ISMES	G.La Barbera	P1	Red	**MOD1**: Uncoupled: Duncan & Chang	-	OMEGA	-	15 min. CPU
ISMES	A. Bani			**MOD2**: Uncoupled	-			15 min. CPU
ENEL	G. Mazza			- Duncan & Chang for Rockfill				
				- Drucker-Prager for Filters				
				- Extended Cam-Clay for the core				
				MOD3: Coupled:	**MOD3**			3 min. CPU
				- Drucker-Prager for Rockfill				
				- Drucker-Prager for Filters				
				- Extended Cam-Clay for the core				
U. NAPOLI	L. Pagano	P2	Green	Modified Cam-Clay		ABAQUS	Pentium 450 XEON	3 hours
	A. Desideri			Coupled for the Till of the core only			500Mb RAM	
	F. Vinale							
	F. Sorvillo							
							DEC-Alpha 3000	Construction in 9 steps: 7 hours
CEMAGREF	P. Anthiniac	P3	Blue	Non associated flow rule	Non associated flow rule	S.I.C.3		Impounding in 12 steps: 8 hours
CEMAGREF	S. Bonelli			Elastoplastic model	elastoplastic model			
Coyne et Bellier	A. Carrère							
ESM2/IMT	O. Débordes							

5.0 PRESENTATION AND COMPARISON OF RESULTS

Most of the answers to the questions that were asked within the actual theme could be presented by means of tables and figures.

5.1 LOCATION OF MAXIMA AND MINIMA OF DISPLACEMENTS

They are given in table 4.

5.2 LOCATION OF MAXIMA AND MINIMA OF EFFECTIVE STRESSES

They are given in table 5.

5.3 DISPLACEMENTS ALONG HORIZONTAL LINE HH

Horizontal and vertical displacements along the horizontal line HH located at the elevation +100 m were required for both end of construction and end of displacements. The upstream part of this line should be influenced by the wetting of the upstream rockfill. The displacements along the line HH are shown in figures 3 and 4.

5.4 DISPLACEMENTS ALONG VERTICAL LINE VV

Horizontal and vertical displacements along the vertical line VV located at 75 m upstream of the center line of the dam. Being located into the reservoir, this line should show the influence of wetting on the upstream rockfill. The displacements along the line VV are shown in figures 5 and 6.

5.5 DISPLACEMENTS ALONG INCLINOMETER #4

Horizontal and vertical displacements along the inclinometer #4 which is located into the till of the core are required. The displacements along the inclinometer #4 are shown in figures 7 and 8.

5.6 DISPLACEMENTS ALONG INCLINOMETER #5

Horizontal and vertical displacements along the vertical inclinometer #5 located 77 m downstream of the central vertical line of the dam. Being located downstream within the dry rockfill, and at equal distance from the central line to the vertical line VV - located upstream within the wetted rockfill -, the results regarding this inclinometer are aimed to be compared to those which are calculated in the case of the vertical line. The displacements along the inclinometer #5 are shown in figures 9 and 10.

5.7 INFLUENCE OF RESERVOIR FILLING ON LINE VV AND INCLINOMETER #5

The influence of reservoir filling and its differential impacts are discussed. In fact, a direct comparison of the displacements calculated along the vertical line VV (X=-75 m) and the inclinometer #5 (X=+77 m) are shown in the case of Ismes-Enel and Cemagref et al.

5.7.1 Influence of reservoir filling in the case of Ismes-Enel

The horizontal displacements (figure 11) and vertical displacements (figure 12) produced by Ismes-Enel are shown for both the vertical line VV and the inclinometer #5 in the case of « end of construction » and « end of reservoir filling ».

5.7.1.1 Horizontal displacement (Ismes-Enel)

It could be noted that the horizontal displacements at « end of construction » are located at about the elevation +90 m and are comparable in both the line VV (ΔH = -0,36 m) and the inclinometer #5 (ΔH = +0,42 m). However, the wetting provoked by the filling of the reservoir produces a higher horizontal displacement in the case of line VV because it is located into the rockfill under the reservoir. Figure 11 shows a total horizontal displacement at « end of reservoir filling » of (-1,0 m) for line VV and (+0,80 m) for inclinometer #5. The additional horizontal displacement due to the collapse by wetting of the upstream rockfill located along the vertical line VV is 0,65 m. The additional horizontal displacement due to the water acting as quasi-horizontal elemental forces distributed along the impervious core is 0,40 m.

5.7.1.2 Vertical displacement (Ismes-Enel)

It could be noted that the vertical displacements at « end of construction » are located at about the elevation +90 m and are comparable in both the line VV and the inclinometer #5 (ΔV = -1,0 m). However, the wetting provoked by the filling of the reservoir produces a much higher vertical displacement in the case of line VV because it is located into the rockfill under the reservoir. Figure 12 shows a total horizontal displacement at « end of reservoir filling » of (-1,45 m) for line VV and (+1,10 m) for inclinometer #5. The additional vertical displacement due to the collapse by wetting of the upstream rockfill located along the vertical line VV is 0,45 m. The additional vertical displacement due to « reservoir filling » is only 0,10 m.

5.7.2 Influence of reservoir filling in the case of Cemagref et al.

The horizontal displacements (figure 13) and vertical displacements (figure 14) produced by Cemagref et al. are shown for both the vertical line VV and the inclinometer #5 in the case of « end of construction » and « end of reservoir filling ».

5.7.2.1 Horizontal displacement (Cemagref et al.)

It could be noted that the horizontal displacements at « end of construction » are located near the crest of the dam near the elevation +100 m to 120 m. Moreover it is found that the horizontal displacements in the case of inclinometer #5 are towards upstream (ΔH = - 0,05 m at elevation +90 m), while it should be moving downstream. The horizontal displacements at the bottom of line VV are also directed downwards while it should be moving towards upstream. At the elevation +100 m, a major change in the direction of the horizontal displacement is found to occur leading obviously to a concentration of shear stresses.

The filling of the reservoir appears to produce a higher horizontal displacement in the case of line VV because it is located into the rockfill under the reservoir. Figure 13 shows a total horizontal displacement at « end of reservoir filling » of (-0,16 m at elevation +120 m) for line VV and (+0,15 m at elevation +125 m near the crest of the dam) for inclinometer #5. The additional horizontal displacement due to the wetting of the upstream rockfill located displacements along the vertical line VV is 0,11 m. The additional horizontal displacement due to the water acting as

quasi-horizontal elemental forces distributed along the impervious core is 0,15 m in the case of inclinometer #5.

5.7.2.2 Vertical displacement (Cemagref et al.)

The shape of the vertical displacements at the « end of construction » phase both in the case of the line VV and the inclinometer #5 are similar and the values are comparable. The line VV shows a higher displacement with almost (-1,0 m at elevation +80 m) and the inclinometer showing a displacement of (-0,9 m at elevation +90 m).
The effect of the wetting is more pronounced in the case of the vertical line VV. The additional displacement due to the collapse in line VV is evaluated to about 0,50 m, while in the case.

5.8 TRANSIENT PIEZMETRIC RESPONSE IN THREE PIEZOMETERS

The transient piezometric response of three different piezometers (P11, P12 and P13) - located at elevation +100 m and distributed from the upstream to the downstream part of the core - were required. Figures 15 shows the measured and calculated results. Some important discrepancies are noticed in this case.

5.9 PREDICTION OF A PECULIAR BEHAVIOUR

The analysis of the results presented for this theme did not allow for the determination of the peculiar behavior as it was observed in the field. It is recalled that a crack appeared near the crest, in the upper part of the dam. However, both participants Ismes-Enel (P1) and Cemagref et al. (P2) pointed out the importance of the deformations. The latter was more specific by showing that excessive deformations are taking place into the upstream filter.

Table 4 Location of maxima and minima of displacements

			Algebraic Maximum	Location		Algebraic Minimum	Location		By
				X (m)	Y (m)		X (m)	Y (m)	
Horizontal displacement (m)									
		Model							
End of construction		MOD1				-0.8	8.65	128.2	P1
		MOD2				-0.53	43	110.4	P1
		MOD3				-0.52	17.8	91.4	P1
						0.29	80.7	155.5	P2
			0.14	134.66	98.26	-0.23	-145.63	91.44	P3
End of impoundment			0.71	23.9	167				P1
			-	-	-	-	-	-	P2
			0.3	15.67	127.87	-0.14	-56.49	134.47	P3
Vertical displacement (m)									
		Model							
End of construction		MOD1				-2.53	-26.3	134.8	P1
		MOD2				-2.02	-35.5	128.2	P1
		MOD3				-1.6	31.9	110.3	P1
						- 0.87	17.2	98.9	P2
			0	399.99	14.51	-1.12	92.64	91.12	P3
End of impoundment						-0.49	-39.6	160.3	P1
			-	-	-	-	-	-	P2
			0	399.99	14.51	-1.33	-56.49	134.47	P3

P1 Ismes-Enel
P2 U. Napoli
P3 Cemagref & al.

Note 1: positive horizontal displacement is for a left to right displacement.
Note 2: positive vertical displacement is for a settlement.

Table 5 Location of maxima and minima of effective stresses

			Algebraic Maximum (note 1)	Location		Algebraic Minimum (note 2)	Location		By
				X (m)	Y (m)		X (m)	Y (m)	
Max. Horiz. Eff. Stress (kPa)									
		Model							
End of construction		MOD1				-2258	-60.8	27.4	P1
		MOD2				-2244	-60.8	27.4	P1
		MOD3				-2355	-60.8	27.4	P1
						-2568	-54.3	27.96	P2
			3.28	-190.91	78.84	-1154.2	-58.49	29.37	P3
End of impoundment						-2534	8	24.5	P1
			-	-	-	-	-	-	P2
			19.44	-3.75	173.27	-1157	7.56	29.15	P3
Max. Vertic. Eff. Stress (kPa)									
		Model							
End of construction		MOD1				-3605	-60.8	27.4	P1
		MOD2				-3598	-60.8	27.4	P1
		MOD3				-3246	-60.8	27.4	P1
						-3889	-6.1	24.9	P2
			9.29	163.31	78.35	-4161	-58.49	29.37	P3
End of impoundment						-4420	8	24.5	P1
			-	-	-	-	-	-	P2
			9.64	-15.94	172.39	-4501	7.56	29.15	P3

P1 Ismes-Enel
P2 U. Napoli
P3 Cemagref & al.

Note 1 : negative stress is for a compression.
Note 2 : positive stress is for a tension.

6.0 CONCLUDING REMARKS BY THE FORMULATOR

6.1 TYPE AND QUALITY OF THE DATA SUGGESTED FOR THE THEME

In the opinion of the formulator, the Duncan and Chang hyperbolic model apply to the dams whose soil materials are not brought up to or near failure. When the soil material reaches or overcomes the peak of the stress-strain curve, the hyperbolic model could only be adapted and used with great care, but is not the suitable model.

This was specifically recalled by Prof. Duncan in Denver (June 2nd, 1999) who was the author of the keynote lecture dedicated to earthfill dams. However, Prof. Duncan was more restrictive, arguing that the hyperbolic Duncan and Chang could be used only in the case of well designed and well built earth dams. The parameters proposed for the actual theme were based on this model but all the bulk laboratory data (data and triaxial curves) available were also given to the participants.

6.2 TARGET NO.1 OF THEME B2

The main target of theme B2 of this BW was to point out and recognize the difficulties associated with the determination of the geotechnical parameters related to a rockfill that is collapsible under wetting. Despite the difficulty related to the determination of the parameters, it is suitable to recall the following conclusions :

- The Duncan and Chang rockfill parameters that were made available represent an acceptable starting point. It was shown in the papers of the participants who succeeded in interpreting the given parameters in order to built their own parameters.

- Ismes-Enel succeeded in using different models to address the problem of a numerical difficulty in using the Duncan and Chang model. The authors succeeded also in the determination of large displacements or collapse due to the wetting of the upstream rockfill.

- Cemagref, Coyne et Bellier and EM2/IMT succeeded in their interpretation of the whole phenomenon since they have depicted the potential of an opening movement near the upper part of the upstream filter. This phenomenon is rather universal for all zoned earth dams :

    - The collapsible rockfill tends to move the filter towards the upstream
    - The water forces that are acting on the upstream face of the core tend to move the filter towards the downstream.

- Comparison of the displacements along the vertical line VV, located in the upstream shell, and the inclinometer No.5, located in the downstream shell, provide a good estimate of the effect of collapse by wetting. In fact, inclinometer No.5 tend to move horizontally towards the downstream, while the displacements along the line VV show a strong settlement in the reservoir filling case. It should be recalled that the line VV and the inclinometer No.5 are

located symmetrically, at a distance of 75 m from the central axis passing through the core of the dam.

6.3 TARGET NO.2 OF THEME B2

The second target of theme B2 of this BW was to compare the calculated and measured piezometric level in a series of three piezometers (i.e. piezometers P11 (upstream), P12 (center) and P13 (downstream) are located in the lower part of the core).

An important (but universal) discrepancy between the calculated and measured piezometric levels was noticed (fig.15). In fact, it is found that the calculated piezometric levels are lower than the measured piezometric levels, particularly near the downstream part of the core, where a higher amount of pore pressure seams to dissipate. In figure 16, an expected linear headloss of pore water pressures at steady-state are compared to the piezometric measurements : an important discrepancy is noticed particularly near the downstream face of the core. The actual question regarding the development of pore pressures in the cores, as it is proposed by the formulator, is undoubtedly a difficult one. It is a fundamental problem that need further research and discussions. This BW was in fact considered by the formulator as a great opportunity to raise « the problem of the transient seepage and the high pore pressures in the core of dams » to the specialists and to the ad-hoc committee.

For the time being, different arguments were proposed in the literature. it is recognized that most of the available seepage models assimilate the advancing water front into the impervious core material, during the reservoir filling phase, to the saturated front. This is not totally correct, since a certain amount a air could be trapped in the inter-granular voids. More than one passage of the water front and a higher water level could be needed in order to really saturate the impervious material of the core. In parallel, one could examine the case of the high back-pressure that is required ine the laboratory before a soil material such a till reaches the saturation. Such a back-pressure could reach a cellular pressure of 700 kPa which corresponds to a water column of about 70 m.

6.4 LESSON FROM THE ACTUAL CASE

An important crack appeared near the crest, in the upstream part of the dam, when the reservoir level reached 75% of the maximum level. As to explain this peculiar behavior, it could be noted that the combination of the settlement of the upstream rockfill and the horizontal movement towards downstream could enhance the opening of a crack in the transition zone. Both movements are conducting to a lack of confinement leading to the opening of a crack.

The importance of the upstream transitions and filters was decisive in the actual case. Both zones could play the role of a filler in the case of the developed of unexpected cracks. On the other hand, it could be recalled that the reduction of the compaction level of the transitions and filters could not only play a major role in preventing or reducing the arching between these zones and the

core, but also to permit to these zones to play properly their role of fillers in case of cracks development.

ACKNOWLEDGEMENTS

The formulator of theme B2 of the 5th Benchmark Workshop wish to thank Dr. David Harris (USBR), Larry Stevens (USCOLD), Kent Murphy (Hydro-Québec) and Pasquale Palumbo (Ismes) for their involvement in the preparation the conference.

Gérard Verzeni, Dam safety director and Phuong Nguyen, head Dams and Civil Works, both from Hydro-Québec, are thanked by the ad-hoc committee and the contributors to the workshop for allowing the case study regarding a Hydro-Québec large dam.

REFERENCES

PAPER CONTRIBUTIONS TO THE 5TH BENCHMARK WORKSHOP :

G.La Barbera[1], A.Bani[1], G.Mazzà[2] , 1999. Numerical Modelling of the First Fill of LG-2 Zoned Rockfill Dam.
1 ISMES S.p.A. – Seriate (Italy), 2 ENEL S.p.A. Research – Milano (Italy).

Pagano, A. Desideri, F. Vinale, F. Sorvillo, 1999. Prediction of the Behavior of a Zoned Earth Dam During Construction and Impounding.
University of Naples "Federico II".

Patrice Anthiniac[1,3], Stéphane Bonelli[1], Alain Carrère[2] - Olivier Débordes[3], 1999. Hydro-Plastic Analysis of LG-2 Rockfill Dam During Construction and Impoundment Stages. 1 Cemagref, division Ouvrages Hydrauliques et Equipements pour l'Irrigation, Le Tholonet BP 31, 13612 Aix-en-Provence - France ; 2 Coyne et Bellier ,9 allée des Barbanniers, 92632 Gennevilliers Cedex - France ; 3 ESM2/IMT Technopôle de Château-Gombert 13451 Marseille Cedex20 - France.

DATABOOK PREPARED BY THE FORMULATOR

Bachir N. Touileb, 1999. Theme B2. Embankment dams - First fill of a rockfill dam : a case study : LG-2 rockfill dam.
Hydro-Québec.

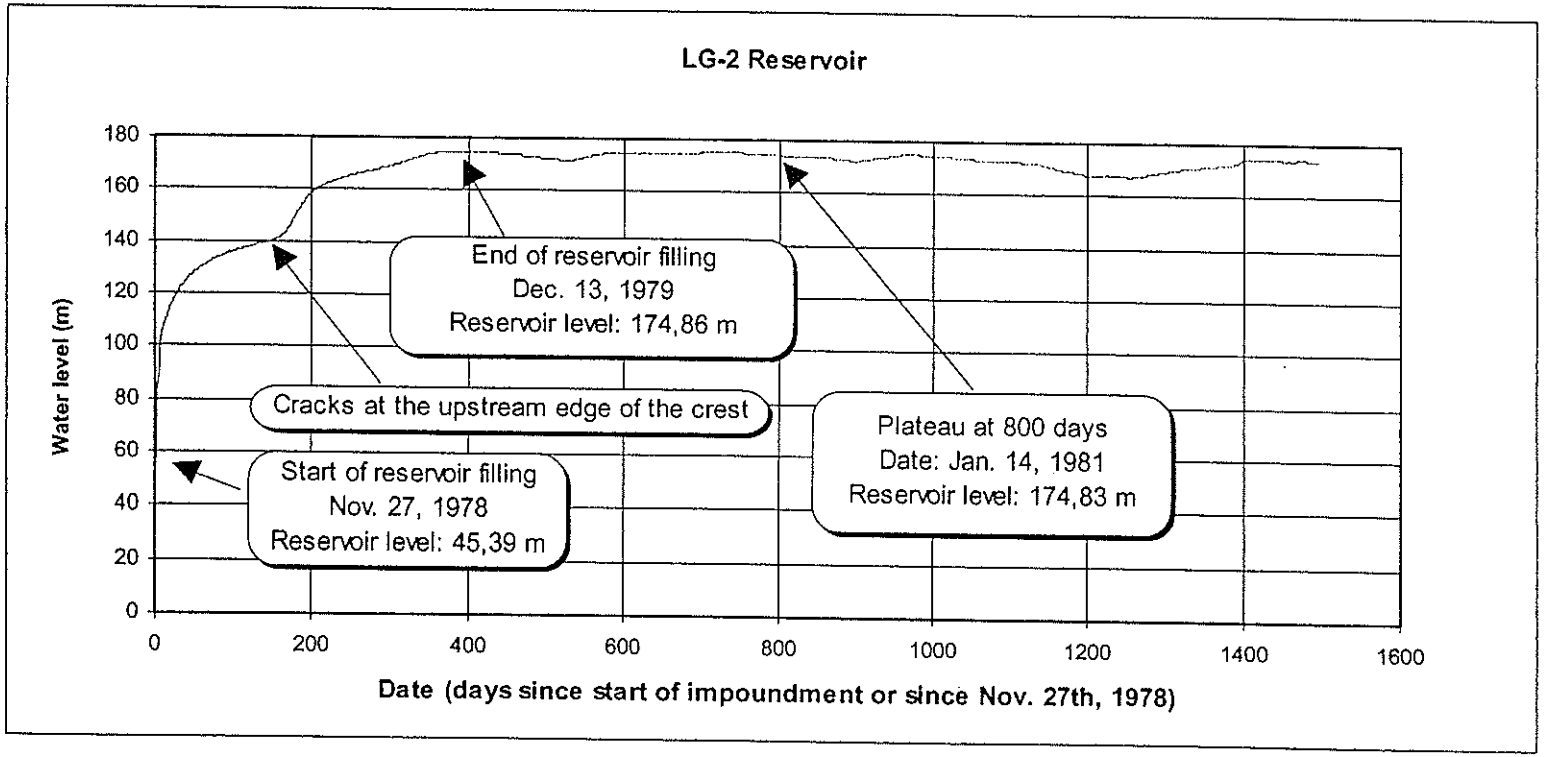

Figure 1 LG-2 . Reservoir filling curve

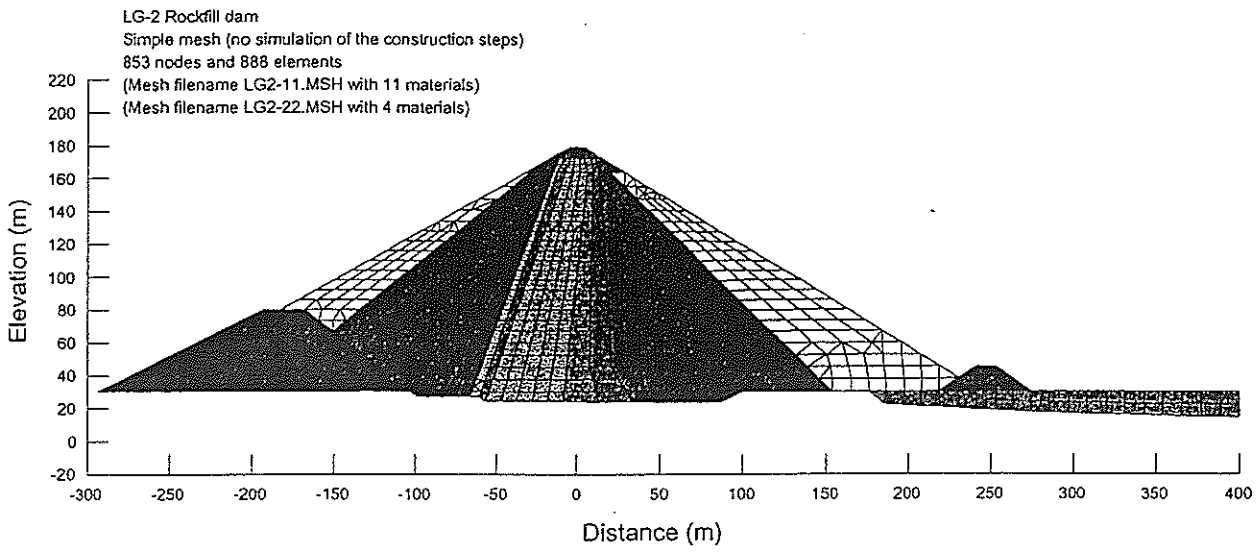

Figure 2 LG-2 rockfill dam. Finite element mesh

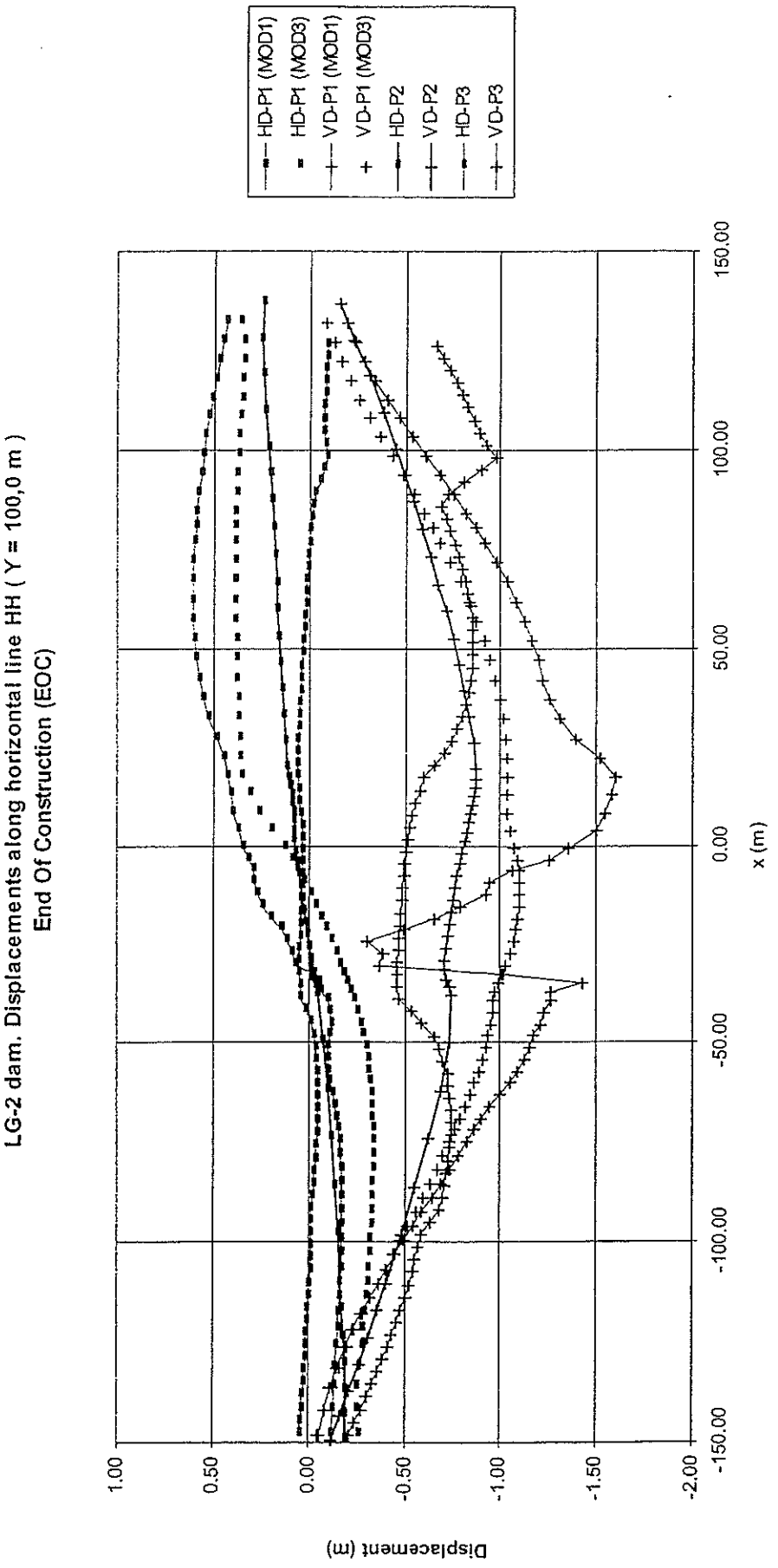

Figure 3 Horizontal (HD) and Vertical (VD) displacements at end of construction along horizontal line HH

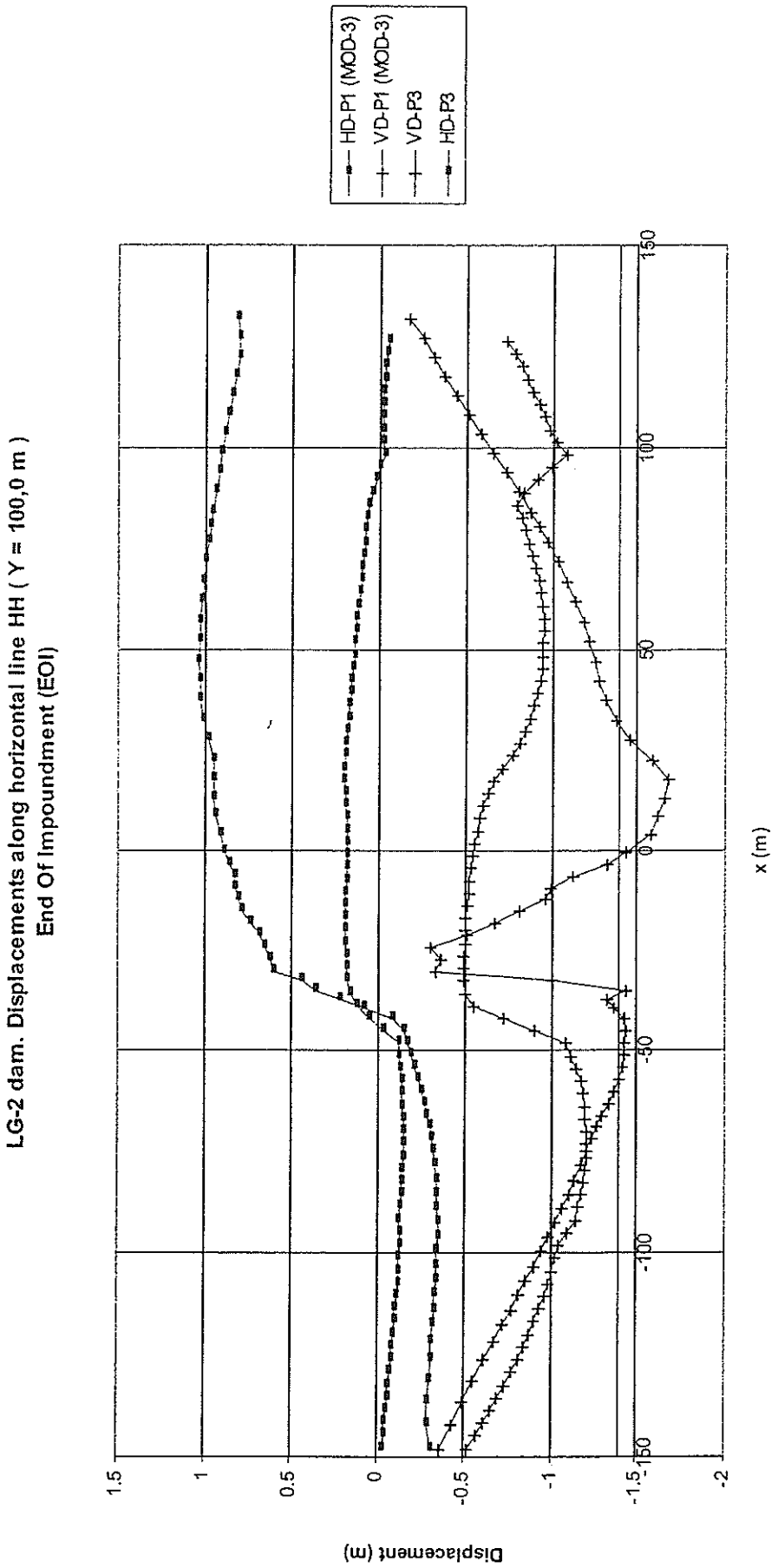

Figure 4 Horizontal (HD) and Vertical (VD) displacements at end of impoundment along horizontal line HH

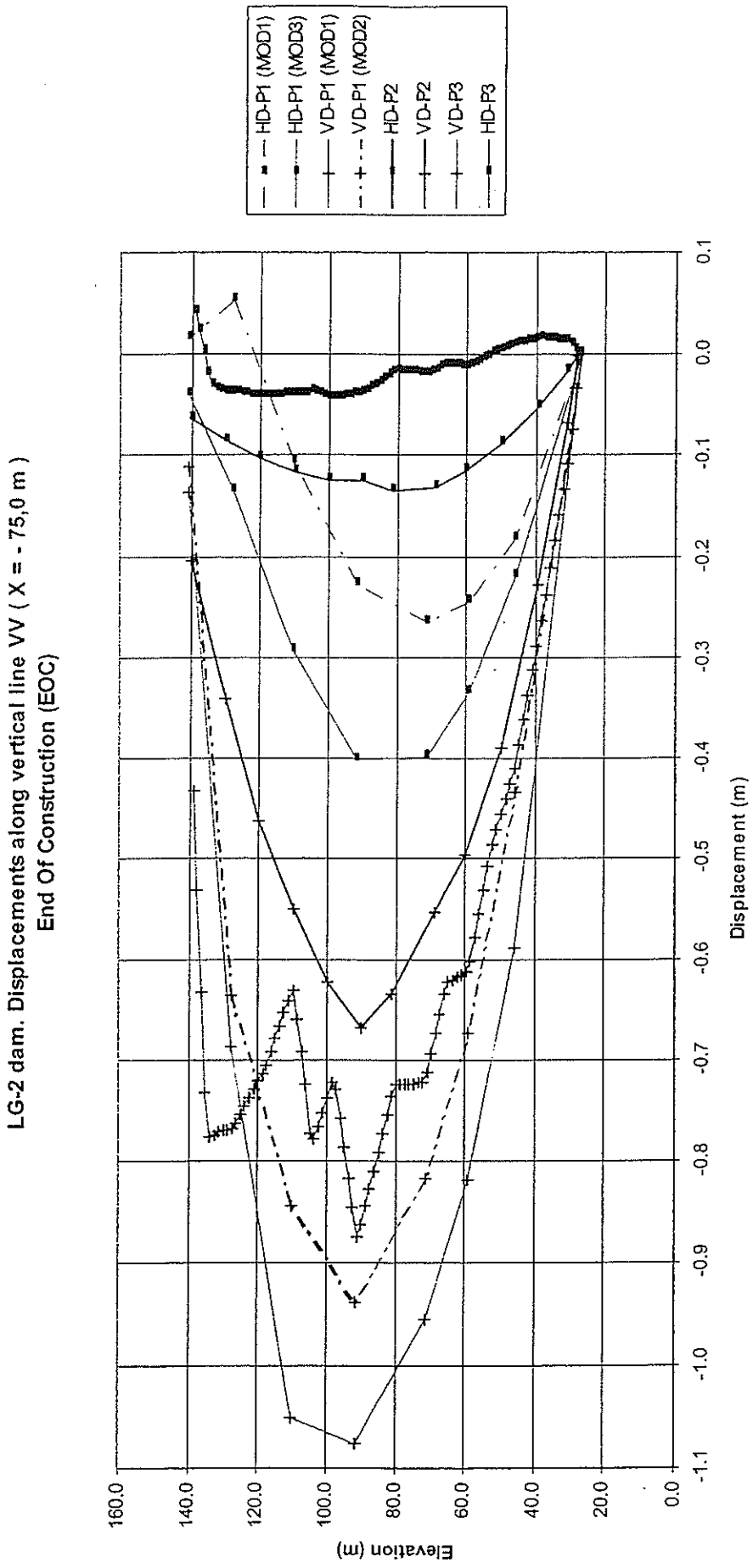

Figure 5 Horizontal displacements (HD) and Vertical displacements (VD) at end of construction along vertical line VV

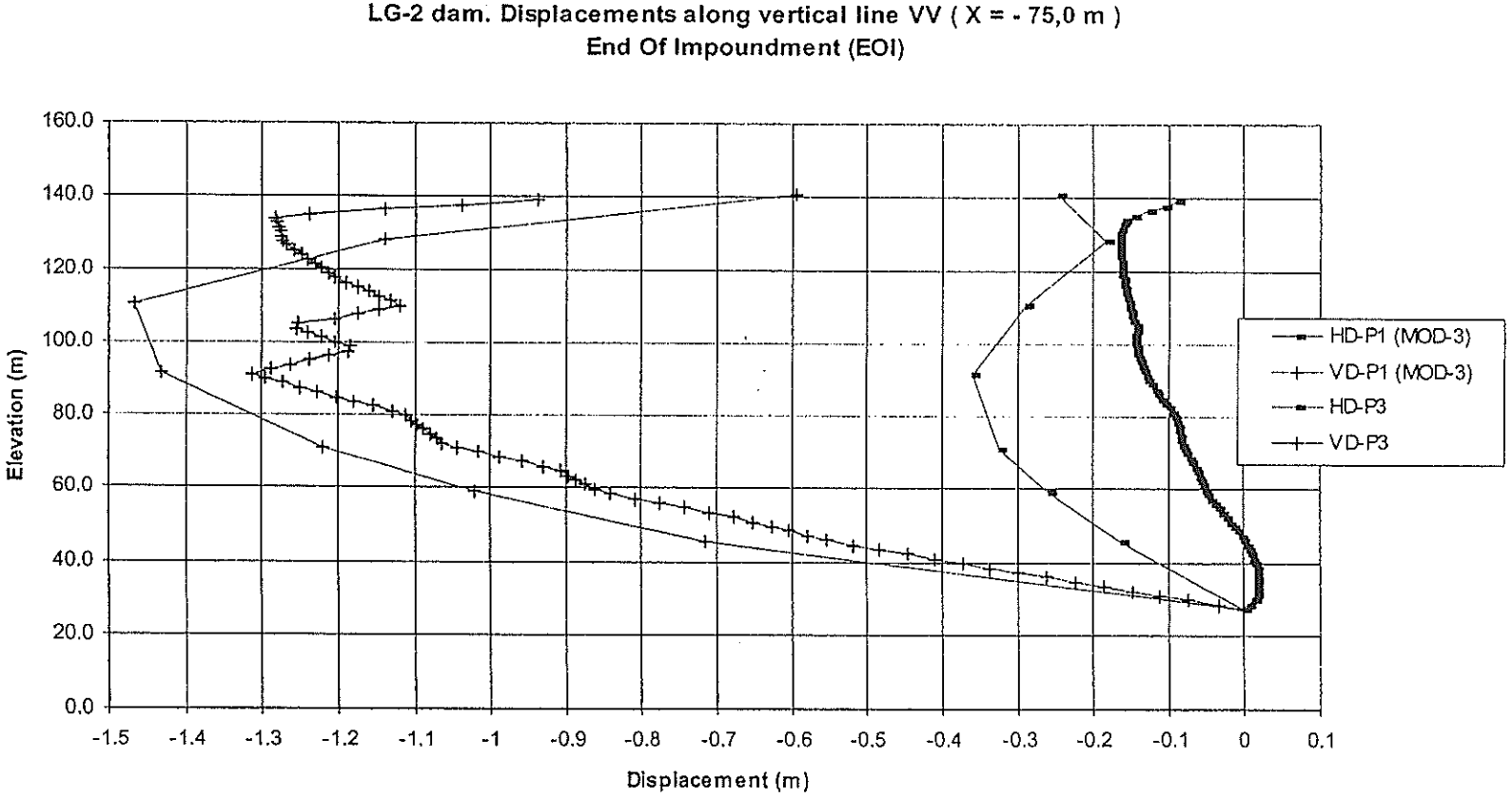

Figure 6 Horizontal displacements (HD) and Vertical displacements (VD) at end of construction along vertical line VV

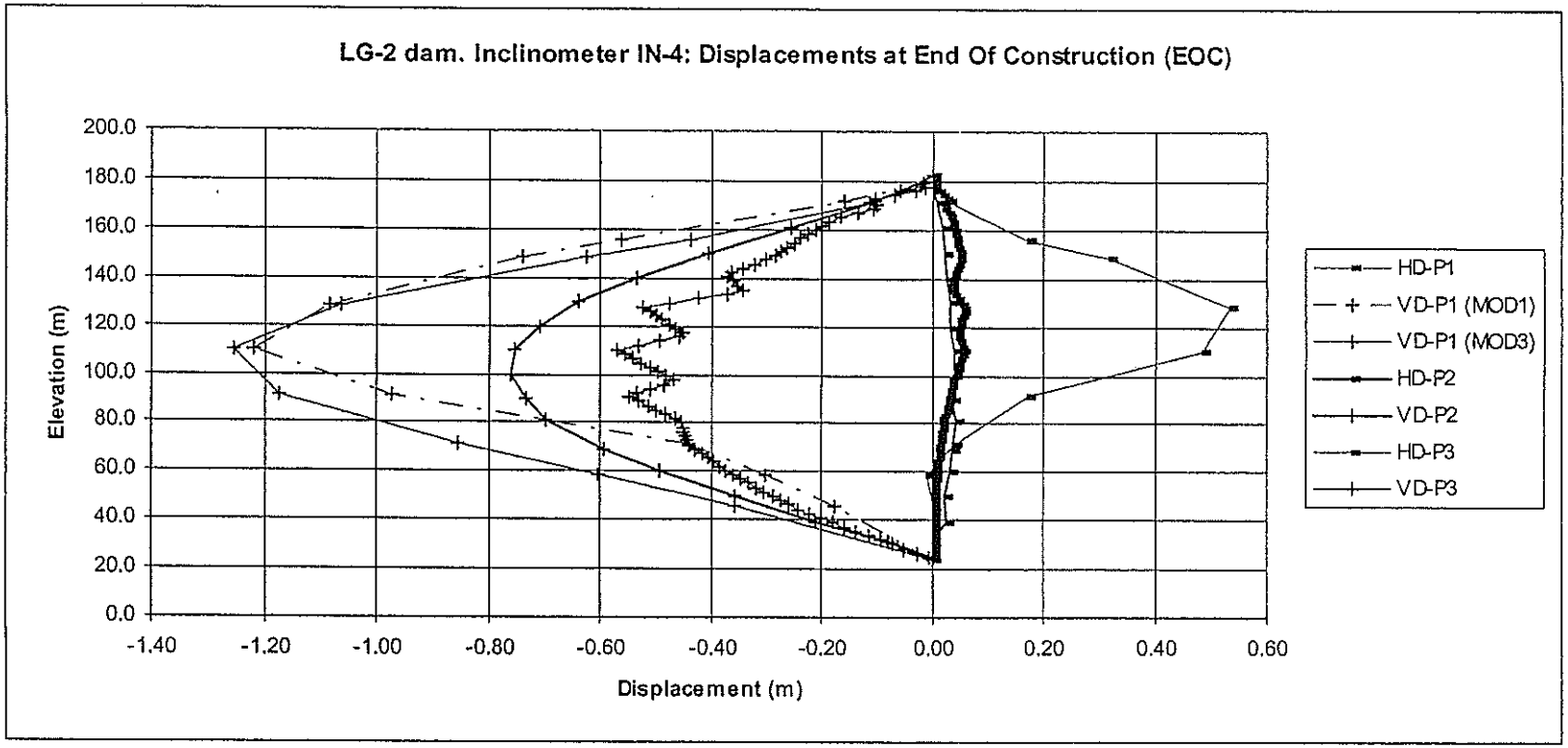

Figure 7 Horizontal displacements (HD) and Vertical displacements (VD) at end of construction along inclinometer #4

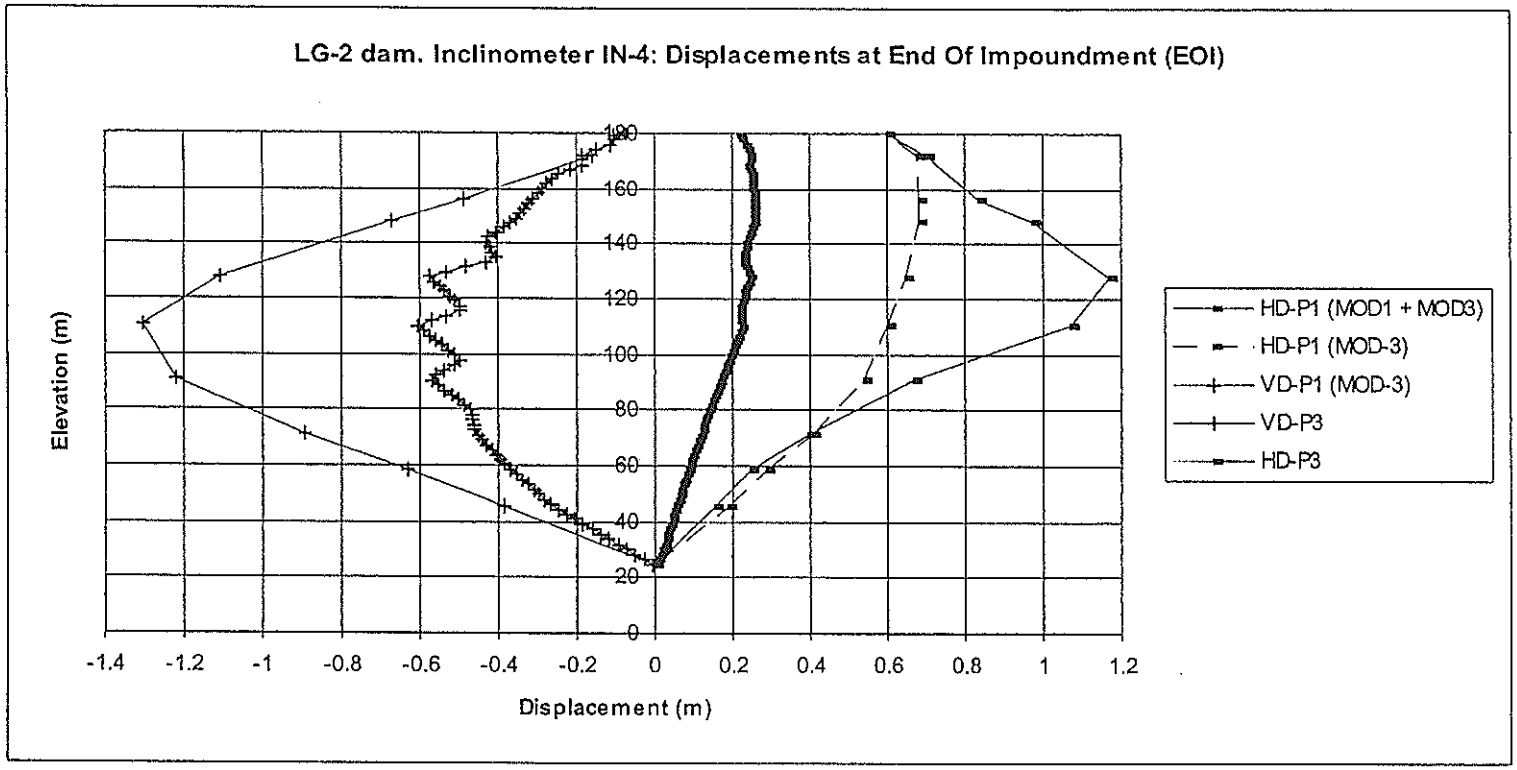

Figure 8 Horizontal displacements (HD) and Vertical displacements (VD) at end of impoundment along inclinometer #4

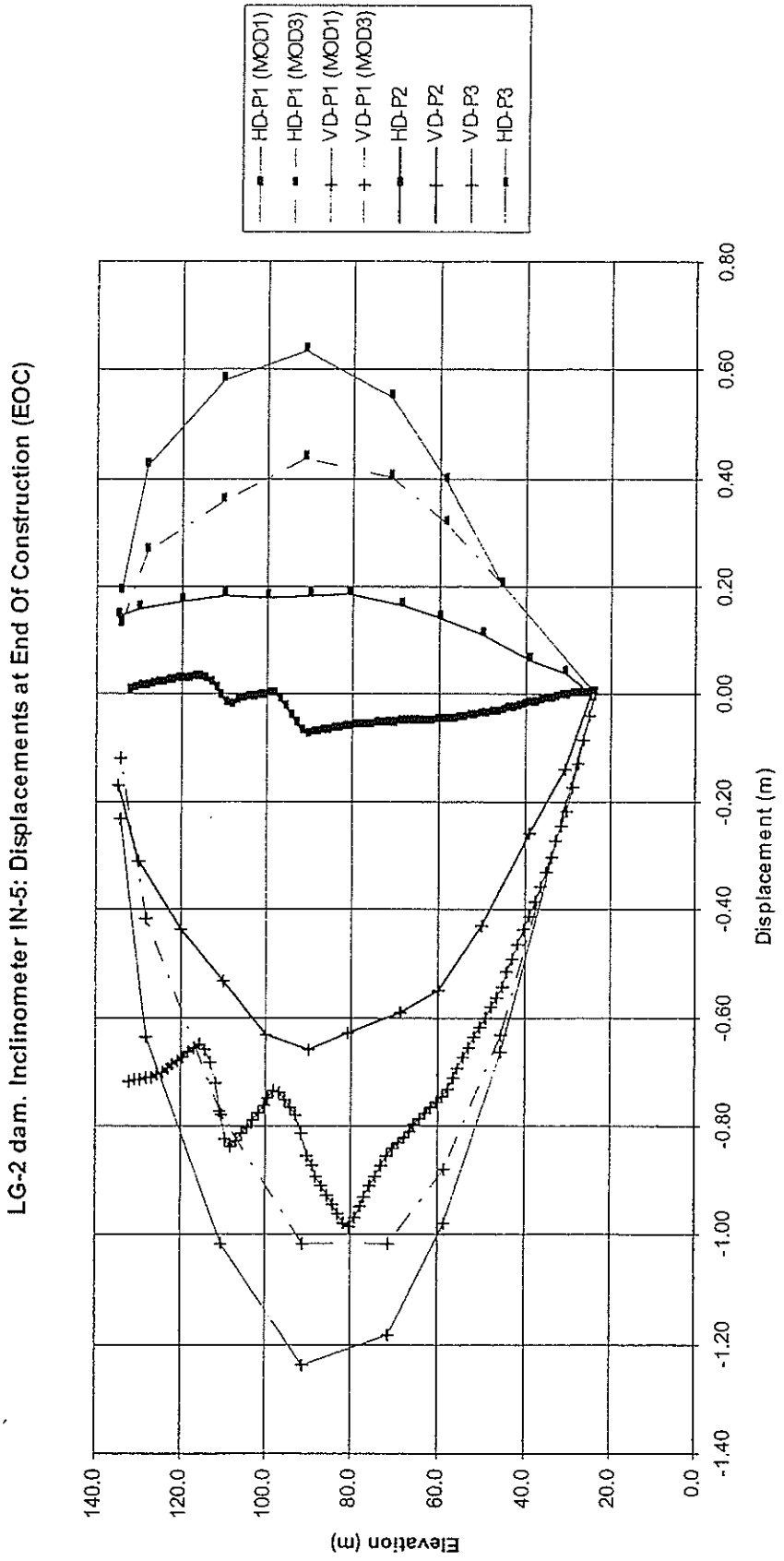

Figure 9 Horizontal displacements (HD) and Vertical displacements (VD) at end of construction along inclinometer #5

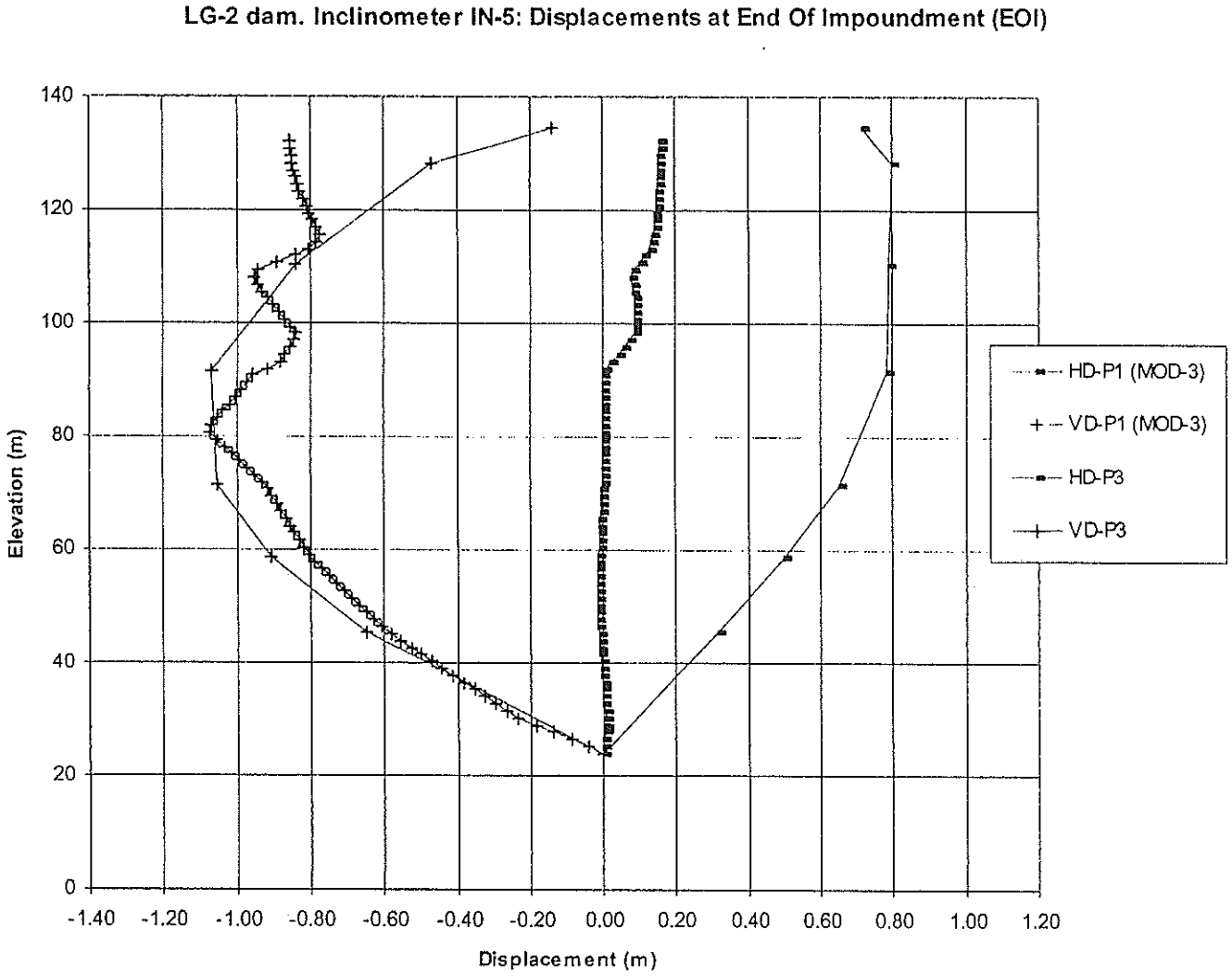

Figure 10 Horizontal displacements (HD) and Vertical displacements (VD) at end of impoundment along inclinometer #5

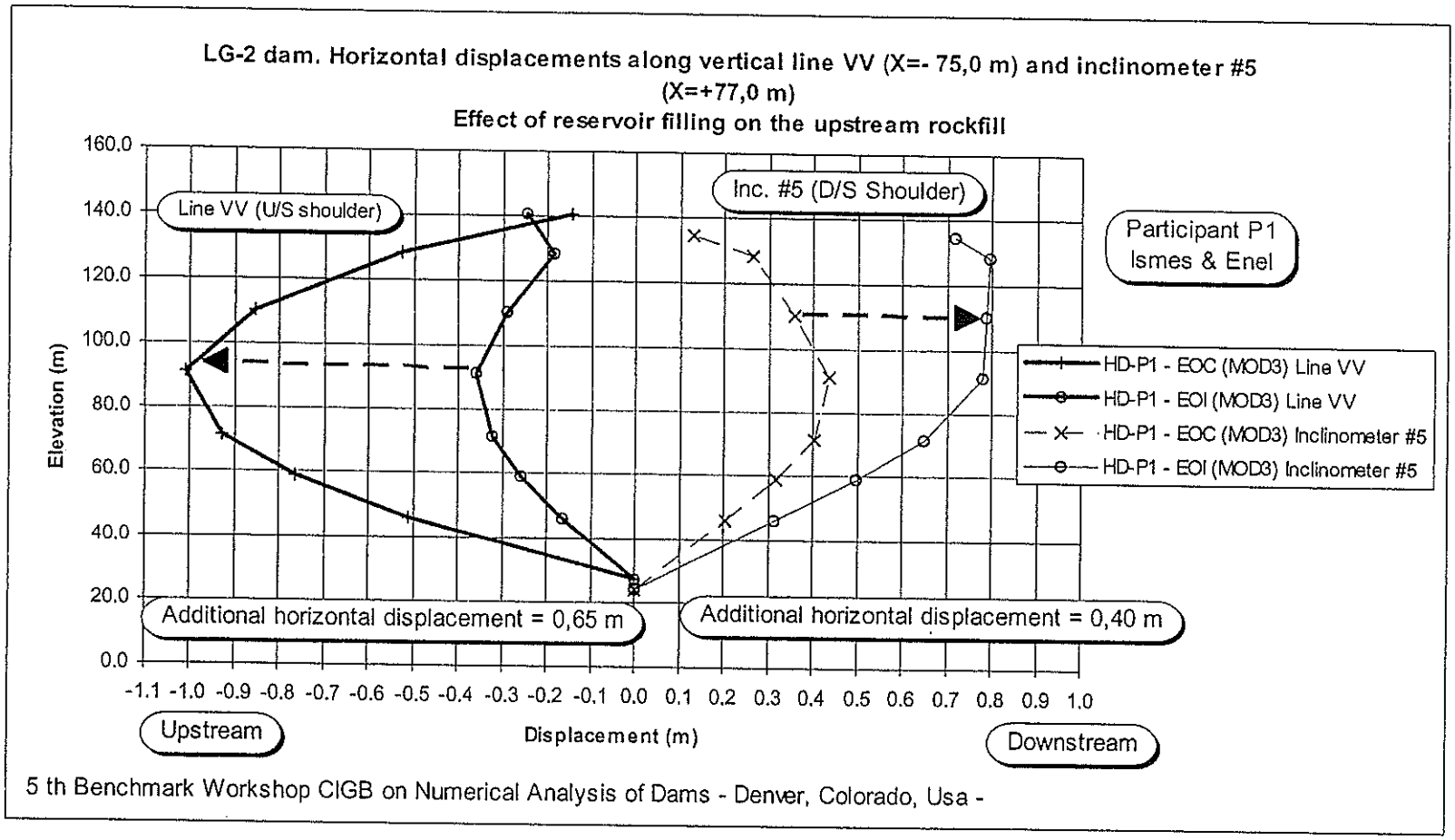

Figure 11 Horizontal displacements (HD) along vertical line VV and inclinometer #5

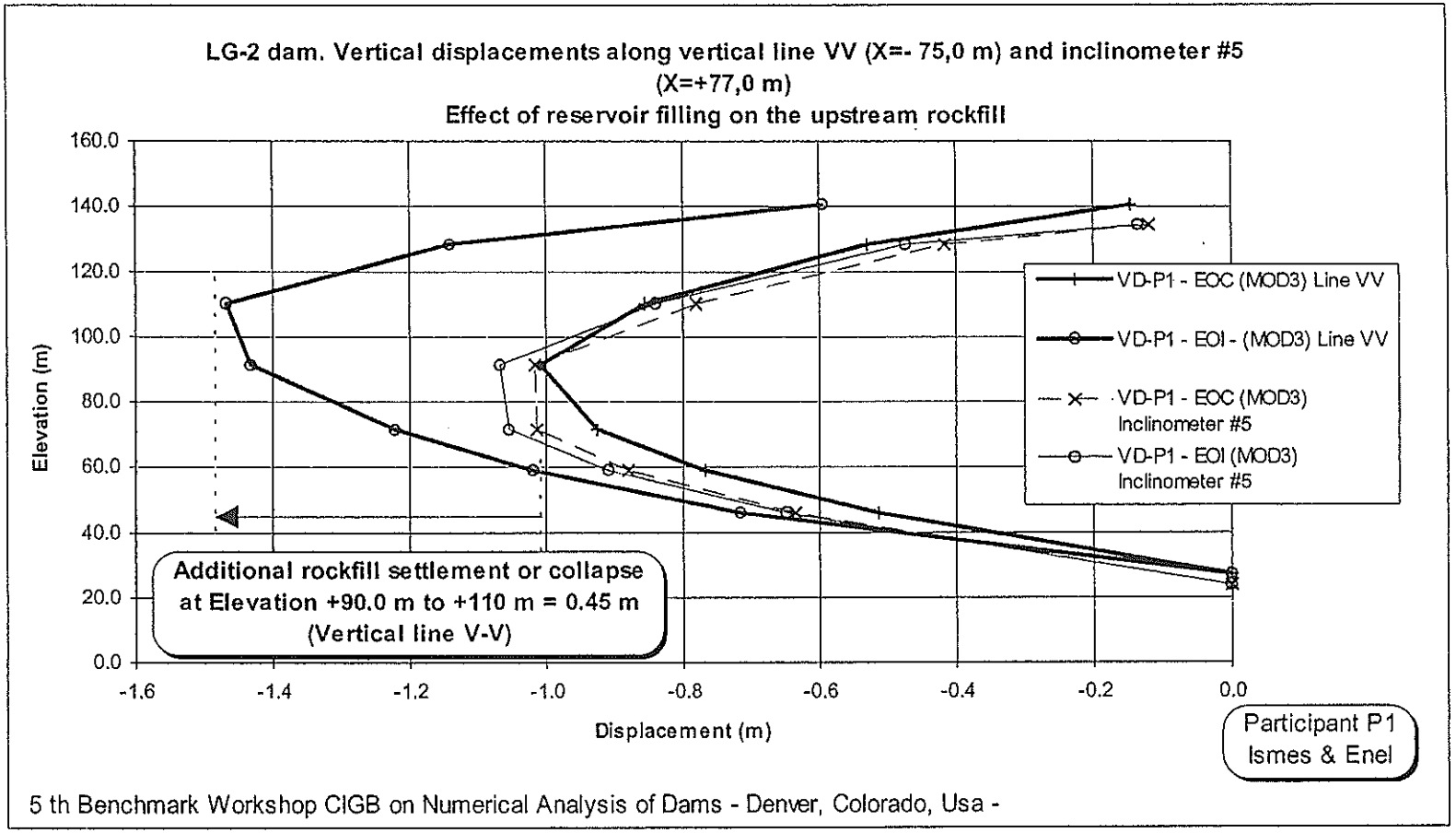

Figure 12 Vertical displacements (VD) along vertical line VV and inclinometer #5

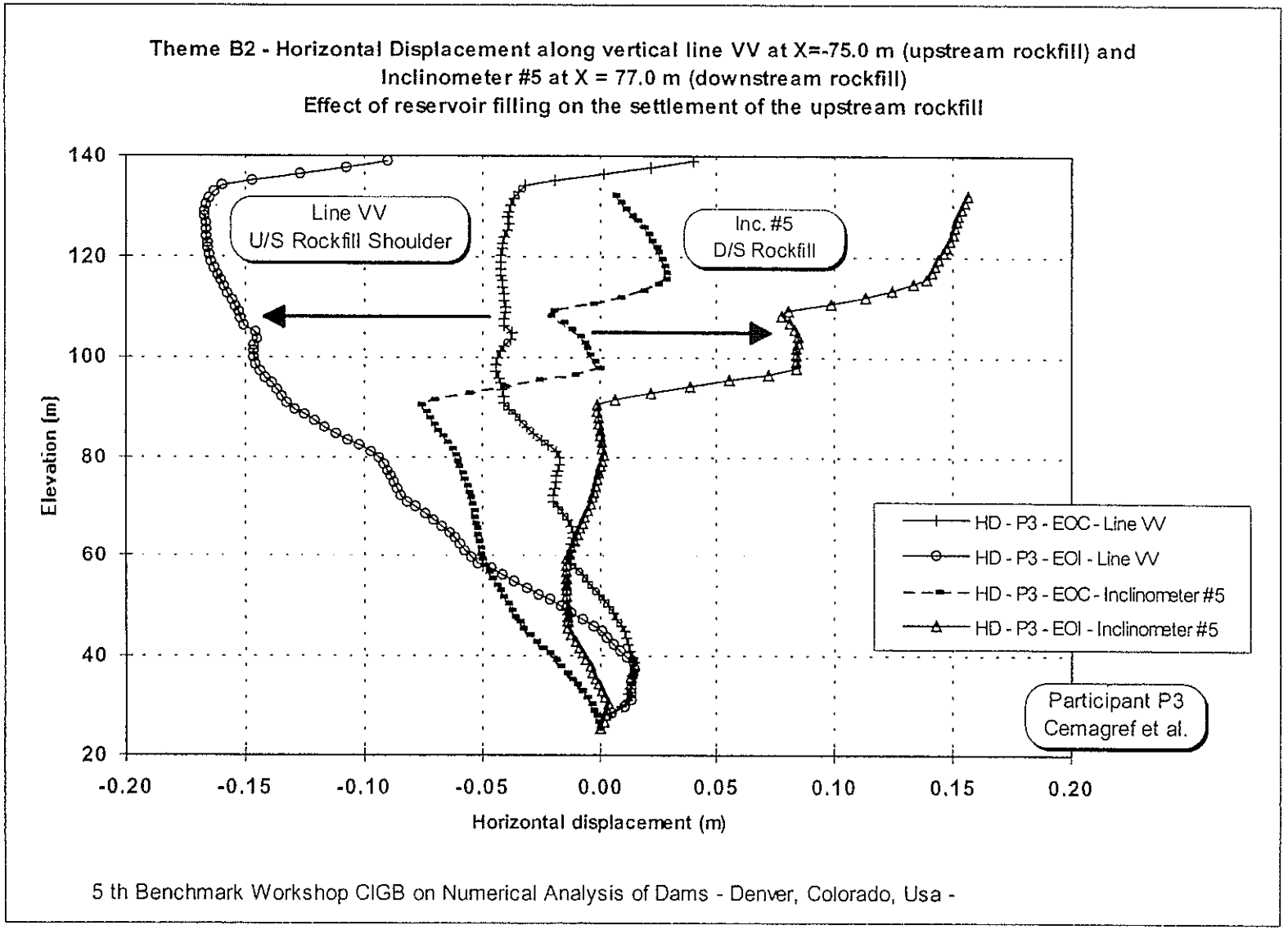

Figure 13 Horizontal displacements (HD) along vertical line VV and inclinometer #5

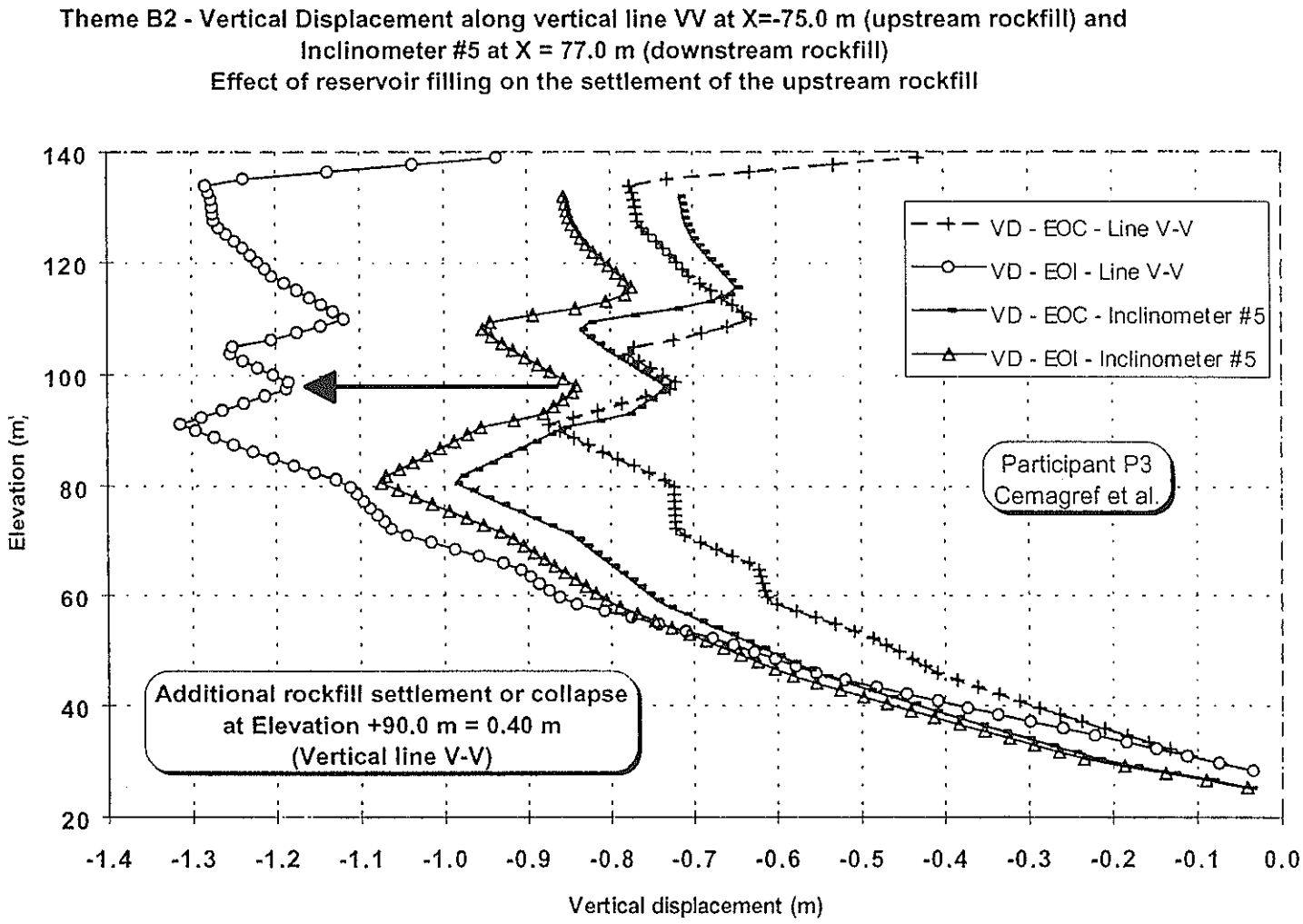

5 th Benchmark Workshop CIGB on Numerical Analysis of Dams - Denver, Colorado, Usa -

Figure 14 Vertical displacements (VD) along vertical line VV and inclinometer #5

Figure 15 LG-2. Piezometric levels at first filling conditions. Comparison of results.

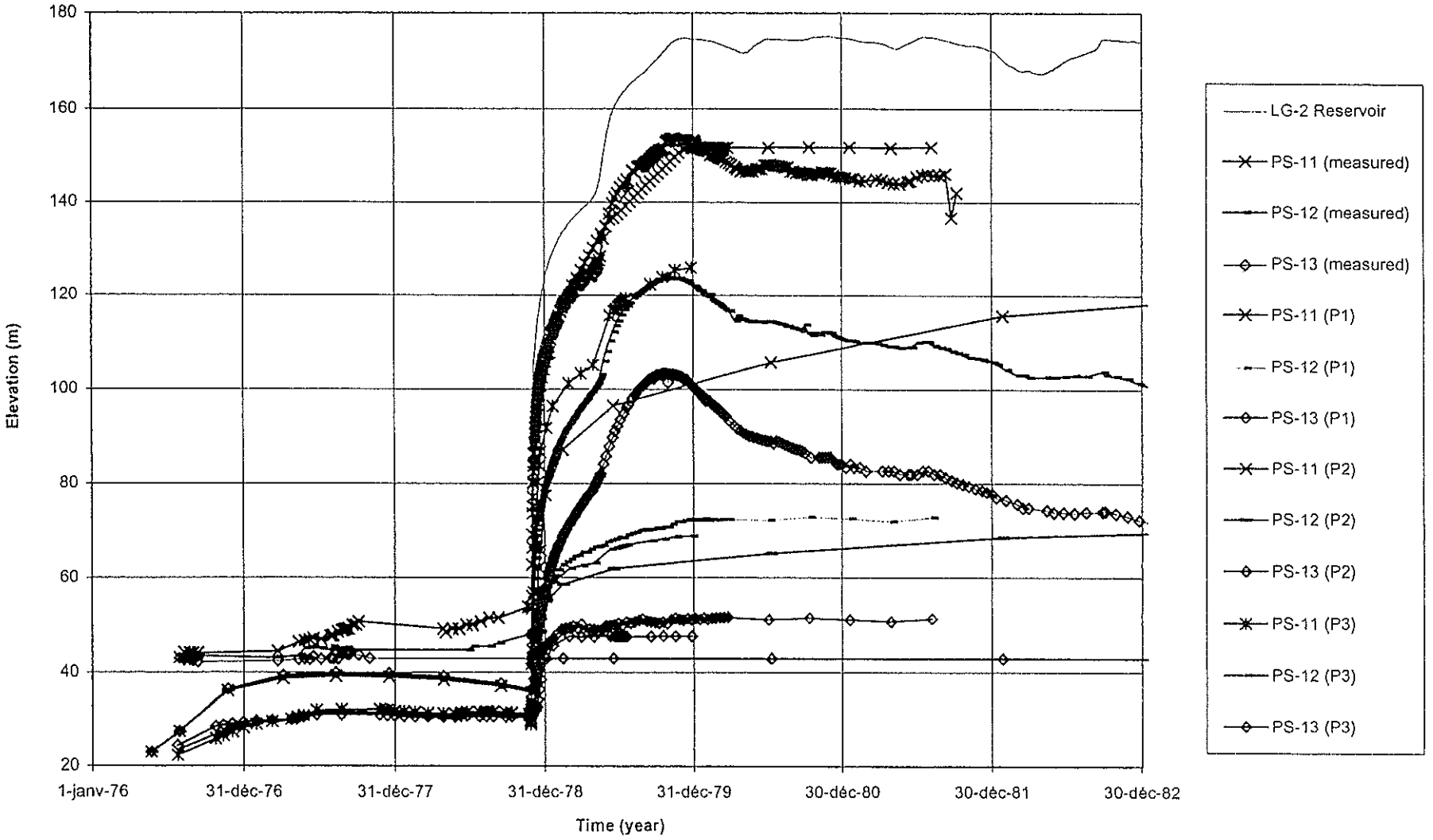

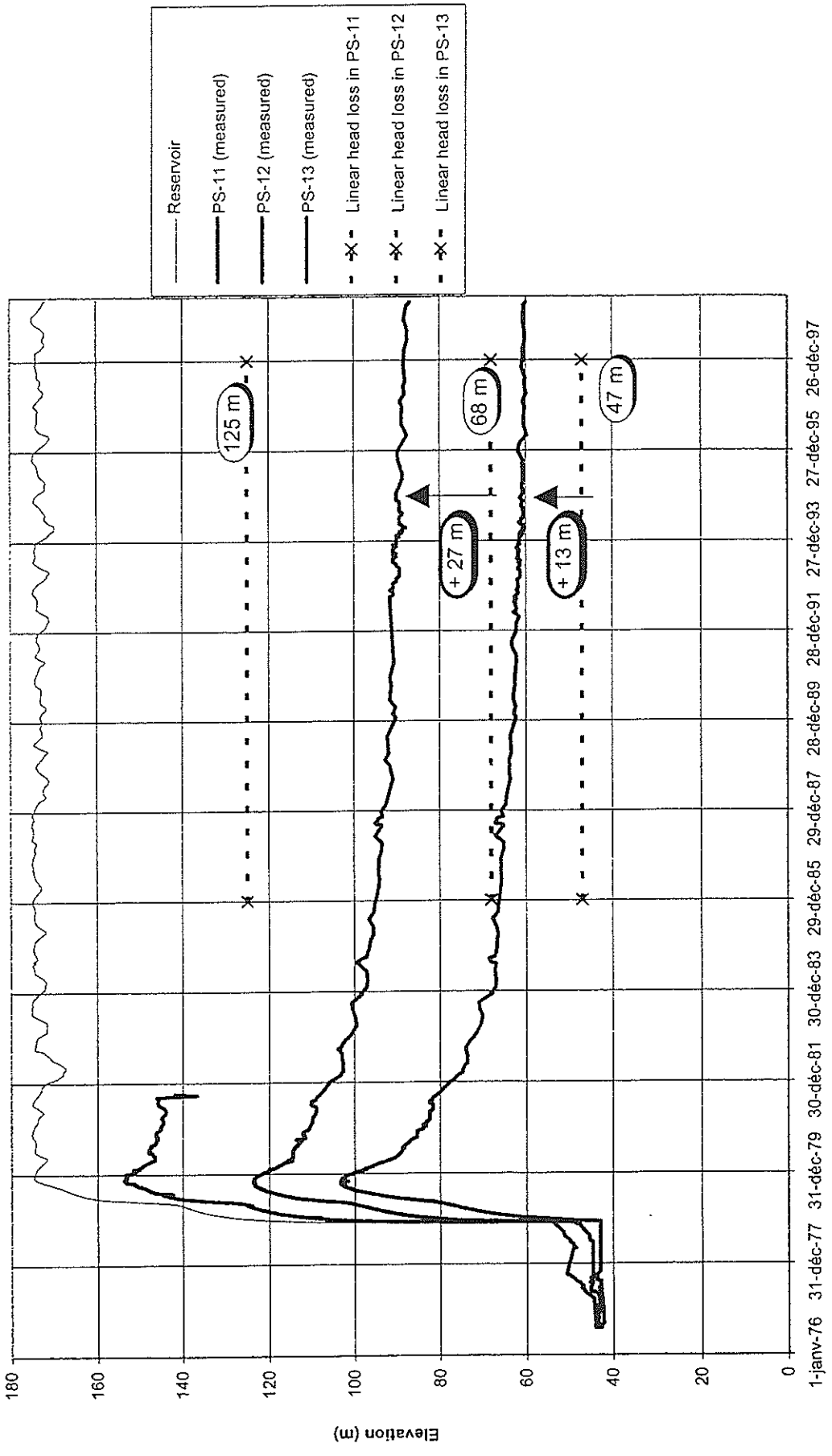

Figure 16 LG-2. Piezometric levels at first filling conditions. Expected and measured levels.

FIFTH ICOLD BENCHMARK WORKSHOP ON NUMERICAL ANALYSIS OF DAMS
DENVER (COLORADO U.S.A.), JUNE 2-5, 1999

THEME B2

NUMERICAL MODELLING OF THE FIRST FILL OF LG-2 ZONED ROCKFILL DAM

G.LA BARBERA*, A.BANI*, G.MAZZÀ**

ABSTRACT

The construction history and the first filling (considering the «wetting collapse» phenomena) of LG-2 zoned earth dam (Canada) have been simulated through numerical analyses performed with the OMEGA finite element code. Three different analyses have been carried out to simulate the construction phase, adopting both the uncoupled and the coupled approach. Three different constitutive models have been considered: the hyperbolic non-linear Duncan-Chang (1970), the modified Cam-Clay (ECAM extended Cam Clay model) and the Drucker-Prager. In the coupled analysis the consolidation phenomena has been assumed to develop on the clayey core materials only.
A quite cumbersome procedure have been adopted in order to simulate the first reservoir impounding.
The results obtained from construction history simulation with the adoption of different constitutive models (displacements and stresses) were in quite good agreement.

1. INTRODUCTION

The paper presents the results of the analyses which have been carried out for the LG-2 dam, part of the Phase One of the La Grande Riviere Complex (Canada). It is a zoned earth and rockfill embankment having a maximum height of 157 m, with a crest length of 2836 m.
The cross section of the rockfill structure has a slightly inclined upstream central core, made out of compacted moraine. Upstream and downstream, the fine material of the core is protected by filter and transition zones. The dam shells are

* ISMES S.p.A. - Seriate (Italy)
** ENEL S.p.A. Research - Milano (Italy)

made of rockfill.
Three analyses were carried out in order to simulate the construction phase: for the first two analyses the one-phase uncoupled approach has been adopted; for the third one the coupled approach. The first uncoupled analysis (Mod-1) has been performed adopting the non-linear hyperbolic soil model (Duncan and Chang, 1970), according to Workshop suggested parameters. The second uncoupled analysis (Mod-2)has been performed using Ecam soil model (Fusco, 1994) for clay core material simulation, Drucker-Prager model for filters material simulation and Duncan - Chang for the simulation of all remaining materials. The third coupled analysis has been performed adopting Ecam model for clay core material and Drucker-Prager for all the remaining materials.
The analyses performed for the first filling simulation procedure has been run adopting the uncoupled approach and the Ecam and Drucker-Prager models.
The computer program used for the analysis is *OMEGA*, a 2D 3D f.e.m. code for the numerical solution of non-linear analysis of both one phase (solid or fluid) and two phases solid-fluid medium subjected to static and dynamic load conditions. This code has been developed by ISMES S.p.A. on the basis of the theoretical formulation presented in [5], [6], [7], [8].

The numerical computation have been carried out on the HP 9000 computer at the ISMES computer facilities in Bergamo.

2. BRIEF DESCRIPTION OF THE ADOPTED CONSTITUTIVE MODELS

Both one-phase solid and coupled two phase solid-fluid formulation associated to an incremental elasto-plastic deformation theory have been adopted. A plane strain hypothesis has also been considered.

Duncan and Chang (1970) model
The implemented non-linear elastic hyperbolic model is based on the work of Duncan and Chang (1970). It respect the following main hypothesis:

- the failure condition is represented by a Mohr-Coulomb surface defined as

$$\frac{(\tilde{\sigma}_1-\tilde{\sigma}_3)(1-\sin\varphi)}{2(c\cos\varphi-\tilde{\sigma}_1\sin\varphi)}=1 \qquad (1)$$

where:

$\tilde{\sigma}_1$ and $\tilde{\sigma}_3$ are the maximum and minimum principal stress values at failure (compression stresses are supposed to be negative);

c and φ are material parameters;

- material response is controlled by a stress level parameter defined as

$$s = \begin{cases} \dfrac{s_1}{s_2} & \text{for } s_2 > 0 \\ 1 & \text{for } s_1 = s_2 = 0 \\ 10. & \text{for } s_1 \neq 0\ s_2 \leq 0 \end{cases}$$

where:

$s_1 = (\sigma_1 - \sigma_3)(1 - sin\varphi)$

$s_2 = 2(c\cos\varphi - \sigma_1 sin\varphi)$

If s=1 the representative stress point in p,q plane falls on the Mohr-Coulomb yield surface; if s>1 representative stress point falls externally to yield surface and if s<1 it is strictly internal to yield surface.

- under triaxial loading conditions the maximum compressive stress σ_a (axial)vs the maximum compressive strain ε_a (axial) and the minimum compressive strain ε_0 (horizontal)vs the maximum compressive strain ε_a (axial) can be represented by hyperbolic curves.

The following sign convention was adopted:

$\sigma_a = -\sigma_3 \qquad \varepsilon_a = -\varepsilon_3$

$\sigma_0 = -\sigma_1 \qquad \varepsilon_0 = -\varepsilon_1$

For loading conditions:

$$E_t = \begin{cases} E_0(1-R\cdot s)^2 & \text{when } 0 \leq s \leq 1 \\ 0.01\, p_a & \text{when } s = 1 \end{cases} \qquad (2)$$

$$\nu = \nu_t = \frac{\nu_0}{(1-A)^2} \qquad \text{with} \qquad (3)$$

$\nu = 0$ when $\nu_t < 0$

$\nu = 0.49$ when $\nu_t > 0.49$

where

$$E_0 = Kp_a\left(\frac{|\bar{\sigma}_1|}{p_a}\right)^n \qquad (4)$$

$$\nu_0 = G - F\cdot\log\left(\frac{|\bar{\sigma}_1|}{p_a}\right) \qquad (5)$$

$$\bar{\sigma}_1 = \frac{c}{\tan\varphi} - \sigma_1 \qquad (6)$$

$$A = \frac{D}{E_i}(\sigma_1 - \sigma_3)(1 - R\cdot s)$$

Pa atmospheric pressure

K Modulus number (initial slope in $(\sigma_a - \sigma_0)/Pa$ vs ε_a diagram for σ_0=Pa

R Failure ratio

n exponent controlling the rate of change of E_0 with σ_0

G initial slope in the ε_0 vs ε_a diagram for σ_0=Pa

D factor controlling the asintote in the ε_0 vs ε_a diagram for σ_0=Pa

F exponent controlling the rate of change of ν_0 with σ_0

(ECAM) Extended Cam-Clay model

ECAM model respects the following hypothesis:

- isotropic material;
- linear elasticity inside the yield surface;
- associate flow rule G ≡ F;
- strain hardening;
- yield function F(p,q,θ,k)=0 of the type shown in Fig.1.

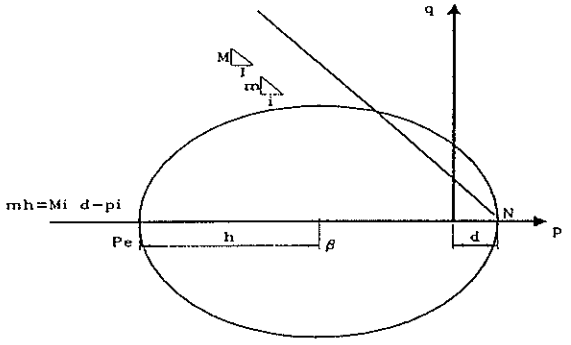

Fig. 1 - Extended Cam-Clay(ECAM) yield surface in p-q plane

In particular ECAM model requires the following material parameters definition:

E	Young modulus;
ν	Poisson coefficient;
c	cohesion;
ϕ	friction angle;
$\overline{V}$	specific volume;
λ	slope of virgin line;
χ	slope of swelling line;
OCR	over consolidation ratio;
r	ECAM yield parameter.

The critical state function results:

$f = q + M \cdot p - N \qquad (q = -Mp + N)$

The mathematical formulation for M and N parameters differ according to the adopted failure criteria, namely :

for Drucker-Prager failure criteria:

$$M = \frac{6\sin\phi}{3-\sin\phi} \qquad (8)$$

$$N = \frac{6c\cos\phi}{3-\sin\phi}$$

for Mohr-Coulomb failure criteria:

$$M = \frac{3\sin\phi}{\sqrt{3}\cos\theta - \sin\theta\sin\phi} \qquad (9)$$

$$N = \frac{3c\cos\phi}{\sqrt{3}\cos\theta - \sin\theta\sin\phi}$$

The yield function can be mathematically represented as follows:

$$F = (p-\beta)^2 + \frac{q^2}{m^2} - h^2 \qquad (10)$$

where:

$\beta = d - r \cdot h$

$d = c \cdot \tan^{-1}\phi$

$m = r \cdot M$ where r is a given constant value defined as:

$$r = \frac{m\,(\theta = 30°)}{M\,(\theta = 30°)}$$

The Drucker_Prager failure criteria has been adopted in the performed analysis.

Drucker-Prager model

The elastic-perfectly plastic Drucker-Prager constitutive model inscribed to the Mohr-Coulomb was adopted (Fig. 2). Plastic deformations were calculated considering an associated flow rule.

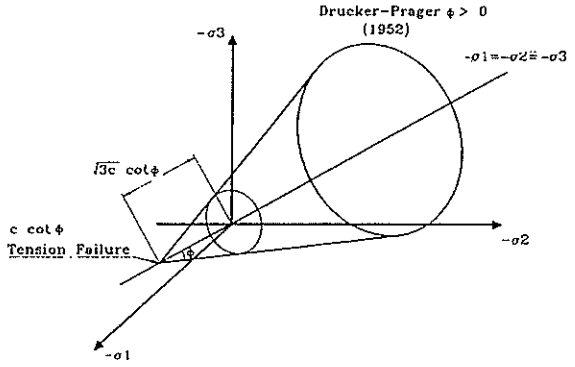

Fig. 2 - Drucker-Prager yield surface in principal stress space

3. RESERVOIR IMPOUNDING MODELLING

The main effects produced by reservoir impounding have been simulated adopting the strategy described as follows:

- independent simulation of seepage phenomena. The hydraulic heads variation between two subsequent calculation times t_n and t_{n-1} have been used as input data, at the same time interval, in the structural analysis;
- pressure load on the wet upstream face of the dam;
- simulation of wetting collapse phenomena by mean of an empirical numerical procedure.

Wetting collapse modelling procedure

The main steps of the procedure used to simulate wetting collapse phenomena are the same explained by Nobari-Duncan (1972). They are described in the following (Fig.3):

- *evaluation of relaxed principal stresses after saturation* by mean of two simplified analyses:
  - A) Instantaneous construction of the dam considering dry parameters and gravity loads
  - B) Instantaneous construction of the dam imposing displacements evaluated at previous step A and gravity

loads. In saturated zones wet parameters have been considered.

- *evaluation of displacements induced by wetting collapse (Analysis A)*:
  for each impounding phase *(n)* displacements induced by wetting collapse have been evaluated by mean of a simplified analysis. The following loads conditions have been considered:
  - instantaneous construction of the dam;
  - same initial stress distribution as in previous load step, but subtracting the evaluated relaxed stresses in the new saturated zones;
  - loads acting in the previous load step *n-1*;
  - wet parameters in all saturated zones.
- *Evaluation of displacements induced by impounding loads (Analysis B)*:
  for each reservoir impounding phase, displacements induced by impounding loads have been evaluated by mean of a simplified analysis subdivided in two load steps:
  - instantaneous construction of the dam considering the same loads and parameters as in the corresponding phase of the previous analysis A. Initial stress distribution corresponding to the final stress distribution evaluated at the end of Analysis A. Young modulus in the saturated zone has been adopted as $Es=4E_0$, where E_0 is the Young modulus adopted in the construction phase.
  - application of the incremental hydraulic loads
- *Total displacements evaluation*
  Total displacements have been obtained by adding the component displacements evaluated on both A and B analyses as previously described.

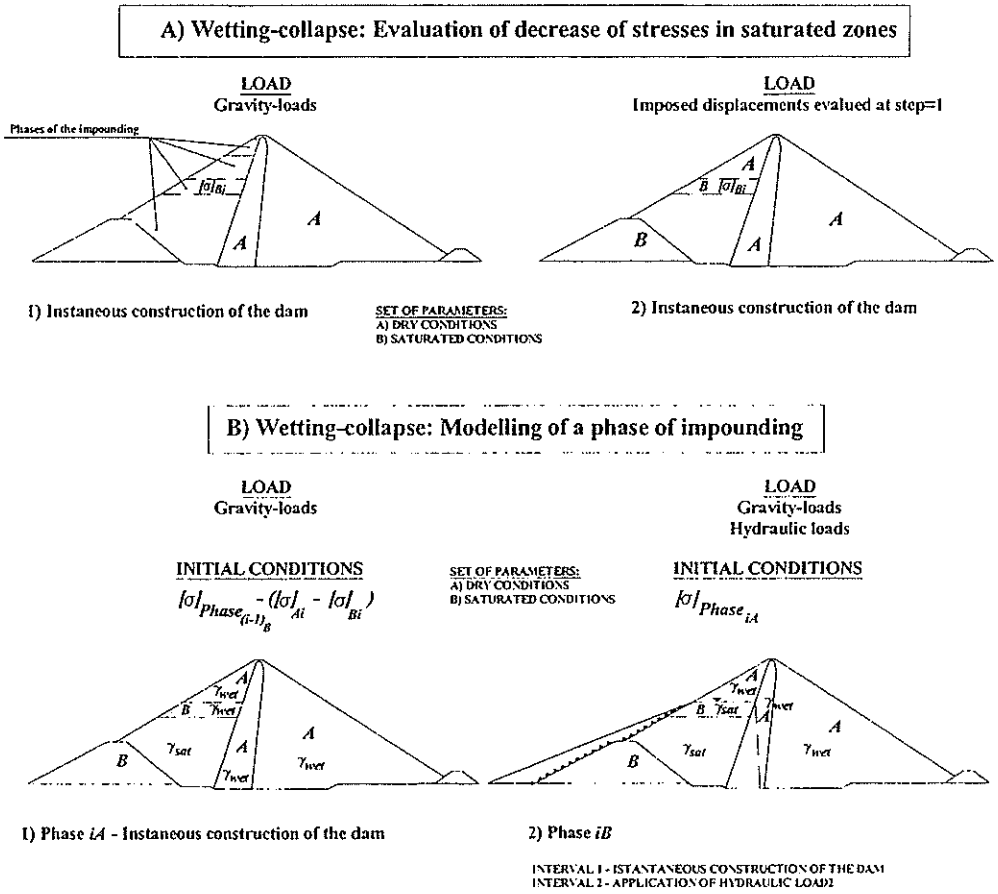

Figure 3

4. ADOPTED MESH

Two finite element meshes have been carried out for the cross section of the dam: the first one for the structural analyses; the second one for the seepage analyses. They are represented in figures 4a and 4b. The first one consists of 833 elements and 2610 nodes. Two different type of elements are present: isoparametric 8-nodes quadrangular and 6-nodes triangular elements. Numerical integration for the two types of elements

was performed using respectively the Gauss (with four integration points) and the Radau rule (with three integration points).
The second mesh consists of 1641 elements and 3418 nodes and is composed of 6-nodes triangular elements. Number and position of the nodes of the first mesh are the same as in the second one.

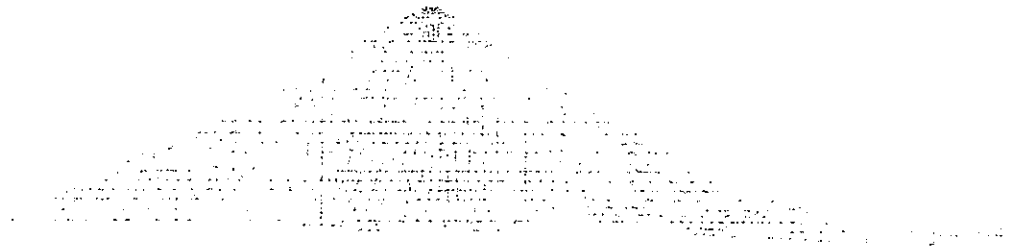

Fig. 4a - Adopted mesh in structural analyses

Fig. 4b - Adopted mesh in seepage analyses

5. BOUNDARY CONDITIONS

The adopted boundary conditions are:

Structural analyses
null horizontal and vertical displacements at the base; null horizontal displacements on the vertical sides of the foundation domain.
In the coupled analyses null excess pore pressure on lateral an upper boundaries of the core.

Seepage analyses
Upstream dam face under water level and upstream soil foundation zone: imposed hydraulic head equal to water table level; base impervious (no flow conditions); downstream zone of foundation soil: imposed hydraulic head equal to the ground level.

The downstream dam face was considered as a seepage surface. Initially all the node along the face are prescribed (head h equal to elevation y of the point). Afterwards in the nodes at which an entering flow (q>0.)was evaluated no flow condition is imposed. If in any of such nodes the evaluated pore pressure, after some iteration, becomes positive, they are fixed imposing h=y.

6. MATERIAL PARAMETERS

The simplified model, considering only four material zones, was adopted. The different materials are represented in Figure 5. The adopted materials parameters are reported in Tables 1 and 2. In Table 1 parameters relevant to Duncan_Chang model are reported. They are the same as those proposed by the Organising Committee.

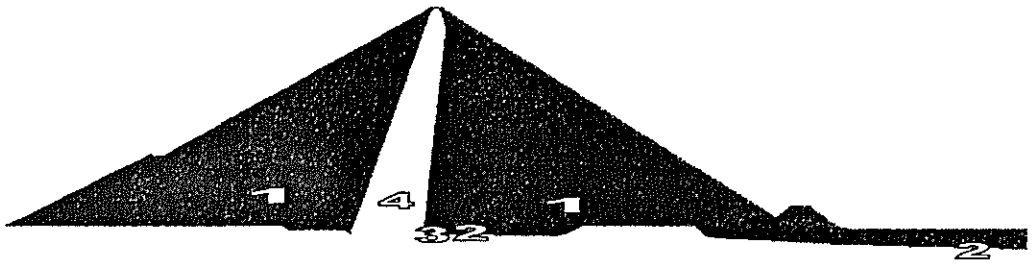

Dam Material considered in the finite element mesh	
Dam Upstream and Downstream outer rockfill	1
Rockfill of the upstream cofferdam	1
Selected rip-rap stones of the dam	1
Moraine of the dam core	4
Dam Upstream and Downstream inner rockfill and Rockfill of the downstream cofferdam	1
Upstream transition of the dam	2
Upstream filter of the dam	3
Downstream filter of the dam	3
Downstream transition of the dam	2
Rip-rap cushion of the dam	2
Dense sand and gravel under the downstream toe	2

Fig. 5 - Defined material zones

In Table 2 the parameters relevant to Ecam and Drucker_Prager models are reported. Consolidation parameters have been estimated from the available data. Strength parameters are the same as those adopted for Duncan_Chang model but transformed in the equivalent ones c^e and φ^e in order to obtain the Drucker_Prager yield surface inscribed to the Mohr-Coulomb one.

Such models require also a secant Young modulus definition. It was estimated for all materials from available triaxial curves and from theoretical curves obtained in the plane ($(\sigma_1-\sigma_3)$ - ε_a) adopting the Duncan-Chang model. After some preliminary analyses, an average confining pressure of 500 kPa and an average deformation of 2-3% have been considered.
For the core material a permeability ratio of $K_h / K_v = 4$ has been adopted.

More details regarding the choice of the parameters is given in the appendix.

Adopted parameters for the model of Wong and Duncan(1974)

	K		*N*	R_f	*G*	*F*	*D*
(see note below)	(1)	(2)	(1);(2)	(1);(2)	(1);(2)	(1);(2)	(1);(2)
Core	1100	1100	0.50	0.50	0.35	0.06	8.8
Filters	2300	2000	0.40	0.70	0.40	0.10	21.4
Transitions	1400	1000	0.38	0.67	0.25	0.06	9.9
Rockfill	500	300	0.36	0.72	0.23	0.08	5.6

Note:
(1) Construction phase
(2) Reservoir impoundment phase
• Apparent cohesion corresponding to the unsaturated state

Table 1

Ecam model (core) and Drucker-Prager

	Core		*Filters*		*Transitions*		*Rockfill*	
(see note Table 1)	(1)	(2)	(1)	(2)	(1)	(2)	(1)	(2)
γ (kN/m^3)	22.6	22.95	21.22	22.79	20.12	22.32	21.22	23.11
C*(kPa)	123.	10.	0.	0.	0.	0.	0.	0.
φ* (°)	25.	25.	28.08	27.25	27.67	26.83	28.48	26.83
ν	0.3	0.3	0.35	0.35	0.3	0.3	0.25	0.25
E (Kpa)	250000	250000	90000	75000	80000	70000	50000	35000
λ	0.015	0.015	-	-	-	-	-	-
χ	0.005	0.005	-	-	-	-	-	-
Vs_{tot}	1.3	1.52	-	-	-	-	-	-
OCR	4.0	4.0	-	-	-	-	-	-
K_h (m/s)	4.0e-7	4.0e-7	-	1.0e-4	-	1.0e-4	-	1.0e-3
K_v (m/s)	1.0e-7	1.0e-7	-	1.0e-4	-	1.0e-4	-	1.0e-3

Note:
(1) Construction phase
(2) Reservoir impoundment phase

*) Equivalent friction angle φ^e for Drucker_Prager failure criteria

Table 2

7. PERFORMED ANALYSES

The following analyses have been carried out on the main cross section of the dam, namely:

Construction phase

1. *Mod-1* - Uncoupled analysis - Duncan-Chang model for all materials;
2. *Mod-2* - Uncoupled analysis - Ecam model for the core, Drucker-Prager for the filters, Duncan-Chang for the transitions;
3. *Mod-3* - Coupled analysis - Ecam model for the core, Drucker-Prager for the others materials.

Reservoir impounding phase

4. *Seepage analysis*
5. *Four phases* of impounding simulated by mean of 8 different and subsequent uncoupled analyses (two analyses for each phase) - Ecam model for the core, Drucker-Prager for the others materials

Initial conditions

In order to simulate the over consolidation due to material compaction an initial stress state has been considered for all materials dam. An isotropic initial stress state of 20 kPa has been applied for Mod-1 analysis; 35 kPa for Mod-1 and Mod-2 analyses. In this case OCR values has been reduced in order to have the same initial plasticity surface as Mod-3 analysis.

In seepage analysis initial pore pressure distribution was the same as the excess pore water pressure distribution evaluated at the end of construction.

Construction phases

The construction sequence proposed by Organising Committee was adopted. Ten construction layers were considered.
The cofferdam and the thin foundation downstream layer were applied in the first construction phase.

Impounding phases

The impounding phases adopted in the analyses are defined in Table 3:

	Elevation (m s.l.m.)	*Time (days from impounding begining)*
Phase 1	110.	14
Phase 2	128.	54
Phase 3	156.	194
Phase 4	175.	374

Table 3

Main remarks on the obtained results

The results of the performed analyses are plotted according to the proposed templates.
The requested displacements results are shown in Figures 6-9 (end of construction) and 10-13 (post construction).
The hydraulic head evolution since the end of construction is reported in Figure 14.
The contours of effective stresses (Figures 15, 16, 18) and of post construction displacements (Figure 17) are also reported.

Tables 4 and 5 reports maximum stresses and displacements values at the end of construction and after construction.

Maximum stresses and displacements at the end of construction

	Mod-1 (D.C.)			Mod-2 (D.C. + D.P.+Ecam)			Mod-3 (D.P. + Ecam)		
	X-coor (m)	Y-coor (m)	Value (Kpa;m)	X-coor (m)	Y-coor (m)	Value (Kpa;m)	X-coor (m)	Y-coor (m)	Value (Kpa;m)
σ'_x	-60.8	27.4	-2258	-60.8	27.4	-2244	-60.8	27.4	-2355
σ'_y	-60.8	27.4	-3605	-60.8	27.4	-3598	-60.8	27.4	-3246
δ_x *	8.65	128.2	0.8	43.0	110.4	0.53	17.8	91.4	0.52
δ_y *	-26.3	134.8	-2.53	-35.5	128.2	-2.02	31.9	110.3	-1.6

*Directly calculated diplacement (comprise settlement of own layer after placing)

Table 4

Maximum stresses and displacements at the end of first reservoir impounding

	Mod-3 (D.P. + Ecam)		
	X-coor (m)	Y-coor (m)	Value (Kpa;m)
σ'_x	8.0	24.5	-2534
σ'_y	8.0	24.5 m	-4420
δ_x *	23.9	167.0 m	0.71
δ_y *	-39.6	160.3	-0.49

* Displacement evaluated after end of construction

Table 5

Construction phase

The maximum calculated settlement has been obtained with Duncan_Chang model (Mod-1) and its value is about 253 cm. It occurs close to the upstream zone of filter-core contact at elevation of about 130 m s.l.m. On the other hand, the maximum settlement with Ecam and Drucker-Prager models (Mod-3) occurs in downstream rockfill, at about 110 m height, and it is about 160 cm.
The calculated maximum horizontal displacements is about 80 cm for Mod-1 analysis and about 50 cm for the other models.

The differences between the result obtained with the different adopted models are evident especially in the core (Figures 7b and 9a).

The calculated effective stress distribution is quite similar in the three performed analyses (Figures 15-16). The most important difference can be noted in the lower part of the core, where in the Mod-1 analysis effective compressive stresses are greater than those calculated in the filters. For the other two cases the situation is exactly opposite.

Impounding phase

The maximum calculated post construction settlement in the upstream rockfill is about 50 cm (Figure 17). The maximum calculated horizontal displacement is about 71 cm toward downstream direction (on downstream face at elevation of about 165 m) and about 26 cm toward upstream direction (on upstream face at elevation of about 135 m).
It was evaluated the different contribution on the displacements development due to wetting collapse and buoyancy and water load. The first cause is prevalent for the settlement (Figure 13b); the second one for horizontal displacements (Figure 13a).
Horizontal displacements on the crest, after the first phase of reservoir impounding, are directed in upstream direction. Afterward they progressively increase toward downstream direction (figure 12a).

After impounding the effective stresses decreased in the upstream zone of the dam, especially at the upstream core-filter contact zone. Effective stresses have strongly increased on the downstream side of the core, close to the base (Figure 18).

7. REQUIRED COMPUTATION TIME

The uncoupled analyses with the Duncan-Chang model (Mod-1 and Mod-2) required a CPU time of about 15 minutes; while the coupled analysis with Ecam-D.P. models (Mod-3) about 3 min.

The simplified analysis for the simulation first reservoir impounding required a CPU time of about 1 min. for each phase.

8. CONCLUDING REMARKS

The whole set of results obtained from the carried out analyses for the Fifth Benchmark Workshop are presented and discussed in this paper.

Two different approaches (coupled and uncoupled) and three models - hyperbolic Duncan-Chang model, Ecam for clayey materials and Drucker-Prager models - were considered to simulate the construction phase of the dam.
An acceptable agreement among the results obtained with different models were found. Some discrepancies are evident in the dam core both for settlements and stress distribution.

The solution with Duncan Chang model presented some numerical difficulties and some doubt arose about the strong differential settlement calculated at contact zone between upstream filter and core.

The wetting collapse phenomena has been simulated by mean of an empirical procedure, which main steps consist in a series of simplified and subsequent analyses. The obtained results are in agreement with the measurements taken on other dams of similar typology and dimension to LG-2 dam (i.e. El Infernillo dam).

9. REFERENCES

[1] Biot M.A. (1941). General theory of three dimensional consolidation J Appl. Phis.

[2] Biot M.A. (1956). The theory of propagations of elastic waves in a fluid saturated porous solid. J. Acou.Soc.Am., 168 191.

[3] Duncan J.M., and Chang C.Y. (1970) "Non-linear analysis of stress and strain in the soils"
Journ. of Soil Mech. and Found. Div. Asce, Vol.96, N0.SM%, pp.1629-1653.

[4] Fusco A. (1985). Continuum mechanics and finite element numerical solutions in geomechanics. Ph. D. Thesis, University of Ottawa.

[5] Fusco A. (1993). Numerical analysis for engeeners. Monograph CIMNE, N.19

[6] Fusco A. (1993). The Continuum Mechanics Theory for engeeners. Monograph CIMNE, N.20

[7] Fusco A. (1993).The Finite Element Method for engeeners. Monograph CIMNE, N.21
[8] Fusco A., Cervera M.(1993).Coupled solid-pore fluid problems solved by Finite Elements. Monograph CIMNE, N.22
[9] La Barbera G., Bani A., Mazzà G. (1994), Evaluation of pore pressure and settlements of an embankment dam under static loadings". Third Icold Benchmark Workshop on Numerical Analysis of Dams, Paris 1994.
[10] La Barbera G., Bani A., Mazzà G. (1994), Effect of large settlements on an embankment dam". Fourth Icold Benchmark Workshop on Numerical Analysis of Dams, Madrid 1996.

Appendix

Evaluation of the parameters for Drucker-Prager and ECAM (Extended Cam Clay) models derived from the data provided by the specifications.

Drucker-Prager model

The model needs, for each material, a secant deformability modulus consistent with the strains that the structure will undergo during the application of the loads. From preliminary analyses an average deformation of 2-3% has been estimated at the end of construction.

Afterwards, deformation moduli have been evaluated assuming an average confinement stress of 500 kPa and considering both the available triaxial tests and the stress-strain($(\sigma_1 - \sigma_3) - \varepsilon_a$) curves obtained from the Duncan-Chang model.

ECAM (Extended Cam Clay) model

The model needs the following additional parameters:

Total specific volume defined as:

$$V_{tot} = 1 + e_0$$

λ and χ (normal consolidation and overconsolidation) parameters defined as $\lambda = C_c/2.3$ and $\chi = C_r/2.3$ where C_c and C_r are the compression and re-compression indices. These indices are obtained from σ'_c- e curves of Theme B2 specifications (Annex 6).

Moreover, a cohesion of 10 kPa has been assumed for satured conditions.

In the table shown in the next page, the values of the parameters adopted in the analyses are reported.

In the seepage analysis the Specific Storage coefficient has also to be evaluated:

$$S_s = gg\ [(1 - n)\ \alpha + n\beta]$$

where

$\alpha = 1/B$

B = volumetric deformation modulus

β = water compressibility (4.8 E -07 1/kPa)

n = porosity

The values of S_s computed and calibrated on the basis of preliminary analyses are:

Core	1.0E -03	1/m
Filtres	1.0E -03	1/m
Trans. Zone	1.0E -03	1/m
Rockfill	1.0E -04	1/m

Finally, the ratio between horizontal and vertical permeabilities has been assumed equal to $K_h/K_v = 4$.

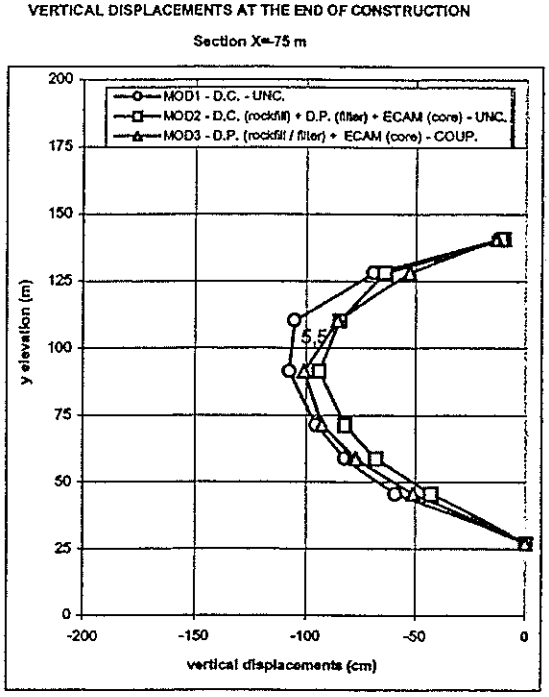

Fig. 6a

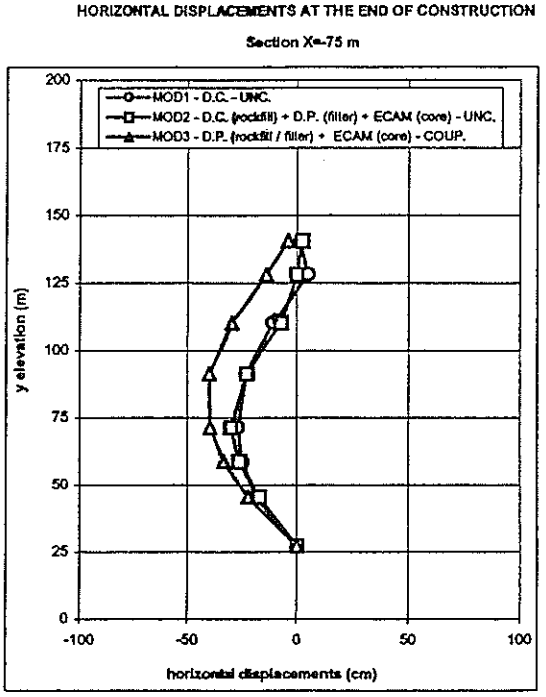

Fig. 6b

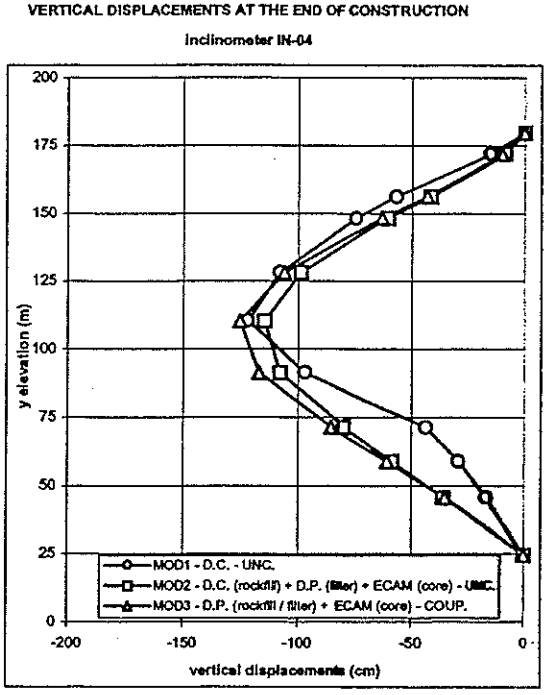

Fig. 7a

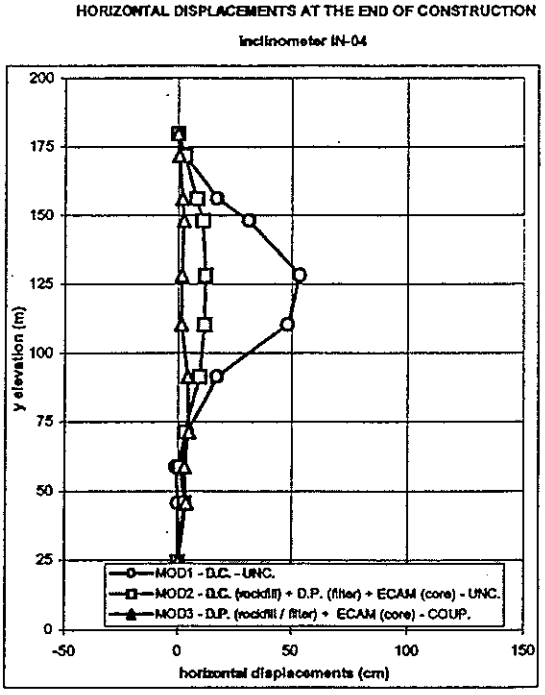

Fig. 7b

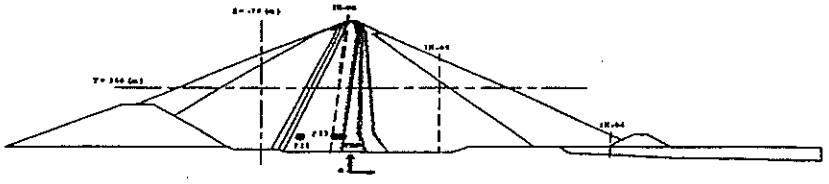

VERTICAL DISPLACEMENTS AT THE END OF CONSTRUCTION

Inclinometer IN-05

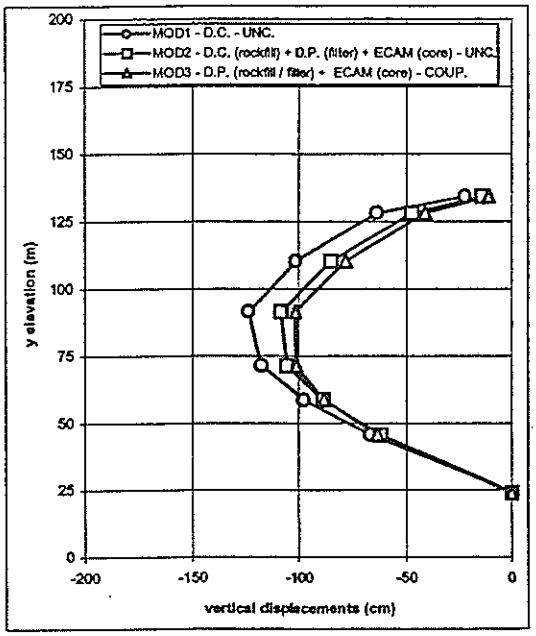

Fig. 8a

HORIZONTAL DISPLACEMENTS AT THE END OF CONSTRUCTION

Inclinometer IN-05

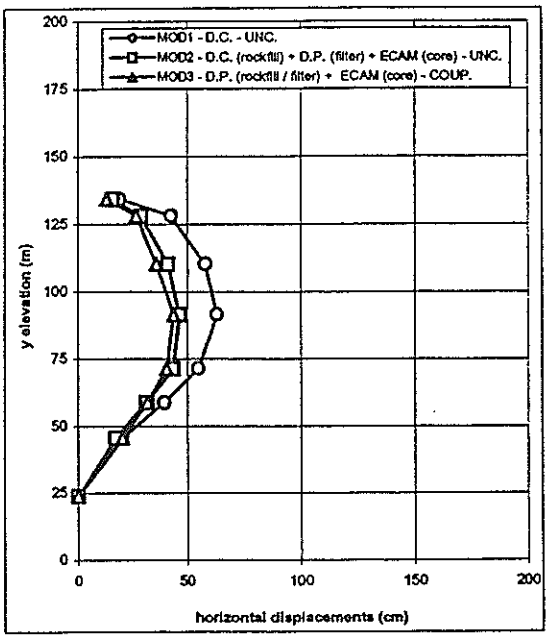

Fig. 8b

VERTICAL DISPLACEMENTS AT THE END OF CONSTRUCTION

Section Y=100 m

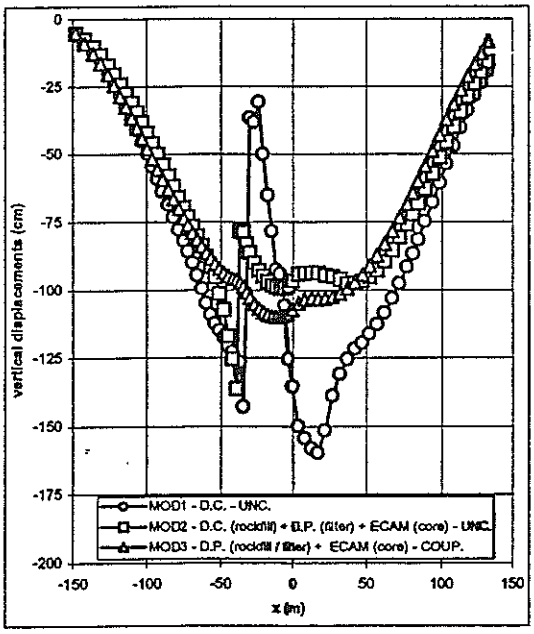

Fig. 9a

HORIZONTAL DISPLACEMENTS AT THE END OF CONSTRUCTION

Section Y=100 m

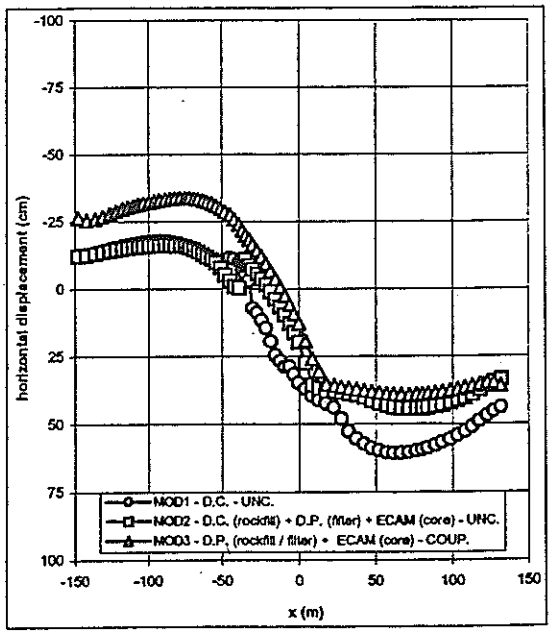

Fig. 9b

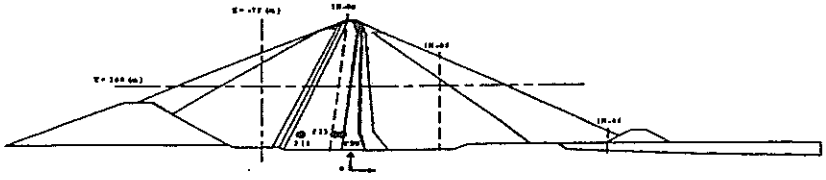

POST CONSTRUCTION - HORIZONTAL DISPLACEMENTS AT THE END OF FIRST IMPOUNDING - MOD3 - vertical sections

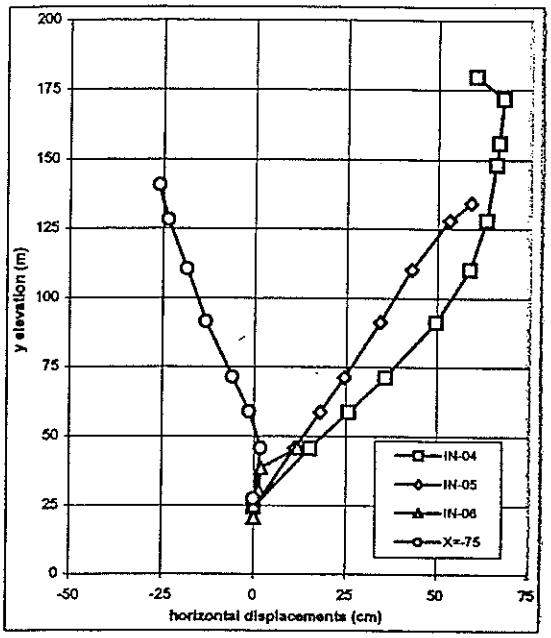

Fig. 10a

POST CONSTRUCTION - VERTICAL DISPLACEMENTS AT THE END OF FIRST IMPOUNDING - MOD3 - vertical sections

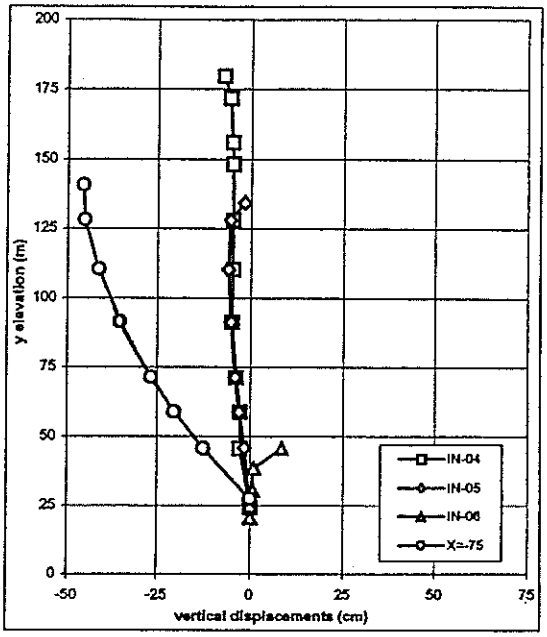

Fig. 10b

POST CONSTRUCTION - HORIZONTAL DISPLACEMENTS AT THE END OF FIRST IMPOUNDING - MOD3 - horizontal section at Y=100 m

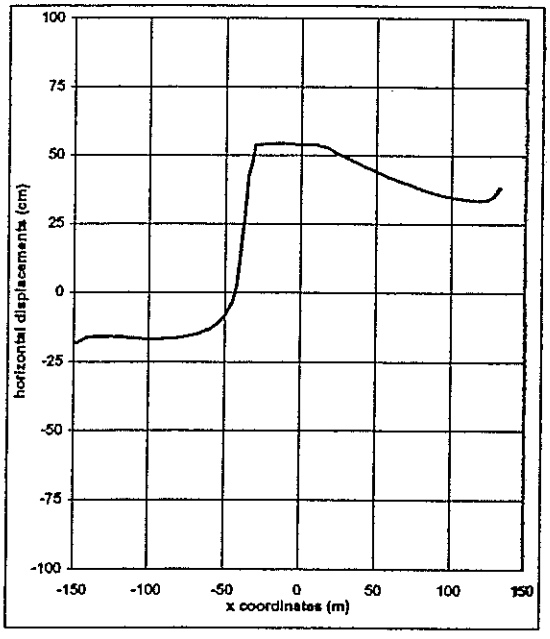

Fig. 11a

POST CONSTRUCTION - VERTICAL DISPLACEMENTS AT THE END OF FIRST IMPOUNDING - MOD3 - horizontal section at Y=100 m

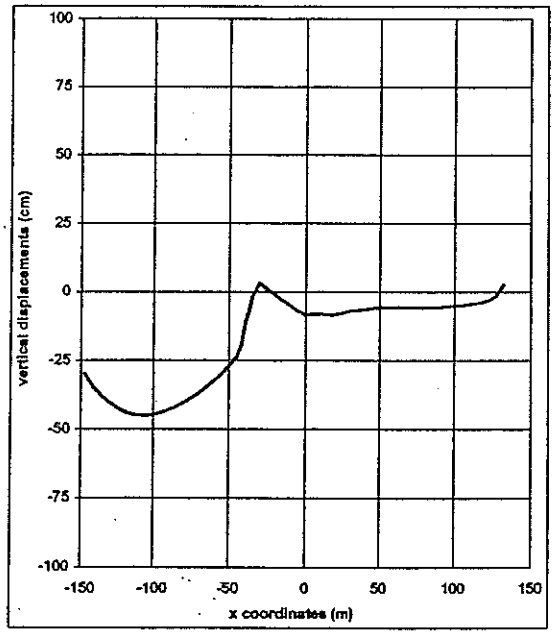

Fig. 11b

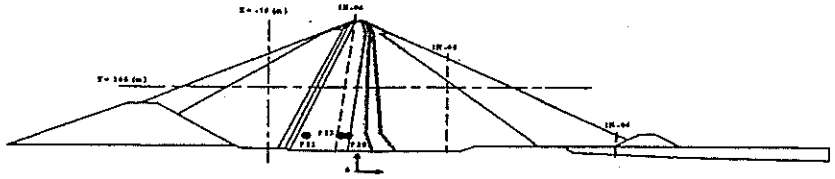

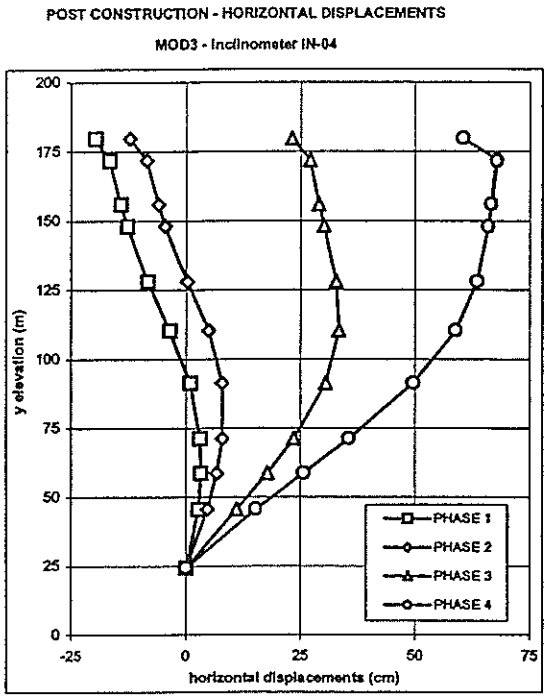

Fig. 12a

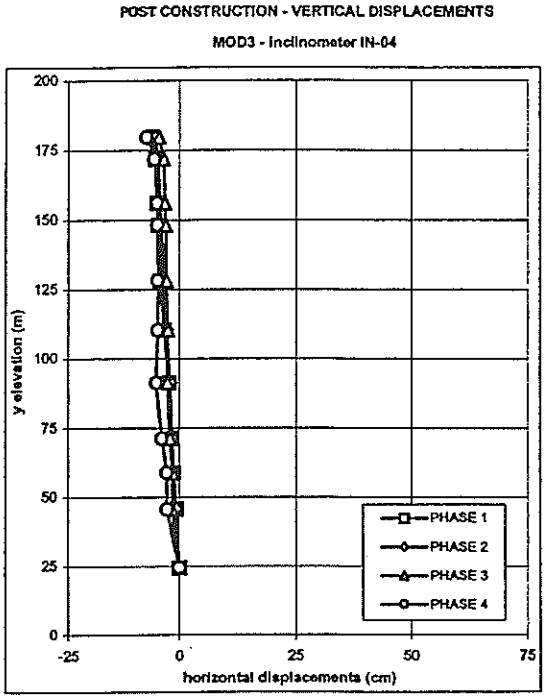

Fig. 12b

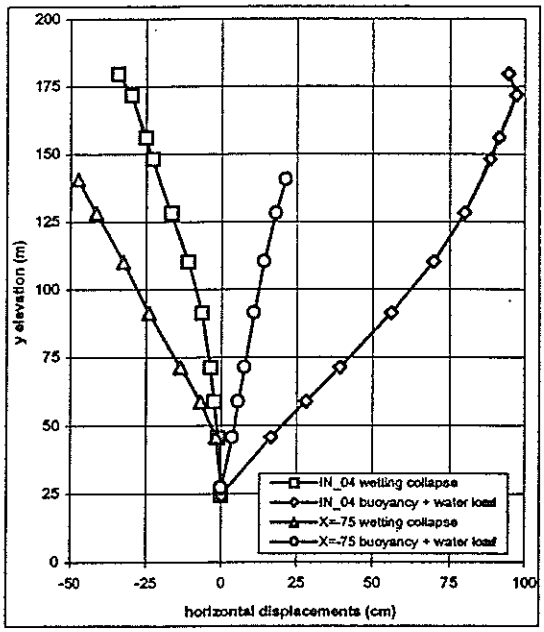

Fig. 13a

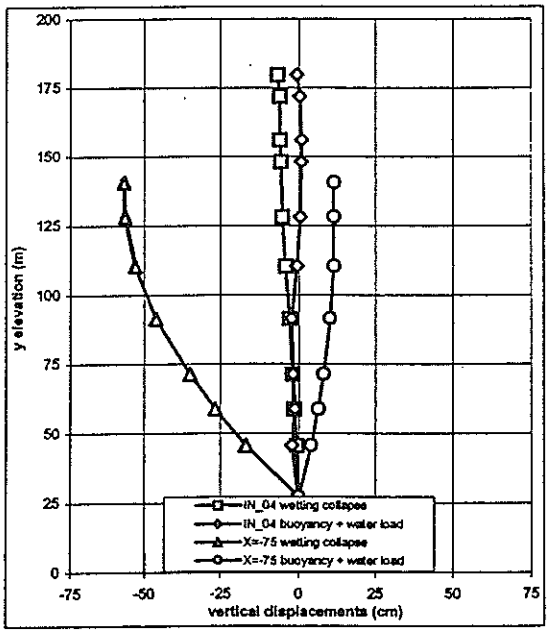

Fig. 13b

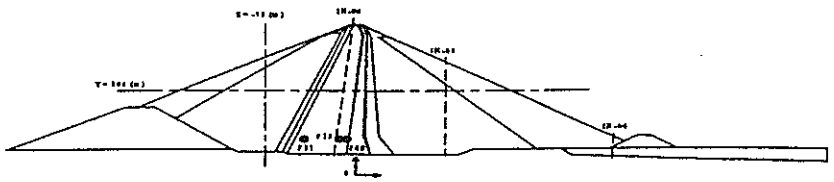

5th. ICOLD BENCHMARK WORKSHOP - 1999 - THEME B2

PROGRESSION OF HYDRAULIC HEAD SINCE THE END OF CONSTRUCTION

SEEPAGE MODEL

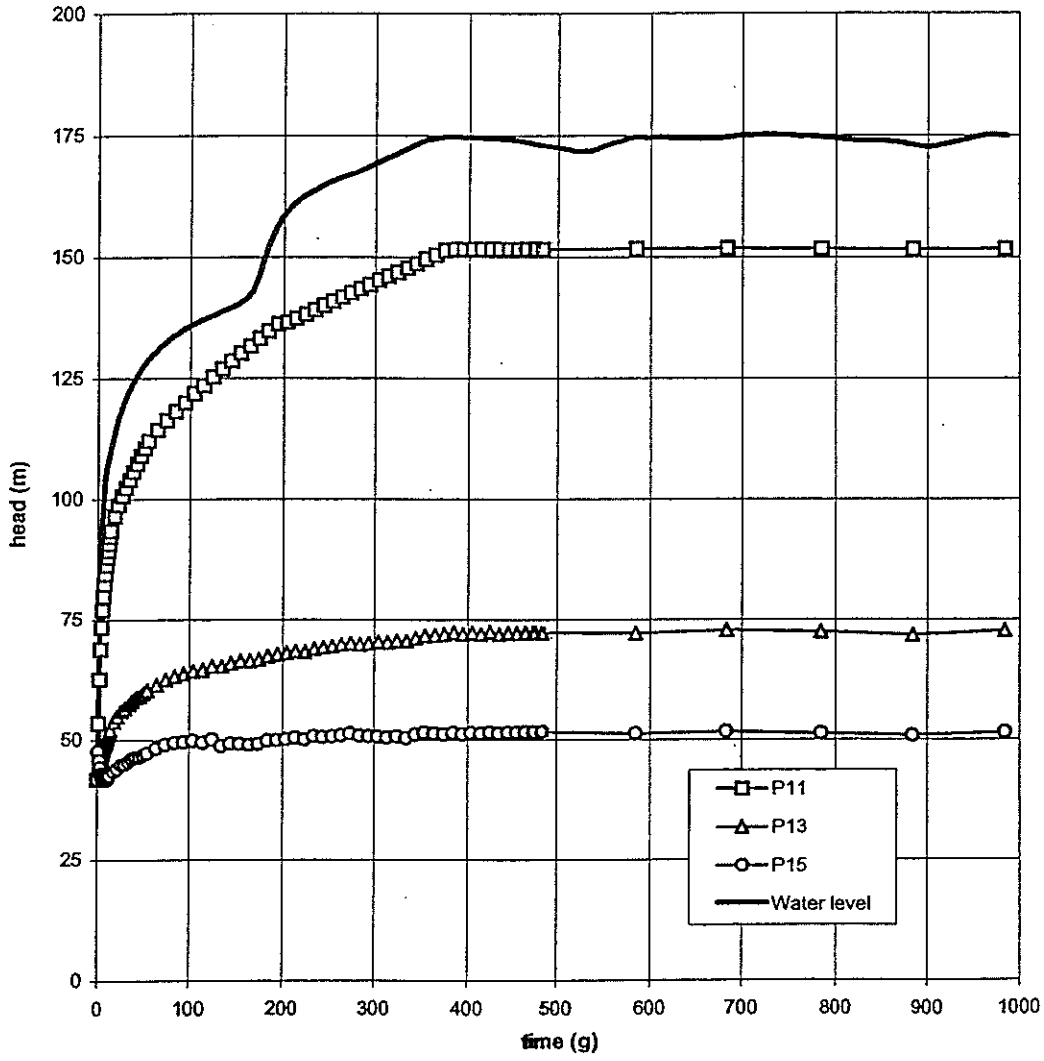

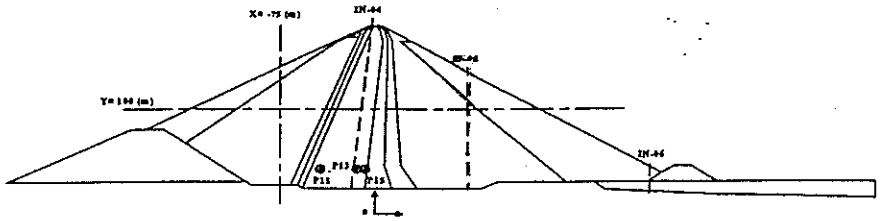

Fig. 14

EFFECTIVE VERTICAL STRESS AT END OF CONSTRUCTION

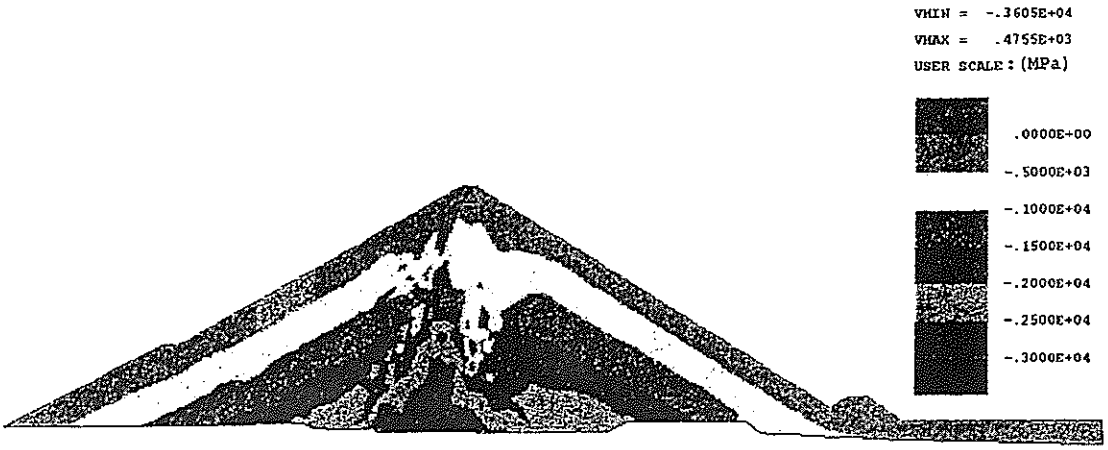

MOD1 - DUNCAN CHANG - UNC.

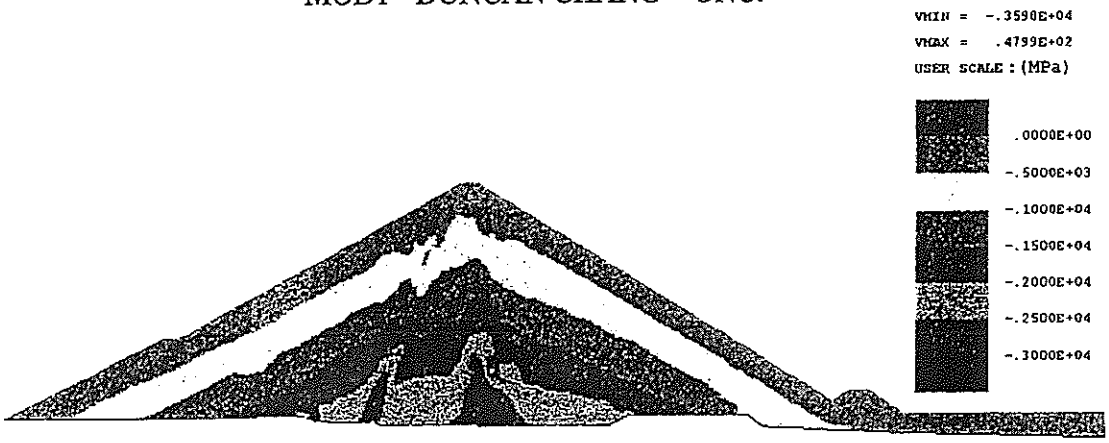

MOD2 - D.C. (rockfill) + D.P. (filter) + ECAM (core) - UNC.

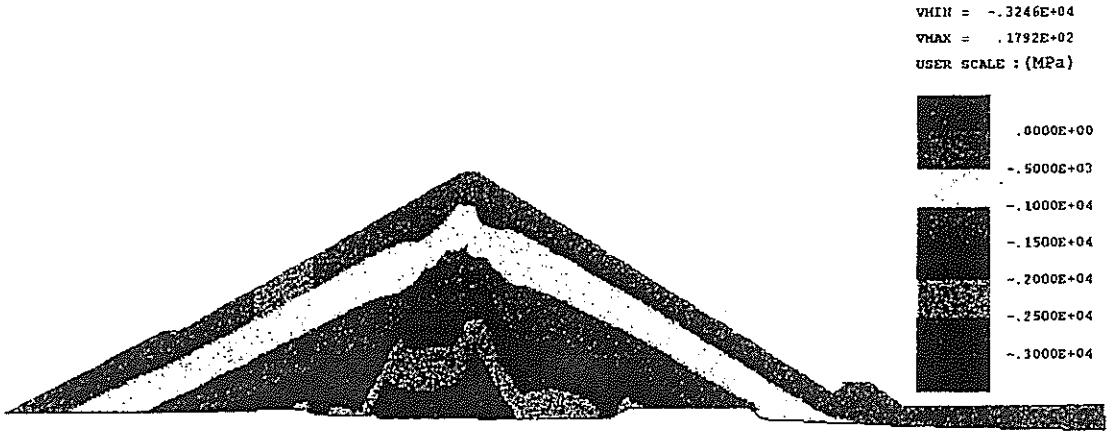

MOD3 - D.P. (rockfill/filter) + ECAM (core) - COUP.

Fig. 15

5th. ICOLD Benchmark Workshop - Theme B2

EFFECTIVE HORIZONTAL STRESS AT END OF CONSTRUCTION

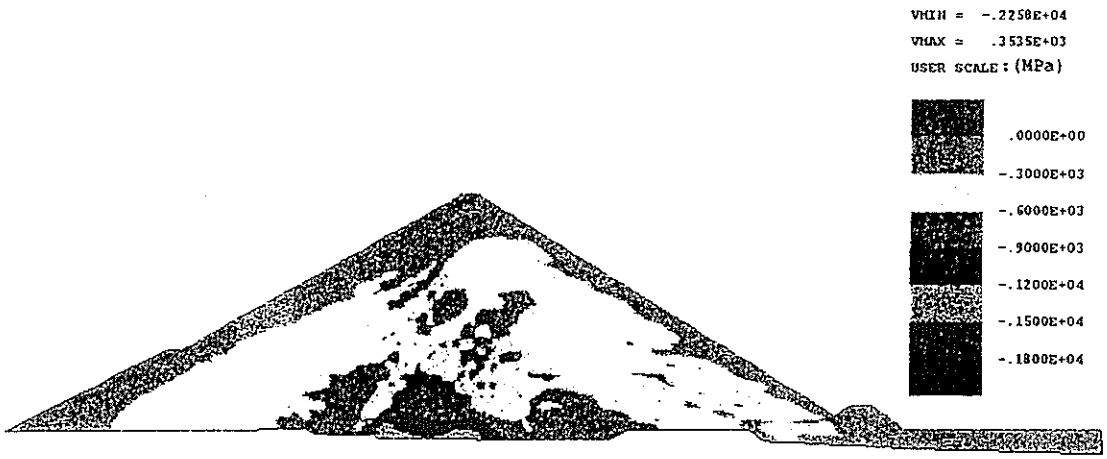

MOD1 - DUNCAN CHANG - UNC.

MOD2 - D.C. (rockfill) + D.P. (filter) + ECAM (core) - UNC.

MOD3 - D.P. (rockfill/filter) + ECAM (core) - COUP.

Fig. 16

5th. ICOLD Benchmark Workshop - Theme B2

MOD3 - D.P. (rockfill/filter) + ECAM (core)

Post construction displacements at the end of first impounding

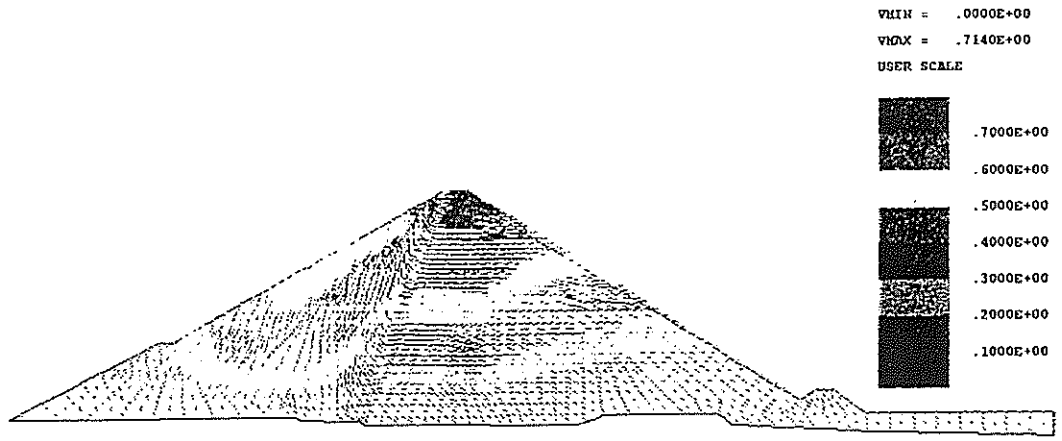

Displacaments Vectors

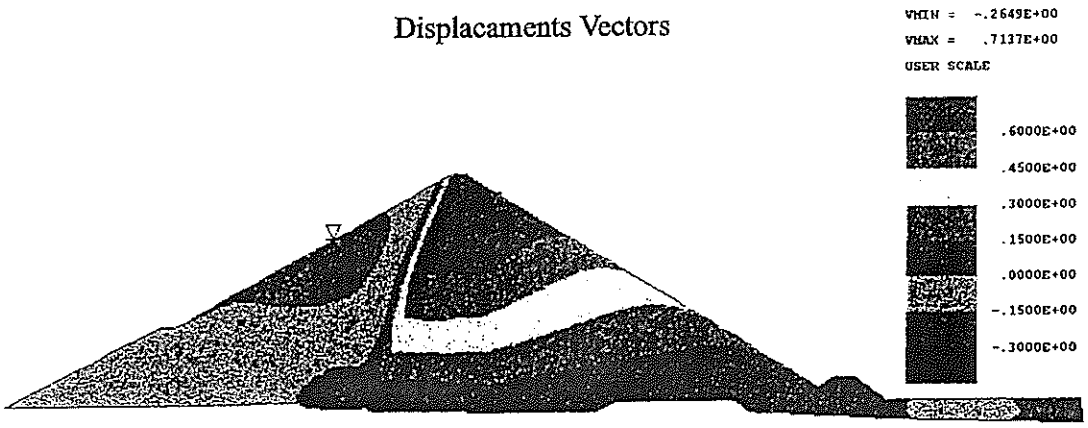

Horizontal Displacements

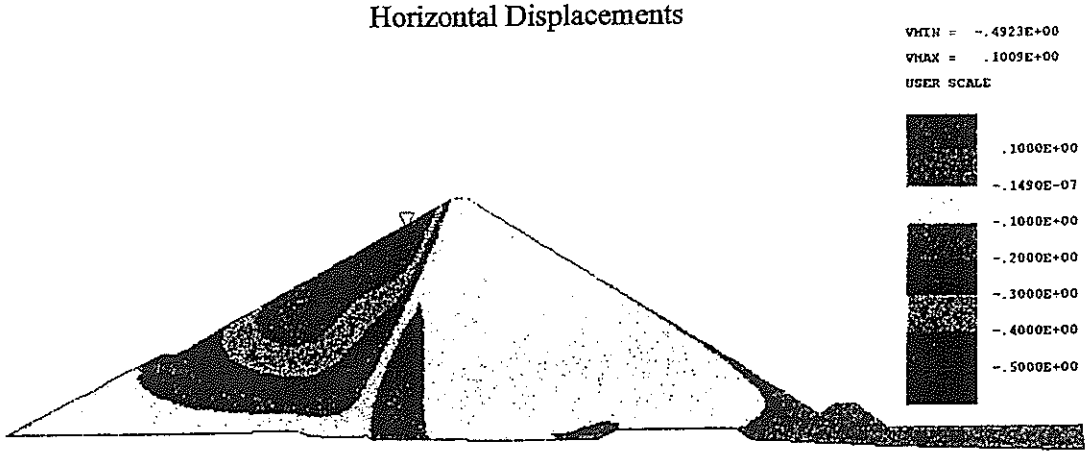

Vertical Displacements

Fig. 17

5th. ICOLD Benchmark Workshop - Theme B2

MOD3 - D.P. (rockfill/filter) + ECAM (core)

Post construction stress at the end of first impounding

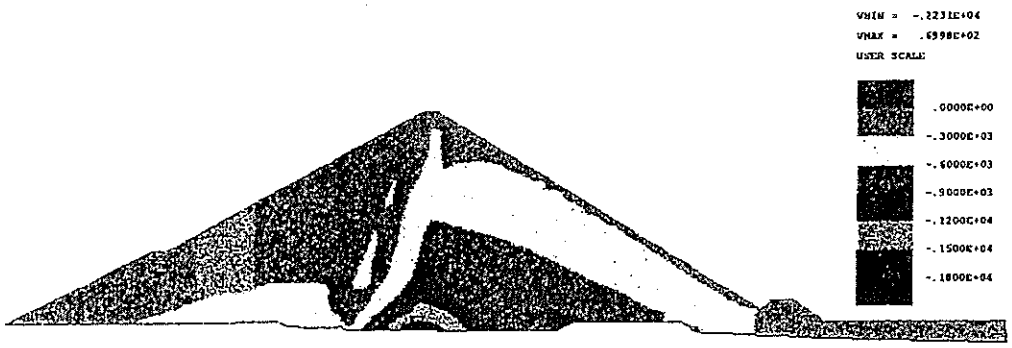

Effective Horizontal Stress

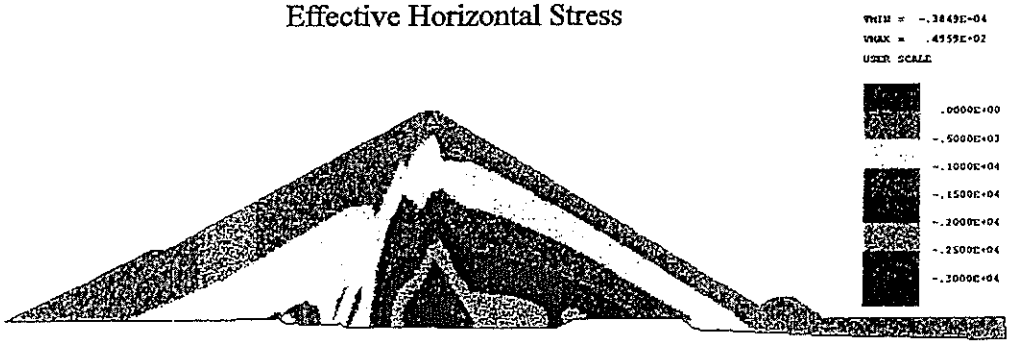

Effective Vertical Stress

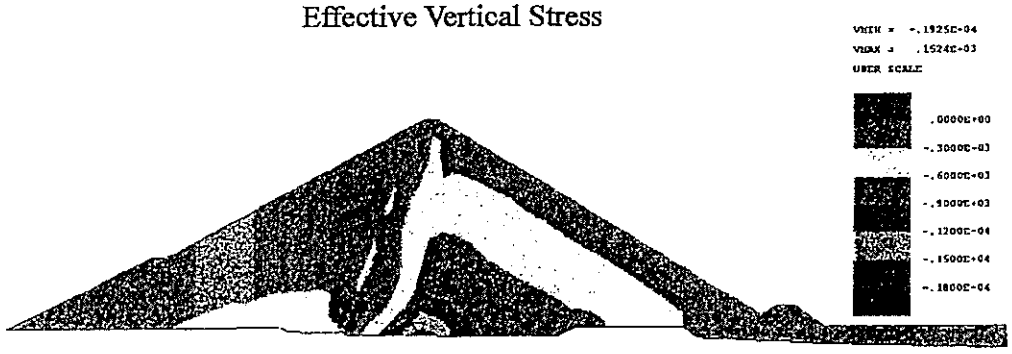

Effective Principal Max Stress

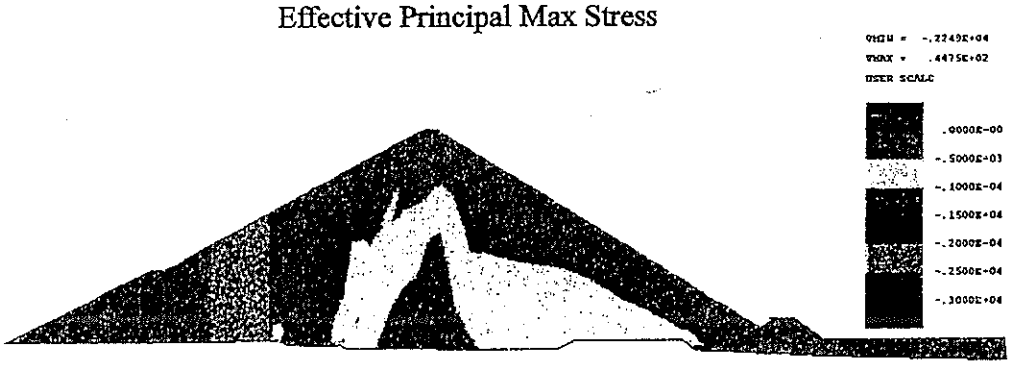

Effective Principal Min Stress

Fig. 18

tend initially to grow due to the reduction in void ratio induced by the overburden weight and, subsequently, to reduce because of both the stiff response of soil skeleton that does not allow further increments in positive pore pressure and the high permeability of the medium that facilitates a downward oriented seepage through the core. At the end of impounding the pore pressure field coincides with the one at steady state.

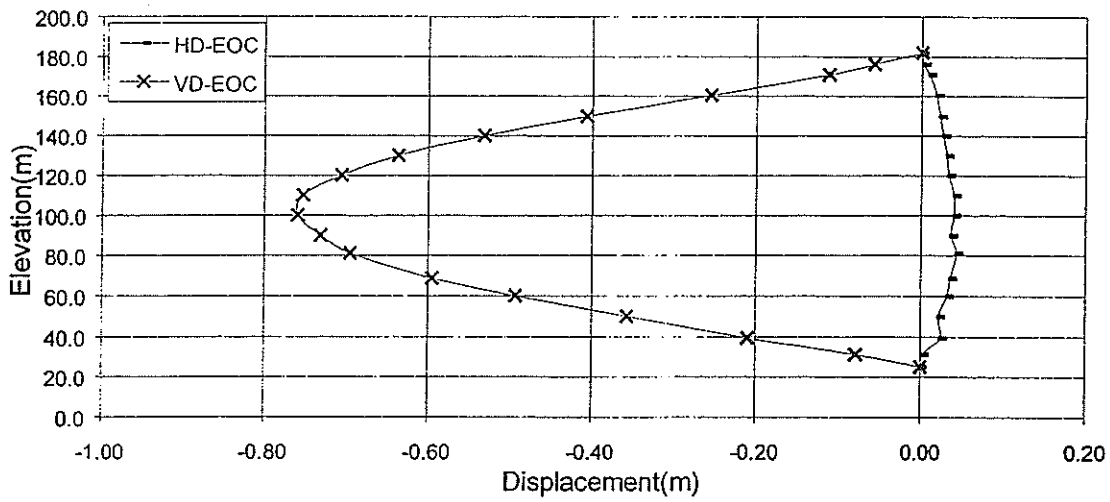

Fig.1. Inclinometer IN-4: Displacement at the End of Construction

on PC Workstation PENTIUM 450 XEON (500 Mb RAM, 9GB HD). The run time has been of about 3 hours.

MODEL PARAMETERS

The problem has been simplified by assuming for the filters, transitions and rockfills the same mechanical and physical properties, except the soil unit weight.

slope of critical state line, M	1.5048
Normal compression index, λ	0.00926
Swelling-recompression index, κ	0.00250
Poisson's ratio, ν	0.30
size of the yield locus, p'_{co} (kPa)	640
initial saturation degree, S_{ro}	0.82
residual pore water pressure, u_{w0} (kPa)	-200
residual mean effective stress, p'_o (kPa)	164
initial void ratio, e_o	0.240
permeability coefficient, k (Sr=1) (m/s)	$4 \cdot 10^{-7}$
dry unit weight, γ_d (kN/m^3)	21.07

Table 1 - Physico-mechanical parameters of the core

Parameters have been derived from the experimental triaxial compression curves obtained on rockfill of EL-Infiernillo shoulders. For the core the parameters of table 1 have been obtained from the experimental results provided by the benchmark promoters.

RESULTS

The results are plotted in Figs 1-9 according to requirements of the benchmark promoters.
Collapse effects during the first impounding were not simulated because there were not enough experimental data about the sensitivity of mechanical properties of rockfill to saturation. The displacement field during impounding remains unchanged (Figs.1 to 8), because collapse was not taken into account and also because construction materials are very stiff when subjected to elastic swelling. During construction piezometric heads at elevation 43 m (Fig.9)

proportional to pore pressure when pore pressure exceeds the atmospheric pressure (Pagano, 1997). This strategy was proven to induce pore pressure values very close to zero at the boundary under saturated conditions and was successfully verified (Pagano,1997) in predicting the saturation line through a homogeneous earthfill dam.

MODELING OF ROCKFILL BEHAVIOUR

The very high permeability of rockfill materials used for the shells permits to hypothesize free draining behavior, and, consequently, to follow a uncoupled approach (equilibrium + stress-strain relationship) where only soil skeleton behavior is accounted for. A elastoplastic isotropic hardening stress-strain relationship has been used. The yield locus is a straight line in the q-p' plane that, when forced to rotate due to stress changes, produces deviatoric plastic strain. Therefore, the hardening law relates the slope of the yield locus to the accumulated deviatoric plastic strain.

DISCRETIZATION OF THE PROBLEM

For the shells 8-node isoparametric reduced integration elements (quadratic displacements) were used; while for the core, where the analysis is coupled, the additional degree of freedom pore pressure is defined at the corner nodes (quadratic displacements, linear pore pressure). The finite element mesh is made of 906 elements and 2873 nodes. A staged construction has been carried out by progressively activating 17 layers with time, according to the experimental fill level versus time relationship. Each layer is made of two or three rows of elements.
Impounding stages have been simulated after the analysis of construction stages. At a given stage of impounding the real pore pressure distribution has been applied on the upstream boundary of the core. The core foundation has been assumed impermeable while the not wetted core boundary has been modeled as a seepage surface (see above the relationship between v_n and u_w). The full water level has been reached in 30 steps, each of one carried out in a time obtained from the curve of the water level versus time.

ANALYSIS TOOLS

The analysis of construction and impounding stages has been carried out by using the finite element code ABAQUS, running

$$\sigma' = \sigma - S_r u_w \mathbf{I} \qquad (1)$$

where:
σ=total stress tensor
S_r=degree of saturation
u_w=pore water pressure
$\mathbf{I}$=unit tensor
A Modified Cam-Clay type stress-strain relationship has been used.
The water retention characteristic curve has been assumed to linearly relate the point expressing the initial conditions in terms of degree of saturation S_{r0} and suction u_{w0} to the point S_r=1 - u_w=0.

Initial state and boundary conditions

Important features of a coupled analysis such as that just described are the definition of the initial values of pore pressures and stress components, as well as of appropriate hydraulic boundary conditions.

The assignment of initial values of pore pressures is problematic, due to the uncertain knowledge of suction acting within the soil when placed (usually not measured) and the extreme sensitivity of the prediction to this variable. The weight of the placed soil is treated like an external load, so that total stress components are initially set to zero. Initial values of negative pore pressure u_{w0}, degree of saturation S_{r0} and effective stress σ'_{i0} components have to be in equilibrium, so that, according to (1) it follows that:

$$\sigma'_{x0} = \sigma'_{y0} = \sigma'_{z0} = -S_{r0} u_{w0} \qquad (2)$$

During numerical simulation of construction and impounding stages care must be taken in modifying the hydraulic boundary conditions consistently with the pore pressure changes occurring at the boundary itself. The hydraulic conditions at the core boundary are uniquely defined only at the impervious foundation and along the part of the lateral boundary wetted by the reservoir. Along the remaining boundary null flow rate must be assumed while pore pressure is negative, and null pore water pressure must be forced if pore pressure values tend to exceed the atmospheric pressure. An effective method to simulate this behavior is to relate at the boundary the flow rate v_n to the current value of pore pressure u_w, by assuming that flow rate is equal to zero when pore pressure is negative, and

PREDICTION OF THE BEHAVIOR OF A ZONED EARTH DAM DURING CONSTRUCTION AND IMPOUNDING

L. Pagano*, A. Desideri+, F. Vinale**, F. Sorvillo++

This paper summarizes the theory and numerical tools used for the prediction of the LG-2 dam behavior during construction and impounding stages. A coupled approach has been assumed for the core while filters, transitions and shells have been analyzed following a uncoupled approach, according with their high permeability determining a free draining behavior. Details are provided about initial conditions and hydraulic boundary conditions defined within the core consistently with the set of differential equations assumed, which take into account the initial unsaturated state of the material.

MODELING OF CORE BEHAVIOR

Set of governing equations

The core has been modeled by using a coupled unsaturated approach consisting of the solution of the following set of equations:

- soil equilibrium equation
- water continuity equation
- water retention characteristic curve (i.e. relationship between degree of saturation S_r and pore pressure u_w)
- stress-strain constitutive equation

Air continuity equation is eliminated by the assumption of air pressure constantly equal to the atmospheric pressure. In this case the degree of saturation remains as field variable in the water continuity equation, ensuring, for $S_r<1$, a dependence of soil compressibility on the slope of the water retention characteristic curve. The stress-strain relationship is defined referring to a "single" effective stress tensor σ' defined as:

* PhD,, Dipartimento di Ingegneria Geotecnica, Universitàdi Napoli "Federico II", Via Claudio 21, 80125 Naples, Italy
+ Prof., Dipartimento di Ingegneria Geotecnica, Universitàdi Napoli "Federico II", Via Claudio 21, 80125 Naples, Italy
** Prof., Dipartimento di Ingegneria Strutturale e Geotecnica, Universitàdi Roma "La Sapienza", Via Montedoro 28, 00196 Rome, Italy
++ Student, Dipartimento di Ingegneria Geotecnica, Universitàdi Napoli "Federico II", Via Claudio 21, 80125 Naples, Italy

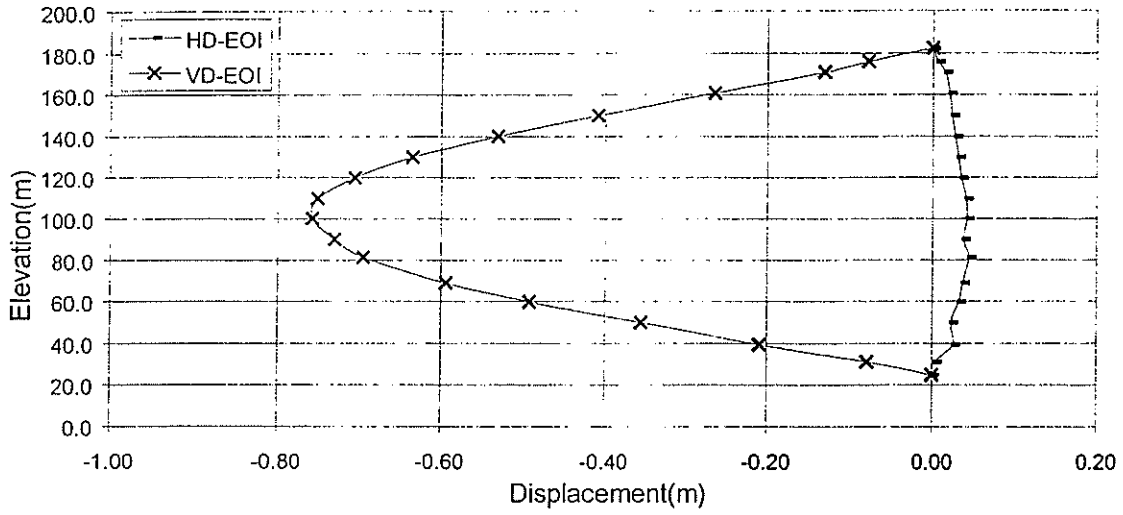

Fig.2. Inclinometer IN-4: Displacement at the End of Impounding

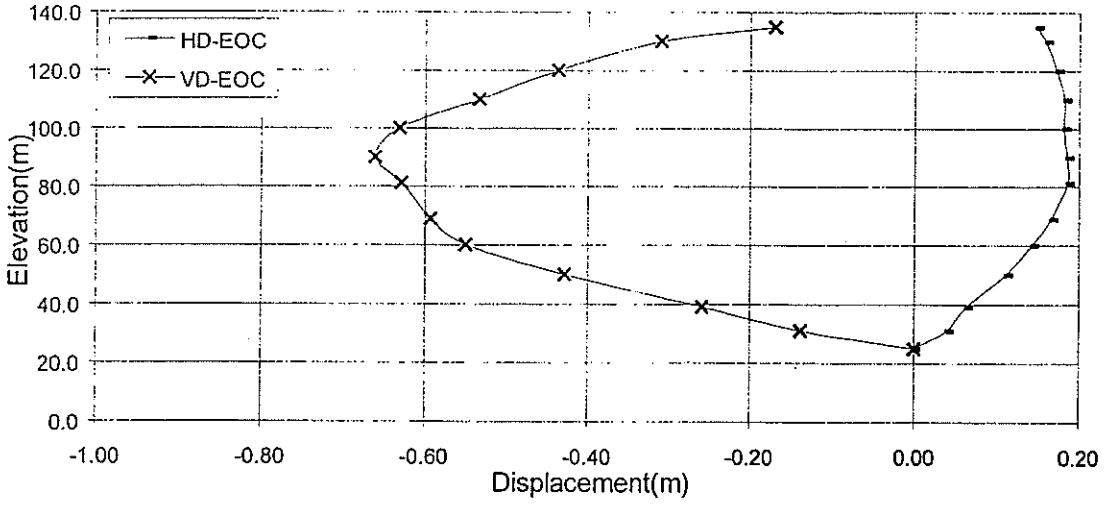

Fig.3. Inclinometer IN-5: Displacement at the End of Construction

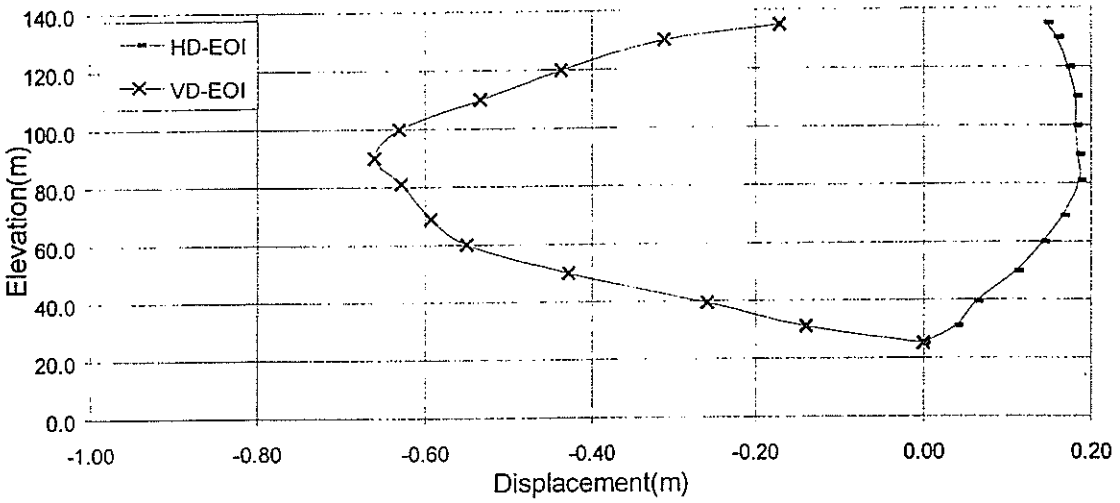

Fig.4. Inclinometer IN-4: Displacement at the End of Impounding

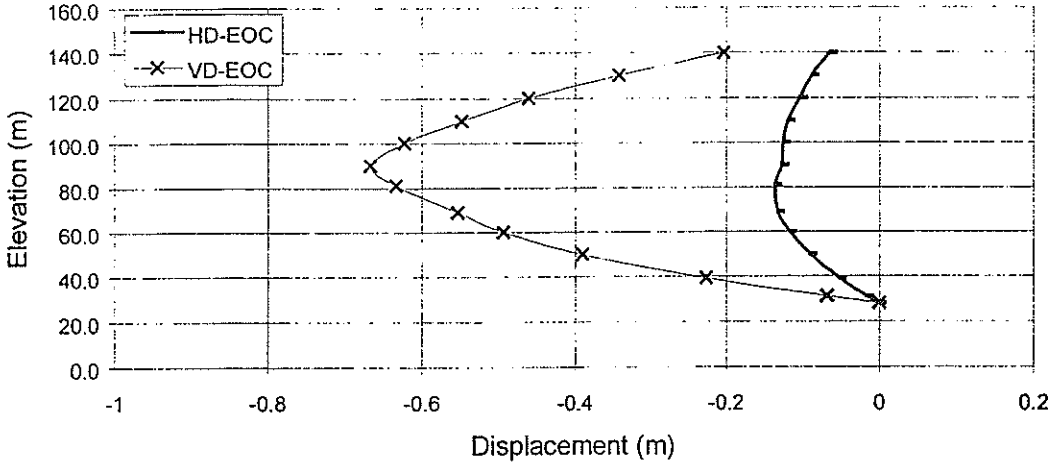

Fig.5. Displacement along vertical line V-V (x=-75.0 m) at the End of Construction

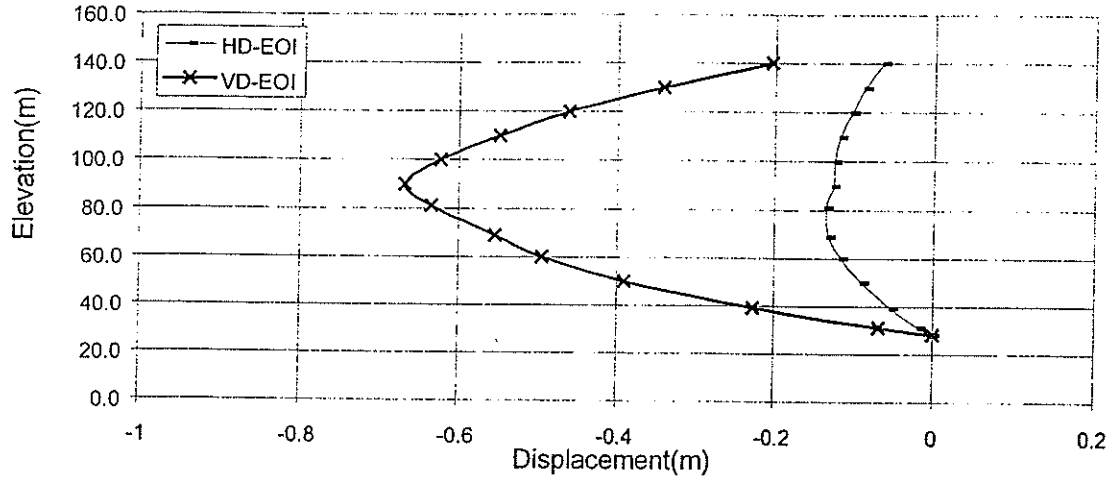

Fig.6. Displacement along vertical line V-V (x=-75.0 m) at the End of Impounding

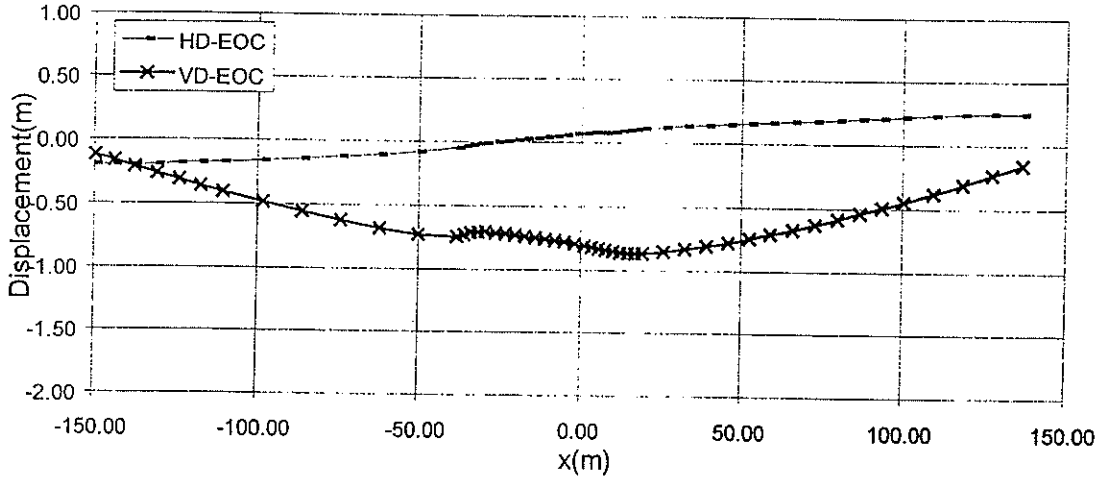

Fig.7. Displacement along horizontal line H-H (y=100 m) at the End of Construction

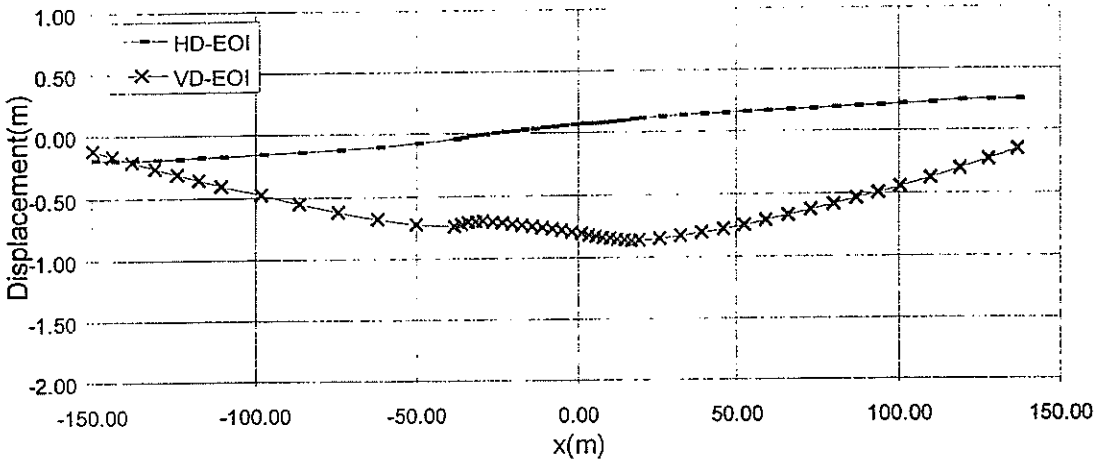

Fig.8. Displacement along horizontal line H-H (y=100 m) at the End of Impounding

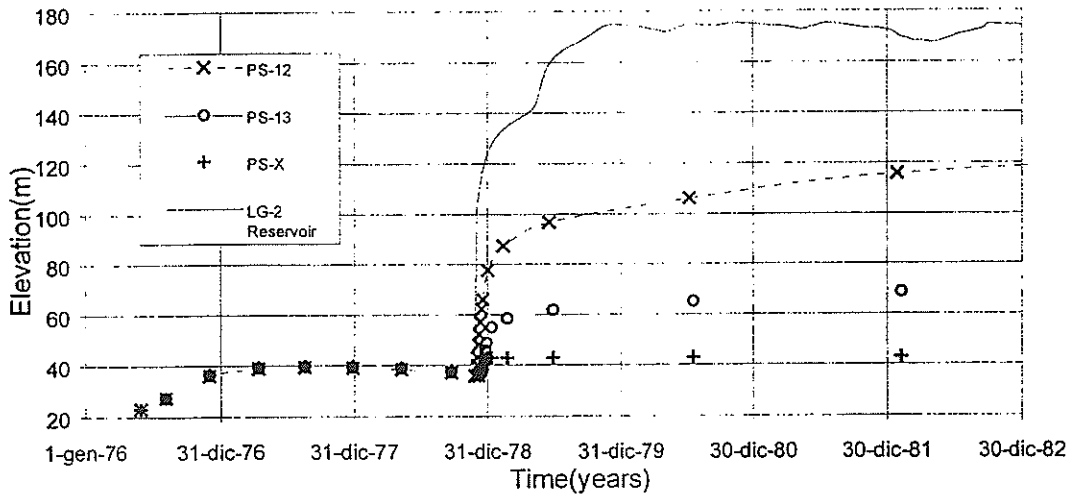

Fig.9. Piezometric response under construction stages

REFERENCES

PAGANO L. **Steady state and transient unconfined seepage analysis for earthfill dams.** *Proc. VIII ABAQUS Users' Conference. Milano,* 1997

HYDRO-PLASTIC ANALYSIS OF LG-2 ROCKFILL DAM DURING CONSTRUCTION AND IMPOUNDING STAGES

Patrice Anthiniac [1,2] Stéphane Bonelli [1] Olivier Débordes [2]

INTRODUCTION

This contribution to the theme B2 of the Fifth Benchmark Workshop on Numerical Analysis of Dams presents a fully coupled hydro-mechanical analysis of the construction and impounding stages of the LG-2 rockfill dam. The originality of this contribution lies in the physical model used : the hydroplastic model. This model has been developed to solve the problem of rockfill collapse modelling. A correct simulation of settlements in upstream shell during impounding is the main objective of this analysis.

THE PHYSICAL MODEL

Modelling collapse of rockfill material with the hyperbolic model (Duncan & Chang 1970) or other models requires a change in modulus. For one material, two sets of parameters are considered (dry and wet). The procedure used to change modulus gives acceptable results but is not scientifically lawful. We propose to simulate the global rockfill behavior (dry-wet) with one single set of parameters, using a new constitutive model : the hydroplastic model.

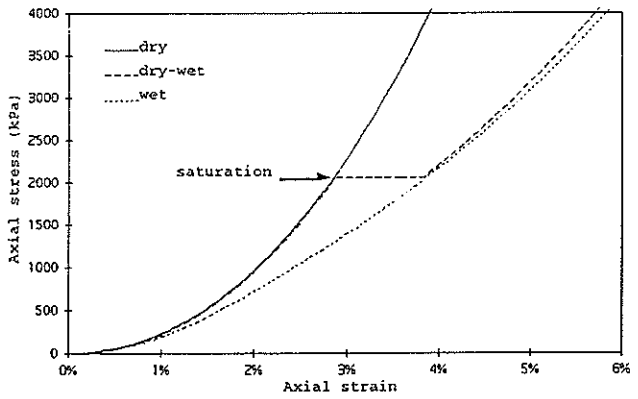

Figure 1. Influence of saturation on oedometric path; Phenomenon of rockfill collapse.

[1] Cemagref, Hydraulics and Irrigation Engineering Research Unit
Le Tholonet BP 31, 13612 Aix-en-Provence - France
[2] Laboratory of Mechanic and Acoustic, Numerical Model Unit
ESM2/IMT Technopôle de Château-Gombert 13451 Marseille Cedex20 - France

The hydroplastic model is an elastoplastic model based on the C.J.S. model (Cambou 1988) developed for granular materials. The C.J.S. model is composed by :

- a non-linear elasticity;
- two plastic mechanisms (deviatoric and spheric);
- the characteristic state concept;
- a non-linear isotropic hardening associated with each plastic mechanism.

Hydric state effect and characteristics of rockfill mechanical behavior described below are introduced in the C.J.S model :

- a decreased secant angle of friction with water;
- a decreased consolidation pressure with water;
- an increased compressibility with water;
- a curved failure envelope;
- the phenomenon of particle crushing in contact areas.

The relationship suggested by Barton (Barton 1981) is used to take into account the curved failure envelope. This relationship, initially developed for rock joints, is completed with the hydric state effect :

$$\varphi_r' = \varphi_b' - R\log\left(\frac{\sigma_n - u}{\sigma_c^*}\right) \quad , \quad \sigma_c^* = d(1-\alpha S_h)\sigma_{c0}$$

where σ_n is the total normal stress, u the pore pressure and S_h the hydric state of block surface (0 = dry ; 1 = wet).

Each parameters has a physical meaning associated with :

- the parent rock
  - φ_b' : basic angle of friction
  - σ_{c0} : dry uniaxial compressive strength
  - $1-\alpha$: ratio between saturated and dry strength

- the shape and the arrangement of the blocks
  - d : parameter dependent on gradation
  - R : parameter dependent on porosity and angularity

Lade (Lade 1996) has evaluated the degree of grain breakage for sand under high stresses from the plastic work. The same argument is used to estimate particle crushing in contact areas for rockfill materials. Consequences of grain crushing on mechanical behavior are introduced in the model using a theory developed by Hicher (Daouadji & Hicher 1997). The hydric state effect is added :

Consolidation pressure :

$$p_c = \left(1 - \beta \; X \; S_h\right) p_{c0} \qquad , \qquad X = \frac{W_p^d}{B + W_p^d}$$

$W_p^d = \int \sigma : d\varepsilon_p^d$: deviatoric plastic work

X : mobilization of grain crushing

β, B : parameters (hydric state influence).

MAIN ASSUMPTIONS FOR COUPLED ANALYSIS

• The mesh used for the mechanical problem was the mesh suggested for the Workshop. Only the core mesh was used for the hydraulical problem.

• 5 types of materials were used : moraine of the dam core, filters, transitions, rockfills and downstream toe alluvium.

• The constitutive model of the materials was the hydroplastic model described above, excepted for the downstream toe alluvium for which the Mohr-Coulomb model has been chosen.

• The initial degree of saturation in the core is 0.83, corresponding to a succion of 200kPa. The filters, transitions and rockfill materials are initially dry. The preconsolidation stress is 200kPa in the core and 100kPa in other materials.

• The boundary conditions are given in figure 2 and figure 3.

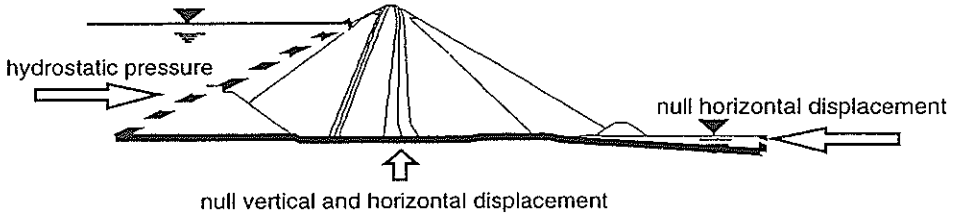

Figure 2. Mechanical boundary conditions.

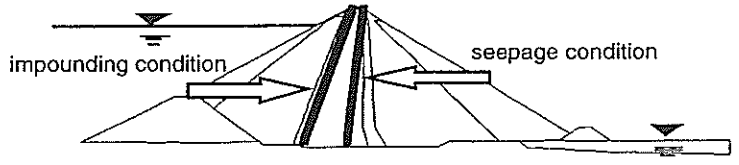

Figure 3. Hydraulical boundary conditions.

PARAMETERS CALIBRATION

Parameters calibration of C.J.S. model has been the subject of a detailed method (Cambou 1988). Barton relationship parameters are identified with abaqus and physical datas (Barton 1981).

Parameter α (water effect on secant angle of friction) is identified from dry and saturated triaxial tests. Parameters β and B (water effect on consolidation pressure and compressibility) are not easily identified from experimental tests and are evaluated on dams with back-analysis.

Application to the LG-2 case study :

Available datas are :
- drained triaxial tests and hyperbolic parameters for core and filter materials;
- hyperbolic parameters for transitions and rockfill.

Review of calibration methods used :

<table>
<tr><th>MATERIAL</th><th colspan="2">DEVIATORIC BEHAVIOR</th><th>SPHERIC BEHAVIOR</th><th>WATER EFFECTS</th></tr>
<tr><td></td><td>Failure</td><td>Stiffness</td><td>Compressibility</td><td></td></tr>
<tr><td>Core</td><td rowspan="5">Barton Abaqus</td><td colspan="2" rowspan="2">Curve fitting with experimental tests</td><td>No water effects</td></tr>
<tr><td>Filters</td><td rowspan="3">Calibration with dry and wet hyperbolic parameters (stiffness and friction angle)</td></tr>
<tr><td>Transitions</td><td>Curve fitting with triaxial responses of the hyperbolic model</td><td>Curve fitting with triaxial responses of the hyperbolic model (set 1) or with oedometric responses of the hyperbolic model (set 2)</td></tr>
<tr><td>Rockfill</td></tr>
</table>

Table 1. Parameters calibration method for LG-2 case study.

No water effect is taken into account for the moraine due to the material gradation (no particle crushing under stress range considered) and the initially wet condition.

For other materials, parameters describing water effects are identified from dry and wet hyperbolic parameters :

- α from dry and wet friction angles;
- β and B from dry and wet stiffness (adjusted on volume change of hyperbolic triaxial responses)

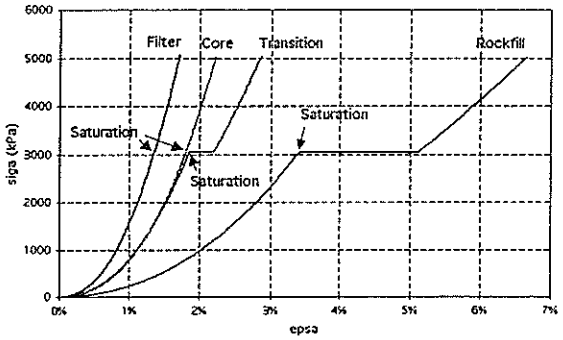

Figure 4. Oedometric test simulations - LG-2 materials - Saturation under constant axial stress 3MPa.

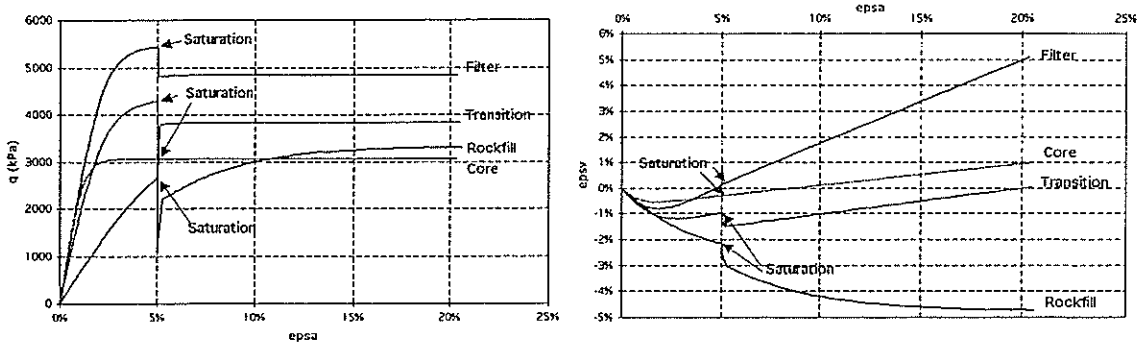

Figure 5. Triaxial test simulations - LG-2 materials - Confining pressure 1MPa - Saturation under constant axial strain 5%.

On figure 4, saturation doesn't seem to influence odeometric behavior of filters. In fact, only a water effect on secant angle of friction has been introduced. Material gradation involves no particle crushing under stress range used.

NUMERICAL MODEL

Continuum medium equations

The coupled numerical model is based on Terzaghi theory and on the principle of effective stresses (Bishop principle $\sigma_m=\sigma'_m-S_r u$). The main equations are given by the continuum

medium equations (traction is positive). The influence of the air-phase is omitted.

$$\begin{cases} \text{Equilibrium equation :} & \vec{\nabla}_x \cdot \vec{\vec{\sigma}} - ((1-n)\rho_s + nS_r\rho_w)g\vec{e}_y = \vec{0} \\ \text{Mass-conservation equation :} & n\rho_w \dot{S}_r + S_r\rho_w \dot{\varepsilon}^v + \vec{\nabla}_x \cdot \vec{\mathbf{m}} = 0 \end{cases}$$

The anisotropic Darcy law is introduced in the last term of the mass-conservation equation. The retention and relative permeability curves are of Van-Genuchten/Mualem type in unsaturated zones.

Numerical formulation for space and time discretization

The fully implicit Euler scheme and the Newton-Raphson method are used for both mass-conservation and equilibrium equations. Spatial integration is reduced. At each spatial integration point, the elastoplastic model is written as an ordinary differential equation. A five order explicit scheme of Dormand&Prince with adaptative time sub-steps is used (Bonelli 1993).

RESULTS AND DISCUSSIONS

Effective stresses

- The major principal effective stress is located in the base of the upstream filter at the end of construction.

- The weigth of rockfill shoulders is partially transferred to the adjacent filter zones due to the different compressibilities of the various zones in the dam. Rockfill shoulders are "hanging" on the core.

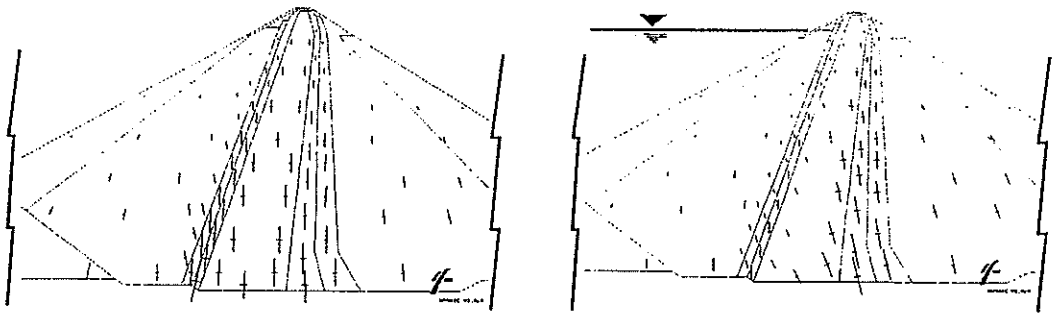

Figure 6. Principal effective stresses at the end of construction (left) and at the end of impoundment (right).

• During impounding, effective stresses are lower in the upstream part of the dam due to the pore pressure development. A load transfer occurs towards the core and the downstream filter. Highest vertical effective stress is located in the base of the downstream filter at the end of impounding.

Pore pressure

• During construction, no pore pressure development occurs in the core.

• The steady state is reached at the end of impounding. The free surface is located along the downstream face of the core.

Remark : the presence of air in the core is not considered.

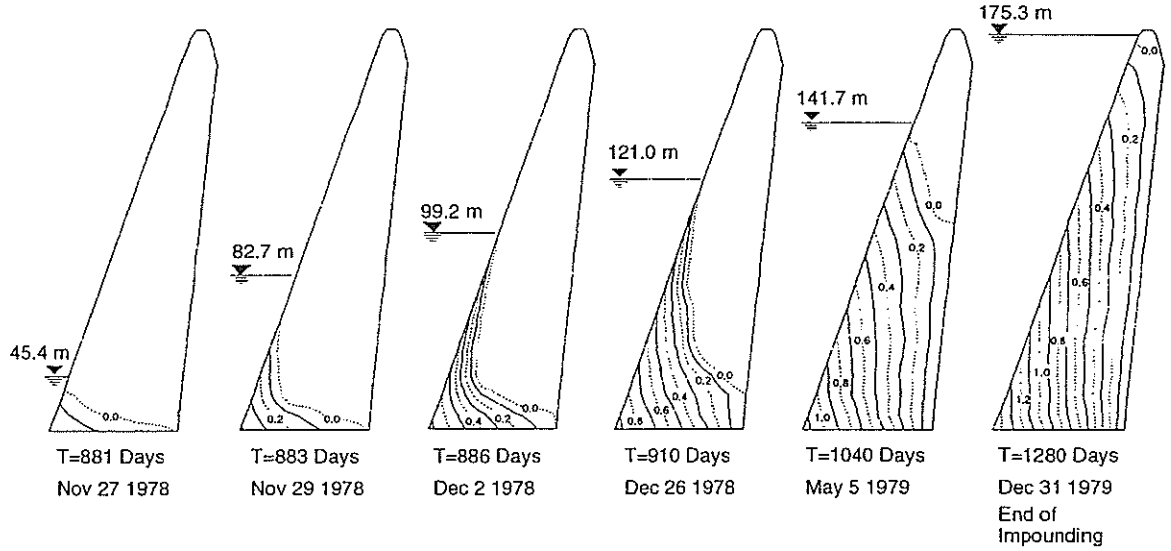

Figure 7. Pore pressure in the core (MPa) - Evolution with time during impoundment.

Displacements

• Settlements in the upstream shoulder during impounding

Considerable settlements occur in the upstream rockfill shell due to the collapse phenomenon. Maximal settlements occuring during impounding are about 50cm and are located in 2/3 of the height of the dam, on the upstream face.

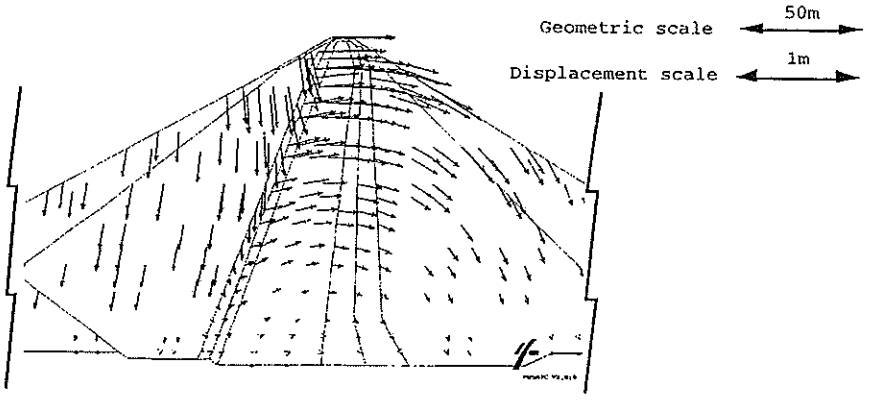

Figure 8. Displacement vectors during impounding (m)
(displacements = dis. at the end of impoudment - dis. at the end of construction).

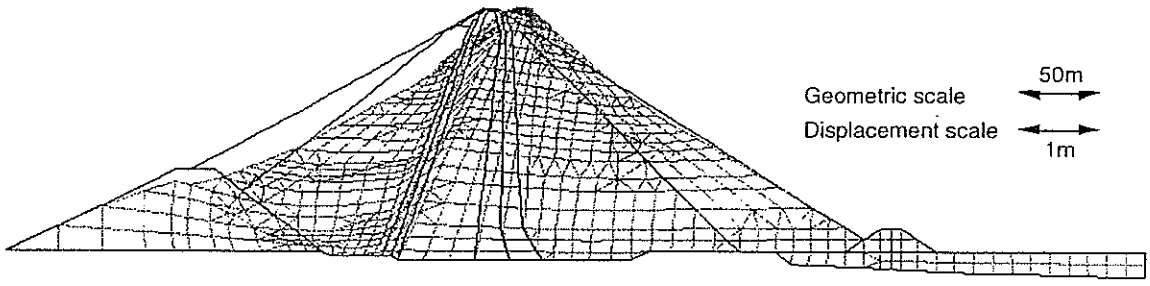

Figure 9. Deformed mesh
(displacements = dis. at the end of impoudment - dis. at the end of construction).

• Movements of the core during impounding

Initially the core was deflected towards the upstream side as a consequence of the additionnal settlements in the submerged parts of rockfill. When the water level was raised further, beyond midheight of the dam, increasing water pressure reversed the upstream movements so that finally, the core was pressed downstream of its original position.

About vertical displacements, at first, the crest settles due to the upstream shell collapse, then, in a second time, buoyancy forces cause an unloading. Differential settlements between the upstream side of the crest and the middle of the crest during impoundment can be observed on figure 10.

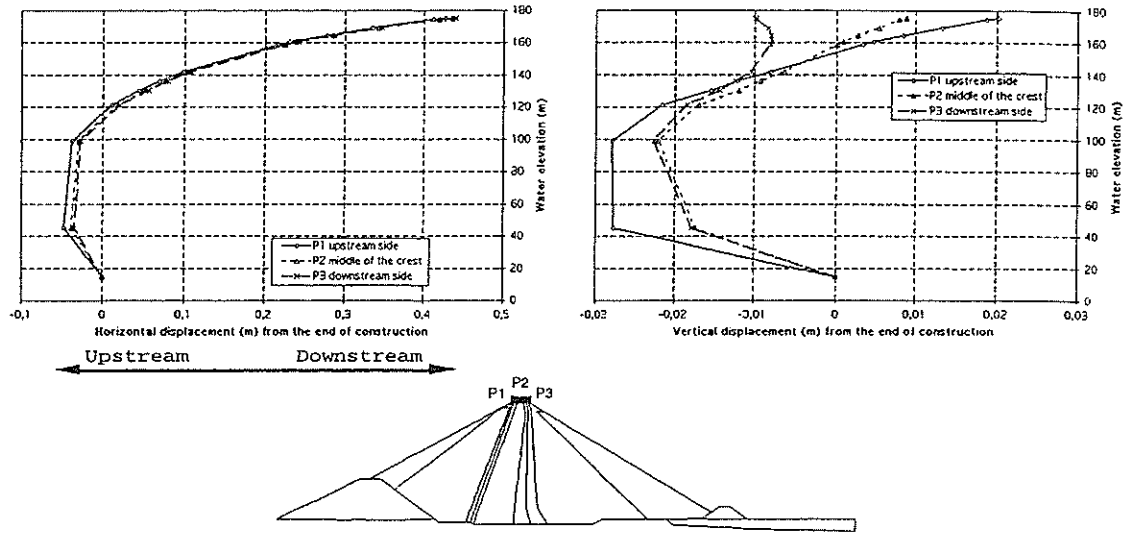

Figure 10. Displacement evolution with water level rise at points P1, P2 and P3, located on the crest.
(displacements = total dis. - dis. at the end of construction).

• Comparisons between upstream shell and downstream shell movements during impounding

Figure 11 allows to perform comparisons between upstream and downstream shell behavior during impoudment stage. Large and quick settlements occur in upstream rockfill shoulder due to collapse phenomenon. Then buoyancy forces produce an unloading after that the rockfill has been submerged. The downstream shell settles continuously with water level rise but displacements are smaller. These settlements are a consequence of the stresses increase in downstream shell due to load transfer during impouding. We can observe that settlements increase when water level raises beyond midheight of the dam, i.e. when unloading occurs in the upstream shell. Horizontal displacements have an upstream direction on the upstream side and a downstream direction on the downstream side. Upstream movement is a consequence of collapse phenomenon in upstream shell. Downstream movement is due to water load on the core.

• Differential settlements

Displacements along horizontal line HH (elevation = 100m) show that differential settlements between upstream rockfill and upstream filters are about 60cm. These differential settlements can cause cracks in filters near the top of the dam, where filter thickness is thin.

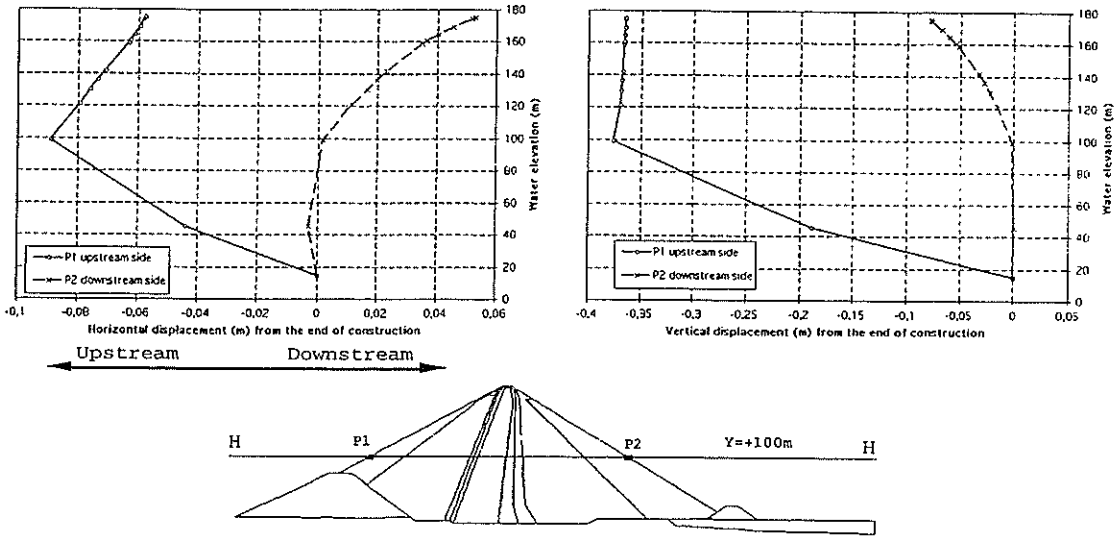

Figure 11. Displacement evolution with water level rise at points P1 and P2, located at 100m elevation, respectively on the upstream and downstream face of the dam.
(displacements = total dis. - dis. at the end of construction).

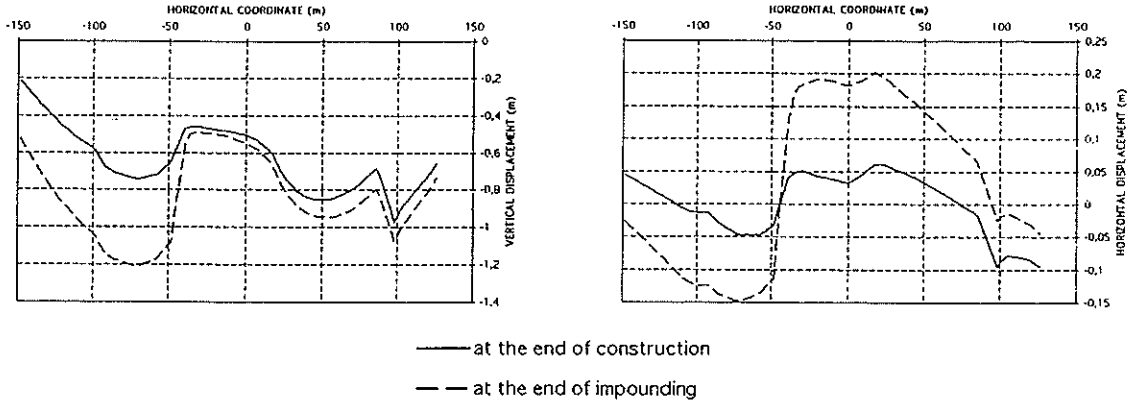

Figure 12. Displacements along horizontal line H-H (Elevation Y=+100m).

CONCLUDING REMARKS

The hydroplastic analysis of LG-2 rockfill dam during impounding has obtained large settlements in upstream shell and a transverse displacement of the core (upstream then downstream). The key-point of this analysis was the parameters calibration. Available datas were insufficient for an accurate identification. Experimental dry-wet tests for transitions and rockfill materials were required. The parameters calibration was made indirectly from hyperbolic

parameters supplied. Neverthless, the whole set of results obtained by the hydroplastic model were found to be in accordance with in-situ results of LG-2 dam. The collapse of rockfill was well reproduced qualitatively and quantitatively. The hydroplastic model allowed to follow the LG-2 behavior evolution during construction and impounding, with one single set of parameters per material.

ACKNOWLEDGEMENT

This work is supported by the 'Région Provence Alpes Côte d'Azur'.
The authors are grateful to A.CARRERE (Coyne et Bellier) for his helpful comments and advices.

REFERENCES

ANTHINIAC P. 1999. Modélisation du comportement hydromécanique des enrochements. Thèse de doctorat, Université Aix-Marseille II, à paraître.

BARTON N. & KJAERNSLI B. 1981. Shear strength of Rockfill. J. Geotechnical Engineering ASCE 107(GT7): 873-891.

BONELLI S. 1993. Contribution à la résolution de problèmes élastoplastiques de mécanique des sols et d'écoulement non saturés par la méthode des éléments finis. Thèse de doctorat, Université Aix-Marseille II, 253 p.

BREITKOPF P. & TOUZOT G. 1992. Architecture des Logiciels et Langages de Modélisation , Revue européenne des éléments finis, vol. 1, N°3, pp 33-368.

CAMBOU B. & JAFARI K. 1988. A constitutive model for granular materials based on two plasticity mechanisms. In Saada & Bianchi (eds), Constitutive Equations for Granular Non-Cohesive Soils: 149-167. Rotterdam: Balkema.

DAOUADJI A. & HICHER P.Y.1997. Modelling of grain breakage influence on mechanical behavior of sands. in Numerical Models in Geomechanics, Pietruszczak & Pande (eds), Balkema, Rotterdam, pp 69-74.

DUNCAN J.M. & CHANG C-Y. 1970. Nonlinear analysis of stress and strain in soils. J. Soil Mech.Found. Division ASCE 96(SM5): 1629-1653.

KJAERNSLI B., VALSTAD T. & HOEG K. 1992. Rockfill Dams Design and construction - Hydropower Development vol.10. Norway: Norwegian Institute of Technology.

LADE V.P., YAMAMURO J.A., BOPP P.A. 1996. Significance of particle crushing in granular materials , J. Geotechnical Engineering ASCE, vol.122, n°4, pp 309-316.

MARSAL R.J. 1973. Mechanical properties of rockfill. In John Wiley and Sons (eds), Embankment Dam Engineering - (Casagrande Volume): 109-200. New York.

OZANAM O. & LA BARBERA G. 1994a. Evaluation of pore pressure and settlements of an embankment dam under static loading - Synthesis. 3rd Benchmark Workshop on Numerical Analysis of Dams. Theme B1. Gennevilliers, France 29-30 sept.

EVALUATING SLIDING STABILITY ALONG ROCK-CONCRETE INTERFACE: HUNGRY HORSE DAM CASE STUDY

G. Fernández[1], E. de A. Gimenes[1], A. Abdulamit[2], M. Maniaci[1]

ABSTRACT:

Foundations of concrete dams can be subjected to loading and unloading due to variations in reservoir levels and ambient temperature during annual operation cycles, resulting in changes in stress levels and joint openings. Case histories where complete monitoring data on uplift pressures, displacements and leakage rates are available can be used to understand hydromechanical interaction in dam-foundation systems and validate predictive numerical models. This paper is focused on the application of discontinuous coupled hydromechanical models to analyze the actual monitored behavior of Hungry Horse Dam, owned and operated by the U.S. Bureau of Reclamation. The dam has a detailed uplift pressure, leakage rate and structure displacement monitoring system, offering a complete case study to validate numerical analyses. It is known that the mechanism of joint opening and crack propagation at the foundation is governed by the redistribution of effective normal stresses along the dam-rock interface triggered by reservoir filling. This stress redistribution was simulated for Hungry Horse dam using a Distinct Element Method code (UDEC 3.0) and the significance of various degrees of foundation drainage efficiency was evaluated. The results indicated that the presence of effective drains is important not only in maintaining a higher level of effective normal stresses along the interface but also to provide a more uniform shear stress distribution thus minimizing the potential of progressive failure along the interface.

INTRODUCTION

For the last twenty years, several research groups (Quadros, 1982; Goodman et al., 1983; Celestino, 1983; Guimarães, 1987; Kafritsas and Einstein, 1987; Lemos, 1987; Amadei et al., 1990; EPRI, 1992; Kovári and Bergamin, 1994; Cervenka, 1994; Fontana et al., 1997; Ebeling et al., 1997)

[1] Department of Civil and Environmental Engineering, University of Illinois at Urbana-Champaign, IL
[2] Department of Hydraulic Structures, Technical University of Civil Engineering, Bucharest, Romania

have been carrying out studies to understand the factors controlling joint opening, uplift pressures and crack propagation in concrete dams and their foundations due to a raise in reservoir levels. The majority of these studies was undertaken to test models based on idealized field conditions. Some studies reported on actual observed behavior of dam foundations and a few elaborated on the main factors controlling this behavior.

This paper presents coupled hydromechanical analyses to simulate the mechanical-hydraulic interaction between joint opening and effective normal stresses along the concrete-rock interface of Hungry Horse dam. The geology of Hungry Horse dam is well documented and its instrumentation includes complete measurements of foundation total heads along the dam-rock interface, displacements of the concrete structure and leakage rates. There are several features of this dam including a grout curtain, the presence of discontinuities within the rock foundation and some three-dimensional (3-D) arching of water loads towards the dam abutment that were not simulated in this first stage of modeling. A second stage to simulate some of these features is currently being carried out as part of a research effort to develop an integrated procedure to analyze and interpret the structural behavior of concrete dams. Other case histories of well mapped and adequately instrumented dam foundations with abundant data on joint opening and crack propagation are also being evaluated (Gimenes, 1999 in prep.; Gimenes et al., 1999).

GEOLOGIC CONDITIONS

Hungry Horse Dam is located on the South Fork of the Flathead River, around elevation 1000 m, in northwestern Montana, near Glacier National Park. It is an arch gravity structure, built between 1948 and 1953, with a maximum height of 197 m, and an average downstream batter of 0.6H:1V. At the time of its completion, it was the second highest concrete dam in the world (Hungry Horse Powerplant, 1958). The crest extends over a distance of 645 m between the two abutments, along elevation 1087 m (Fig. 1a). The dam has a slightly curved geometry and precooling of the concrete mass was carried out during construction to ensure tight contact at the joints between blocks.

The high mountains and ridges of the Hungry Horse area are sedimentary rocks that were covered by two or possibly three

sheets of glacial till of Quaternary Age. The dam is founded on the Siyeh Limestone, a dolomitic impure limestone with varying amounts of siliceous, argillaceous and dolomitic materials.

The dam site is cut by four well developed joint sets (figure 1a). Joints in the first two sets are relatively steep, and strike/dip N45°W/53°SW, semi-parallel to the valley and N63°E/80°SE, semi-perpendicular to the valley, respectively. The joints are relatively continuous, often open and filled with clay. Joints in the third set, which strike N38°E and dip 80°NW, are less continuous and open than those in the other two sets.

A fourth set of joints is associated with the bedding planes, which strike N38°W, semi-parallel to the valley, dipping gently 30°NE upstream. The thickness of the limestone beds ranges from a couple of centimeters to a few meters. The combination of the two main joint sets 1 and 2, together with the bedding plane, isolate rock wedges below the dam foundation which can displace under reservoir loading. Weathering has been recognized along many of the joints in the first 30 to 50 m below ground surface, gradually decreasing with depth.

During foundation excavation, several fracture zones associated with the steep joint sets were found mainly in the left (i.e. south) abutment. Some of these zones were large enough to require excavation of trenches for material removal and execution of upstream and downstream cutoff shafts. A bedding seam, developed by shearing of competent limestone beds during mountain building and folding, was found in the left abutment. The shear plane was filled with clay up to 10 cm thick. It was decided to treat the seam by washing it with high-pressure water to dislodge the clay and subsequently grout the void.

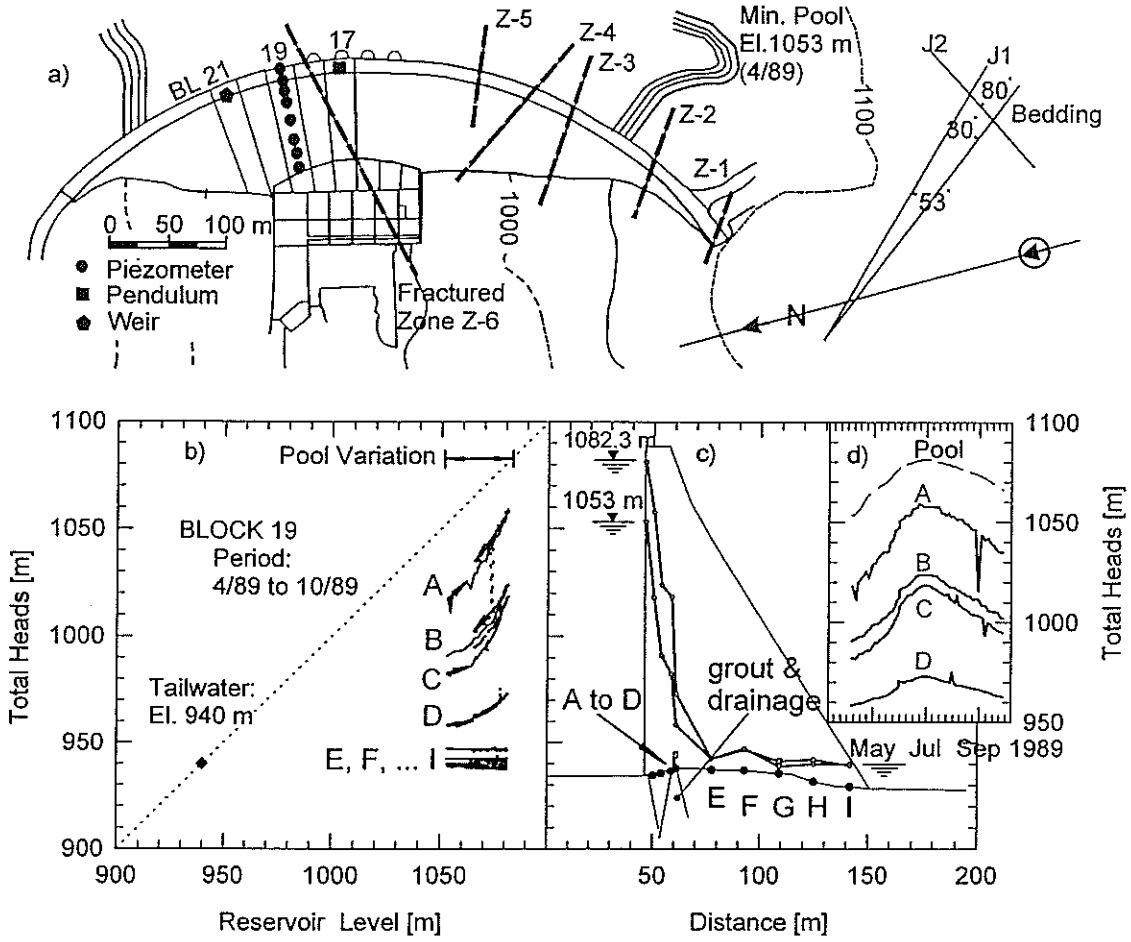

Figure 1. HUNGRY HORSE DAM. Plan view, location of instrumentation and total heads.
Period: April 1989 to October 1989. a) plan view; b) total head curves; c) total head distributions during reservoir filling; d) pool level and total heads during the period

MONITORED DAM BEHAVIOR

At Hungry Horse Dam, standpipe piezometers, pendulum and weirs were used to monitor uplift pressures at the dam-rock interface and concrete structure displacements. Data obtained from foundation monitoring are shown in Figures 1 and 2. The database of total heads is available in the literature (EPRI, 1992). Complementary data to assess leakage rates and structure displacements were obtained from unpublished monitoring records (USBR, unpubl).

Total Head Measurements at the interface joint

Total heads measured along the dam-rock interface at various distances from the upstream are plotted against reservoir levels for Block 19 (Figure 1b). Each plot is provided with a 45° inclined line through the origin, which corresponds to total heads in the discontinuities being equal to reservoir levels. The vertical distance between the 45° line and the total head curves provides quantitative information regarding head loss and effective normal stress along the dam-rock interface as the reservoir is filled. The slope of the total head curves reflects changes in permeability along the dam-rock interface as the reservoir is filled. A steep change in slope indicates a rapid increase in joint opening, concurrent with significant reductions of effective normal stresses. Considerable hysteresis in total head curves takes place due to a possible joint mismatch during reverse shearing as the reservoir is lowered to the minimum level.

The point at which the total head curve exhibits a pronounced change in slope provides an estimate of the critical reservoir elevation at which significant hydromechanical interaction begins to take place for a certain location. At any reservoir elevation beyond this critical value, the vertical distance from the total head curves to the 45° line (full reservoir head) provides a numerical estimate of the minimum effective normal stress remaining at that location.

As shown in Figure 1b, four measurements (A, B, C and D) were taken at various locations between the grout curtain and drainage gallery. None of the total head curves of points A, B, C, D reach the 45° line, indicating that a positive effective normal stress remains in the upstream portion of the dam-rock interface at maximum reservoir elevation. At a given reservoir level, the points closer to the upstream face show the higher total head values, indicating a gradual loss of head away from the reservoir. The change in the slope of curves A, B, C and D in Figure 1b shows the various reservoir levels at which significant increases in joint opening begin to take place at various locations away from the dam face. It is important to note that in spite of the joint opening shown by the slope changes, the effective normal stresses remain positive at all these locations.

The remaining measuring points (E, F, G, H, I) along the interface are located downstream of the drainage gallery and show no increase of total head and no slope changes as the reservoir level increases. This behavior indicates the efficiency of the combined action of the grout curtain and drainage gallery in practically eliminating uplift pressures.

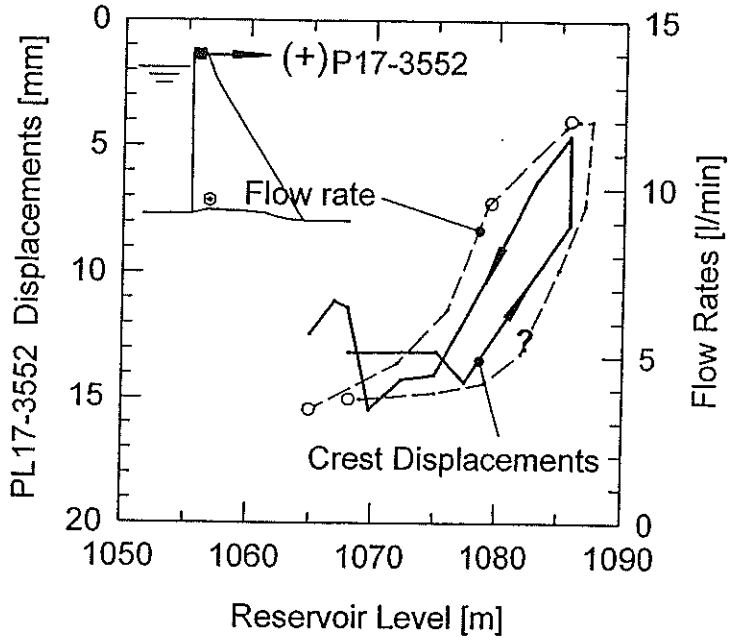

Figure 2. HUNGRY HORSE DAM. Monitored dam crest displacements and leakage rates.
Period: April 1984 to April 1985

Measured Displacements and Flow Rates

Crest dam displacements and leakage rates for Hungry Horse Dam are shown in Figure 2. The structure displaces upstream with reservoir filling, due to dilation of the downstream concrete slope during the hot summer months. This thermal effect is commonly observed in dams with low fluctuations in reservoir level. However, thermal effects do not seem to affect the behavior of the dam-rock interface, where total head curves exhibit a nonlinear shape controlled by reservoir elevation. Leakage rates in the gallery for Hungry Horse Dam are also shown in Figure 2. Readings were only taken four times a year, making it difficult to determine the shape of the flow rate curve for this dam. Increasing the frequency of these measurements could be beneficial for

future investigations.

DISTINCT ELEMENT INCREMENTAL ANALYSIS

Introduction

The mechanical and hydraulic behavior of Hungry Horse Dam and its foundation was analyzed with the Distinct Element Method code UDEC 3.0 (Itasca, 1996). Two main capabilities were considered in selecting this numerical code: a) the capability to handle changes in fracture permeability due to changes in effective normal stresses as the reservoir elevation is incrementally raised; and b) the capability to geometrically reproduce the existing irregular topography of the dam-rock interface. The model was tested by analyzing laboratory tests on irregular and planar joints with discussion of results presented in the appendix.

The analysis of the dam-rock interface was carried out considering three cases: (1) no uplift pressures; (2) uplift along the dam-rock interface with 100% drain efficiency and (3) uplift along the dam-rock interface with 0% drain efficiency. In case 1, only the effect of mechanical loads due to the reservoir are taken into account. In cases 2 and 3, in addition to the reservoir loads, the coupled effect of seepage and resulting uplift pressures along the dam-rock interface are included. Cases 2 and 3 are lower and upper bounds for the effect of uplift pressures, respectively.

An advantage of this modeling approach is that the effect of seepage along the interface does not need to be given as an input of external forces acting at the base of the dam. Instead, the distribution of pore pressures is a result from the analyses and depends on the hydraulic-mechanical parameters along the dam-rock interface, as well as the drain efficiency and the relative stiffness of the dam and its foundation.

The objective is to simulate the concrete-rock interface behavior during reservoir filling by incrementally increasing the water thrust on the dam and rock surface upstream, while concurrently increasing pore pressures at the heel of the dam. This incremental approach allows to evaluate the factor of safety against sliding at the end of each step and to estimate the flood level at which failure is imminent

(ICOLD, 1999). The condition of imminent failure is defined by determining the reservoir elevation at which the factor of safety against sliding approaches unity.

Dam Model Description and Computation Steps

A simplified two-dimensional distinct element model was developed to simulate the dam and rock foundation which are assumed to be elastic deformable masses separated by a single joint at the dam-rock interface. It is assumed that the interface joint conducts all the flow.

Both dam and foundation are discretized in a finite difference mesh to compute internal stresses and deformations. A higher degree of discretization is applied around the interface joint where the water flow is concentrated and hydromechanical interaction is expected. Model geometry and boundary conditions are indicated in Figure 3a. Model boundaries are placed at a horizontal distance from the structural equivalent to 2 to 3 times the height of the dam to avoid stress perturbations. Mechanical boundary conditions (Figure 3b) include fixing the bottom boundary of the model and allowing movement only in the vertical direction along lateral boundaries. Hydraulic boundary conditions include impermeable lateral and bottom boundaries. At each incremental loading stage, water loads are applied to the dam and rock surface upstream while concurrently applying corresponding reservoir pressures at the heel of the dam. Water pressures corresponding to the tailrace elevations are applied at the toe of the dam. In the case of 100% drain efficiency, atmospheric pressure was prescribed at the outlet of the drain, inside the drainage gallery.

The analyses were carried out in two stages (Figure 3b). Stage one corresponds to dam construction, while stage two includes the incremental raising of reservoir levels. The weight of the underlying rock is neglected in this model because no other main discontinuities are included in the rock foundation. During the first stage, stresses within the dam and foundation are generated by the weight of the dam. Resulting joint closures are controlled by the compressibility of the interface joint. During the second loading stage, additional stresses are generated by the application of water loads on the dam and foundation. Coupled hydromechanical computations are concurrently carried out to estimate the

corresponding uplift pressures and flow rates along the interface joint.

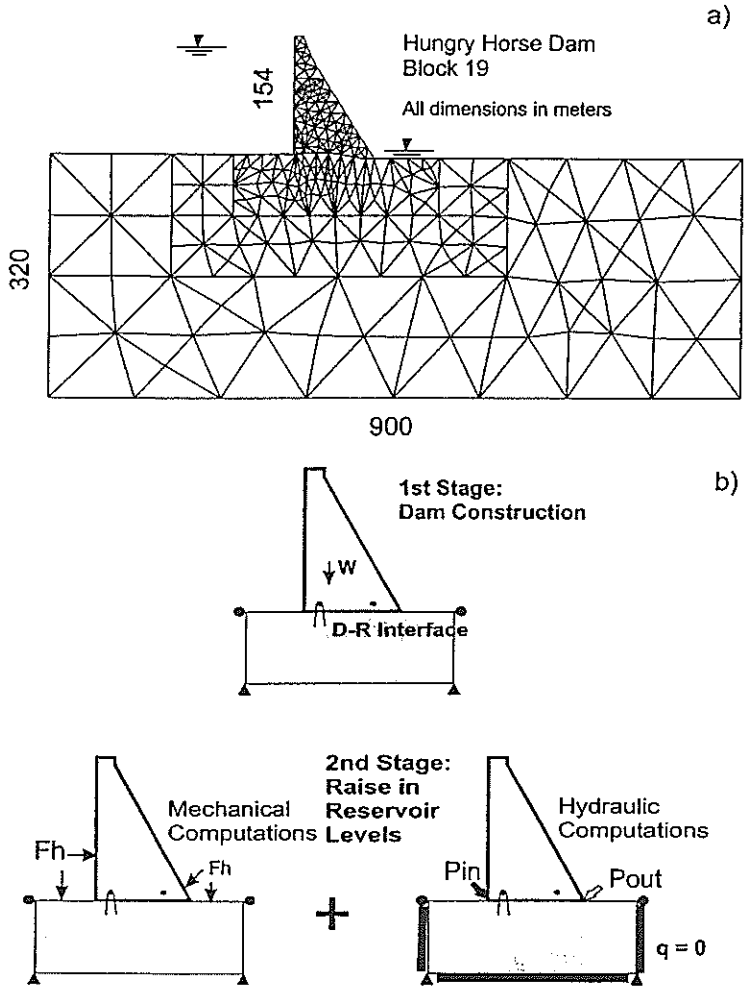

Figure 3 - HUNGRY HORSE DAM. Distinct Element Model.
a) finite difference discretization of dam-foundation system
b) stages for incremental analysis

Mechanical and Hydraulic Properties of Pertinent Materials

Mechanical and hydraulic properties of the concrete, rock mass and dam-rock interface are given in Table 1. Properties are assumed to be equal throughout the domain in all computation steps. Rock and concrete are assumed to be homogeneous, isotropic, impervious materials characterized by elastic parameters, since internal stress levels are a fraction of their unconfined strength. The dam-rock interface joint is assumed to be permeable, with stress dependent permeability characterized by mechanical and hydraulic parameters.

Joint compressibility and permeability are governed by the nonlinear relationship between mechanical aperture and effective normal stress (Alvarez et al., 1995) shown in Figure 4a. During loading, significant joint closure takes place at low values of effective normal stresses. However, the magnitude of the closure per unit of stress decreases significantly as the stress level increases. The above relationship was assumed to be linear for the unloading condition allowing an increase in joint opening rate before reaching a zero effective normal stress condition.

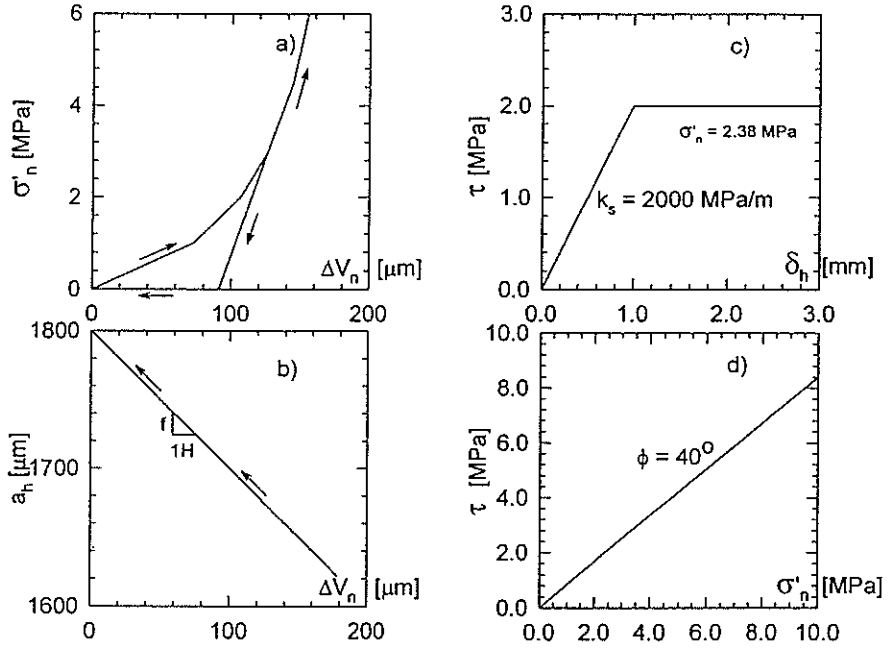

Figure 4. HUNGRY HORSE DAM. Mechanical and hydraulic properties for the dam-rock interface.

A one to one correspondence between hydraulic apertures and joint opening (coefficient f) was assumed prior to the critical point where an increased rate of joint opening takes place, as shown in Figure 4b. Beyond this critical point the maximum hydraulic aperture was limited to 1800 μm. To simulate the effect of 100 % drain efficiency, drains were modeled as high stiffness fractures, to minimize displacements during loading. Hydraulic apertures of drainage fractures were similar to those of the dam-rock interface.

Table 1. Mechanical and Hydraulic Parameters for Dam Model

INTACT ELASTIC BLOCKS	ROCK	CONCRETE	UNITS
Unit Weight	0	24	KN/m^3
Shear Modulus	8000	8300	MPa
Bulk Modulus	13300	11100	MPa
Young's Modulus	20000	20000	MPa
Poisson's Ratio	0.25	0.20	
JOINT MECHANICAL PROPERTIES	**DAM-ROCK INTERFACE**	**DRAINS**	**UNITS**
Tensile Strength	0	0	MPa
Cohesion Intercept	0	0	MPa
Friction Angle	40	40	^{0}
Dilation Angle	0	0	^{0}
Initial Normal Stiffness	9000	100000	MPa/m
Maximum Joint Closure	200	50	μm
Shear Stiffness	2000	100000	MPa/m
JOINT HYDRAULIC PROPERTIES	**DAM-ROCK INTERFACE**	**DRAINS**	**UNITS**
Initial Hydraulic Aperture	1800	1800	μm
Residual Hydraulic Aperture	10	10	μm
Coefficient f	1.0	1.0	

Discussions of Dam Model Results

Pore pressures, effective normal stresses, leakage rates, interface joint opening and structure displacements were computed with the numerical model and were compared to measured values at several locations along the interface. These values are presented in Figures 5 to 7, for cases 1 to 3, respectively.

The estimated values of key parameters are plotted in Figures 5a to 7d against reservoir levels, in the same format

used to report the monitored data. Computed values of stresses and displacements along the interface are shown in Figures 5e to 7g, in a format typical of coupled hydromechanical laboratory test results.

The full scale behavior of the dam-foundation system can be explained by evaluating the values of key parameters along the interface for different reservoir levels. At point B, located upstream of the drainage gallery, the effective stress decreases rapidly as the reservoir level rises, reaching nil values beyond a reservoir elevation of 1070 m (Figures 5b, 6b, 7b). Concurrently, the computed joint opening at these locations shows a large increase at the 1070 m reservoir elevation. This behavior corresponds well with the sharp increase in pore pressures measured at 1070 m reservoir elevation. On the other hand, effective normal stresses increase as the reservoir level rises and follow the nonlinear loading portion of the joint compressibility curve at the downstream of the dam (Point I in Figures 5f, 6f, 7f).

For the case of 0% drain efficiency (Figure 7a) computed values of pore pressures near the upstream toe (Points B, E) increase almost parallel to the 45° line as the reservoir level rises, indicating very low head losses in this area of the interface. Concurrently, the pore pressures computed near the downstream toe (Point I) show a significant lower value. Model simulation indicates that drain efficiency (100%) reduces the magnitude and the rate of increase of pore pressures along the entire interface as the reservoir level rises (Figure 6a). However, computed pore pressure values for 100% efficiency are still higher than measured values and do not exhibit the sharp increase in the slope shown by the measured data around a reservoir level of 1070m. This difference may be due to the effect of the grout curtain, the presence of foundation fractures and/or the three-dimensional load distribution towards the dam abutments, which were not simulated in the model.

Computed flow rates for cases 2 and 3 exhibit an almost linear relationship with reservoir levels (Figures 6c, 7c). However, measured flow rates exhibit a nonlinear dependency on reservoir levels and are significantly lower than computed flows. Modifications in the calibration process are presently being implemented to improve this condition. The increase in drain efficiency to 100% divides the flow along the interface. The difference in flow rates between Point B,

upstream of the drainage gallery, and Point I, at the downstream toe, corresponds to the flow rate diverted to the drains.

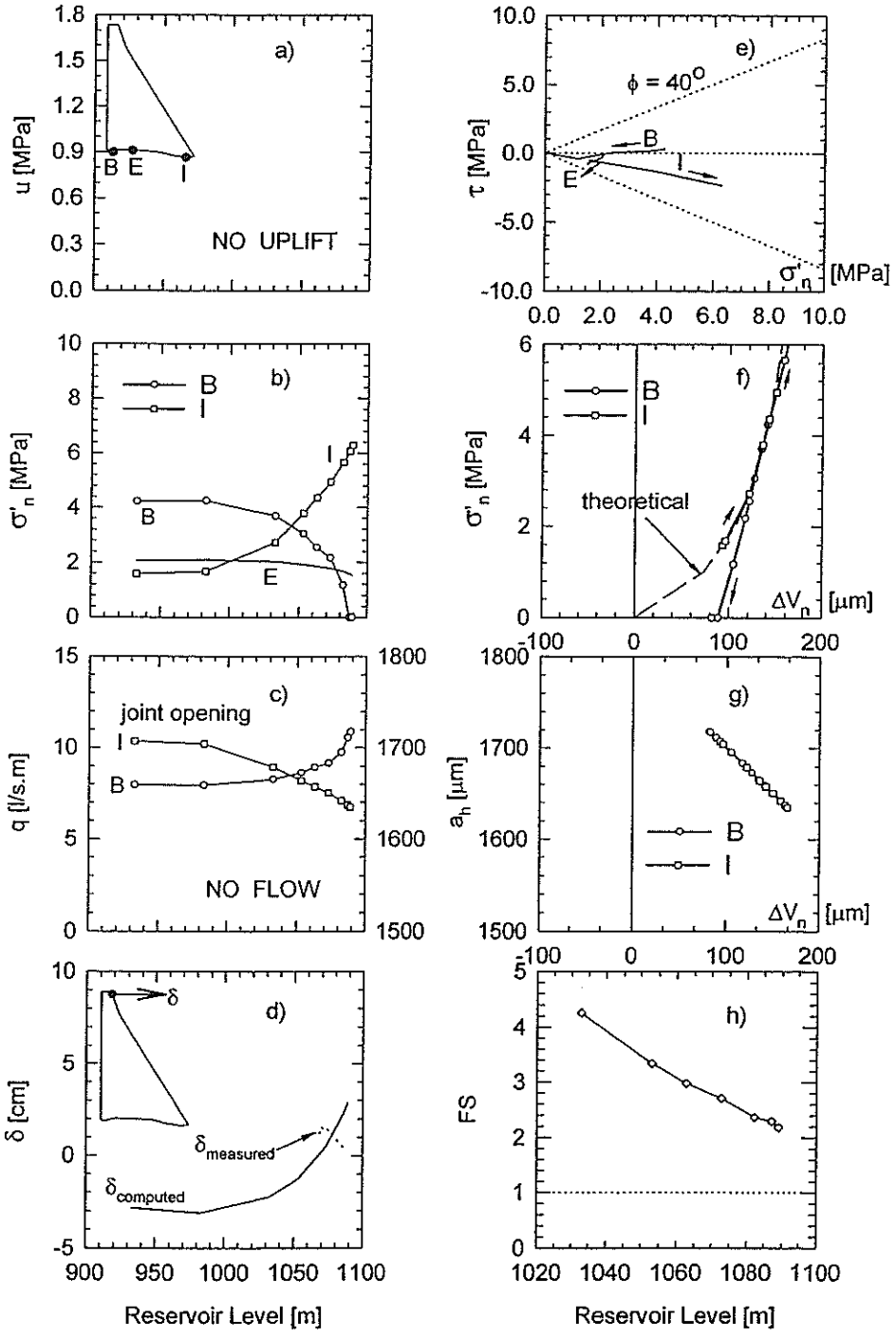

Figure 5. HUNGRY HORSE DAM. Distinct element incremental analysis. Case 1 - No uplift pressures along the interface

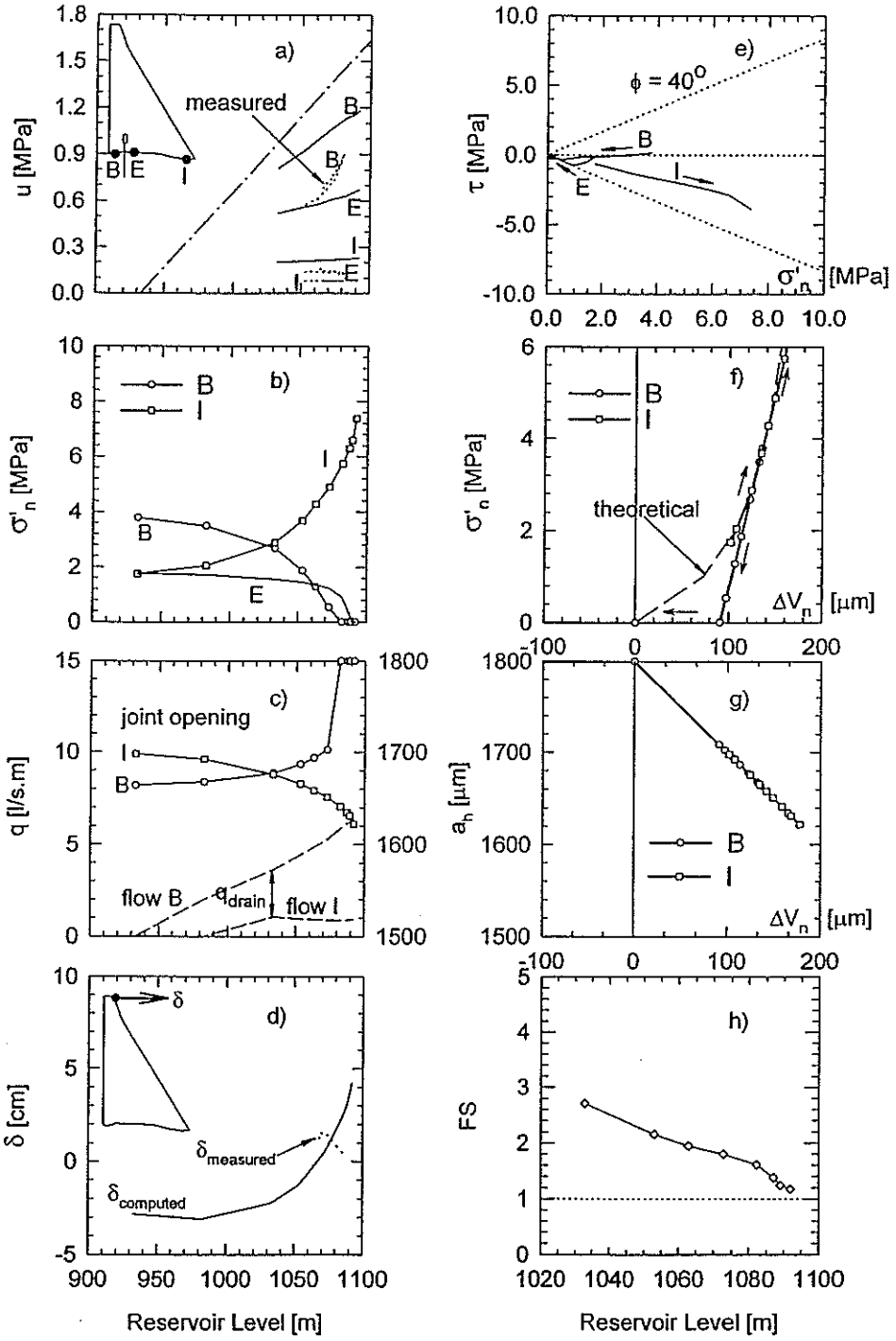

Figure 6. HUNGRY HORSE DAM. Distinct element incremental analysis. Case 2 - 100% drain efficiency.

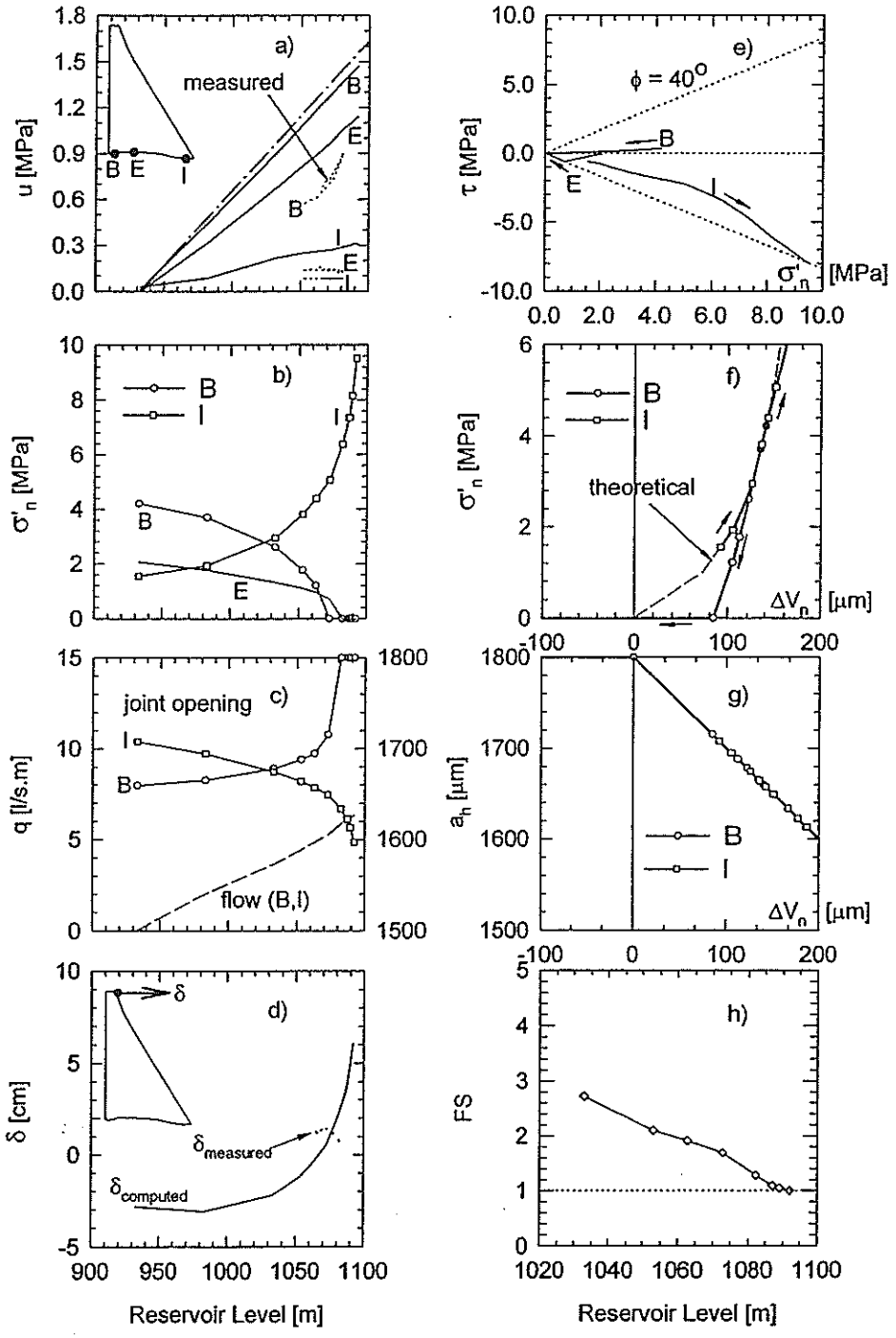

Figure 7. HUNGRY HORSE DAM. Distinct element incremental analysis. Case 3 - 0% drain efficiency.

Increased drain efficiency or absence of uplift pressures can reduce computed structure displacements considerably, especially at higher reservoir levels (Figures 5d, 6d, 7d). Thermal effects could explain the difference between the trend of measured and computed displacements with respect to reservoir levels.

Stress paths followed by points B, E and I along the dam-rock interface during reservoir filling are shown in Figures 5e, 6e, 7e. As the reservoir level increases, points in the upstream zone typically undergo a reduction in effective normal stresses. All points experience an increase in shear stress as the reservoir level increases. The upstream points B and E reach the failure envelope below maximum reservoir elevation and displace along the failure envelope towards the origin. On the other hand, at Point I, at the downstream toe, effective normal and shear stresses always increase as the reservoir levels rise. The increase is almost linear for the case of no uplift pressures along the interface. However, the increase in shear stress at Point I becomes non-linear and gradually accelerates towards the failure envelope as drain efficiency decreases.

A progressive reduction of factor of safety against sliding was computed as the reservoir elevations increased until a marginal condition was reached. Computed factors of safety along the dam-rock interface are shown in Figures 5h, 6h, 7h. A computed imminent failure flood level for 0% drain efficiency was estimated at 1089 m (2 m above the crest elevation). The case of 100% drain efficiency would increase the factor of safety to 1.24 at a reservoir elevation of 1089 m. If uplift pressures are not considered at all increases the factors of safety increases to 2.19 for the elevation 1089 m.

Distribution of stresses and openings along the interface

Computed distributions of stresses, pore pressures and relative joint openings along the interface are shown in Figure 8 for maximum operating level (El. 1082.3 m). Relative joint openings refer to a benchmark aperture corresponding to zero effective normal stresses across the joint. Thus "closed" joints have positive hydraulic apertures being capable of conducting water and experiencing pore pressures along their surface.

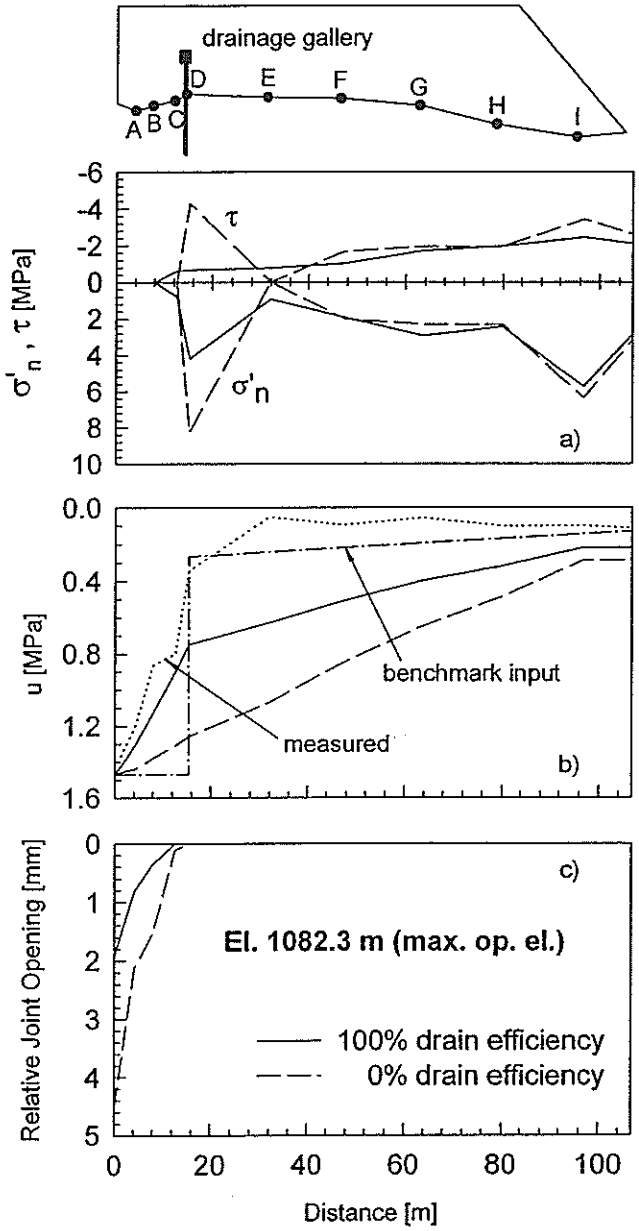

Figure 8. HUNGRY HORSE DAM. Distributions at normal maximum level (Elevation 1082.3 m) for cases 2 (100% drain efficiency) and 3 (0% efficiency): a) effective normal and shear stresses; b) pore pressures; c) relative joint openings

The effective normal and shear stress distributions along the interface (Figure 8a) indicate stress concentrations around the geometrical irregularity at point D, in the upstream zone. High stress values are also shown at the toe (Point I) and are due to the reservoir-induced stress redis-

tribution along the interface. Points close to the heel of the dam are at zero effective normal and shear stresses. Increased drain efficiency is responsible for a more uniform stress distribution along the interface thus minimizing the potential for progressive failure at highly stressed points and enhancing the stability against sliding.

Computed uplift pressures decrease linearly across the interface for the case of 0% drain efficiency (Figure 8b). Uplift pressures decrease more rapidly across the interface with 100% drain efficiency, with a sharp drop at the drain location. The uplift force, which is equal to the area under the pore pressure distribution, is reduced by approximately 1/3 due to drain efficiency. Computed and measured pore pressure distributions along the interface show a similar trend in the reduction of pore pressures away from the reservoir. However, the measured values of pore pressures were significantly lower than the values computed in the model. This difference can be explained by the presence of the grout curtain, the 3-D load load arching towards the dam abutments and/or the presence of foundation fractures which were not simulated in the model.

In the upstream zone, relative joint openings decrease from 5 mm to 2 mm with increase drain efficiency (Figure 8c). The portion of the interface where positive joint openings were computed ("cracked" zones) extends only within the first 15 - 20% of the dam-rock interface. However, even in the case of 0% drain efficiency, the magnitude uplift pressures in these zones does not reach full reservoir heads, in contrast to the prescribed design guidelines (FERC, 1991) in current engineering practice.

Smoothened stress distributions

The effect of stress concentrations on factors of safety and imminent failure levels was investigated by smoothening contact normal and shear stresses around geometrical irregularities along the dam-rock interface at different reservoir elevations.

The imminent failure levels were slightly lower than the levels computed without smoothened stress distributions. The imminent failure flood levels were estimated at elevations below the dam crest, between 1070 and 1082 m, for 0% and 100% drain efficiency, respectively.

The computed factors of safety were also reduced 25-40% of the nominal values estimated without smoothened stress distributions. The factor of safety corresponding to maximum operating reservoir elevation assuming 100% drain efficiency changed from 1.24 to 0.95, which would result in an unstable condition. This prediction obviously does not correspond to the actual dam behavior, which has shown an adequate structural behavior at maximum operating levels.

SUMMARY AND CONCLUSIONS

This paper is focused on the application of discontinuous coupled hydromechanical models to analyze the concrete-rock interface of Hungry Horse Dam. A two-dimensional Distinct Element Model was developed using the computer code UDEC 3.0 for a cross section at block 19 of the dam. The effects of changes in fracture permeability induced by changes in effective stresses and shear displacements along the dam-rock interface were taken into account in the model. One of the objectives was also to estimate the flood level at which sliding failure is imminent (factor of safety equal to one).

Main results of the analyses are summarized in Figure 9 considering three cases: (1) no uplift pressures; (2) uplift along the dam-rock interface with 100% drain efficiency and (3) uplift along the dam-rock interface with 0% drain efficiency.

The imminent failure flood level for Hungry Horse Dam, for a 0% drain efficiency was estimated at Elevation 1089 m (2 m above crest level). With 100% drain efficiency the factor of safety increases to 1.24. Factors of safety and imminent failure flood levels were also estimated with smoothened normal and shear stress distributions. The factor of safety at maximum operating reservoir elevation assuming a 100% drain efficiency resulted in an unstable condition (0.95). This prediction obviously does not correspond to the actual dam behavior, which has shown an adequate structural behavior at maximum operating levels.

A graphical representation of the influence of the uplift pressure on the change of effective normal stress along the interface as the reservoir level increases is shown in Figure 9a, for Points B and E. The normal stress at Point B,

assuming no uplift pressures, is compared with the corresponding normal stress with 0% drain efficiency. A similar comparison is also shown for point E, slightly downstream of the drainage gallery.

Reduction in effective normal stresses results from the overturning moment as well as the development of pore pressures along the dam-rock interface. It is important to emphasize that uplift pressures not only directly reduce the effective normal stresses along the interface but also contribute to increase the overturning moment. The contribution of these phenomena is shown by the vertical distance u* between the effective normal stress curves corresponding to cases 1 and 3 (Figure 9a) which shows that the reduction of effective normal stress induced by pore pressure becomes increasingly significant as the reservoir level rises.

The study also showed the efficiency of the drains in maintaining a higher level of effective normal stresses. High drain efficiency also results in relatively uniform shear stress distributions along the interface, minimizing the potential for progressive failure along highly stressed contact zones.

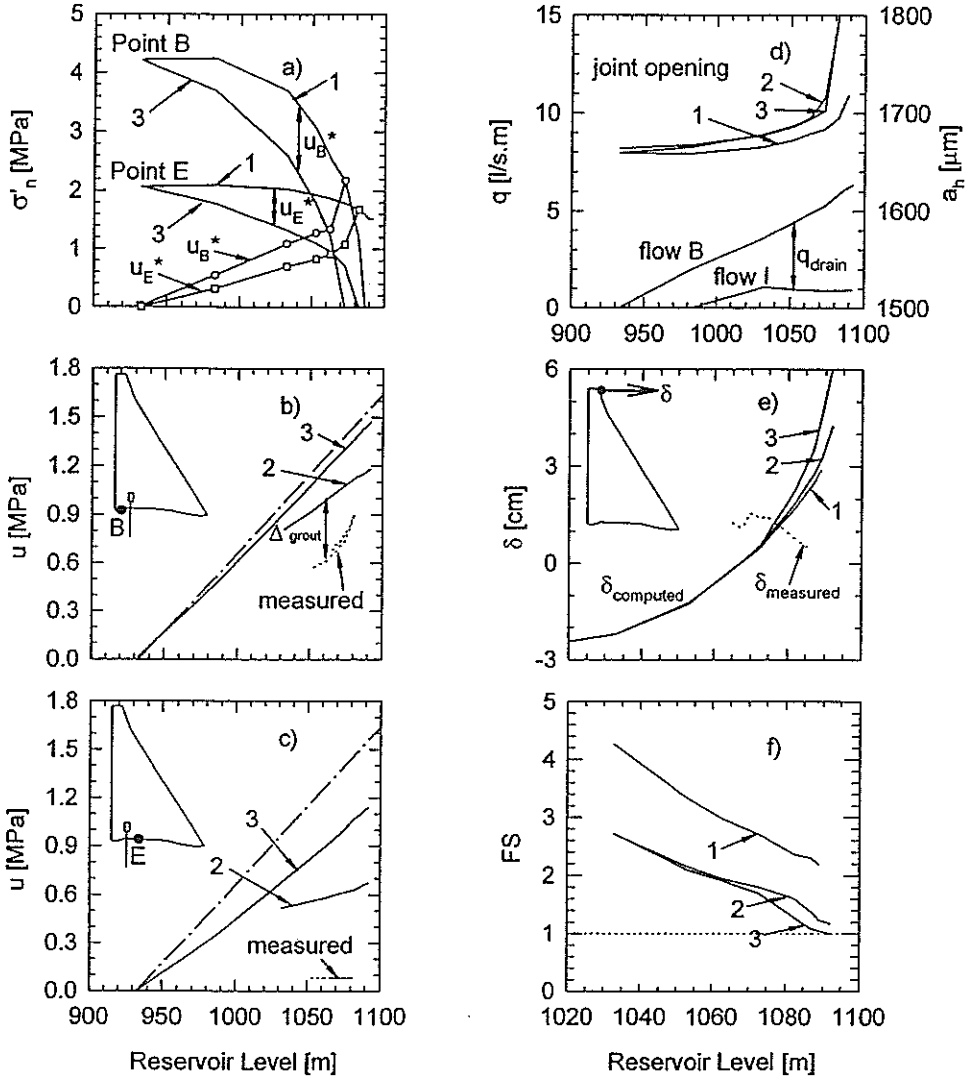

Figure 9. HUNGRY HORSE DAM. Summary of results for cases 1 (no uplift), 2 (100% drain efficiency) and 3 (0% drain efficiency): a) effective normal stresses at points B and E b) pore pressures at point B c) pore pressures at point E d) flow rates and joint openings e) crest displacements f) imminent failure flood level.

An advantage of this modeling approach is that the effect of seepage along the interface does not need to be given as an input of external forces acting at the base of the dam. Instead, the distribution of pore pressures is given by the analyses and depends on the hydraulic and mechanical parameters along the dam-rock interface, as well as the drain ef-

ficiency and the relative stiffness of the dam and its foundation.

Another advantage of the modeling approach is the possibility to incorporate existing mapped discontinuities (faults, fractures and joints) in the dam foundation. This is a fundamental premise, which is site specific if faults, fractures and shear zones are appropriately identified. The effect of treatment of these features can also be simulated.

A comparison of computed and measured pore pressures along the interface indicates a close correspondence in the tendency for the reduction of pore pressures downstream of the reservoir. However, the magnitudes of the computed pore pressures are slightly higher than the measured ones. In addition, computed leakage rates are at least an order of magnitude larger than measured values.

In our opinion, the main causes of discrepancy between actual behavior and behavior predicted in the numerical analyses can be summarized as follows:

1) the grout curtain installed at the heel of the dam was not simulated in the model;
2) the 3-D arching of water loads towards the dam abutments was not reproduced. Because the arched geometry of the dam and the pre-cooling of the concrete mass this effect can be of some significance;
3) the present simplified model considered the bedrock as a relatively impermeable elastic mass without taking into account the presence of discontinuities; and
4) the degree of finite difference mesh refinement along the dam-rock interface affects the distributions of contact stresses, pore water pressures and joint openings. Thus, increasing mesh refinement could improve model predictions.

Continuing efforts are presently being carried out to enhance modeling capabilities and improve simulation of in situ conditions.

ACKNOWLEDGEMENTS

The authors gratefully acknowledge the National Science Foundation (Grant CMS 96-10545) and CAPES (Brazilian Government Agency) for providing financial support for the devel-

opment of this research project. The United States Bureau of Reclamation is also acknowledged for supplying unpublished monitoring records of Hungry Horse Dam to complement this study. Help from Mr. Carlos A. Regalado and Mr. Joon-Shik Moon in collecting and processing information on project history, instrumentation, and geology was greatly appreciated by the authors.

REFERENCES

Alvarez, T.A., Cording, E.J. and Mikhail, R.A.,1995. Hydromechanical Behavior of Rock Joints. A reinterpretation of Published Experiments. In: Daemen and Schultz (Editors), 35th U.S. Symposium on Rock Mechanics, pp. 665-671.

Amadei, B., Illangasekare, T., Chinnaswamy, C. and Morris, D.I., 1990. Reducing uplift pressures in concrete gravity dams. Water Power and Dam Construction(feb.): 13-17.

Celestino, T.B.,1983. Modelos Matemáticos no Projeto de Fundações de Barragens de Concreto. In: ABMS (Editor), Simpósio sobre a Geotecnia da Bacia do Rio Paraná, São Paulo, Brazil.

Cervenka, J., 1994. Discrete Crack Modeling in Concrete Structures. Ph. D Thesis, University of Colorado, Boulder, Colorado, 287 pp.

Ebeling, R.M., Pace, M.E. and Morrison, E.E., 1997. Evaluating the Stability of Existing Massive Concrete Gravity Structures Founded on Rock. REMR-CS-54, U.S. Army Engineer Waterways Experiment Station, Vicksburg, Mississippi.

EPRI, 1992. Uplift Pressures, Shear Strengths , and Tensile Strengths for Stability Analysis of Concrete Gravity Dams. 2917-05 Volumes 1-3, Electric Power Research Institute, Palo Alto, California.

FERC, 1991. Engineering Guidelines, Federal Energy Regulatory Commission, Washington, DC.

Fontana, O., Egger, P. and Descoeudres, F., 1997. Barrage D'Albigna: Etude des Ecoulementes et des Deformations Couplees dans le Massif de Fondation. Mandat RY 86, Ecole Polytechnique Federale de Lausanne, Lausanne, Suisse.

Gimenes, E.de A., 1999 in prep. Hydromechanical Evaluation of Flow Behavior in Rock Foundations of Concrete Gravity Dams. Ph.D. Thesis, Department of Civil and Envi-

ronmental Engineering, University of Illinois at Urbana-Champaign, Urbana, IL.
Gimenes, E.de A., Fernández, G. and Abdulamit, A.,1999. Monitored Hydromechanical Behavior of Concrete Gravity Dam Foundations, Proceedings, 37th U.S. Rock Mechanics Symposium. Balkema, Rotterdam, Vail, Colorado.
Goodman, R.E., Amadei, B. and Sitar, N., 1983. Uplift Pressure in Crack below Dam. Journal of Energy Engineering, Volume 109(#4): 207-221.
Guimarães, M.C.B., 1987. Um estudo comparativo de métodos de avaliação de subpressões em estruturas de concreto. M. Sc. Thesis, Escola Politécnica, Universidade de São Paulo, São Paulo, Brazil, 218 pp.
Itasca, 1996. Universal Distinct Element Code. Version 3.0. Vol. I, II, III, Itasca Consulting Group, Minneapolis, Minnesota.
Kafritsas, J.C. and Einstein, H.H.,1987. Coupled flow/deformation analysis of a dam foundation with the distinct element method. In: D. Farmer, Desai, Glass and Neumann (Editor), Proceedings, 28th U.S Rock Mechanics Symposium. Balkema, Rotterdam, Universtity of Arizona, Tucson, pp. 481-489.
Kovári, K. and Bergamin, S.,1994. Joint Opening and Head Distribution in the Foundation Rock of the Albigna Gravity Dam, Seventh International IAEG Congress. Balkema, Rotterdam, Lisbon, pp. 3797-3806.
Lemos, J.V., 1987. A Distinct Element Model for Dynamic Analysis of Joint Rock with Application to Dam Foundations and Fault Motion. Ph.D. Thesis, University of Minnesota, 295 pp.
Quadros, E.F., 1982. Determinação das características do fluxo de água em fraturas de rochas. M. Sc. Thesis, Escola Politécnica, Universidade de São Paulo, São Paulo, Brazil.

APPENDIX

Laboratory Shear Test Model

As a first step for the validation of the dam model, results from laboratory direct shear tests were analyzed using UDEC 3.0. The geometry, material properties, and boundary conditions of the laboratory test model correspond to those used by Patton (1966) in his experiments on artificial joints molded out of plaster of Paris.

Patton tested both planar and irregular joints in the laboratory (Figure 10a). The samples consisted of two halves 25 mm high by 75 mm long. Irregular joint samples were molded with two 5 mm high teeth, inclined 35° with the horizontal direction. During the test, shearing loads, horizontal and vertical displacements were monitored. Properties for the block material and joint are summarized in Table 2.

Table 2. Mechanical properties for laboratory tests

INTACT RIGID BLOCKS	PLASTER OF PARIS	UNITS
Unit Weight	10.7	KN/m^3
Shear Modulus	N/A	MPa
Bulk Modulus	N/A	MPa
Young's Modulus	N/A	MPa
Poisson's Ratio	N/A	

MECHANICAL PROPERTIES	JOINT	UNITS
Tensile Strength	0	MPa
Cohesion Intercept	0	MPa
Friction Angle	31	^{0}
Dilation Angle	0	^{0}
Initial Normal Stiffness	9000	MPa/m
Maximum Joint Closure	200	μm
Shear Stiffness	2000	MPa/m

Measured and computed values of shear strength of planar and irregular joints are in good agreement up to a normal load of approximately 720 N (Figure 10b). For normal loads above that level, irregular joint samples start shearing the intact material at the base of the teeth. The numerical model is not following the same behavior beyond that normal load because the blocks were assumed to be rigid and thus it is only possible to ride the irregularities.

Measured and computed shear load-displacement and joint dilation curves are shown in Figure 10c for a normal load of 471.5 N. Measured values for peak and residual shear

strength agree with the shear strength computed for irregular and planar joints, respectively. The computed shear strength is constant with horizontal displacement because the top block is sliding along the teeth, therefore computed vertical displacements increase gradually as sliding takes place. Measured shear loads decrease with horizontal displacement due to shearing of irregularities above the base of the teeth. Also, because the irregular joint is actually being sheared, measured vertical displacement is different than the computed value. However, the overall behavior of the numerical model resembles the known behavior of real fractures during shearing at low normal loads and thus can be used to simulate sliding along an irregular dam-rock interface.

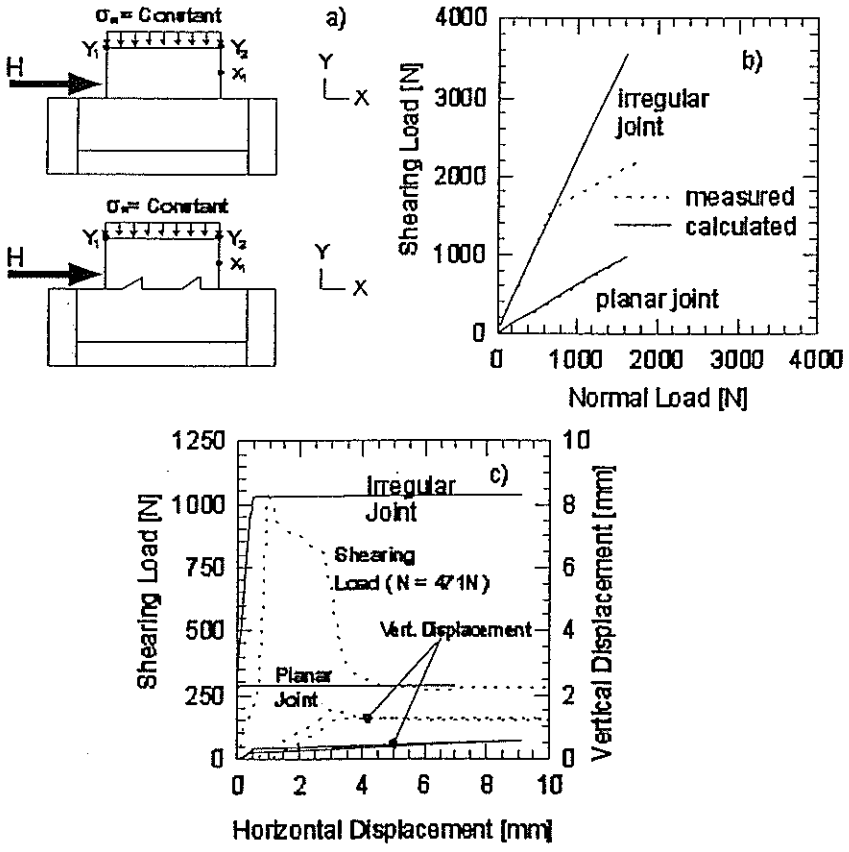

Figure 10 - Shear test on joints (after Patton, 1966). Laboratory test model results.
a) sample geometries; b) joint shear strength;
c) joint dilation and joint deformability curves

SEISMIC STRENGTHENING OF CONCRETE GRAVITY DAMS

Hongyuan Zhang[1] and Tatsuo Ohmachi[2]

ABSTRACT

Concrete gravity dams designed in compliance with the present specification are likely to experience cracking under intense shaking like maximum credible earthquakes. Dangerous cracking in dam body should be prevented in advance to ensure the serviceability of dams. In this paper, some measures to prevent cracking of concrete gravity dams are presented. The measures are, for example, adjustment of dam section, local reinforcement and post-tension technique. The adjustment of dam section will reduce the tensile stress in dam body and avoid the occurrence of cracking. Local reinforcement at possible cracking positions is expected to resist the propagation of cracks and reduce the damage of dam body, although it might not prevent the initial cracking. Post-tension technique exerts pre-compressive stress in dams to offset the tensile stress during earthquakes. Effects of these measures are evaluated by numerical simulation. It is shown that these measures could improve the cracking-resistant behavior of concrete gravity dams effectively.

INTRODUCTION

Concrete dams should be designed to resist two levels of earthquakes: level one is design base earthquake and level two is maximum credible earthquake. Although there are only a few examples of earthquake-induced damage in concrete dams (Hall, 1988), this fact could not give us the confidence regarding the safety of concrete dams since concrete dams have rarely experienced intensive earthquake excitations. The tremendous damage caused by the 1995 Hyogoken-nanbu earthquake demonstrated that the earthquake resistance of structures designed in compliance with the present specification is insufficient under near-field earthquakes, so the dam safety under intensive excitations must be evaluated carefully.
Because concrete can not sustain highly tensile stress, concrete

[1]Dr. Eng., Department of Built Environment, Tokyo Institute of Technology, 4259, Nagatsuda, Midori-ku, Yokohama 226-8502,JAPAN
[2]Dr. Eng., Professor, ditto

gravity dams are likely to experience cracking during large earthquakes. Once cracking occurs, it will propagate deeply inside the dam body. Even though cracks in dam body do not imply the failure of dam immediately, they represent the defects that alter the structural resistance and may lead to failure of dam body. So the cracking of concrete is an important factor in the safety evaluation of gravity dams and any possible cracking in dam body should be prevented in advance to ensure the dam safety under large earthquakes.

This study deals with seismic strengthening of concrete gravity dams. Finite element method with the smeared crack model is used to predict the cracking position and extent in dam body under large earthquakes. Some possible measures to prevent the cracking of dam body are considered. These measures are, for example, adjustment of dam section, local reinforcement and post-tension technique. A concrete gravity dam designed in compliance with the present specification is taken as an example and the effect of strengthening measures is checked by numerical examples.

SEISMIC CRACKING IN CONCRETE GRAVITY DAMS

Assumptions for Analysis

A 102^{m}-high concrete gravity dam designed in compliance with the present specification is supposed as an example to analyze cracking of dam body under large earthquakes. The cross-section of the dam-reservoir system is shown in Figure 1. The nonlinear finite element method with the smeared crack model is used to simulate the seismic cracking procedure in the dam body (Zhang,1998). In the calculation, dam body is idealized as a two-dimensional one rested on a rigid foundation. Hydrodynamic pressure on the upstream face of dam is represented by an added mass technique according to Westergaad's formula.

The material properties of dam concrete are listed in Table 1. Fracture energy of dam concrete can not be determined accurately from experimental results and it is generally considered to be in the range of 175 ~ 310N/m (Bhattacharjee, 1992). For dynamic calculation, the elastic modulus, strength and fracture energy of concrete are increased by 10% to account approximately for the strain rate effect.

The Pacoima dam basement record in the 1994 Northridge earthquake is scaled to have a maximum acceleration of 300cm/s^2 as the input ground motion in this study, as shown in Figure 2. In this record, the duration of intensive shaking is very short and the intensive

shaking just has several pulses. These features show that it is a typical near-field earthquake record. Furthermore, as it is observed at an existing dam site, the record containing characteristics of dam site seems appropriate for the present analysis.

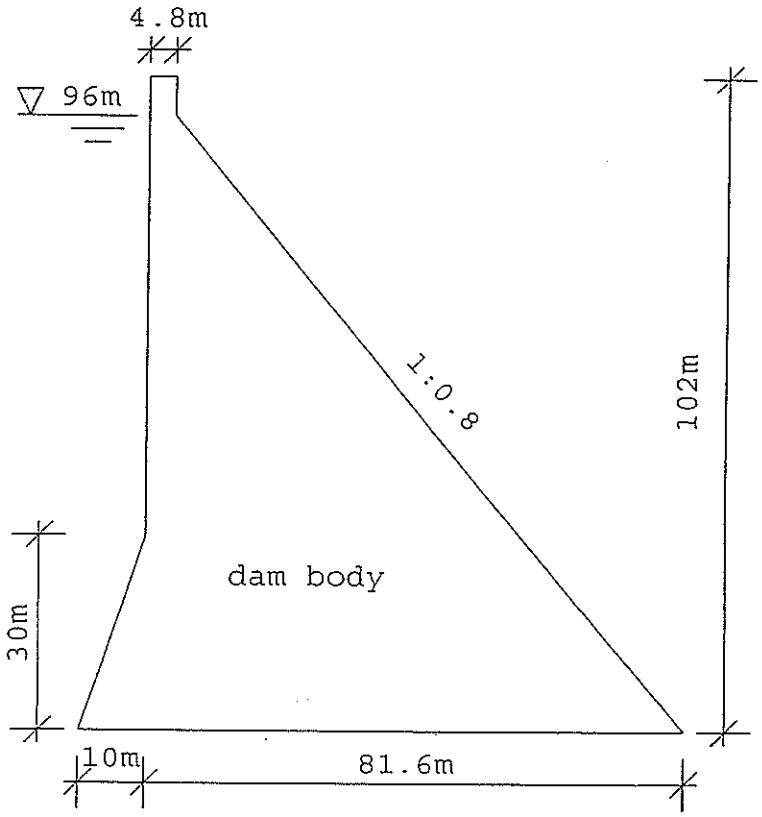

Figure 1. Concrete gravity dam

Table 1. Material properties of dam concrete

Elastic modulus	25000MPa
Poisson ratio	0.2
Density	2400kg/m^3
Tensile strength	2.0MPa
Compressive strength	20.0MPa
Damping ratio	0.05

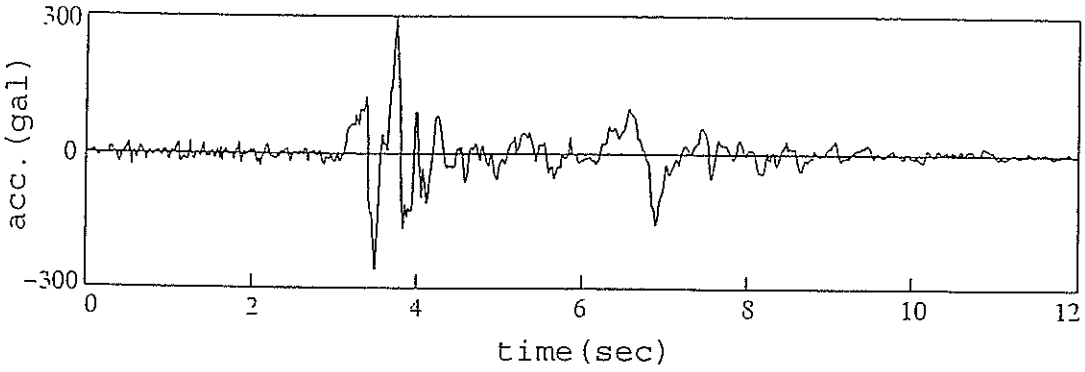

Figure 2. Input ground motion

Seismic Response of Dam Body

Under the intensive excitation as shown in Figure 2, cracking occurs in the dam body. The displacement response at dam crest is shown in Figure 3. Cracking state of dam body at several selected times is shown in Figure 4, in which the cracked elements are represented by dots at the element centers. According to the calculation results, cracking initiates at the dam heel at 3.51s and propagates along the dam base until 3.59s. At 4.37s, when the dam crest shows its maximum displacement in the upstream direction, cracking occurs on the downstream face and develops inside the dam body in the direction perpendicular to the downstream face. But when the dam begins to swing towards the downstream direction at 3.71s, the cracking propagation at the downstream face stops sooner. At 4.51s, new cracking occurs at the discontinuity of upstream face and propagates in the horizontal direction until 4.53s.

Although earthquake-induced tensile stress in the dam body is local and transient, it will still cause severe cracking of dam body due to the brittle behavior of concrete.

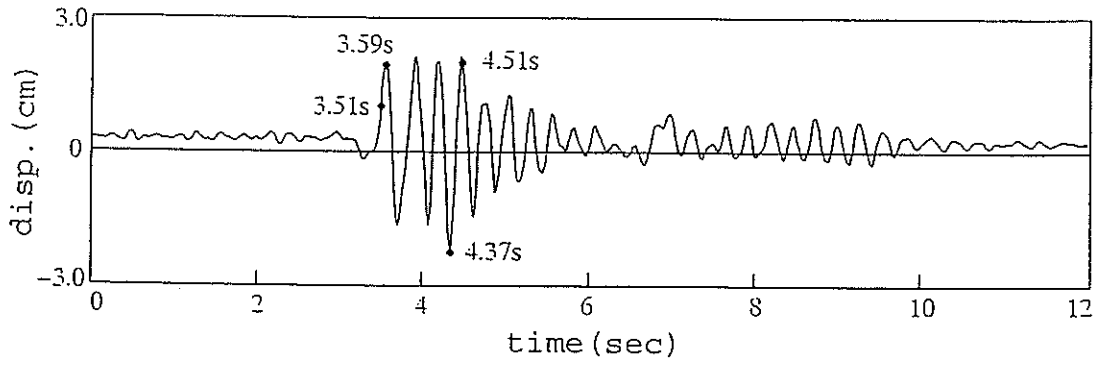

Figure 3. Response of dam crest

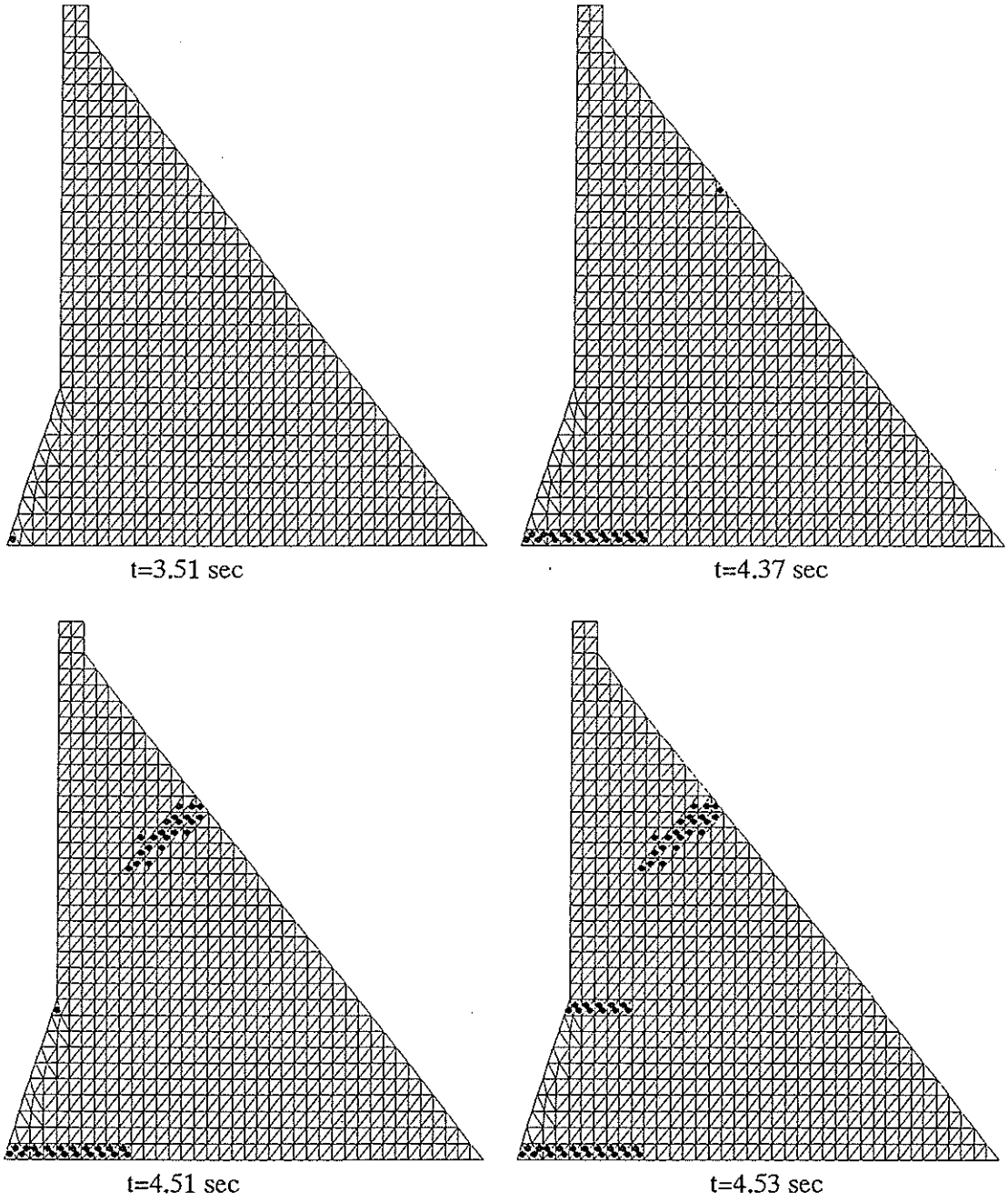

Figure 4. Cracking of dam body

SEISMIC STRENGTHENING OF CONCRETE GRAVITY DAMS

Especially after the 1995 Hyogoken-nanbu earthquake, the safety of concrete gravity dams under near-field earthquakes is a matter of concern in Japan. This is partly because concrete gravity dams designed in compliance with the present specification will

experience tensile stress under near-field earthquakes and partly because the tensile stress might cause severe cracking of dam body. Hence, practical measures must be adopted to ensure the safety of dam body under near-field earthquakes.

Adjustment of dam section

During earthquakes, tensile stress in the dam body is caused by water pressure on the upstream face and inertia force of dam body. These forces are not only dependent on the ground motion but also dependent on the profile of the dam. For example, hydrostatic pressure depends on the gradient of upstream face. For vertical upstream face, the hydrostatic pressure is horizontal and most unfavorable. Inclined upstream face can reduce the hydrostatic pressure in the horizontal direction and the vertical component of hydrostatic pressure on the inclined upstream face is favorable to the safety of dam body. On the other hand, sudden slope change of dam face will lead to stress localization at the discontinuity and severe cracking might occur there under intensive earthquakes. Hence abrupt change in dam face slope should be avoided.

Based on the above consideration, we can adjust the dam profile to reduce tensile stress in the dam body. For the dam section shown in Figure 1, a gentler upstream slope could reduce the tensile stress at the heel of dam body. At the same time, the slope should transit smoothly to the vertical part of upstream face to avoid stress localization at discontinuity. From this point of view, a suitable upstream slope is shown in Figure 5. The fillet slope near the heel is gentler than that of original dam but it becomes steeper gradually and transits smoothly to the vertical part of upstream face.

With the modified profile shown in Figure 5, seismic response of the dam is calculated similarly. There is no cracking occurred in the dam body during the earthquake. To investigate the effect of section modification, linear earthquake response of dam body with the original and modified section is compared. The maximum tensile stresses at the heel, upstream discontinuity and on the downstream face for the two sections are compared in Table 2. It can be seen that the improvement of the fillet slope evidently reduces tensile stress at the heel as well as at the upstream discontinuity. As for the tensile stress on the downstream face, it is lower than the tensile strength of concrete even in the original section for the linear response.

The above example demonstrates that tensile stress in the dam body is dependent on the dam profile, and that a suitable shape of upstream slope can help us to keep tensile stress at lower

level even under large earthquakes. Thus, the option of dam profile is a very important factor in the design of concrete gravity dams in order to increase the earthquake-resistant capacity of dam body.

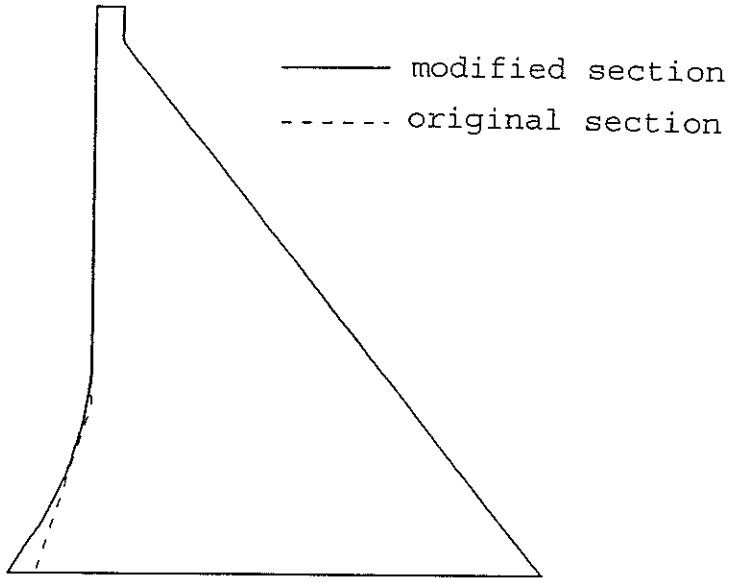

Figure 5. Modified profile of dam section

Table 2. Comparison of maximum tensile stress (MPa)

	original shape	modified shape
heel	3.27	1.98
upstream discontinuity	2.37	1.92
downstream face	1.90	1.85

Local reinforcement

Reinforcing steel is widely used in the modern construction of concrete structures, including concrete gravity dams to improve the cracking-resistant behavior of dam body. Effects of reinforcing steel on preventing cracks in concrete gravity dams are discussed here. From economical point of view, steel bars are usually allocated at possible cracking regions only. As an example, the reinforcing region is illustrated by cross marks in Figure 6.

In the analysis of reinforced concrete, bond slip between concrete and steel is disregarded, and the reinforcement bars

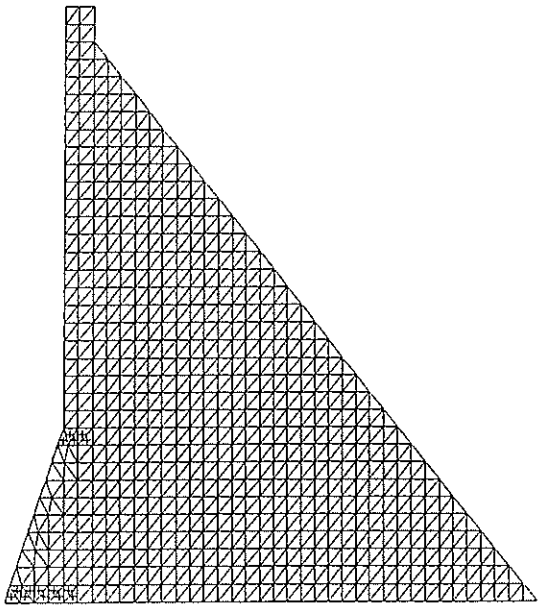

Figure 6. Local reinforcement

are smeared throughout the concrete element (Suidan, 1973). The property of steel can be expressed as

$$D_s = E_s \begin{bmatrix} p_x & 0 & 0 \\ 0 & p_y & 0 \\ 0 & 0 & 0 \end{bmatrix} \quad (1)$$

in which E_s is the elasticity modulus of steel, and p_x and p_y are the median ratios of steel bars in the x and y directions. This property will be added to that of concrete to represent the mixed property of reinforced concrete.

The elasticity modulus of steel is generally 200000MPa. In this example, the diameter of steel bars is taken as 50mm and the maximum aggregate size of concrete is assumed to be 120mm. The pure interval between steel bars, which should be larger than 1.5 times of the maximum aggregate size of concrete, is set to 200mm here. Then the median ratios of steel are 0.0314 in the x and y directions.

Based on the above assumption, seismic response of the reinforced dam is calculated. With the local reinforcement, cracking does not occur at the upstream discontinuity, but occurs along the dam base during the earthquake, as shown in Figure 7. According to Table 2 showing linear calculation results for the plain concrete dam, the maximum tensile stress at the upstream discontinuity is a little higher than the strength of concrete, but the maximum tensile stress at the heel is much higher than

the strength. Consequently, adding the steel bars cannot prevent the occurrence of cracking due to the tensile stress. On the other hand, the cracking region along the dam base in the case with steel bars is smaller than that in the case without steel bars, showing that adding the steel bars is effective to prevent propagation of cracks.

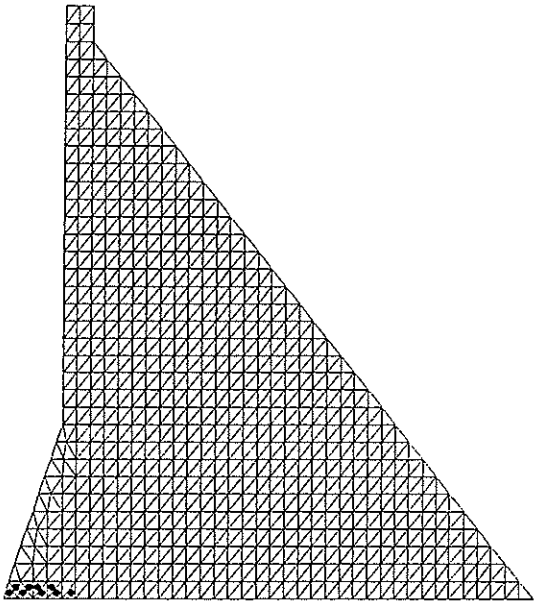

Figure 7. Cracking of dam with local reinforcement

According to the linear calculation result, tensile stress exceeding the strength of concrete along the dam base develops in a small region near the heel, as shown in Figure 8. But because of the brittle feature of plain concrete, the occurrence of cracking causes stress redistribution in the structure. The stress redistribution leads to the propagation of crack, and the highly tensile stress in a small region near the heel will cause large cracking region along the base of the plain concrete dam. Reinforcing the possible cracking region by steel bars could resist the stress redistribution and reduces crack propagation. As a result, the cracking region can be limited by reinforcing with steel bars.

Although earthquake-induced cracking should be prevented, if possible, to ensure linear response of dam body under maximum credible earthquakes is sometimes too expensive or impossible. In such a case, localized cracking of concrete may be accepted under maximum credible earthquakes if the cracking is far from endangering the integrity and safety of dam body (USBOR, 1977). From this viewpoint, local reinforcement is an effective method for the seismic strengthening of concrete gravity dams.

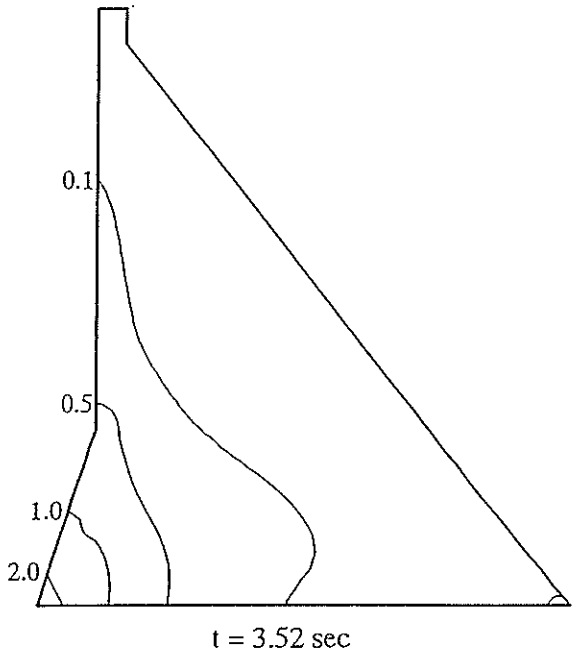

Figure 8. Distribution of tensile stress (MPa)

Post-tension technique

Post-tension technique is an effective method to improve the load carrying capability of concrete structures and it is already applied to concrete gravity dams to rehabilitate earthquake-induced cracking. For the seismic strengthening of concrete gravity dams, the reasonable arrangement of cables and the adequate post-tension forces must be carefully determined by numerical simulation, to ensure the dam safety against cracking. Generally, post-tension cables should be arranged in the direction perpendicular to the possible cracking. For the concrete gravity dam shown in Figure 1, horizontal cracking will occur at the heel and/or upstream discontinuity during the near-field earthquake, as predicted in nonlinear analysis. Thus cables to prevent the upstream cracking are arranged in the vertical direction. As for the downstream cracking, because the tensile stress on the downstream face is lower than the tensile strength of concrete for the linear response of dam body, the downstream cracking will not occur if the upstream cracking is prevented. So the post-tension cables are just considered to prevent the upstream cracking.

The requirement of post-tension force must be evaluated carefully because over-strengthening might cause cracking of the dam body. To check the effect of strengthening, seismic response of the post-tensioned dam is simulated by the finite element

method. Initial tension force in cables is simulated as concentrated load at the anchorage. Cables are modeled as truss elements which have axial stiffness only (Leger, 1994). The amount of cables, their location and post-tension force are adjusted until the scheme satisfies the objective of allowing no cracks in the dam body during the earthquake.

A post-tension configuration to prevent cracking of dam body under the earthquake is shown in Figure 9. The diameter of the cables is 63mm. Four cables are densely arranged near the heel of dam body because highly tensile stress will occur there during the earthquake. The post-tension forces in the cables are listed in Table 3. From P1 to P4, the post-tension force reduces gradually to avoid over-strengthening.

The difference between the post-tension technique and other strengthening method is that the post-tension force is applied to the dam body as external force. Because of this, the post-tension scheme needs to take into consideration of the structural resistance, in order not to endanger the safety of dam body.

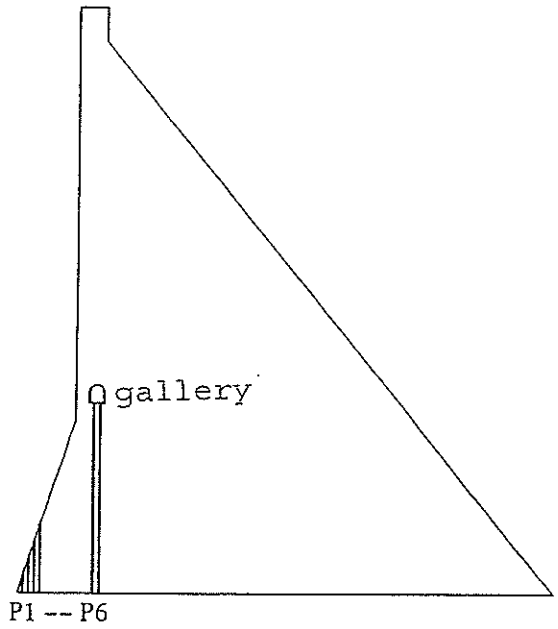

Figure 9. Post-tension configuration

Table 3. Post-tension forces in the cables (kN)

P1	P2	P3	P4	P5	P6
2500	2000	1500	1000	2000	2000

CONCLUSION

To improve the dam safety under very strong earthquakes, seismic strengthening of concrete gravity dams is discussed in this paper. Numerical simulation shows that the suggested measures are effective to prevent the occurrence and propagation of cracking in concrete gravity dams. Conclusions can be listed as follows.
(1) Concrete gravity dams are likely to experience cracking under intensive excitations, especially at the heel of dam body and upstream discontinuity.
(2) A gentle and smooth upstream face could reduce the tensile stress in the dam body and avoid the occurrence of cracking.
(3) Reinforcing bars cannot prevent the occurrence of cracking under highly tensile stress, but it can resist the propagation of cracks and reduce the damage of dam body.
(4) Post-tension cables can strengthen the dam body effectively, if it is adequately designed.

REFERENCES

Bhattacharjee S. S. and Leger P.: Concrete constitutive models for nonlinear seismic analysis of gravity dams --- state-of-the-art, Can. J. Civil Eng., 19, 492-509, 1992

Hall J. F.: The dynamic and earthquake behavior of concrete dams: review of experimental behavior and observational evidence, Soil Dyn. Earthquake Eng., 7, 58-121, 1988

Leger P. and Mahyari A. T.: Finite element analysis of post-tensioned gravity dams for floods and earthquakes, Dam Eng., 5(3), 5-27, 1994

Suidan M. and Schnobrich W. C.: Finite element analysis of reinforced concrete, J. Struct. Division., ASCE, 99, 2109-2122, 1973

United States Department of the Interior Bureau of Reclamation: Design of gravity dams, Denver, Colorado, 1977

Zhang H. and Ohmachi T.: 2 dimensional analysis of seismic cracking in concrete gravity dams, Dam Eng., JSDE, 8, 93-101, 1998

DEFORMATION ANALYSIS OF THE BAISHAN ARCH DAM

ZHANG Jinping, CHEN Zhonghua, LI Libing[1]

ABSTRACT

In this paper the observed displacements of the Baishan Arch Dam are analyzed using distribution model. In the model for 1D displacement distribution, such as the measuring points on one pendulum wire, the component attributable to the water load is expressed as the fitting polynomial for the calculation results by means of finite element method (FEM) modified by one coefficient of correction. An overall knowledge on the behavior of the whole section can be acquired. The 2D distribution model for describing the radial displacement of the whole dam is also illustrated.

GENERAL

The Baishan Arch Dam is located on the Second Songhua River in Huadian County, Jilin Province in northeastern China. Main construction work of the Baishan Project started in May 1975, and impoundment of the reservoir on November 16, 1982. The first unit was commissioned on December 30, 1983. Now all the 5 units with total capacity of 1,500MW are in operation (Fig. 1).

The climate is north continental with minimum temperatures reaching -45. The V-shaped valley is of appreciable width, with bedrock of sound migmatite, except for a small portion of basalt at the left abutment. There are a number of faults, veins and weathered zones in the dam foundation. Generally speaking, the topography and geology are suitable for an arch dam.

The Baishan Hydropower Station comprises an arch dam with 4 crest spillway openings and 3 outlets at mid height, an underground power plant on the right bank with 3 generating units, 300MW each, an underground switch station and on the

1.ZHANG Jinping, Senior Engineer, CHEN Zhonghua, Professor and Senior Engineer, LI Libing, Engineer. China Institute of Water Resources and Hydropower Research, P.O. Box 366, Beijing 100038, China, Tel: 0086-10-68530689, Fax: 0086-10-68518286, E-mail: iwhrxld@public.bta.net.cn

left bank, a surface powerhouse with a capacity of 2×300MW, and an appurtenant switch station.

The arch dam is divided into 39 blocks along its entire arch length, each 16m in width excepting the spillway blocks being 18m in width. The four spillway sections are in blocks No.14, 16, 18 and 20 with sill elevation at 404m. The major project features and the main geometric data of the dam are listed in Tables 1 and 2.

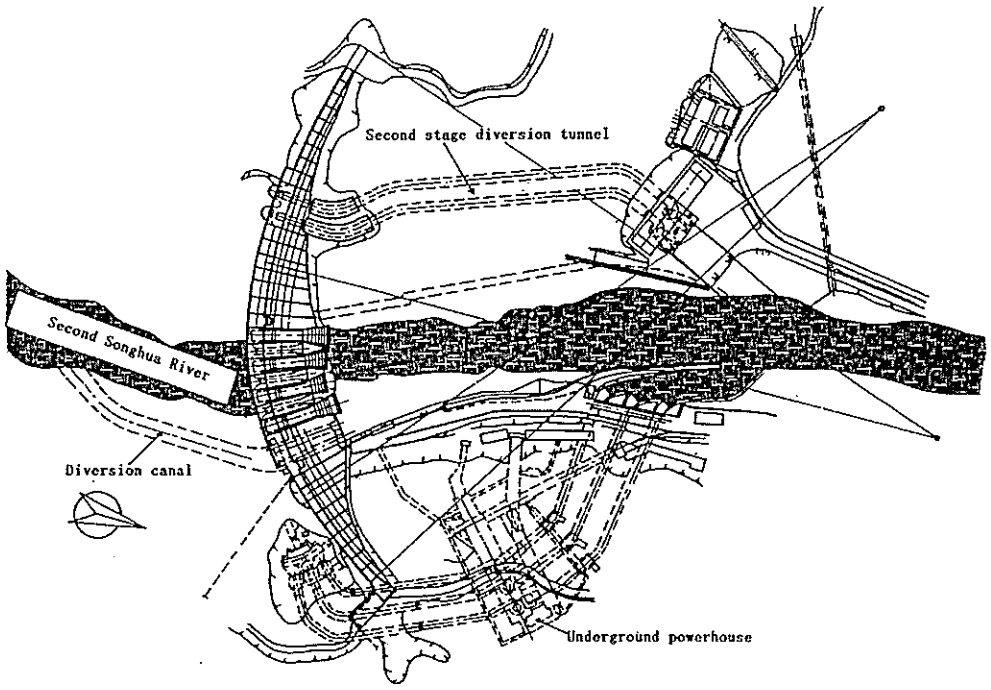

Fig. 1 General layout of Baishan Dam.

Table 1 Major project features

Items	Indices
Long term average discharge	$23m^3/s$
Max Probable Flood Discharge	$32,200\ m^3/s$
Design Flood	$19,100\ m^3/s$
Reservoir water level at PMF	423.45m
Reservoir water level at design flood (p=0.1%)	418.30m
Normal high water level:	413.00m
Total reservoir storage:	$6.5 \times 10^9\ m^3$
Installed capacity	5 × 300 MW
Annual energy output	2.037 TWh

Table 2 Main geometric data of the dam

Items	Indices
Type	Three circle arch dam
Height	149.5m
Crest length	676.5m
Base thickness	63.7m
Radius of arch at the middle	770m
At both sides	320m
Max central angle	77°22′
Width to height ratio	4.525
Thickness to height ratio	0.426
Volume	1.66×10^6 m^3

MONITORING INSTRUMENTATION SYSTEM

Conventional monitoring system was designed to evaluate the safety of the dam. For brevity, only the instruments for deformation monitoring are introduced here.

There is one reversed pendulum wire installed in each of the blocks No.2, 21, and 36. In block 32 there is a pair of reversed pendulum wires. And in blocks No. 6, 10, 17 and 26, one pendulum wire is used in combination with one reversed pendulum wire. (Fig. 2) There are measuring points at El. 423, El. 418, El. 375 and El. 340 as well as in the grouting gallery. Measuring points totals 29. The triangulation survey is also performed to monitor the deformation of the dam and valley slopes.

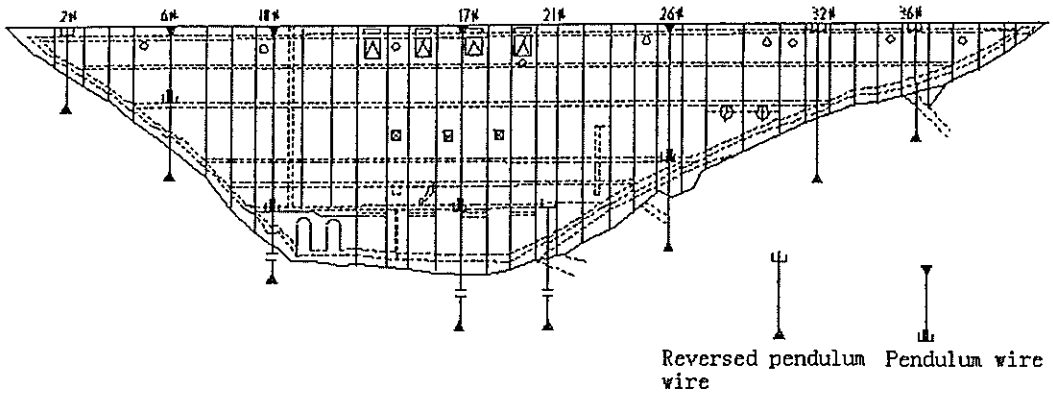

Fig.2 Layout of pendulum and reversed pendulum wires.

The grouting to fill the crown joints was completed in May, 1985. The first pendulums were put into use in the beginning of 1983 and all of them have been in operation since August 25, 1985. From then on, the series of measured data are rather complete.

A data processing system was developed on the computer to treat all measured data for the dam safety during the operation period. Both the analysis of the observed data collected up to now and the results of the past visual inspections indicate the normal performance of the dam. Here, our analysis is focused on the observed radial displacements of the dam at measuring points on these pendulums and reversed pendulums.

FINITE ELEMENT ANALYSIS

The finite element analysis was carried out for processing the measured deformation data in the dam and it's foundation at the Baishan Project. In this paper, only displacement calculations at different upstream water levels are introduced. The objective of the analysis was to help

1) establish numerical hybrid model for monitoring displacements, i.e. the hybrid displacement distribution model described later, in which the deformation law of component due to water load can be formulated with the aid of the calculated results .

2) judge if the water load induced component of the displacements read from pendulums and triangulation survey

show a normal deformation trend under the upstream water load as predicted by the F. E. A.

The purpose of the calculation was different from the deformation and stress analysis for the design purpose, where the mesh may be comparable with multi-arch-cantilever analysis and topography can be simplified. Therefore, the mesh adopted in the above mentioned calculations was more carefully designed. The mesh covers an area of 3km by 3 km with the topography input by a drawing board so that the all triangulation survey stations can be included properly. Fig. 3 shows the part of mesh near the dam. There are 3518 nodes and 3375 elements in the whole mesh.

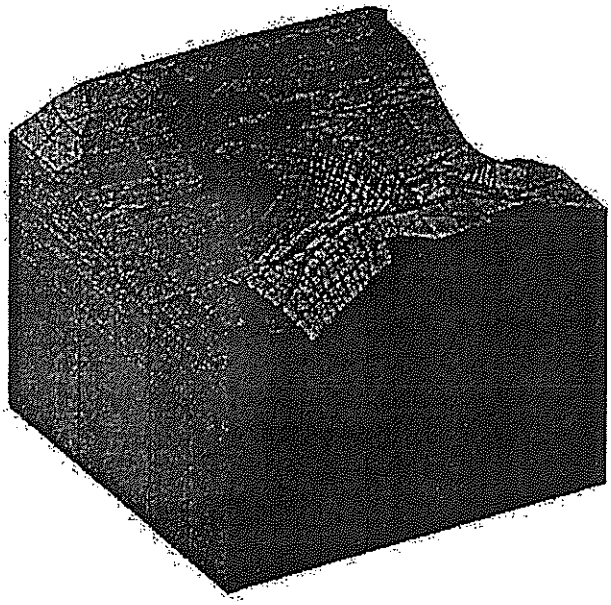

Fig. 3 A part of the discretized mesh for FEM calculation.

The material parameters were adopted by reviewing the design documents and technical reports provided by the designer. Since the foundation and abutment rock is sound enough, elastic model both for dam and foundation rock was considered adequate to offer an overall pattern of the deformation of the dam under upstream water load. Seven rock regions can be divided with different Young's modulus ranging from 8,000 to 27,000 MPa while a modulus of 30,000 MPa was adopted for the concrete of more than 10 years old.

Since the variation of downstream water depth is very small, the main water load is governed by upstream water level. 11 different upstream water levels were taken in

simulating the rise and down of the water level in the reservoir during the operation period, ranging from El. 300 to El. 423.5. By assuming that the dam is impermeable, the water load in rock mass can be treated either as body forces by the seepage analysis with drainage and grouting curtains considered, or as the surface load by assuming a distribution curve for the uplift under the dam. Since the observed uplift water head could not give sufficient information to make the assumption, trial calculations have been performed for both seepage body forces and assumed uplift pressures. The calculations showed that the results obtained by assuming a conventional curve for the uplift pressure distribution fit the observed displacement data much better. This may be because the method for estimating seepage body forces is not suitable for the rock mass in which no dense homogeneous fissures exist.

The displacements of dam and its foundation were calculated and the values at the triangulation survey stations were interpolated which were further checked against the observed displacements. Obviously, a perfect agreement between the calculated and observed data could not be attained for such a complex structure and so large an area of rock mass with geological uncertainties. The aim of the trial calculations is to get an overall agreement of the deformation tendency in the dam and it's foundation. It is adequate to give a sound base for further data processing in the computer monitoring system for the Baishan Dam developed by the authors. The calculated results stored in the database include the displacements versus upstream water levels on radial sections of the dam and at survey stations.

THE DISPLACEMENT DISTRIBUTION MODEL

Supposing the principle of displacement superposition is applicable, then it follows that the radial displacement of the dam at any point, δ, can be resolved into three parts:

$$\delta = \delta(h) + \delta(T) + \delta(t) \qquad (1)$$

in which, $\delta(h)$, $\delta(T)$ and $\delta(t)$ are components accounting for the effect of water load, temperature and time respectively.

For the 1D distribution of displacements, such as the deflection of cantilevers or deformation of arch rings, Equ.(1) takes the following form:

$$\delta = \delta(h,x) + \delta(T,x) + \delta(t,x) \quad (2)$$

in which, x is an variable representing spatial position of points.

In Equ.(2), all the three components are nonlinear bivariate functions, for which no specific mathematical expressions with definite mechanical meaning are available in any means. However, they can be transformed to generalized linear regression problems. Supposing continuity in the displacement distribution with respect to spatial location of the medium (dam body and foundation), all these component functions can be expanded into power series. Taking the first as an example, it can be expressed as follows:

$$\delta(h,x) = \sum_{j=0}^{n}\sum_{i=0}^{m} a_{ij} x^j h^i \quad (3)$$

When n and m are large enough, an asymptotical bivariate polynomial with sufficient accuracy can be obtained for the function to be approximated. The component functions representing the effects of temperature and time can be treated in the same manner. The coefficients of the governing equation including all three components can be determined as the regression factors using linear stepwise regression method.

The hybrid statistic model for one dimension displacement distribution can be expressed as follows:

$$\delta = A\delta(h,x) + \delta(T,x) + \delta(t,x) \quad (4)$$

in which, $\delta(h,x)$, taking the form of Equ. (3), is a bivariate polynomial fitting the calculated results, obtained by using finite element method, at the measuring points and A is a coefficient of correction.

As for the 2D problems, there is no essential difference from Equs. (2) or (4), except that one more variable y is introduced as the other dimension of space. With the aid of

this kind of 2D model, the overall field of radial displacement of the dam body can be studied in a general way.

On the basis of the 6 series of radial displacements (all of 120 data points) of the 6 measuring points on the pendulum and reversed pendulum in the block No. 17, the crown cantilever of the dam, a hybrid model was established:

$$\begin{aligned}\delta = &-72.043 + 0.872F(h,x) + 47.674x - 3.386x^3 + 0.069T_1x^3 - 2.685T_1^3x \\ &- 0.003T_1x^5 - 0.195T_1^3 - 0.043T_1^4 + 0.166T_2^4 + 0.030T_2^4 - 0.016T_2^3x^2 \\ &- 0.012T_2x^5 - 0.005T_2^5x^4 - 0.159Tx + 0.012Tx^3 - 0.24\times10^{-7}T^4 - 0.005Tx^5\end{aligned} \tag{5}$$

in which, F(h,x), the above mentioned polynomial obtained by fitting the calculated results using finite element as mentioned above, is determined as follows after trial:

$$\begin{aligned}F(h,x) = &-4.068 - 4.653h^2 + 0.267x^3 + 20.529h^3 - 2.691hx^3 + 10.909h^4 \\ &- 0.002x^6 - 0.203hx^5 + 0.101h^2x^4 + 1.479h^3x^3 + 1.425h^4x^2\end{aligned} \tag{6}$$

and, x is used to represent the spatial position of points, T_1 the average temperature of the seven days before the time of measurement, T_2 the average temperature of the sixty days before the time of measurement, T the duration of time and h the water level, all after non-dimentionalizing.

For Equ.(4), the multiple correlation coefficient R is 0.999 and standard deviation S is 0.252mm.

In Fig.4, each curve stands for the deflection of the cantilever at certain water level. It is clear that the calculation results of FEM are well fitted.

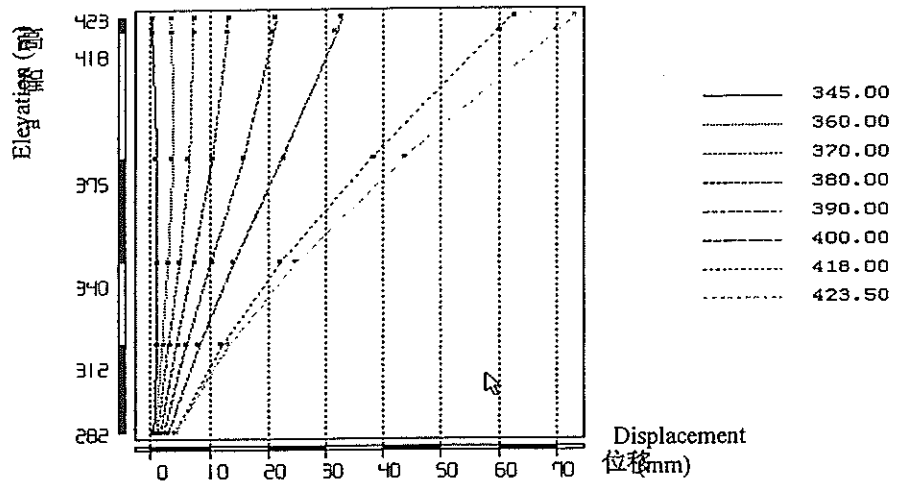

Fig.4 The family of fitting curves for FEM calculation results.

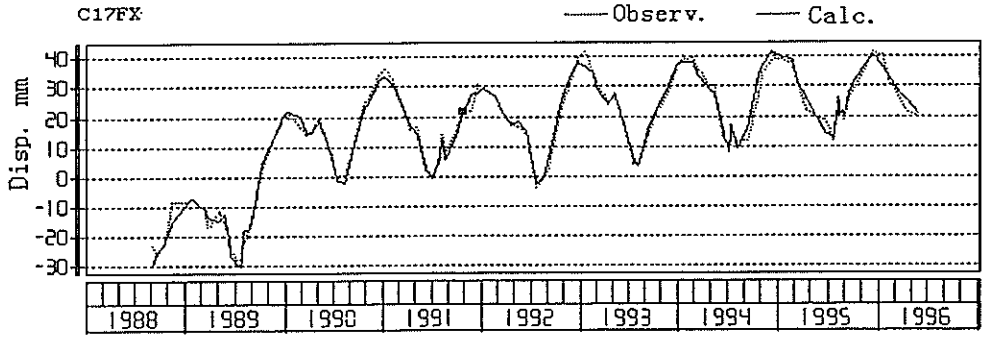

Fig.5 The graph of radial displacement at point C17FX degenerated from the 1D distribution model.

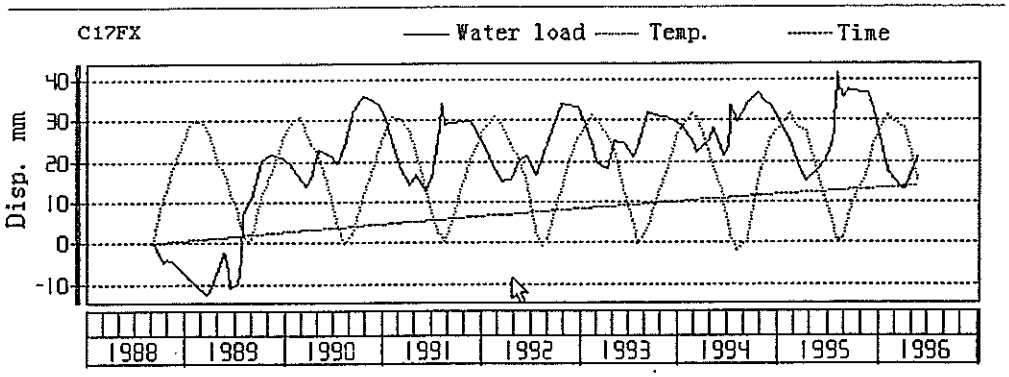

Fig. 6 The graph of displacement components at point C17FX.

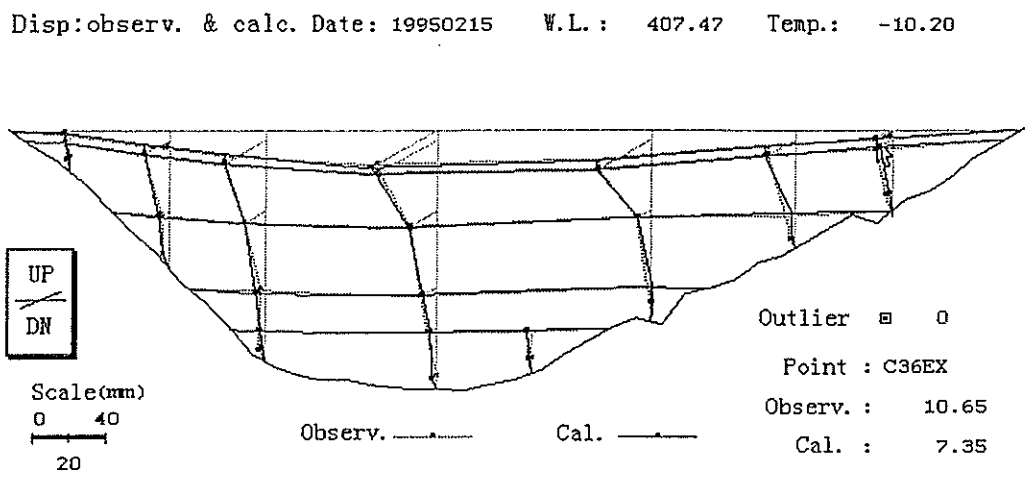

Fig. 7 The radial displacement fields: observed vs. Computed.

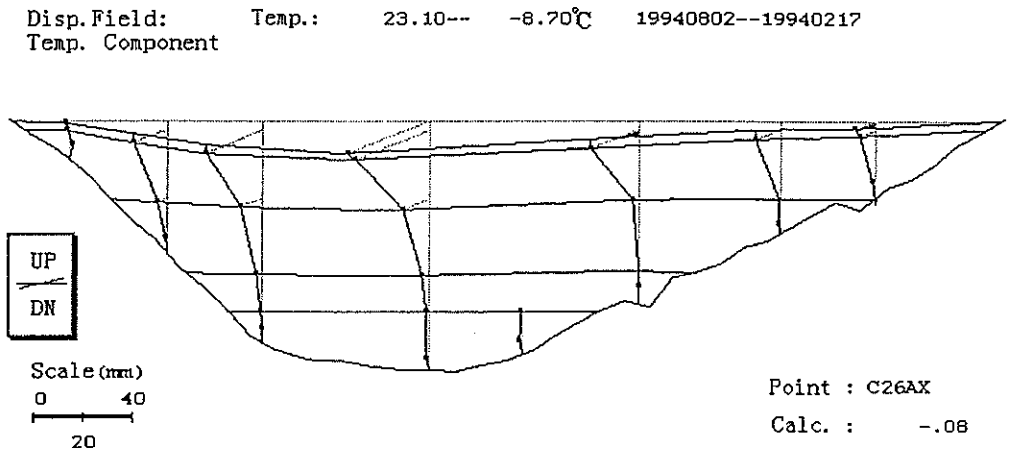

Fig. 8 The radial displacement field: component due to temperature.

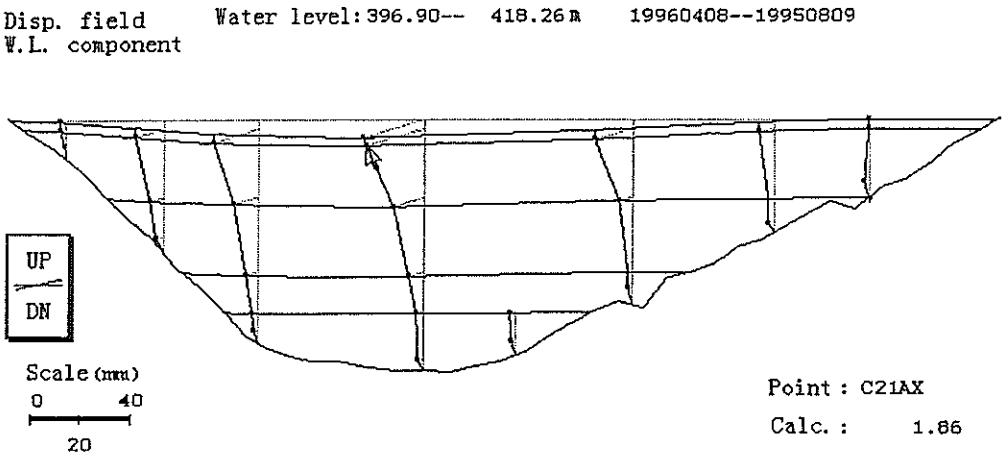

Fig. 9 The radial displacement field: component due to water load.

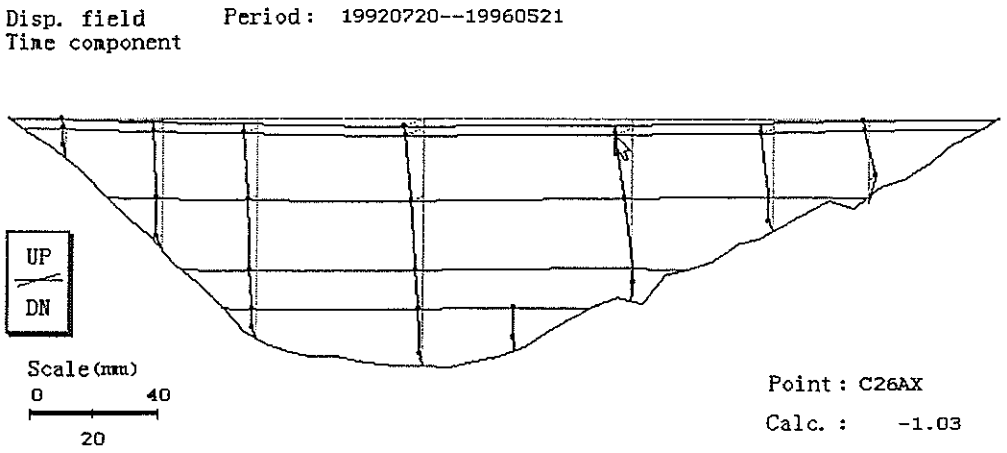

Fig. 10 The radial displacement field: component due to time.

In Equ.(5), the coefficient of correction is 0.872. Quite different from the case that the coefficient of correction varies in the range of from 0.7 to 1.1 for the points on the same (reversed) pendulum wire when the single point hybrid model is adopted, here only one coefficient of correction is necessary to describe the displacement at all the six points under different water loads. Moreover, the hybrid statistic model for displacement distribution can be used to obtain the degenerated model for any single point. Figs. 5 and 6 show the degenerated model for the point C17FX. The results are fairly satisfactory in terms of accuracy or the capacity of prediction in comparison with the single point hybrid model.

Based on the results of observation on the 27 measuring points, one 2D model of displacement distribution is established for a certain period:

$$
\begin{aligned}
Y = & -3.111 - 2.314h^4 - 0.076xy - 0.345x^3y^2 - 0.001y^6 + 0.549x^4y^2 - 0.924x^5y \\
& - 0.459x^6 + 0.186hxy^4 - 0.408hx^3y^2 + 2.26hx^5 + 0.41T_1xy^3 - 0.049T_1x^2y^3 \\
& - 0.004T_1^3y^2 + 4.164T_2x + 0.720T_2^2 - 1.120T_2y^2 - 3.156T_2x^2 + 0.220T_2y^4 \\
& + 0.201T_2xy^3 + 0.326T_2x^4 - 0.085T_2^5x^2y - 0.006T_2^3y^2 - 0.036T_2y^5 - 0.097T_2xy^4 \\
& + 0.079T_2x^2y^3 - 0.081T_2x^5 - 0.680\times10^{-4}Ty^3 + 0.591\times10^{-4}Ty^3 \\
& - 0.122\times10^{-9}T^3x^2 - 0.254\times10^{-4}Tx^3y^2 + 0.138\times10^{-4}Tx^5
\end{aligned}
\qquad (7)
$$

in which, y is a nondimensionalized variable with respect to the horizontal location of points parallel to the direction of the arch rings, all other variable mean the same as above.

For Equ. (7), the multiple correlation coefficient R is 0.978 and standard deviation S is 1.76mm.The fairly high multiple correlation coefficient and low standard deviation confirm the good fitting of the regression equation.

Figs.7 shows the computed and observed fields of the radial displacement of the dam at recorded highest water level. Figs. 8 through 10 show separately the fields of displacement distribution attributable to the effects of water load, temperature and time respectively.

Needless to say, using one model alone to describe the distribution of the radial displacement of the dam with satisfactory accuracy provides much convenience for data analysts and operation management in looking through the constantly increased data to get an overall knowledge of the behavior of the structure in operation.

The value of the correction coefficient in Equ (4) could give a guide to evaluate the validity of the input elastic modulus in an average sense for the elastic FEA, while an overall comparison of the measured displacements with the interpolated results of FEA could also provide information for the back analysis. The input elastic moduli were estimated about 10 to 20% higher in fitting the observed data.

CONCLUSIONS

1.The displacement distribution models were established and implemented in the data processing system for safety monitoring on computer for the Baishan Arch Dam. An overall picture of the dam deformation can be shown during operation period for monitoring.

2.Elastic finite element analyses were performed to predict a general deformation trend of the dam and help establish the hybrid displacement distribution model. The deformation law predicted by FEA agreed well with that shown by the measured data as far as the displacements induced by water load were concerned. It provided one important proof that the integrality of the arch dam is good enough to make the dam work as a whole.

REFERENCES

1. The Northeast Investigation and Design Institute of China: The Report on the stress analysis of the Baishan Arch Dam. June, 1987 (in Chinese).

2. The Technical Specification for the Safety Monitoring of Concrete Dam SDJ 336-89, issued jointly by the Ministry of Energy and the Ministry of Water Resources (in Chinese).

3. CHEN, Zongliang and ZHANG, Jinping: Introduction to the French Techniques for Safety Monitoring of Dams. March, 1988(in Chinese).

4. ZHANG, Jinping and ZHUANG, Wankang: A Mathematical Model of Displacement Distribution for Dam Monitoring. Journal of Hydraulic Engineering, No.5, 1991, Chinese Hydraulic Engineering Society (in Chinese).

5. ZHANG, Jinping and CHEN, Zhonghua, Data Processing and Displaying of Displacement Field Distribution Model for Dams, Applied Basic Research of the Three Gorges Project", Vol. 2, pp424-429. Geology Press, Beijing, 1997 (in Chinese).

USCOLD

United States Committee on Large Dams
1616 Seventeenth Street, Suite 483
Denver, Colorado 80202
Phone: 303-628-5430
Fax: 303-628-5431
E-mail: stephens@uscold.org
Internet: www.uscold.org/~uscold